Synthesis and Biological Characterization of Natural and Designed Sugars

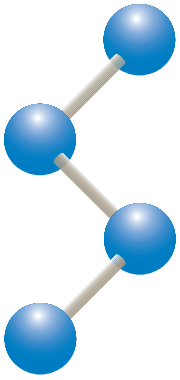

THE SCRIPPS RESEARCH INSTITUTE

J. L. Kiappes

Lincoln College

The Skaggs Institute
for Chemical Biology
Department of Chemistry
The Scripps Research Institute

Antiviral Drug Discovery Unit
Oxford Glycobiology Institute
Department of Biochemistry
University of Oxford

Submitted in partial fulfillment
of the requirements for the degree of

Doctor of Philosophy

Hilary Term 2014

Supervisors: Prof. K. C. Nicolaou and Prof. Nicole Zitzmann

Abstract

Carbohydrates represent a keystone among biological molecules. Well known as a source of energy, sugars also form the backbone of various biopolymers, act as markers and receptors for cellular communication and modulate lipid and protein functions. As such a powerful class, carbohydrates represent a useful pool from which both nature and man have drawn structures to produce biologically active compounds with a variety of modes of action. Beyond their importance to biology, sugars have represented attractive synthetic targets to chemists given their densely functionalized scaffolds.

The work presented in this thesis aims to employ synthetic chemistry to provide both natural and designed carbohydrates in order to carry out biological studies to improve our understanding of these compounds' particular effects. In the first part, a synthesis is developed for the carboline disaccharide domain of the cytotoxic enediyne, shishijimicin A. The route employs a Reetz–Müller-Starke reaction to install the domain's quaternary center, with addition of a carboline dianion to complete the target.

Iminosugars represent the focus of the second portion of the thesis. These polyhydroxylated alkaloids have long been investigated for their ability to mimic single sugars, inhibiting various glycosidases and glycosyltransferases. The endocyclic nitrogen atom of members of this class can act as a functional handle for alkylation, with increased chain length increasing both potency of enzyme inhibition and toxicity *in cellula*. Specific iminopyranose structures with D-*gluco* stereochemistry have broad-spectrum antiviral activity, while those with D-*galacto* stereochemistry are antiviral with respect to hepatitis C, but not other genetically related viruses. Reported herein are syntheses of classes of iminosugars to determine the influence of both *N*-alkylation chain length and iminopyranose stereochemistry on the spectrum of antiviral activity. Complementing antiviral activity with isolated enzyme inhibition assays, the work aims to identify new targets for next generation antivirals.

Finally, the prototypical iminosugar, D-deoxynojirimycin, is conjugated to a second natural product, D-α-tocopherol. By replacing the more common normal alkyl group with a lipid, the goal was to reduce cellular toxicity, while also taking advantage of the natural active transport for the lipid to increase uptake of the drug. Surprisingly, this change provided a marked shift in selectivity of enzyme inhibition and antiviral ability. In order to fully characterize the mechanism, the mentioned enzymatic and antiviral studies were supplemented with lipidomic, STED-microscopy and pharmacokinetic investigations.

Take chances!
Make mistakes!
Get messy!

—Ms. Frizzle
The Magic School Bus

To my parents

Acknowledgements

I would like to begin by thanking my two supervisors, Profs. Nicole Zitzmann and K.C. Nicolaou. I had the good fortune of many learning experiences under the guidance of each of you. Thank you, K.C., for helping me to develop my synthetic and problem solving skills. Nicole- thank you for being willing to take on a synthetic chemist as a student, and not only allowing, but encouraging me to pursue new scientific adventures.

In addition to my supervisors, I received exceptional support from Prof. Raymond Dwek, whose dedication to the Glycobiology Institute, the Skaggs-Oxford program, and all of the scientists with whom he works is inspiring.

Work is not done in isolation, and it is with the benefit of exceptional coworkers that the work in this thesis was possible: Dr. Jochen Becker, Dr. Pietro Roversi, Emma Dixon, Alex Caputo, Simon Spiro, and Drew Sayce among others. I am especially indebted to Mrs. Michelle Hill and Dr. Joanna Miller, without whose patience, dedication and enthusiasm, I never would have learned nearly as much biology as I have, nor been able to collect the wealth of antiviral data contained herein.

Thanks is due to a number of collaborators—Prof. Atsushi Kato, Dr. Norica Branza-Nichita, Dr. Dom Alonzi, Dr. Claude Wolf, Prof. George Fleet, Dr. Jakub Chojnacki, and Prof. Christian Eggeling, all of whom provided their time and expertise to strengthen the work presented here. Dr. Alexander Weymouth-Wilson and Dr. Ieuan Davies gave me the chance to work at Dextra to perform large scale synthesis; I am very grateful for this experience.

I appreciate the useful suggestions, comments, and advice from my thesis examiners: Prof. Sabine Flitsch, Prof. Ian Wilson, and Dr. Mark Wormald; as well as my other Scripps thesis committee members: Prof. Dale Boger and Prof. Jim Paulson. The feedback provided by all of you greatly helped in improving this thesis. I would particularly like to thank Ian and Mark for their ongoing guidance not only about my thesis work, but my development as a scientist more generally.

Without the people who populated my life outside of lab—Heather, Marisa, Amanda, Katie, Erin, and Alexandros—I don't think I could have maintained my sanity, especially at the end. My chemistry teachers, Cindy Foley and Karla Lowerre, have been a reliable source of support, wise cracks, and wisdom that has always encouraged me.

Finally, I want to thank my family; in particular, my siblings, Anna and Ed, and my parents. Mom and Dad, you were my first teachers, and I'm still learning from you. You've been on this journey with me the longest- thanks for believing in me, even when I've had my doubts.

Contents

List of Figures

List of Schemes

List of Tables

List of Abbreviations, Acronyms and Symbols

$[\alpha]_{\mathrm{D}}^{25}$	specific rotation at 25 °C at the sodium D-line
Å	angstrom
AB	part of an AB spin system
Ac	acetyl
AF	ambiguous fit
Alloc	allyloxycarbonyl
aq.	aqueous
α-Toc	D-α-tocopherol
α-TTP	α-tocopherol transport protein
Bn	benzyl
br	broad
brsm	based on recovered starting material
BSA	bovine serum albumin
BVDV	bovine viral diarrhea virus
°C	degree Celsius
ca.	circa

calcd	calculated
CI	confidence interval
cm	centimeter
CMC	critical micelle concentration
CNX	calnexin
CRT	calreticulin
δ	NMR chemical shift in ppm downfield from tetramethylsilane
DAJ	1-deoxyallonojirimycin
d	doublet in NMR data; otherwise, day
DAST	diethylaminosulfur trifluoride
DENV	dengue virus
DGJ	1-deoxygalactonojirimycin
DIBAL-H	di(*iso*-butyl)aluminium hydride
DIJ	1-deoxyidonojirimycin
DMAP	4-(*N,N*-dimethylamino)pyridine
DMEM	Dulbecco's modified Eagle's media
DMF	*N,N*-dimethylformamide
DMJ	1-deoxymannojirimycin
DMP	Dess–Martin periodinane
DMSO	dimethyl sulfoxide
DNA	deoxyribonucleic acid
DNJ	1-deoxynojirimycin

dr	diastereomeric ratio
DRJ	1-deoxyaltronojirimycin
DTJ	1-deoxytalonojirimycin
DUJ	1-deoxygulonojirimycin
EDEM	ER degradation-enhancing α-mannosidase-like protein
EDTA	ethylenediaminetetraacetic acid
ELISA	enzyme-linked immunosorbent assay
equiv	equivalent
ERAD	ER-associated degradation
ER	endoplasmic reticulum
ESI	electrospray ionization
Et	ethyl
EU	endotoxin units
FCS	heat inactivated fetal calf serum
ffu	focus forming unit
Fmoc	fluorenylmethyloxycarbonyl
FOS	free oligosaccharide
FTIR	Fourier transform infrared spectroscopy
g	gram
GalCer	galactosylceramide
GBA	β-glucocerebrosidase, acid β-glucosidase, GCase
GCS	glucosylceramide synthase

GlcCer	glucosylceramide
GluI	ER α-glucosidase I
GluII	ER α-glucosidase II
GM3	monosialodihexosylganglioside
GSL	glycosphingolipid
h	hour
HBSS	Hank's buffered salt solution
HBV	hepatitis B virus
HCV	hepatitis C virus
HIV	human immunodeficiency virus
HMBC	heteronuclear multiple-bond correlation
HPLC	high-performance liquid chromatography
HRMS	high resolution mass spectrometry
HS	heat inactivated horse serum
Hz	Hertz
IC_{50}	half maximal inhibitory concentration
IF	immunofluorescence
IMS	industrial methylated spirits
i-Pr	*iso*-propyl
IR	infrared
IV	intravenous
J	NMR coupling constant

Jc1Luc	luciferase construct of HCV Jc1 chimera
K_a	acid dissociation constant
kb	kilobase
kg	kilogram
KHMDS	potassium bis(trimethylsilyl)amide
L	liter
LRMS	low resolution mass spectrometry
M	molar
MALDI	matrix-assisted laser-desorption ionization
m	multiplet
MDMΦ	monocyte derived macrophage
Me	methyl
MEM	minimum essential media
µF	microfarad
µg	microgram
mg	milligram
MHz	megahertz
µL	microliter
µM	micromolar
min	minute
mL	milliliter
mm	millimeter

mM	millimolar
mmol	millimole
MOI	multiplicity of infection
mol	mole
m.p.	melting point
MS	molecular sieves
MTS	3-(4,5-dimethylthiazol-2-yl)-5-(3-carboxymethoxyphenyl)-2-(4-sulfophenyl)-2*H*-tetrazolium, inner salt
Nap	2-naphthylmethyl
ng	nanogram
NI	no inhibition (at tested concentrations)
NJ	nojirimycin
nm	nanometer
nM	nanomolar
NMO	*N*-methylmorpholine-*N*-oxide
NMR	nuclear magnetic resonance
NOE	nuclear Overhauser effect
NS2-F	forward primer for BVDV NS2 coding sequence
NS2-R	reverse primer for BVDV NS2 coding sequence
NS	not significant
OST	oligosaccharyltransferase
PBS-T	PBS plus 0.1% (v/v) Tween-20
PBS	phosphate buffered saline

PCR	polymerase chain reaction
PDI	protein disulfide isomerase
PE	phosphoethanolamine
pet ether	petroleum ether, 40 – 60 °C fraction
pg	picogram
pH	$-\log_{10}$ of the H^+ concentration in M
Ph	phenyl
pK_a	$-\log_{10} K_a$
PO	oral delivery, *per os*
ppm	parts per million
PTLC	preparative thin layer chromatography
q	quartet
qRT-PCR	quantitative reverse transcription-polymerase chain reaction
quin	quintet
RLU	relative luciferase units
R_f	retention factor
s	singlet in NMR data; otherwise, second
sat.	saturated
SM	sphingomyelin
S_N2	bimolecular nucleophilic substitution
t	triplet
TBS	*tert*-butyldimethylsilyl

t-Bu	*tert*-butyl
$TCID_{50}$	50% tissue culture infective dose
TFA	trifluoroacetic acid
Tf	trifluoromethylsulfonyl
THF	tetrahydrofuran
TLC	thin layer chromatography
TMS	trimethylsilyl
TOF	time of flight
TPAP	tetrapropylammonium perruthenate
Ts	*p*-toluenesulfonyl
UDP	uridine diphosphate
UGGT	UDP-glucose:glycoprotein glycosyltransferase
UT	untreated control
UV	ultraviolet
V	volt
v/v	volume/volume
ν_{max}	wavenumber at maximum absorption
w/v	weight/volume

Notes on Nomenclature

Unless otherwise noted, the numbering and names are based upon the conventions endorsed by the International Union of Pure and Applied Chemistry.[1]

A notable exception to this is the naming of iminopyranoses and derivatives, where names are based on the the "*N*B-DNJ" nomenclature widely accepted in the iminosugar field. Alkylations are assigned one or two letter abbreviations (Table 1), while each iminopyranose stereochemistry is assigned based on the corresponding aldohexose (Figure 1).

Table 1: Iminosugar Nomenclature - Alkyl Groups

Alkyl Group	Iminosugar Abbreviation
Methyl	M
Ethyl	E
Propyl	R
Butyl	B
Pentyl	P
Hexyl	X
Heptyl	H
Octyl	O
Nonyl	N
Decyl	D
Undecyl	Md
Dodecyl	Ed
Tridecyl	Rd
Tetradecyl	Bd
Pentadecyl	Pd
Hexadecyl	Xd
Heptadecyl	Hd
Octadecyl	Od

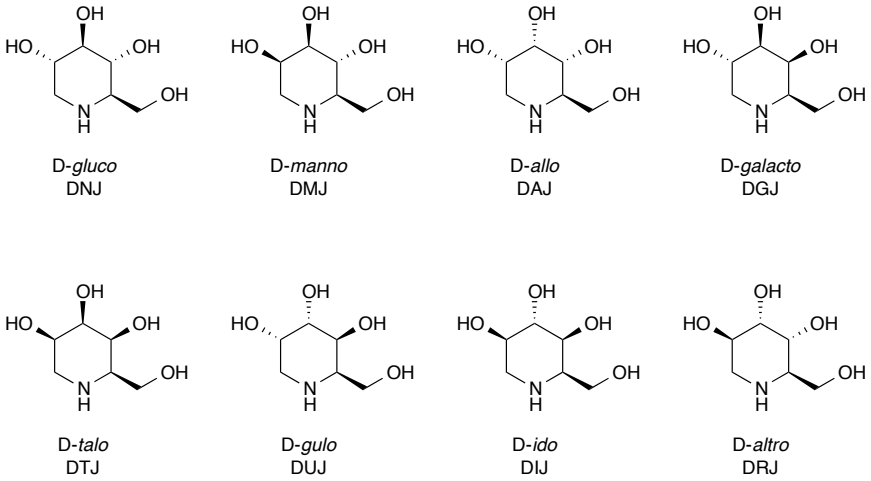

Figure 1: *Abbreviations for Iminopyranoses.*

Structures of glycans are drawn according to the Oxford system of glycan nomenclature,[2] with a color scheme adapted from the Consortium for Functional Glycomics (Figure 2). The color and shape of each sugar indicate the monosaccharide unit. The angle of lines between monosaccharides indicate the points of attachment of the glycosidic bonds, while the pattern of the bond indicates whether it is an α or β linkage.

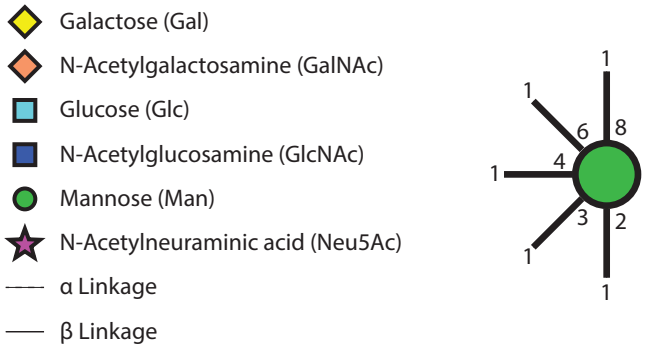

Figure 2: *Key to Glycan Nomenclature.*

Wisdom begins in wonder.

—Socrates

1

A Brief Introduction

When presented with the word "sugar," most minds will turn to a single specific substance, the sweet, white solid present in nearly every kitchen. However, this is just one specific disaccharide, sucrose **1** (Figure 1.1), made up of two simple sugars, glucose **2** and fructose **3**.

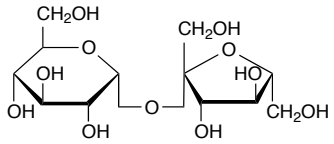

1

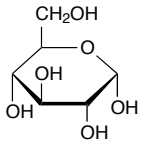

2

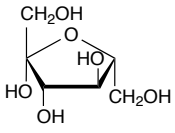

3

Figure 1.1: *Structure of Table Sugar.* The structure of the table sugar disaccharide, sucrose **1**, and its constituent monosaccharides, glucose **2** and fructose **3**.

The ubiquity of sugars extends beyond the kitchen, however. As monosaccharides and in various oligomeric and polymeric forms, sugars are perhaps the most pervasive

of all biological molecules. They serve as energy currency (adenosine triphosphate **4**, Figure 1.2), storage (glycogen **5**), and source (the variety of sugars in our diet including **1**). As an integral part of both primary and secondary metabolism, they warrant the interest and respect of both chemists and biologists.

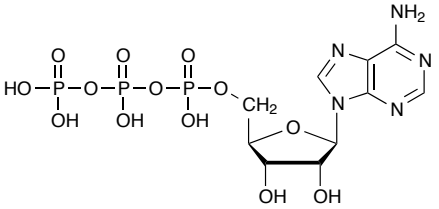

4

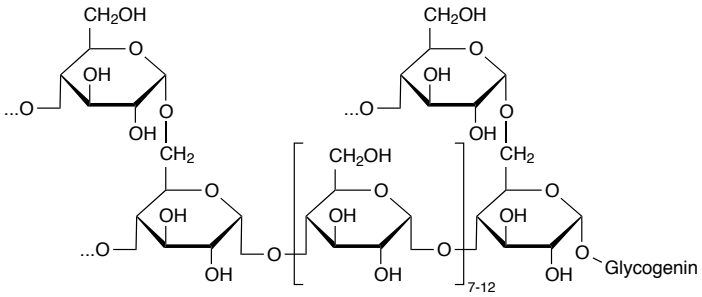

5

Figure 1.2: *Structures of Adenosine Triphosphate and Glycogen.* Adenosine triphosphate **4**, ATP, serves as the energy currency of the cell. A pentose, ribose, is modified with the purine base, adenine, and the reactive triphosphate. It is this functional group which stores the energy, as hydrolysis to adenosine diphosphate releases 30.5 kJ/mol of Gibbs' free energy.[3] Glycogen **5** is a polymer of glucose, acting as a storage form of the monosaccharide. Glycogenin is a protein that forms a homodimer, which serves as both an enzyme for initiating glycogen synthesis as well as the core to which the reducing end of glycogen is bound.[4] The main chain of the glycogen is connected by $\alpha(1\rightarrow4)$ glycosidic linkages; however, there is a branching point every 8–13 glucose residues, with the secondary arms diverging via an $\alpha(1\rightarrow6)$ linkage.

Synthesis provides a tool to make new sugars, as well as rare natural ones in larger amounts so that we can piece together the role this myriad molecules plays, and the far reach they truly have.

The first part of this thesis focuses solely on the synthesis of the saccharide domain of a potently cytotoxic natural product, shishijimicin A.

Following this, an introduction to another class of natural products, iminosugars, is provided along with an overview of the various metabolic pathways with which they

interfere.

The three next chapters explore the structure-activity relationships of iminosugars: first, the value of *N*-alkylation is evaluated as part of the optimization of high throughput antiviral assays. Next, these assays are put to use to investigate the importance of iminopyranose stereochemistry to the antiviral ability of an iminosugar. Finally, an iminosugar is conjugated to a second natural product, D-α-tocopherol, radically changing the molecule's biological effects, which are characterized in detail.

Aims of the Thesis:

- Develop a synthesis of the carboline-saccharide domain of the marine natural product, shishijimicin A. (Chapter 2)
- Improve understanding of the structure activity relationships of iminosugars for inhibition of specific pathways and for antiviral ability. (Chapters 3 – 6)

Οὐδὲν τοῖς θαρροῦσιν ἀνάλωτον

—Alexander the Great

2

Synthesis of the Carboline Disaccharide Domain of Shishijimicin A

2.1 Enediyne Natural Products

Isolated from the thin encrusting orange ascidian *Didemnum proliferum*, the shishijimicins (A – C, **6** – **8**, respectively; Figure 2.1)[6] and namenamicin **9**[7] represent the only members of the enediyne class that originate from marine sources. Enediynes are defined by the presence of a conjugated system of two carbon-carbon triple bonds separated by a single carbon-carbon double bond; isolated natural products of the class contain this series of functional groups in either a nine- or ten-membered ring.

The shishijimicins all carry the same ten-membered enediyne aglycone or "warhead," calicheamicinone **10**, which they also share with namenamicin and calicheamicin γ_1^{I}.[8] The martial moniker for this domain arises from the fact that it exhibits potent cytotoxicity via double stranded DNA cleavage. This deadly activity has earned the

The work presented in this chapter has been published.[5]

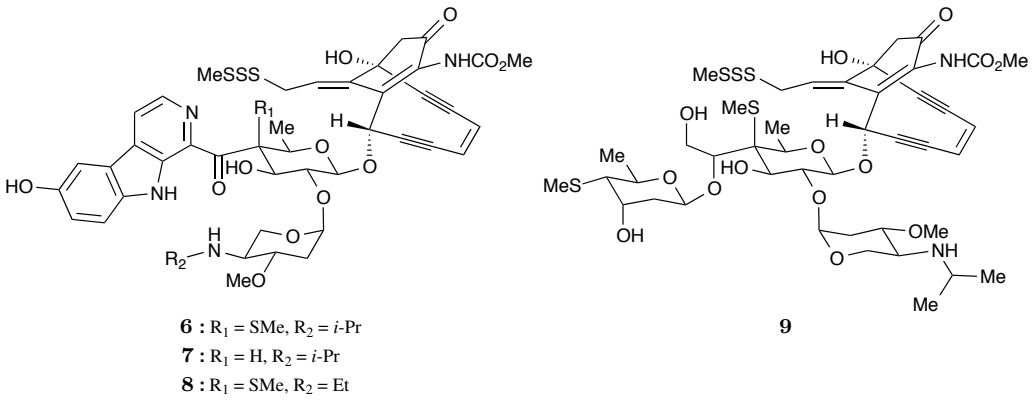

6 : R_1 = SMe, R_2 = *i*-Pr
7 : R_1 = H, R_2 = *i*-Pr
8 : R_1 = SMe, R_2 = Et

9

Figure 2.1: *Structures of shishijimicin A* ***6****, B* ***7****, C* ***8*** *and namenamicin* ***9****.*

archetypal class member, calicheamicin, a place in history as the poison supposedly used to kill Alexander the Great.[9]

In order to cleave DNA, the calicheamicinone must first be primed by nucleophilic cleavage of the trisulfide. In a cellular environment, glutathione has been shown to act as the nucleophile, unveiling a primary thiolate (Figure 2.2).[10] This moiety then does an intramolecular Michael-type addition to one of the bridgehead positions of the ten-membered enediyne. As the attacked carbon atom is forced to rehybridize from sp^2 to sp^3, the arrangement of the whole ring changes, and the termini of the enediyne become closer (3.43[11] to 3.16 Å). This shift in geometry permits a Bergman cyclization, producing a benzene diradical.[12] This subsequently abstracts two protons from the sugar backbone of DNA, initiating the process of strand cleavage with the exact mechanism depending upon the site of abstraction (Figure 2.3).[13]

While **10** is conserved amongst a number of natural products, they are each differentiated by the saccharide domain attached to it. In the case of calicheamicin γ_1^{I}, the aryloligosaccharide binds to the minor groove of DNA,[14;15] and imparts selectivity for 5′-TCCT-3′ and 5′-TCTC-3′ sequences.[16] The amino substituent is obligate for the DNA cleavage activity, with Myers suggesting that it aids in deprotonation of the thiol of glutathione for activation.[10] Not only can the aryloligosaccharide deliver the warhead intracellularly, but by binding on its own, it can disrupt DNA-protein interactions, acting as a transcription inhibitor.[17]

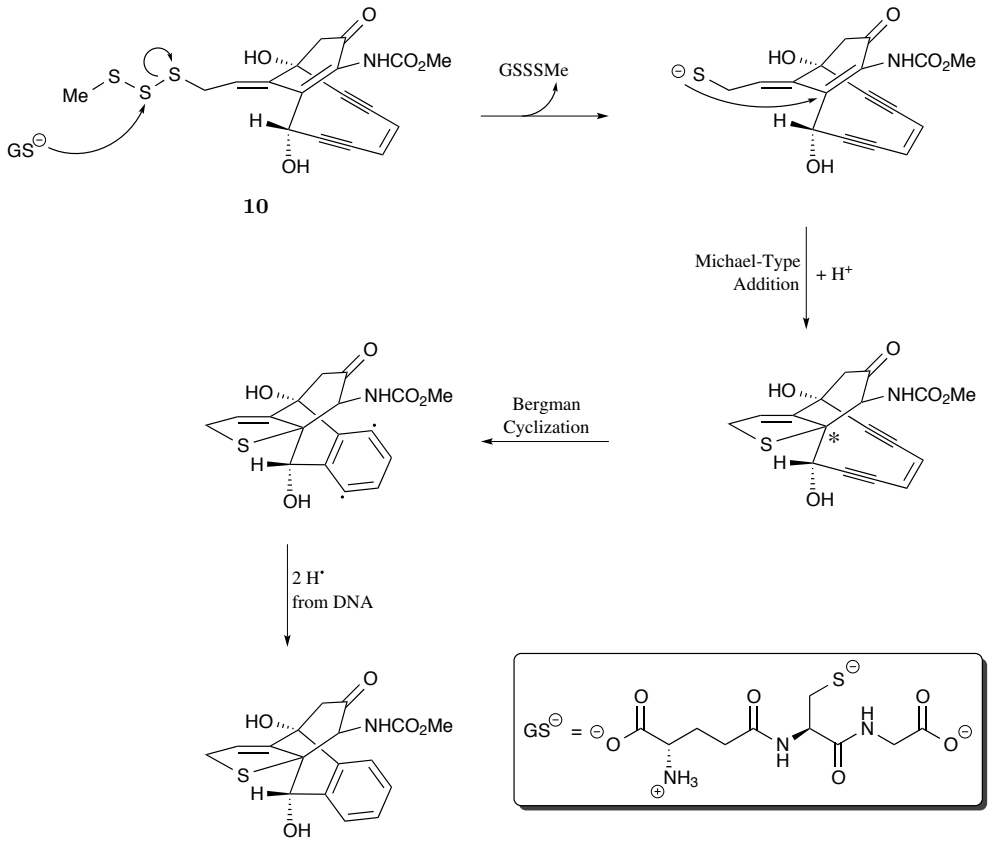

Figure 2.2: *Activation and Bergman Cyclization of Calicheamicinone **10**.* Deprotonated glutathione (GS^-) attacks the trisulfide moiety of **10**. Although addition to the outer and middle sulfur atoms are kinetically preferred, the equilibrium is funneled to the indicated route by its trapping via Michael addition. The conjugate addition causes rehybridization at the labelled carbon (∗), resulting in the two terminal alkynyl carbons becoming close enough to undergo a Bergman cyclization. The electrocyclic reaction provides the diradical, which abstracts a proton from each strand of DNA, starting the cleavage pathway indicated in Figure 2.3.

With this combination of molecular architectures, potent biological properties and medical potential, this class of natural products has captured the imagination of chemists, biologists and clinicians since its discovery. Thus, investigations of members of this family of compounds led to important advances in fundamental science and, by conjugating to antibodies to direct the cytotoxicity, practical applications in cancer chemotherapy.[18–24] In the two clinically approved calicheamicin conjugates, the antibody is attached via a linker to the molecular warhead (Figure 2.4).[25–27] As this moiety is conserved in the shishijimicins, antibody-drug conjugates could be prepared from synthetic shishijimicins in the same way.

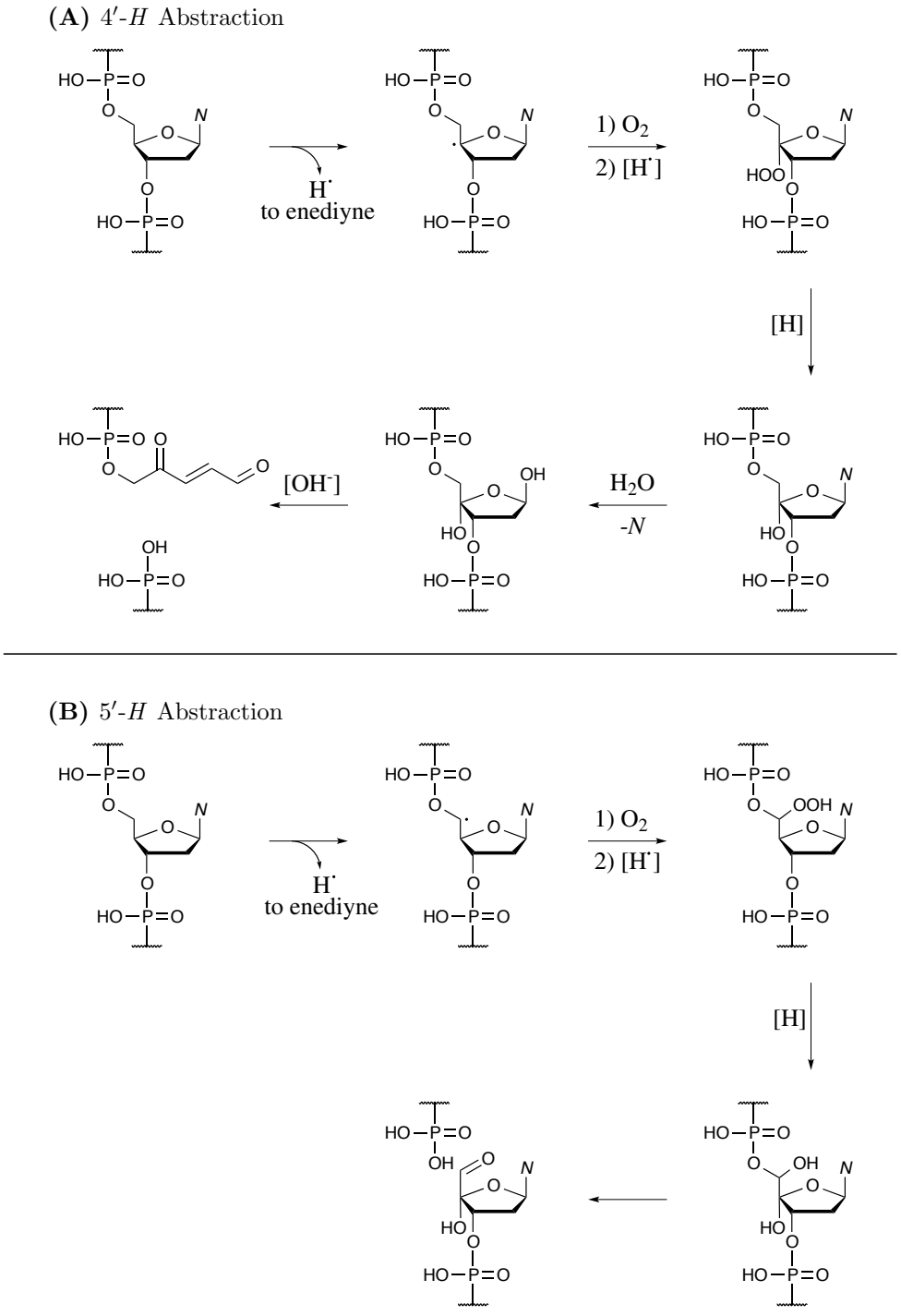

Figure 2.3: *Radical Pathways of DNA Strand Cleavage.* After hydrogen abstraction by the enediyne at either the 4′ or 5′ position of DNA, a series of oxidation and reduction reactions quench the radical and eventually result in hydrolyzable compounds. In these figures, *N* represents any DNA base.

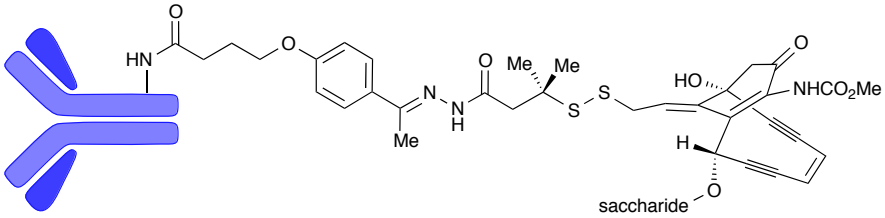

Figure 2.4: *Structure of the Calicheamicin-Antibody Linker.* Gemtuzumab ozogamicin and inotuzumab ozogamicin, the two clinically approved calicheamicin derivatives, employ anti-CD33 and anti-CD22 antibodies, respectively, to direct the cytotoxic molecule to leukemic cells. The linker which tethers the enediyne is stable at physiological pH (7.4), but permits two cleavage events under specific conditions.[25] The first takes place in the lysosome after cellular uptake; the acidic environment (pH 4) catalyzes hydrolysis of the hydrazone, severing the enediyne from the antibody. As with the trisulfide of the natural product (Figure 2.2), the disulfide bond of the synthetic derivative is cleaved by glutathione, at which point the mechanism is identical to that of natural calicheamicins. Though this figure only shows one drug molecule per antibody, the linker allows attachment to any terminal amine on the antibody, and the approved drugs contain an average of 2.5 moles of enediyne per mole of antibody.[26;27]

What sets the shishijimicins apart from all other enediynes is their unique carboline structural motif. Indeed, β-carboline is known to intercalate into double-stranded DNA,[28–38] and a number of β-carbolines have been shown to cleave DNA under photoirradiation conditions.[39] Shishijimicin A (**6**) displays the most potent toxicity of the shishijimicin family (Table 2.1). In light of these observations and the extreme scarcity of shishijimicin A, its total synthesis and that of its carboline disaccharide domain are deemed important.

Table 2.1: *Marine Enediyne Cytotoxicity.*[6]

Cell Line	CC_{50} (pg/mL)			
	6	**7**	**8**	**9**
3Y1	2.0	3.1	4.8	13
HeLa	1.8	3.3	6.3	34
P388	0.47	2.0	1.7	3.3

2.2 Retrosynthetic Analysis of Shishijimicin A

Using a glycosylation disconnection analogous to that in syntheses of calicheamicin,[40–44] one obtains calicheamicinone **10** and the targeted disaccharide fragment **11** (Figure 2.5). Subsequent retrosynthetic rupture of **11** revealed carboline deriva-

tive **12**, methylthio sugar **13**, and *N*-alloc aminoglycosyl fluoride **14** as the required building blocks.

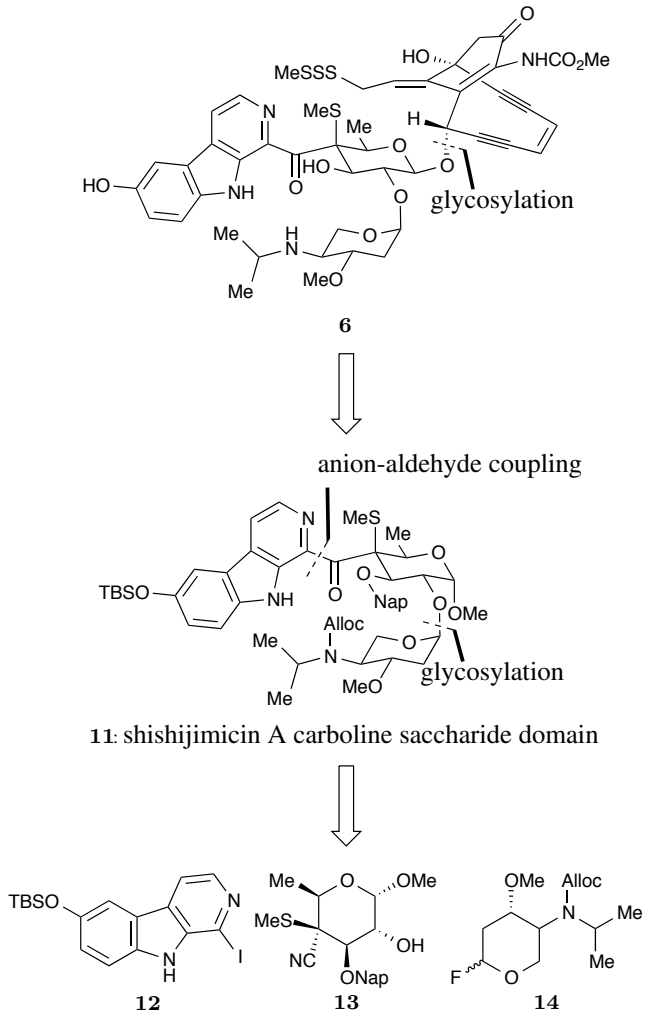

Figure 2.5: *Retrosynthetic Analysis of Shishijimicin A* ***6*** *and its Carboline Disaccharide Domain* ***11****.*

2.3 Synthesis of the Carboline Disaccharide Domain

Scheme 2.1 summarizes the developed expedient route to carboline derivative **12** starting with 5-methoxytryptamine **15**. Thus, **15** was sequentially treated with triphosgene (60 – 70 °C) and 30% HBr in glacial acetic acid (100 °C) to afford the rather insoluble dihydrocarboline **16** in 72% overall yield. The fully aromatized carboline **17** was obtained from the latter compound through oxidation in the presence of 10%

Pd/C in refluxing cumene (4 d, 68% yield). Previous studies[45;46] with carboline dianions employed bromide derivatives; however, in this case, the bromide was obtained in rather low yield (*i.e.* <40%), prompting us to target the corresponding iodide derivative. Toward this end, and capitalizing on the reactivity of the hydroxypyridine moiety of compound **17**, the latter was transformed first to its triflate (Tf_2O, pyridine) and then to its iodide in the same pot by iodide displacement (NaI, TfOH) in 61% overall yield.[47] Exchange of protecting group within the so-obtained iodo-β-carboline **18** (BBr_3 – demethylation; TBSOTf – silylation) led to the desired carboline block **12** in 55% overall yield.

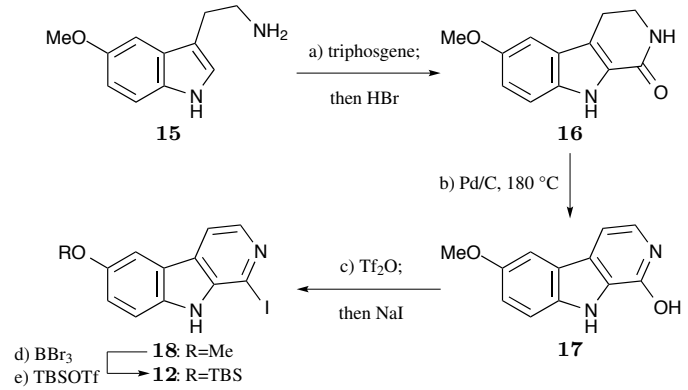

Scheme 2.1: *Synthesis of β-Carboline Intermediate **12**.* Reagents and conditions: Et_3N (2.5 equiv), triphosgene (0.5 equiv), PhMe , 60 – 70 °C, 20 min; then HBr, 100 °C, 30 min, 72%; b) 10% Pd/C (200 weight %), cumene, 180 °C, 4 d, 68%; c) pyridine (1.2 equiv), Tf_2O (1.1 equiv), MeCN, 0 → 25 °C; then NaI (5.0 equiv), TfOH (2.1 equiv), 25 °C, 61%; d) BBr_3 (8.0 equiv), CH_2Cl_2, –78 → 25 °C, 1.75 h; e) *i*-Pr_2NEt (5.0 equiv), TBSOTf (1.3 equiv), DMF, 0 → 25 °C, 1 h, 55% over the two steps. Tf = trifluoromethylsulfonyl, TBS = *tert*-butyldimethylsilyl, DMF = *N,N*-dimethylformamide.

With the carboline coupling partner in hand, attention turned to the synthesis of the central unit of the molecule, namely the methylthio sugar **13**. Successful construction of this intermediate commenced with differentially protected glycoside **19**[48;49] and proceeded as shown in Scheme 2.2. Cleavage of the benzylidene group under acidic conditions (TsOH) liberated the 1,3-diol system **20** (80% yield), whose tosylation (TsCl, Et_3N, DMAP cat.) furnished monotosylate **21** in 89% yield. Subsequent reduction of the tosylate **21** with $LiAlH_4$ led smoothly to 6-deoxymethylpyranoside **22** in 94% yield. The remaining hydroxyl group within **22** was then oxidized with

NMO in the presence of TPAP (cat.), yielding ketone **23** (84% yield). Aiming for the eventual installment of the quaternary center bearing the methylthio and nitrile groups in the growing molecule, ketone **23** was treated with TMSSMe and TMSOTf in CH_2Cl_2 at –78 – 0 °C to furnish dithioketal **24** in 94% yield. Careful monitoring of the temperature for this reaction was important, as warming above 0 °C resulted in formation of by-products in which the anomeric methoxy group was replaced with a methylthio substituent.

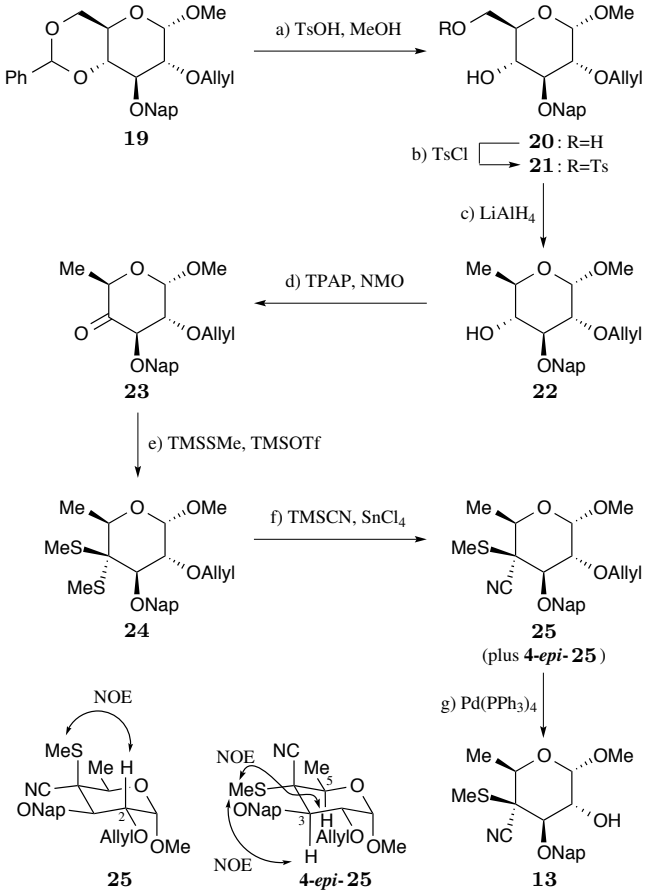

Scheme 2.2: *Synthesis of Thiosugar Intermediate **13**.* Reagents and conditions: a) TsOH (0.5 equiv), $MeOH/CH_2Cl_2$ (4:1), 25 °C, 48 h, 80%; b) Et_3N (1.3 equiv), TsCl (1.1 equiv), DMAP (0.1 equiv), CH_2Cl_2, 25 °C, 8 h, 89%; c) $LiAlH_4$ (3.0 equiv), THF, 45 °C, 2.5 h, 94%; d) NMO (3.0 equiv), TPAP (0.1 equiv), CH_2Cl_2, 0 → 25 °C, 8 h, 84%; e) TMSSMe (2.2 equiv), TMSOTf (1.5 equiv), 4 Å MS, CH_2Cl_2, –78 → 0 °C, 20 min, 94%; f) TMSCN (1.5 equiv), $SnCl_4$ (1.1 equiv), CH_2Cl_2, 0 °C, 3 h, 75%, *dr* ca. 2:1; g) $Pd(PPh_3)_4$ (1.1 equiv), AcOH, 80 °C, 2 h, 77%. Nap = 2-naphthylmethyl, Ts = *p*-toluenesulfonyl, DMAP = 4-dimethylaminopyridine, THF = tetrahydrofuran, NMO = *N*-methylmorpholine *N*-oxide, TPAP = tetra-*n*-propylammonium perruthenate, TMS = trimethylsilyl, MS = molecular sieves.

To complete the construction of the central carbon center bearing the required methylthio

and nitrile groups, the Reetz–Müller-Starke reaction was called upon.[50] This method had been successful previously on dithioketals but not demonstrated on carbohydrates such as **24**, where the anomeric methoxy group may lead to complications. Despite these fears, it was observed that, under the conditions originally reported by Reetz and Müller-Starke (*i.e.* TMSCN, $SnCl_4$, CH_2Cl_2, 0 °C), dithioketal **24** reacted to afford the expected methylthio nitrile **25** as a ca. 2:1 diastereomeric mixture and in 75% combined yield. The structures of the chromatographically separated isomers **25** (major, desired) and **4-*epi*-25** (minor, undesired) were assigned by ^{1}H NMR spectroscopic analysis. Specifically, the desired isomer **25** exhibited a diagnostic nuclear Overhauser effect (NOE) between the methylthio group protons and the *C*-2 proton, whereas the undesired epimer did not (see chair structures **25** and **4-*epi*-25** in Scheme 2.2). In support of the stereochemical assignment of **4-*epi*-25** were the NOEs exhibited between its methylthio group protons and those of *C*-3 and *C*-5. All that remained to generate the targeted fragment **13** was the deallylation of intermediate **25**, a reaction that proceeded smoothly, and in 77% yield, in the presence of $Pd(PPh_3)_4$.

The remaining carbohydrate unit, glycosyl fluoride **14**, was prepared from the known amino glycoside **26**,[51;52] as summarized in Scheme 2.3. The Alloc group was chosen as a protecting group for the secondary amine moiety instead of the Fmoc group employed in previous work,[41;43;53] due to the anticipated basic conditions of the carboline coupling. Thus, treatment of **26** with allyl chloroformate in the presence of K_2CO_3 and 18-crown-6 led to carbamate **27** (98% yield), whose exposure to AcOH:H_2O (5:1) at 95 °C liberated lactol **28** (70% yield; 90% based on recovered starting material). Finally, glycosyl fluoride **14** was formed from the latter compound through the action of DAST in 64% yield.

With all three required fragments available, their coupling and elaboration to the targeted carboline disaccharide domain **11** became the next task. Scheme 2.4 summarizes the accomplishment of this goal. Coupling of carbohydrate fragment **13** with glycosyl donor **14** proceeded smoothly following the Mukaiyama protocol.[51;54;55] Thus, in the

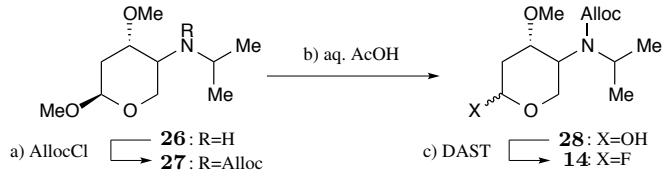

Scheme 2.3: *Synthesis of Amino Sugar Intermediate **14**.* Reagents and conditions: a) AllocCl (3.0 equiv), K_2CO_3 (6.0 equiv), 18-crown-6 (0.2 equiv), THF, 0 → 25 °C, 8 h, 98%; b) AcOH:H_2O (5:1), 95 °C, 8 h, 70% yield, 90% yield based on 22% recovered **31**; c) DAST (3.0 equiv), 4 Å MS, THF, –78 → –30 °C, 2 h; then 0 °C, 15 min, 64%. Alloc = allyloxycarbonyl, DAST = diethylaminosulfur trifluoride.

presence of $AgClO_4$ and $SnCl_2$ under anhydrous conditions (4 Å molecular sieves), the mixture afforded, stereoselectively, disaccharide **29** in 85% yield (based on **13**). The anomeric stereochemistry of the (1,4)-glycosidic linkage was confirmed by NMR coupling constant analysis. The anomeric proton displayed only $J < 5$ Hz, indicating a lack of axial-axial interactions. Direct addition of the dianion derived from carboline fragment **12** to disaccharide nitrile **29** gave a complex mixture of products, necessitating the intermediacy of aldehyde **30**. The latter was produced from **29** by DIBAL-H reduction (88% yield). Reaction of this aldehyde with the dianion generated from iodocarboline derivative **12** (KHMDS, Et_2O, –20 °C; then *t*-BuLi, –78 °C; then **30**) resulted in the formation of the corresponding coupling product as a mixture of diastereomeric alcohols (*dr* ca. 1:1; 70% yield based on 50% recovered starting material).[45] This mixture was then oxidized with MnO_2 to afford the targeted ketone **11** in 74% yield.

2.4 Conclusions and Future Directions

The described chemistry comprises the first reported route to the carboline disaccharide domain of shishijimicin A, demonstrating the application of the Reetz–Müller-Starke reaction and of the carboline dianion coupling in complex situations. The highly convergent synthesis provided the target **11** in 8% yield over the 11-step longest linear sequence from protected glucose **19** to the carboline disaccharide domain **11** of shishijmicin A (**6**), paving the way for an eventual total synthesis of the natural product itself. Indeed, such work is currently underway, with an aim to prepare

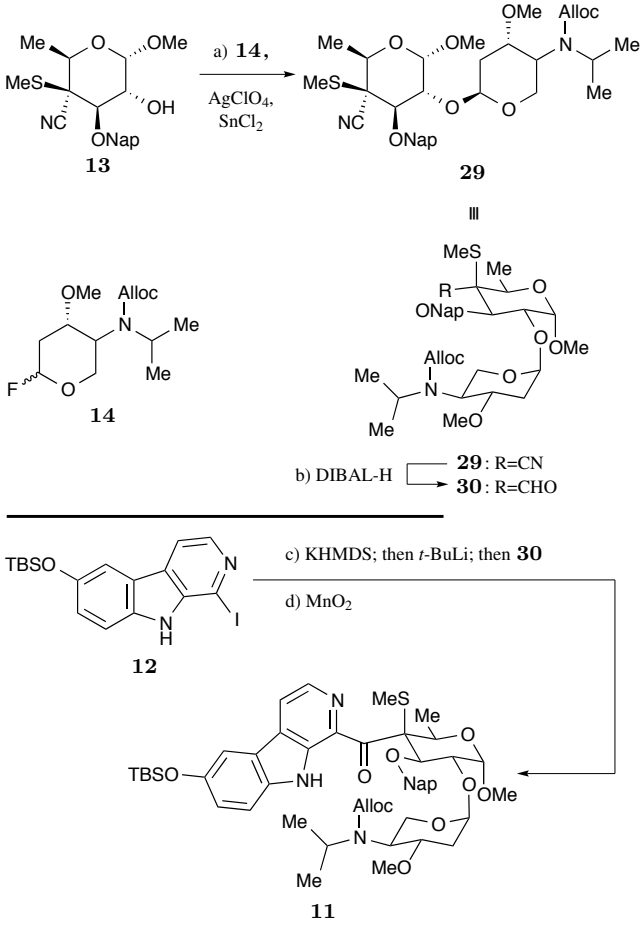

Scheme 2.4: *Endgame of Carboline Disaccharide Domain* ***11*** *Synthesis.* Reagents and conditions: a) Glycosyl donor **14** (2.2 equiv), $AgClO_4$ (3.3 equiv), $SnCl_2$ (3.3 equiv), 4 Å MS, THF, –78 °C, 1 h; then –78 → –30 °C, 2 h, 85% based on **13**; b) DIBAL-H (1.5 equiv), CH_2Cl_2, –78 → 0 °C, 1 h, 88%; c) carboline iodide **12** (2.3 equiv), KHMDS (2.5 equiv), Et_2O, –20 °C, 30 min; then *t*-BuLi (6.9 equiv), –78 °C, 30 min; then aldehyde **30** (1.0 equiv), –78 °C, 2 h; then –30 °C, 10 min, 35% yield based on **30**, 70% based on 50% recovered **30**; g) MnO_2 (150 equiv), CH_2Cl_2, 25 °C, 8 h, 74%. DIBAL-H = di(*iso*-butyl)aluminium hydride, KHMDS = potassium bis(trimethylsilyl)amide.

and evaluate the utility of shishijimicin A-antibody conjugates. Preparation of the aryloligosaccharide, in addition to enabling synthetic studies, allows pursuit of interaction studies with DNA. These can characterize whether the glycan displays binding to specific sequences, which, together with the binding data of calicheamicin γ_1^{I}, will provide a foundation for a more methodical study of the structure–activity relationships of DNA binding sugars.

2.5 General Procedures

All reactions were carried out under an argon atmosphere with anhydrous solvents under anhydrous conditions, unless otherwise noted. Anhydrous acetonitrile (MeCN), benzene, diethyl ether (Et_2O), *N,N*-dimethylformamide (DMF), tetrahydrofuran (THF), toluene, and methylene chloride (CH_2Cl_2) were obtained by passing commercially available pre-dried, oxygen-free formulations through activated alumina columns. Yields refer to chromatographically and spectroscopically (^{1}H NMR) homogeneous materials, unless otherwise stated. Reagents were purchased at the highest commercial quality and used without further purification, unless otherwise stated. Reactions were monitored by thin layer chromatography (TLC) carried out on 0.25 mm E. Merck silica gel plates (60F-254) using UV light as visualizing agent and an ethanolic solution of phosphomolybdic acid and cerium sulfate as a developing agent. Acros Organics silica gel (60, particle size 0.035–0.07 mm) was used for flash column chromatography. Preparative thin layer chromatography (PTLC) separations were carried out on 0.25 or 0.50 mm E. Merck silica gel plates (60F-254). NMR spectra were recorded on Bruker DRX-600, DRX-500, or AMX-400 instruments and calibrated using residual undeuterated solvent ($CDCl_3$: $\delta_H = 7.26$ ppm, $\delta_C = 77.16$ ppm; DMSO-d_6: $\delta_H = 2.50$ ppm, $\delta_C = 39.52$ ppm; C_6D_6: $\delta_H = 7.16$ ppm, $\delta_C = 128.06$ ppm; toluene-d_8: $\delta_H = 7.09, 7.00, 6.98, 2.09$ ppm, $\delta_C = 137.86, 129.24, 128.33, 125.49, 20.40$ ppm)[56] as an internal reference. The following abbreviations were used to designate the multiplicities: s = singlet, d = doublet, t = triplet, q = quartet, quin = quintuplet, m = multiplet, br = broad, AB = part of an AB spin system. IR spectra were recorded on a Perkin-Elmer Spectrum 100 FT-IR spectrometer. Electrospray ionization (ESI) mass spectrometry (MS) experiments were performed on an API 100 Perkin Elmer SCIEX single quadrupole mass spectrometer at 4000V emitter voltage. High-resolution mass spectra (HRMS) were recorded on a VG ZAB-ZSE mass spectrometer using MALDI (matrix-assisted laser-desorption ionization) or ESI (electrospray ionization). Optical rotations were recorded on a Perkin-Elmer Model 343 polarimeter at 589 nm, and are reported in units of 10^{-1} ($^\circ cm^2 g^{-1}$).

2.6 Selected Experimental and Physical Data

All tabulated NMR spectra described in this section may be found in Appendix A.

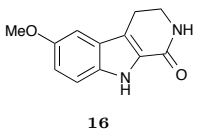

16

6-Methoxy-3,4-dihydro-2*H*-pyrido[3,4-b]indol-1(9*H*)-one 16: 5-Methoxytryptamine **15**[i] (1.902 g, 10.0 mmol, 1.0 equiv) was dissolved in toluene (200 mL) by heating the mixture at 80 °C. The solution was cooled to 50 °C and triethylamine (3.48 mL, 25.00 mmol, 2.5 equiv) was added. A solution of triphosgene (1.484 g, 5.00 mmol, 0.5 equiv) in toluene (20 mL) was added dropwise within 5 min to the vigorously stirred reaction mixture. The mixture was stirred at 60 – 70 °C for 20 min before HBr (30% in glacial acetic acid, 2.32 mL) was added. The reaction mixture was heated at reflux for 30 min and then cooled to 25 °C. H_2O (50 mL) and EtOAc (100 mL) were added, and the layers were separated. The aqueous layer was extracted with EtOAc (2 × 100 mL) and CH_2Cl_2 (2 × 100 mL). The combined organic layers were dried ($MgSO_4$), filtered and concentrated under reduced pressure. The residue was taken up in EtOAc (50 mL), and the suspension was concentrated under reduced pressure at 40 °C to a volume of 25 mL. The suspension was cooled to 25 °C, and the precipitate was decanted. The solution was removed via pipette, and the precipitate was washed with EtOAc (20 mL) to give **16** (2.327 g, 10.77 mmol, 72% yield) as a yellowish-white solid. **16**: $R_f = 0.31$ (silica gel, EtOAc); m.p. >250 °C (CH_2Cl_2); IR (neat) ν_{max} = 3392, 3347, 3187, 3078, 2992, 2967, 2906, 2830, 1653, 1543, 1493, 1467, 1445, 1391, 1327, 1296, 1279, 1250, 1226, 1214, 1193, 1109, 1024, 983, 931, 911, 839, 808, 775, 755, 716, 682 cm^{-1}; ^1H NMR (600 MHz, DMSO-d_6) δ = 11.42 (s, 1 H), 7.51 (br s, 1 H), 7.27 (d, J = 8.8 Hz, 1 H), 7.05 (d, J = 2.5 Hz, 1 H), 6.86 (dd, J = 8.8, 2.5 Hz, 1 H), 3.76 (s, 3 H), 3.49 (td, J = 7.0, 2.5 Hz, 2 H), 2.88 (t, J = 7.0 Hz, 2 H) ppm; ^{13}C NMR (150 MHz, DMSO-d_6): δ = 161.8, 153.5, 132.3, 127.7, 125.1, 117.7,

[i]Prepared by dissolving commercial 5-methoxytryptamine hydrochloride (5.0 g) in H_2O (70 mL) and heating the solution in a steam bath at 55 °C. At the same temperature, the solution was adjusted to pH = 12 with 20% (weight/volume, w/v) aq. KOH solution (ca. 9 mL, added dropwise). The suspension was slowly cooled to 25 °C, and the precipitate was filtered, washed with cold water (50 mL) and dried in a desiccator over P_2O_5 to give the free base as a white powder which could be stored for several days at room temperature over P_2O_5.

115.1, 113.3, 100.7, 55.3, 41.2, 20.4 ppm; HRMS (ESI-TOF): calcd for $C_{12}H_{12}N_2O_2$ [M + H^+]: 217.0971, found 217.0973.

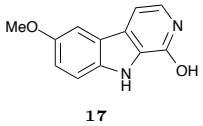

17

6-Methoxy-9*H*-pyrido[3,4-b]indol-1-ol 17: Finely powdered hydrocarboline **16** (1.293 g, 5.98 mmol, 1.0 equiv) was suspended in cumene (300 mL) and the mixture was purged with argon for 30 min. Pd/C (10% Pd, 1.293 g, 100 weight-%) was added, and the mixture was heated at reflux (180 °C oil bath) for 48 h. The reaction mixture was cooled to 60 °C, and additional Pd/C (10% Pd, 1.293 g, 100 weight-%) was added. The mixture was heated at reflux (180 °C oil bath) for 48 h until completion of the reaction (as monitored by TLC) and then cooled to 60 °C. EtOH (100 mL) was added, and the suspension was heated to reflux and filtered while still hot in order to avoid crystallization of the hydroxypyridine. Without being allowed to dry, the catalyst was washed with hot EtOH (200 mL). It is important that the catalyst was never allowed to dry completely, as this would have posed a combustion danger. The solvent was evaporated under reduced pressure to give pyridine **17** (875 mg, 4.09 mmol, 68% yield) as a white solid. **17**: R_f = 0.08 (silica gel, EtOAc); m.p. >250 °C (CH_2Cl_2); IR (neat) ν_{max} = 3316, 3145, 3007, 2956, 2924, 2850, 1643, 1609, 1497, 1454, 1419, 1402, 1298, 1272, 1217, 1195, 1169, 1122, 1092, 1070, 1021, 891, 837, 811, 872, 714 cm^{-1}; ^{1}H NMR (500 MHz, DMSO-d_6): δ = 11.75 (s, 1 H), 11.29 (br s, 1 H), 7.53 (d, J = 2.5 Hz, 1 H), 7.41 (d, J = 8.9 Hz, 1 H), 7.05 (dd, J = 8.9, 2.5 Hz, 1 H), 7.03 (m, 1 H), 6.96 (d, J = 6.8 Hz, 1 H), 3.82 (s, 3 H) ppm; ^{13}C NMR (150 MHz, DMSO-d_6): δ = 155.8, 153.5, 134.1, 128.5, 124.0, 123.9, 122.2, 117.0, 113.3, 102.4, 99.8, 55.5 ppm; HRMS (ESI-TOF): calcd for $C_{12}H_{10}N_2O_2$ [M + H^+]: 215.0815, found 215.0812.

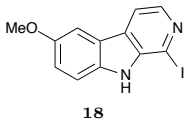

18

1-Iodo-6-methoxy-9*H*-pyrido[3,4-b]indole 18: To a stirred suspension of hydroxypyridine **17** (30 mg, 0.14 mmol, 1.0 equiv) and pyridine (13 µL, 0.16 mmol, 1.15 equiv) in MeCN (3 mL) at 0 °C (ice/water bath) was added Tf_2O (26 µL, 0.15 mmol, 1.10 equiv). The solution was warmed to 25 °C within 15 min and then stirred at 25 °C for 1 h. During this time, the suspension became a homogeneous solution. The solution was

then cooled back to 0 °C. While flushing with argon, freshly dried NaI (104.9 mg, 0.70 mmol, 5.00 equiv) was added, followed by dropwise addition of anhydrous TfOH (26 µL, 0.29 mmol, 2.10 equiv). The solution was warmed to 25 °C within 1 h, and then stirred at 25 °C for 18 h. The solution was diluted with EtOAc (7 mL) and H_2O (7 mL). While cooling to 0 °C, the pH of the aqueous layer was adjusted to 10 with 10 M NaOH aq. solution. The layers were separated, and the organic layer was washed with 5% aq. $Na_2S_2O_3$ (5 mL), 1 M aq. NaOH (5 mL), and brine (5 mL). The organic layer was then dried (Na_2SO_4), filtered and concentrated under reduced pressure. The residue was purified by flash column chromatography (silica gel, EtOAc:hexanes = 1:4) to give iodide **18** (28 mg, 0.09 mmol, 61% yield) as clear, colorless needle-like crystals. **18**: R_f = 0.30 (silica gel, EtOAc:hexanes = 1:4); m.p. = 173 °C (decomposition, Et_2O); IR (neat) ν_{max} = 3416, 3116, 3049, 2954, 2925, 2854, 1717, 1634, 1580, 1540, 1495, 1465, 1436, 1420, 1376, 1289, 1216, 1160, 1058, 1033, 1020, 914, 857, 820, 761 cm^{-1}; ^1H NMR (600 MHz, C_6D_6): δ = 8.13 (d, J = 5.1 Hz, 1 H), 7.33 (br s, 1 H), 7.27 (d, J = 5.1 Hz, 1 H), 7.22 (d, J = 2.5 Hz, 1 H), 7.14 (dd, J = 8.9, 2.3 Hz, 1 H), 6.68 (d, J = 8.9 Hz, 1 H), 3.44 (s, 3 H) ppm; ^{13}C NMR (150 MHz, C_6D_6): δ = 155.3, 140.4, 139.8, 134.6, 128.8, 123.5, 119.4, 114.9, 113.5, 104.0, 102.3, 55.7 ppm; HRMS (ESI-TOF): calcd for $C_{12}H_9IN_2O$ [M + H^+]: 324.9832, found 324.9833.

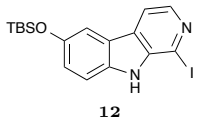

12

1-Iodo-6-(*tert*-butyldimethylsilyloxy)-9*H*-pyrido[3,4-b]indole 12: Methyl ether **18** (270 mg, 0.83 mmol, 1.0 equiv) was dissolved under argon in CH_2Cl_2 (60 mL) and the solution was cooled to –78 °C (dry ice/acetone bath). BBr_3 (1 M in CH_2Cl_2, 6.71 mL, 6.71 mmol, 8.0 equiv) was added, and the solution was stirred at –78 °C for 15 min. The mixture was warmed to 25 °C within 15 min and then stirred at 25 °C for 1.5 h. The solution was cooled back to –78 °C and quenched with sat. aq. $NaHCO_3$ (7.5 mL) and H_2O (7.5 mL). After warming to 25 °C, the reaction mixture was diluted with CH_2Cl_2 (150 mL) and H_2O (15 mL). The pH was adjusted to 7–8 with sat. aq. $NaHCO_3$ solution. The layers were separated, and the aqueous layer was extracted

with CH_2Cl_2 (2 × 75 mL). The combined organic layers were dried (Na_2SO_4), filtered and concentrated under reduced pressure to give crude alcohol as a pale yellow solid, which was dried under high vacuum overnight. The residue was dissolved in DMF (4.5 mL) under argon, and the solution was cooled to 0 °C (ice/water bath). *i*-Pr_2NEt (0.73 mL, 4.17 mmol, 5.0 equiv) was added, followed by TBSOTf (0.25 mL, 1.08 mmol, 1.3 equiv). The mixture was warmed to 25 °C and then stirred for 1 h. The mixture was cooled back to 0 °C and quenched with 1 M aq. NH_4Cl solution (9.0 mL). The mixture was warmed to 25 °C, diluted with H_2O (75 mL) and extracted with EtOAc (3 × 120 mL). The combined organic layers were dried (Na_2SO_4), filtered and concentrated under reduced pressure. Toluene (2 × 15 mL) was added to the crude product to azeotropically remove the DMF under reduced pressure. The residue was purified by flash column chromatography (silica gel, EtOAc:hexanes = 1:4) to give silyl ether **12** (193 mg, 0.45 mmol, 55% yield for the two steps) as pale yellow, needle-like crystals. **12**: R_f = 0.50 (silica gel, EtOAc:hexanes = 1:4); m.p. = 121 – 122 °C (Et_2O); IR (neat) ν_{max} = 3419, 3126, 3050, 2954, 2928, 2895, 2856, 2742, 1633, 1576, 1539, 1488, 1462, 1389, 1361, 1327, 1273, 1258, 1206, 1166, 1080, 1065, 1006, 950, 883, 851, 838, 823, 780 cm^{-1}; ^1H NMR (400 MHz, C_6D_6): δ = 8.07 (d, J = 5.1 Hz, 1 H), 7.45 (dt, J = 2.4, 0.6 Hz, 1 H), 7.40 (s, 1 H), 7.20 (dd, J = 5.1, 0.7 Hz, 1 H), 7.05 (dd, J = 8.8, 2.4 Hz, 1 H), 6.68 (dd, J = 8.7, 0.6 Hz, 1 H), 1.07 (s, 9 H), 0.18 (s, 6 H) ppm; ^{13}C NMR (100 MHz, C_6D_6): δ = 150.5, 140.5, 140.0, 135.1, 123.9, 123.1, 115.0, 113.1, 112.2, 102.1, 100.6, 26.3, 18.8, –4.0 ppm; HRMS (ESI-TOF): calcd for $C_{17}H_{21}IN_2OSi$ [M + H^+]: 425.0541, found 425.0539.

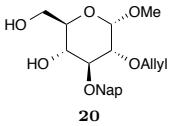

20

Diol 20: To protected glucose **19**[48;49] (5.30 g, 11.46 mmol, 1.0 equiv) and TsOH (1.09 g, 5.73 mmol, 0.5 equiv) were added MeOH (40.0 mL) and CH_2Cl_2 (10.0 mL). The mixture was stirred at 25 °C for 48 h. The reaction mixture was quenched with sat. aq. $NaHCO_3$ solution (40 mL), and the layers were separated. The aqueous layer was then extracted with CH_2Cl_2 (2 × 75 mL). The combined organic layers were dried ($MgSO_4$), filtered and concentrated under reduced pressure. The crude product was purified by flash

column chromatography (silica gel, EtOAc:hexanes = 1:9 → 100% EtOAc) to give diol **20** (3.42 g, 9.14 mmol, 80% yield) as a white solid. **20**: R_f = 0.08 (silica gel, EtOAc:hexanes = 1:1); $[\alpha]_D^{25}$ = +29.0 ($CHCl_3$, c = 2.90); IR ν_{max} (film): 3432, 2924, 1726, 1423, 1362, 1092, 1052 cm^{-1}; ^1H NMR (400 MHz, $CDCl_3$): δ = 7.87 – 7.78 (m, 4 H), 7.52 – 7.44 (m, 3 H), 6.03 – 5.90 (m, 1 H), 5.32 (dm, J = 17.2 Hz, 1 H), 5.23 (dm, J = 10.4 Hz, 1 H), 5.15 (d, J = 11.8 Hz, 1 H), 4.85 (d, J = 11.8 Hz, 1 H), 4.82 (d, J = 3.4 Hz, 1 H), 4.27 – 4.17 (m, 2 H), 3.88 – 3.71 (m, 1 H), 3.67 – 3.60 (m, 1 H), 3.60 – 3.53 (m, 1 H), 3.49 (dd, J = 9.5, 3.5 Hz, 1 H), 3.44 (s, 3 H), 2.31 (d, J = 2.3 Hz, 1 H), 1.93 (t, J = 6.4 Hz, 1 H) ppm; ^{13}C NMR (100 MHz, $CDCl_3$): δ = 136.5, 135.0, 133.7, 133.4, 128.9, 128.3, 128.1, 127.1, 126.6, 126.4, 126.2, 118.3, 98.6, 81.6, 80.2, 75.8, 72.7, 71.2, 70.8, 62.9, 55.6 ppm; HRMS (ESI-TOF): calcd for $C_{21}H_{26}O_6$ [M + Na^+]: 397.1621 found 397.1632.

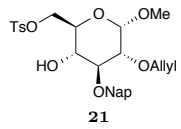

21

Tosylate 21: To a stirred solution of **20** (5.10 g, 13.6 mmol, 1.0 equiv) in CH_2Cl_2 (100 mL) at 25 °C was added triethylamine (2.47 mL, 17.7 mmol, 1.3 equiv) followed by *p*-tolunesulfonylchloride (2.86 g, 15.0 mmol, 1.1 equiv) and 4-dimethylaminopyridine (0.2 g, 1.4 mmol, 0.1 equiv). The resulting mixture was stirred at that temperature for 8 h. The mixture was diluted with Et_2O (200 mL) and passed through a pad of silica gel, eluting with Et_2O. The eluent was concentrated under reduced pressure. The crude residue was purified by flash column chromatography (silica gel, EtOAc:hexanes = 1:1) to give tosylate **21** (6.40 g, 12.1 mmol, 89% yield) as a white solid. **21**: R_f = 0.44 (silica gel, EtOAc:hexanes = 1:1); $[\alpha]_D^{25}$ = +15.8 ($CHCl_3$, c = 1.20); IR ν_{max} (neat): 3513, 2922, 1726, 1598, 1452, 1360, 1176, 1057, 977, 815 cm^{-1}; ^1H NMR (500 MHz, $CDCl_3$): δ = 7.87 – 7.75 (m, 6 H), 7.51 – 7.44 (m, 3 H), 7.32 (d, J = 8.0 Hz, 2 H), 5.99 – 5.89 (m, 1 H), 5.31 (dq, J = 17.2, 1.5 Hz, 1 H), 5.22 (dq, J = 10.3, 1.3 Hz, 1 H), 5.12 (ABd, J = 11.7 Hz, 1 H), 4.84 (ABd, J = 11.7 Hz, 1 H), 4.77 (d, J = 3.5 Hz, 1 H), 4.26 – 4.23 (m, 2 H), 4.21 – 4.17 (m, 2 H), 3.75 (t, J = 10.0 Hz, 1 H), 3.73 – 3.69 (m, 1 H), 3.51 – 3.43 (m, 2 H), 3.39 (s, 3 H), 2.43 (s, 3 H), 2.24 (d, J = 3.0 Hz, 1 H) ppm; ^{13}C NMR (125 MHz, $CDCl_3$): δ = 145.0, 136.2, 134.8, 133.5, 133.3, 133.2,

130.0, 128.7, 128.20, 128.18, 128.16, 127.0, 126.5, 126.3, 126.0, 118.3, 98.3, 81.1, 79.7, 75.6, 72.6, 69.6, 69.2, 69.1, 55.6, 21.9 ppm; HRMS (ESI-TOF): calcd for $C_{28}H_{32}O_8S$ [M + Na^+]: 551.1710 found 551.1715.

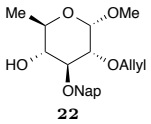

22

6-Deoxypyranoside 22: To a solution of tosylate **21** (1.86 g, 3.5 mmol, 1.0 equiv) in THF (25.0 mL) at 0 °C (ice/water bath) was slowly added $LiAlH_4$ (1.0 M in THF, 10.6 mL, 10.6 mmol, 3.0 equiv). The solution was warmed to 45 °C and stirred for 2.5 h. The solution was cooled back to 0 °C and quenched with ice (0.3 g), aq. NaOH (3 M, 0.6 mL), and H_2O (1.0 mL) successively. After stirring for 30 min, the suspension was filtered, and the residue was washed with EtOAc (15 mL). The solution was diluted with sat. aq. NH_4Cl (15 mL), and the layers were separated. The organic layer was dried ($MgSO_4$), filtered and concentrated under reduced pressure. The crude product was purified by flash column chromatography (silica gel, EtOAc:hexanes = 1:4 → 1:1) to give 6-deoxypyranoside **22** (1.18 g, 3.3 mmol, 94% yield) as a colorless oil. **22**: R_f = 0.44 (silica gel, EtOAc:hexanes = 1:1); $[\alpha]_D^{25}$ = +26.0 ($CHCl_3$, c = 1.40); IR ν_{max} (film): 3458, 2923, 1726, 1461, 1365, 1102, 1054, 920, 816 cm^{-1}; ^1H NMR (500 MHz, $CDCl_3$): δ = 7.87 – 7.79 (m, 4 H), 7.52 – 7.44 (m, 3 H), 6.02 – 5.92 (m, 1 H), 5.32 (dm, J = 17.2 Hz, 1 H), 5.22 (dm, J = 10.8 Hz, 1 H), 5.10 (ABd, J = 11.8 Hz, 2 H), 4.83 (ABd, J = 11.8 Hz, 2 H) 4.77 (d, J = 3.5 Hz, 1 H), 4.21 (dm, J = 6.0 Hz, 2 H), 3.75 (t, J = 9.2 Hz, 1 H), 3.70 – 3.62 (m, 1 H), 3.51 (dd, J = 9.6, 3.6 Hz, 1 H), 3.43 (s, 3 H), 3.21 (td, J = 9.2, 2.5 Hz, 1 H), 2.18 (d, J = 2.5 Hz, 1 H), 1.26 (d, J = 6.2 Hz, 3 H) ppm; ^{13}C NMR (125 MHz, $CDCl_3$): δ = 136.3, 134.9, 133.5, 133.2, 128.6, 128.1, 127.9, 126.9, 126.3, 126.1, 125.9, 118.0, 98.1, 81.3, 80.2, 75.5, 75.4, 72.3, 67.0, 55.2, 17.8 ppm; HRMS (ESI-TOF): calcd for $C_{21}H_{26}O_5$ [M + Na^+]: 381.1672 found 381.1678.

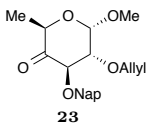

23

Ketone 23: To a solution of alcohol **22** (2.55 g, 7.12 mmol, 1.0 equiv) in CH_2Cl_2 (15 mL) was added NMO (2.50 g, 21.36 mmol, 3.0 equiv) at 25 °C. The solution was then cooled to 0 °C (ice/water bath). TPAP (250 mg, 0.71 mmol, 0.1 equiv) was added. The solution was warmed to

25 °C within 1 h, and then stirred at the same temperature for 8 h. Upon evaporation of the solvent, the crude product was purified by flash column chromatography (silica gel, EtOAc:hexanes = 1:19 → 1:9) to give ketone **23** (2.13 g, 5.98 mmol, 84% yield) as a colorless oil. **23**: R_f = 0.50 (silica gel, EtOAc:hexanes = 1:1); $[\alpha]_D^{25}$ = +84.3 ($CHCl_3$, c = 1.25); IR ν_{max} (film): 2987, 2937, 1734, 1447, 1361, 1195, 1147, 1049, 923, 819 cm^{-1}; ^1H NMR (600 MHz, $CDCl_3$): δ = 7.87 – 7.80 (m, 4 H), 7.57 (dd, J = 8.4, 1.5 Hz, 1 H), 7.49 – 7.44 (m, 2 H), 5.93 (dddd, J = 17.1, 10.4, 6.5, 5.4 Hz, 1 H), 5.29 (dq, J = 17.4, 1.6 Hz, 1 H), 5.21 (dq, J = 10.3, 1.2 Hz, 1 H), 5.10 (ABd, J = 11.5 Hz, 1 H), 4.90 (d, J = 3.5 Hz, 1 H), 4.82 (ABd, J = 11.5 Hz, 1 H), 4.45 (d, J = 10.2 Hz, 1 H), 4.35 (ddt, J = 12.9, 5.2, 1.3 Hz, 1 H), 4.24 – 4.17 (m, 2 H), 3.76 (dd, J = 10.1, 3.5 Hz, 1 H), 3.51 (s, 3 H), 1.31 (d, J = 6.5 Hz, 3 H) ppm; ^{13}C NMR (150 MHz, $CDCl_3$): δ = 203.6, 135.4, 134.6, 133.4, 133.2, 128.3, 128.1, 127.8, 126.9, 126.2, 126.1, 126.0, 118.3, 98.6, 82.8, 80.6, 74.5, 73.4, 69.2, 56.2, 13.9 ppm; HRMS (ESI-TOF): calcd for $C_{21}H_{24}O_5$ [M + Na^+]: 379.1516 found 379.1527.

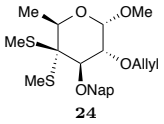

24

Dithioketal 24: To ketone **23** (100.0 mg, 0.28 mmol, 1.0 equiv) in CH_2Cl_2 (3.4 mL) under argon were added molecular sieves (4 Å, 168.0 mg). The solution was stirred at 25 °C until all of the ketone had dissolved. The solution was then cooled to –78 °C (dry ice/acetone bath) and stirred for 30 min in order to allow all moisture to be absorbed by the molecular sieves. TMSSMe (90 µL, 0.62 mmol, 2.2 equiv) was added to the solution, followed by addition of TMSOTf (80 µL, 0.42 mmol, 1.5 equiv). The reaction mixture was stirred at –78 °C for an additional 15 min, then the mixture was warmed to 0 °C (ice/water bath) within 10 min. After stirring at 0 °C for 5 min, the reaction mixture was quenched with sat. aq. $NaHCO_3$ (10 mL) and diluted with EtOAc (7 mL). The biphasic mixture was filtered through Celite. The layers were separated, and the aqueous layer was extracted with EtOAc (2 × 15 mL). The combined organic layers were washed with brine (15 mL), dried ($MgSO_4$), filtered, and concentrated under reduced pressure. The crude product was purified by flash column chromatography (silica gel, EtOAc:hexanes = 1:9 → 1:4) to give dithioketal **24** (114.4 mg, 0.26 mmol,

94% yield) as a yellow oil. **24**: R_f = 0.41 (silica gel, EtOAc:hexanes = 1:4); $[\alpha]_D^{25}$ = +51.5 ($CHCl_3$, c = 1.20); IR ν_{max} (film): 2923, 2850, 1732, 1458, 1362, 1266, 1100, 1049, 816 cm^{-1}; ^1H NMR (600 MHz, $CDCl_3$): δ = 7.86 – 7.78 (m, 4 H), 7.58 (dd, J = 8.4, 1.5 Hz, 1 H), 7.50 – 7.43 (m, 2 H), 5.99 – 5.90 (m, 1 H), 5.28 (dq, J = 17.3, 1.6 Hz, 1 H), 5.18 (dq, J = 10.3, 1.2 Hz, 1 H), 5.03 (ABd, J = 10.7 Hz, 1 H), 4.95 (ABd, J = 10.7 Hz, 1 H), 4.81 (d, J = 3.9 Hz, 1 H), 4.28 (ddt, J = 12.7, 5.5, 1.3 Hz, 1 H), 4.23 – 4.12 (m, 3 H), 3.95 (d, J = 9.4 Hz, 1 H), 3.43 (s, 3 H), 2.31 (s, 3 H), 2.16 (s, 3 H), 1.41 (d, J = 6.5 Hz, 3 H) ppm; ^{13}C NMR (150 MHz, $CDCl_3$): δ = 136.5, 135.0, 133.4, 133.0, 128.1, 128.0, 127.8, 126.6, 126.4, 126.1, 125.9, 117.8, 98.7, 83.0, 79.0, 73.0, 70.6, 65.9, 55.4, 16.2, 13.6, 12.6 ppm; HRMS (ESI-TOF): calcd for $C_{23}H_{30}O_4S_2$ [M + Na^+]: 457.1478 found 457.1484.

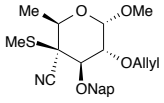

25

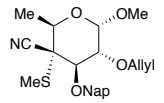

4-*epi*-25

Nitriles 25 and 4-*epi*-25: To a stirred solution of **24** (0.83 g, 1.91 mmol, 1.00 equiv) in CH_2Cl_2 (20 mL) at 0 °C (ice/water bath) were added TMSCN (0.28 g, 2.85 mmol, 1.50 equiv) and $SnCl_4$ (1 M in CH_2Cl_2, 2.0 mL, 2.0 mmol, 1.05 equiv). The resulting mixture was stirred at 0 °C for 3 h and then quenched with sat. aq. $NaHCO_3$ solution (20 mL). The resulting mixture was extracted with ether (2 × 20 mL), dried ($MgSO_4$), filtered and concentrated under reduced pressure. The crude residue was purified by flash column chromatography (silica gel, EtOAc:hexanes = 1:1) to give a mixture of nitriles **25** and **4-*epi*-25** (0.55 g, 1.33 mmol, 75% yield, ca. 2:1 *dr*) as a colorless oil. The two diastereoisomers were separated by PTLC (silica gel, EtOAc:hexanes 1:1), with assignment of the epimers by NOE studies. **25** (major nitrile): R_f = 0.47 (silica gel, MeOH:CH_2Cl_2 = 1:199); $[\alpha]_D^{25}$ = +53 ($CHCl_3$, c = 0.90); IR ν_{max} (film): 2928, 2232, 1443, 1344, 1139, 1100, 1034, 922, 820 cm^{-1}; ^1H NMR (600 MHz, $CDCl_3$): δ = 7.86 – 7.80 (m, 4 H), 7.54 (dd, J = 8.4, 1.5 Hz, 1 H), 7.50 – 7.46 (m, 2 H), 5.99 – 5.92 (m, 1 H), 5.32 (dq, J = 17.2, 1.5 Hz, 1 H), 5.23 (dq, J = 10.3, 1.5 Hz, 1 H), 5.05 (ABd, J = 10.5 Hz, 1 H), 5.05 (ABd, J = 10.5 Hz, 1 H), 4.78 (d, J = 3.8 Hz, 1 H), 4.36 (q, J = 6.4 Hz, 1 H), 4.30 (ddt, J = 12.7, 5.4, 1.4 Hz, 1 H), 4.27 (d, J = 9.5 Hz, 1 H), 4.18 (ddt, J = 12.7,

6.5, 1.2 Hz, 1 H), 4.05 (dd, J = 9.5, 3.8 Hz, 1 H), 3.44 (s, 3 H), 2.41 (s, 3 H), 1.48 (d, J = 6.4 Hz, 3 H) ppm; ^{13}C NMR (150 MHz, $CDCl_3$): δ = 135.3, 134.7, 133.4, 133.2, 128.3, 128.1, 127.8, 127.3, 126.6, 126.2, 126.2, 118.2, 116.9, 98.7, 82.1, 76.6, 76.6, 73.1, 67.6, 55.8, 53.9, 16.8, 16.0 ppm; HRMS (ESI-TOF): calcd for $C_{23}H_{27}NO_4S$ [M + Na^+]: 436.1553 found 436.1559. **4-*epi*-25** (minor nitrile): R_f = 0.53 (silica gel, MeOH:CH_2Cl_2 = 1:199); $[\alpha]_D^{25}$ = +104 ($CHCl_3$, c = 0.40); IR ν_{max} (film): 2928, 2232, 1721, 1453, 1341, 1196, 1107, 1041, 819, 751 cm^{-1}; ^{1}H NMR (600 MHz, $CDCl_3$): δ = 7.86 – 7.80 (m, 4 H), 7.51 – 7.45 (m, 3 H), 5.93 – 5.85 (m, 1 H), 5.27 (dq, J = 17.2, 1.5 Hz, 1 H), 5.18 (dq, J = 10.3, 1.2 Hz, 1 H), 5.16 (ABd, J = 11.5 Hz, 1 H), 5.02 (ABd, J = 11.3 Hz, 1 H), 4.84 (d, J = 3.5 Hz, 1 H), 4.24 (ddt, J = 12.6, 5.5, 1.3 Hz, 1 H), 4.16 (ddt, J = 12.7, 6.4, 1.2 Hz, 1 H), 3.93 (d, J = 9.7 Hz, 1 H), 3.89 – 3.83 (m, 1 H), 3.75 (dd, J = 9.7, 3.6 Hz, 1 H), 3.45 (s, 3 H), 2.40 (s, 3 H), 1.51 (d, J = 6.4 Hz, 3 H) ppm; ^{13}C NMR (150 MHz, $CDCl_3$): δ = 135.7, 134.4, 133.4, 133.1, 128.1, 127.8, 127.5, 126.2, 126.1, 126.0, 125.7, 118.4, 115.2, 98.4, 82.1, 79.1, 76.6, 73.0, 68.3, 55.8, 54.9, 16.9, 16.2 ppm; HRMS (ESI-TOF): calcd for $C_{23}H_{27}NO_4S$ [M + Na^+]: 436.1553 found 436.1556.

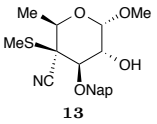

13

Alcohol 13: To a stirred solution of **25** (74 mg, 0.179 mmol, 1.0 equiv) in AcOH (2 mL) at 25 °C was added $Pd(PPh_3)_4$ (0.124 g, 0.107 mmol, 0.6 equiv). The resulting mixture was heated to 80 °C for 2 h. The mixture was quenched with sat. aq. $NaHCO_3$ solution (20 mL). The resulting mixture was extracted with Et_2O (2 × 20 mL), dried ($MgSO_4$), and concentrated under reduced pressure. The crude residue was purified by flash column chromatography (silica gel, CH_2Cl_2 → CH_2Cl_2:Et_2O = 99:1) to give alcohol **13** (51 mg, 0.137 mmol, 77% yield) as a colorless oil. **13**: R_f = 0.41 (silica gel, MeOH:CH_2Cl_2 = 1:99); $[\alpha]_D^{25}$ = +120 ($CHCl_3$, c = 0.73); IR ν_{max} (film): 3483, 2927, 2232, 1732, 1341, 1138, 1090, 1037, 920, 820 cm^{-1}; ^{1}H NMR (600 MHz, $CDCl_3$): δ = 7.88 – 7.80 (m, 4 H), 7.57 (d, J = 8.5 Hz, 1 H), 7.52 – 7.45 (m, 2 H), 5.09 (ABd, J = 11.0 Hz, 1 H), 5.06 (ABd, J = 11.0 Hz, 1 H), 4.76 (d, J = 3.9 Hz, 1 H), 4.33 (q, J = 6.1 Hz, 1 H), 4.25 (td, J = 9.1, 4.0 Hz, 1 H), 4.06 (d, J = 9.3 Hz, 1 H), 3.43 (s, 3 H), 2.43 (s, 3

H), 2.12 (d, J = 8.9 Hz, 1 H), 1.50 (d, J = 6.2 Hz, 3 H) ppm; ^{13}C NMR (150 MHz, $CDCl_3$): δ = 135.0, 133.4, 133.3, 128.5, 128.2, 127.9, 127.4, 126.4, 126.3, 126.3, 117.0, 99.5, 83.0, 76.1, 69.8, 68.1, 55.9, 53.2, 16.8, 15.8 ppm; HRMS (ESI-TOF): calcd for $C_{20}H_{23}NO_4S$ [M + Na^+]: 396.1240 found 396.1235.

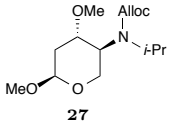

27

Carbamate 27: Allyl chloroformate (1.16 g, 9.61 mmol, 3.0 equiv) was added to a solution of **26**[52] (0.654 g, 3.20 mmol, 1.0 equiv) in THF (10 mL) at 0 °C (ice/water bath). K_2CO_3 (2.65 g, 19.2 mmol, 6.0 equiv) was added, followed by 18-crown-6 (170 mg, 0.6 mmol, 0.2 equiv). The mixture was warmed to 25 °C over 2 h, then stirred at 25 °C for a further 8 h. The mixture was quenched with sat. aq. NH_4Cl (20 mL). The aqueous layer was extracted with Et_2O (3 × 20 mL). The combined organic layers were washed with brine (20 mL), dried (Na_2SO_4), filtered and concentrated under reduced pressure. The crude residue was purified by flash column chromatography (EtOAc:hexanes = 1:1) to give carbamate **27** (0.90 g, 3.13 mmol, 98% yield) as a white foam. **27**: R_f = 0.50 (silica gel, EtOAc:hexanes = 1:1); $[\alpha]_D^{25}$ = –66.2 ($CHCl_3$, c = 2.73); IR ν_{max} (film): 2934, 1696, 1440, 1307, 1281, 1127, 1051, 993, 960, 901 cm^{-1}; ^{1}H NMR (600 MHz, $CDCl_3$): δ = 5.98 – 5.85 (m, 1 H), 5.39 – 5.23 (m, 1 H), 5.23 – 5.13 (m, 1 H), 4.75 (d, J = 2.2 Hz, 1 H), 4.63 – 4.51 (m, 2 H), 4.08 (m, 3 H), 3.41 (bs, 1 H), 3.30 (s, 3 H), 3.28 (s, 3 H), 2.28 (dd, J = 12.7, 3.7 Hz, 1 H), 1.48 (t, J = 10.6 Hz, 1 H), 1.27 –1.12 (m, 6 H) ppm; ^{13}C NMR (150 MHz, $CDCl_3$): δ = 171.2, 156.7, 155.5, 133.3, 132.9, 132.7, 117.9, 117.1, 99.1, 72.7, 71.7, 65.8, 65.7, 60.5, 60.0, 56.9, 54.9, 47.6, 36.0, 21.6, 21.0, 20.9, 20.3, 14.3 ppm; HRMS (ESI-TOF): calcd for $C_{14}H_{25}NO_5$ [M + Na^+]: 310.1625 found 310.1630.

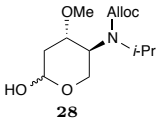

28

Lactol 28: A solution of **27** (0.90 g, 3.13 mmol, 1.0 equiv) in AcOH (5 mL) and H_2O (1 mL) was heated to 95 °C for 8 h. Upon cooling, toluene (20 mL) was added and the darkened mixture was concentrated. Azeotropic removal of AcOH with toluene (10 mL) was repeated four times. The crude residue was purified by flash column chromatography (silica gel, EtOAc:hexanes = 3:2) to give inseparable mixture of lactol anomers **28** and the

equivalent aldehyde (0.60 g, 2.20 mmol, 70% yield, 90% yield brsm) as a colorless oil. **28**: R_f = 0.31 (silica gel, EtOAc:hexanes = 1:1); IR ν_{max} (film): 3407, 2965, 2935, 1673, 1440, 1307, 1283, 1142, 1101, 1050, 1016, 1000, 925, 771 cm^{-1}; ^1H NMR (500 MHz, toluene-d_8, 80 °C): δ = see spectrum on 205. The spectrum shows a ratio of 23.5:13.7:1 (anomer 1 : anomer 2 : aldehyde); ^{13}C NMR (125 MHz, toluene-d_8, 80 °C): δ = 155.4, 155.2, 134.1, 134.0, 117.1, 117.0, 95.5, 93.0, 74.7, 72.7, 65.7, 64.2, 61.0, 58.2, 57.4, 56.4, 56.2, 48.9, 48.6, 39.4, 37.1, 21.3, 21.2, 21.0, 20.9 ppm; HRMS (ESI-TOF): calcd for $C_{13}H_{23}NO_5$ [M + Na^+]: 296.1468 found 296.1468.

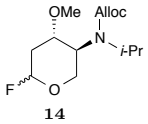

14

Fluoride 14: Powdered 4 Å molecular sieves (1.0 g) were added to a stirred solution of lactol **28** (0.355 g, 1.30 mmol, 1.0 equiv) in THF (10 mL). The mixture was cooled to –78 °C (dry ice/acetone bath) and DAST (0.627 mL, 3.90 mmol, 3.0 equiv) was added dropwise over 15 min. The temperature was allowed to slowly rise to –30 °C over 2 h and then held at 0 °C (ice/water bath) for 15 min. The reaction mixture was diluted with Et_2O (20 mL) and quickly filtered through a pad of Celite, followed by washing with Et_2O (2 × 20 mL). The filtrate was extensively washed with cold sat. aq. $NaHCO_3$ (8 × 10 mL), dried ($MgSO_4$), filtered and concentrated under reduced pressure. The residue was quickly filtered through a short plug of silica gel (hexanes → EtOAc:hexanes = 1:1) to give glycosyl fluoride **14** (0.229 g, 0.83 mmol, 64% yield) as a mixture of anomers (ca. 2:1 *dr*). The ^1H NMR spectrum contained too much overlap for individual assignment of most peaks to a specific anomer; however, the singlets of the methoxy peaks allowed estimation of the diastereomeric ratio. **14**: R_f = 0.57 (silica gel, EtOAc:hexanes = 1:1); IR ν_{max} (film): 2972, 2935, 1690, 1435, 1308, 1280, 1165, 1101, 1062, 979, 959, 908, 771 cm^{-1}; ^1H NMR (600 MHz, $CDCl_3$): δ = 6.01 – 5.88 (m, 1 H), 5.69 (d, J = 51.9 Hz, 0.7 H), 5.43 (dd, J = 8.0, 2.7 Hz, 0.3 H), 5.37 – 5.25 (m, 1 H), 5.25 – 5.16 (m, 1 H), 4.68 – 4.53 (m, 2 H), 4.50 – 3.70 (m, 3 H), 3.64 – 3.54 (m, 1 H), 3.32 (s, 1 H), 3.32 (s, 2H), 2.54 – 2.43 (m, 1 H), 1.68 – 1.46 (m, 1 H), 1.30 – 1.06 (m, 6 H) ppm; ^{13}C NMR (150 MHz, $CDCl_3$): δ = 155.1, 145.5, 133.2, 133.0, 132.8, 119.0, 117.3, 108.3, 108.2, 106.9, 106.7, 101.4, 72.2, 71.0, 66.1, 65.8, 63.4, 62.1, 57.3, 56.0,

55.4, 48.3, 47.8, 35.8, 29.8, 21.5, 21.3, 22.0, 20.4 ppm; HRMS (ESI-TOF): calcd for $C_{13}H_{22}FNO_4$ [M + Na^+]: 298.1425 found 298.1423.

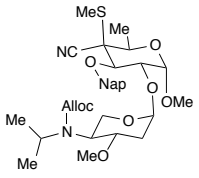

29

Glycoside 29: A mixture of anhydrous $AgClO_4$ (75 mg, 360 µmol, 3.3 equiv) and $SnCl_2$ (70 mg, 360 µmol, 3.3 equiv) was dried by azeotropic removal of benzene (2 × 2 mL). The salts were then suspended in THF (2 mL), and powdered, activated 4 Å molecular sieves (100 mg) were added. The suspension was stirred in the dark at 25 °C for 15 min and then cooled to –78 °C (dry ice/acetone bath). The solution was stirred at –78 °C for 30 min to allow all moisture to be absorbed by the molecular sieves. A solution of fluoride **14** (65 mg, 240 µmol, 2.2 equiv) and alcohol **13** (39 mg, 110 µmol, 1.0 equiv) in THF (2 mL) was added slowly to this solution, and the mixture was stirred at –78 °C for 1 h. The reaction mixture was allowed to warm slowly to –30 °C over 2 h, diluted with Et_2O (20 mL), and filtered through Celite. The resulting solution was washed with sat. aq. $NaHCO_3$ (2 × 20 mL) and brine (20 mL), dried ($MgSO_4$), filtered and concentrated. The resulting residue was purified by flash column chromatography (silica gel, EtOAc:hexanes = 1:9 → 2:3) to give glycoside **29** (56 mg, 90 µmol, 85% yield based on **13**) as a colorless oil. **29**: R_f = 0.72 (silica gel, EtOAc:hexanes = 1:1); $[\alpha]_D^{25}$ = +32.4 ($CHCl_3$, c = 1.80); IR ν_{max} (film): 2932, 2237, 1695, 1441, 1308, 1133, 1105, 1034, 963, 819 cm^{-1}; ^1H NMR (500 MHz, toluene-d_8, 80 °C): δ = 7.75 (s, 1 H), 7.66 – 7.61 (m, 2 H), 7.60 – 7.56 (m, 1 H), 7.46 (dd, J = 8.4, 1.7 Hz, 1 H), 7.25 – 7.19 (m, 2 H), 5.88 – 5.78 (m, 1 H), 5.16 (dd, J = 17.3, 1.6 Hz, 1 H), 5.01 – 4.95 (m, 3 H), 4.90 (d, J = 11.1 Hz, 1 H), 4.78 (d, J = 2.5 Hz, 1 H), 4.53 (d, J = 5.4 Hz, 2 H), 4.43 – 4.22 (m, 5 H), 4.11 – 4.03 (m, 1 H), 3.38 (dd, J = 10.3, 4.9 Hz, 1 H), 3.36 – 3.28 (m, 1 H), 3.22 (s, 3 H), 3.10 (s, 3 H), 2.30 (s, 3 H), 2.23 – 2.18 (m, 1 H), 1.45 (d, J = 6.4 Hz, 3 H), 1.37 – 1.30 (m, 1 H), 1.21 (d, J = 6.7 Hz, 3 H), 1.08 (d, J = 6.8 Hz, 3 H) ppm; ^{13}C NMR (125 MHz, toluene-d_8, 80 °C): δ = 155.2, 136.1, 134.2, 134.2, 134.0, 129.3, 128.4, 127.2, 126.4, 126.4, 126.3, 125.5, 117.0, 100.7, 82.9, 76.6, 68.3, 65.7, 61.4, 58.0, 54.9, 48.6, 37.0, 21.4, 21.0, 21.0, 17.9, 15.7 ppm; HRMS (ESI-TOF): calcd for $C_{33}H_{44}N_2O_8S$ [M + Na^+]: 651.2710 found

651.2714.

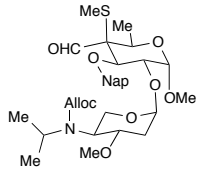

30

Aldehyde 30: To a stirred solution of **29** (70 mg, 110 µmol, 1.0 equiv) in CH_2Cl_2 (1.4 mL) at –78 °C (dry ice/acetone bath) was added DIBAL-H (1 M in CH_2Cl_2, 0.17 mL, 170 µmol, 1.5 equiv). The resulting mixture was stirred for 30 min at –78 °C, then for 30 min at 0 °C. The mixture was quenched with H_2O (0.5 mL) and sat. aq. $NaHCO_3$ solution (15 mL) at 0 °C. The resulting mixture was extracted with Et_2O (3 × 20 mL), dried ($MgSO_4$), filtered and concentrated under reduced pressure. The crude residue was purified by flash column chromatography (silica gel, Et_2O:CH_2Cl_2 = 1:19) to furnish **30** (61 mg, 97 µmol, 88% yield) as a colorless oil. **30**: R_f = 0.24 (silica gel, MeOH: CH_2Cl_2 = 1:49); $[\alpha]_D^{25}$ = +8.6 ($CHCl_3$, c = 0.41); IR ν_{max} (film): 2928, 1696, 1441, 1135, 1108, 1045, 993, 963, 816 cm^{-1}; ^1H NMR (500 MHz, toluene-d_8, 70 °C): δ = 9.43 (s, 1 H), 7.68 (s, 1 H), 7.64 – 7.55 (m, 3 H), 7.35 (dd, J = 8.4, 1.7 Hz, 1 H), 7.24 – 7.18 (m, 2 H), 5.91 – 5.79 (m, 1 H), 5.18 (d, J = 17.1 Hz, 1 H), 5.04 – 4.99 (m, 2 H), 4.95 (dd, J = 27.6, 11.3 Hz, 2 H), 4.86 (d, J = 3.8 Hz, 1 H), 4.64 (d, J = 9.7 Hz, 1 H), 4.54 (d, J = 5.5 Hz, 2 H), 4.47 (dd, J = 9.8, 3.7 Hz, 1 H), 4.40 (br s, 1 H), 4.07 (dd, J = 12.9, 6.5 Hz, 2 H), 3.41 (dd, J = 11.4, 4.8 Hz, 2 H), 3.24 (s, 3 H), 3.07 (s, 3 H), 2.21 (ddd, J = 12.9, 4.7, 1.6 Hz, 1 H), 2.07 (s, 3 H), 1.37 – 1.30 (m, 2 H), 1.26 (d, J = 6.5 Hz, 3 H), 1.22 (d, J = 6.7 Hz, 3 H), 1.11 (d, J = 6.8 Hz, 3 H) ppm; ^{13}C NMR (125 MHz, toluene-d_8, 50 °C): δ = 197.7, 155.1, 137.7, 137.4, 137.3, 137.0, 134.0, 134.0, 133.6, 128.4, 126.5, 126.3, 126.0, 116.9, 101.1, 100.6, 80.0, 76.3, 68.3, 67.4, 65.6, 61.2, 57.6, 56.0, 55.3, 48.1, 36.8, 30.3, 21.3, 16.3, 12.6, 1.4 ppm; HRMS (ESI-TOF): calcd for $C_{33}H_{45}NO_9S$ [M + Na^+]: 654.2707 found 654.2715.

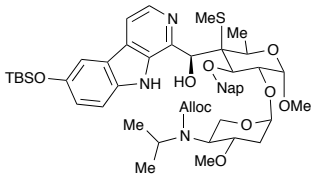

11'

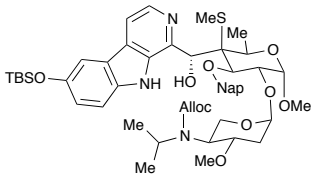

epi-11'

Alcohols 11′ and *epi*-11′: Iodide **12** (25 mg, 0.059 mmol, 2.3 equiv) was azeotroped with toluene (2 × 5 mL) under reduced pressure, then dried over P_2O_5 under vacuum. The flask was then charged with argon. Et_2O (1.0 mL) was added, and the solid was dissolved completely by stirring at 20–25 °C. The solution was cooled to –20 °C (dry ice/acetone bath). KHMDS (0.5 M in toluene, 0.13 mL, 65 µmol, 2.5 equiv) was added in order to deprotonate the carboline nitrogen atom, and the mixture was stirred for 30 min at –20 °C. The solution was then cooled to –78 °C (dry ice/acetone bath), and *t*-BuLi (1.75 M in toluene, 0.10 mL, 177 µmol, 6.9 equiv) was added dropwise. The reaction mixture was stirred at –78 °C for 30 min. Aldehyde **30** (17 mg, 26 µmol, 1.0 equiv) was azeotroped with toluene (2 × 5 mL) under reduced pressure and then dried over P_2O_5 under vacuum. The material was then dissolved in Et_2O (0.5 mL) under argon. The solution was then cannulated dropwise into the solution of the dianionic carboline at –78 °C. The cannula was further rinsed with Et_2O (0.5 mL) to ensure complete transfer of the aldehyde. The reaction was stirred at –78 °C for 2 h, warmed to –30 °C, then stirred at –30 °C for an additional 10 min. The mixture was quenched at –30 °C with AcOH (0.1 mL) and sat. aq. $NaHCO_3$ (10 mL), then it was warmed to 25 °C. The resulting mixture was extracted with EtOAc (2 × 30 mL), dried (Na_2SO_4), filtered and concentrated under reduced pressure. Due to observed decomposition on standing, the alcohols were used directly in the next step. The crude residue was purified for characterization by preparative TLC (silica, Et_2O:hexanes = 1:1) to give alcohols **11′** and ***epi*-11′** (4 mg each, 9 µmol total, 35% yield based on **30**, 70% yield brsm) as pale yellow oils. Both alcohols decomposed under the elevated temperatures required for NMR analysis (due to hindered rotation of the alloc carbamate), so the material was characterized spectroscopically after the following step. **11′** or ***epi*-11′**: R_f = 0.37 (silica gel, EtOAc/hexanes, 4:6); $[\alpha]_D^{25}$ = +12 ($CHCl_3$, c = 0.18); IR ν_{max} (film): 3382, 2926, 1693, 1485, 1460, 1259, 1094, 1047, 806 cm^{-1}; HRMS (ESI-TOF): calcd for $C_{50}H_{67}N_3O_{10}SSi$ [M + H^+]: 930.4389

found 930.4383. ***epi*-11′** or **11′**: R_f = 0.26 (silica gel, EtOAc:hexanes = 4:6); $[\alpha]_D^{25}$ = +1.1 ($CHCl_3$, c = 0.45); IR ν_{max} (film): 3448, 2956, 2928, 2955, 1694, 1485, 1462, 1260, 1093, 1047, 810 cm^{-1}; HRMS (ESI-TOF): calcd for $C_{50}H_{67}N_3O_{10}SSi$ [M + H^+]: 930.4389 found 930.4383.

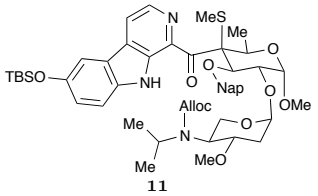

11

Ketone 11: To a stirred solution of a mixture of alcohols **11′** and ***epi*-11′** (8 mg, 8.7 µmol, 1.0 equiv) in CH_2Cl_2 (3.0 mL) at 25 °C was added activated MnO_2 (120 mg, 1.32 mmol, 150 equiv), and the resulting mixture was stirred for 8 h. The mixture was filtered and concentrated under reduced pressure. The crude residue was purified by preparative TLC (silica gel, Et_2O:hexanes = 1:1) to give ketone **11** (6 mg, 6.4 µmol, 74% yield) as a bright yellow oil. **11**: R_f = 0.38 (silica gel, Et_2O:hexanes = 1:1); $[\alpha]_D^{25}$ = +3.3 ($CHCl_3$, c = 0.18); IR ν_{max} (film): 3346, 2927, 1664, 1483, 1461, 1282, 1125, 1100, 1036, 885, 809 cm^{-1}; ^{1}H NMR (500 MHz, toluene-d_8, 65 °C): δ = 9.82 (s, 1 H), 8.12 (d, J = 4.8 Hz, 1 H), 7.35 (d, J = 1.9 Hz, 1 H), 7.31 – 7.12 (m, 7 H), 6.74 (d, J = 8.7 Hz, 1 H), 6.57 (d, J = 9.3 Hz, 1 H), 6.19 – 6.07 (m, 1 H), 5.94 (br s, 1 H), 5.38 – 5.01 (m, 5 H), 4.91 (d, J = 12.1 Hz, 1 H), 4.69 – 4.36 (m, 5 H), 4.43 (d, J = 12.0 Hz, 1 H), 4.07 (br s, 1 H), 3.70 – 3.41 (m, 6 H), 3.12 (s, 3 H), 2.80 (s, 3 H), 2.30 (br s, 1 H), 1.50 – 1.40 (m, 1 H), 1.35 (d, J = 6.5 Hz, 3 H), 1.27 (d, J = 6.0 Hz, 3 H), 1.18 (d, J = 5.8 Hz, 3 H), 1.07 (s, 9 H), 0.23 (s, 6 H) ppm; ^{13}C NMR (125 MHz, toluene-d_8, 65 °C): δ = 155.5, 150.8, 137.2, 136.9, 136.7, 134.5, 133.8, 133.4, 132.2, 126.4, 126.02, 125.98, 125.0, 123.2, 122.4, 118.9, 117.3, 113.0, 111.8, 101.6, 100.4, 84.5, 75.7, 68.8, 65.9, 61.6, 58.4, 56.2, 55.6, 42.7, 37.4, 26.3, 21.7, 18.8, 17.0, 15.4, –3.96 ppm; In order to find weaker carbon signals, an HMBC was performed. Additional ^{13}C determined by HMBC (600 MHz, toluene-d_8, 60 °C): δ = 80.9, 76.0, 73.2, 71.6 ppm; HRMS (ESI-TOF): calcd for $C_{50}H_{65}N_3O_{10}SSi$ [M + H^+]: 928.4232 found 928.4227.

It has become evident that a reevaluation of the biological role of oligosaccharides is necessary.

—Prof. Raymond Dwek, CBE, FRS

3

Iminosugars as Therapeutics

3.1 Introduction

Iminosugars are monosaccharide mimics with at least one nitrogen-containing cycle in their structure. In 1966, Inouye reported the first isolation of an iminosugar from natural sources, nojirimycin (NJ) **32D** (Figure 3.1) from *Streptomyces* bacteria, and observed its antibacterial effects.[57;58] Chemical synthesis of "heteroses"[59] (sugars where the endocyclic oxygen is replaced with a different heteroatom: nitrogen, phosphorus or sulfur) had, however, already been underway for a number of years.[60–66]

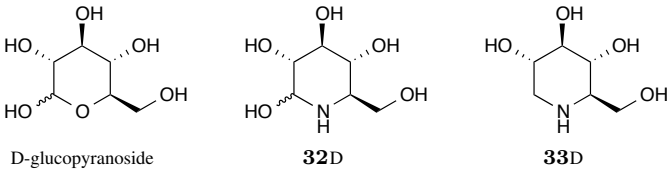

Figure 3.1: *Structures of Nojirimycin and 1-Deoxynojirimycin.*The two archetypal iminosugars, D-nojirimycin **32D** and D-1-deoxynojirimycin **33D**, with D-glucopyranoside for comparison.

Nojirimycin is unstable: decomposing under both neutral and acidic conditions and necessitating formation of its bisulfite adduct for purification.[58] As such, research

focused instead on its hydrogenated form. This reaction effects reduction of the anomeric carbon of nojirimycin, providing D-1-deoxynojirimycin (DNJ) **33D**, whose synthesis was first reported by Paulsen in 1966.[67–69] In addition to being synthetically accessible, DNJ was found to be a natural product a decade after the first report of its preparation, when it was isolated from mulberry trees *Morus alba*.[70]

As mentioned above, the first report of an iminosugar natural product included its promising biological activity.[57] By mimicking monosaccharides, iminosugars are able to act as competitive inhibitors of a myriad of glycosidases and glycosyltransferases, and, as a result of this activity, iminosugars (and plants rich in them) have a long history as therapeutics, recommended as herbal remedies for diabetes in both Eastern[71] and Western medicine.[59] With the passage of time, the focus of iminosugar studies have shifted from the novelty of molecular structures to their development as useful medicines and molecular tools. These efforts have resulted in clinically approved pharmaceuticals for diabetes mellitus and genetic glycolipid storage disorders,[72–74] as well as a number of candidates for the treatment of viral infections.

3.2 Iminosugar Structure

Natural iminosugars can be grouped by their cyclic scaffold into 5 classes (Figure 3.2), with both nojirimycin and deoxynojirimycin falling into the piperidine class. Perhaps unsurprisingly, this subgroup of iminosugars was the first pursued given the direct analogy between their structure and that of pyranose sugars (*e.g.*, D-glucopyranoside). Generally, but not always,[75] piperidine iminosugars competitively inhibit enzymes whose substrate have the same stereochemistry.

Though not studied in this thesis, there are four other natural classes of iminosugars. Pyrrolidines are 5-membered rings that visually resemble ketoses, such as fructose **3** (Figure 1.1), but are still often inhibitors of glucosidases. 2,5-dideoxy-2,5-imino-D-mannitol **36** (DMDP) is the most abundant natural iminiosugar,[81] a potent inhibitor of several β-glucosidases[82] and was the first pyrrolidine to be isolated from natural

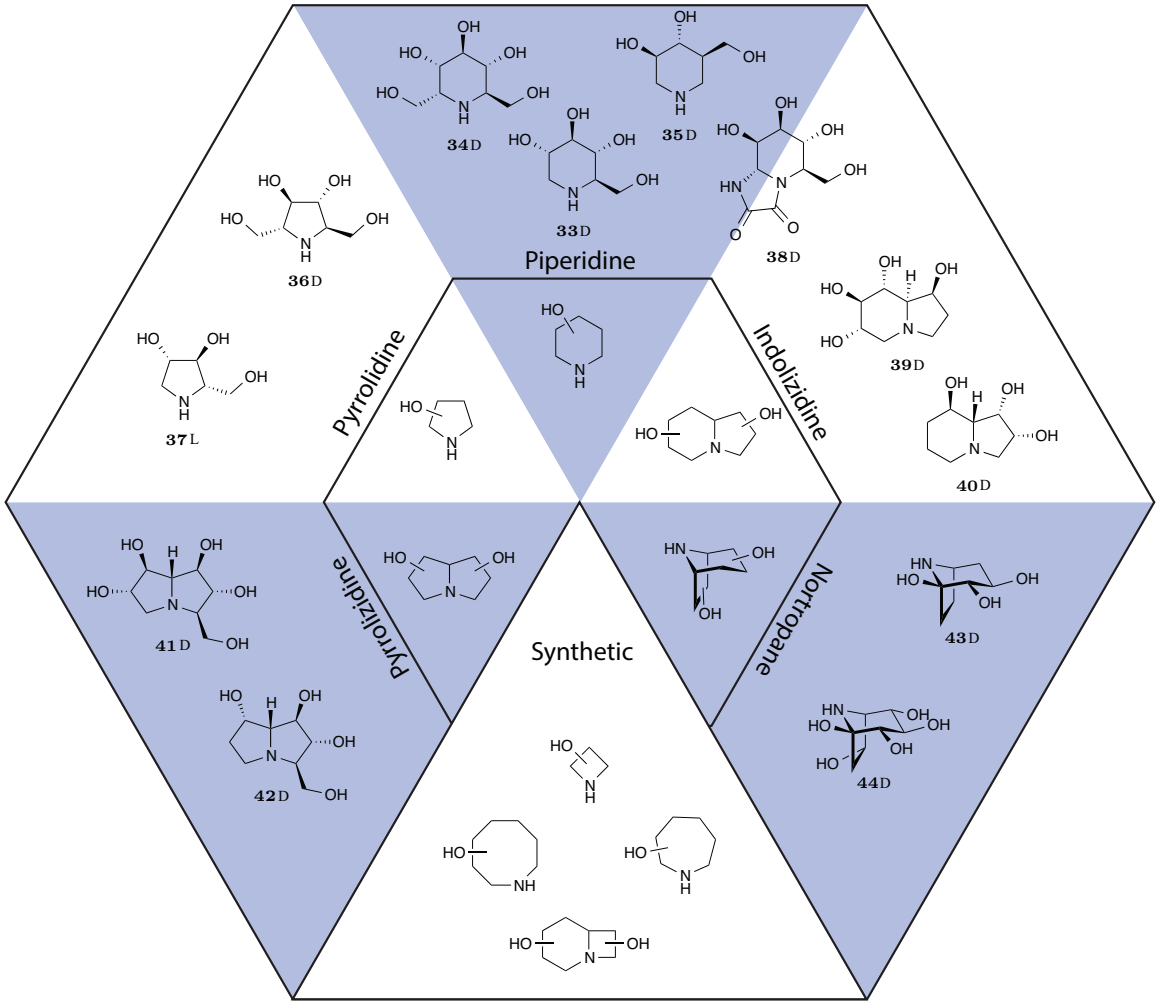

Figure 3.2: *Natural and Synthetic Structural Classes of Iminosugars.* The inner hexagon contains the characteristic framework of each natural iminosugar class, while the outer hexagon provides specific examples of isolated compounds. (Piperidine) DNJ **33**, α-homonojirimycin **34**, isofagomine, **35**; (Pyrrolidine) 2,5-dideoxy-2,5-imino-D-mannitol **36**, 1,4-dideoxy-1,4-imino-L-arabinitol **37**; (Indolizidine) castanospermine **39**, australine **42**; (Pyrrolizidine) casuarine **41**, swainsonine **40**; (Nortropane) calystegine A_3 **43**, calystegine C_1 **44**; (Piperidine-Indolizidine Hybrid) kifunensine **38**. (Synthetic Scaffolds) Iminosugars have been designed and synthesized with molecular architectures not yet isolated from nature, including azetidines,[76;77] azepanes,[78;79] 8-membered iminosugars,[76] and azetidine analogues of the bicyclic classes.[80]

sources in 1976.[83] Because of the ring contraction relative to piperidines, enzyme inhibition profiles are less predictable than for the 6-membered class. Recent work preparing D-DMDP **36D** and its 9 stereoisomers helped to elucidate the behavior of these compounds as a group.[82] Indolizidine and pyrrolizidines represent the bicyclic analogues of piperidines and pyrrolidines, respectively, with the presence of the second ring limiting conformational flexibility. The nortropane class is unique, being based

upon a bridged scaffold.

In pursuit of novel iminosugars, synthetic chemists have pushed the boundaries of iminosugar space further, invoking skeletons of both larger[76;78;79] and smaller rings.[76;77]

3.3 Glycosidases and their Inhibition

Glycosidases, or glycoside hydrolases, can be broadly defined as enzymes that catalyze the cleavage of a glycosidic bond to liberate an alcohol and either a mono- or oligosaccharide as a hemiacetal. Those that cleave only a single terminal sugar are referred to as *exo*-glycosidases, while *endo*-glycosidases release an oligosaccharide via hydrolysis of an internal linkage (Figure 3.3).

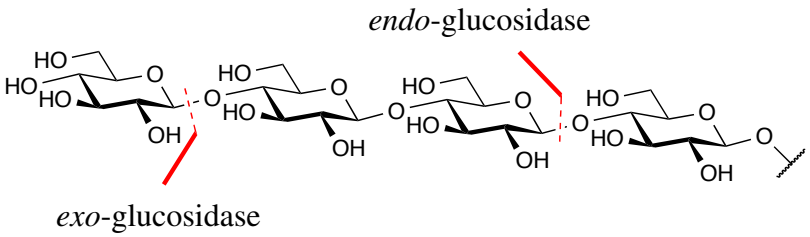

Figure 3.3: *Sites of Glycosidase Action. Exo*-glycosidases (here, specifically a glucosidase) cleave only the terminal sugar of an oligosaccharide. In contrast, *endo*-glycosidases can cleave multiple saccharide residues by cleaving closer to the reducing end of the oligosaccharide; one example of an *endo* site is marked, though an enzyme which cleaves any of the three non-terminal glycosidic linkages would be classified as *endo*.

The second major dichotomy of glycosidases concerns whether the anomeric stereochemistry is inverted or retained (Figure 3.4). The enzymatic chemistry is performed by two conserved acidic residues in the active site for both of these classes.[84;85] In the instance of inverting glycosidases, the hydrolysis proceeds via a concerted mechanism (Figure 3.5). The two catalytic residues simply serve as acid and base, respectively, in order to protonate the departing alcohol to improve its leaving group ability, while the other simultaneously hydrogen bonds to one of the hydrogen atoms of the water molecule to render the attached oxygen atom more nucleophilic.

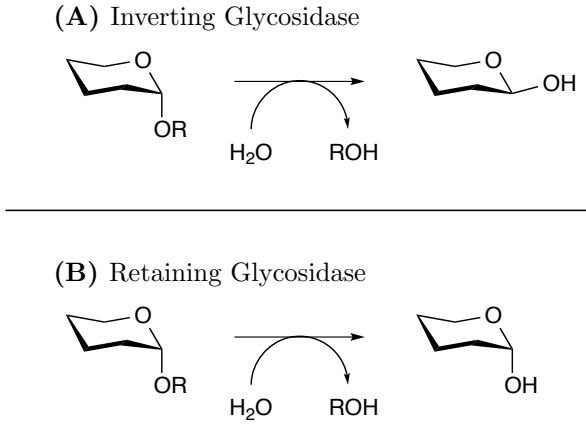

Figure 3.4: *Reactions Catalyzed by Inverting (A) and Retaining (B) Glycosidases.*

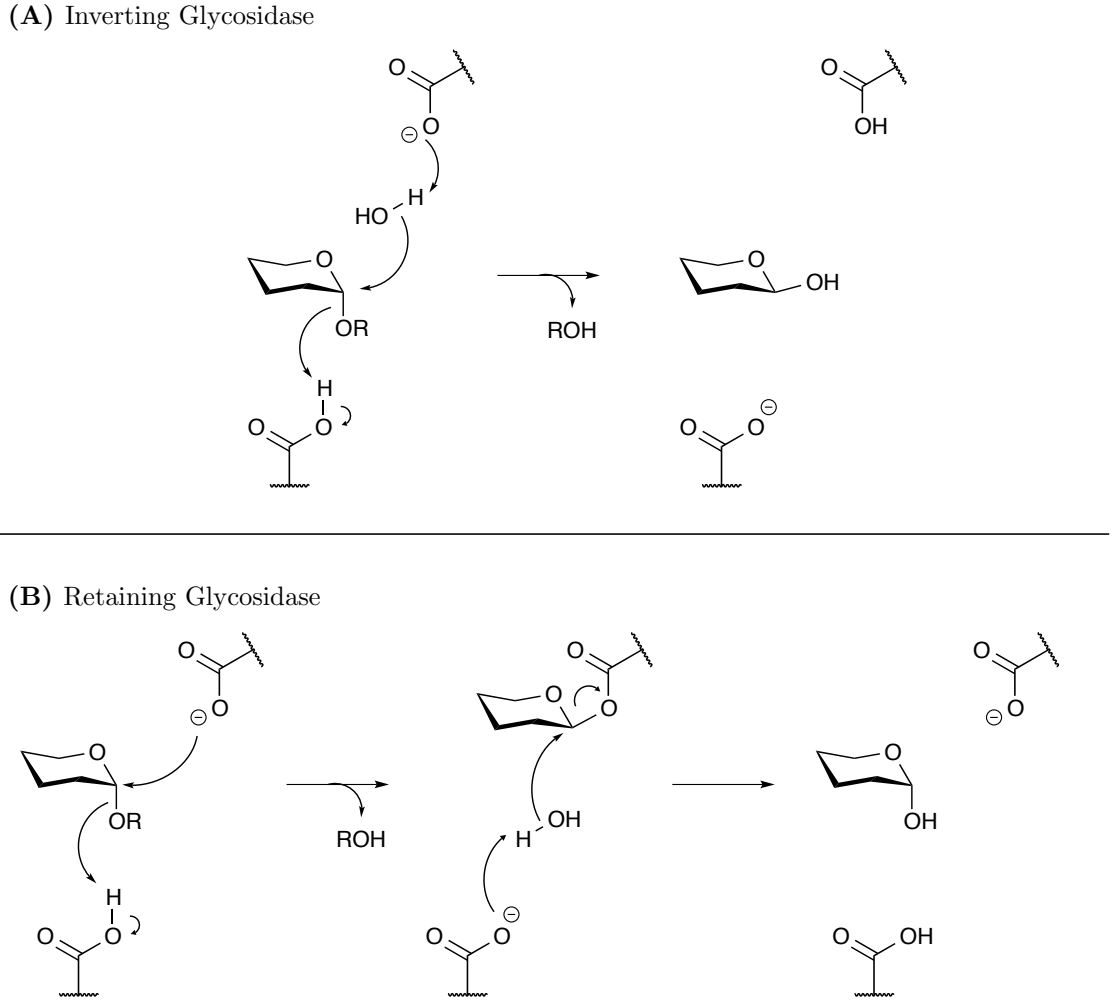

Figure 3.5: *Mechanism of Glycoside Hydrolysis as Catalyzed by Glycosidases*

Retaining glycosidases, in contrast, operate via a 2-step mechanism, with the double inversion at the anomeric center resulting in the observed overall retention of stereochemistry. In the first step, one of the catalytic residues, as before, activates the leaving group by protonation, however the second carboxylate in this instance acts as a nucleophile to form a covalent linkage between the enzyme and substrate. After formation of glycosyl-enzyme, the aglycone departs the active site and is replaced by a molecule of water. The residue which served as an acid in the first inversion now acts as base to deprotonate the water as it attacks the anomeric carbon of the sugar. As the hemiacetal forms, the link to the enzyme is cleaved, regenerating the nucleophilic catalyst. Some retaining glycosidases, rather than proceeding by this "classical" mechanism, invoke either an anchimeric (*e.g* the carbonyl oxygen of an *N*-glycosamine)[86–92] or tyrosine[93;94] nucleophile, rather than the archetypal acidic residue.

The difference in the two mechanisms is reflected in the structure of the glycosidase active site. The distance between the catalytic pair is 9.0 – 9.5 Å for inverting enzymes, whereas the distance is much shorter (4.8 – 5.3 Å) in members of the retaining class.[95] The larger cavity in inverting enzymes allows room for the arrangement of the four reacting species, while the smaller size of the retaining glycosidase active site provides the necessary close proximity to allow formation of the glycosyl-enzyme covalent adduct.

In the concerted step of the inverting and each step of the retaining mechanism, the S_N2 type mechanism causes the build up of positive charge at the neighboring endocylic oxygen, as it donates electron density to the carbon atom from which the leaving group is departing. Protonated iminosugars are proposed to be analogs of this transition state[96] (Figure 3.6), though this model is not undisputed in the field.[97;98] Consistent with this model, however, is the selectivity of D-DNJ **33D** and IFG **35D** for α- and β-glucosidases respectively. These enzymes are predominantly retaining, and so the nucleophilic catalystic residue is in close enough proximity to stabilize the positively charged transition state. The geometric presentation of the residue relative

to the substrate is different depending upon the adaptation of the enzyme to α- or β-linked substrates, as the nucleophile has to approach the anomeric carbon from the side opposite the leaving group's departure. When the iminosugar structures are aligned to overlay the hydroxylation patterns with that of D-glucose, the endocyclic nitrogen occupies a different position in the enzyme: DNJ's nitrogen atom being closer to the counterion in an α-glucosidase; IFG's, to that in a β-glucosidase, consistent with the experimental inhibitory data of the compounds.

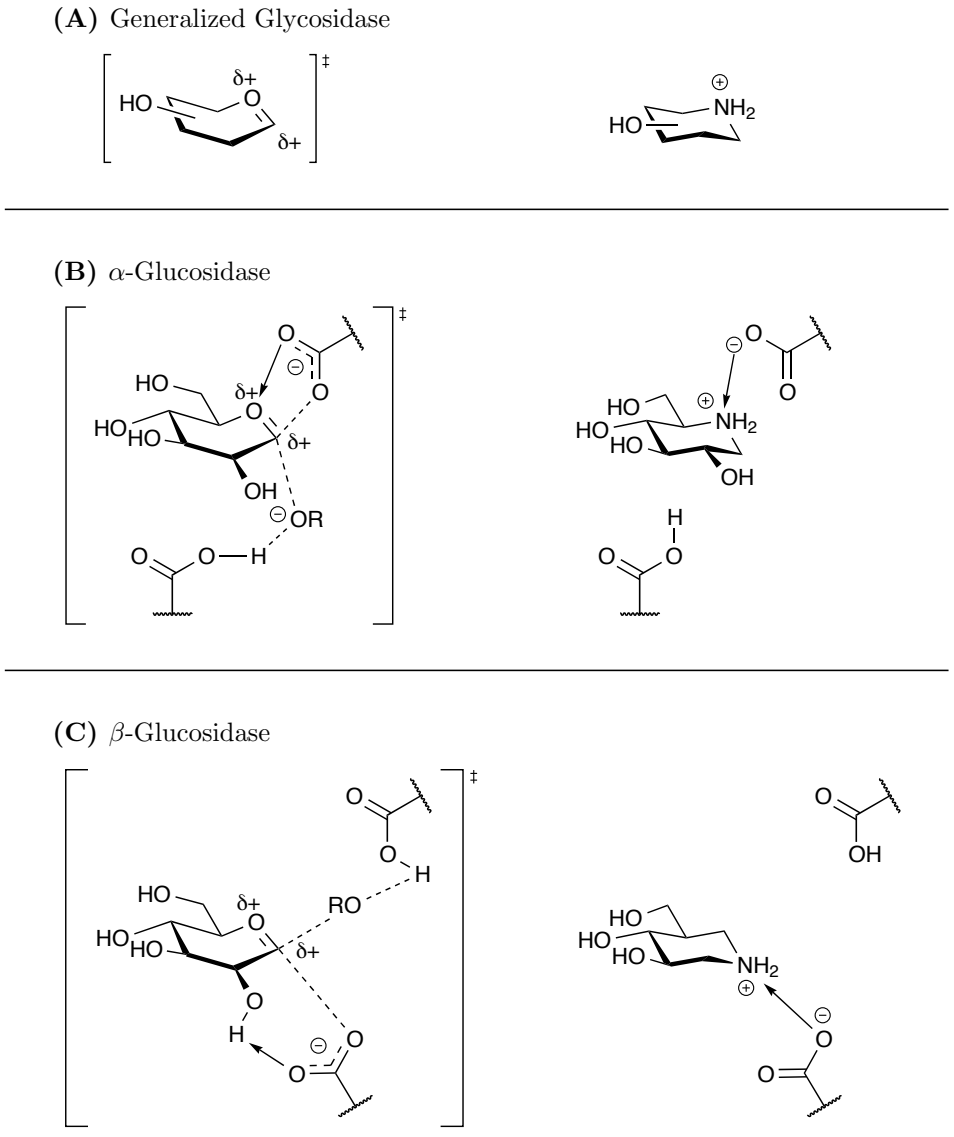

Figure 3.6: *Comparison of Iminosugars and Glycosidase Transition States*

In both mechanisms, in order for the reaction to proceed, one of the catalytic residues

must be protonated and the other deprotonated, so the activity of glycosidases is particularly pH dependent.[99] Inhibition by an iminosugar introduces a third pH sensitive moiety. In studies of β-glucosidases, iminosugars bind to enzymes preferentially in a state where only one of the three groups is protonated.[100] For these reasons an important consideration in inhibitor design is pK_{a} of the candidate molecule, as well as the pH of the local compartment where the enzyme is located. Intracellular pH can vary from 4.7 in lysosomes to 7.2 in the endoplasmic reticulum (ER) to as high as 8 in the mitochondria in mammalian cells.[101]

Having examined the way iminosugars interact on a molecular level with an individual glycosidase, understanding their influence on the various cellular pathways of which these enzymes are a part is critical for analyzing their ability to exert therapeutic effects. Among these, two of the most integral metabolic processes will be discussed: glycosylation of N-linked glycoproteins and sphingolipids.

3.4 Protein Glycosylation

N-linked glycosylation occurs on the lumenal side of the ER membrane as the nascent protein is being translated and translocated into the ER. Rather than being built up on the target glycoprotein, the 14-sugar N-linked glycan is synthesized as a dolichol conjugate, often referred to as the lipid linked oligosaccharide, before being transferred onto the protein *en bloc* by oligosaccharyltransferase (OST, EC 2.4.1.119) (Figure 3.7). Glycosylation occurs at the terminal nitrogen atom of the Asn side chain in either Asn-X-Ser or Asn-X-Thr motifs,[102] and rarely Asn-X-Cys,[103–106] where X is any amino acid other than proline. However, not every occurrence of these motifs is occupied by a glycan; Thr-containing motifs are glycosylated 40 times more efficiently than those containing Ser.[107;108] The complete set of factors determining site occupancy remains an area of active research.[109]

The biosynthesis of the glycan occurs at the ER membrane, with the first steps occuring on the cytosolic face. Dolichol is initially phosphorylated, followed by the ad-

dition of GlcNAc-phosphate[110] and then the sequential conjugation of individual sugars, with GlcNAc-uridine diphosphate (UDP) and Man-UDP acting as the pyranose sources.[111–116] Once the lipid-linked oligosaccharide has reached the $Man_5GlcNAc_2$ state, a flippase encoded by the gene RFT1 inverts the glycosylated dolichol[117–121] so that the final anabolic steps may be carried out in the lumen.[122–127] Rather than the nucleotide sugars that serve as cytosolic monosaccharide sources, the lumenal glycosyltransferases employ dolichol phosphate-linked glucose and mannose. These conjugates are prepared on the cytosolic face from the UDP-sugars, with the dolichol acting as a vehicle for crossing the membrane. After the assembly of the $Glc_3Man_9GlcNAc_2$ species, OST performs the oligosaccharide transfer. The thus-obtained glycoprotein may then be further modified, and the dolichol pyrophosphate either recycled or catabolized.[128]

All N-linked glycans begin as this $Glc_3Man_9GlcNAc_2$ species, before the terminal sugars are trimmed to eventually give rise to three different glycan classes. ER α-glucosidase I (GluI) cleaves the terminal glucose, while ER α-glucosidase II (GluII) removes each of the next two glucose residues sequentially (Figure 3.8). The resulting $Man_9GlcNAc_2$ species is the base upon which oligosaccharides of the high mannose class are built. Alternatively, ER α-mannosidase I,[i] (ER ManI), ER α-mannosidase II (ER ManII), and Golgi α-mannosidase I (Golgi ManI) cleave 4 mannose residues providing a substrate for GlcNAc transferse which conjugates a GlcNAc to the terminus of the α1,3-branch of the glycan. $GlcNAcMan_5GlcNAc_2$ may either be further elaborated to hybrid glycans or the remaining two terminal mannose residues removed by Golgi α-ManII to yield the foundation of complex glycans.[132]

DNJ **33** and *N*-alkylated derivatives thereof, as well as castanospermine **39**, can inhibit both GluI and GluII,[133] impeding further processing of the glycan. Likewise, ER ManI can be inhibited by the 2-epimer of DNJ, D-deoxymannojirimycin (DMJ)

[i] While GluI and GluII are known to be localized to the ER, the localization of ER ManI is more controversial. Multiple recent studies[129–131] have shown the protein to localize to the Golgi apparatus.

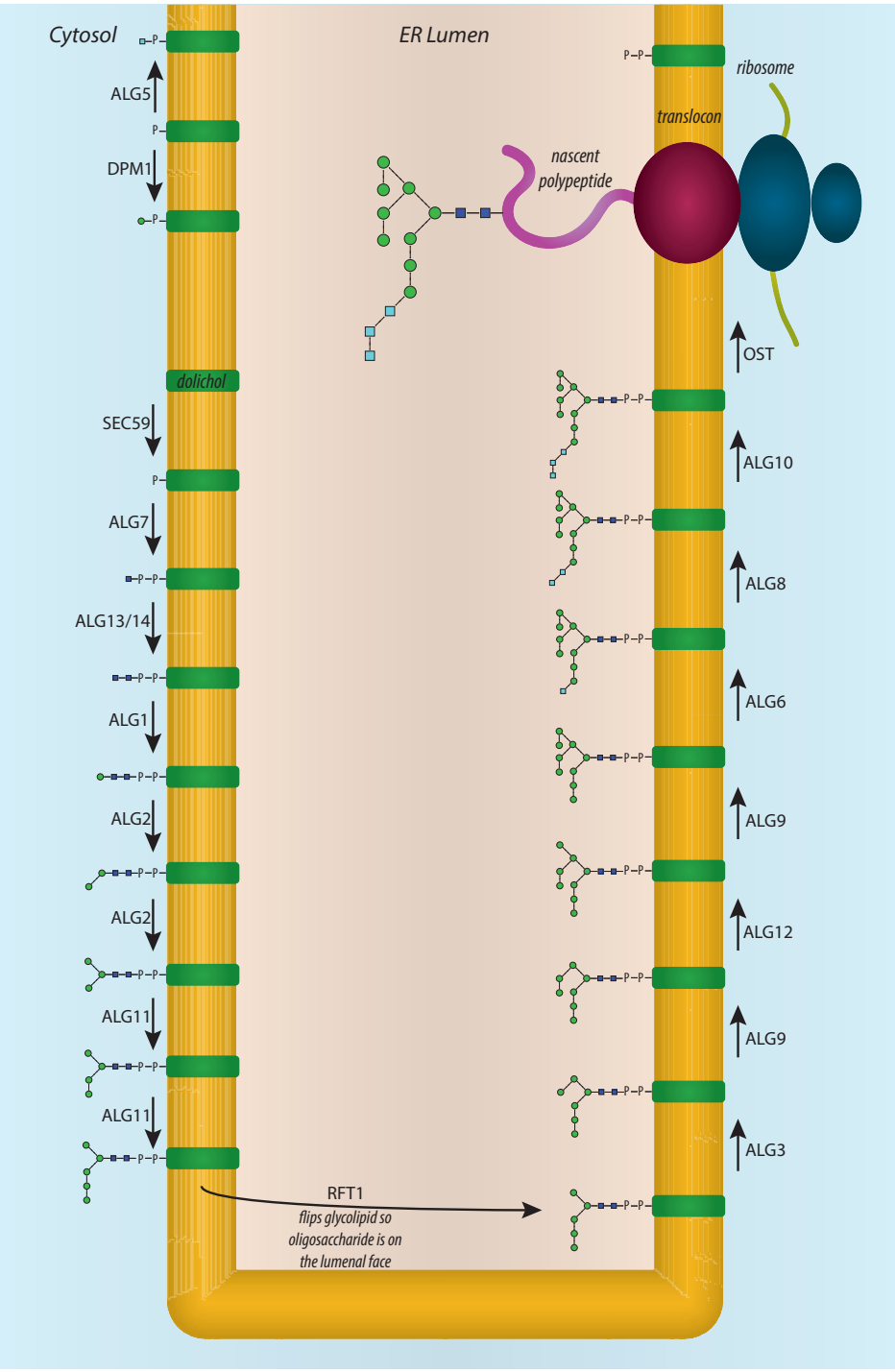

Figure 3.7: *N-linked Glycan Biosynthesis.* With the exception of OST, the arrow labels in the figure represent gene names which encode the enzyme that catalyzes the indicated reaction, as there are not yet widely accepted names for these molecules. Cytosolic reactions use monosaccharide-UDP as the source of GlcNAc and Man, while lumenal reactions use the dolichol phosphate monosaccharides, whose biosynthesis is shown in the upper left of the figure.

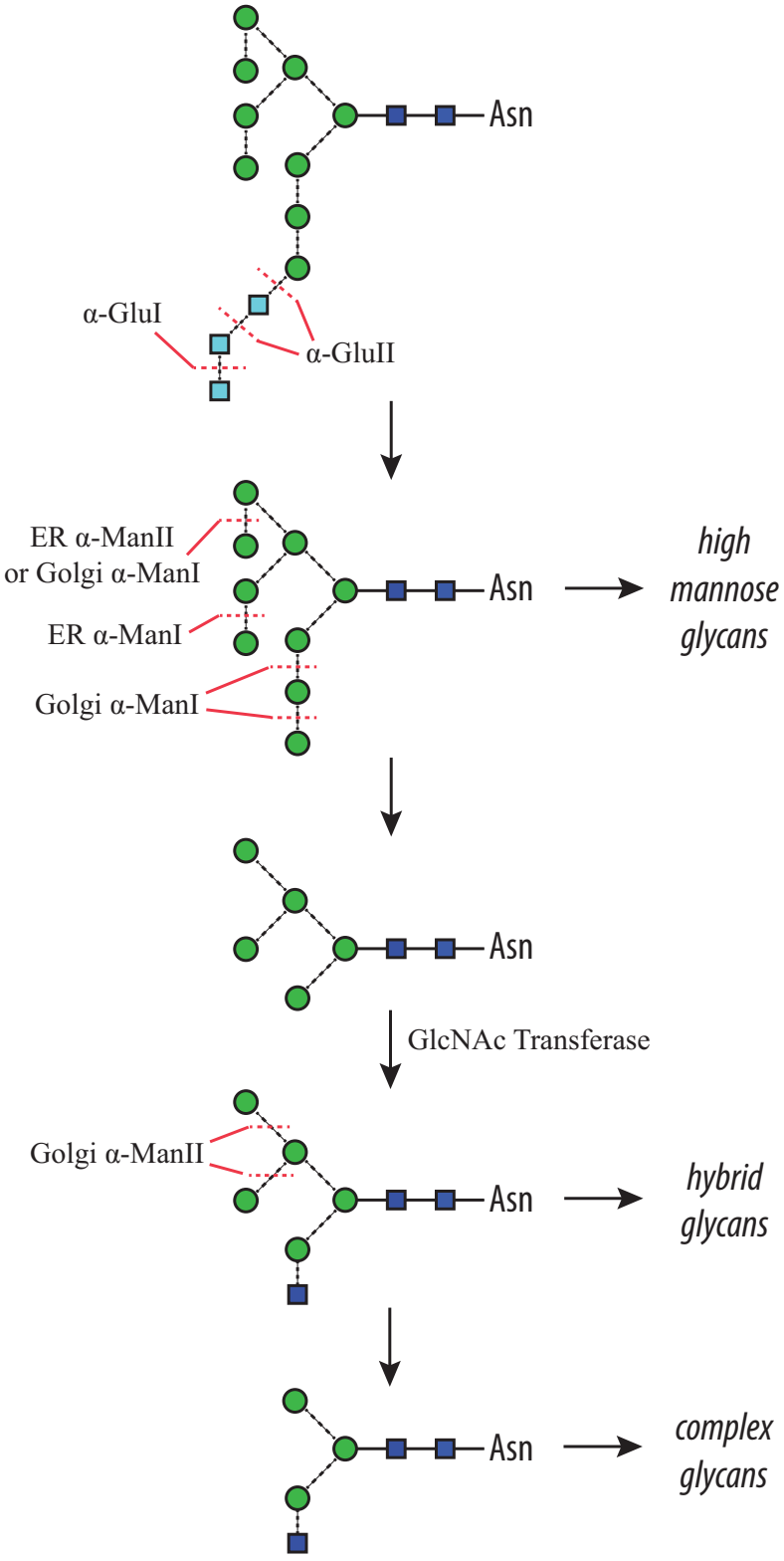

Figure 3.8: *N-linked Glycan Processing.* Red lines indicate the cleavage sites of each labelled enzyme.

45D. However, in the instance of GluI and/or GluII inhibition, golgi endomannosidase can shunt material to the high mannose intermediate by cleaving the terminal tetrasaccharide (Glc_3Man) at once rather than sequentially.[134]

Although glycan processing can be salvaged by the endomannosidase, sequential trimming of the terminal glucose residues of the N-glycan plays a crucial role in the proper folding of glycoproteins.[134–139] After the sequential removal of the two terminal glucose residues by ER GluI and ER GluII, the $Glc_1Man_9GlcNAc_2$ glycan is bound by the lectin domain of either the membrane protein, calnexin (CNX), or soluble protein, calreticulin (CRT) (Figure 3.9). CNX and CRT mediate interaction between the glycoprotein and ER-resident chaperones (*e.g.* ERp57). These chaperones aid the proteins to achieve their native fold. In particular, a number of protein disulfide isomerases (PDI) allow proper matching of cysteines into disulfide bridges.[135;140]

The final glucose of the N-glycan is removed by ER GluII. If the protein has achieved native fold, it is processed as normal and exported to the Golgi for packaging. If however, it remains incorrectly folded, UDP-glucose:glycoprotein glycosyltransferase (UGGT) acts as a means of quality control, reattaching a terminal glucose, so that the protein may interact with CNX or CRT again. The mechanism by which UGGT recognizes the misfolding of such a wide array of proteins is not known. However, bioinformatic analysis shows sequence homology of 4 putative PDI regions within UGGT, suggesting that the recognition might occur via surface (i.e. mismatched) disulfide bonds (unpublished results by Dr. P. Roversi and P. McIvor).

ER ManI acts as the "timer" of the CNX/CRT cycle.[141] The longer a misfolded protein is resident in the ER, the more likely it is to have a terminal mannose cleaved from the middle branch of the oligosaccharide.[ii] UGGT has much lower affinity for glycoproteins with fewer than 9 mannose residues.[138;143] However, GluII still removes the glucose from the $GluMan_8GlcNAc_2$, releasing N-$Man_8GlcNAc_2$ glycoprotein, which

[ii]ER ManI has also recently been shown to exert control over protein folding quality control independently of its enzymatic activity and active site. This alternate mechanism invokes a separate region of the protein binding misfolded proteins that have reached the Golgi, in order to promote their retrograde transport to the ER where it can be degraded via ERAD.[142]

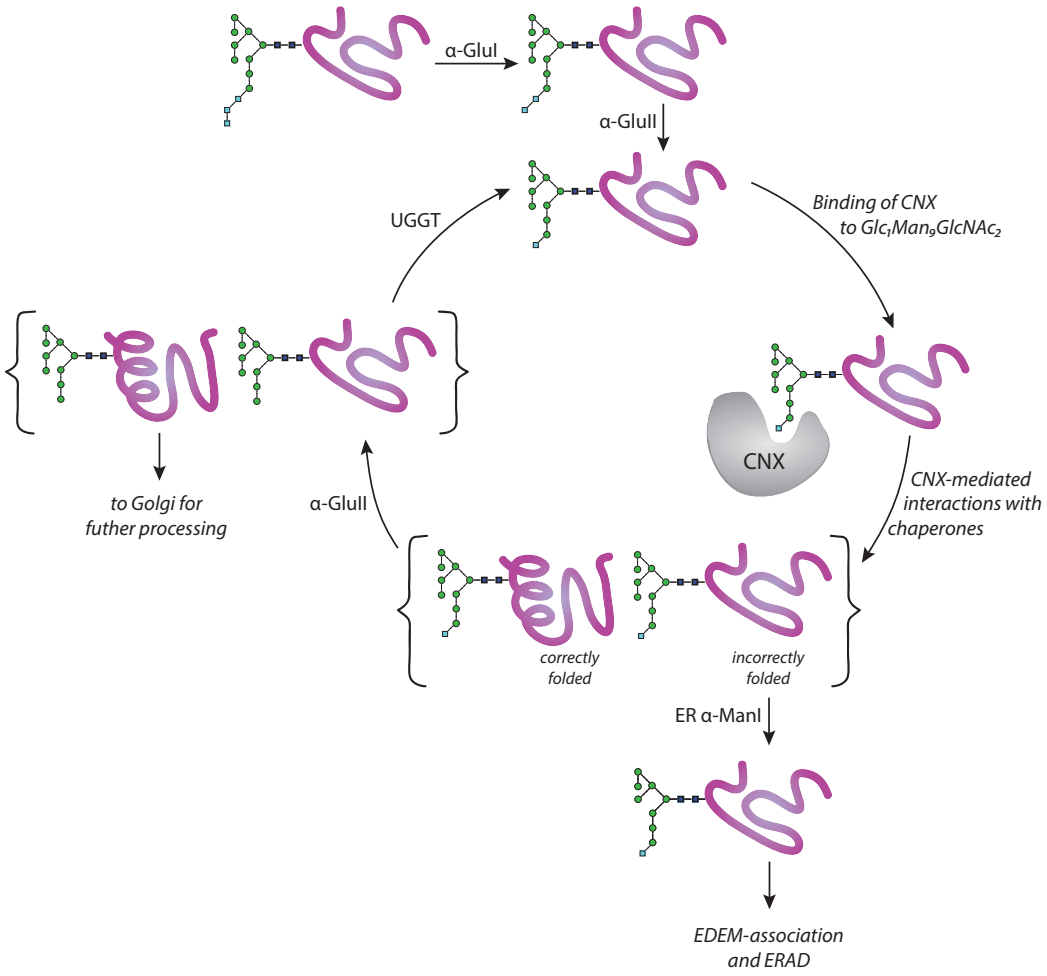

Figure 3.9: *Calnexin Cycle.*

can be bound by ER degradation-enhancing α-mannosidase-like protein (EDEM), directing it for ER-associated degradation (ERAD).[144] The protein is reverse translocated to the cytosol, where the glycoprotein is cleaved into a free oligosaccharide (FOS) and protein by a glycopeptidase, after which the protein is degraded by the proteasome.[144]

Via their inhibition of GluI and GluII, iminosugars not only result in improperly glycosylated proteins, but also abrogate the ability of glycoproteins to interact with the CNX/CRT cycle. The inhibition of the two enzymes means that newly synthesized proteins with unprocessed N-glycans cannot reach the monoglucosylated state necessary to interact with CNX/CRT and their associated chaperones. When these misfolded proteins are catabolized by ERAD, the glucosylated FOS produced can

act as a biomarker of the extent of GluI and GluII inhibition.[145] Because GluII also removes the final glucose from the N-glycan, treatment with iminosugars causes proteins already in the cycle to be trapped within it due to the continued presence of the motif to which the CNX/CRT lectins bind.[146]

The inability to be folded by the CNX-mediated chaperones results in various outcomes depending upon the protein. Under treatment of *N*B-DNJ, tyrosinase is misfolded in B16 mouse melanoma cells, and the protein is unable to bind copper; despite this, it is properly trafficked to the melanosome. Without active tyrosinase, the cells are deficient in pigment resulting in a much lighter phenotype that can be observed visually.[134;135;146;147] In contrast, under treatment of iminosugars, one of the pestivirus envelope glycoproteins, E^{rns}, maintains its RNase activity, demonstrating that CNX/CRT interaction is not obligate for native folding of the active site; instead secretion of the protein is inhibited by the treatment.[137] Though iminosugars influence these two glycoproteins in almost exactly opposite ways, together they demonstrate the fundamental importance of native glycosylation for both the function and localization of proteins.

3.5 Glycosphingolipid Metabolism

Glycolipids are the second repertoire of sugar conjugates influenced by iminosugar treatment. A particular point of importance to sphingolipids is their association with lipid nanodomains (also called lipid "rafts").[148] These regions were in fact discovered due to the observation that glycosphingolipids selectively accumulated in regions of membranes, rather than freely diffusing.[149] Lipid nanodomains, in addition to being relatively enriched in sphingolipids, have increased amounts of cholesterol, whose rigid polycyclic structure imposes higher order than found in the surrounding membrane.[150] The rafts help maintain heterogeneity of cellular membranes, so that proteins may be segregated to different regions.

Before they can form nanodomains however, glycosphingolipids must be biosynthesized. Sphingosine, the lipid foundation of the sphingolipid class (Figure 3.10A), is initially acylated by a fatty acid to form a ceramide, with the identity of the acyl chain varying by species.[151] From ceramide, the biosynthesis diverges, depending on the modification to the primary alcohol of ceramide. Phosphocholine modification of the alcohol provides sphingomyelin, while the alcohol may instead be glycosylated (with either a single glucose or galactose) to provide a cerebroside, the simplest glycosphingolipids.

Much like the biosynthesis of the N-linked oligosaccharide, glycosphingolipids are built up by the sequential addition of monosaccharide residues (Figure 3.10B), with the process taking place on the ER and Golgi membranes. The first sugar is added by glucosylceramide synthase (GCS) on the cytoplasmic side of the ER membrane to form glucosylceramide (GlcCer),[152–154] or the ceramide flips to the lumenal side of the membrane where ceramide galactosyltransferase converts it to galactosylceramide (GalCer).[155;156] In both cases, the lipid is transferred to the lumenal side of the cis-Golgi stack. It is here that all further elaboration of the glycan takes place.[151]

Catabolism of glycolipids can take place on the outer leaflet of the plasma membrane, but primarily occurs in lysosomes. Of particular interest with respect to the study of iminosugars is β-glucocerebrosidase, a lysosomal enzyme that breaks GlcCer down into glucose and ceramide. This enzyme, together with the reciprocal GCS enzyme, are both inhibited by alkylated DNJ compounds.

Mutations which result in impaired or ablated β-glucocerebrosidase activity are associated with the genetic lysosomal storage disorder, Gaucher's disease, which results from the accumulation of GlcCer in cells. Iminosugars can be employed to treat the disease in two different ways. The first, substrate reduction therapy, invokes the iminosugar inhibition of GCS, which reduces the amount of GlcCer. Because less substrate for β-glucocerebrosidase is present, the impaired enzyme is able to maintain balance as would be achieved with the wild type enzyme.[157–159]

(A) Sphingolipid class structures

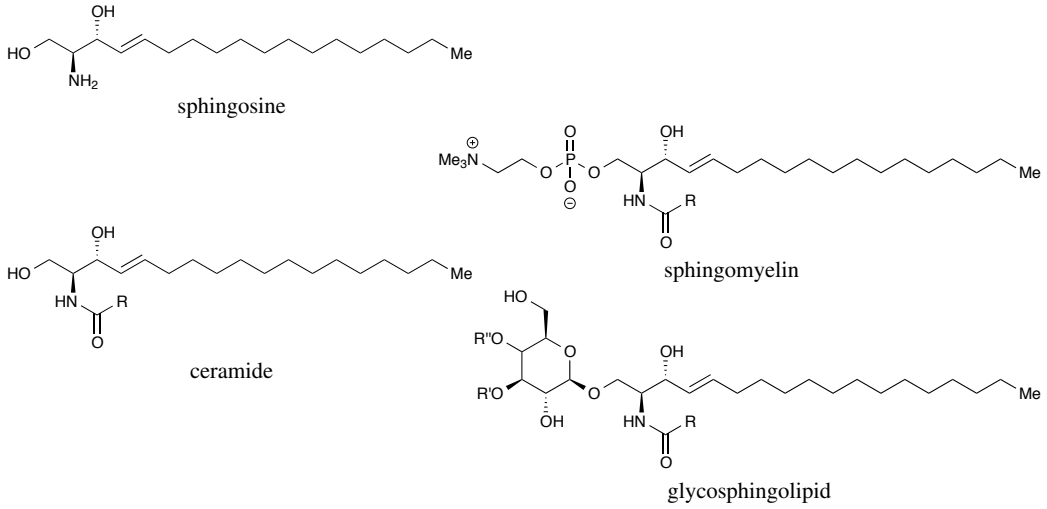

(B) Anabolism of Glycosphingolipids

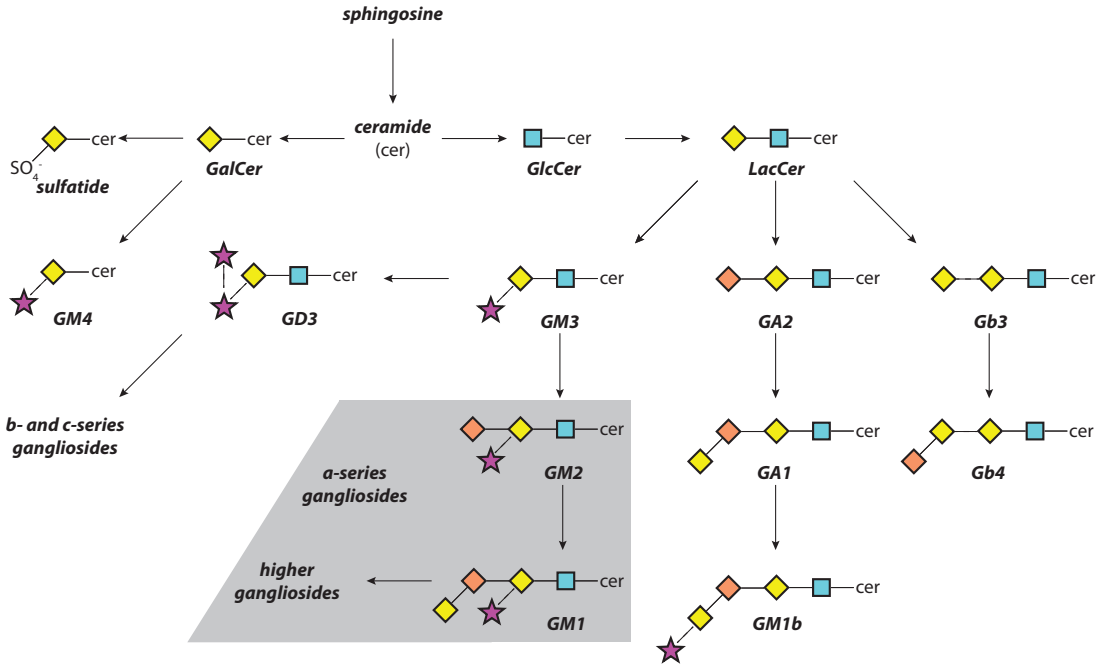

Figure 3.10: *Glycosphingolipid Structure and Metabolism.*

Alternatively, the affinity of iminosugars for the impaired enzyme itself can be exploited as part of active-site-specific chaperone therapy. For certain mutants, the enzyme has an intact active site in terms of sequence, but misfolding elsewhere in the protein due to the mutation that leads to ERAD of the enzyme, rather than normal trafficking. The iminosugar can serve as a template around which the active site can coalesce and the rest of the enzyme may, in turn, properly fold. With native folding restored, the enzyme is packaged via the Golgi as normal. Once in the lysosome, the inhibitor is competed out of the active site by the high levels of substrate, resulting in an overall increase in the amount of β-glucocerebrosidase activity, despite the use of an inhibitor.[59]

Glycolipid turnover is driven by the movement of exosomes, endosomes, and lysosomes throughout the cell. For this reason, the half-life of glycosphingolipids depends upon the cell type and growth rate of cells, with reported half-life values values varying from 2 h to 3 d.[151] So despite the fact that incorporation of new ceramide into glycolipids occurs almost instantaneously after the beginning of iminosugar treatment,[158] it can often take a while before levels reach treatment steady state.

3.6 Viruses

Hepatitis C virus (HCV), hepatitis B virus (HBV), dengue virus (DENV) and HIV collectively result in more than 65 million new infections and over 2.5 million deaths worldwide each year (Table 3.1). While there is a prophylactic vaccine for HBV, none of the other viruses have such a measure. There are no specific clinical treatments for DENV, while those available for HIV and HCV often have severe side effects and are expensive.[160–164] While HIV treatments have improved over time in terms of both side effects and cost, the current dearth of treatments that are both effective and affordable for the other viruses and the wide reach of all of these viruses makes the development of antivirals an area of active interest, in particular broad-spectrum antivirals given the prevalence of coinfection of HCV, HBV and HIV.

Table 3.1: Statistics of Worldwide Chronically Infected Population, Annual New Infections and Annual Virus-related Deaths (including associated complications).[165–168]

Virus	Chronically Infected	New Infections per year	Virus-related deaths per year
DENV	N/A	50,000,000	22,000
HBV	240,000,000	10,000,000	780,000
HCV	150,000,000	3,000,000	500,000
HIV	35,000,000	2,100,000	1,500,000

Because many viruses depend upon glycoproteins for proper envelope formation and cell entry, the activity of GluI and GluII is critical for viruses. As such, the use of iminosugars as antivirals has been an area of active research since the 1980s,[169–171] with other disruptors of protein glycosylation such as tunicamycin[172] and bromoconduritol[173] dating back even further. At that time, the mechanism of action was simply considered alteration to the glycosylation of viral proteins, as the importance of protein glycosylation for folding via the CNX/CRT pathway was then unknown. Indeed, iminosugar treatments are known to decrease secretion of infectious virus,[174–178] and this hypothesis has served as the basis of various clinical antiviral trials. Further supporting this mechanism is the fact that glucosidase inhibiting iminosugars have shown broad-spectrum activity against a number of enveloped viruses (i.e. those viruses that have a lipid membrane) *in vitro*, including both DNA and RNA viruses, with effects shown against members of *Herpesviridae, Hepadnaviridae, Retroviridae, Togaviridae, Flaviviridae, Coronaviridae, Paramyxoviridae, Rhabdoviridae, Filoviridae, Arenaviridae, Bunyaviridae* and *Orthomyxoviridae*.[179]

The choice of *N*N-deoxygalactonojirimycin (*N*N-DGJ, **46**) as a control, which does not inhibit GluI and GluII, in bovine viral diarrhea virus (BVDV) experiments revealed the presence of a second antiviral mechanism of action.[180] After further study, this first direct-acting antiviral mechanism of action of iminosugars was identified as inhibition of the viroporin, p7, a target conserved between BVDV and HCV.[177;181;182] Iminosugars of both D-DNJ and D-DGJ stereochemistry with long alkyl chains (C_9) have been demonstrated to inhibit HCV p7 in black lipid membranes, while the same iminosugars with butyl rather than nonyl alkylation do not inhibit the current facili-

tated by the viroporin. Examination of other iminosugar groups has never been done to determine if DNJ and DGJ are privileged stereochemistries or if all iminopyranoses can effect this inhibition. Additionally, while *N*-butyl iminosugars do not inhibit p7, and *N*-nonyl do, the intermediate alkylations have never been investigated to establish the minimum critical length.

Until now, these have been the two mechanisms presumed responsible for the therapeutic potential of iminosugars with respect to viruses. However, some iminosugars demonstrated antiviral activity without an identified mechanism of action.[170;183]

Since iminosugars are known to disrupt glycolipid synthesis, one of the aims of the thesis is to investigate whether glycolipid inhibition induces an antiviral effect. Many viral receptors are associated with lipid rafts, and disruption of lipid homeostasis has been proposed as an antiviral target for a number of viruses.[184–188] Targeting the glycosylation of lipids specifically has never been reported or proposed previously. Particularly in the case of the hepatitis viruses that are known to depend heavily on lipids and membrane make up, glycolipid targeting is a promising prospect.

Targeting of ER GluI and GluII as well as glycosphingolipids (GSL) have the additional benefit of being host targets upon which viruses do (in the case of GluI and GluII) and might (GSL) depend. Despite the high rate of virus mutation, development of a mutation sufficient to overcome this dependence is unlikely as opposed to a directly acting antiviral therapy.[189]

The viruses selected to be studied in this work are three members of *Flaviviridae* each representing a separate genus: HCV (*hepacivirus*), DENV (*flavivirus*), and BVDV (*pestivirus*). The three viruses have similar genomic organization (Figure 3.11) and cellular life cycle, but differ in most other ways. HCV is a strictly human virus, while DENV infects humans alternately with *Aedes aegypti* vector, and BVDV is a bovine virus. HCV and BVDV both have a p7 viroporin and cause predominantly chronic infections, while DENV lacks an ion channel and produces acute infections.

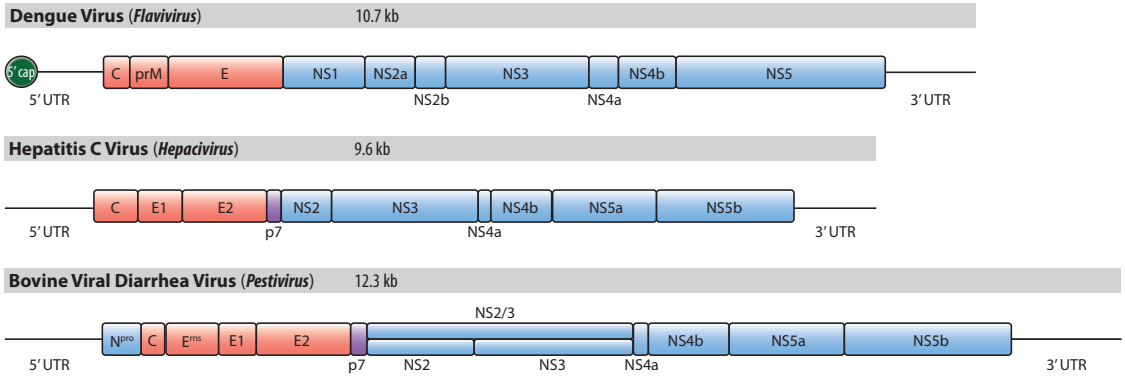

Figure 3.11: *Representative Genomes of the* Flaviviridae *Genera.* Structural proteins are indicated in red, while nonstructural are in blue. HCV and BVDV contain the viroporin, p7, which has not been confirmed to be either present or absent in the particle, and so is displayed in purple.

In Chapter 6, the effects of a novel iminosugar are also investigated in HBV and HIV virus systems. Not only are both medically relevant, but HBV (the only DNA virus studied in this work) represents a virus phenotypically similar to, but genotypically distinct from, HCV.

3.7 Enzymes

As part of the anticipated screening of compounds to elucidate the mechanisms by which iminosugars are antiviral, a collaboration was established with Prof. Atsushi Kato (University of Toyama; Toyama, Japan), who has a large panel of enzymes against which to test inhibition.[190] Among those available, a subset was selected to evaluate the iminosugars to be prepared with three major considerations: (i) known or suspected antiviral mechanisms; (ii) enzymes implicated in undesired side effects of clinical iminosugars; and (iii) screening against enzymes with as many different substrate stereochemistry specificities (i.e. glucosidases, galactosidases, mannosidases, etc) as available.

The most critical enzyme included in the panel was rat liver ER α-glucosidase II, as a known cellular target of iminosugar inhibition and keystone to the best characterized iminosugar antiviral mechanism. While the relative importance of ER α-glucosidase I

versus II inhibition to the antiviral effect is not known, mammalian ER α-glucosidase I was, unfortunately, unavailable to be included.

Given the well documented activity of the *N*B and *N*N derivatives of both D-DNJ and D-DGJ as inhibitors of glycosphingolipid metabolism, human glucocerebrosidase and glucosylceramide synthase were selected to be part of the screen. As mentioned previously, iminosugar interaction with these two enzymes can treat the genetic disorder, Gaucher disease, via pharmacological chaperone and substrate reduction therapy, respectively. A third included sphingolipid glycosidase, human lysosomal α-galactosidase, breaks down globoside Gb3 into LacCer (Figure 3.10), and mutations in the enzyme result in another lysosomal storage disorder, Fabry disease. While the potential for iminosugars to treat these diseases justified inclusion of the enzymes, all three also influence the cellular glycosphingolipidome. The importance of these lipids to lipid nanodomains, and lipid nanodomains to viral receptors, the study of inhibition of these glycolipid processing enzymes enabled investigation into the correlation between glycolipid manipulation and antiviral potency.

Digestion enzymes from the intestinal brush membrane (maltase, isomaltase, sucrase, cellobiase, lactase) were selected, as a common undesired side effect of iminosugar therapy is gastrointestinal distress due to inhibition of theses enzyme ablating ability to digest sugars and starches from the diet.[191] As compounds were evaluated for therapeutic potential, selectivity of inhibition for targeted enzymes versus these off target effects is an important factor in comparing candidates.

Anticipating inclusion of iminosugars with various stereochemistry (Chapter 5), enzymes of other selectivities (α- and β-galactosidases, α- and β-mannosidases, α-L-rhamnosidase, and α-L-fucosidase) were included (Table 3.2) to ensure that as many different enzymatic geometric selectivities as possible were evaluated.

Table 3.2: *Enzyme Commission Numbers of Screened Isolated Enzymes*

Enzyme	EC Number
α-Glucosidase	
Rat intestinal maltase	3.2.1.20
Rat intestinal isomaltase	3.2.1.10
Rat intestinal sucrase	3.2.1.48
Human lysosome	3.2.1.20
Rat liver ER, II	3.2.1.84
β-Glucosidase	
Bovine liver	3.2.1.21
Rat intestinal cellobiase	3.2.1.21
Human glucocerebrosidase	3.2.1.45
α-Galactosidase	
Human lysosome	3.2.1.22
β-Galactosidase	
Bovine liver	3.2.1.23
Rat intestinal lactase	3.2.1.108
α-Mannosidase	
Jack beans	3.2.1.24
β-Mannosidase	
Snail	3.2.1.25
α-L-Rhamnosidase	
Penicillium decumbens	3.2.1.40
α-L-Fucosidase	
Bovine kidney	3.2.1.51
β-Glucuronidase	
Bovine liver	3.2.1.31
α,α-Trehalase	
Porcine kidney	3.2.1.28
Amyloglucosidase	
Aspergillus niger	3.2.1.3
Glucosyltransferase	
HL-60 glucosylceramide synthase	2.4.1.80

3.8 Aims of the Second Portion of the Thesis

As established in this chapter, both nature and synthesis have provided an array of various iminosugars, with an even wider array of enzyme inhibition profiles and selectivities. However, the subset of the molecular class screened for antiviral activity remains largely limited to variously alkylated forms of D-DNJ[178;180;192–196] This bounded exploration of iminosugar space limits the degree to which other mechanistic targets can be identified, despite the evidence in the literature of these "orphaned" antiviral iminosugars, whose mode of action remain unclear.[170;183] In an effort to better map out the antiviral terrain of the iminosugar class, stereoisomers of the archetypal iminosugar, D-DNJ, were prepared, along with their *N*B and *N*N derivatives (Chapter 5). To screen these compounds efficiently, medium to high throughput screens were developed and optimized for HCV, BVDV and DENV (Chapter 4). Finally, a natural product heterodimer of D-DNJ and D-(+)-α-tocopherol was synthesized. As a unique structure, the activity of the conjugate was characterized not only in terms of isolated enzyme and antiviral assays, but also examined for pharmacokinetic properties and effects on cellular metabolism.

The best way to have a good idea is to have a lot of ideas.

—Linus Pauling

4

Optimization of Antiviral Assays and the Effects of DNJ *N*-Alkylation Chain Length on Antiviral Potency

4.1 Introduction

Given the plan to prepare a library of iminosugars to be screened, the aim was to develop medium- to high-throughput antiviral assays for the three selected members of *Flaviviridae*: HCV, BVDV, and DENV. In the screening of an iminosugar or any compound of interest as an antiviral, the assay has two distinct phases. The first stage involves the infection of naive cells and the subsequent treatment of the infected cells with the potential therapeutic. After an incubation of set length, the cell supernatant, which contains virus produced by the treated cells, is harvested. This collected virus is characterized in terms of particle quantity, virus infectivity or both in the second step of the assay to determine the effects, if any, of the treatment.

Iminosugar inhibition of ER α-glucosidases or of the viroporin, p7, reduces the amount of infectious virus.[174–178] Use of quantitative polymerase chain reaction (qPCR) to

measure amount of secreted viral nucleic acid is both quantitative and high-throughput, and in this regard might seem a good method for screening. However, it is feasible for an antiviral to reduce the infectivity of secreted virus, with[194] or without[197] an effect on either virus expression or secretion. For this reason, it was decided to consider assays that determine the infectious titer of virus secreted from treated cells, so that a compound can be identified as antiviral regardless of whether it inhibits entry, expression, secretion, or infectivity.

As model compounds for optimization of these assays, the *N*-*n*-alkyl-D-DNJ series was selected, as members of this class are antiviral against all three viruses of interest.[176;177;180;193] While unmodified D-DNJ **33D**, *N*B-D-DNJ **47D**, and *N*N-D-DNJ **48D** (Figure 4.1)have been tested against all of these systems, a more complete series of homologues has only been tested against BVDV (C_4 – C_{10}, C_{12}, C_{14}, C_{16} and C_{18}; *N.B.* the C_{16} and C_{18} compound were *cis*-alkenyl).[180]

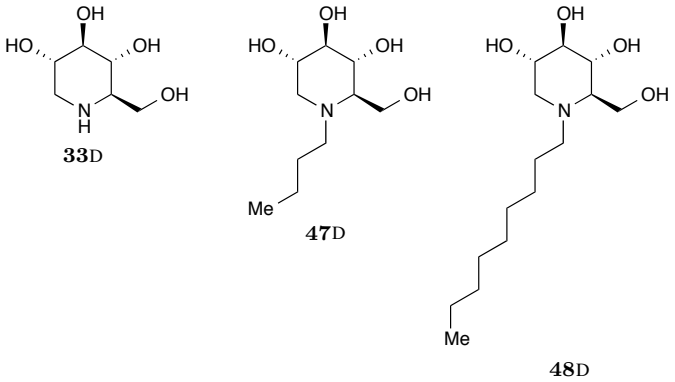

Figure 4.1: *Structures of* D-*DNJ* ***33D****, NB-*D-*DNJ* ***47D****, and NN-*D-*DNJ* ***48D****.*

Length of the *N*-alkylation has no appreciable effect on inhibition of isolated ER α-glucosidase I and II.[198] However, *N*N-DNJ induces FOS more potently in treated cells compared to NB-DNJ, likely due to the fact that alkylation increases cellular uptake, particularly as iminosugars must cross both the plasma and ER membranes to reach ER GluI and GluII. In contrast to the trend in ER glycoprotein processing enzymes, there is a direct correlation between chain length and ability to inhibit the glycolipid processing enzymes, glucosylceramide synthase and β-glucocerebrosidase, both when isolated and *in cellula*.[158;198] As these enzymes are resident on the cytosolic face of

the ER and in the lysosome, respectively,[199] iminosugars only need to penetrate the plasma membrane.

Independent of these metabolic effects, longer alkyl chains impart more potent cytotoxicity. Given their hydrophobic tails and hydrophilic head groups, longer chained iminosugars closely resemble the structures of common detergents, such as *n*-octyl-β-D-glucoside. Unlike the cytotoxic mechanism of some detergents, however, the iminosugar toxicity is independent of caspase-mediated apoptosis.[200] Further, the toxicity was observed when cells were treated with concentrations below the critical micelle concentrations (CMC) of the respective iminosugars. Studies of cellular protein and lipid retention indicate that the toxicity is mediated by mechanical disruption of treated cell membranes, but without membrane solubilization.[200]

Specifically relevant to inhibition of hepaci- and pestiviruses, alkyl chain length is critical for inhibition of p7, with *N*N-DNJ inhibiting the ion channel activity, while *N*B-DNJ is unable to do so.[181;182] Much like the antiviral data, however, the intermediate alkyl chain lengths have never been examined for p7 inhibition to determine whether this is a molecular trait which gradually increases with increasing chain length, or an activity that simply requires a critical minimum length.

Given these numerous alkylation-dependent effects on uptake, cytotoxicity, and inhibition potency, the *N*-*n*-alkyl-D-DNJ series represents not only positive controls for assay optimization, but a previously unmined resource for antiviral mechanism elucidation.

4.2 Antiviral Assay Optimization

4.2.1 DENV

4.2.1.1 From MDMΦ to Huh7 Cells

The initial DENV assay used primary human monocyte-derived macrophages (MDMΦ) for the testing of antiviral effect, with a subsequent plaque assay on LLC-MK_2.[201]

The use of primary human MDMΦ cells to investigate drug treatments has a number of incontrovertible advantages. As primary cells, they lack the mutations that impart immortality to a cell line, and, as long as a sufficient number of donors is employed, represent the outbred state of the human population. This variation can provide useful information, not only about antiviral effects, but also about any cytotoxic effects of the drugs.[178]

While donor-to-donor variation is useful in fully characterizing the biological effects of a promising compound, it represents a limitation in screening. Because multiple blood samples from the same donor were not available during the course of this project, cytotoxicity and antiviral assays had to be run in parallel so that cells from the same donor were used for both experiments. Given the set volume of blood per sample, only a limited number of cells can be obtained from each donor, meaning that there are not sufficient cells to screen a titration of a library of compounds against each donor. Furthermore, IC_{50} values measured in primary human MDMΦ cells can vary by as much as two $\log_{10}$ units,[178] so numerous donors are required for each compound to provide data that can be compared between drugs.

Balancing these benefits and weaknesses, it was determined that an initial screen in a cell line should be used to identify promising compounds, with the primary cell assay remaining the system for thorough investigation as a subsequent step. Human hepatoma Huh7-derived cell lines were selected for three primary reasons: (a) the cells are permissive to DENV;[202–205] (b) DENV has been detected in the liver tissue of naturally infected humans,[206] and NS3 protein detected specifically in hepatocytes;[207] (c) HCV assays are also carried out in Huh7-derived lines, so more direct comparisons between the two viral systems can be made, aiding in identification of mechanisms as either broad-spectrum or virus-specific.

To maximize the throughput of the assay, it was optimized in 96-well plates. Initially, various cell seeding densities and multiplicities of infection (MOI) were screened for 2 and 4 d to ensure that a plaqueable titer was achieved (Figure 4.2). For assays lasting 2 d, the observed viral titer was relatively independent of MOI, but depended on the

cell seeding density. Of note, the highest seeding density tested (1×10^5 cells/well) produced a lower infectious titer of virus than a well seeded at 3×10^4 cells/well. Cell confluence is known to not influence DENV production in the BHK-21/15 cells, another mammalian cell line;[208] however, HCV replication is higher in growing Huh7 and Huh8 cells than in confluent ones.[209–211] Indeed, the cells seeded at 1×10^5 cells/well reached confluence by the end of the two day assay, while those at lower densities had not. In the case of HCV, the reduction in HCV replication was found to be due not simply to cytostasis (as serum starvation did not recreate the effects seen at confluence), and could be partially recovered with nucleotide supplementation.[211] Further experiments are necessary to characterize whether the trends seen with DENV can be explained in the same way but are outside the scope required for optimization of an antiviral screening assay.

At the end of a 4 d assay, the titer of virus in the supernatant had decreased by more than two orders of magnitude relative to the 2 d assay (data not shown), an effect observed previously in other cell types- both cell lines (BHK-21/15[208]) and primary cells (MDMΦ, personal communication with A. Sayce, Oxford Glycobiology Institute). In order to maximize titer (and accordingly, the window of potential inhibition by compounds) and economize virus use, a 2 d assay with 2×10^4 cells/well seeding density and MOI of 0.1 was evaluated to be best according to these criteria. The average titer of virus produced from Huh7.5 cells is approximately 1 $\log_{10}$ unit higher than that observed for MDMΦ, meaning that there is a larger window over which virus inhibition can be observed.

With assay parameters determined, the next step was to investigate whether iminosugar IC_{50} values demonstrate the same trends in Huh7.5 cells as in primary MDMΦ. Four iminosugars (*N*B-, *N*N-, M*O*N-, and *N*AP-DNJ) were evaluated by the optimized assay, and compared to literature values for MDMΦ (Figure 4.3).[178] While IC_{50} values were not identical between the two cell types, the values and relative trends were similar, indicating that the conditions are suitable for screening.

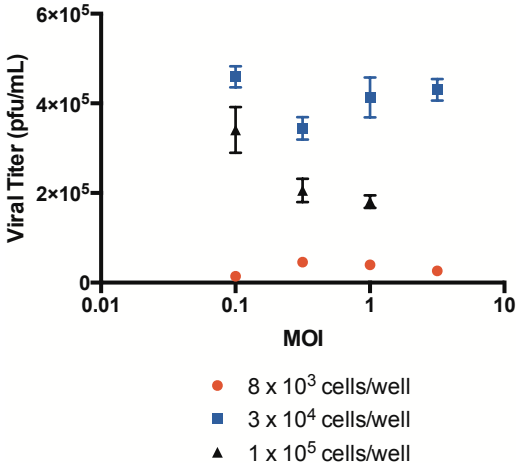

Figure 4.2: *Optimization of DENV Infection in Huh7.5 Cells.* Huh7.5 cells were seeded at the indicated density and incubated overnight. Supernatant was removed, and the cells were inoculated with DENV2 16681 at the indicated MOI (assuming cells doubled overnight) in quadruplicate. After 2 d, the supernatant was harvested, and the titer of infectious virus in the supernatant was evaluated in triplicate by plaque assay on LLC-MK_2 monolayers. Values shown are the mean with propagated error presented as standard error of the mean.

4.2.1.2 Selection of Titer Measurement Method

As explained in the previous section, plaque assay was the standard method that had been used to evaluate viral titer. While robust and quantitative, as a 12-well plate confluent monolayer assay, it requires a vast quantity of cells and media (approx. 3×10^6 LLC-MK_2 cells and 24 mL of media for evaluation of each individual analyte). To make the assay more efficient, optimization of a 96-well viral titration assay was undertaken.

Initially, a coworker, Dr. J. Miller, investigated a focus-forming unit (ffu) assay using immunohistochemistry and reading by Elispot reader. Foci could be observed by eye on a light microscope, but individual foci were too small to be accurately counted by the reader (data not shown). While manual counting could have been pursued, scoring each well as either positive or negative for infection would proceed faster, particularly if infected cells were detected by immunofluorescence (IF) rather than immunohistochemistry. With wells scored in this binary fashion, a 50% tissue culture infective dose ($TCID_{50}$) assay was pursued.

(A)

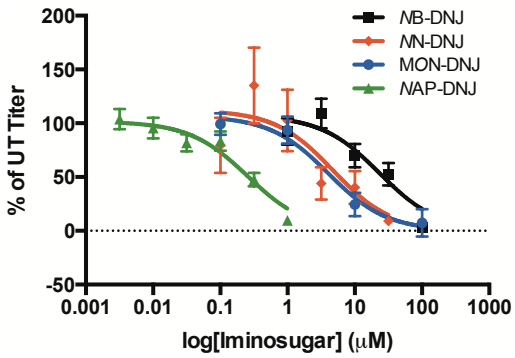

(B)

Iminosugar	IC_{50} in MDMΦ[178] (μM)	IC_{50} in Huh7.5 (μM) Fitted Value	95% CI
*N*B-DNJ	6.00	26.7	15.0 – 49.4
*N*N-DNJ	0.91	5.92	2.18 – 15.7
M*O*N-DNJ	3.09	4.58	2.13 – 10.1
*N*AP-DNJ	0.04	0.26	0.17 – 0.40

Figure 4.3: *Comparison of Iminosugar Inhibition of DENV by Cell Type.* (A) Adhered Huh7.5 cells were inoculated with DENV2 16681 at a MOI of 0.1. After inoculation, the cells were incubated with drug treatment in triplicate. Following 2 d incubation, the supernatants were harvested, and the infectious viral titer determined by plaque assay on LLC-MK_2 monolayers in triplicate. The average titer with each treatment was determined and converted to a percentage of the average untreated titer. Values are shown as the mean with standard error of the mean. Each data set was fitted with a three parameter Hill plot using Prism 6. (B) Comparison of the fitted iminosugar IC_{50} values and 95% confidence interval (CI) in Huh7.5 cells to those reported[178] for primary MDMΦ. The Huh7.5 IC_{50} values were interpolated from the curves fitted by Prism.

As with the plaque assay, the $TCID_{50}$ assay served as a method to measure infectious virus titer in the supernatant of infected cells that were either treated with iminosugars or left untreated. To evaluate the feasibility of the assay, DENV from a known stock was initially employed as the analyte. The supernatants to be analyzed were serially diluted to produce a series of 8 10-fold dilutions. The prepared dilutions were used to inoculate naive cells in 6 technical replicates. The infected cells were incubated for 3 days. After the incubation, the cells were fixed, permeabilized and stained for immunofluorscence with anti-E protein antibody 3H5 as the primary antibody. As a negative control, D1.3 antibody was included as an IgG1 isotype control. Each well was scored as either positive or negative, and the dose of each analyte required to in-

fect half of the wells calculated according to the method of Reed and Muench.[212] The wells treated with D1.3 were all negative. Furthermore, the evaluated dilution series included at least one dilution that was sufficiently dilute to be completely negative.

4.2.1.3 Final Assay Design

With the Huh cells demonstrated to be infectable and $TCID_{50}$ titration evaluated, all that remained was to determine whether it was sufficiently sensitive to observe the titre reduction caused by iminosugars. Huh7-Lunet-hCD81-GLuc cells[213] were infected and incubated with M*O*N-DNJ treatments as described in the previous section. The supernatants were then evaluated for infectious virus by immunofluorescent $TCID_{50}$ assay (Figure 4.4). Because the analytes are evaluated as serial 10-fold dilutions and each well is scored in a binary fashion, the assay is not quantitative enough to evaluate an IC_{50} (decrease in viral titre by 50%). Despite being less quantitative, the $TCID_{50}$ value is 10-fold higher than the titre measured by plaque assay, providing a still larger window over which inhibition may be demonstrated. The maximum concentration of 100 µM M*O*N-DNJ tested showed a 2.21 order of magnitude decrease in $TCID_{50}$ compared to the untreated control. Fitting the data as percentage of control (4.4B), the IC_{50} of M*O*N-DNJ was determined as 3.09 µM, comparable to the value of 4.58 µM observed by plaque assay and identical to that determined in MDMΦ (*cf.* Figure 4.3B).

4.2.2 HCV

A luciferase construct of the Jc1 chimera of HCV (Jc1Luc) has previously been reported,[214] which was viewed as a promising starting point for an anti-HCV screening assay.[215;216] The firefly luciferase is inserted in the ORF of the HCV RNA, such that one molecule of luciferase is expressed for every molecule of the viral polyprotein expressed, so measurement of luciferase levels is a surrogate for the amount of viral expression.

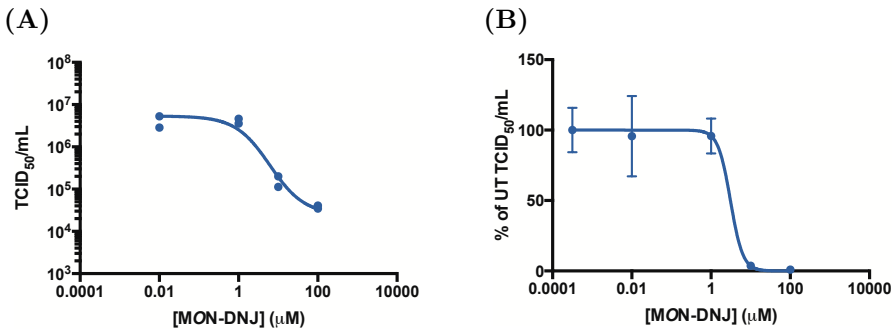

Figure 4.4: *Evaluation of MON-DNJ Inhibition of DENV by $TCID_{50}$ Assay.* (A) Huh7-Lunet-hCD81-GLuc cells were seeded at 2×10^4 cells/well and incubated overnight. The cells were inoculated with DENV 16681 at MOI = 0.1 (assuming that cells doubled overnight), and then incubated with UV4 at the indicated concentrations in duplicate. After 2 d, the supernatant was harvested, and the titer of virus was evaluated by $TCID_{50}$ assay on LLC-MK_2 cells in octuplicate. Individual replicate values are shown. (B) The data described in A is presented as percentage of untreated control. Each point represents the mean, with error bars indicating standard error of the mean. In both cases, data was fitted with a three parameter Hill plot using Prism 6.

Attempts to transfect Huh7.5 and Huh7-Lunet-hCD81-GLuc cells with Jc1Luc RNA were successful. 3 d after transfection, both cell types were approximately 10% infected, as measured by immunofluorescence of HCV core (Figure 4.5). As the infected cells were passaged, a plate was set up to measure luciferase activity, with levels of luciferase expression high enough to obtain a standard curve (Figure 4.5B). Together, these data confirmed successful electroporation of RNA for both the HCV polyprotein and reporter luciferase.

However, progress of the infection diverged by cell type. Even after subculturing the transfected cells for three weeks, the level of infection in Huh7.5 cells did not increase. In contrast, over the course of culturing for two weeks, the level of infection in Huh7-Lunet-hCD81-GLuc increased to approximately 30%. Supernatant removed from these Jc1Luc transfected cells could also be used to infect naive Huh7-Lunet-hCD81-GLuc cells. As the infection only progressed in the Huh7-Lunet-hCD81-GLuc cells, this system was carried forward into assay development.

Transfected cells were seeded directly into an opaque 96-well plate. After incubating in the presence of drug for 4 days, the supernatants were removed and used to inoculate naive Huh7-Lunet-hCD81-GLuc cells. However, after a three day incubation of the

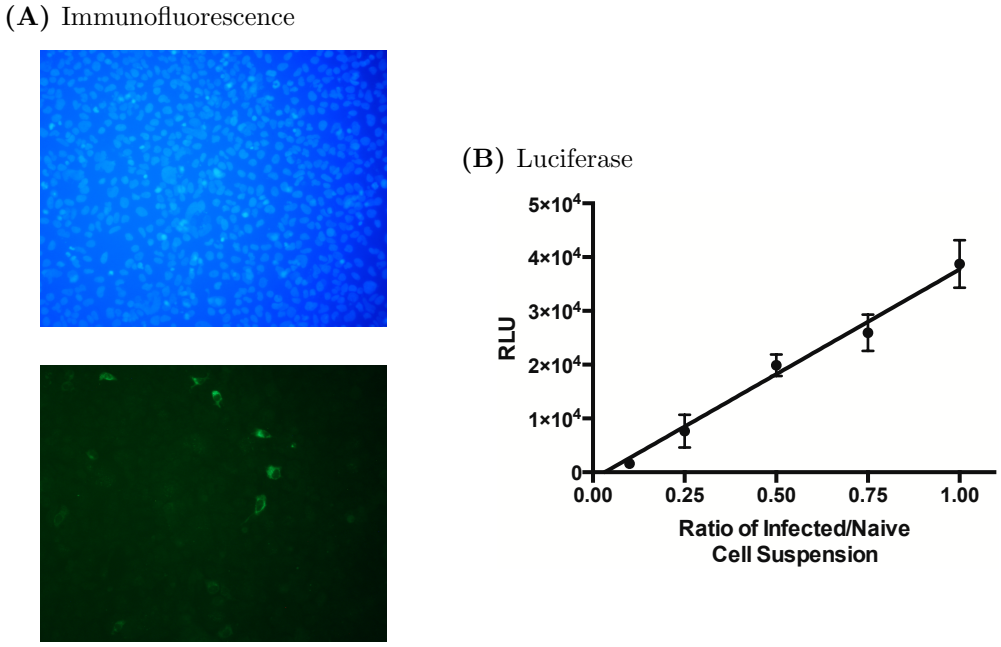

Figure 4.5: *Transfection of Huh7.5 Cells with Jc1Luc.* (A) After electroporating Huh7.5 cells with Jc1Luc RNA, cells were incubated in a 48-well plate for 72 h, then fixed and stained according to the HCV immunofluorescence protocol: DAPI staining cell nuclei (top panel, 20 × magnification), and a FITC-labelled secondary antibody indicating the presence of HCV core protein (lower panel, 20 × magnification). (B) Jc1Luc-transfected and naive cells were each prepared as a cell suspension at 2×10^5 cells/mL. Cells were seeded as a mixture of the two suspensions at the indicated ratios in triplicate. After incubating for 18 h, the cells were lysed and luciferase levels measured. Values are reported as relative luciferase units (RLU) as the mean of the triplicate with standard deviation.

subsequent infection, luciferase levels were undetectable (data not shown). In order to try and increase the titer of virus produced during the initial drug treatment, a viral stock of Jc1Luc was cultured from transfected cells, rather than using transfected cells in the assay directly. When the Jc1Luc virus stock was titered, the concentration was found to be < 10 ffu/mL even after concentration. As such, preparation of a Jc1Luc stock with sufficiently high titer to obtain higher infection levels than transfection was impracticable.

Without being able to perform a second step infectivity assay, the luciferase system only provided information about drug effects on HCV expression, but indicated nothing about either secretion or infectivity. For this reason, attention was returned to the Jc1 chimera system (without luciferase), as this virus is more infectious in cell

culture. The $TCID_{50}$ assay developed for DENV was adapted to be used to evaluate HCV (§ 4.8.5.6), as well as BVDV (§ 4.8.7.4), so that all three virus systems would be measured analogously.

4.3 Synthesis of *N*-*n*-Alkyl DNJ Series

Before the alkyl series could be prepared, the conserved D-DNJ iminosugar **33D** had to be synthesized. D-Glucuronolactone **49D** was used as the chiral starting point for the synthesis, employing the route developed by Best *et al.* (Scheme 4.1).[217] The hydroxyl groups on *C*-1 and C-2 were tandem protected with acetone in the presence of acid catalyst (H_2SO_4), providing acetonide **50D** in 65% yield. After this protection, a single alcohol group remained exposed to be used as a handle for installation of the eventual endocyclic nitrogen atom. To effect a net retention in stereochemistry, sequential S_N2 reactions were invoked: first, triflation (Tf_2O, pyridine, –30 °C) and nucleophilic attack with CF_3CO_2Na to provide the epimeric L-*ido* lactone **51L** (97% yield); and subsequently, a second triflation under identical conditions and a second inversion with NaN_3 ($\leq$ –30 °C) to provide azide **52D** in 76% yield. In order for the inversion with azide to be successful, it was imperative that the temperature be maintained below –30 °C, otherwise side reactions would occur, in particular nucleophilic attack by the DMF solvent to provide formyl ester rather than the desired azide.

After installing the masked amine with proper stereochemistry, the *C*-4 and *C*-6 alcohol groups were unmasked by sequential reductions by DIBAL-H (–78 °C) and $NaBH_4$ (–10 °C) to reveal idol **53D** in 87% yield over the two steps. To complete the synthesis, the anomeric center and vicinal alcohol were deprotected (H_2O, DOWEX 50WX8, 60 °C), followed by hydrogenation (Pd/C) to reduce the azide to a secondary amine and close the iminopyranose ring via reductive amination, providing D-DNJ **33D** in 71% yield and 30% overall yield from **49D**.

With D-DNJ **33D** in hand, the alkyl series was prepared by reductive amination (H_2, Pd/C) to prepare the series of homologs (Scheme 4.2).

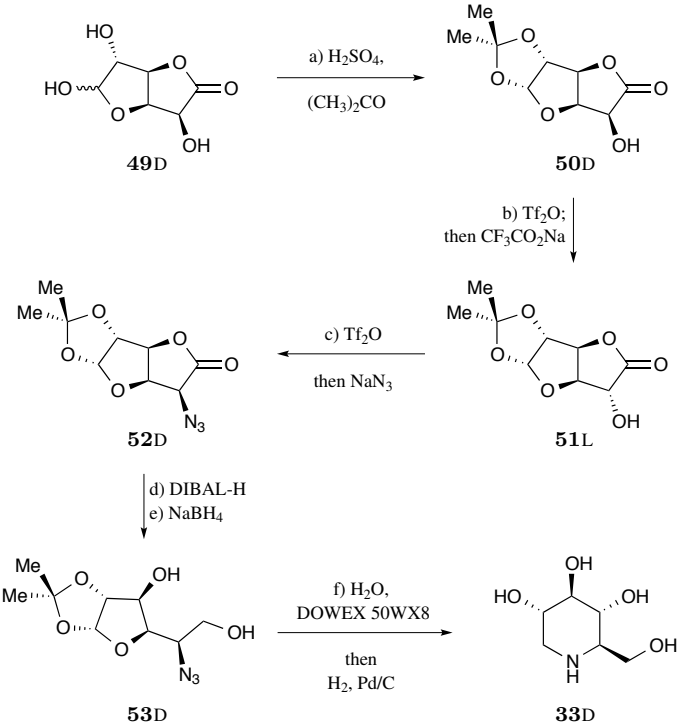

Scheme 4.1: *Synthesis of* D*-1-Deoxynojirimycin.* Reagents and conditions: a) H_2SO_4, $(CH_3)_2CO$, 25 °C, 5 h, 65%; b) Tf_2O (1.1 equiv), pyridine (3.0 equiv), CH_2Cl_2, –40 °C, 2 h; CF_3CO_2Na (2 equiv), DMF, –30 → 25 °C, 97%; c) Tf_2O (1.1 equiv), pyridine (3.0 equiv), CH_2Cl_2, –40 °C, 2 h; NaN_3 (1.2 equiv), DMF, –30 °C, 76%; d) DIBAL-H (3.0 equiv), CH_2Cl_2, –78 °C, 2 h; e) $NaBH_4$ (0.4 equiv), MeOH, –10 °C, 1 h, 84% over the 2 steps; f) DOWEX 50WX8 (H^+ form, 150 weight-%), H_2O, 70 °C, 3 h; H_2, Pd/C (50 weight-%), 18 h, 71% over the 2 steps.

4.4 Enzyme Inhibition by *N*-*n*-Alkyl DNJ Series

While the DNJ series had been previously screened for inhibition of ER α-glucosidases and glucosylceramide synthase,[158;198] they were sent to Prof. Atsushi Kato (University of Toyama; Toyama, Japan) to be tested against the full panel of enzymes described in Chapter 3 (Table 4.1). Maltase, isomaltase, sucrase, cellobiase and trehelase were used as partially purified tissue extracts, and as such inhibition was evaluated with the respective natural substrates. Glucosylceramide synthase was employed as a partially purified cellular extract. The remaining members of the panel were used in pure form, with the *p*-nitrophenyl glycoside as the substrate. Inhibition of each enzyme by each inhibitor was measured in triplicate.

As previously observed, the entire series potently inhibits α-glucosidases, with essen-

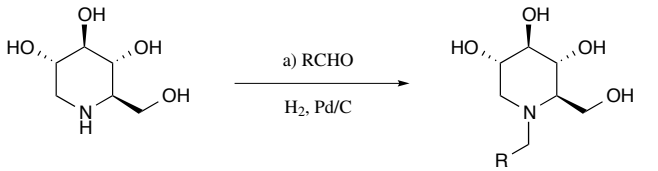

33D

R = H	*N*M-DNJ	**54**D
R = Me	*N*E-DNJ	**55**D
R = Et	*N*R-DNJ	**56**D
R = Pr	*N*B-DNJ	**47**D
R = Bu	*N*P-DNJ	**57**D
R = C_5H_{11}	*N*X-DNJ	**58**D
R = C_8H_{17}	*N*N-DNJ	**48**D

Scheme 4.2: *Alkylation by Reductive Amination of* D*-DNJ.* Reagents and conditions: a) aldehyde (15 equiv), Pd/C (50 weight-%), H_2O:dioxane (various ratios), 25 °C, 24 h.

tially no effect of alkylation. The two glycolipid metabolism enzymes (glucosylceramide synthase and β-glucocerebrosidase) show increased inhibition with increased alkylation length. The largest "jump" in the potency of inhibition occurs between *N*R-D-DNJ and *N*B-D-DNJ for GCS, and between *N*B-D-DNJ and *N*P-D-DNJ for GCase.

Beyond these enzymes of particular interest, the whole series showed potent inhibition of α,α-trehalase and weak inhibition of amyloglucosidase, both logical results as these digestion enzymes liberate terminal glucose residues from oliogsaccharides. The inhibition of both of these enzyme show no clear trend of the effect of alkylation.

Surprisingly, alkyl-D-DNJ compounds showed weak inhibition of α-L-rhamnosidase, which cleaves monosaccharides with a stereochemistry different to that of glucose. Other than the requirement of the presence of alkylation, there is no defined trend as the length of alkylation increases.

4.5 Inhibition of Infectious Virus Release by *N*-*n*-Alkyl DNJ Series

Before beginning antiviral assays, the iminosugar stock solutions were tested for the presence of endotoxin (Table 4.2). A component of bacterial membranes, endotoxin is a lipopolysaccharide that can induce an immune response which would manifest

Table 4.1: *IC_{50} of N-n-Alkyl DNJs against Isolated Enzymes*

	IC_{50}[a, b] (μM)						
Enzyme	D-DNJ **33D**	*N*M-D-DNJ **54D**	*N*E-D-DNJ **55D**	*N*R-D-DNJ **56D**	*N*B-D-DNJ **47D**	*N*P-D-DNJ **57D**	*N*X-D-DNJ **58D**
α-Glucosidase							
Rat intestinal maltase	0.16	0.41	0.99	2.2	1.7	1.2	0.91
Rat intestinal isomaltase	0.79	4.7	8.0	5.6	1.6	1.7	2.4
Rat intestinal sucrase	0.51	0.49	0.44	0.7	0.43	0.36	0.39
Human lysosome	0.37	2.3	6.0	2.4	2.1	1.2	0.99
Rat liver ER, II	16	28	34	24	13	6.7	3.9
β-Glucosidase							
Bovine liver	NI	NI	NI	NI	NI	NI	NI
Rat intestinal cellobiase	271	92	964	627	742	341	412
Human glucocerebrosidase	402	332	290	620	350	28	18
α-Galactosidase							
Human lysosome	217	NI	NI	NI	NI	NI	NI
β-Galactosidase							
Bovine liver	NI	NI	NI	NI	NI	NI	NI
Rat intestinal lactase	41	15	294	221	175	138	120
α-Mannosidase							
Jack beans	NI	NI	NI	NI	NI	NI	NI
β-Mannosidase							
Snail	NI	NI	NI	NI	NI	NI	NI
α-L-Rhamnosidase							
Penicillium decumbens	NI	473	322	174	366	554	583
α-L-Fucosidase							
Bovine kidney	NI	NI	NI	NI	NI	NI	NI
β-Glucuronidase							
Bovine liver	NI	NI	NI	NI	NI	NI	NI
α,α-Trehalase							
Porcine kidney	64	78	151	208	54	16	9.9
Amyloglucosidase							
Aspergillus niger	781	61	687	339	876	508	739
Glucosyltransferase							
HL-60 glucosylceramide synthase	NI	NI	NI	606	24	17	58

[a] NI : No inhibition (less than 50% inhibition at 1 mM).

[b] Reported IC_{50} values represent the mean of three measurements.

as an apparent antiviral effect. Three compounds had detectable levels of endotoxin, two of these (**54D** and **55D**), while considered very low, were above the tissue culture media guarantee threshold of ≤ 0.01 EU/mL. All of these compounds were evaluated for antiviral ability despite these results, but they should be borne in mind when considering the analysis of antiviral effects.

Table 4.2: *Endotoxin Levels in* D*-DNJ Series Stock Solutions*

Iminosugar	[Endotoxin], (EU/mL)[a]
D-DNJ **33D**	0.006
*N*M-D-DNJ **54D**	0.099
*N*E-D-DNJ **55D**	0.040
*N*R-D-DNJ **56D**	< 0.005
*N*B-D-DNJ **47D**	< 0.005
*N*P-D-DNJ **57D**	< 0.005
*N*X-D-DNJ **58D**	< 0.005

[a] EU: endotoxin units

All compounds were examined at 4 $\log_{10}$ dilutions against HCV and BVDV, and 5 $\log_{10}$ dilutions against DENV, starting at the highest non-toxic dose as evaluated by MTS assay (data not shown). Titrations curves of $TCID_{50}$/mL *vs.* iminosugar concentration are shown in Figure 4.6 – Figure 4.12, with summary statistics in Table 4.3, Table 4.4, and Table 4.5. Data were fitted with GraphPad Prism, using a three variable Hill plot model, with the limitation that the bottom of the curve be > 0. For each fit, a comparison was made with a horizontal line using the extra sum-of-squares F-test, with $p < 0.05$ required to reject the horizontal line.

Iminosugars showed the most substantial reduction of infectious titer in DENV, followed by BVDV and HCV. Considering the full curves, most of the iminosugars had similar profiles in each of the three viruses, with unalkylated D-DNJ and *N*M-D-DNJ having the most variable behavior comparing the three viruses. D-DNJ demonstrated a dose dependent antiviral effect only with respect to DENV, while *N*M-D-DNJ exhibited an inhibition of both DENV and BVDV, but not HCV.

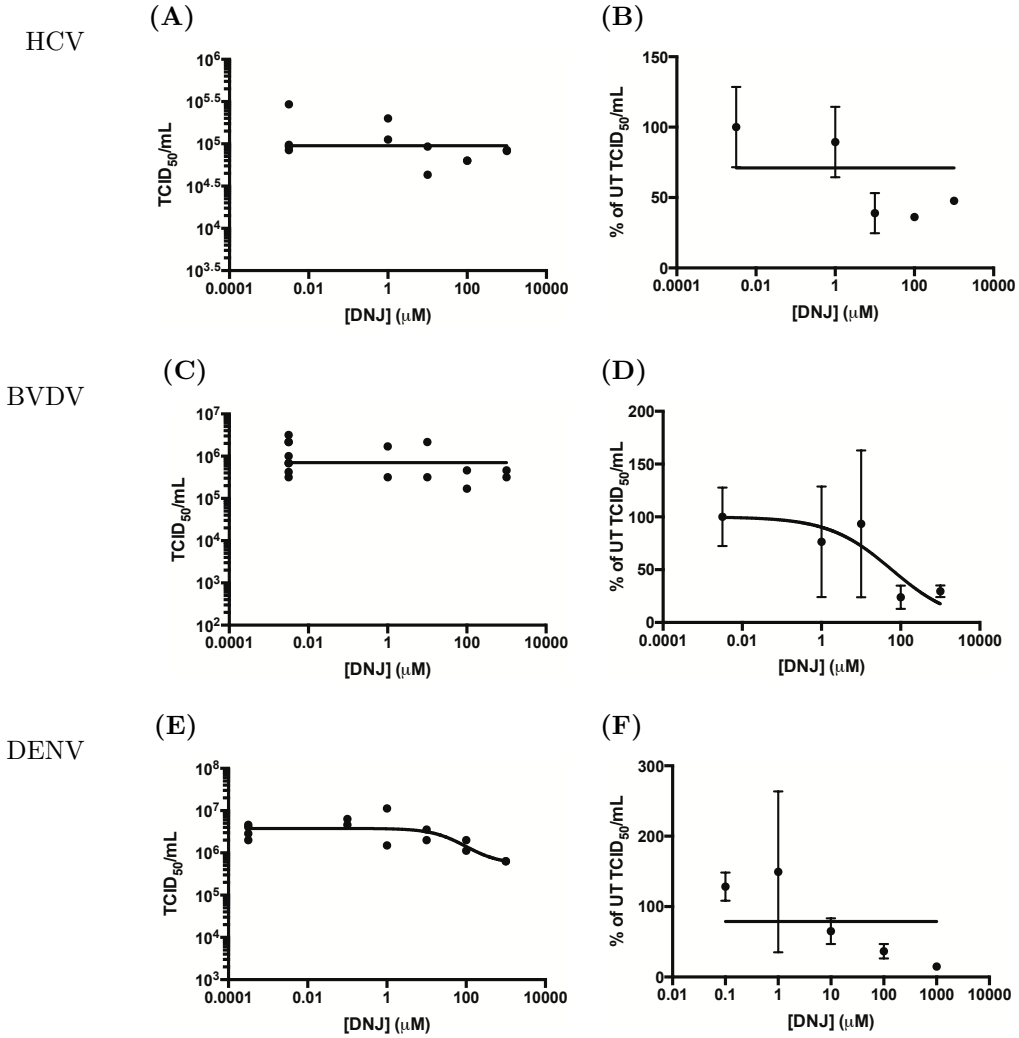

Figure 4.6: *Antiviral Effects of* D*-DNJ.* (A) Huh7-Lunet-hCD81-GLuc cells were infected with Jc1 HCV (MOI = 0.2) and then incubated with media containing D-DNJ at the indicated concentrations in duplicate. After 4 d, the cell supernatant was harvested, and the titer of infectious virus from each well was measured by immunofluorescence endpoint dilution assay on naive Huh7-Lunet-hCD81-GLuc cells, calculating by the method of Reed and Muench.[212] Each point indicates an individual replicate value. (B) The data of A are presented as percentage of untreated control. Each point is the mean with error bars representing standard error of the mean. (C) MDBK cells were infected with Pe515-ncp strain BVDV (MOI = 10) and then incubated with media containing D-DNJ at the indicated concentrations in duplicate. After 2 d, the cell supernatant was harvested, and the titer of infectious virus from each well was measured by immunofluorescence endpoint dilution assay on naive MDBK cells, calculating by the method of Reed and Muench.[212] Each point indicates an individual replicate value. (D) The data of C are presented as percentage of untreated control. Each point is the mean with error bars representing standard error of the mean. (E) Huh7-Lunet-hCD81-GLuc cells were infected with 16681 DENV2 and then incubated with media containing D-DNJ at the indicated concentrations in duplicate. After 2 d, the cell supernatant was harvested, and the titer of infectious virus from each well was measured by immunofluorescence endpoint dilution assay on naive LLC-MK_2 cells, calculating by the method of Reed and Muench.[212] Each point indicates an individual replicate value. (F) The data of E are presented as percentage of untreated control. Each point is the mean with error bars representing standard error of the mean. In each case, the data were fitted using Prism 6, with a comparison of fits between a horizontal line and a three parameter Hill plot, using the extra sum-of-squares F test to determine the better fit.

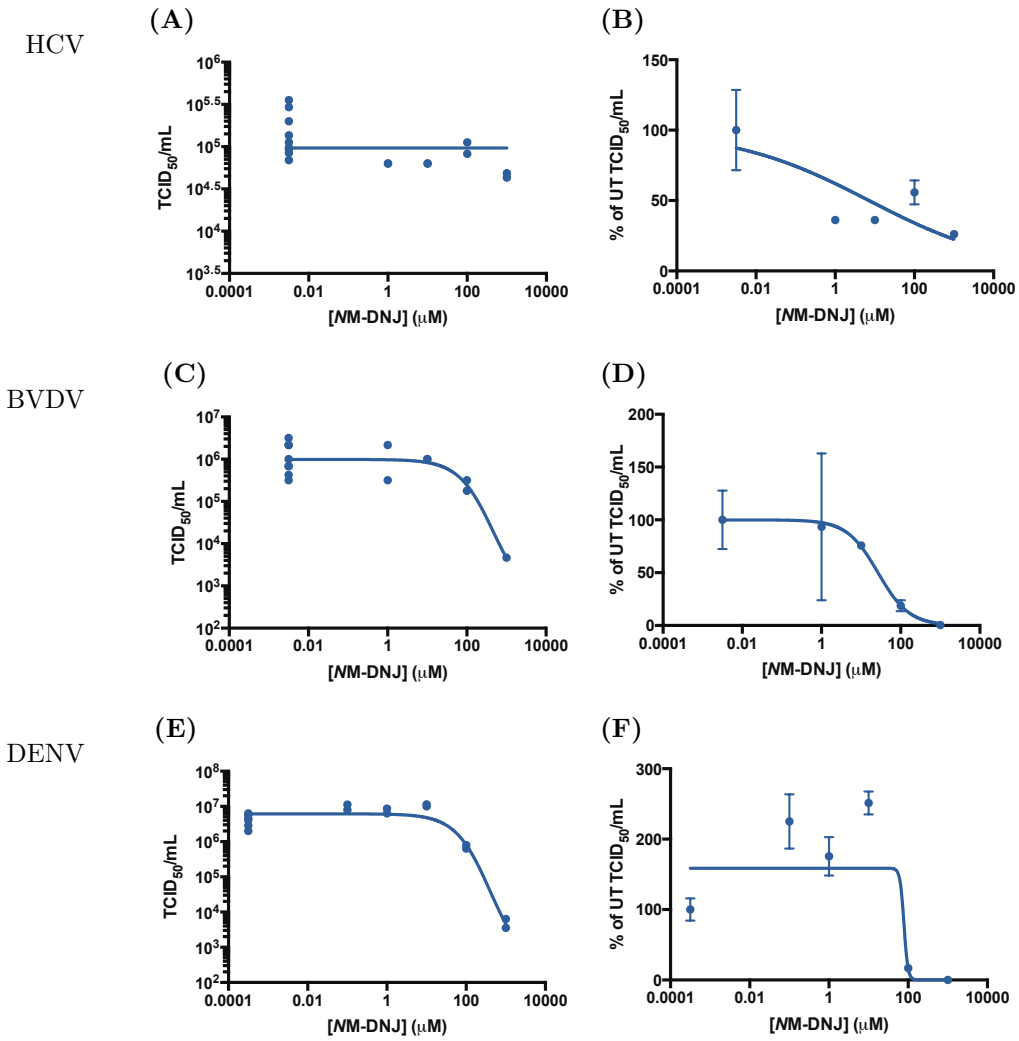

Figure 4.7: *Antiviral Effects of NM-D-DNJ.* (A) Huh7-Lunet-hCD81-GLuc cells were infected with Jc1 HCV (MOI = 0.2) and then incubated with media containing *N*M-D-DNJ at the indicated concentrations in duplicate. After 4 d, the cell supernatant was harvested, and the titer of infectious virus from each well was measured by immunofluorescence endpoint dilution assay on naive Huh7-Lunet-hCD81-GLuc cells, calculating by the method of Reed and Muench.[212] Each point indicates an individual replicate value. (B) The data of A are presented as percentage of untreated control. Each point is the mean with error bars representing standard error of the mean. (C) MDBK cells were infected with Pe515-ncp strain BVDV (MOI = 10) and then incubated with media containing *N*M-D-DNJ at the indicated concentrations in duplicate. After 2 d, the cell supernatant was harvested, and the titer of infectious virus from each well was measured by immunofluorescence endpoint dilution assay on naive MDBK cells, calculating by the method of Reed and Muench.[212] Each point indicates an individual replicate value. (D) The data of C are presented as percentage of untreated control. Each point is the mean with error bars representing standard error of the mean. (E) Huh7-Lunet-hCD81-GLuc cells were infected with 16681 DENV2 and then incubated with media containing *N*M-D-DNJ at the indicated concentrations in duplicate. After 2 d, the cell supernatant was harvested, and the titer of infectious virus from each well was measured by immunofluorescence endpoint dilution assay on naive LLC-MK_2 cells, calculating by the method of Reed and Muench.[212] Each point indicates an individual replicate value. (F) The data of E are presented as percentage of untreated control. Each point is the mean with error bars representing standard error of the mean. In each case, the data were fitted using Prism 6, with a comparison of fits between a horizontal line and a three parameter Hill plot, using the extra sum-of-squares F test to determine the better fit.

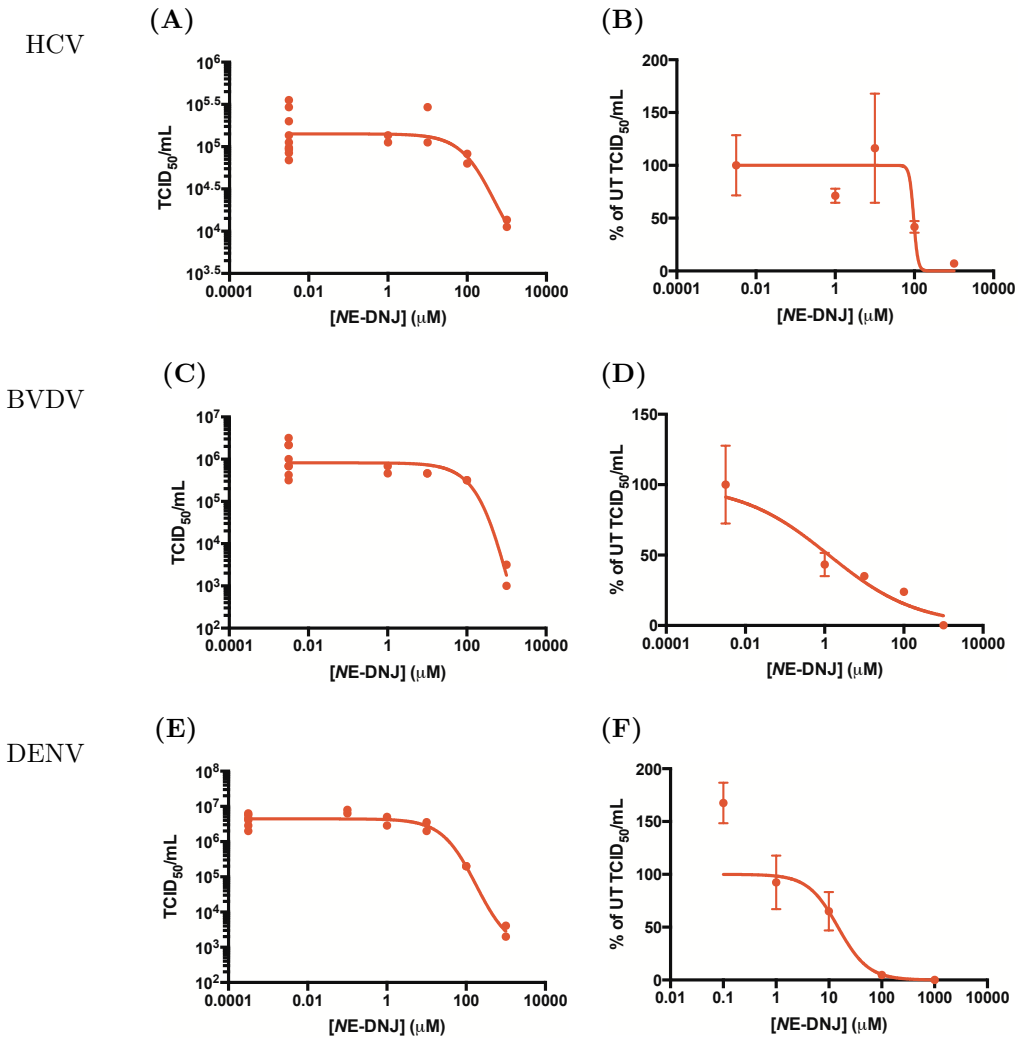

Figure 4.8: *Antiviral Effects of NE-D-DNJ.* (A) Huh7-Lunet-hCD81-GLuc cells were infected with Jc1 HCV (MOI = 0.2) and then incubated with media containing *N*E-D-DNJ at the indicated concentrations in duplicate. After 4 d, the cell supernatant was harvested, and the titer of infectious virus from each well was measured by immunofluorescence endpoint dilution assay on naive Huh7-Lunet-hCD81-GLuc cells, calculating by the method of Reed and Muench.[212] Each point indicates an individual replicate value. (B) The data of A are presented as percentage of untreated control. Each point is the mean with error bars representing standard error of the mean. (C) MDBK cells were infected with Pe515-ncp strain BVDV (MOI = 10) and then incubated with media containing *N*E-D-DNJ at the indicated concentrations in duplicate. After 2 d, the cell supernatant was harvested, and the titer of infectious virus from each well was measured by immunofluorescence endpoint dilution assay on naive MDBK cells, calculating by the method of Reed and Muench.[212] Each point indicates an individual replicate value. (D) The data of C are presented as percentage of untreated control. Each point is the mean with error bars representing standard error of the mean. (E) Huh7-Lunet-hCD81-GLuc cells were infected with 16681 DENV2 and then incubated with media containing *N*E-D-DNJ at the indicated concentrations in duplicate. After 2 d, the cell supernatant was harvested, and the titer of infectious virus from each well was measured by immunofluorescence endpoint dilution assay on naive LLC-MK_2 cells, calculating by the method of Reed and Muench.[212] Each point indicates an individual replicate value. (F) The data of E are presented as percentage of untreated control. Each point is the mean with error bars representing standard error of the mean. In each case, the data were fitted using Prism 6, with a comparison of fits between a horizontal line and a three parameter Hill plot, using the extra sum-of-squares F test to determine the better fit.

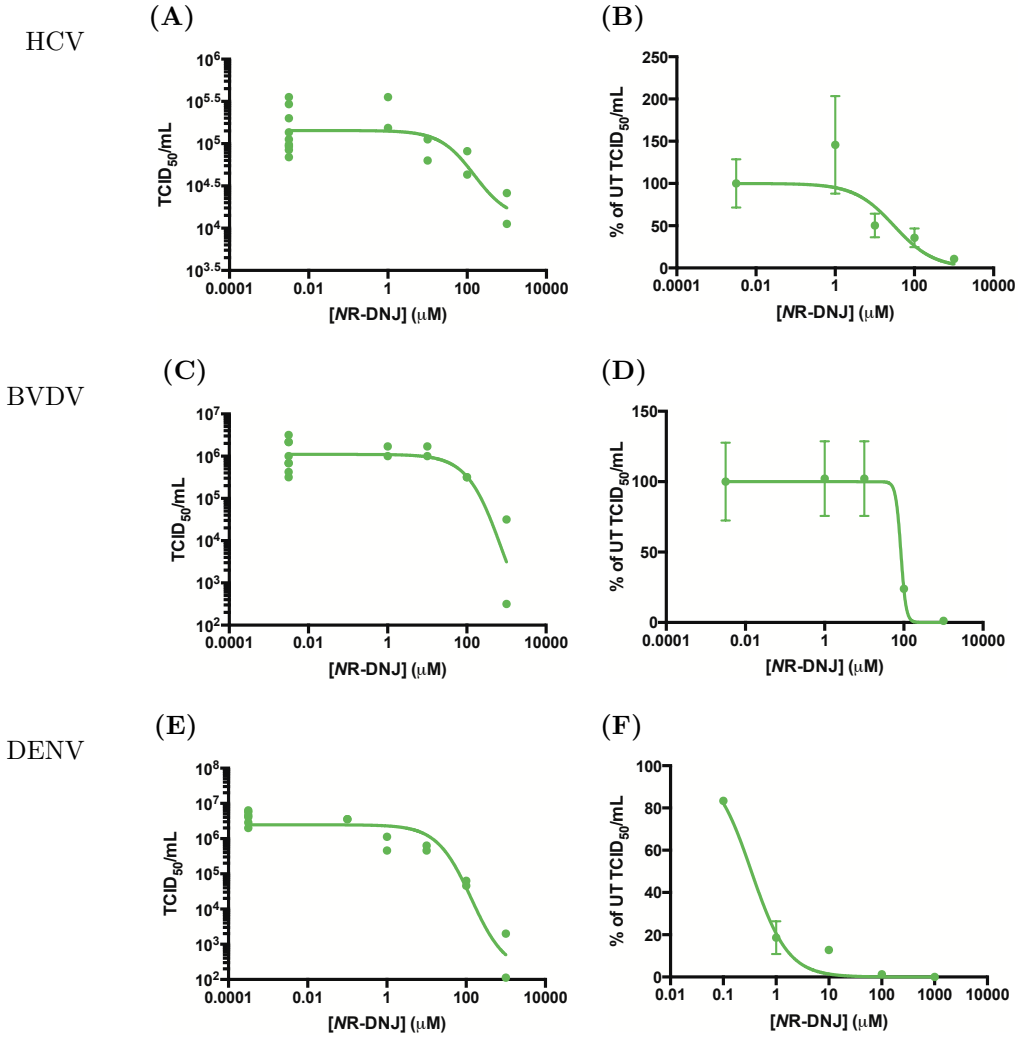

Figure 4.9: *Antiviral Effects of NR-D-DNJ.* (A) Huh7-Lunet-hCD81-GLuc cells were infected with Jc1 HCV (MOI = 0.2) and then incubated with media containing *N*R-D-DNJ at the indicated concentrations in duplicate. After 4 d, the cell supernatant was harvested, and the titer of infectious virus from each well was measured by immunofluorescence endpoint dilution assay on naive Huh7-Lunet-hCD81-GLuc cells, calculating by the method of Reed and Muench.[212] Each point indicates an individual replicate value. (B) The data of A are presented as percentage of untreated control. Each point is the mean with error bars representing standard error of the mean. (C) MDBK cells were infected with Pe515-ncp strain BVDV (MOI = 10) and then incubated with media containing *N*R-D-DNJ at the indicated concentrations in duplicate. After 2 d, the cell supernatant was harvested, and the titer of infectious virus from each well was measured by immunofluorescence endpoint dilution assay on naive MDBK cells, calculating by the method of Reed and Muench.[212] Each point indicates an individual replicate value. (D) The data of C are presented as percentage of untreated control. Each point is the mean with error bars representing standard error of the mean. (E) Huh7-Lunet-hCD81-GLuc cells were infected with 16681 DENV2 and then incubated with media containing *N*R-D-DNJ at the indicated concentrations in duplicate. After 2 d, the cell supernatant was harvested, and the titer of infectious virus from each well was measured by immunofluorescence endpoint dilution assay on naive LLC-MK_2 cells, calculating by the method of Reed and Muench.[212] Each point indicates an individual replicate value. (F) The data of E are presented as percentage of untreated control. Each point is the mean with error bars representing standard error of the mean. In each case, the data were fitted using Prism 6, with a comparison of fits between a horizontal line and a three parameter Hill plot, using the extra sum-of-squares F test to determine the better fit.

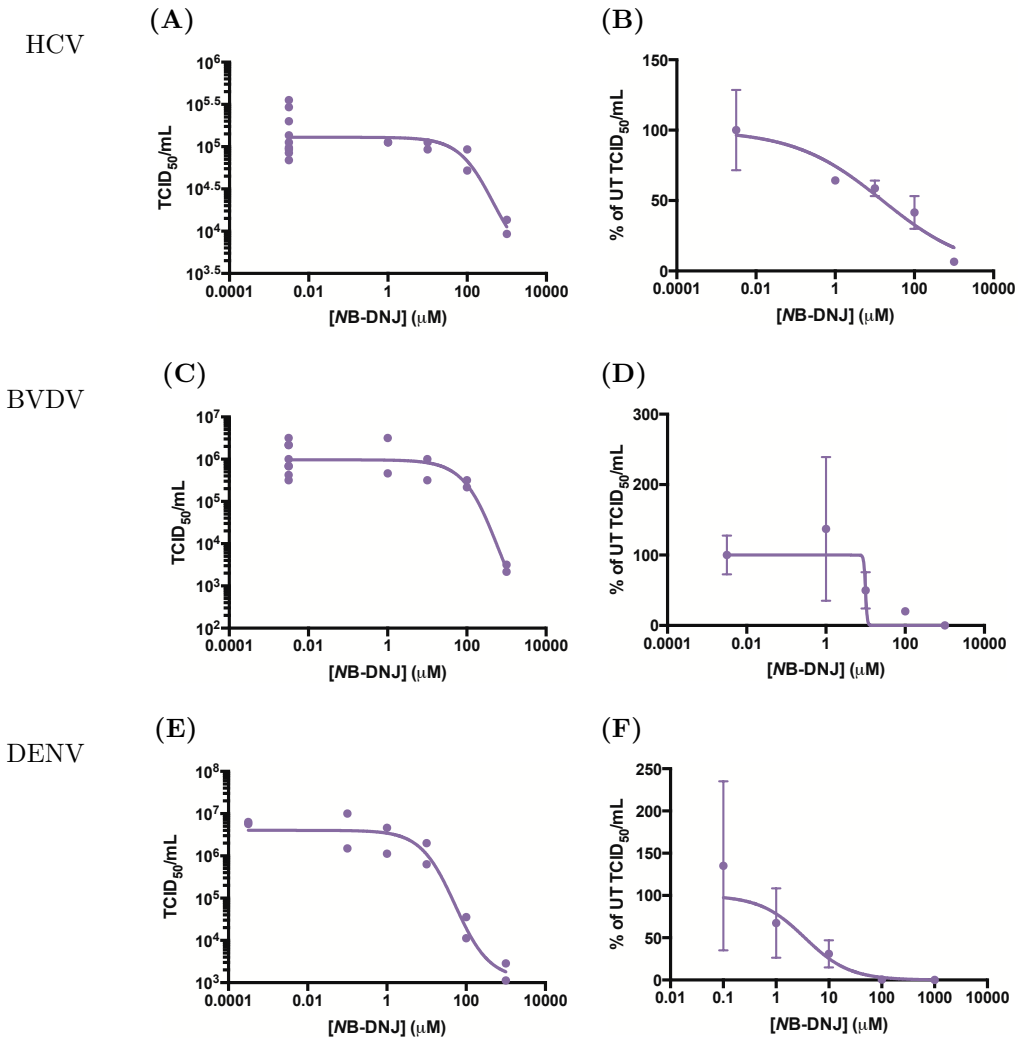

Figure 4.10: *Antiviral Effects of NB-D-DNJ.* (A) Huh7-Lunet-hCD81-GLuc cells were infected with Jc1 HCV (MOI = 0.2) and then incubated with media containing *N*B-D-DNJ at the indicated concentrations in duplicate. After 4 d, the cell supernatant was harvested, and the titer of infectious virus from each well was measured by immunofluorescence endpoint dilution assay on naive Huh7-Lunet-hCD81-GLuc cells, calculating by the method of Reed and Muench.[212] Each point indicates an individual replicate value. (B) The data of A are presented as percentage of untreated control. Each point is the mean with error bars representing standard error of the mean. (C) MDBK cells were infected with Pe515-ncp strain BVDV (MOI = 10) and then incubated with media containing *N*B-D-DNJ at the indicated concentrations in duplicate. After 2 d, the cell supernatant was harvested, and the titer of infectious virus from each well was measured by immunofluorescence endpoint dilution assay on naive MDBK cells, calculating by the method of Reed and Muench.[212] Each point indicates an individual replicate value. (D) The data of C are presented as percentage of untreated control. Each point is the mean with error bars representing standard error of the mean. (E) Huh7-Lunet-hCD81-GLuc cells were infected with 16681 DENV2 and then incubated with media containing *N*B-D-DNJ at the indicated concentrations in duplicate. After 2 d, the cell supernatant was harvested, and the titer of infectious virus from each well was measured by immunofluorescence endpoint dilution assay on naive LLC-MK_2 cells, calculating by the method of Reed and Muench.[212] Each point indicates an individual replicate value. (F) The data of E are presented as percentage of untreated control. Each point is the mean with error bars representing standard error of the mean. In each case, the data were fitted using Prism 6, with a comparison of fits between a horizontal line and a three parameter Hill plot, using the extra sum-of-squares F test to determine the better fit.

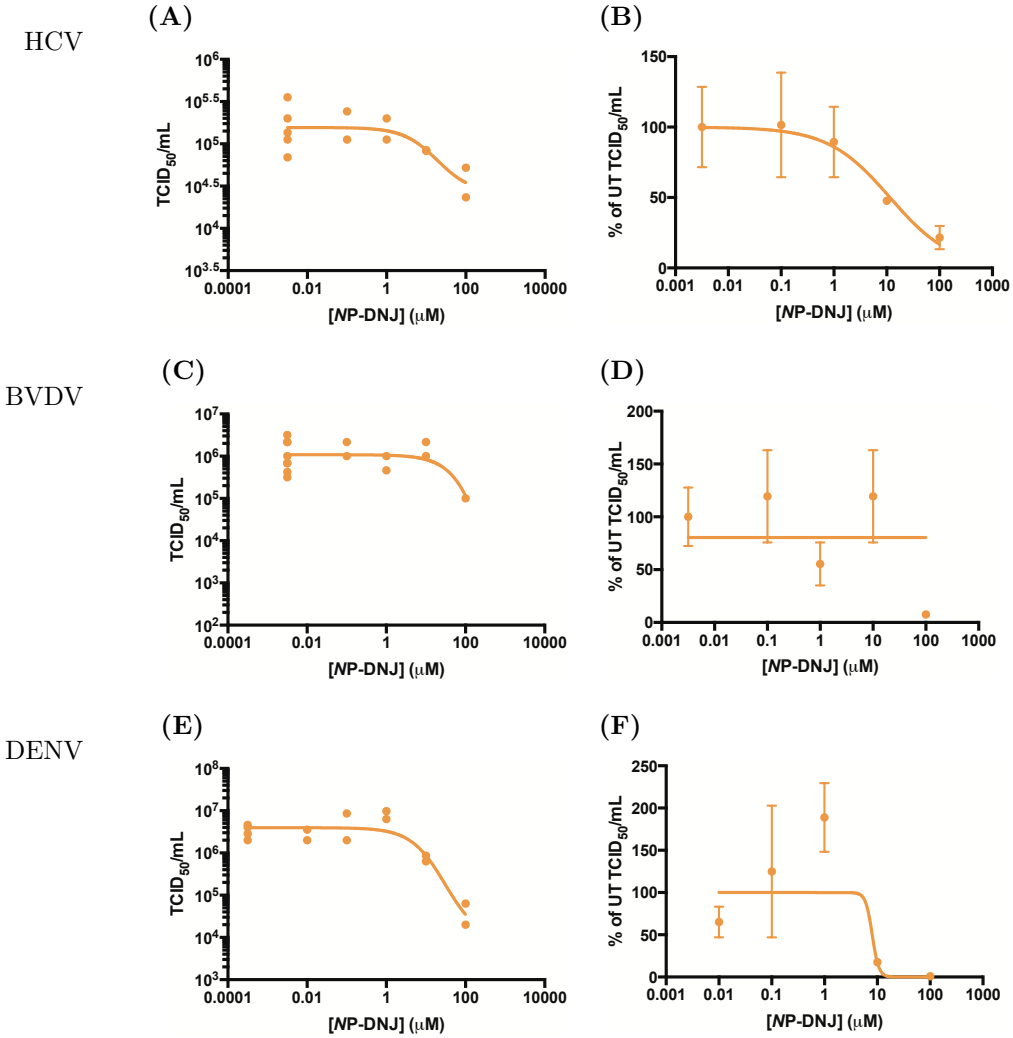

Figure 4.11: *Antiviral Effects of NP-D-DNJ.* (A) Huh7-Lunet-hCD81-GLuc cells were infected with Jc1 HCV (MOI = 0.2) and then incubated with media containing *N*P-D-DNJ at the indicated concentrations in duplicate. After 4 d, the cell supernatant was harvested, and the titer of infectious virus from each well was measured by immunofluorescence endpoint dilution assay on naive Huh7-Lunet-hCD81-GLuc cells, calculating by the method of Reed and Muench.[212] Each point indicates an individual replicate value. (B) The data of A are presented as percentage of untreated control. Each point is the mean with error bars representing standard error of the mean. (C) MDBK cells were infected with Pe515-ncp strain BVDV (MOI = 10) and then incubated with media containing *N*P-D-DNJ at the indicated concentrations in duplicate. After 2 d, the cell supernatant was harvested, and the titer of infectious virus from each well was measured by immunofluorescence endpoint dilution assay on naive MDBK cells, calculating by the method of Reed and Muench.[212] Each point indicates an individual replicate value. (D) The data of C are presented as percentage of untreated control. Each point is the mean with error bars representing standard error of the mean. (E) Huh7-Lunet-hCD81-GLuc cells were infected with 16681 DENV2 and then incubated with media containing *N*P-D-DNJ at the indicated concentrations in duplicate. After 2 d, the cell supernatant was harvested, and the titer of infectious virus from each well was measured by immunofluorescence endpoint dilution assay on naive LLC-MK_2 cells, calculating by the method of Reed and Muench.[212] Each point indicates an individual replicate value. (F) The data of E are presented as percentage of untreated control. Each point is the mean with error bars representing standard error of the mean. In each case, the data were fitted using Prism 6, with a comparison of fits between a horizontal line and a three parameter Hill plot, using the extra sum-of-squares F test to determine the better fit. *Data collected in collaboration with Dr. J. Miller and M. Hill.*

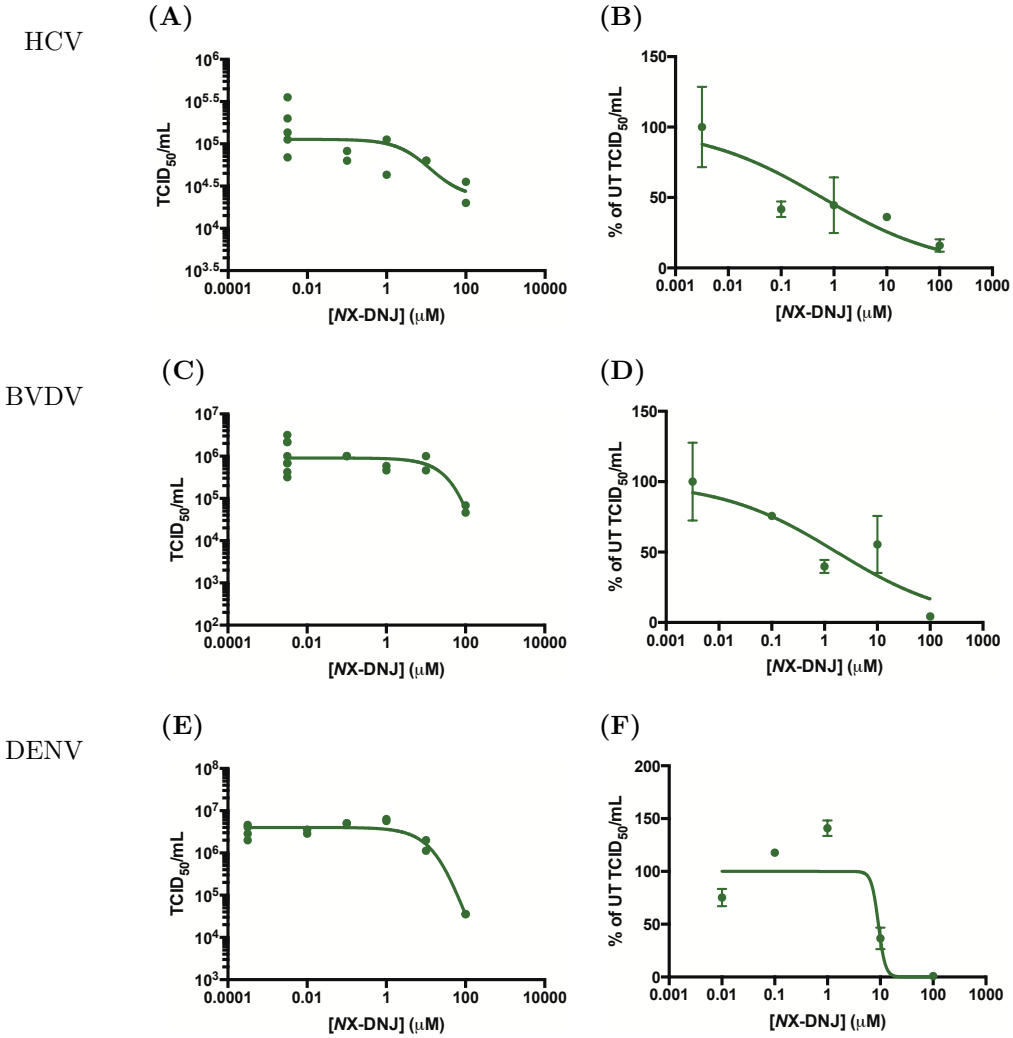

Figure 4.12: *Antiviral Effects of NX-D-DNJ.* (A) Huh7-Lunet-hCD81-GLuc cells were infected with Jc1 HCV (MOI = 0.2) and then incubated with media containing *N*X-D-DNJ at the indicated concentrations in duplicate. After 4 d, the cell supernatant was harvested, and the titer of infectious virus from each well was measured by immunofluorescence endpoint dilution assay on naive Huh7-Lunet-hCD81-GLuc cells, calculating by the method of Reed and Muench.[212] Each point indicates an individual replicate value. (B) The data of A are presented as percentage of untreated control. Each point is the mean with error bars representing standard error of the mean. (C) MDBK cells were infected with Pe515-ncp strain BVDV (MOI = 10) and then incubated with media containing *N*X-D-DNJ at the indicated concentrations in duplicate. After 2 d, the cell supernatant was harvested, and the titer of infectious virus from each well was measured by immunofluorescence endpoint dilution assay on naive MDBK cells, calculating by the method of Reed and Muench.[212] Each point indicates an individual replicate value. (D) The data of C are presented as percentage of untreated control. Each point is the mean with error bars representing standard error of the mean. (E) Huh7-Lunet-hCD81-GLuc cells were infected with 16681 DENV2 and then incubated with media containing *N*X-D-DNJ at the indicated concentrations in duplicate. After 2 d, the cell supernatant was harvested, and the titer of infectious virus from each well was measured by immunofluorescence endpoint dilution assay on naive LLC-MK_2 cells, calculating by the method of Reed and Muench.[212] Each point indicates an individual replicate value. (F) The data of E are presented as percentage of untreated control. Each point is the mean with error bars representing standard error of the mean. In each case, the data were fitted using Prism 6, with a comparison of fits between a horizontal line and a three parameter Hill plot, using the extra sum-of-squares F test to determine the better fit.

Table 4.3: *Effect of* D*-DNJ Series on Infectious HCV Secretion*

Iminosugar	$IC_{50}{}^{a}$ (µM)	95% $CI^{a,b}$
D-DNJ **33D**	NA	NA
*N*M-D-DNJ **54D**	7.16	0.005 – AF
*N*E-D-DNJ **55D**	95.9	AF
*N*R-D-DNJ **56D**	14.7	0.03 – AF
*N*B-D-DNJ **47D**	15.7	0.10 – AF
*N*P-D-DNJ **57D**	11.5	0.48 – AF
*N*X-D-DNJ **58D**	0.60	0.006 – 78.5

[a] NA : Not applicable; the data was fitted with a horizontal line.
[b] AF : The fitted curve was ambiguous and a complete 95% confidence interval cannot be reported.

Table 4.4: *Effect of* D*-DNJ Series on Infectious BVDV Secretion*

Iminosugar	$IC_{50}{}^{a}$ (µM)	95% $CI^{a,b}$
D-DNJ **33D**	59.7	1.38 – AF
*N*M-D-DNJ **54D**	26.8	20.0 – 36.2
*N*E-D-DNJ **55D**	1.28	0.04 – 11.0
*N*R-D-DNJ **56D**	84.3	AF
*N*B-D-DNJ **47D**	10	AF
*N*P-D-DNJ **57D**	NA	AF
*N*X-D-DNJ **58D**	1.70	0.02 – AF

[a] NA : Not applicable; the data was fitted with a horizontal line.
[b] AF : The fitted curve was ambiguous and a complete 95% confidence interval cannot be reported.

Table 4.5: *Effect of* D*-DNJ Series on Infectious DENV Secretion*

Iminosugar	$IC_{50}{}^{a}$ (µM)	95% $CI^{a,b}$
D-DNJ **33D**	49.4	2.44 – 937.6
*N*M-D-DNJ **54D**	85.7	AF
*N*E-D-DNJ **55D**	14.9	2.54 – 117.8
*N*R-D-DNJ **56D**	0.34	0.09 – 1.21
*N*B-D-DNJ **47D**	3.52	0.29 – 41.4
*N*P-D-DNJ **57D**	0.34	AF
*N*X-D-DNJ **58D**	9.20	AF

[a] NA : Not applicable; the data was fitted with a horizontal line.
[b] AF : The fitted curve was ambiguous and a complete 95% confidence interval cannot be reported.

4.6 Discussion

Initial forays into the development of higher throughput antiviral screening assays demonstrated the success with which Huh7 derived cell lines can be employed as a cell system for culturing DENV. Both Huh7.5 and Huh7-Lunet-hCD81-GLuc cells were infected with 16681 DENV2, and produced virus of 10-fold higher titer over the course of two days than that obtained from primary MDMΦ cells. While the medically relevant variation of primary cells was sacrificed by switching to a cell line, this removed the limitations that result from the limited cells available from a given blood donation. Furthermore, the homogeneity of the cells allowed for more direct comparison of different iminosugars.

The $TCID_{50}$ assay was selected as a method for viral titer determination as an alternative to both plaque and focus forming assays. Because the $TCID_{50}$ assay requires only scoring a well as positive or negative, reading of the assay is faster and more efficient than the counting of individual plaques and foci required by the other assays. Compared to the plaque assay, fewer cells and reagents were required to determine $TCID_{50}$, making the assay more cost effective. The initial test of the overall method with M*O*N-DNJ in the DENV system suggested not only that the screen could provide an indication of the presence of antiviral activity, but also provide a comparable IC_{50} to that measured by other methods.

Further use of the $TCID_{50}$ technique to evaluate the antiviral effects of the *N*-*n*-alkyl DNJ series, however, revealed limitations of the method. Because individual foci or plaques are not counted, the quantitative specificity of the assay is limited by the size of the dilution step and number of replicate wells of each dilution. That is to say, in the case of DENV, where the dilution step size in the $TCID_{50}$ assay is 10-fold, a difference in titre of at least 10-fold is clearly demonstrated, however a reduction of less than 90% in the viral titre can be within the error of the assay. This may be alleviated somewhat by using smaller dilutions (as with the half $\log_{10}$ dilution steps used in the HCV and BVDV assays). However, with its binary evaluation, the results

of a $TCID_{50}$ assay are inherently step-like in nature, as opposed to the continuous readout of the plaque and focus assays.

When screening whether a compound has any antiviral activity, only the highest nontoxic dose is tested initially. For this purpose, the $TCID_{50}$ assay is ideal. Because higher concentrations of the drug cannot be used (due to toxicity), the drug does not warrant further investigation if the treatment does not reduce the viral titer by at least 90% compared to untreated. Once a compound has been identified as promising, a plaque or focus forming assay is better suited to IC_{50} determination, which involves fitting the viral titer not as a raw value, but as a percentage of the untreated control. Though the $TCID_{50}$ assay is more sensitive in terms of minimum measurable titer, the larger window of potential titer reduction does not provide useful information in the percentage curve, with all reductions of more than 2 orders of magnitude being practically identical in terms of percentage. Similarly, the less quantitative nature provides less detailed information for fitting close to the inflection point of the fitted curve, the points most critical to IC_{50} value determination. This combination results in the fitting of $TCID_{50}$ data as a percentage of the untreated $TCID_{50}$ (Panels B, D, and F of Figure 4.6 – Figure 4.12) being almost universally ambiguous. 95% confidence intervals could not be calculated for the IC_{50} values for several of the iminosugars in each of the viral systems due to these ambiguous fits (Table 4.3, Table 4.4, and Table 4.5). Indeed, even in cases where intervals for IC_{50} could be fitted, they spanned ranges close to 3 orders of magnitude (2.44 to 937.6 µM for D-DNJ against DENV). The counting of individual infectious particles provides more quantitative data which allows for more exact fitting of a dose-response curve, and would be the better method for characterization of antiviral potency.

Given the ambiguous fit of IC_{50} values, the relative potency of tested DNJ derivatives were evaluated by comparing the reduction in $TCID_{50}$ of all of the candidates at the same concentration. *N*P-D-DNJ and *N*X-D-DNJ demonstrated higher cytotoxicity than the compounds with shorter alkylation, so the amount of viral inhibition for each

virus was compared for each iminosugar at 100 µM (Figure 4.13), the highest non-toxic dose of *N*P- and *N*X-DNJ that was tested. Two distinct alkylation-dependent trends emerged. In the case of HCV and BVDV, as the alkyl chain length increases, the inhibition of infectious virus release at 100 µM of iminosugar is constant from unalkylated up to *n*-butyl, but potency sequentially increases with the *n*-pentyl and *n*-hexyl. DENV displays a pattern distinct from the two other viruses. In this instance, iminosugars become increasingly potent from D-DNJ through *N*B-D-DNJ, plateauing through the rest of the examined series.

In terms of overall trends, it is not surprising that the net effect in both patterns is increasing potency as length increases, as iminosugar alkylation has previously been shown to improve cellular uptake.[198] However, this does not explain the differences among the viruses, particularly because the DENV and HCV culture systems employ the same cell line. While the difference could be due to viral-induced changes in cellular iminosugar uptake, the similarity in trends between HCV and BVDV (which tested in different cell lines) indicate that the trend might correspond to the relative importance of mechanisms of action to each virus.

Two potential explanations for the trend in HCV and BVDV readily present themselves. The first, as indicated by the isolated enzyme inhibition data (Table 4.1), is the fact that glycolipid enzymes are inhibited more potently by iminosugars with longer *N*-alkylation chains. The iminosugar inhibits the enzyme by acting as a ceramide mimic,[218] and the longer chains better approximate the lipid tail of the natural substrate. In particular, human glucocerebrosidase is more potently inhibited by *N*P-DNJ (IC_{50} = 28 µM) and *N*X-DNJ (IC_{50} = 18 µM) than those with shorter chains ($IC_{50} \geq 290$ µM).

Alternatively, both HCV and BVDV contain the viroporin p7, while DENV does not. It is known that iminosugars can inhibit the electrophysiological activity of this pore-forming protein, with this capability being dependent on the compound's alkylation.[177;181] Compounds with *N*-butyl alkylation have no effect on the pore, while those with *N*-nonyl alkylation can completely abrogate activity.[181] The chain lengths

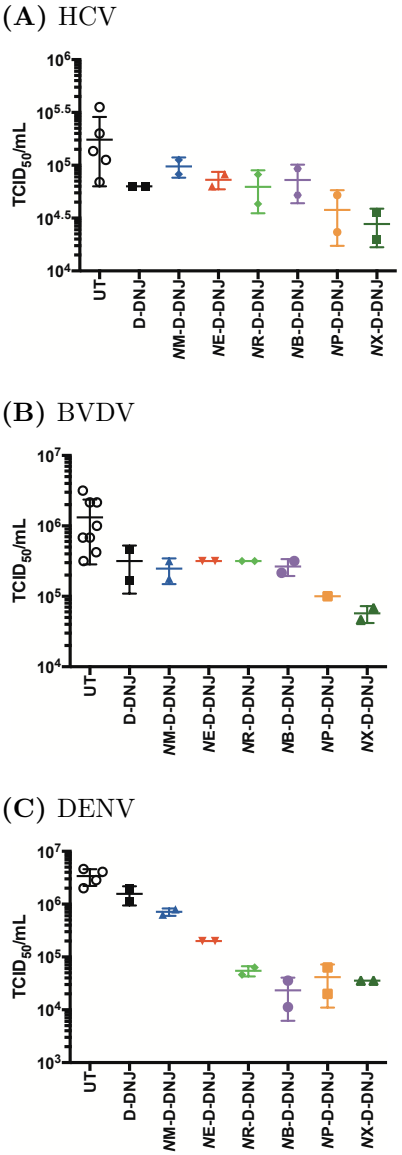

Figure 4.13: *Comparison of N-n-*D*-DNJ Antiviral Effects at 100 µ*M. (A) Huh7-Lunet-hCD81-GLuc cells were infected with Jc1 HCV (MOI = 0.2) and then incubated with media containing 100 µM of the indicated DNJ derivative in duplicate. After 4 d, the cell supernatant was harvested, and the titer of infectious virus from each well was measured by immunofluorescence endpoint dilution assay on naive Huh7-Lunet-hCD81-GLuc cells, calculating by the method of Reed and Muench.[212] (B) MDBK cells were infected with Pe515-ncp strain BVDV (MOI = 10) and then incubated with media containing 100 µM of the indicated DNJ derivative in duplicate. After 2 d, the cell supernatant was harvested, and the titer of infectious virus from each well was measured by immunofluorescence endpoint dilution assay on naive MDBK cells, calculating by the method of Reed and Muench.[212] (C) Huh7-Lunet-hCD81-GLuc cells were infected with 16681 DENV2 and then incubated with media containing 100 µM of the indicated DNJ derivative in duplicate. After 2 d, the cell supernatant was harvested, and the titer of infectious virus from each well was measured by immunofluorescence endpoint dilution assay on naive LLC-MK_2 cells, calculating by the method of Reed and Muench.[212] In all panels, each point indicates an individual replicate value. The data for each virus were analysed by a one-way ANOVA using Prism 6. Neither HCV ($p = 0.25$) or BVDV ($p = 0.23$) showed statistically significant variation among the treatments, while there was in DENV ($p = 0.003$). However, the only significant differences were between each alkylated iminosugar and untreated.

between 4 and 9 have not been studied previously to determine p7 inhibition activity. It is possible that inhibition of the viral protein's activity simply requires alkylation of longer than 4 carbons, with longer chains inhibiting the channel more potently. In order to investigate this hypothesis, isolated electrophysiology experiments with p7 and these intermediate chain-length iminosugars need to be carried out.

4.7 Conclusions

After evaluating the feasibility of several options, the $TCID_{50}$ assay was selected as the screen for HCV, DENV, and BVDV. Due to its higher efficiency in terms of time, methodology and cost, it is well suited to determining whether a compound is antiviral or not. However, when characterizing the potency, the more quantitative methods of plaque and focus forming assays are more appropriate.

Examining the enzyme inhibition profiles of the synthesized D-DNJ series, the compounds unsurprisingly demonstrated more potent inhibition of glucose-processing enzymes than those evolved to cleave sugars with different stereochemistry. For most of the enzymes studied, the alkyl chain had little influence on inhibition, with the notable exceptions of β-glucocerebrosidase and glucosylceramide synthase. Because both of these enzymes act upon glycolipids, it makes sense that they are sensitive to alkylation, as this mimics the lipophilic chain of the ceramide-based substrates of these enzymes.

With respect to inhibition of infectious virus release, longer alkyl chains corresponded to more potent antiviral effect in all three virus systems overall; however, the trend in how this changed with the addition of each individual methylene group varied. HCV and BVDV showed an increase in antiviral effect only with butyl and longer chains. This correlates to the chain lengths that demonstrate potent inhibition of the glycolipid enzymes, indicating that this mechanism could potentially be antiviral with respect to these two viruses. However, both of these viruses have a p7 viroporin. It is known that *N*B-DNJ is not a p7 inhibitor, while *N*N-DNJ is, so a second potential

explanation for the antiviral trend observed is that ability to inhibit p7 requires any chain length longer than 4 carbon atoms and the increasing antiviral potency is mirroring a p7 effect. In contrast to these viruses, treatment of DENV showed increasing potency from no alkylation up to butyl, rather than the increase starting there.

While work remains to be done to fully elucidate the mechanistic explanation for the influence of DNJ alkylation on antiviral activity, the collected data suggest that anti-DENV activity results from a different combination (or differently weighted combination) of mechanisms of action than for the other two members of the *Flaviviridae*.

4.8 Biological Materials and Methods

4.8.1 Cells

Human monocytic cell line HL60 (ATCC) was maintained in RPMI 1640 media (PAA) supplemented with 2 mM L-glutamine (Sigma), 100 µg/mL streptomycin (Sigma), 100 U/mL penicillin (Sigma) and 10% (volume/volume, v/v) heat-inactivated (56 °C, 30 min) fetal calf serum (FCS, Seralab). Human hepatoma cell lines, Huh7.5 (Apath, LLC) and Huh7-Lunet-hCD81-GLuc (Twincore), were cultured in Dulbecco's modified Eagle media (DMEM) with GlutaMax™ (Gibco) supplemented with 100 µg/mL streptomycin, 100 U/mL penicillin, 100 µM MEM non-essential amino acids (Gibco) and 10% (v/v) FCS. Madin–Darby Bovine kidney cell line MDBK (ECACC) was maintained in DMEM with GlutaMax™ supplemented with 100 µg/mL streptomycin, 100 U/mL penicillin and 10% (v/v) heat inactivated horse serum (HS, Sigma). Monkey kidney cell line LLC-MK_2 was cultured in M199 media (Gibco) supplemented with 2 mM L-glutamine, 100 µg/mL streptomycin, 100 U/mL penicillin and 20% (v/v) FCS. Subsequently, these are referred to as growth media for each cell line.

Unless otherwise indicated, cell passages were carried out by washing twice with phosphate buffered saline (PBS, Gibco) and lifting with trypsin + ethylenediaminetetraacetic acid (EDTA) (Sigma), and all cell incubations were carried out at 37 °C and 5% CO_2 unless otherwise indicated.

All cells were maintained as mycoplasma free, with regular verifications by polymerase chain reaction (PCR).

4.8.2 Viruses

HCV Jc1 and Jc1-Luc plasmids were provided by Prof. R. Bartenschlager, University of Heidelberg, Germany.

DENV2 strain 16681 (a gift from Prof. E. Gould, Centre for Ecology and Hydrology, Oxford, United Kingdom) was propagated in the C6/36 cell line.

BVDV strain Pe515-ncp (a gift from Prof. J. McCauley, Institute for Animal Health, Compton, United Kingdom) was propagated in the MDBK cell line.

4.8.3 Cell Viability

Cell viability was measured using the CellTiter 96® AQ_{ueous} One Solution Cell Proliferation MTA (3-(4,5-dimethylthiazol-2-yl)-5-(3-carboxymethoxyphenyl)-2-(4-sulfophenyl)-2*H*-tetrazolium, inner salt) Assay (Promega) according to the manufacturer's instruction. Briefly, cells were seeded at the indicated density (Table 4.6) in 100 µL of growth media in each well of a sterile 96-well plate. 100 µL of 2× each drug treatment were added in triplicate. As controls, wells with 200 µL growth media with and without cells were also included in triplicate. The cells were incubated with drug for the indicated length of time. After the incubation, 20 µL of MTS reagent was added. After a further one to two hour incubation, the absorbance at 490 nm was measured on a Molecular Devices SpectraMax M5 microplate reader. The endpoint for evaluation was taken when untreated cells had an absorbance reading of approximately 1.

Table 4.6: *MTS Assay Parameters*

Cell Type	Seeding Density (cells/well)	Assay Length (d)
Huh7-Lunet-hCD81-GLuc	5×10^3	4
MDBK	1×10^4	2

Absorbances were averaged across replicates, and corrected for background by subtracting the value for media-only wells. Each drug treatment was then evaluated as a percentage of untreated cells.

4.8.4 LAL Assay for Endotoxin

Endotoxin levels in the prepared iminosugars were measured using the PyroGene® Recombinant Factor C Endotoxin Detection Assay (Lonza) according to the manufacturer's instructions, except that rather than the recommended pyrogen-free vials,

HPLC vials (Waters) that were cleansed of pyrogens by heating at 250 °C for 30 min were employed.

4.8.5 HCV

4.8.5.1 Preparation of Infectious Virus

Stocks of infectious HCV were prepared from plasmid according to the protocol of Kato *et al.*.[219] Competent DH5α *Escherichia coli* (*E. coli*, New England Biolabs) were transformed to incorporate the Jc1 or Jc1-Luc plasmid. Transformed *E. coli* were cultured overnight, and DNA was isolated using an EndoFree Plasmid Maxi Kit (Qiagen) according to the manufacturer's instructions. The identity of the DNA was confirmed by PCR sequencing (Table 4.7). The DNA was linearized by digestion with MluI (Invitrogen), subsequently purified by phenol/$CHCl_3$ extraction, digested with mung bean nuclease (New England Biolabs) to provide ligatable ends, treated with proteinase K (Ambion) to remove contaminating proteins and purified a second time by phenol/$CHCl_3$ extraction. *In vitro* transcription using the MegaScript T7 transcription kit (Ambion) according to the manufacturer's instructions provided RNA, with the parent DNA being digested afterwards with DNase (Roche). The product RNA size was confirmed by 6% acrylamide gel analysis. The RNA could be electroporated directly or stored at –80 °C for up to 4 months.

For electroporation, Huh7 derived cells (either Huh7.5 or Huh7-Lunet-hCD81-GLuc) were lifted with trypsin/EDTA, and the trypsin was then inactivated with growth media, and the cells pelleted (290 × *g*, 5 min, 4 °C). The cells were washed three times with OptiMEM I reduced serum media (Gibco) by resuspending and pelleting. The cells were resuspended in OptiMEM I a final time, counted, and 1×10^7 cells were pelleted. The pellet was resuspended in 1 mL of Cytomix buffer. 400 µL of the cell suspension were mixed with 10 µg of the RNA, and the complete mixture transferred to an Gene Pulser/MicroPulser electroporation cuvette (0.4 cm gap, Bio-Rad) and electroporated using a Gene Pulser Xcell (Bio-Rad) at 260 V and 950 µF. 1 mL of

Table 4.7: Primers for HCV Sequencing

Primer Name	Sequence
JC1-For	5′-ACC TGC CCC TAA TAG GGG CGA-3′
JC-594F	5′-TAT ACG GGA ATG AGG GAC TCG-3′
JC1025F	5′-TGC GAG AAA GTG GGG AAT GC-3′
JC1452F	5′-TCG TTG TCA TCC TTC TGT TGG C-3′
JC-2002F	5′-CAC GTG GAT GAA CTC TTC TGG CTA-3′
JC2602F	5′-GCT GGT CAT CTT GCA CGC TGC-3′
JC4168F	5′-TGG CAT CAA TCC CAA CAT TAG G -3′
JC4374F	5′-TCA GAC TAA CTG TGC TGG CTA CGG-3′
JC4795F	5′-TGT CTC ACG CAG TCA GCG-3′
JC5336F	5′-TAG CTG GAG GAG TCC TGG CAG-3′
JC-5829F	5′-CAC CGG CTT TGT CGT CAG TG-3′
JC-5980R	5′-CAT AGA GGG CTT CTC GCC AGA-3′
JC-6320R	5′-GAC TTC AAA AAT TGG CTG ACC TC-3′
JC-6519R	5′-CAG GTG TTC ATG CAG GTT TTA GGC-3′
JC7712F	5′-CCC GAA GAG GAA AAG TTG CC-3′
JC8085F	5′-CCA AAA ATG AGG TGT TCT GCG TG-3′
JC8464F	5′-GTT CAA CAG CAA GGG TCA AAC C-3′
JC8602F	5′-AAT GCT GGT ATG CGG CGA TG-3′
JC1-luc 930F	5′-ATA CGA TTT TGT ACC AGA-3′
J6-700R	5′-ACC CAC GTT GCG CGA CCT-3′
JFH1-4300R	5′-ATC GCA TAT GAT GAT GTC-3′
JFH1-3601F	5′-CGG AGC TGG CAA CAA GAC-3′
JFH1-5750F	5′-CGT TGT CGA CCA GTA CCA-3′
JFH1-7890R	5′-GCC GCT AGC TTG ATG TCC-3′
JFH1-850R	5′-GTA AGT TCC CTG TTG CAA-3′

growth media was added to the cuvette and the cells thoroughly resuspended. The cells were either seeded as described in the luciferase assay (§ 4.8.5.4) or the entire aliquot of cells placed into a 175 cm^2 tissue culture flask with 24 mL of growth media to produce a virus stock.

If placed into the tissue culture flask, the media was replaced 24 h after electroporation, and the cells were passaged every 3 d for 15 d, collecting the supernatant and storing at 4 °C. After the harvesting of final supernatant, it was concentrated in a Vivaspin® 20 centrifugal concentrator with a molecular weight cut off of 50,000 (Sartorius), aliquoted and stored at –80 °C.

4.8.5.2 Immunofluorescence

Cells were washed once with PBS, and then fixed with MeOH:Acetone (1:1) at room temperature for 10 min. The cells were washed three times with PBS with 0.1% (v/v) Tween-20 (Fisher) (PBS-T) and blocked with 3% (w/v) bovine serum albumin (BSA) in PBS-T for 1 h. After washing three times with PBS-T, the cells were incubated with 2 µg/mL mouse monoclonal anti-hepatitis C virus core 1b [C7-50] antibody (Abcam) in PBS-T for 1 h. The cells were washed three times with PBS-T, and incubated with 4 µg/mL Alexa Fluor® 488 donkey anti-mouse antibody (Invitrogen Molecular Probes) in PBS-T for 1 h. The cells were washed a final three times with PBS-T, and Vectashield with 4′,6-diamidino-2-phenylindole (DAPI) (Vector Laboratories, 1:100 dilution in PBS) was added to stain cell nuclei. The plates were imaged on an inverted Nikon Eclipse TE200-U microscope no sooner than 15 min after the addition of Vectashield, but, if stored at 4 °C, could be reliably observed for at least 10 d.

4.8.5.3 Titering of Virus Stock

Huh7-Lunet-hCD81-GLuc cells were seeded in a sterile 96-well plate at a density of 1×10^4 cells/well in 100 µL of growth media and incubated for 18 h. Serial 10-fold dilutions of the stock to be evaluated were prepared in growth media. Supernatant was removed from the cells, and each well was inoculated with 50 µL of virus dilution, with 8 replicates of each dilution. After incubating for 3 d, the cells were fixed and stained according to the HCV IF protocol (§ 4.8.5.2). Foci were counted in the highest dilution with $\geq$ 10 foci/well. Titer was calculated in units of focus forming units (ffu)/mL.

4.8.5.4 Luciferase Assay

Transfected Huh7 cells (2×10^4 cells/well) were seeded in an opaque, white, sterile 96-well plate in 100 µL of growth media directly after transfection. After 6 h, the

supernatant was removed, and replaced with 200 µL fresh media. The cells were incubated for 4 d.

100 µL of supernatant was removed, and expression of firefly (*Photinus pyralis*) luciferase was measured using the Bright-Glo™ Luciferase Assay System (Promega) according to the manufacturer's instructions.

4.8.5.5 Antiviral Assay

Huh7-Lunet-hCD81-GLuc cells were seeded in a sterile 96-well plate at a density of 5×10^3 cells/well in 100 µL of growth media. After an 18 h incubation, the supernatant was removed, and the wells were inoculated for 4 h with 100 µL of Jc1 HCV at an MOI of 0.2. The inoculum was removed and replaced with 200 µL of growth media with drug at the indicated concentration in duplicate, and the infected cells were incubated with drug for 4 d. The supernatant was harvested and infectious viral titer assessed immediately in the $TCID_{50}$ assay.

4.8.5.6 $TCID_{50}$ Assay

Huh7-Lunet-hCD81-GLuc cells were seeded in a sterile 96-well plate at a density of 2×10^4 cells/well in 100 µL of growth media and incubated for 18 h. The supernatants to be evaluated were diluted 1:100 in growth media, and 5 serial half-$\log_{10}$ dilutions were subsequently prepared in the same media. Supernatant was removed from the cells, and wells were inoculated in quadruplicate with 50 µL of analyte. After 4 h, the inoculum was removed and replaced with 100 µL of growth media.

The plates were incubated for 3 d, then fixed and stained according to the HCV IF protocol (§ 4.8.5.2). Based upon Alexa Fluor® 488 staining, each well was scored as either positive ($\geq$ 5 stained cells) or negative. $TCID_{50}$ values were calculated according to the method of Reed and Muench.[212]

4.8.6 DENV

4.8.6.1 Antiviral Assay

Huh7 derived cells were seeded in a sterile 96-well plate (1×10^4 cells/well for Huh7.5, 2×10^4 cells/well for Huh7-Lunet-hCD81-GLuc) in 100 µL of growth media. After 18 h incubation, the supernatant was removed, and the wells inoculated for 2 h with 50 µL of DENV2 16681 strain at an MOI of 0.1. The inoculum was removed and replaced with 200 µL of growth media with drug at the indicated concentration in duplicate, and the infected cells were incubated with drug for 2 d. The supernatant was harvested and stored at –80 °C.

4.8.6.2 Plaque Assay

LLC-MK_2 cells were lifted with trypsin-EDTA and prepared as a single cell suspension at a density of 1.2×10^5 cells/mL in growth media. The cells were then seeded in sterile 12-well plates with 2 mL/well of cell suspension. Before placing the plates into the incubator, they were gently and uniformly tapped to distribute the cells evenly across the well. After 18 h, the cells were observed by light microscope to confirm the formation of an 80 – 100% evenly confluent cell monolayer.

1.8% (w/v) agarose was prepared by adding 7.2 g of SeaPlaque Agarose (Lonza) to 400 mL of MilliQ H_2O. In order to sterilize the solution it was autoclaved.

The supernatants to be evaluated were diluted 1:10 in minimum essential media (MEM, Gibco) supplemented with 100 µg/mL streptomycin, 100 U/mL penicillin, and 10% (v/v) FCS. Three serial 10-fold dilutions were subsequently prepared in the same media. The supernatant was removed from the monolayers, and the cells were washed once with Hank's buffered salt solution (HBSS, Gibco). After removal of the wash, the cells were inoculated with 100 µL of analyte and 100 µL of the supplemented MEM used to prepare the virus dilutions. The plates were placed on a seesaw-style rocker at room temperature to incubate. After 90 min, the inoculum was

removed and 1 mL of 1:1 (v/v) first overlay (Table 4.8):1.8% agarose (preheated to 37 °C) was added to each well. The agarose was allowed to set at room temperature before being returned to the incubator.

Table 4.8: *1st Overlay for LLC-MK2*[a]

Component	Volume (mL)
HBSS A[b]	50
HBSS B[c]	50
100× MEM Vitamins (Gibco)	10
50× MEM Amino Acids (Gibco)	10
FCS	50
L-Glutamine (200 mM)	6
7.5% aq. $NaHCO_3$, pH = 8.2 (Invitrogen)	20
100× penicillin/streptomycin	10

[a] After combining the listed ingredients, 200 mL of MilliQ H_2O were added, and the pH was adjusted to 8.2 with 2 M NaOH and 2 M HCl, then MilliQ H_2O was added to a final volume of 500 mL. The solution was filter sterilized before use.
[b] See Table 4.9
[c] See Table 4.10

Table 4.9: *Hank's Buffered Salt Solution A*

Component	Mass (g)
NaCl	160.0
KCl	8.0
$MgSO_4 \cdot 7\,H_2O$	2.0
$MgCl_2 \cdot 6\,H_2O$	2.0
$CaCl_2 \cdot 2\,H_2O$	2.8

[a] MilliQ H_2O was added to a final volume of 1 L, and the solution was autoclaved to sterilize before use.

After incubating for 4 d, 1 mL of the complete second overlay mixture was added to each well and allowed to set before returning plates to the incubator. The complete mixture was prepared by pre-equilibrating second overlay (Table 4.11) and 1.8% agarose at 37 °C. Immediately before addition to the cells, second overlay and 1.8% agarose were mixed (1:1 v/v), and neutral red (Sigma, 0.75 mL of 6 g/L stock) was added to complete the overlay mixture. After a further 18 h, plaques were observed and counted from the underside of the plate by eye.

Table 4.10: *Hank's Buffered Salt Solution B*

Component	Mass (g)
Na_2HPO_4	1.2
KH_2PO_4	1.2
Glucose	20.0

[a] MilliQ H_2O was added to a final volume of 1 L, and the solution was filter sterilized before use.

Table 4.11: *2^{nd} Overlay for LLC-MK$_2$*

Component	Volume (mL)
HBSS A[b]	50
HBSS B[c]	50
100× MEM Vitamins	10
50× MEM Amino Acids	10
L-Glutamine (200 mM)	6
100× penicillin/streptomycin	10

[a] After combining the listed ingredients, 300 mL of MilliQ H_2O were added, and the pH was adjusted to 6.3 with 2 M NaOH and 2 M HCl, then MilliQ H_2O was added to a final volume of 500 mL. The solution was filter sterilized before use.
[b] See Table 4.9
[c] See Table 4.10

4.8.6.3 $TCID_{50}$ Assay

LLC-MK_2 cells were seeded in a sterile 96-well plate at a density of 2×10^4 cells/well in 100 µL of growth media and incubated for 18 h. The supernatants to be evaluated were diluted 1:10 in MEM supplemented with 100 µg/mL streptomycin, 100 U/mL penicillin, and 2.5% (v/v) FCS. 7 serial 10-fold dilutions were subsequently prepared in the same media. Supernatant was removed from the cells, and wells were inoculated in hextuplicate with 50 µL of analyte. After 2 h, the inoculum was removed and replaced with 100 µL of MEM supplemented with 100 µg/mL streptomycin, 100 U/mL penicillin, and 0.5% (v/v) FCS.

The plates were incubated for 3 d, then washed three times with PBS and fixed with 4% (v/v) paraformaldehyde in PBS at 4 °C for 1 h. After washing three times with

PBS, cells were permeabilized with PBS + 0.5% Triton X-100 (PBS-TX) for 15 min and subsequently incubated with 5 µg/mL 3H5 monoclonal antibody (prepared from hybridoma HB-46, ATCC) for 1 h. The 3H5 antibody recognizes DENV E protein. The cells were then washed three times with PBS and incubated with 4 µg/mL Alexa Fluor® 488 donkey anti-mouse antibody in PBS-TX for 1 h. The cells were washed a final three times with PBS, and Vectashield with DAPI (1:100 dilution in PBS) was added to stain cell nuclei. The plates were imaged on an inverted Nikon Eclipse TE200-U microscope no sooner than 15 min after the addition of Vectashield. Based upon Alexa Fluor® 488 staining, each well was scored as either positive ($\geq$ 5 stained cells) or negative. $TCID_{50}$ values were calculated according to the method of Reed and Muench.[212]

4.8.7 BVDV

4.8.7.1 Antiviral Assay

MDBK cells were seeded in a sterile 96-well plate at a density of 1×10^4 cells/well in 100 µL of growth media. After an 18 h incubation, the supernatant was removed, and the wells were inoculated for 2 h with 100 µL of BVDV Pe515-ncp strain at an MOI of 10. The inoculum was removed and replaced with 200 µL of growth media with the drug at the indicated concentration in duplicate, and the infected cells were incubated with drug for 2 d. The supernatant was harvested and used immediately for the $TCID_{50}$ assay.

4.8.7.2 Immunofluorescence assay

Cells were washed three times with PBS and fixed with 4% (v/v) paraformaldehyde in PBS for 1 h. After washing three times with PBS, cells were blocked with 5% chick serum (Sigma) for 2 h, washed three times with PBS, and permeabilized with PBS + 1% Triton X-100 for 20 min. After permeabilization, the cells were washed three times with PBS-T and incubated with WB103/105 monoclonal antibody to

pestivirus (Animal Health and Veterinary Laboratories Agency, 1:500 dilution in PBS-T of 1 mg/mL 50% (w/v) glycerol stock) for 1 h. WB103/105 is a 1:1 mixture of two monoclonal antibodies which recognizes the NS2/3 protein of BVDV. After the incubation, the cells were washed three times with PBS-T. Incubation with secondary antibody and DAPI proceeded as described for HCV IF (§ 4.8.5.2).

4.8.7.3 Titering of Virus Stock

MDBK cells were seeded in a sterile 96-well plate at a density of 2×10^4 cells/well in 100 µL of growth media and incubated for 18 h. Serial 10-fold dilutions of the stock to be evaluated were prepared in growth media. Supernatant was removed from the cells, and each well was inoculated with 100 µL of virus dilution, with 8 replicates of each dilution. After incubating for 24 h, the cells were fixed and stained according to the BVDV IF protocol (§ 4.8.7.2). Foci were counted in the lowest dilution with ≥10 foci/well. Titer was calculated in units of ffu/mL.

4.8.7.4 $TCID_{50}$ Assay

MDBK cells were seeded in a sterile 96-well plate at a density of 2×10^4 cells/well in 100 µL of growth media for 18 h. The supernatants to be evaluated were diluted 1:100 in growth media, and 5 serial 10-fold dilutions were subsequently prepared in the same media. Supernatant was removed from the cells, and wells were inoculated in quadruplicate with 100 µL of analyte. After 4 h, the inoculum was removed and replaced with 100 µL of growth media.

The plates were incubated for 1 d, then the plates were fixed and stained according to the BVDV immunofluorescence protocol (§ 4.8.7.2). Based upon Alexa Fluor® 488 staining, each well was scored as either positive (≥ 5 stained cells) or negative. $TCID_{50}$ values were calculated according to the method of Reed and Muench.[212]

4.9 General Synthetic Procedures

All reactions were carried out under an argon atmosphere under anhydrous conditions, unless otherwise noted. Anhydrous tetrahydrofuran (THF), *N,N*-dimethylformamide (DMF), and methylene chloride (CH_2Cl_2) were obtained as commercially available pre-dried, oxygen-free formulations and used without further purification. Yields refer to chromatographically and spectroscopically (^{1}H NMR) homogeneous materials, unless otherwise stated. Reagents were purchased at the highest commercial quality and used without further purification, unless otherwise stated. Reactions were monitored by thin-layer chromatography (TLC) carried out on 0.25 mm E. Merck silica gel plates (60F-254) using UV light as visualizing agent and an ethanolic solution of phosphomolybdic acid and cerium sulfate as a developing agent. Merck Geduran silica gel (60, particle size 0.040–0.063 mm) was used for flash column chromatography. NMR spectra were recorded on Varian Unity Inova 500 or Bruker AVII-400 instruments and calibrated using residual undeuterated solvent as an internal reference.[56] Electrospray ionization (ESI) mass spectrometry (MS) experiments were performed on an API 100 Perkin Elmer SCIEX single quadrupole mass spectrometer at 4000V emitter voltage. HRMS were recorded on a Bruker μTOF mass spectrometer using ESI.

4.10 Selected Synthesis Experimental Data

NMR spectra for compounds tested in biological assays are included in Appendix B.

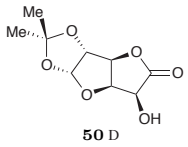

50 D

1,2-*O*-Isopropylidene-α-D-glucurono-3,6-lactone 50D: D-Glucuronolactone **49D** (62.5 g, 355 mmol, 1.0 equiv) was suspended in acetone (1.5 L) and agitated with a mechanical stirrer. Concentrated H_2SO_4 (60 mL) was added over 15 min. The reaction mixture was stirred at 25 °C for 5 h. The acid was quenched with solid $NaHCO_3$ (1950 g) and filtered. The filtrate was concentrated under reduced pressure. The residue was recrystallized from hot toluene to provide **50D** (49.9 g, 229 mmol, 65% yield) as white crystals. Spectral data were identical to those previously reported.[217]

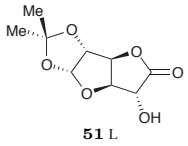

51 L

1,2-*O*-Isopropylidene-β-L-idurono-3,6-lactone 51L: Lactone **50D** (5.00 g, 23.1 mmol,1.0 equiv) was dissolved in CH_2Cl_2 (50 mL). After addition of pyridine (5.0 mL, 62.1 mmol, 2.7 equiv), the solution was cooled to –40 °C (dry ice/acetone bath). Tf_2O (5.0 mL, 29.7 mmol, 1.3 equiv) was added dropwise to the solution. The solution was stirred for 2 h, maintaining the temperature of the bath between –40 and –30 °C. The reaction mixture was diluted with CH_2Cl_2 (200 mL) and washed with aq. HCl (2 M, 3 × 100 mL). The organic layer was dried ($MgSO_4$), filtered and concentrated under reduced pressure, maintaining the temperature below 30 °C during concentration. The thus obtained residue (1.0 equiv) was dissolved in DMF (25 mL). CF_3CO_2Na (6.30 g, 46.3 mmol, 2.0 equiv) was added to the solution portionwise. The solution was stirred at room temperature for 18 h. The reaction mixture was diluted with sat. aq. $NaHCO_3$ (150 mL), and the mixture was extracted with EtOAc (3 × 100 mL). The combined organic layers were dried ($MgSO_4$), filtered and concentrated under reduced pressure. The residue was purified by flash column chromatography (silica gel, EtOAc:pet ether = 1:4 → 2:3) to provide L-iduronolactone **51L** (4.84 g, 22.4 mmol, 97% yield) as white crystals. Spectral data were identical to those previously reported.[217]

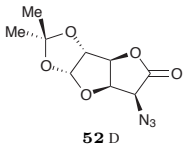

52 D

5-Azido-5-deoxy-1,2-*O*-isopropylidene-α-D-glucurono-3,6-lactone 52D: L-Iduronolactone **51L** (4.84 g, 22.4 mmol, 1.0 equiv) was dissolved in CH_2Cl_2 (125 mL). After addition of pyridine (5 mL, 62.1 mmol, 2.8 equiv), the solution was cooled to –40 °C (dry ice/acetone bath). Tf_2O (5.0 mL, 29.7 mmol, 1.3 equiv) was added dropwise to the solution. The solution was stirred for 2 h, maintaining the temperature of the bath between –40 and –30 °C. The reaction mixture was diluted with CH_2Cl_2 (100 mL) and washed with aq. HCl (2 M, 3 × 100 mL). The organic layer was dried ($MgSO_4$), filtered and concentrated under reduced pressure, maintaining the temperature below 30 °C during concentration. The obtained white solid was used directly in the next reaction. Triflate (assumed 22.4 mmol, 1.0 equiv) was dissolved in DMF (25 mL), and the solution cooled to –30 °C (dry ice/acetone bath). NaN_3 (1.85 g, 28.4 mmol, 1.3 equiv) was added to the solution portionwise. The solution was stirred for 2 h, maintaining the reaction between –40 and –30 °C at all times. The reaction mixture was diluted with brine (20 mL) and H_2O (80 mL). The mixture was extracted with EtOAc (1 × 200 mL, 2 × 100 mL). The combined organic layers were dried ($MgSO_4$), filtered and concentrated under reduced pressure. The residue was purified by flash column chromatography (silica gel, EtOAc:pet ether 1:4 → 2:3) to provide azide **52D** (4.08 g, 16.9 mmol, 76% yield) as a white crystalline solid. Spectral data were identical to those previously reported.[217]

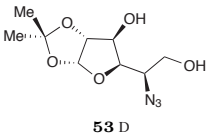

53 D

5-Azido-5-deoxy-1,2-*O*-Isopropylidene-α-D-glucofuranose 53D: Azidolactone **52D** (4.08 g, 16.9 mmol, 1.0 equiv) was dissolved in CH_2Cl_2 (30 mL), and the solution cooled to –78 °C (dry ice/acetone bath). DIBAL-H (1.5 M in toluene, 19 mL, 29 mmol, 1.7 equiv) was added to the solution dropwise. The solution was stirred for 2 h at the same temperature. The reaction was quenched with dropwise addition of EtOAc (3.0 mL) at –78 °C, then diluted with CH_2Cl_2 (250 mL) and 1.2 M aq. Rochelle salt (250 mL). The layers were stirred vigorously for 18 h and then separated. The aqueous layer was extracted with CH_2Cl_2 (6 × 75 mL). The combined organic layers

were dried ($MgSO_4$), filtered and concentrated under reduced pressure. The crude product (assumed 16.9 mmol, 1.0 equiv) was dissolved in MeOH (50 mL), and the solution cooled to –20 °C (dry ice/acetone bath). $NaBH_4$ (0.30 g, 7.9 mmol, 0.5 equiv) was added to the solution in a single portion, and the solution stirred for 1 h at the same temperature. The reaction was quenched with glacial AcOH (0.5 mL), concentrated under reduced pressure and purified by flash column chromatography (silica gel, EtOAc:pet ether 1:1 → EtOAc) to provide diol **53D** (3.62 gram, 14.9 mmol, 88% over the two steps) as a white crystalline solid. Spectral data were identical to those previously reported.[217]

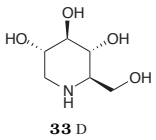

33 D

D-1-Deoxynojirimycin (D-DNJ) 33D: D-*gluco*-diol **53D** (3.62 g, 14.9 mmol, 1.0 equiv) was dissolved in H_2O (50 mL). Dowex 50WX8 (H^+ form) (6.0 g) was added, and the suspension stirred at 70 °C for 3 h. The reaction mixture was filtered, washing the resin with a further portion of H_2O (25 mL). Pd/C (10% Pd, 1.75 g, 50 weight-%) was added and the reaction stirred under H_2 balloon for 24 h. The Pd/C was removed by filtering through glass microfiber (GF/B filter). The iminosugar was purified by strong cation exchange chromatography (Dowex 50WX8, H^+ form), washing with H_2O and eluting with 1:4 conc. NH_4OH:H_2O. The combined ammoniacal fractions were concentrated to provide D-DNJ **33D** (1.72 g, 10.6 mmol, 71% yield) as an oil which crystallized upon standing. **33D**: ^{1}H NMR (400 MHz, D_2O): δ = 3.92 (AB dd, J = 11.7, 3.0 Hz, 1 H), 3.72 (AB dd, J = 11.7, 6.2 Hz, 1 H), 3.58 (ddd, J = 10.8, 9.1, 5.2 Hz, 1 H), 3.41 (t, J = 9.1 Hz, 1 H), 3.32 (dd, J = 9.9, 9.1 Hz, 1 H), 3.21 (dd, J = 12.4, 5.2 Hz, 1 H), 2.64 (ddd, J = 9.5, 6.2, 3.0 Hz, 1 H), 2.55 (dd, J = 12.4, 10.8 Hz, 1 H) ppm; HRMS (ESI): calcd for $C_6H_{13}NO_4$ [M + H^+]: 164.0923, found 164.0919.

Reductive amination: Iminosugar (1 equiv) and aldehyde (15 equiv) were dissolved in a 2:1 1,4-dioxane:H_2O mixture. Pd/C (50 weight-%) was added, and the reaction vessel purged with argon then hydrogen. The reaction was stirred under H_2 balloon overnight. The alkyl-iminosugar was purified by strong cation exchange chromatograph (Dowex 50WX8), washing with H_2O and eluting with 1:4 conc. NH_4OH:MeOH.

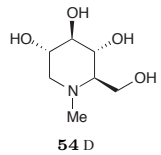

54 D

***N*M-D-DNJ 54D**: ^{1}H NMR (400 MHz, D_2O): δ = 3.90 (AB dd, J = 12.8, 2.5 Hz, 1 H), 3.82 (AB dd, J = 12.9, 2.7 Hz, 1 H), 3.55 (ddd, J = 10.8, 9.2, 5.0 Hz, 1 H), 3.38 (t, J = 9.5 Hz, 1 H), 3.27 (t, J = 9.2 Hz, 1 H), 2.96 (dd, J = 11.5, 5.0 Hz, 1 H), 2.35 (s, 3 H), 2.23 (t, J = 11.1 Hz, 1 H), 1.99 (d, J = 9.9 Hz, 1 H) ppm; HRMS (ESI): calcd for $C_7H_{15}NO_4$ [M + H^+]: 178.1079, found 178.1075.

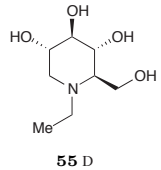

55 D

***N*E-D-DNJ 55D**: ^{1}H NMR (400 MHz, D_2O): δ = 3.90 (AB dd, J = 12.9, 2.5 Hz, 1 H), 3.83 (AB dd, J = 13.0, 2.7 Hz, 1 H), 3.54 (td, J = 10.1, 4.9 Hz, 1 H), 3.38 (t, J = 9.5 Hz, 1 H), 3.26 (t, J = 9.2 Hz, 1 H), 3.01 (dd, J = 11.3, 5.0 Hz, 1 H), 2.87 (dd, J = 13.9, 7.1 Hz, 1 H), 2.77 – 2.62 (m, 1 H), 2.36 – 2.17 (m, 2 H), 1.03 (t, J = 7.2 Hz, 3 H) ppm; HRMS (ESI): calcd for $C_8H_{17}NO_4$ [M + H^+]: 192.1236, found 192.1231.

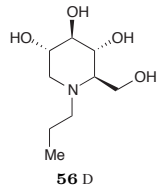

56 D

***N*R-D-DNJ 56D**: ^{1}H NMR (400 MHz, CD_3OD): δ = 3.93 – 3.78 (m, 2 H), 3.52 – 3.42 (m, 1 H), 3.38 – 3.33 (m, 1 H), 3.12 (t, J = 9.0 Hz, 1 H), 2.99 (dd, J = 11.2, 4.9 Hz, 1 H), 2.75 (ddd, J = 13.4, 10.2, 6.3 Hz, 1 H), 2.54 (ddd, J = 13.3, 9.9, 5.6 Hz, 1 H), 2.17 (t, J = 10.9 Hz, 1 H), 2.11 (dt, J = 9.6, 2.8 Hz, 1 H), 1.52 (ddd, J = 16.7, 8.8, 5.4 Hz, 2 H), 0.90 (t, J = 7.4 Hz, 3 H) ppm; HRMS (ESI): calcd for $C_9H_{19}NO_4$ [M + H^+]: 206.1387, found 206.1389.

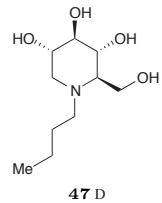

47 D

***N*B-D-DNJ 47D**: ^{1}H NMR (400 MHz, CD_3OD): δ = 3.89 – 3.80 (m, 2 H), 3.51 – 3.43 (m, 1 H), 3.38 – 3.33 (m, 1 H), 3.12 (t, J = 9.1 Hz, 1 H), 2.98 (dd, J = 11.2, 5.0 Hz, 1 H), 2.85 – 2.74 (m, 1 H), 2.63 – 2.51 (m, 1 H), 2.17 (t, J = 10.8 Hz, 1 H), 2.10 (dt, J = 9.6, 2.7 Hz, 1 H), 1.53 – 1.41 (m, 2 H), 1.37 – 1.26 (m, 2 H), 0.95 (t, J = 7.3 Hz, 3 H) ppm; HRMS (ESI): calcd for $C_{10}H_{21}NO_4$ [M + H^+]: 220.1549, found 220.1543.

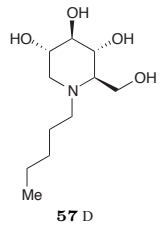

57 D

***N*P-D-DNJ 57D**: ^{1}H NMR (400 MHz, CD_3OD): δ = 3.91 – 3.79 (m, 2 H), 3.47 (ddd, J = 10.5, 9.3, 4.9 Hz, 1 H), 3.38 – 3.33 (m, 1 H), 3.12 (t, J = 9.1 Hz, 1 H), 2.98 (dd, J = 11.2, 4.9 Hz, 1 H), 2.79 (dt, J = 13.4, 8.3 Hz, 1 H), 2.63 – 2.51 (m, 1 H), 2.17 (t, J = 10.9 Hz, 1 H), 2.13 – 2.07 (m, 1 H), 1.50 (quin, J = 7.9 Hz, 2 H), 1.42 – 1.31 (m, 2 H), 1.26 (dtd, J = 15.1, 7.0, 4.0 Hz, 2 H), 0.92 (t, J = 7.2 Hz, 3 H) ppm; HRMS (ESI): calcd for $C_{11}H_{23}NO_4$ [M + H^+]: 234.1705, found 234.1699.

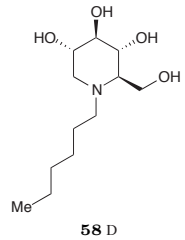

58 D

***N*X-D-DNJ 58D**: ^{1}H NMR (400 MHz, CD_3OD): δ = 3.90 – 3.80 (m, 2 H), 3.52 – 3.42 (m, 1 H), 3.38 – 3.33 (m, 1 H), 3.12 (t, J = 9.0 Hz, 1 H), 2.98 (dd, J = 11.2, 4.9 Hz, 1 H), 2.86 – 2.72 (m, 1 H), 2.58 (dt, J = 13.7, 6.9 Hz, 1 H), 2.17 (t, J = 10.8 Hz, 1 H), 2.11 (d, J = 9.5 Hz, 1 H), 1.49 (quin, J = 7.2 Hz, 2 H), 1.38 – 1.24 (m, 6 H), 0.92 (t, J = 6.6 Hz, 3 H) ppm; HRMS (ESI): calcd for $C_{12}H_{25}NO_4$ [M + H^+]: 248.1862, found 248.1856.

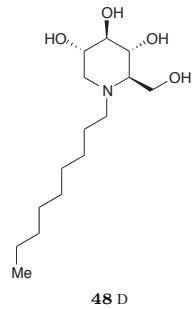

48 D

***N*N-D-DNJ 48D**: ^{1}H NMR (400 MHz, CD_3OD): δ = 3.91 – 3.80 (m, 2 H), 3.48 (ddd, J = 10.5, 9.1, 4.8 Hz, 1 H), 3.36 (t, J = 9.3 Hz, 1 H), 3.13 (t, J = 9.1 Hz, 1 H), 3.00 (dd, J = 11.2, 4.9 Hz, 1 H), 2.87 – 2.75 (m, 1 H), 2.66 – 2.54 (m, 1 H), 2.26 – 2.11 (m, 2 H), 1.50 (dq, J = 14.8, 7.5 Hz, 2 H), 1.39 – 1.21 (m, 14 H), 0.90 (t, J = 6.7 Hz, 3 H) ppm.

...denn die Ueberzeugung, dass der geometrische Bau des Moleküls selbst bei Spiegelbildformen einen so grossen Einfluss auf das Spiel der chemischen Affinitäten ansübe, konnte meiner Ansicht nach nur durch neue thatsächliche Beobachtungen gewonnen werden.

—Emil Fischer

5

Influence of Iminopyranose Stereochemistry on Enzyme and Virus Inhibition

5.1 Introduction

Recognition of the importance of substrate stereochemistry to enzyme affinity extends as far back as the 1890s, when Emil Fischer first proposed the "lock and key" model of enzymes. In fact, his model was based on observations of the enzyme class discussed here, namely the glycosidases. Fischer noted the geometric preferences of *Invertin* (later, yeast β-fructosidase) and *Emulsin* (a mixture of glycosidases extracted from almonds).[220] Although direct stereochemical analogues have made predictions of iminosugar activity straightforward initially, questions about the relationship between stereochemistry and enzyme inhibition have increased with exploration of non-6-membered ring sizes[76–79;82] and identification of noncompetitive inhibition by iminosugars.[221]

As discussed in Chapter 3, a number of iminopyranose stereochemistries have demonstrated antiviral activity. D-DMJ compounds are able to inhibit viruses by disrupting

proper glycosylation,[222] while D-DGJ compounds with sufficiently long alkylation can inhibit the BVDV and HCV p7 ion channels.[177;181;182] D-DNJ compounds can operate via both of these mechanisms. Given the varied antiviral activities of these three stereoisomers, synthesis of the other 13 iminopyranoses (Figure 5.1) was deemed a worthwhile effort in order to fully elucidate which piperidine iminosugar stereochemical arrangements correlate with antiviral properties. As the slightly different three-dimensional configurations of the isomers impart variable selectivity towards enzymes, this stereoisomeric library of iminosugars could identify as yet unknown mechanisms of virus inhibition. Because the structures are constitutionally identical, they act as ideal controls for one another, allowing comparisons to be easily made between them.

Though all 8 relative stereochemistries of DNJ have been synthetically prepared previously,[67–69;217;223–328] never have all 16 absolute stereochemistries been obtained by a unified route from a single starting material. In order to obtain the library of DNJ stereoisomers, the synthetic plan was designed to complement work by the group of Prof. G. W. J. Fleet (Department of Chemistry, University of Oxford). A series of recent papers have detailed the versatility of 3,6-glucuronolactone **50** as a chiral pool foothold from which a variety of iminsugars can be prepared.[82;217;329–331] By preparing all 16 compounds from the two enantiomers of glucuronolactone, the versatility of this inexpensive starting material was further demonstrated.

5.2 Synthesis of Iminopyranose Stereoisomers

In essence, the route to all of the stereoisomers was inspired by that described in the previous chapter for D-*gluco* DNJ. To obtain the other stereoisomers, each stereocenter of glucuronolactone **50** needed to be inverted independently. The D-*gluco* synthesis exposes each hydroxyl group sequentially, except that of C4 is involved in an intramolecular acetal throughout the entire sequence. For this reason, it was not possible to invert the center in a straightforward manner. As such, only the eight

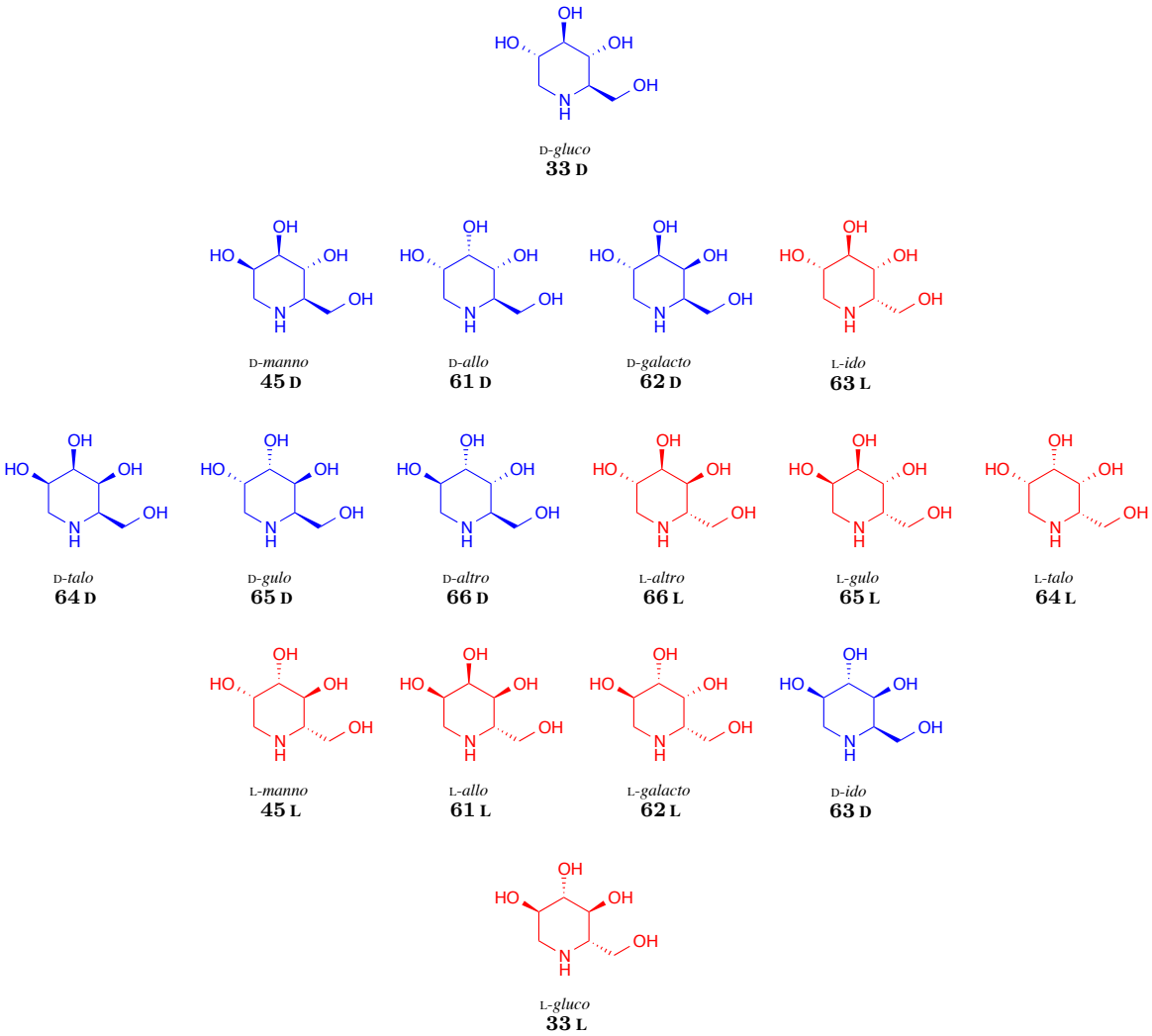

Figure 5.1: *Structures of Iminopyranose Stereoisomers.* The stereoisomers are organized vertically by stereochemical similarity to D-glucose. D-DNJ **33D** is identical in configuration to the monosaccharide. The second row is epimeric to D-glucose, the third differing by two stereocenters, the fourth row by three stereocenters, and the bottom compound is the enantiomeric L-DNJ **33D**. D-Isomers are shown in blue, while L-isomers are shown in red.

stereoisomers with *R*-configuration at C4 can be prepared from D-glucuronolactone **50D**.

To cover all of the stereochemical space available to the iminopyranose target, the enantiomeric starting material, L-glucuronolactone, was prepared on large scale at local industrial collaborator, Dextra (Reading, United Kingdom). D-Glycero-D-guloheptono-γ-lactone **67D** was protected as the benzylidene **96D** (Scheme 5.1). Although this leaves three hydroxyl groups unprotected, only two of them exist in a vic-

inal relationship susceptible to periodate cleavage ($NaIO_4$) which resulted in aldehyde **69L**. Equilibration in aqueous trifluoroacetic acid (TFA) yielded L-glucuronolactone **49L**. Protection with acetone in the presence of acid catalyst (H_2SO_4), as described for the enantiomer in Chapter 4, provided the acetonide **50L** from which the iminopyranose synthesis could begin, with a yield of 42% over the four steps from **67D**. As both enantiomers of this material were in hand, all 16 stereoisomers were theoretically accessible. For the sake of brevity, the synthesis of each stereoisomer of DNJ is shown as the scheme for its D-enantiomer; the L-forms are obtained by an identical series of reactions on the enantiomeric starting material.

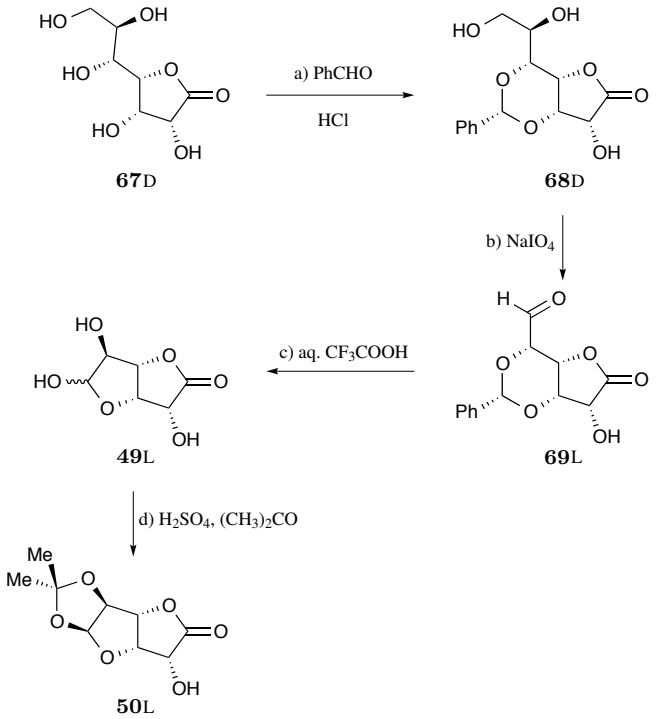

Scheme 5.1: *Synthesis of* L*-Glucuronolactone Acetonide.* Reagents and conditions: a) PhCHO (6.2 equiv), HCl, 25 °C, 2.5 h; b) $NaIO_4$ (1.4 equiv), 10:1 THF:H_2O, 40 °C, 3 h; c) 9:1 TFA:H_2O, 45 °C, 2 h; d) H_2SO_4, $(CH_3)_2CO$, 20 °C, 3.5 h, 42% yield over the four steps from **67D**.

Inversion of C5 represented the most straightforward isomer to obtain. D-*gluco* DNJ (as discussed in Chapter 4) required double inversion to introduce the nitrogen with overall retention; reaching the opposite configuration at this atom simplified the procedure, adding the azide directly to the triflate of glucuronolactone **50**, to obtain iduronolactone **70** after the single inversion (Scheme 5.2). In order to obtain the

D-*ido* isomer, L-glucuronolactone **50L** must be used as the starting material. After installation of the azide (Tf_2O, pyridine; NaN_3, 98% yield), the route matched that of D-*gluco*: sequential reduction with DIBAL-H (–78 °C) and $NaBH_4$ (–10 °C) to provide diol **71L** in 54% yield. From there, removal of the acetonide and reductive amination by hydrogenation yielded D-1-deoxyidonojirimycin (D-DIJ) **63D** (96% yield), with an overall yield of 50% from acetonide **50L**.

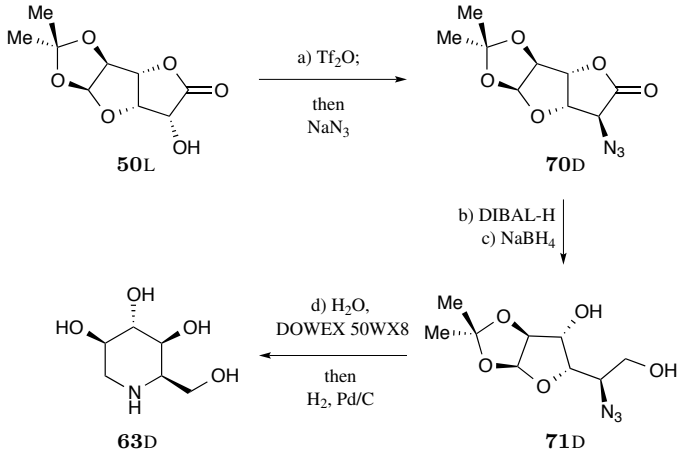

Scheme 5.2: *Synthesis of* D-*1-Deoxyidonojirimycin.* Reagents and conditions: a) Tf_2O (1.1 equiv), pyridine (3.0 equiv), CH_2Cl_2, –40 °C, 2 h; NaN_3 (1.2 equiv), DMF, –30 °C, 98%; b) DIBAL-H (3.0 equiv), CH_2Cl_2, –78 °C, 2 h; c) $NaBH_4$ (0.4 equiv), MeOH, –10 °C, 1 h, 54% over 2 steps; d) DOWEX 50WX8 (H^+ form, 150 weight-%), H_2O, 70 °C, 3 h; H_2, Pd/C (50 weight-%), 18 h, 96%.

In order to invert C3 and obtain D-1-deoxyallonojirimycin (D-DAJ) **61D**, the synthesis was diverted from the D-*gluco* route after formation of diol **53D**. From there, the primary alcohol of C6 could be selectively protected with TBSCl to provide silyl ether **72D** in 67% yield (Scheme 5.3), leaving only the C3 hydroxyl group exposed. While previous inversions took advantage of an α carbonyl to promote S_N2 reactivity, the C3 alcohol had no such activation. Instead, the center was inverted by an oxidation-reduction sequence (Dess–Martin periodinane [DMP], then $NaBH_4$), affording D-*allo* silyl ether **73D** (95% yield over the two steps). The hydride is selectively delivered from the top face of **72D**, as the bottom face of the tetrahydrofuran system is blocked by the ring of the acetonide group. The TBS ether was cleaved with TBAF to unveil diol **74D** (99% yield). The now standard acetonide deprotection-cyclization

procedure provided D-DAJ **61D** in 95% yield from the diol and 37% from acetonide **50D**.

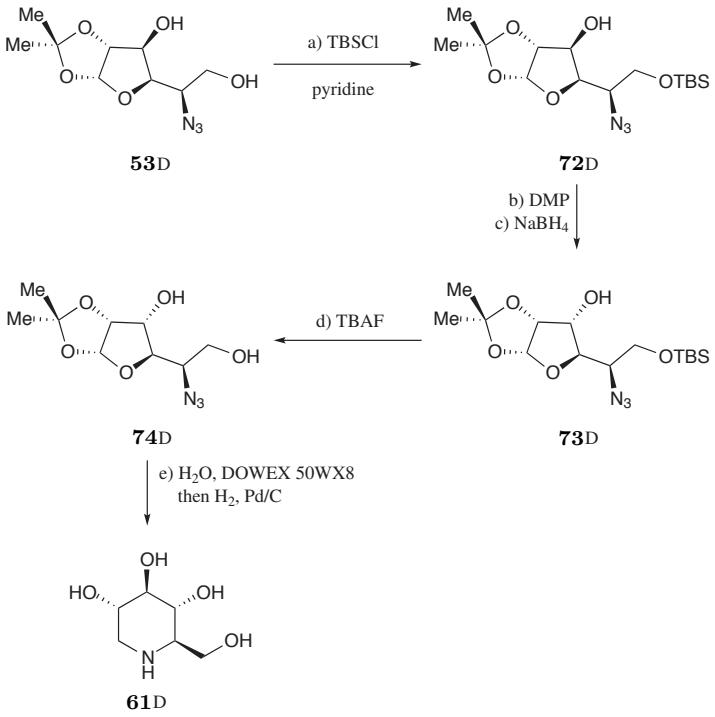

Scheme 5.3: *Synthesis of* D*-1-Deoxyallonojirimycin.* Reagents and conditions: a) TBSCl (1.7 equiv), pyridine, 25 °C, 67%; b) DMP (1.5 equiv), CH_2Cl_2, 25 °C, 18 h,; c) $NaBH_4$ (0.4 equiv), MeOH, –10 °C, 1 h, 95% over 2 steps; d) TBAF (1.3 equiv), THF, 25 °C, 2 h, 99%; e) DOWEX 50WX8 (H^+ form, 150 weight-%), H_2O, 70 °C, 3 h; H_2, Pd/C (50 weight-%), 18 h, 95%.

Although the acetonide and silyl ether could be removed deprotected simultaneously, the stepwise deprotection allows for simpler purification, as the fully deprotected compound is a mixture of anomers rather than a single compound and the anomers are far more polar than **74**.

The same reaction sequence provided D-1-deoxytalonojirimycin (D-DTJ) **64D** in 44% overall yield from D-*ido* diol **71D** (Scheme 5.4) and 23% yield from **50L**.

To isolate C2 for modification, the two free alcohols of **53D** were simultaneously protected as benzyl ethers (BnBr, NaH) to provide fully protected **78D** in 85% yield (Scheme 5.5). Because the anomeric position is already in the proper oxidation state for the reductive amination, the acetonide functional group was initially cleaved in MeOH with AcCl to provide the mixture of epimeric methyl glycosides, leaving only

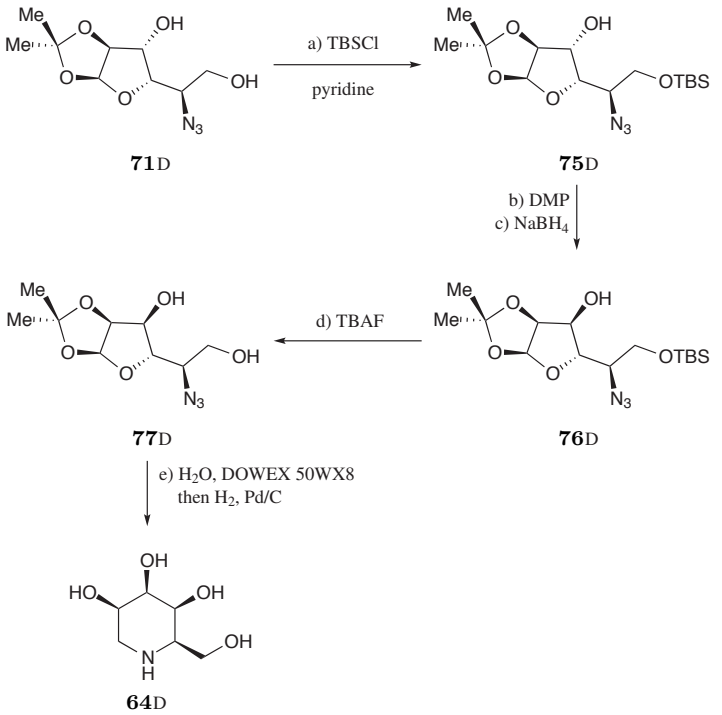

Scheme 5.4: *Synthesis of* D*-1-Deoxytalonojirimycin.* Reagents and conditions: a) TBSCl (1.7 equiv), pyridine, 25 °C, 65%; b) DMP (1.5 equiv), CH_2Cl_2, 25 °C, 18 h; c) $NaBH_4$ (0.4 equiv), MeOH, –10 °C, 1 h, 89% over 2 steps; d) TBAF (1.3 equiv), THF, 25 °C, 2 h, 92%; e) DOWEX 50WX8 (H^+ form, 150 weight-%), H_2O, 70 °C, 3 h; H_2, Pd/C (50 weight-%), 18 h, 83%.

the C2 hydroxyl group unmasked. The hydroxyl group was successfully converted to the corresponding triflate (Tf_2O, pyridine, –40 °C); however, the substrate was resistant to S_N2 substitution by CF_3CO_2Na.

As an alternative route to favor the desired inversion, acid catalyzed hydrolysis (TsOH, 80 °C) removed the acetonide, unmasking both C2 and the anomeric position. Oxidation (K_2CO_3, I_2) of the lactol to a lactone collapsed the anomeric pair to a single compound **79D** (58% yield over two steps). In addition to acting as a protecting group for the anomeric position, the carbonyl activated the C2 substituent toward S_N2 to overcome the difficulty faced in the methyl glycoside system. Converting the α-hydroxylactone to the triflate (Tf_2O, pyridine, –40 °C) allowed attack by trifluoroacetate (CF_3CO_2Na, DMF), which upon basic work up, hydrolyzed resulting in the desired D-*manno* configured **80D** (93% yield). Hydrogentation conditions (H_2, Pd/C) effected both the cyclization and removal of the benzyl protecting groups

resulting in D-DMJ **45D** (96% yield, 27% from acetonide **50D**). The order of the reactions during the final step was determined by tracking of the reaction by mass spectrometry.

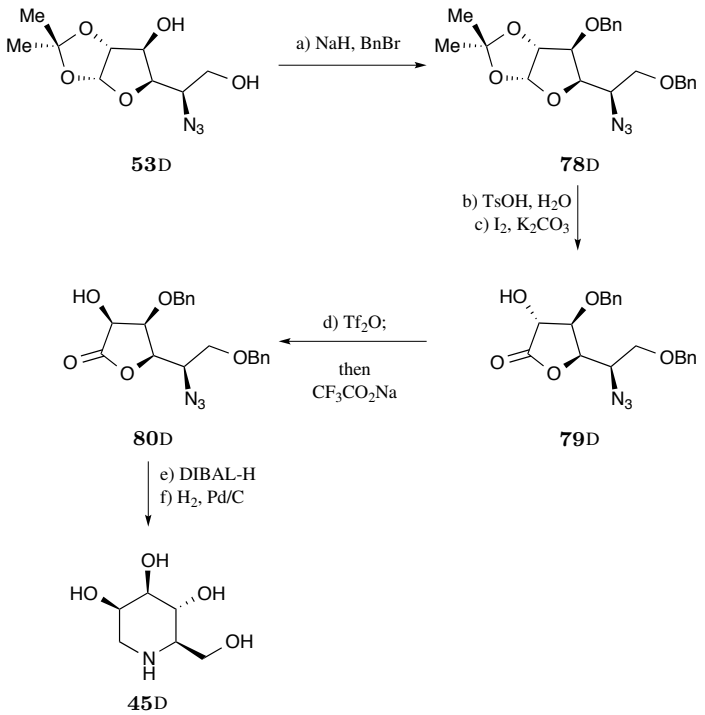

Scheme 5.5: *Synthesis of* D*-1-Deoxymannojirimycin.* Reagents and conditions: a) BnBr (3.0 equiv), NaH (2.9 equiv), DMF, –10 → 25 °C, 14 h, 85%; b) TsOH (2.2 equiv), 7:1 1,4-dioxane:H_2O, 80 °C, 3 h; c) K_2CO_3 (2.0 equiv), I_2 (2.0 equiv), *t*-BuOH, 100 °C, 3 h, 58% over 2 steps; d) Tf_2O (1.1 equiv), pyridine (3.0 equiv), CH_2Cl_2, –40 °C, 2 h; CF_3CO_2Na (2 equiv), DMF, –30 → 25 °C, 93%; e) DIBAL-H (3.0 equiv), CH_2Cl_2, –78 °C, 2 h; f) H_2, Pd/C (50 weight-%), 18 h, 96% over 2 steps.

This method of inverting C2 was employed to provide the final three relative stereochemistry, by performing the sequence on the diols with D-*ido* **71D**, D-*allo* **74D**, and D-*talo* **77D** to provide D-1-deoxygulonojirimycin (D-DUJ) **65D** (Scheme 5.6, 24% from acetonide **50L**), D-1-deoxyaltronojirimycin (D-DRJ) **66D** (Scheme 5.7, 12% from acetonide **50D**), and D-DGJ **62D** (Scheme 5.8, 14% from acetonide **50L**), respectively. It is important to note that the order of inversion is critical for the stereochemistries that require inversion of both C2 and C3. The oxidation-reduction sequence to manipulate C3 relies upon C2 to direct hydride addition in the second step. As such, C3 must be inverted first (as described here) to obtain the target compounds.

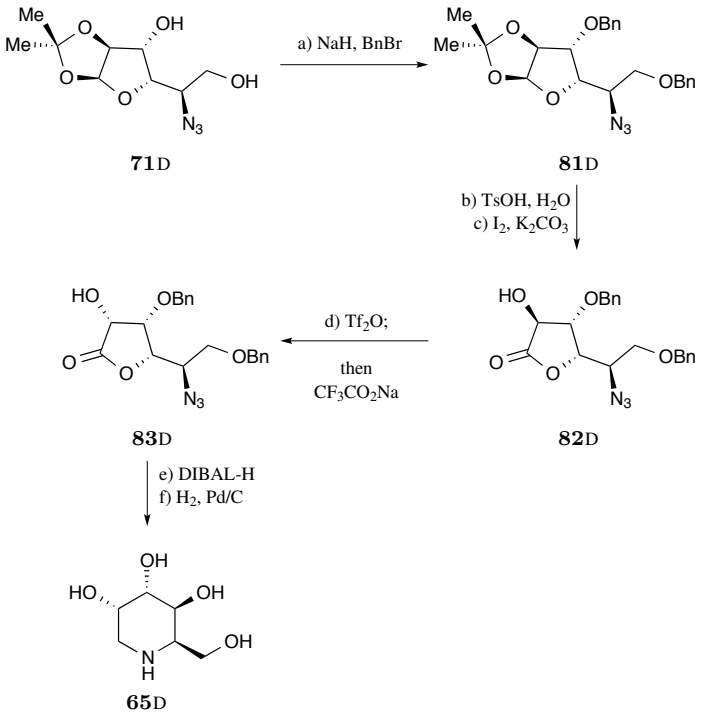

Scheme 5.6: *Synthesis of* D*-1-Deoxygulonojirimycin.* Reagents and conditions: a) BnBr (3.0 equiv), NaH (2.9 equiv), DMF, –10 → 25 °C, 14 h, 96%; b) TsOH (2.2 equiv), 7:1 1,4-dioxane:H_2O, 80 °C, 3 h; c) K_2CO_3 (2.0 equiv), I_2 (2.0 equiv), *t*-BuOH, 100 °C, 3 h, 65% over 2 steps; d) Tf_2O (1.1 equiv), pyridine (3.0 equiv), CH_2Cl_2, –40 °C, 2 h; CF_3CO_2Na (2 equiv), DMF, –30 → 25 °C, 77%; e) DIBAL-H (3.0 equiv), CH_2Cl_2, –78 °C, 2 h; f) H_2, Pd/C (50 weight-%), 18 h, 96% over two steps.

Alkylation proceeded as described for D-DNJ in Chapter 4.

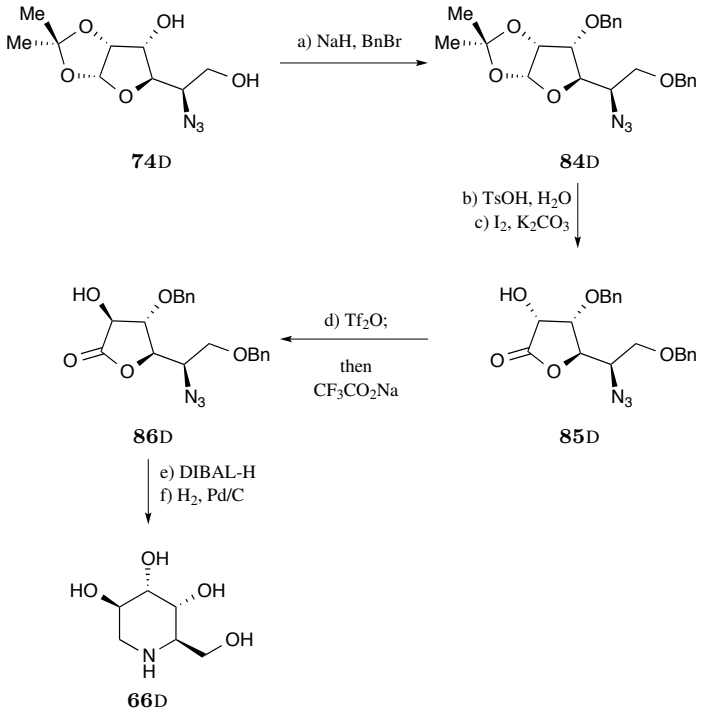

Scheme 5.7: *Synthesis of* D*-1-Deoxyaltronojirimycin.* Reagents and conditions: a) BnBr (3.0 equiv), NaH (2.9 equiv), DMF, –10 → 25 °C, 14 h, 99%; b) TsOH (2.2 equiv), 7:1 1,4-dioxane:H_2O, 80 °C, 3 h; c) K_2CO_3 (2.0 equiv), I_2 (2.0 equiv), *t*-BuOH, 100 °C, 3 h, 43% over 2 steps; d) Tf_2O (1.1 equiv), pyridine (3.0 equiv), CH_2Cl_2, –40 °C, 2 h; CF_3CO_2Na (2 equiv), DMF, –30 → 25 °C, 72%; e) DIBAL-H (3.0 equiv), CH_2Cl_2, –78 °C, 2 h; f) H_2, Pd/C (50 weight-%), 18 h, 97% over 2 steps.

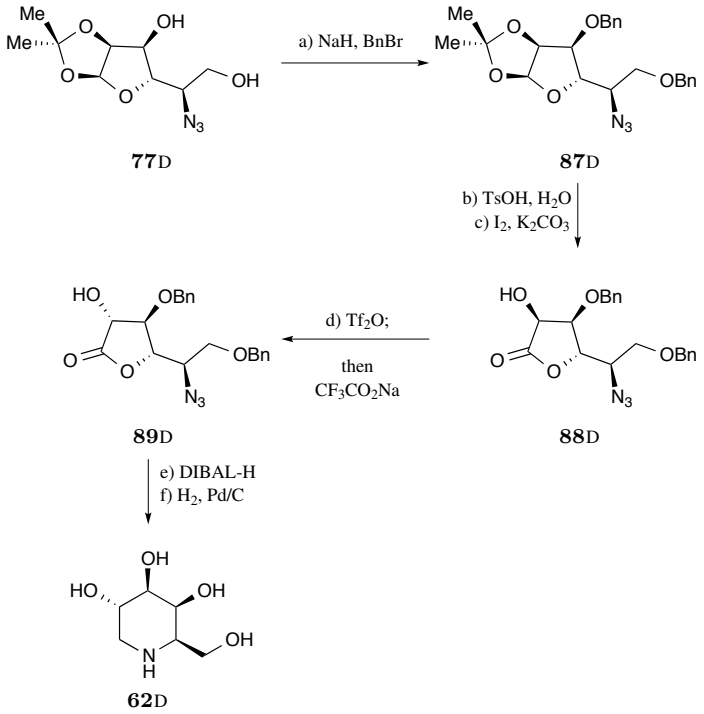

Scheme 5.8: *Synthesis of* D*-1-Deoxygalactonojirimycin.* Reagents and conditions: a) BnBr (3.0 equiv), NaH (2.9 equiv), DMF, –10 → 25 °C, 14 h, 77%; b) TsOH (2.2 equiv), 7:1 1,4-dioxane:H_2O, 80 °C, 3 h; c) K_2CO_3 (2.0 equiv), I_2 (2.0 equiv), *t*-BuOH, 100 °C, 3 h, 79%; d) Tf_2O (1.1 equiv), pyridine (3.0 equiv), CH_2Cl_2, –40 °C, 2 h; CF_3CO_2Na (2 equiv), DMF, –30 → 25 °C, 88%; e) DIBAL-H (3.0 equiv), CH_2Cl_2, –78 °C, 2 h; f) H_2, Pd/C (50 weight-%), 18 h, 93%.

5.3 Enzyme Inhibition by Iminopyranoses

Each of the compounds was screened for inhibition up to a concentration of 1 mM in the same panel of isolated enzymes described in Chapter 3 by Prof. Atsushi Kato (University of Toyama; Toyama, Japan). While several compounds remain to be evaluated, the current results already reveal a number of trends (Table 5.1, Table 5.2, and Table 5.3).

The most potent inhibitors of each enzyme were generally the iminosugars whose stereochemical arrangement matched that of the natural substrate. Indeed, the D-*gluco* series inhibited α-glucosidases with low and submicromolar IC_{50} values (0.16 – 2.1 µM), and the D-*galacto* iminosugar was measured to have an IC_{50} of 61 nM against human lysosomal α-galactosidase. In contrast, the β-glucosidases and β-galactosidases were inhibited less potently than their α counterparts providing further support to the model that deoxynojirimycins bind better to the active site of α-glycosidases due to the alignment of the iminosugar's cationic nitrogen atom with the carboxylate residue of the enzyme (Figure 3.6B). Also, of note, the D-*manno* compounds, despite stereochemical agreement with the substrate, demonstrated only weak inhibition of the jack bean α-mannosidase tested, in line with previous literature reports.[291]

Ability of other stereoisomers to inhibit each enzyme largely followed the trend that greater similarity (i.e. more identical stereocenters) correlates with more potent inhibition. However, each stereocenter's inversion did not have an equal effect. Considering the three epimers of D-*gluco*, L-*ido* (C5 epimer) demonstrated the most potent inhibition of α-glucosidases (IC_{50} from 8.4 – 55 µM), followed by D-*manno* (C2 epimer, IC_{50} from 10 – 92 µM), while D-*galacto* (C4 epimer) showed no inhibition of two α-glucosidases and poor inhibition of the other two (IC_{50} of 362 and 340 µM). These results indicate that *R*-configuration at C4 is critical for inhibition of the α-glucosidase class. This was further validated, as other stereoisomers with *S*-configuration at C4 (D-*ido* and D-*talo*) also show poor inhibition of the α-glucosidases ($IC_{50} \geq 762$ µM).

In a similar trend, the galactosidases were inhibited only by the epimers of D-*galacto*, with D-*talo* (C3 epimer) inhibiting the examined α-galactosidase preferentially, and D-*gluco* (C4 epimer) conversely inhibiting the β-galactosidases.

Unexpectedly, the glycolipid processing enzymes, human glucocerebrosidase (a β-glucosidase) and human glucosylceramide synthase (a glucosyltransferase) show greater promiscuity with respect to inhibitor stereochemistry, and a strong dependence upon *N*-alkylation, with longer alkyl chains correlating to greater potency. All of the *N*-nonyl modified iminosugars are inhibitors of both enzymes, though the enzymes have different stereochemical preferences. D-*Gluco*, L-*ido*, and both *talo* enantiomers more potently inhibit the synthase, while D-*manno* was relatively selective for the glucocerebrosidase.

Table 5.1: *IC_{50}s of* D-*DNJ,* D-*DGJ, and* D-*DMJ series against Isolated Enzymes*

	IC_{50}[a] (μM)					
	D-*gluco*		D-*galacto*		D-*manno*	
Enzyme	D-DNJ **33D**	*N*B-D-DNJ **47D**	D-DGJ **62D**	D-DMJ **45D**	*N*B-D-DMJ **94D**	*N*N-D-DMJ **95D**
α-Glucosidase						
Rat intestinal maltase	0.16	1.7	362	10	39	21
Rat intestinal isomaltase	0.79	1.6	NI	92	108	98
Rat intestinal sucrase	0.51	0.43	340	37	34	37
Human lysosome	0.37	2.1	NI	21	125	15
Rat liver ER, II	16	13	NI	521	597	19
β-Glucosidase						
Bovine liver	NI	NI	NI	NI	NI	600
Rat intestinal cellobiase	271	742	123	NI	NI	NI
Human glucocerebrosidase	402	350	NI	NI	NI	6.8
α-Galactosidase						
Human lysosome	217	NI	0.061	816	NI	NI
β-Galactosidase						
Bovine liver	NI	NI	NI	NI	NI	433
Rat intestinal lactase	41	175	94	206	NI	NI
α-Mannosidase						
Jack beans	NI	NI	NI	763	NI	NI
β-Mannosidase						
Snail	NI	NI	NI	NI	NI	NI
α-L-Rhamnosidase						
Penicillium decumbens	NI	366	NI	NI	NI	NI
α-L-Fucosidase						
Bovine kidney	NI	NI	876	599	NI	NI
β-Glucuronidase						
Bovine liver	NI	NI	NI	NI	NI	NI
α,α-Trehalase						
Porcine kidney	64	54	NI	NI	NI	190
Amyloglucosidase						
Aspergillus niger	781	876	NI	NI	NI	703
Glucosyltransferase						
HL-60 glucosylceramide synthase	NI	24	NI	NI	284	50

[a]NI : No inhibition (less than 50% inhibition at 1 mM).

Table 5.2: *IC_{50}s of* D*-DTJ and* L*-DTJ series against Isolated Enzymes*

	IC_{50}[a] (μM)					
		D-*talo*			L-*talo*	
Enzyme	D-DTJ **64D**	*N*B-D-DTJ **92D**	*N*N-D-DTJ **93D**	L-DTJ **64L**	*N*B-L-DTJ **92L**	*N*N-L-DTJ **93L**
α-Glucosidase						
Rat intestinal maltase	NI	NI	667	135	NI	229
Rat intestinal isomaltase	NI	NI	NI	620	NI	992
Rat intestinal sucrase	1000	NI	NI	326	864	160
Human lysosome	NI	NI	801	163	NI	212
Rat liver ER, II	NI	NI	NI	NI	NI	497
β-Glucosidase						
Bovine liver	NI	NI	806	NI	NI	NI
Rat intestinal cellobiase	NI	NI	NI	NI	NI	NI
Human glucocerebrosidase	NI	NI	364	NI	NI	71
α-Galactosidase						
Human lysosome	3.0	254	47	NI	NI	NI
β-Galactosidase						
Bovine liver	NI	NI	640	NI	NI	118
Rat intestinal lactase	100	NI	454	NI	NI	NI
α-Mannosidase						
Jack beans	NI	NI	NI	571	NI	NI
β-Mannosidase						
Snail	NI	NI	NI	NI	NI	NI
α-L-Rhamnosidase						
Penicillium decumbens	695	42	6.2	NI	NI	NI
α-L-Fucosidase						
Bovine kidney	NI	NI	NI	NI	NI	393
β-Glucuronidase						
Bovine liver	NI	NI	NI	493	NI	584
α,α-Trehalase						
Porcine kidney	NI	NI	NI	NI	NI	NI
Amyloglucosidase						
Aspergillus niger	NI	NI	NI	NI	NI	NI
Glucosyltransferase						
HL-60 glucosylceramide synthase	NI	255	15	NI	71	5.5

[a] NI : No inhibition (less than 50% inhibition at 1 mM).

Table 5.3: *IC_{50}s of* D*-DIJ and* L*-DIJ series against Isolated Enzymes*

	IC_{50}[a] (μM)				
	D-*ido*		L-*ido*		
Enzyme	D-DIJ **63D**	*N*B-D-DIJ **90D**	L-DIJ **63L**	*N*B-L-DIJ **90L**	*N*N-L-DIJ **91L**
α-Glucosidase					
Rat intestinal maltase	NI	NI	8.4	71	24
Rat intestinal isomaltase	762	NI	55	480	220
Rat intestinal sucrase	1000	NI	22	49	45
Human lysosome	NI	NI	12	104	21
Rat liver ER, II	NI	NI	752	NI	38
β-Glucosidase					
Bovine liver	NI	NI	NI	NI	396
Rat intestinal cellobiase	220	NI	NI	NI	883
Human glucocerebrosidase	58	NI	NI	NI	40
α-Galactosidase					
Human lysosome	NI	NI	356	NI	NI
β-Galactosidase					
Bovine liver	NI	NI	NI	NI	67
Rat intestinal lactase	37	NI	677	433	159
α-Mannosidase					
Jack beans	NI	NI	NI	NI	NI
β-Mannosidase					
Snail	NI	NI	NI	NI	NI
α-L-Rhamnosidase					
Penicillium decumbens	NI	NI	NI	NI	887
α-L-Fucosidase					
Bovine kidney	NI	NI	NI	NI	258
β-Glucuronidase					
Bovine liver	NI	NI	NI	NI	NI
α,α-Trehalase					
Porcine kidney	NI	NI	NI	NI	NI
Amyloglucosidase					
Aspergillus niger	NI	NI	NI	NI	207
Glucosyltransferase					
HL-60 glucosylceramide synthase	NI	NI	NI	4.7	0.58

[a] NI : No inhibition (less than 50% inhibition at 1 mM).

5.4 Inhibition of Infectious Virus Release

After screening for toxicity in the Huh7-Lunet-hCD81-GLuc and MDBK cell lines up to a maximum concentration of 1 mM, the maximum nontoxic dose of each compound was evaluated for antiviral effect with respect to HCV, BVDV, and DENV in cell culture. For each virus, the $TCID_{50}$ of the supernatant of treated cells was evaluated by endpoint dilution assay as described in Section 4.8. *N*-nonyl derivatives were evaluated at 100 µM, while all other compounds were tested at 1 mM (Figure 5.2).

The alkylation series of D-*gluco* produced two different inhibition patterns (Chapter 4), one for DENV and the other for HCV and BVDV. In contrast, the results of the compounds screened here show a similar pattern of hits for all three viruses, with titer values showing statistically significant differences ($p < 0.001$ for the three viruses) between treatments. *N*B-D-DNJ, *N*B-D-DMJ, *N*N-D-DMJ and *N*N-D-DTJ demonstrated a significant effect in all three viral systems, while D-DGJ produced a small but significant effect in the DENV system (Table 5.4). The reductions in viral titer for *N*N-D-DMJ (100 µM) and *N*N-D-DTJ (100 µM) were similar to that resulting from treatment with *N*B-D-DNJ (1 mM), indicating that they are comparable to but not more potent than previously examined iminosugars. *N*B-D-DMJ (1 mM) produced an effect in each viral system approximately half that caused by *N*N-D-DMJ.

As a second way of comparison, all compounds were screened at a uniform concentration of 100 µM (Figure 5.3), as this was the maximum nontoxic concentration of the *N*-nonyl iminosugars. In this situation, the difference in potency between the nonyl derived compounds from the others is even more pronounced as the only two iminosugars showing a statistically significant effect at 100 µM (Table 5.5).

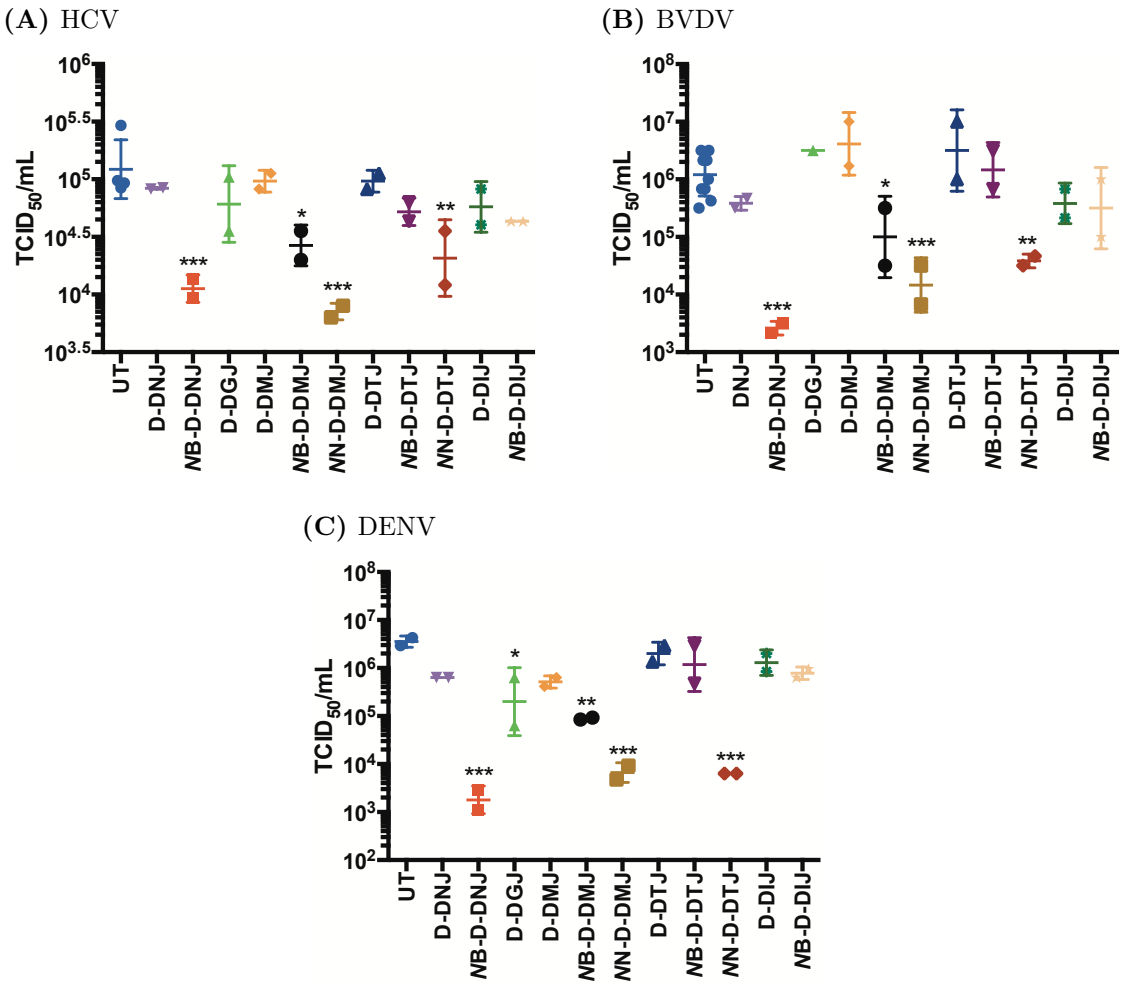

Figure 5.2: *Screen of* D*-DMJ,* D*-DTJ,* D*-DIJ, and* D*-DGJ Series.* (A) Huh7-Lunet-hCD81-GLuc cells were infected with Jc1 HCV (MOI = 0.2) and then incubated with media containing the indicated iminosugar at the highest non-toxic concentration (100 µM for *N*N-D-DMJ and *N*N-D-DTJ, 1 mM for all others) in duplicate. After 4 d, the cell supernatant was harvested, and the titer of infectious virus from each well was measured by immunofluorescence endpoint dilution assay on naive Huh7-Lunet-hCD81-GLuc cells, calculating by the method of Reed and Muench.[212] (B) MDBK cells were infected with Pe515-ncp strain BVDV (MOI = 10) and then incubated with media containing 100 µM of the indicated iminosugar at the highest non-toxic concentration (100 µM for *N*N-D-DMJ and *N*N-D-DTJ, 1 mM for all others) in duplicate. After 2 d, the cell supernatant was harvested, and the titer of infectious virus from each well was measured by immunofluorescence endpoint dilution assay on naive MDBK cells, calculating by the method of Reed and Muench.[212] (C) Huh7-Lunet-hCD81-GLuc cells were infected with 16681 DENV2 and then incubated with media containing 100 µM of the indicated iminosugar at the highest non-toxic concentration (100 µM for *N*N-D-DMJ and *N*N-D-DTJ, 1 mM for all others) in duplicate. After 2 d, the cell supernatant was harvested, and the titer of infectious virus from each well was measured by immunofluorescence endpoint dilution assay on naive LLC-MK$_2$ cells, calculating by the method of Reed and Muench.[212] In all panels, each point indicates an individual replicate value, with horizontal bars marking the mean value of each treatment and error bars representing standard deviation. The data for each virus were analysed by a one-way ANOVA using Prism 6. All three viruses showed significant effects of some treatments ($p < 0.001$ in all cases). Treatments significantly different from untreated are indicated: *:$p < 0.05$; **:$p < 0.01$; ***:$p < 0.001$.

Table 5.4: *Summary of Antiviral Effects of Screened Iminosugars at Maximum Concentration.*

Iminosugar	HCV Reduction in $\log_{10}(\text{TCID}_{50}/\text{mL})^a$	p value	BVDV Reduction in $\log_{10}(\text{TCID}_{50}/\text{mL})^a$	p value	DENV Reduction in $\log_{10}(\text{TCID}_{50}/\text{mL})^a$	p value
*N*B-D-DNJ **47D**	1.0	< 0.001	2.7	< 0.001	3.3	< 0.001
D-DGJ **62D**	NS	-	NS	-	1.3	0.011
*N*B-D-DMJ **94D**	0.7	0.013	1.1	0.033	1.6	0.002
*N*N-D-DMJ **95D**	1.2	< 0.001	1.9	< 0.001	2.7	< 0.001
*N*N-D-DTJ **93D**	0.8	0.004	1.5	0.002	2.8	< 0.001

[a]NS : Not significant; the comparison of treatment to untreated was not identified as significant ($p > 0.05$).

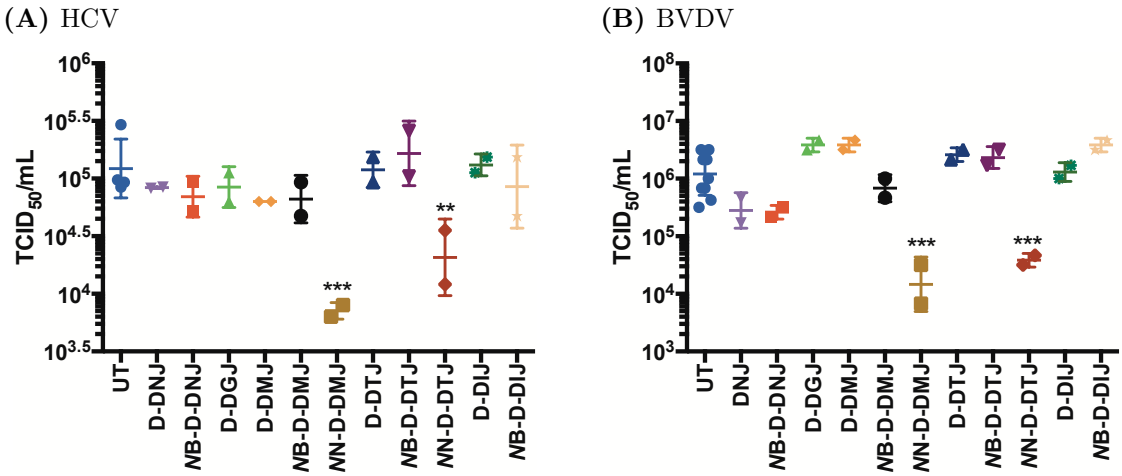

Figure 5.3: *Screen of* D*-DMJ,* D*-DTJ,* D*-DIJ, and* D*-DGJ Series at 100 µM.* (A) Huh7-Lunet-hCD81-GLuc cells were infected with Jc1 HCV (MOI = 0.2) and then incubated with media containing 100 µM of the indicated iminosugar in duplicate. After 4 d, the cell supernatant was harvested, and the titer of infectious virus from each well was measured by immunofluorescence endpoint dilution assay on naive Huh7-Lunet-hCD81-GLuc cells, calculating by the method of Reed and Muench.[212] (B) MDBK cells were infected with Pe515-ncp strain BVDV (MOI = 10) and then incubated with media containing 100 µM of the 100 µM ofindicated iminosugar in duplicate. After 2 d, the cell supernatant was harvested, and the titer of infectious virus from each well was measured by immunofluorescence endpoint dilution assay on naive MDBK cells, calculating by the method of Reed and Muench.[212] In both panels, each point indicates an individual replicate value, with horizontal bars marking the mean value for each treatment and error bars representing standard deviation. The data for each virus were analysed by a one-way ANOVA using Prism 6. All three viruses showed significant effects of some treatments ($p < 0.001$ for HCV and $p < 0.001$ for BVDV). Treatments significantly different from untreated are indicated: **:$p < 0.01$; ***:$p < 0.001$. *Data collected in collaboration with Dr. J. Miller and M. Hill.*

Table 5.5: *Summary of Antiviral Effects of Screened Iminosugars at 100 µM.*

Iminosugar	HCV Reduction in $\log_{10}(\text{TCID}_{50}/\text{mL})$	HCV p value	BVDV Reduction in $\log_{10}(\text{TCID}_{50}/\text{mL})$	BVDV p value
*N*N-D-DMJ **95D**	1.2	< 0.001	1.9	< 0.001
*N*N-D-DTJ **93D**	0.8	0.008	1.5	< 0.001

5.5 Discussion

Screening of the compounds for inhibition of isolated enzymes revealed that the majority of enzymes are inhibited most potently by mimics of the sugars they have evolved to cleave. Considering α-glucosidases, the stereochemistry of C4 as R seems to be of particular importance. In contrast, the glycosphingolipid metabolic enzymes are more sensitive with respect to iminosugar alkylation than to stereochemistry of the aza-sugar itself. This propensity to be more potently inhibited by lipophilic iminosugars could likely be explained by the fact that the native substrates themselves are lipids. Co-crystallization trials are currently under way with human β-glucocerebrosidase and the N-nonyl derivatives to bring clarity both to how the alkylation improves binding, as well as how the enzyme active site accommodates such a variety of inhibitor stereochemistries. Specifically, there is interest in whether the iminosugar conformation shifts to fill the active site or whether there are shifts in residues to compensate the various presentations of hydroxyl groups of the inhibitors.

As the D- and L-DTJ series inhibit the glycolipid enzymes without inhibition of the gastrointestinal glucosidases, these compounds are promising leads for the treatment of Gaucher's disease that might prove to have better side effect profiles if the effects observed *in vitro* are conserved *in vivo*.

With respect to antiviral ability, the two most promising leads identified up to this point are NN-D-DMJ and NN-D-DTJ, with both of these compounds demonstrating antiviral ability against all three members of *Flaviviridae* tested: HCV, BVDV, and DENV. While the long alkyl chain is in line with reports of features necessary for viroporin p7 inhibition, DENV lacks this protein or any ion channel, indicating that this could not be the sole mechanism of antiviral activity for these compounds.

NN-D-DMJ also inhibits α-glucosidases, including ER α-glucosidase II, so it is possible that its antiviral ability could be exerted *via* disruption of viral glycoprotein folding by inhibition of the ER α-glucosidases that regulate entry into the CNX/CRT cycle. However, NN-D-DTJ does not inhibit α-glucosidases at the concentrations

that it was found to be antiviral, meaning that a novel mechanism of antiviral activity has likely been identified. While this could be via the glycosphingolipid pathway inhibition, other compounds that inhibit glucosylceramide glucosyltransferase (e.g. *N*B-D-DTJ) are not antiviral, suggesting that this is not the correct explanation.

Although neither *N*N-D-DMJ nor *N*N-D-DTJ show inhibition of the mannosidases included in the isolated enzyme panel, D-DMJ and its *N*-alkyl derivatives are inhibitors of ER ManI, ER ManII, and Golgi ManI.[134] Inhibition of these enzymes involved in N-glycan processing would result in viral glycoproteins with abnormal glycans, potentially influencing the proper packaging and export of the proteins. This mechanism is consistent with the fact that NB-D-DMJ effected a decrease in infectious virus titer in all three virus culture systems. The difference between the therapeutic outcome of the *N*-nonyl and *N*-butyl compounds can be understood as analogous to the trend of DNJ compounds, with longer alkylation improving cellular uptake of the iminosugar.[198] Furthermore, *N*N-D-DTJ might operate by the same mechanism as D-DTJ is the C4 epimer of D-DMJ; differing by only one stereocenter, it is reasonable that the structure could still inhibit the ER and Golgi mannosidases. In order to investigate whether this mechanism is at work, the compounds could be tested for inhibition of the enzymes in isolated form or the FOS produced by treated cells could be examined. Alternatively, the viral glycoproteins of both treated and untreated samples could be isolated by immunoprecipitation with a glycan-independent antibody, and the glycans subsequently cleaved and analyzed by mass spectrometry.

5.6 Conclusions

Synthetic routes were developed to turn each enantiomer of glucuronolactone into 8 of the iminopyranose stereoisomers, with D-glucuronolactone providing those that have *R*-stereochemistry at C4 and L-glucuronolactone, the *S*-configuration. All of the D-iminopyranoses have been prepared, demonstrating that every relative DNJ

stereochemistry is available from glucuronolactone. Additionally, several of the L-stereoisomers have been prepared in order to characterize the ability of the compounds to inhibit viruses and isolated enzymes.

The antiviral assays identified three compounds as antiviral against all three members of *Flaviviridae* examined: *N*B-D-DMJ, and the more potently antiviral *N*N-D-DMJ and *N*N-D-DTJ. Though the known antiviral mechanisms of iminosugars (ER glucosidase inhibition and p7 inhibition) can explain the inhibition of some of these compounds against some of these viruses, neither of these mechanisms can explain the broad-spectrum inhibition of all three identified compounds, indicating that at least one previously unidentified mechanism of antiviral activity must be at work.

Future work will seek to identify exactly what this new mechanism or these new mechanisms are. Based on the enzymatic inhibition here, glycolipid metabolism might be considered. The *N*-nonyl compounds are both inhibitors of glucosylceramide metabolism; however, *N*B-D-DMJ inhibits the anabolic but not catabolic enzyme, comparable to *N*B-D-DTJ, which is not antiviral. Alternatively, the antiviral effect might be due to alteration of the N-glycan composition by inhibition of the ER and Golgi mannosidases.

Experimentally, the rest of the iminosugar library are currently being screened for enzyme inhibition and antiviral ability, and promising compounds, including those identified in this chapter, will be evaluated for dose-response relationships over a wider concentration range, rather than simply at a single concentration.

Looking further forward, a major limitation in providing antiviral doses of iminosugars has been that they cause gastrointestinal distress as described in Chapter 3. As *N*N-D-DTJ does not inhibit these off-target enzymes, it could be a promising point from which to pursue the next generation of antiviral iminosugars.

5.7 Selected Synthesis Experimental Data

Alkylation of iminosugars was carried out by the reductive amination procedure described in Section 4.9. NMR spectra for compounds tested in biological assays are included in Appendix B.

5.7.1 Synthesis of 1,2-*O*-Isopropylidene-α-L-glucurono-3,6-lactone

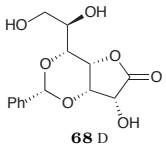

68 D

3,5-*O*-Benzylidene-D-glycero-D-guloheptono-1,4-lactone 68D: D-Glycero-D-guloheptono-γ-lactone **67D** (255 g, 1.20 mol, 1.0 equiv) was suspended in benzaldehyde (750 mL, 7.42 mol, 6.2 equiv) with a mechanical stirrer at 25 °C. HCl (32%, 75 mL) was added in a single portion. The resulting mixture was stirred at that temperature for 2.5 h. Pet ether (2 L) was added at a rate of 15 mL/min with vigorous stirring. After completion of the addition, the mixture was stirred for a further 30 min. The suspension was filtered to provide a white solid. The solid was returned to the reaction flask, and, after blanketing with Ar, suspended in Et_2O (875 mL). The suspension was stirred vigorously for 30 min, then filtered. The filter cake was washed with a further portion of Et_2O (625 mL) and then dried in a vacuum oven overnight to provide crude **68D** as a white solid which was used in the next step without further purification. **68D**: $R_f = 0.43$ (EtOAc:industrial methylated spirits (IMS):H_2O = 45:5:1).

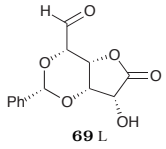

69 L

2,4-*O*-Benzylidene-L-glucurono-3,6-lactone 69L: Diol **68D** (163.03 g, 550 mmol, 1.0 equiv) was dissolved in 10:1 THF:H_2O (1.243 L) in a 2-L reaction vessel. While stirring vigorously with a mechanical stirrer, the mixture was heated to an internal temperature of 40 °C. After stabilizing at this temperature, $NaIO_4$ (151.81 g, 710 mmol, 1.3 equiv) was added portion-wise over 40 min. During the addition, the temperature of the heating jacket was lowered to 35 °C, and the temperature of the reaction mixture

was maintained between 39 and 45 °C. After the final addition, the jacket temperature was returned to 40 °C, and the mixture was stirred at the same temperature for 1 h. TLC indicated that the reaction was not complete, so a further single portion of $NaIO_4$ (16.16 g, 76 mmol, 0.14 equiv) was added. The mixture was stirred for 1 h at the same temperature, then cooled to 20 °C. The reactor was drained and rinsed out with 10:1 THF:H_2O (440 mL). The initially drained reaction mixture was filtered. The filter cake was washed first with the rinse of the reaction vessel, and then by 10:1 THF:H_2O (110 mL). The filtrate was concentrated under reduced pressure to provide crude **69L** as a white solid which was used in the next step without further purification. **69L**: $R_f = 0.68$ (EtOAc:IMS:H_2O = 45:5:1).

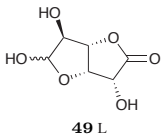

49 L

L-glucurono-3,6-lactone 49L: Aldehyde **69L** (assumed 1.2 mol) was suspended in 9:1 TFA:H_2O (750 mL). The reaction mixture was connected to a rotary evaporator and rotated at atmospheric pressure in a 45 °C water bath. After 15 min, the suspended solid had dissolved completely. 2 h after rotating had commenced, the solution was concentrated under reduced pressure at the same temperature. Toluene (2 × 500 mL) was added to azeotropically remove the TFA under reduced pressure. H_2O (1.5 L) and EtOAc (400 mL) were added, and the layers were separated. The organic layer was extracted with H_2O (150 mL). The combined aqueous layers were washed with EtOAc (300 mL) and concentrated under reduced pressure. Toluene (3 × 500 mL) was added to the crude product to azeotropically remove H_2O. **49L** was obtained as a pale orange solid which was used in the next step without further purification. **49L**: $R_f = 0.47$ (EtOAc:IMS:H_2O = 45:5:1).

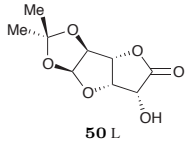

50 L

1,2-*O*-Isopropylidene-α-L-glucurono-3,6-lactone 50L: Acetone (1.9 L) and H_2SO_4 (conc., 63 mL) were combined, and the mixture added to L-glucuronolactone **49L** (assumed 1.2 mol). The mixture was connected to a rotary evaporator and rotated at atmospheric pressure in a 30 °C water bath. After 30 min, the starting material had dissolved completely. The water bath temperature was reduced to 20 °C, and the mixture was

rotated for 3.5 h at the same temperature. The mixture was quenched with solid $NaHCO_3$ (1951.66 g) and stirred at 25 °C for 12 h. The mixture was filtered, and the filter cake washed with acetone (2 L). To remove finer particulate matter, the filtrate was filtered through a GF/A filter, and the subsequent filter cake washed with acetone (50 mL). The filtrate was concentrated under reduced pressure. Toluene (2 × 500 mL) was added to the crude product to azeotropically remove H_2O. The residue was purified by medium pressure chromatography (silica gel, heptane → heptane:acetone = 3:1) and dried under reduced pressure. The obtained white solid was recrystallized from toluene to provide **50L** (108 g, 500 mmol, 42% yield over the four steps) as white needles. **50L**: $R_f = 0.27$ (acetone:pet ether = 3:7); spectral data were identical to those previously reported.[332]

5.7.2 Synthesis of D-1-Deoxyidonojirimycin

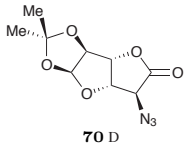

70 D

5-Azido-5-deoxy-1,2-*O*-isopropylidene-β-D-idurono-3,6-lactone 70D: L-Glucuronolactone **50L** (5.35 g, 25.0 mmol, 1.0 equiv) was dissolved in CH_2Cl_2 (55 mL). After addition of pyridine (5.4 mL, 67 mmol, 2.7 equiv), the solution was cooled to –40 °C (dry ice/acetone bath). Tf_2O (5.4 mL, 32 mmol, 1.3 equiv) was added dropwise to the solution. The solution was stirred for 2 h, maintaining the temperature of the bath between –40 and –30 °C. The reaction mixture was diluted with CH_2Cl_2 (100 mL) and washed with aq. HCl (2 M, 3 × 100 mL). The organic layer was dried ($MgSO_4$), filtered and concentrated under reduced pressure, maintaining the temperature below 30 °C during concentration. The obtained white solid was used directly in the next reaction. Triflate (assumed 25 mmol, 1.0 equiv) was dissolved in DMF (25 mL), and the solution cooled to –30 °C (dry ice/acetone bath). NaN_3 (2.00 g, 30.8 mmol, 1.2 equiv) was added to the solution portionwise. The solution was stirred for 2 h, maintaining the reaction between –40 and –30 °C at all times. The reaction mixture was diluted with brine (20 mL) and H_2O (80 mL). The mixture was extracted with EtOAc (1 × 200 mL, 2 × 100 mL). The combined organic layers were dried

($MgSO_4$), filtered and concentrated under reduced pressure. The residue was purified by flash column chromatography (silica gel, EtOAc:pet ether 1:4 → 2:3) to provide azide **70D** (5.90 g, 24.5 mmol, 98% yield) as a white crystalline solid. Spectral data were identical to those previously reported.[330]

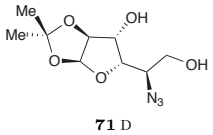

71 D

5-Azido-5-deoxy-1,2-*O*-Isopropylidene-β-D-idofuranose 71D: Azidolactone **70D** (7.18 g, 29.8 mmol, 1.0 equiv) was dissolved in CH_2Cl_2 (150 mL), and the solution cooled to –78 °C (dry ice/acetone bath). DIBAL-H (1.5 M in toluene, 22 mL, 33 mmol, 1.1 equiv) was added to the solution dropwise. The solution was stirred for 2 h at the same temperature. The reaction was quenched with dropwise addition of EtOAc (3.3 mL) at –78 °C. The reaction was then diluted with CH_2Cl_2 (200 mL) and 1.2 M aq. Rochelle salt (200 mL). The layers were stirred vigorously for 18 h. The layers were then separated and the aqueous layer extracted with CH_2Cl_2 (6 × 100 mL). The combined organic layers were dried ($MgSO_4$), filtered and concentrated under reduced pressure. The crude product (5.79 g, assumed 23.8 mmol, 1.0 equiv) was dissolved in MeOH (70 mL), and the solution cooled to –20 °C (dry ice/acetone bath). $NaBH_4$ (0.36 g, 10 mmol, 0.3 equiv) was added to the solution in a single portion, and the solution stirred for 1 h at the same temperature. The reaction was quenched with glacial AcOH (0.4 mL), concentrated under reduced pressure and purified by flash column chromatography (silica gel, EtOAc:pet ether 1:1 → EtOAc) to provide diol **71D** (3.98 gram, 16.2 mmol, 54% over the two steps) as a white crystalline solid. Spectral data were identical to those previously reported.[330]

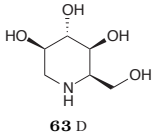

63 D

D-1-Deoxyidonojirimycin (D-DIJ) 63D: D-*ido*-diol **71D** (900 mg, 3.67 mmol, 1.0 equiv) was dissolved in H_2O (10 mL). Dowex 50WX8 (H^+ form) (1.3 g) was added, and the suspension stirred at 70 °C for 3 h. The reaction mixture was filtered, washing the resin with a further portion of H_2O (5 mL). Pd/C (10% Pd, 450 mg, 50 weight-%) was added and the reaction stirred under H_2 balloon for 24 h. The Pd/C was removed by filtering through glass microfiber (GF/B filter). The iminosugar was purified by strong cation

exchange chromatography (Dowex 50WX8, H^+ form), washing with H_2O and eluting with 1:4 conc. NH_4OH:H_2O. The combined ammoniacal fractions were concentrated to provide D-DIJ **63D** (575.4 mg, 3.53 mmol, 96% yield) as a brown oil. **63D**: ^{1}H NMR (500 MHz, D_2O): δ = 3.89 – 3.78 (m, 3 H), 3.74 – 3.67 (m, 2 H), 3.28 (dt, J = 8.1, 5.4 Hz, 2 H), 3.08 (dd, J = 12.9, 3.3 Hz, 1 H), 2.93 – 2.81 (m, 1 H) ppm; HRMS (ESI): calcd for $C_6H_{13}NO_4$ [M + H^+]: 164.0923, found 164.0918.

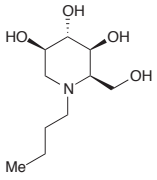

90 D

***N*B-D-DIJ 90D**: ^{1}H NMR (500 MHz, D_2O): δ = 4.04 – 3.89 (m, 2 H), 3.85 (dd, J = 9.7, 5.5 Hz, 1 H), 3.71 (ddd, J = 10.6, 8.7, 5.3 Hz, 1 H), 3.54 (t, J = 9.3 Hz, 1 H), 3.24 (q, J = 5.1 Hz, 1 H), 2.98 (dd, J = 12.6, 5.4 Hz, 1 H) 2.82 (td, J = 11.7, 11.1, 5.7 Hz, 1 H), 2.73 (td, J = 12.7, 11.9, 5.6 Hz, 1 H), 2.64 (t, J = 11.5 Hz, 1 H), 1.58 (dddd, J = 16.9, 13.5, 11.1, 6.7 Hz, 2 H), 1.40 (heptet, J = 7.4 Hz, 2 H), 0.99 (t, J = 7.4 Hz, 3 H) ppm; HRMS (ESI): calcd for $C_6H_{13}NO_4$ [M + H^+]: 220.1543, found 220.1542.

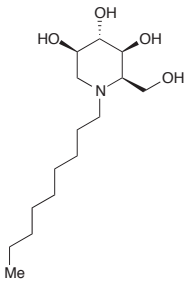

91 D

***N*N-D-DIJ 91D**: ^{1}H NMR (500 MHz, CD_3OD): δ = 3.82 (qd, J = 11.5, 5.6 Hz, , 2 H), 3.69 (dd, J = 8.9, 5.2 Hz, 1 H), 3.57 – 3.48 (m, 1 H), 3.38 (t, J = 8.5 Hz, 1 H), 3.02 (q, J = 5.5 Hz, 1 H), 2.82 – 2.69 (m, 2 H), 2.68 – 2.52 (m, 2 H), 1.51 (dd, J = 13.7, 7.3 Hz, 2 H), 1.41 – 1.21 (m, 14 H), 0.90 (t, J = 6.8 Hz, 3 H) ppm; HRMS (ESI): calcd for $C_{15}H_{31}NO_4$ [M + H^+]: 290.2326, found 290.2323.

5.7.3 Synthesis of D-1-Deoxyallonojirimycin

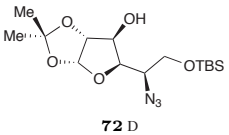

72 D

5-Azido-6-*O*-*tert*-butyldimethylsilyl-5-deoxy-1,2-*O*-isopropylidene-α-D-glucofuranose 72D: D-*Gluco* diol **53D** (3.72 g, 15.2 mmol, 1.0 equiv) was dissolved in pyridine (45 mL). While stirring, TBSCl (3.89 g, 25.8 mmol, 1.7 equiv) was added in a single portion. The reaction mixture was stirred for 18 h. The mixture was diluted with EtOAc (125 mL) and washed with 2 M aq. HCl (3 × 75 mL).The organic layer was

dried ($MgSO_4$), filtered and concentrated under reduced pressure. The residue was purified by flash column chromatography (silica gel, EtOAc:pet ether = 1:19 → 1:3) to give TBS ether **72D** (3.68 g, 10.2 mmol, 67% yield) as a colorless oil. Spectral data were identical to those previously reported.[82]

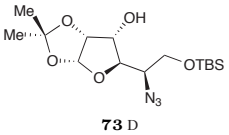

73 D

5-Azido-6-*O*-*tert*-butyldimethylsilyl-5-deoxy-1,2-*O*-isopropylidene-α-D-allofuranose 73D: Alcohol **72D** (3.68 g, 10.2 mmol, 1.0 equiv) was dissolved in CH_2Cl_2 (40 mL), and the solution cooled to 0 °C. Dess–Martin periodinane (6.49 g, 15.3 mmol, 1.5 equiv) was added in a single portion. The mixture was allowed to come to 25 °C and stirred for 18 h. The reaction was diluted with EtOAc (200 mL) and quenched with 1:1 sat. aq. $Na_2S_2O_3$: sat. aq. $NaHCO_3$ (150 mL). The layers were separated, and the organic layer further washed with 1:1 sat. aq. $Na_2S_2O_3$: sat. aq. $NaHCO_3$ (2 × 100 mL). The organic layer was dried ($MgSO_4$), filtered, and concentrated under reduced pressure. The residue was purified by flash column chromatography (silica gel, EtOAc:pet ether = 1:9 → 3:7) to provide the cyclic ketone as a colorless oil. The product (1.0 equiv) was dissolved in EtOH (40 mL), and the solution cooled to –20 °C (dry ice/acetone bath). $NaBH_4$ (0.42 g, 11.1 mmol, 1.1 equiv) was added to the solution in a single portion, and the solution stirred for 1 h at the same temperature. The reaction was quenched with glacial AcOH (0.4 mL) and concentrated under reduced pressure. The residue was dissolved in EtOAc (100 mL) and sat. aq. $NaHCO_3$ (100 mL). The layers were separated. The organic layer was washed with sat. aq. $NaHCO_3$ (100 mL) and brine (100 mL), dried ($MgSO_4$), filtered and concentrated under reduced pressure. The residue was purified by flash column chromatography (silica gel, EtOAc:pet ether = 1:19 → 1:4) to give D-*allo* silyl ether **73D** (3.47 g, 9.65 mmol, 95% yield) as a colorless oil. Spectral data were identical to those previously reported.[82]

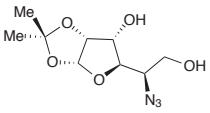

74 D

5-Azido-5-deoxy-1,2-*O*-isopropylidene-α-D-allofuranose 74D: Silyl ether **73D** (100 mg, 280 µmol, 1.0 equiv) was dissolved in THF (3 mL) and the solution cooled to 0 °C (ice/H_2O bath). TBAF (1 M in THF, 0.6 mL, 600 µmol, 2.1 equiv) was added dropwise, and the mixture was allowed to come to room temperature over 1 h. The mixture was concentrated under reduced pressure and purified by flash column chromatography (silica gel, EtOAc:pet ether = 1:1 → EtOAc) to provide D-*allo* diol **74D** (68 mg, 278 µmol, 99% yield) as a white crystalline solid. Spectral data were identical to those previously reported.[82]

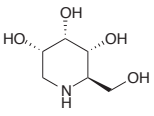

61 D

D-1-Deoxyallonojirimycin (D-DAJ) 61D: D-*allo*-diol **74D** (750 mg, 3.06 mmol, 1.0 equiv) was dissolved in H_2O (10 mL). Dowex 50WX8 (H^+ form) (1.1 g) was added, and the suspension stirred at 70 °C for 3 h. The reaction mixture was filtered, washing the resin with a further portion of H_2O (5 mL). Pd/C (10% Pd, 375 mg, 50 weight-%) was added and the reaction stirred under H_2 balloon for 24 h. The Pd/C was removed by filtering through glass microfiber (GF/B filter). The iminosugar was purified by strong cation exchange chromatography (Dowex 50WX8, H^+ form), washing with H_2O and eluting with 1:4 conc. NH_4OH:H_2O. The combined ammoniacal fractions were concentrated to provide D-DAJ **61D** (473 mg, 2.902 mmol, 95% yield) as a brown oil. **61D**: ^{1}H NMR (500 MHz, D_2O): δ = 4.18 (t, J = 2.7 Hz, 1 H), 3.89 (dd, J = 11.7, 3.1 Hz, 1 H), 3.80 (ddd, J = 11.2, 5.2, 2.8 Hz, 1 H), 3.74 (dd, J = 11.8, 5.8 Hz, 1 H), 3.58 (dd, J = 10.4, 2.9 Hz, 1 H), 2.96 (dd, J = 12.2, 5.1 Hz, 1 H), 2.87 (ddd, J = 10.3, 5.7, 3.0 Hz, 1 H), 2.80 (dd, J = 12.2, 11.2 Hz, 1 H) ppm; HRMS (ESI): calcd for $C_6H_{13}NO_4$ [M + H^+]: 164.0923, found 164.0916.

5.7.4 Synthesis of D-1-Deoxytalonojirimycin

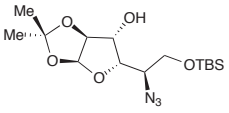

75 D

5-Azido-6-*O*-*tert*-butyldimethylsilyl-5-deoxy-1,2-*O*-isopropylidene-β-D-idofuranose 75D: D-*Ido* diol **71D** (1.26 g, 5.14 mmol, 1.0 equiv) was dissolved in pyridine (16 mL). While stirring, TBSCl (1.31 g, 8.69 mmol, 1.7 equiv) was added in a single portion. The reaction mixture was stirred for 18 h. The mixture was diluted with EtOAc (50 mL) and washed with 2 M aq. HCl (3 × 50 mL).The organic layer was dried ($MgSO_4$), filtered and concentrated under reduced pressure. The residue was purified by flash column chromatography (silica gel, EtOAc:pet ether = 1:19 → 1:3) to give TBS ether **75D** (1.20 g, 3.34 mmol, 65% yield) as a colorless oil. Spectral data were identical to those previously reported.[330]

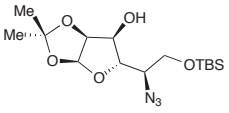

76 D

5-Azido-6-*O*-*tert*-butyldimethylsilyl-5-deoxy-1,2-*O*-isopropylidene-β-D-talofuranose 76D: Alcohol **75D** (1.20 g, 3.34 mmol, 1.0 equiv) was dissolved in CH_2Cl_2 (15 mL), and the solution cooled to 0 °C. Dess–Martin periodinane (2.13 g, 5.02 mmol, 1.5 equiv) was added in a single portion. The mixture was allowed to come to 25 °C and stirred for 18 h. The reaction was diluted with EtOAc (100 mL) and quenched with 1:1 sat. aq. $Na_2S_2O_3$: sat. aq. $NaHCO_3$ (100 mL). The layers were separated, and the organic layer further washed with 1:1 sat. aq. $Na_2S_2O_3$: sat. aq. $NaHCO_3$ (2 × 50 mL). The organic layer was dried ($MgSO_4$), filtered, and concentrated under reduced pressure. The residue was purified by flash column chromatography (silica gel, EtOAc:pet ether = 1:9 → 3:7) to provide the cyclic ketone as a colorless oil. The product (1.0 equiv) was dissolved in EtOH (15 mL), and the solution cooled to –20 °C (dry ice/acetone bath). $NaBH_4$ (127 mg, 3.36 mmol, 1.0 equiv) was added to the solution in a single portion, and the solution stirred for 1 h at the same temperature. The reaction was quenched with glacial AcOH (0.2 mL) and concentrated under reduced pressure. The residue was dissolved in EtOAc (100 mL) and sat. aq. $NaHCO_3$ (100 mL). The layers were separated. The organic layer was washed with sat. aq. $NaHCO_3$ (100 mL) and brine (100 mL), dried ($MgSO_4$), filtered and

concentrated under reduced pressure. The residue was purified by flash column chromatography (silica gel, EtOAc:pet ether = 1:19 → 1:4) to give D-*talo* silyl ether **76D** (1.07 g, 2.98 mmol, 89% yield) as a colorless oil. Spectral data were identical to those previously reported.[330]

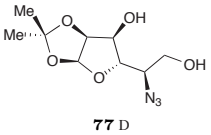

77 D

5-Azido-5-deoxy-1,2-*O*-isopropylidene-β-D-talofuranose 77D: Silyl ether **76D** (1.07 g, 2.98 mmol, 1.0 equiv) was dissolved in THF (15 mL) and the solution cooled to 0 °C (ice/H_2O bath). TBAF (1 M in THF, 3.7 mL, 3.7 mmol, 1.2 equiv) was added dropwise, and the mixture was allowed to come to room temperature over 1 h. The mixture was concentrated under reduced pressure and purified by flash column chromatography (silica gel, EtOAc:pet ether = 1:1 → EtOAc) to provide D-*talo* diol **77D** (670 mg, 2.73 mmol, 92% yield) as a white crystalline solid. Spectral data were identical to those previously reported.[330]

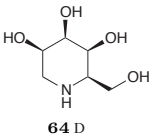

64 D

D-1-Deoxytalonojirimycin (D-DTJ) 64D: D-*talo*-diol **77D** (1.50 g, 6.12 mmol, 1.0 equiv) was dissolved in H_2O (20 mL). Dowex 50WX8 (H^+ form) (2.50 g) was added, and the suspension stirred at 70 °C for 3 h. The reaction mixture was filtered, washing the resin with a further portion of H_2O (20 mL). Pd/C (10% Pd, 750 mg, 50 weight-%) was added and the reaction stirred under H_2 balloon for 24 h. The Pd/C was removed by filtering through glass microfiber (GF/B filter). The iminosugar was purified by strong cation exchange chromatography (Dowex 50WX8, H^+ form), washing with H_2O and eluting with 1:4 conc. NH_4OH:H_2O. The combined ammoniacal fractions were concentrated to provide D-DTJ **64D** (826.6 mg, 5.07 mmol, 83% yield) as a colorless oil. **64D**: $[\alpha]_D^{25}$ = –22.5 (H_2O, c = 1.00); ^{1}H NMR (500 MHz, D_2O): δ = 4.34 – 4.30 (m, 1 H), 4.25 – 4.22 (m, 1 H), 3.96 (d, J = 6.9 Hz, 2 H), 3.92 (t, J = 3.4 Hz, 1 H), 3.61 (dd, J = 13.8, 2.9 Hz, 1 H), 3.48 (td, J = 6.9, 1.7 Hz, 1 H), 3.34 (dd, J = 13.8, 2.0 Hz, 1 H) ppm; HRMS (ESI): calcd for $C_6H_{13}NO_4$ [M + H^+]: 164.0923, found 164.0918.

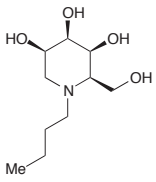

92 D

***N*B-D-DTJ 92D**: ^{1}H NMR (500 MHz, CD_3OD): δ = 3.94 – 3.89 (m, 1 H), 3.84 (dd, J = 5.1, 2.7 Hz, 2 H), 3.80 (d, J = 6.7 Hz, 1 H), 3.56 (t, J = 3.1 Hz, 1 H), 2.95 (dd, J = 12.2, 5.7 Hz, 1 H), 2.71 (dt, J = 13.4, 7.9 Hz, 1 H), 2.61 (dt, J = 13.6, 7.4 Hz, 1 H), 2.56 – 2.42 (m, 2 H), 1.49 (quin, J = 7.8 Hz, 2 H), 1.40 – 1.27 (m, 2 H), 0.94 (t, J = 7.4 Hz, 1 H) ppm; HRMS (ESI): calcd for $C_6H_{13}NO_4$ [M + H^+]: 220.1549, found 220.1543.

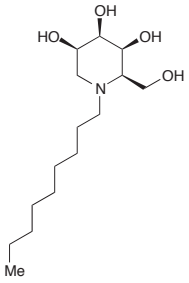

93 D

***N*N-D-DTJ 93D**: ^{1}H NMR (500 MHz, CD_3OD): δ = 3.92 (t, J = 3.2 Hz, 1 H), 3.88 – 3.77 (m, 3 H), 3.57 (t, J = 3.2 Hz, 1 H), 2.96 (dd, J = 12.3, 5.7 Hz, 1 H), 2.72 (dt, J = 15.7, 7.3 Hz, 1 H), 2.66 – 2.58 (m, 1 H), 2.55 – 2.41 (m, 2 H), 1.56 – 1.45 (m, 2 H), 1.37 – 1.22 (m, 14 H), 0.90 (t, J = 6.7 Hz, 3 H) ppm; HRMS (ESI): calcd for $C_6H_{13}NO_4$ [M + H^+]: 290.2331, found 290.2324.

5.7.5 Synthesis of D-1-Deoxymannojirimycin

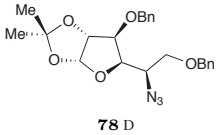

78 D

5-Azido-3,6-di-*O*-benzyl-5-deoxy-1,2-*O*-isopropylidene-α-D-glucofuranose 78D: D-*Gluco* diol **53D** (1.25 g, 5.10 mmol, 1.0 equiv) was dissolved in DMF (15 mL). BnBr (1.83 mL, 15.4 mmol, 3.0 equiv) was added, and the solution was cooled to –10 °C. NaH (360 mg, 15.0 mmol, 2.9 equiv) was added portionwise. The reaction was allowed to warm to 25 °C and stirred at the same temperature for 14 h. The reaction was quenched with MeOH (0.3 mL), diluted with EtOAc (150 mL) and washed with 1:1 brine:H_2O (5 × 100 mL). The organic layer was dried ($MgSO_4$), filtered and concentrated under reduced pressure. The residue was purified by flash column chromatography (silica gel, EtOAc:pet ether = 1:9 → 1:4) to provide dibenzyl ether **78D** (1.84 g, 4.32 mmol, 85% yield) as a colorless oil. Spectral data were identical to those previously reported.[217]

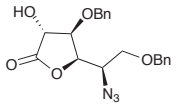

79 D

5-Azido-3,6-di-*O*-benzyl-5-deoxy-D-glucono-1,4-lactone 79D: Dibenzylacetonide **78D** (1.84 g, 4.32 mmol, 1.0 equiv) was dissolved in 7:1 1,4-dioxane:H_2O (12 mL) and the solution heated to 80 °C. TsOH (1.82 g, 9.57 mmol, 2.2 equiv) was added, and further H_2O (3.5 mL) was added at a steady rate over 30 min. The reaction mixture was stirred at the same temperature for 3 h, then allowed to cool to 25 °C. The mixture was quenched with sat. aq. $NaHCO_3$ (100 mL) and extracted with EtOAc (3 × 100 mL). The combined organic layers were dried ($MgSO_4$), filtered, and concentrated under reduced pressure. The residue (1.0 equiv) was dissolved in *t*-BuOH (25 mL), and the solution heated to 100 °C. K_2CO_3 (1.69 g, 12.2 mmol, 2.8 equiv) and I_2 (3.10 g, 12.2 mmol, 2.8 equiv) were added sequentially. The reaction mixture was stirred at the same temperature for 3 h, and then cooled to 25 °C. The mixture was diluted with EtOAc (150 mL) and sat. aq. $Na_2S_2O_3$ (100 mL) and stirred vigorously until the brown iodine color was no longer observed. The layers were separated, and the aqueous layer was extracted with EtOAc (3 × 100 mL). The combined organic layers were dried ($MgSO_4$), filtered, and concentrated under reduced pressure. The residue was purified by flash column chromatography (silica gel, EtOAc:pet ether = 1:19 → 1:3) to provide D-*gluco* lactone **79D** (960 mg, 2.5 mmol, 58% yield) as a colorless oil. Spectral data were identical to those previously reported.[217]

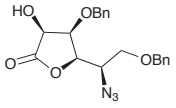

80 D

5-Azido-3,6-di-*O*-benzyl-5-deoxy-D-mannono-1,4-lactone 80D: Lactone **79D** (960 mg, 2.5 mmol,1.0 equiv) was dissolved in CH_2Cl_2 (11 mL). After addition of pyridine (650 µL, 8.1 mmol, 3.2 equiv), the solution was cooled to –40 °C (dry ice/acetone bath). Tf_2O (600 µL, 3.6 mmol, 1.4 equiv) was added dropwise to the solution. The solution was stirred for 2 h, maintaining the temperature of the bath between –40 and –30 °C. The reaction mixture was diluted with CH_2Cl_2 (50 mL) and washed with aq. HCl (2 M, 3 × 25 mL). The organic layer was dried ($MgSO_4$), filtered and concentrated under reduced pressure, maintaining the temperature below 30 °C during concentration. The thus obtained residue (1.0 equiv) was dissolved in DMF (5 mL). CF_3CO_2Na

(680 mg, 5.0 mmol, 2.0 equiv) was added to the solution portionwise. The solution was stirred at room temperature for 18 h. The reaction mixture was diluted with sat. aq. $NaHCO_3$ (50 mL), and the mixture was extracted with EtOAc (3 × 50 mL). The combined organic layers were dried ($MgSO_4$), filtered and concentrated under reduced pressure. The residue was purified by flash column chromatography (silica gel, EtOAc:pet ether = 1:19 → 1:3) to provide D-*manno* lactone **80D** (890 mg, 2.3 mmol, 93% yield) as a colorless oil. Spectral data were identical to those previously reported.[82]

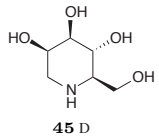

45 D

D-1-Deoxymannojirimycin (D-DMJ) 45D: Hydroxylactone **80D** (1.00 g, 2.6 mmol, 1.0 equiv) was dissolved in CH_2Cl_2 (10 mL), and the solution cooled to –78 °C (dry ice/acetone bath). DIBAL-H (1.5 M in toluene, 5.0 mL, 7.5 mmol, 2.9 equiv) was added to the solution dropwise. The solution was stirred for 2 h at the same temperature. The reaction was quenched with dropwise addition of EtOAc (5.0 mL) at –78 °C. The reaction was then diluted with CH_2Cl_2 (100 mL) and 1.2 M aq. Rochelle salt (100 mL). The layers were stirred vigorously for 18 h. The layers were then separated and the aqueous layer extracted with CH_2Cl_2 (6 × 50 mL). The combined organic layers were dried ($MgSO_4$), filtered and concentrated under reduced pressure. The crude product was dissolved in dioxane (50 mL). Pd/C (10% Pd, 500 mg, 50 weight-%) was added and the reaction stirred under H_2 balloon for 24 h. Glacial AcOH (0.5 mL, 1% final concentration) was added to the mixture, and the reaction was stirred under H_2 balloon for a further 24 h. The Pd/C was removed by filtering through glass microfiber (GF/B filter). The iminosugar was purified by strong cation exchange chromatography (Dowex 50WX8, H^+ form), washing with H_2O and eluting with 1:4 conc. NH_4OH:H_2O. The combined ammoniacal fractions were concentrated to provide D-DMJ **45D** (410.2 mg, 2.5 mmol, 96% yield) as a colorless oil. **45D**: ^{1}H NMR (500 MHz, D_2O): δ = 4.11 (td, J = 3.0, 1.5 Hz, 1 H), 3.93 – 3.83 (m, 2 H), 3.72 (t, J = 9.7 Hz, 1 H), 3.67 (dd, J = 9.6, 3.1 Hz, 1 H), 3.14 (dd, J = 14.3, 2.8 Hz, 1 H), 2.90 (dd, J = 14.4, 1.6 Hz, 1 H), 2.64 (ddd, J = 9.8, 4.6, 3.5 Hz, 1 H) ppm; HRMS (ESI): calcd for $C_6H_{13}NO_4$ [M + H^+]:

164.0923, found 164.0918.

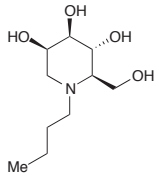

94 D

***N*B-D-DMJ 94D**: ^{1}H NMR (500 MHz, CD_3OD): δ = 3.93 – 3.80 (m, 3 H), 3.67 (t, J = 9.2 Hz, 1 H), 2.99 (dd, J = 12.3, 3.4 Hz, 1 H), 2.82 – 2.73 (m, 1 H), 2.65 – 2.56 (m, 1 H), 2.50 (d, J = 12.3 Hz, 1 H), 2.14 (d, J = 6.0 Hz, 1 H), 1.47 (quin, J = 8.0 Hz, 2 H), 1.32 (dt, J = 13.6, 6.7 Hz, 2 H), 0.94 (t, J = 7.5 Hz, 3 H) ppm; HRMS (ESI): calcd for $C_6H_{13}NO_4$ [M + H^+]: 220.1549, found 220.1544.

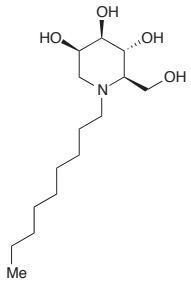

95 D

***N*N-D-DMJ 95D**: ^{1}H NMR (500 MHz, CD_3OD): δ = 3.94 – 3.79 (m, 3 H), 3.67 (t, J = 9.0 Hz, 1 H), 3.61 (q, J = 7.1 Hz, 2 H) 3.06 – 2.96 (m, 1 H), 2.83 – 2.71 (m, 1 H), 2.66 – 2.56 (m, 1 H), 2.51 (d, J = 12.2 Hz, 1 H), 2.20 – 2.09 (m, 1 H), 1.48 (quin, J = 7.7 Hz, 2 H), 1.37 – 1.23 (m, 14 H), 0.90 (t, J = 6.9 Hz, 3 H) ppm; HRMS (ESI): calcd for $C_6H_{13}NO_4$ [M + H^+]: 290.2331, found 290.2325.

5.7.6 Synthesis of D-1-Deoxygulonojirimycin

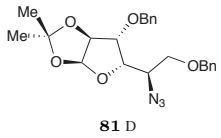

81 D

5-Azido-3,6-di-*O*-benzyl-5-deoxy-1,2-*O*-isopropylidene-β-D-idofuranose 81D: D-*Ido* diol **71D** (3.50 g, 14.3 mmol, 1.0 equiv) was dissolved in DMF (50 mL). BnBr (5.2 mL, 43.7 mmol, 3.0 equiv) was added, and the solution was cooled to –10 °C. NaH (1.00 g, 25 mmol, 1.8 equiv) was added portionwise. The reaction was allowed to warm to 25 °C and stirred at the same temperature for 14 h. The reaction was quenched with MeOH (1.0 mL), diluted with EtOAc (200 mL) and washed with 1:1 brine:H_2O (2 × 100 mL). The organic layer was dried ($MgSO_4$), filtered and concentrated under reduced pressure. The residue was purified by flash column chromatography (silica gel, EtOAc:pet ether = 1:9 → 1:4) to provide dibenzyl ether **81D** (5.85 g, 13.7 mmol, 96% yield) as a colorless oil. Spectral data were identical to those previously reported.[82]

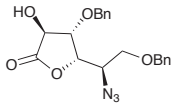

82 D

5-Azido-3,6-di-*O*-benzyl-5-deoxy-D-idono-1,4-lactone 82D: Dibenzylacetonide **81D** (5.85 g, 13.8 mmol, 1.0 equiv) was dissolved in 7:1 1,4-dioxane:H_2O (40 mL) and the solution heated to 80 °C. TsOH (5.75 g, 30.3 mmol, 2.2 equiv) was added, and further H_2O (12.5 mL) was added at a steady rate over 30 min. The reaction mixture was stirred at the same temperature for 3 h, then allowed to cool to 25 °C. The mixture was quenched with sat. aq. $NaHCO_3$ (200 mL) and extracted with EtOAc (3 × 200 mL). The combined organic layers were dried ($MgSO_4$), filtered, and concentrated under reduced pressure. The residue (1.0 equiv) was dissolved in *t*-BuOH (60 mL), and the solution heated to 100 °C. K_2CO_3 (3.66 g, 26.5 mmol, 2.0 equiv) and I_2 (6.72 g, 26.5 mmol, 2.0 equiv) were added sequentially. The reaction mixture was stirred at the same temperature for 3 h, and then cooled to 25 °C. The mixture was diluted with EtOAc (150 mL) and sat. aq. $Na_2S_2O_3$ (100 mL) and stirred vigorously until the brown iodine color was no longer observed. The layers were separated, and the aqueous layer was extracted with EtOAc (3 × 100 mL). The combined organic layers were dried ($MgSO_4$), filtered, and concentrated under reduced pressure. The residue was purified by flash column chromatography (silica gel, EtOAc:pet ether = 1:19 → 1:3) to provide D-*ido* lactone **82D** (3.45 g, 9.0 mmol, 65% yield) as a colorless oil. Spectral data were identical to those previously reported.[82]

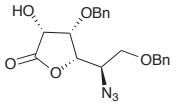

83 D

5-Azido-3,6-di-*O*-benzyl-5-deoxy-D-gulono-1,4-lactone 83D: Lactone **82D** (3.45 g, 9.0 mmol,1.0 equiv) was dissolved in CH_2Cl_2 (35 mL). After addition of pyridine (2.2 mL, 27 mmol, 3 equiv), the solution was cooled to –40 °C (dry ice/acetone bath). Tf_2O (2.0 mL, 12 mmol, 1.3 equiv) was added dropwise to the solution. The solution was stirred for 2 h, maintaining the temperature of the bath between –40 and –30 °C. The reaction mixture was diluted with CH_2Cl_2 (200 mL) and washed with aq. HCl (2 M, 3 × 100 mL). The organic layer was dried ($MgSO_4$), filtered and concentrated under reduced pressure, maintaining the temperature below 30 °C during concentration. The thus obtained residue (1.0 equiv) was dissolved in DMF (15 mL). CF_3CO_2Na

(2.45 g, 18.0 mmol, 2.0 equiv) was added to the solution portionwise. The solution was stirred at room temperature for 18 h. The reaction mixture was diluted with sat. aq. $NaHCO_3$ (150 mL), and the mixture was extracted with EtOAc (3 × 100 mL). The combined organic layers were dried ($MgSO_4$), filtered and concentrated under reduced pressure. The residue was purified by flash column chromatography (silica gel, EtOAc:pet ether = 1:19 → 1:3) to provide D-*gulo* lactone **83D** (2.66 g, 6.94 mmol, 77% yield) as a colorless oil. Spectral data were identical to those previously reported.[82]

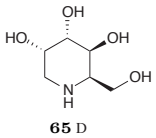

65 D

D-1-Deoxygulonojirimycin (D-DUJ) 65D: Hydroxylactone **83D** (1.88 g, 4.9 mmol, 1.0 equiv) was dissolved in CH_2Cl_2 (20 mL), and the solution cooled to –78 °C (dry ice/acetone bath). DIBAL-H (1.5 M in toluene, 5 mL, 7.5 mmol, 1.5 equiv) was added to the solution dropwise. The solution was stirred for 2 h at the same temperature. The reaction was quenched with dropwise addition of EtOAc (5.0 mL) at –78 °C. The reaction was then diluted with CH_2Cl_2 (100 mL) and 1.2 M aq. Rochelle salt (100 mL). The layers were stirred vigorously for 18 h. The layers were then separated and the aqueous layer extracted with CH_2Cl_2 (6 × 50 mL). The combined organic layers were dried ($MgSO_4$), filtered and concentrated under reduced pressure. The crude product was dissolved in dioxane (50 mL). Pd/C (10% Pd, 940 mg, 50 weight-%) was added and the reaction stirred under H_2 balloon for 24 h. Glacial AcOH (0.5 mL, 1% final concentration) was added to the mixture, and the reaction was stirred under H_2 balloon for a further 24 h. The Pd/C was removed by filtering through glass microfiber (GF/B filter). The iminosugar was purified by strong cation exchange chromatography (Dowex 50WX8, H^+ form), washing with H_2O and eluting with 1:4 conc. NH_4OH:H_2O. The combined ammoniacal fractions were concentrated to provide D-DUJ **65D** (763.1 mg, 4.7 mmol, 96% yield) as a colorless oil. **65D**: ^{1}H NMR (400 MHz, D_2O): δ = 4.00 (ddd, J = 11.4, 5.1, 2.7 Hz, 1 H), 3.93 – 3.86 (m, 2 H), 3.73 – 3.56 (m, 2 H), 3.16 (dd, J = 8.0, 5.7 Hz, 1 H), 3.00 (dd, J = 12.2, 4.8 Hz, 1 H), 2.83 (t, J = 11.7 Hz, 1 H) ppm; HRMS (ESI): calcd for $C_6H_{13}NO_4$ [M + H^+]:

164.0923, found 164.0918.

5.7.7 Synthesis of D-Deoxyaltronojirimycin

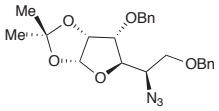

84 D

5-Azido-3,6-di-*O*-benzyl-5-deoxy-1,2-*O*-isopropylidene-α-D-allofuranose 84D: D-*Allo* diol **74D** (3.51 g, 14.3 mmol, 1.0 equiv) was dissolved in DMF (40 mL). BnBr (5.10 mL, 42.9 mmol, 3.0 equiv) was added, and the solution was cooled to –10 °C. NaH (1.66 g, 41.5 mmol, 2.9 equiv) was added portionwise. The reaction was allowed to warm to 25 °C and stirred at the same temperature for 14 h. The reaction was quenched with MeOH (1.0 mL), diluted with EtOAc (100 mL) and washed with 1:1 brine:H_2O (2 × 100 mL). The organic layer was dried ($MgSO_4$), filtered and concentrated under reduced pressure. The residue was purified by flash column chromatography (silica gel, EtOAc:pet ether = 1:9 → 1:4) to provide dibenzyl ether **84** (6.03 g, 14.2 mmol, 99% yield) as a colorless oil. Spectral data were identical to those previously reported.[82]

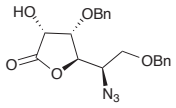

85 D

5-Azido-3,6-di-*O*-benzyl-5-deoxy-D-allono-1,4-lactone 85D: Dibenzylacetonide **84D** (6.03 g, 14.2 mmol, 1.0 equiv) was dissolved in 7:1 1,4-dioxane:H_2O (40 mL) and the solution heated to 80 °C. TsOH (5.94 g, 31.2 mmol, 2.2 equiv) was added, and further H_2O (12.5 mL) was added at a steady rate over 30 min. The reaction mixture was stirred at the same temperature for 3 h, then allowed to cool to 25 °C. The mixture was quenched with sat. aq. $NaHCO_3$ (200 mL) and extracted with EtOAc (3 × 200 mL). The combined organic layers were dried ($MgSO_4$), filtered, and concentrated under reduced pressure. The residue (1.0 equiv) was dissolved in *t*-BuOH (75 mL), and the solution heated to 100 °C. K_2CO_3 (3.93 g, 28.4 mmol, 2.0 equiv) and I_2 (7.21 g, 28.4 mmol, 2.0 equiv) were added sequentially. The reaction mixture was stirred at the same temperature for 3 h, and then cooled to 25 °C. The mixture was diluted with EtOAc (150 mL) and sat. aq. $Na_2S_2O_3$ (100 mL) and stirred vigorously until the brown iodine color

was no longer observed. The layers were separated, and the aqueous layer was extracted with EtOAc (3 × 100 mL). The combined organic layers were dried ($MgSO_4$), filtered, and concentrated under reduced pressure. The residue was purified by flash column chromatography (silica gel, EtOAc:pet ether = 1:19 → 1:3) to provide D-*allo* lactone **85D** (2.33 g, 6.08 mmol, 43% yield) as a colorless oil. Spectral data were identical to those previously reported.[82]

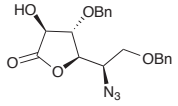

86 D

5-Azido-3,6-di-*O*-benzyl-5-deoxy-D-altrono-1,4-lactone 86D: Lactone **85D** (3.83 g, 10.0 mmol,1.0 equiv) was dissolved in CH_2Cl_2 (45 mL). After addition of pyridine (2.4 mL, 30 mmol, 3 equiv), the solution was cooled to –40 °C (dry ice/acetone bath). Tf_2O (2.2 mL, 13 mmol, 1.3 equiv) was added dropwise to the solution. The solution was stirred for 2 h, maintaining the temperature of the bath between –40 and –30 °C. The reaction mixture was diluted with CH_2Cl_2 (200 mL) and washed with aq. HCl (2 M, 3 × 100 mL). The organic layer was dried ($MgSO_4$), filtered and concentrated under reduced pressure, maintaining the temperature below 30 °C during concentration. The thus obtained residue (1.0 equiv) was dissolved in DMF (25 mL). CF_3CO_2Na (2.72 g, 20.0 mmol, 2.0 equiv) was added to the solution portionwise. The solution was stirred at room temperature for 3 h. The reaction mixture was diluted with sat. aq. $NaHCO_3$ (150 mL), and the mixture was extracted with EtOAc (3 × 100 mL). The combined organic layers were dried ($MgSO_4$), filtered and concentrated under reduced pressure. The residue was purified by flash column chromatography (silica gel, EtOAc:pet ether = 1:19 → 1:3) to provide D-*altro* lactone **86D** (2.77 g, 7.22 mmol, 72% yield) as a colorless oil. Spectral data were identical to those previously reported.[82]

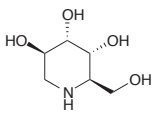

66 D

D-1-Deoxyaltronojirimycin (D-DRJ) 66D: Hydroxylactone **86D** (1.03 g, 2.69 mmol, 1.0 equiv) was dissolved in CH_2Cl_2 (50 mL), and the solution cooled to –78 °C (dry ice/acetone bath). DIBAL-H (1.5 M in toluene, 9.0 mL, 13.4 mmol, 5.0 equiv) was added to the solution dropwise. The solution was stirred for 2 h at the same temperature. The reaction was quenched with dropwise addition of EtOAc (5.0 mL) at –78 °C. The reaction was

then diluted with CH_2Cl_2 (200 mL) and 1.2 M aq. Rochelle salt (200 mL). The layers were stirred vigorously for 18 h. The layers were then separated and the aqueous layer extracted with CH_2Cl_2 (6 × 50 mL). The combined organic layers were dried ($MgSO_4$), filtered and concentrated under reduced pressure. The crude product was dissolved in dioxane (50 mL). Pd/C (10% Pd, 450 mg, 50 weight-%) was added and the reaction stirred under H_2 balloon for 10 h. Aq. HCl (2 M, 40 mL) and $Pd(OH)_2$ (10% $Pd(OH)_2$, 450 mg, 50 weight-%) were added to the mixture, and the reaction was stirred under H_2 balloon for a further 24 h. The catalysts were removed by filtering through glass microfiber (GF/B filter). The iminosugar was purified by strong cation exchange chromatography (Dowex 50WX8, H^+ form), washing with H_2O and eluting with 1:4 conc. NH_4OH:H_2O. The combined ammoniacal fractions were concentrated to provide D-DRJ **66D** (416.4 mg, 2.6 mmol, 97% yield) as a colorless oil. **66D**: ^{1}H NMR (500 MHz, D_2O): δ = 4.01 – 3.98 (m, 1 H), 3.98 – 3.94 (m, 1 H), 3.89 (dd, J = 9.5, 2.7 Hz, 1 H), 3.84 – 3.79 (m, 2 H), 3.08 – 3.01 (dm, J = 14.0 Hz, 1 H), 2.96 – 2.90 (m, 1 H), 2.89 – 2.82 (dm, J = 14.0 Hz, 1 H) ppm; HRMS (ESI): calcd for $C_6H_{13}NO_4$ [M + H^+]: 164.0923, found 164.0926.

5.7.8 Synthesis of D-Deoxygalactonojirimycin

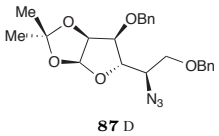

87 D

5-Azido-3,6-di-*O*-benzyl-5-deoxy-1,2-*O*-isopropylidene-β-D-talofuranose 87D: D-*Talo* diol **77D** (2.00 g, 8.16 mmol, 1.0 equiv) was dissolved in DMF (8.5 mL). BnBr (2.94 mL, 24.8 mmol, 3.0 equiv) was added, and the solution was cooled to –10 °C. NaH (980 mg, 25 mmol, 3.0 equiv) was added portionwise. The reaction was allowed to warm to 25 °C and stirred at the same temperature for 14 h. The reaction was quenched with MeOH (1.0 mL), diluted with EtOAc (100 mL) and washed with 1:1 brine:H_2O (2 × 100 mL). The organic layer was dried ($MgSO_4$), filtered and concentrated under reduced pressure. The residue was purified by flash column chromatography (silica gel, EtOAc:pet ether = 1:9 → 1:4) to provide dibenzyl ether **87**

(2.67 g, 6.28 mmol, 77% yield) as a colorless oil. Spectral data were identical to those previously reported.[82]

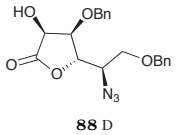

88 D

5-Azido-3,6-di-*O*-benzyl-5-deoxy-D-talono-1,4-lactone 88D: Dibenzylacetonide **87D** (2.67 g, 6.28 mmol, 1.0 equiv) was dissolved in 7:1 1,4-dioxane:H_2O (20 mL) and the solution heated to 80 °C. TsOH (2.70 g, 14.2 mmol, 2.3 equiv) was added, and further H_2O (6.25 mL) was added at a steady rate over 30 min. The reaction mixture was stirred at the same temperature for 3 h, then allowed to cool to 25 °C. The mixture was quenched with sat. aq. $NaHCO_3$ (100 mL) and extracted with EtOAc (3 × 100 mL). The combined organic layers were dried ($MgSO_4$), filtered, and concentrated under reduced pressure. The residue (1.0 equiv) was dissolved in *t*-BuOH (30 mL), and the solution heated to 100 °C. K_2CO_3 (1.83 g, 13.3 mmol, 2.0 equiv) and I_2 (3.36 g, 13.3 mmol, 2.0 equiv) were added sequentially. The reaction mixture was stirred at the same temperature for 3 h, and then cooled to 25 °C. The mixture was diluted with EtOAc (100 mL) and sat. aq. $Na_2S_2O_3$ (50 mL) and stirred vigorously until the brown iodine color was no longer observed. The layers were separated, and the aqueous layer was extracted with EtOAc (3 × 100 mL). The combined organic layers were dried ($MgSO_4$), filtered, and concentrated under reduced pressure. The residue was purified by flash column chromatography (silica gel, EtOAc:pet ether = 1:19 → 1:3) to provide D-*talo* lactone **88D** (1.89 g, 4.93 mmol, 79% yield) as a colorless oil. Spectral data were identical to those previously reported.[82]

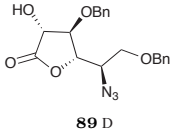

89 D

5-Azido-3,6-di-*O*-benzyl-5-deoxy-D-galactono-1,4-lactone 89D: Lactone **88D** (1.70 g, 4.4 mmol,1.0 equiv) was dissolved in CH_2Cl_2 (20 mL). After addition of pyridine (1.1 mL, 13 mmol, 3 equiv), the solution was cooled to –40 °C (dry ice/acetone bath). Tf_2O (950 µL, 6.0 mmol, 1.4 equiv) was added dropwise to the solution. The solution was stirred for 2 h, maintaining the temperature of the bath between –40 and –30 °C. The reaction mixture was diluted with CH_2Cl_2 (100 mL) and washed with aq. HCl (2 M, 3 × 50 mL). The organic layer was dried ($MgSO_4$), filtered and concentrated under

reduced pressure, maintaining the temperature below 30 °C during concentration. The thus obtained residue (1.0 equiv) was dissolved in DMF (10 mL). CF_3CO_2Na (1.22 g, 9.0 mmol, 2.0 equiv) was added to the solution portionwise. The solution was stirred at room temperature for 18 h. The reaction mixture was diluted with sat. aq. $NaHCO_3$ (100 mL), and the mixture was extracted with EtOAc (3 × 100 mL). The combined organic layers were dried ($MgSO_4$), filtered and concentrated under reduced pressure. The residue was purified by flash column chromatography (silica gel, EtOAc:pet ether = 1:19 → 1:3) to provide D-*galacto* lactone **89D** (1.49 g, 3.9 mmol, 88% yield) as a colorless oil. Spectral data were identical to those previously reported.[82]

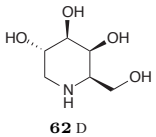

62 D

D-1-Deoxygalactonojirimycin (D-DGJ) 62D: Hydroxylactone **89D** (500 mg, 1.3 mmol, 1.0 equiv) was dissolved in CH_2Cl_2 (50 mL), and the solution cooled to –78 °C (dry ice/acetone bath). DIBAL-H (1.5 M in toluene, 4.3 mL, 6.5 mmol, 5.0 equiv) was added to the solution dropwise. The solution was stirred for 2 h at the same temperature. The reaction was quenched with dropwise addition of EtOAc (5.0 mL) at –78 °C. The reaction was then diluted with CH_2Cl_2 (100 mL) and 1.2 M aq. Rochelle salt (100 mL). The layers were stirred vigorously for 18 h. The layers were then separated and the aqueous layer extracted with CH_2Cl_2 (6 × 50 mL). The combined organic layers were dried ($MgSO_4$), filtered and concentrated under reduced pressure. The crude product was dissolved in dioxane (50 mL). Pd/C (10% Pd, 250 mg, 50 weight-%) was added and the reaction stirred under H_2 balloon for 24 h. Glacial AcOH (0.5 mL, 1% final concentration) was added to the mixture, and the reaction was stirred under H_2 balloon for a further 24 h. The Pd/C was removed by filtering through glass microfiber (GF/B filter). The iminosugar was purified by strong cation exchange chromatography (Dowex 50WX8, H^+ form), washing with H_2O and eluting with 1:4 conc. NH_4OH:H_2O. The combined ammoniacal fractions were concentrated to provide D-DGJ **62D** (198.0 mg, 1.2 mmol, 93% yield) as a colorless oil. **62D**: ^{1}H NMR (500 MHz, D_2O): δ = 4.02 (d, J = 3.0 Hz, 1 H), 3.81 (td, J = 10.4, 5.2 Hz,

1 H), 3.65 (qd, J = 11.5, 6.6 Hz, 2 H), 3.50 (dd, J = 9.7, 3.1 Hz, 1 H), 3.20 (dd, J = 12.7, 5.3 Hz, 1 H), 2.90 (t, J = 6.7 Hz, 1 H), 2.48 (dd, J = 12.7, 11.0 Hz, 1 H) ppm; HRMS (ESI): calcd for $C_6H_{13}NO_4$ [M + H^+]: 164.0923, found 164.0919.

If at first, the idea is not absurd, then there is no hope for it.

—Albert Einstein

6

ToP-DNJ: A Novel Iminosugar-Natural Product Conjugate

6.1 Introduction

As both discussed and studied in Chapters 3 and 4, iminosugars modified by adding unbranched alkyl chains have been extensively investigated. While increasing the length of the chain can increase the potency of *in cellula* enzyme inhibition, it similarly correlates with increased toxicity of the compound and increased tendency towards aggregation.[133;158;198;200] For these reasons, iminosugar drugs that have achieved FDA approval have shorter chains (four or fewer non-hydrogen atoms in length),[72;73] sacrificing lower IC_{50}s in exchange for more favorable toxicity and solubility profiles.

One of the difficulties encountered in the clinical trials of canonical iminosugars as antiviral treatments has been oral delivery of sufficient amounts of the molecule to the tissue and cellular targets of interest.[191;333–335] Although the molecules are not metabolized and are excreted unchanged, large amounts of the compounds cannot be administered, as they inhibit not only the target ER α-glucosidases but also intesti-

nal sucrase-isomaltase and maltase-glucoamylase.[191] The inhibition of these enzyme heterodimers means that sugars consumed as part of the diet cannot be properly processed, leading to severe intestinal distress as a side effect of the treatment. In order to manage these deleterious activities, reduced carbohydrate diets have been developed for the clinically approved iminosugars.[159] However, the ideal would be to eliminate or minimize the ability of the therapeutic iminosugar to inhibit the digestive enzymes.

In an effort to avoid this side effect profile, the Zitzmann group investigated delivery of iminosugars via liposomes. Using this packaging technique, it was demonstrated that iminosugar potency was increased 5 $\log_{10}$-fold for HIV inhibition *in vitro*.[194] The increase in delivery by the method was further confirmed by *in vivo* studies. In treatment of DENV in a lethal antibody-dependent enhancement mouse model, liposome-encapsulated *N*B-DNJ demonstrated efficacy at a concentration 3 orders of magnitude lower than that required for similar effect by free drug.[178] While these studies verify the potential for liposome-encapsulated iminosugars, liposomes have to be administered intravenously (IV), in contrast to the oral availability of iminosugars currently on the market for treatment of other diseases. Although IV drug delivery might be viable for treatment of some acute viruses, it is not practical for treatment of viruses causing chronic disease such as HIV or HCV.

Because of this drawback, attention was turned to designing an antiviral iminosugar that could, like miglustat and miglitol, be orally available, but with greater specificity both in terms of targeted enzymes and with regard to uptake and localization. The D-DNJ headgroup was left unmodified, as this was optimal for inhibition of glucosidase enzymes, with the ER α-glucosidases as the primary intended targets. Rather than substituting the endocyclic nitrogen atom with either a straight-chain aliphatic group or other arbitrary "greasy" substitution (*e.g.*, adamantane),[336;337] it was decided that the substituent should be a natural product. The working hypothesis was that the molecule would be taken up in the same way as this second natural product, allowing for the drug to be directed to both the organs and organelles of interest.

In considering candidate natural products for conjugation, an unexpected finding of the liposome delivery work was considered: liposomes which contained tocopherol (vitamin E) proved antiviral with respect to HCV even if not loaded with iminosugars (unpublished data). Vitamin E is available as over-the-counter gel capsules, and taken at daily doses of as much as 670 mg. This combination of oral availability, low toxicity and observed anti-HCV activity made the molecule an interesting proposal for the natural product portion of the iminosugar hybrid. In fact, vitamin E is actually a mixture of 8 vitamers – 4 tocopherols (α–δ, **97**–**100**; Figure 6.1) and 4 tocotrienols (α–δ, **101**–**104**), with each of these existing as a number of stereoisomers.

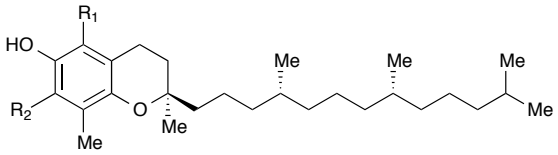

97 : R_1 = Me, R_2 = Me
98 : R_1 = Me, R_2 = H
99 : R_1 = H, R_2 = Me
100: R_1 = H, R_2 = H

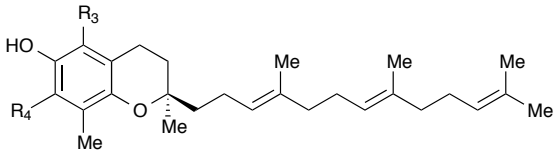

101: R_3 = Me, R_4 = Me
102: R_3 = Me, R_4 = H
103: R_3 = H, R_4 = Me
104: R_3 = H, R_4 = H

Figure 6.1: *Structures of Vitamin E.* The two classes of vitamin E are the tocopherols (**97**–**100**) and tocotrienols (**101**–**104**). The four vitamins within each group differ in the methylation of the aromatic portion of the chroman.

On its own, vitamin E is a component of lipid bilayers and an antioxidant. When exposed to radicals, vitamin E is able to undergo an oxidation reaction (Figure 6.2), providing a sink for these harmful compounds which include reactive oxygen species.[338;339] The reaction is facile enough that it can occur spontaneously, not only in biological systems, but also when tocopherols are exposed to air. D-α-Tocopherol is the most biologically active member of this family of compounds.[340–342] In particular, even though all forms of vitamin E are absorbed from the gut, D-α-tocopherol is selectively accumulated by processing in the liver.[343;344] Because this is the main targeted

organ of HCV and HBV infections, conservation of this biodelivery property is favorable for the desired therapeutic outcome.

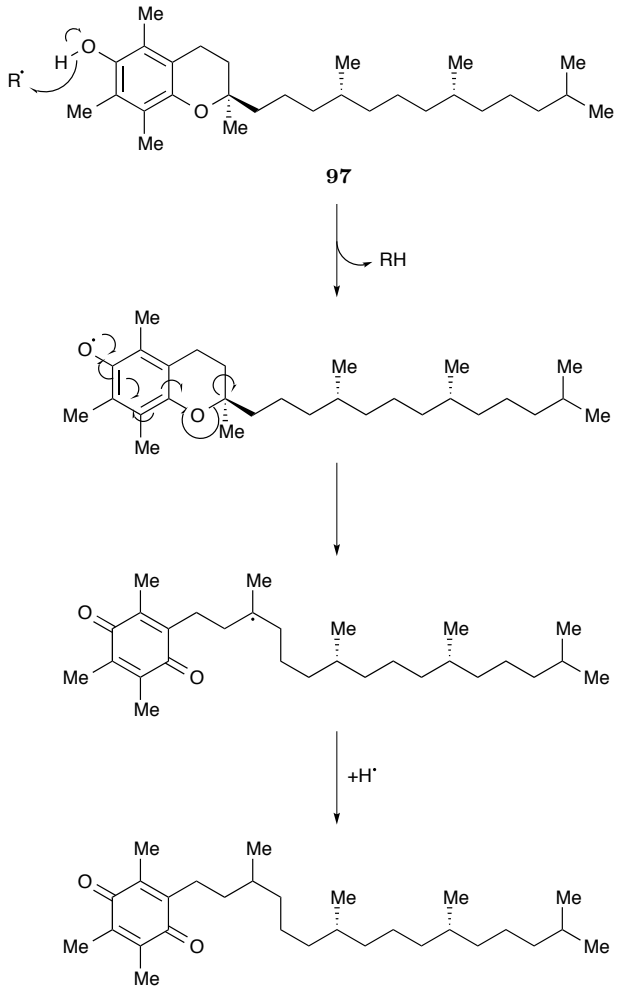

Figure 6.2: *Antioxidant Mechanism of Tocopherol.* Once an oxidant removes a hydrogen radical, the residual radical on the vitamin molecule is stabilized by resonance throughout the hydroquinone system. After formation of the oxidized quinone, the unpaired electron localizes to a tertiary center, the most stable form of unconjugated carbon radical, which can be trapped to form a stable molecule. Though shown here for D-α-tocopherol **97**, all of the forms of vitamin E are capable of the same mechanism.

In designing the D-α-tocopheroxy iminosugar, the concept was to design the compound as a lipid, with distinct hydrophobic and hydrophilic regions, rather than simply as a modified sugar. With this in mind, it was determined that the iminosugar, with its 4 hydrogen bond donors and 5 hydrogen bond acceptors, should be tethered to the hydrophilic end of tocopherol, namely the phenolic oxygen. Beyond fulfilling the lipid design restriction, it also places this free alcohol of the tocopherol to be used

as a chemical handle. This also eliminates the ability of the iminosugar to act as an antioxidant. While this does limit the chemical versatility of the molecule, it also makes it more air-stable, a desirable drug quality.

Rather than attaching the two natural products directly to one another, a 5-carbon alkyl linker was included to provide enough flexibility for both the iminosugar and tocopherol to maintain the necessary independence to inhibit glucose-processing enzymes and be recognized by lipid trafficking enzymes, respectively.

Combining these specifications into a single design resulted in *N*-5-(D-α-Tocopheroxy) Pentyl deoxynojirimycin (ToP-DNJ, **105**, Figure 6.3).

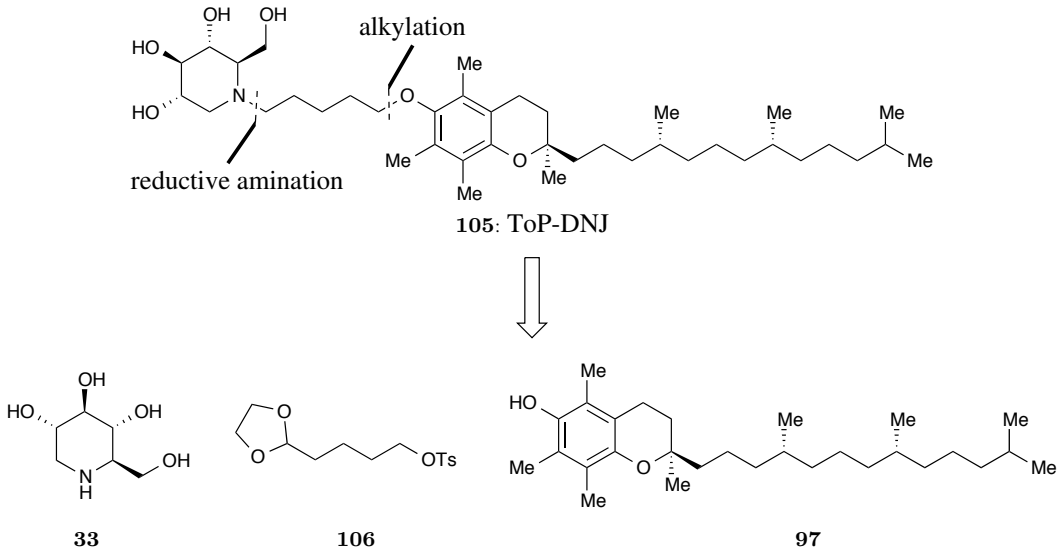

Figure 6.3: *Structure and Retrosynthetic Analysis of ToP-DNJ **105**.*

6.2 Synthesis of ToP-DNJ

Keeping the retrosynthetic analysis presented in Figure 6.3 in mind, the synthesis was begun by targeting the linker. Commercially available pentane-1,5-diol **107** was desymmetrized by protecting one of the equivalent terminal alcohols with BnBr in the presence of Ag_2O to give monobenzyl ether **108** (Scheme 6.2).[345] The remaining free alcohol was oxidized to aldehyde **109** with Dess–Martin periodinane (DMP), providing the proper oxidation state for the eventual reductive amination (75% yield over

two steps). In advance of installing the tocopherol moiety, the aldehyde functionality was masked by refluxing **116** with ethylene glycol and an acid catalyst (TsOH), while removing water by benzene azeotrope and Dean–Stark trap, to smoothly obtain the 1,2-dioxolane **110** (71% yield).

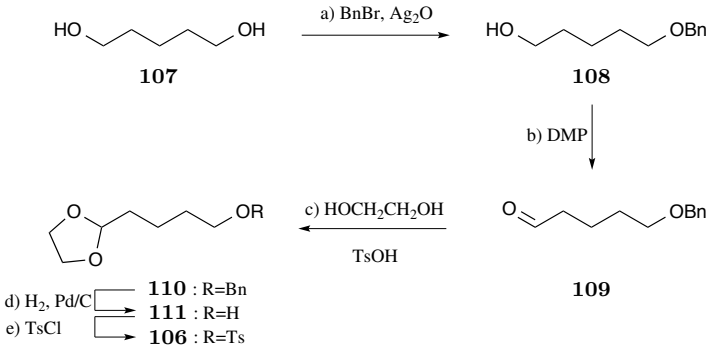

Scheme 6.1: *Synthesis of Pentyl Linker.* Reagents and conditions: a) Ag_2O (1.5 equiv), BnBr (1.1 equiv), CH_2Cl_2, 25 °C, 18 h; b) DMP (1.0 equiv), CH_2Cl_2, 25 °C, 18 h, 75% yield over two steps from **107**; c) ethylene glycol (1.3 equiv), TsOH (catalytic), benzene, 95 °C, 12 h, 71% yield; d) H_2, Pd/C (2.5 weight-%), 1,4-dioxane, 100% yield; e) TsCl (1.1 equiv), Et_3N (1.3 equiv), DMAP (0.1 equiv), CH_2Cl_2.

Now that the two termini were in differing oxidation states, the cleavage of benzyl ether **110** under hydrogenolysis conditions (H_2, Pd/C) provided primary alcohol **111**. In order to install the tocopherol, the alcohol was first converted into tosylate **106** (TsCl, Et_3N, DMAP), which, due to its instability, was immediately treated with deprotonated (NaH) D-α-tocopherol. This S_N2 displacement provided alkylated tocopherol **112**, with 86% yield over the two steps from **111**. Deprotection under acidic conditions (TsOH) with slow addition of water liberated aldehyde **113** (85% yield), preparing the side chain in 39% yield from **107**.

113 and tetra-*O*-benzyl DNJ **114**[337] were reacted with H_2 gas to undergo acid- and palladium-catalyzed reductive amination to afford fully protected ToP-DNJ **115**. Unfortunately, these hydrogenation conditions were not potent enough to cleave the benzyl protecting groups. Instead, a transfer hydrogenation with both cyclohexene and HCO_2NH_4 as H_2 sources provided ToP-DNJ **105** in 11% yield.

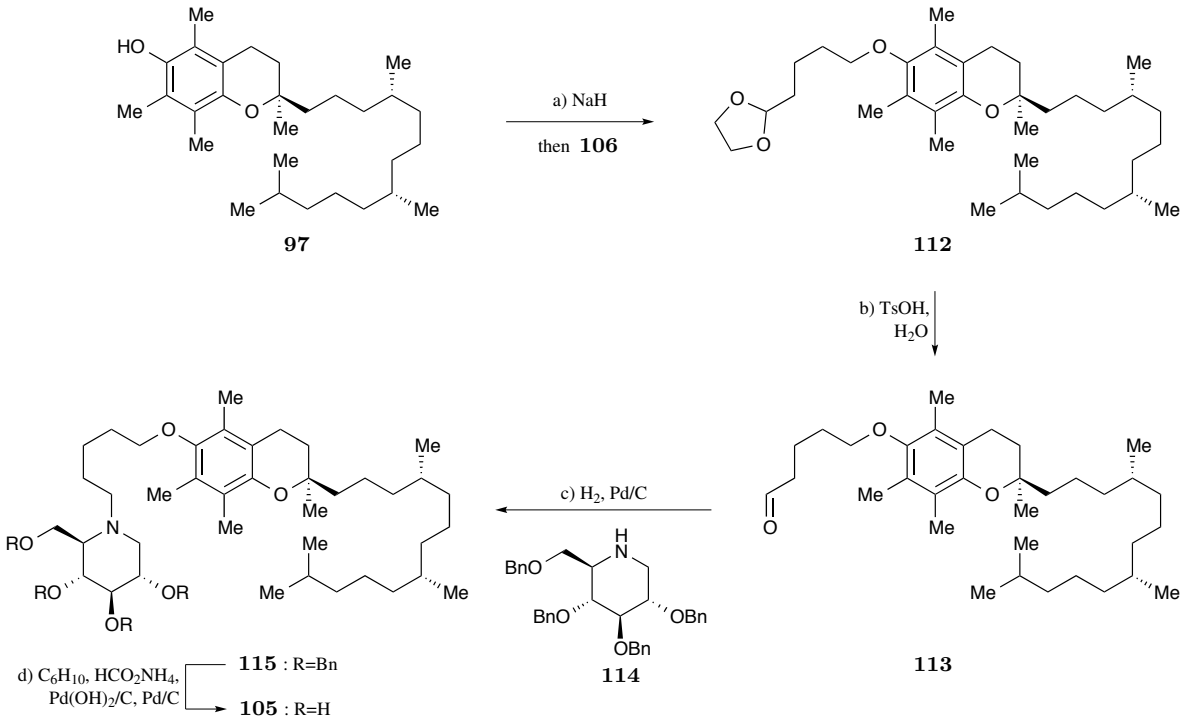

Scheme 6.2: *Synthesis of ToP-DNJ **105*** Reagents and conditions: a) NaH (2.0 equiv), DMF, then **106** (0.9 equiv), 0 – 25 °C, 1 h, then 80 °C, 20 h, 86% yield; b) $TsOH \cdot H_2O$ (2.0 equiv), H_2O:1,4-dioxane (1:8), 90 °C, 3 h, 99% yield; c) tetra-*O*-benzyl DNJ **114**[337] (0.67 equiv), AcOH (catalytic), H_2, Pd/C (10% Pd, 10 weight-%), EtOH, 95 °C, 12 h, 71% yield; d) cyclohexene (10 equiv), HCO_2NH_4 (10 equiv), Pd/C (10% Pd, 25 weight-%), $Pd(OH)_2$/C (20% $Pd(OH)_2$, 25 weight-%), MeOH:EtOH (1:1), 90 °C, 48 h, 11% yield from **113**.

6.3 Toxicity

With the target iminosugar in hand, biological profiling of ToP-DNJ commenced. Toxicity was examined in primary human MDMΦ (5 donors) and a number of cell lines (Table 6.1). CC_{10} was only reached for HepG2 cells, with all other cell types showing less than a 10% decrease in viability. For all other cell types tested, ToP-DNJ showed no toxicity beyond that observed for the DMSO vehicle as measured by MTS assay at the concentrations examined.

Despite the lack of effect as measured by MTS, examining the MDMΦ cells from 3 donors revealed unusual morphologies at a concentrations of 100 µM and higher (Figure 6.4).

While employed as a standard measure of cell viability and toxicity, the MTS assay

Table 6.1: *Cytotoxicity of ToP-DNJ in Cell Culture as Measured by MTS Assay*

Cell Type	CC_{10} (µM)
Cell lines	
Huh7.5	>100
HepG2	83.3 ± 7.5
MDBK	>316
HL60	>316
HEK293T	>100
Primary cells	
MDMΦ	>100

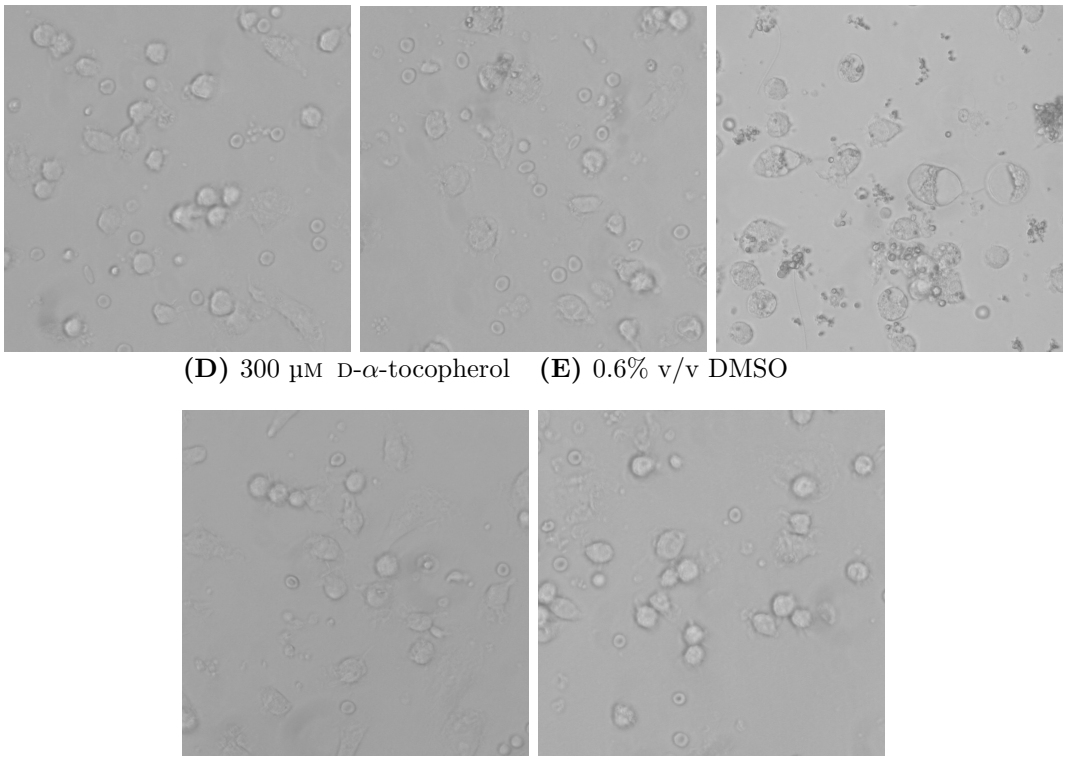

Figure 6.4: *ToP-DNJ Treated MDMΦ Cells.* Primary human MDMΦ cells were incubated with media containing the indicated treatment for 48 h and then observed by light microscopy (200x magnification). D-α-Tocopherol and 0.6% DMSO were included as controls for the lipid tail and solubilization vehicle of ToP-DNJ, respectively. For all treatments, cells resemble untreated (6.4A), except for those treated with the higher dose of ToP-DNJ (6.4C). Under these conditions, the cells have large vacuoles, with this phenotype correlating with increased levels of caspases 3 and 7. The dark debris seen in panel C is precipitated ToP-DNJ, as confirmed by a cell-free control of the same condition (not shown).

is truly a measure of metabolism. As such, an even more rigorous cell viability assay, called ApoToxGlo, was performed on ToP-DNJ treated MDMΦ cells from two donors to further characterize its effects (Figure 6.5). This assay measures intra- and extracellular protease activity to provide a ratio of living to dead cells, providing an indication of both cytotoxicity and cell viability. A third reagent measures the activity of caspases 3 and 7, proteases that act as executioner caspases during apoptosis. By cytotoxicity and cell viability, there was no unfavorable effect of ToP-DNJ up to the maximum tested concentration of 316 µM for either donor. In fact, in donor 2, ToP-DNJ showed a decrease in the dead cell (extracellular) protease activity. With regard to caspase activity, one donor showed no significant effects due to ToP-DNJ, while the other demonstrated an increase in caspase activity at concentrations of 31 µM and higher, reaching a 2-fold increase relative to untreated cells at 316 µM. This divergence between the donors was also reflected in the phenotypic effects of the treatment, with higher caspase activity correlating with a higher proportion of visually affected cells (ca. 80% vs. ca. 20%).

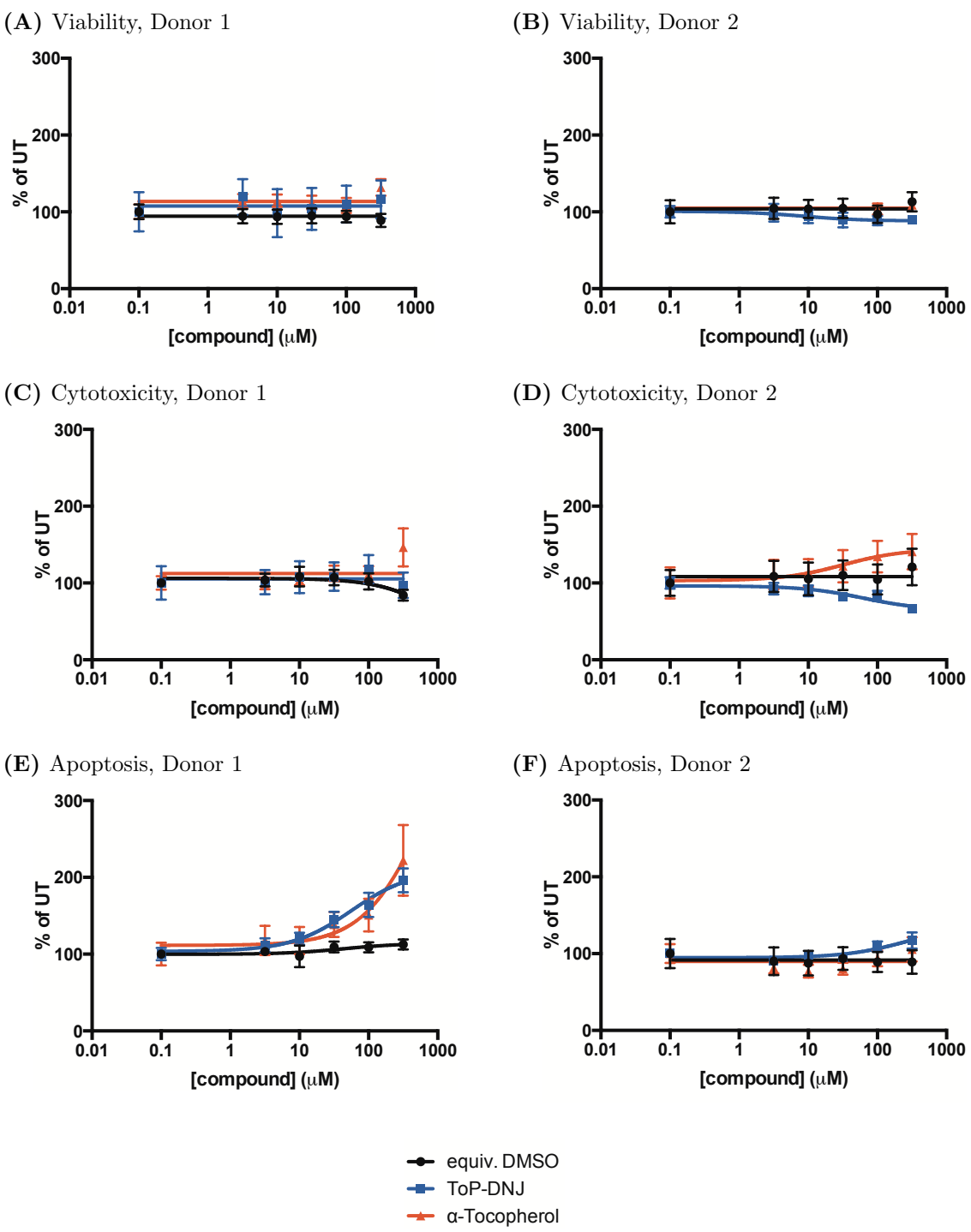

Figure 6.5: *Influence of ToP-DNJ on MDMΦ Cell Health.* Primary human MDMΦ cells were incubated with media containing the indicated treatment for 48 h and then evaluated using the ApoToxGlo cell viability assay. Panels A and B show the normalized levels of intracellular (live cell) protease, an indicator of cell viability; panels C and D, the normalized levels of extracellular (dead cell) protease, an indicator of cytotoxicity; panels E and F, levels of caspsases 3 and 7.

6.4 Inhibition of Isolated Enzymes

In collaboration with the group of Prof. A. Kato (Toyama University; Toyama, Japan), the ability of ToP-DNJ to inhibit individual isolated enzymes was surveyed (Table 6.2 and Table 6.3). ToP-DNJ showed a pronounced selectivity; when tested at concentrations up to 50 µM, the compound showed less than 50% inhibition of all enzymes tested except three: rat liver ER α-glucosidase II (GluII, EC 3.2.1.84), human β-glucocerebrosidase (EC 3.2.1.45) and glucosylceramide synthase (EC 2.4.1.80) demonstrating IC_{50}s of 9.0 µM, 110 nM and 1.0 µM, respectively. The β-glucocerebrosidase is also known as GBA or β-glucosidase. Involved in glycosphingolipid processing, mutations in this enzyme result in the lysosomal storage disorder, Gaucher's disease. Similarly, the glucosylceramide synthase tested, HL60 glucosylceramide glucosyltransferase, is also a component of the glycolipid biosynthetic pathway.

Previously,[218] iminosugar structures have been mapped onto ceramide as an explanation for inhibition of glycosphingolipid metabolism, and the lipid tail of ToP-DNJ fits this model. Indeed, this selectivity of ToP-DNJ for enzymes involved in the processing of glycolipids, specifically glucosylceramides, is not surprising considering the lipid nature of α-tocopherol. In addition to this model, one can map the structure of ToP-DNJ onto that of glucosylceramide (Figure 6.6). The iminosugar head group and straightforward mapping of the carbohydrates and lipid tails, the oxygen atoms of the tocopherol heterocycle could fulfill the role of hydrogen bond acceptors in place of the amide and hydroxyl group of the ceramide.

Table 6.2: *IC_{50} of ToP-DNJ **105** Against Isolated Enzymes*

Enzyme	IC_{50}[a] (µM)
α-Glucosidase	
Rat intestinal maltase	NI
Rat intestinal isomaltase	NI
Rat intestinal sucrase	NI
Human lysosome	NI
Rat liver ER, II	9.0
β-Glucosidase	
Bovine liver	NI
Rat intestinal cellobiase	NI
Human glucocerebrosidase	0.11
α-Galactosidase	
Human lysosome	NI
β-Galactosidase	
Bovine liver	NI
Rat intestinal lactase	NI
α-Mannosidase	
Jack beans	NI
β-Mannosidase	
Snail	NI
α-L-Rhamnosidase	
Penicillium decumbens	NI
α-L-Fucosidase	
Bovine kidney	NI
β-Glucuronidase	
Bovine liver	NI
α,α-Trehalase	
Porcine kidney	NI
Amyloglucosidase	
Aspergillus niger	NI
Glucosyltransferase	
HL-60 glucosylceramide synthase	1.0

[a]NI : No inhibition (less than 50% inhibition at 50 µM). For degree of inhibition at 50 µM, see Table 6.3.

Table 6.3: *Inhibition of Isolated Enzymes by 50 μM ToP-DNJ* ***105***

Enzyme	Inhibition (%)
α-Glucosidase	
Rat intestinal maltase	45.2
Rat intestinal isomaltase	6.1
Rat intestinal sucrase	16.1
Human lysosome	48.2
β-Glucosidase	
Bovine liver	0.0
Rat intestinal cellobiase	9.3
α-Galactosidase	
Human lysosome	15.2
β-Galactosidase	
Bovine liver	0.0
Rat intestinal lactase	9.8
α-Mannosidase	
Jack beans	0.0
β-Mannosidase	
Snail	0.0
α-L-Rhamnosidase	
Penicillium decumbens	3.9
α-L-Fucosidase	
Bovine kidney	0.0
β-Glucuronidase	
Bovine liver	0.0
α,α-Trehalase	
Porcine kidney	0.0
Amyloglucosidase	
Aspergillus niger	0.0

(A)

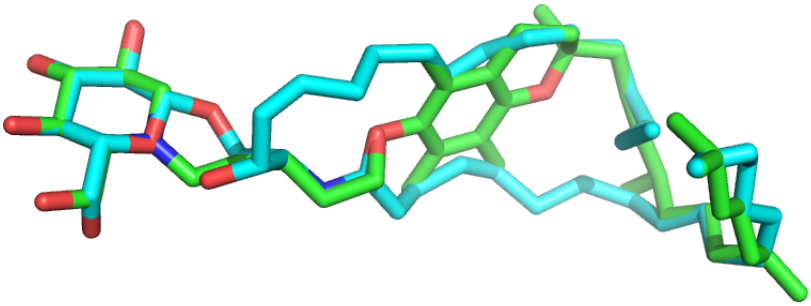

(B)

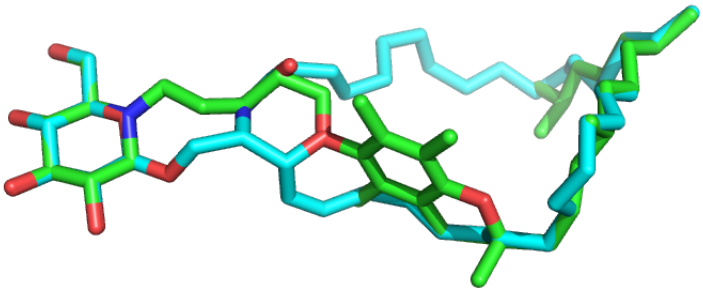

(C)

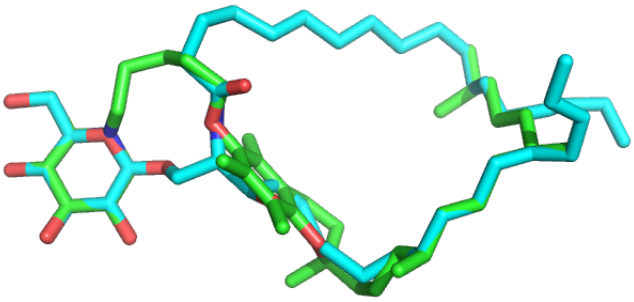

Figure 6.6: *Overlays of ToP-DNJ and GlcCer.* Three different alignments of ToP-DNJ (green) are presented to show how its phenolic oxygen might overlap with each of the heteroatoms of the ceramide chain of GlcCer (cyan): the amide oxygen (A), alcohol oxygen (B), and amide nitrogen (C).

The selectivity for GluII over the other α-glucosidase enzymes is more difficult to explain. GluII and the intestinal enzymes tested are all members of glycoside hydrolase family 31, a group defined by their sequence similarity. Presently, there is a lack of high-resolution structural data for GluII; however, work towards the crystallization of

the enzyme is presently under way. The clearer understanding of the structural distinctions of GluII that this research might provide could allow for a closer examination of the way in which ToP-DNJ preferentially inhibits the ER resident enzyme.

6.5 Inhibition of Selected Cellular Enzymes

To substantiate the data determined for isolated enzymes, ToP-DNJ was further tested for inhibition of enzymes *in cellula* in collaboration with Dr. D. Alonzi (University of Oxford; Oxford, U.K.).

Effects of ToP-DNJ on GluI and GluII were measured in primary MDMΦs (one donor) and Huh7.5, HL60, and MDBK cell lines. By measuring the free oligosaccharides (FOS) by HPLC,[145] cell-dependent inhibition of the ER glucosidases was observed. In the Huh7.5 and MDBK cell lines, ToP-DNJ treatment resulted in no increase of FOS relative to α-tocopherol or DMSO vehicle (see Appendix C). In contrast, both the primary cells and monocytic cell line showed inhibition of the second reaction of GluII (Figure 6.7). However, no increase in the triglucosylated species was observed, indicating a lack of GluI inhibition. In the MDMΦ cells, the ToP-DNJ effect was found to be dose dependent, with FOS detected at both 10 and 100 µM. While FOS levels have been observed to depend on cell type before (unpublished results by D. Alonzi), this is the first instance of an iminosugar causing FOS production in some cell types without any FOS effect observed in others.

A further unusual observation is that, even in the cell types where ToP-DNJ induced FOS, the inhibition was selective. Chromatogrpahic separation of the FOS showed accumulation of only monoglucosylated species, but neither diglucosylated nor triglucosylated (Figure 6.8) glycan levels were affected, suggesting that only the second hydrolysis catalyzed by ER α-GluII is inhibited by ToP-DNJ. To substantiate this hypothesis, isolated enzyme assays of GluI and GluII with native (rather than fluorescent) substrates will be carried out.

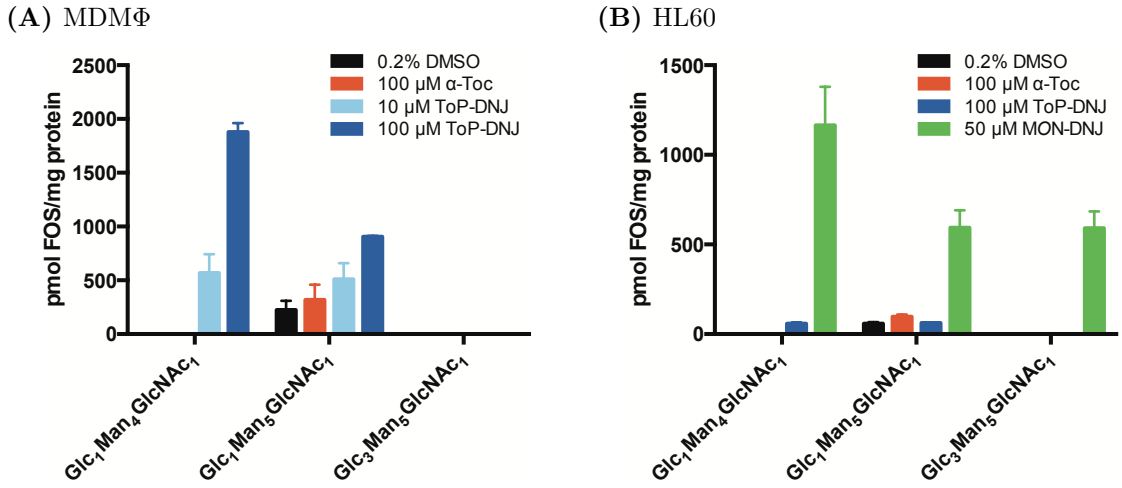

Figure 6.7: *FOS Analysis of ToP-DNJ Treated Cells.* Cells were incubated with the indicated treatment for 24 (HL60) or 48 h (MDMΦ, single donor). FOS were isolated and characterized by HPLC as previously described.[145] The presence of monoglucosylated species indicates inhibition of the second reaction of GluII, while the triglucosylated is a result of GluI inhibition. The MDMΦ results indicate a dose dependent effect of ToP-DNJ on FOS levels, while the HL60 experiment demonstrates that the effect of ToP-DNJ is smaller in comparison to the differently alkylated M*O*N-DNJ. *Data collected in collaboration with Dr. D. Alonzi.*

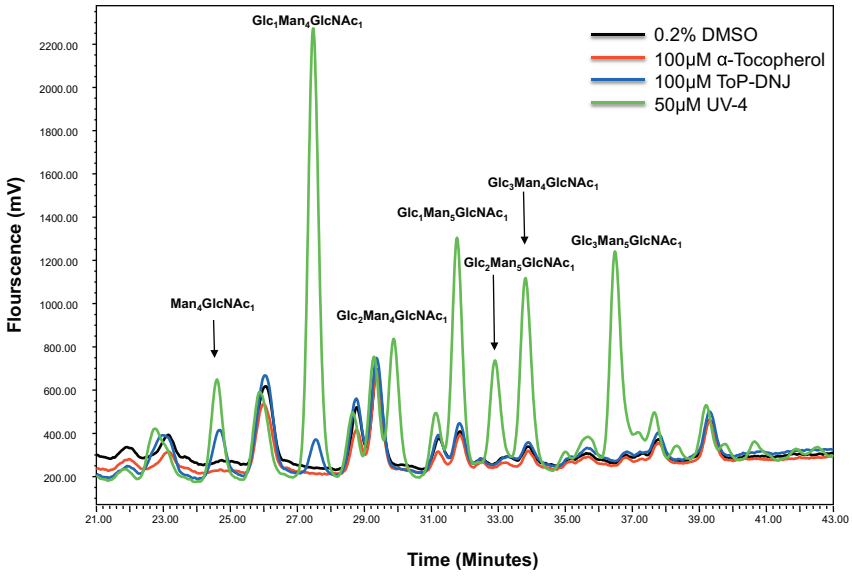

Figure 6.8: *Chromatogram of Treated HL60 Free Oligosaccharides.* HL60 cells were incubated with the indicated treatment for 24 h. FOS were isolated and characterized by HPLC as previously described.[145] The positive control, M*O*N-DNJ, induced accumulation of mono-, di-, and triglucosylated species indicating inhibition of ER α-GluI and both reactions of ER α-GluII. In contrast, ToP-DNJ treatment resulted in accumulation of only the product of the second reaction of GluII. The negative controls (α-tocopherol and DMSO) showed no appreciable levels of any of these species. *Data collected in collaboration with Dr. D. Alonzi.*

When examining glycolipid synthesis, the HL-60 cell line was used because these cells have a simple repertoire of glycolipids, dominated by the monosialylated ganglioside, GM3.[158] When GM3 levels were measured after a 72 h treatment with 50 nM ToP-DNJ, the amount of ganglioside present was reduced by 50% (Figure 6.9). Comparing this to the data obtained for the associated enzyme (HL-60 glucosylceramide glucosyltransferase), the IC_{50} was 20-fold lower in cells versus the isolated enzyme alone. This may be interpreted in a number of ways. Because GM3 is a downstream product of glucosylceramide, this could simply be a result of the decrease of substrate (GlcCer); however, as mentioned in the previous section, ToP-DNJ could act as a mimic of either ceramide, GlcCer or both. If it indeed is a GlcCer mimic, it could inhibit subsequent reactions in the glycosphingolipid biosynthesis pathway. Alternatively, the reduced IC_{50} in cells may be taken as a favorable indicator of uptake or cellular distribution of the drug by the cells, i.e. that an intracellular concentration of 1 µM is achieved with a much lower extracellular concentration.

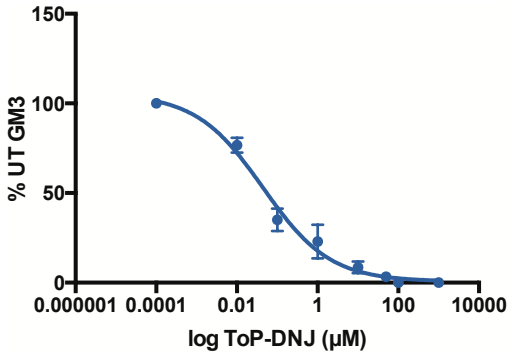

Figure 6.9: *ToP-DNJ Decreases GM3 Levels in HL60 cells.* HL60 cells were incubated for 72 h in the presence of the indicated dose of ToP-DNJ in triplicate. After this time, the cells were harvested and lysed. Lipids were extracted, and their glycans enzymatically released, fluorescently labelled by reductive amination and quantified by normal phase HPLC. The peak area for GM3 in each case allows the relative amount to be calculated. *Data collected by Dr. D. Alonzi.*

6.6 Lipidomics

With the influence of ToP-DNJ on glycolipid processing enzymes documented both in isolation and *in cellula*, it was decided to test the compounds influence on the entire

profile of lipid components in the cell, rather than focusing on specific enzymes. Both HCV-infected and uninfected Huh7.5 cells were treated with 10 µM ToP-DNJ for 96 h, and the amount and variety of lipids were analysed by mass spectrometry (Figure 6.10) by Dr. C. Wolf (APLIPID; Paris, France).[346–353]

As anticipated based on the HL60 results, 10 µM ToP-DNJ demonstrated a statistically significant effect on both GlcCer ($p = 0.006$) and LacCer ($p < 0.001$) levels, with similar effects seen in both naive and HCV-infected Huh7.5 cells. Despite these effects seen on glycerosphingolipids, no statistically significant impact was observed on either of the other metabolically related lipid classes measured, ceramide and sphingomyelin. While D-α-tocopherol shares a number of receptors (SR-BI,[354–356] LDLr,[357;358] NPC1-L1[359])[360] with cholesterol, ToP-DNJ had no influence on the levels of either total cholesterol or the distribution between its free and esterified forms. Further lipid classes examined (diacylglycerides, triacylglycerides, phosphatidylcholine) showed no significant effect with ToP-DNJ treatment, suggesting that the drug does not influence the entirety of the cellular metabolism, but specifically sphingolipid glycosylation (For complete results of the lipidomic report, see Appendix D).

The data set also allowed for investigation of the effects of HCV on the Huh7.5 lipidome. Because of the conservative nature of the statistical analysis (2-way ANOVA with Bonferroni correction), HCV had no statistically significant impact on the mentioned lipids. However, effects trending towards significance were observed both with respect to LacCer ($p = 0.027$) and total cholesterol ($p = 0.029$), with HCV-infection lowering the levels of both lipids. Interestingly, none of the effects of ToP-DNJ directly counteract any of the changes induced by HCV, and in fact, both have a similar effect on LacCer, though the effect of ToP-DNJ is more pronounced.

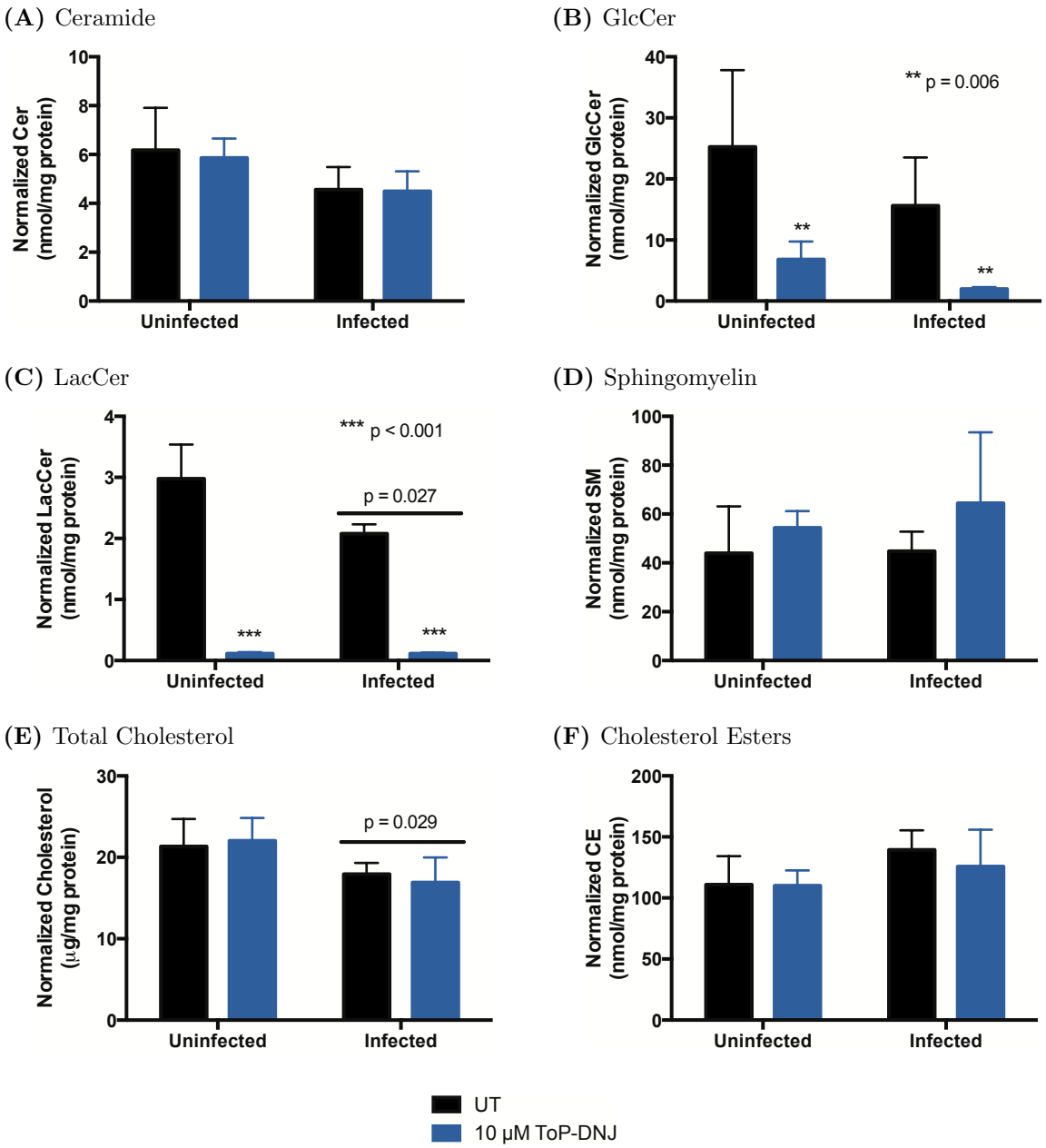

Figure 6.10: *Effects of ToP-DNJ Treatment and HCV Infection on the Huh7.5 Lipidome.* Huh7.5 cells (either HCV-infected or naive) were incubated in the presence of either normal growth media or media supplemented with 10 µM ToP-DNJ. After 4 d, cells were harvested, and lipidomic studies were carried out by LC-MS. Levels of each lipid were normalized to the amount of protein in each sample. The plotted values are the average of triplicates with error indicated by standard deviation. 2-way ANOVA was performed, providing the indicated p-values. In order to determine significance, the Bonferroni correction was invoked, with the only statistically significant effects being the lowering of GlcCer ($p = 0.0062$) and LacCer ($p < 0.0001$) levels by 10 µM ToP-DNJ. HCV infection induced two changes which trended toward significance, lowering the levels of LacCer ($p = 0.0269$) and total cholesterol ($p = 0.0287$). *Data collected in collaboration with Dr. C. Wolf.*

6.7 Antiviral Activity

6.7.1 Dengue Virus

ToP-DNJ was tested for its ability to inhibit DENV in both primary MDMΦ cells and the Huh7-Lunet-hCD81-GLuc cell line (Figure 6.11). Mirroring the cell type-dependent effects found in the FOS studies, ToP-DNJ displayed a dose dependent antiviral effect with respect to DENV in MDMΦ (IC_{50} = 12.7 µM), but not in Huh7-Lunet-hCD81-GLuc cells. This supports the hypothesis that anti-DENV effect is mediated by inhibition of the ER α-glucosidases. As ToP-DNJ inhibits only GluII in MDMΦ at the concentrations (10 – 100 µM) displaying an antiviral effect, it demonstrates that inhibition of GluII alone is sufficient to produce the desired therapeutic outcome. However, the maximum inhibition achieved by ToP-DNJ was 25%, while other iminosugars, which inhibit both ER α-glucosidases, have resulted in >99% reduction in infectious virus titer,[178] suggesting that either inhibition of GluI or inhibition of both enzymes is key for this larger effect.

6.7.2 Bovine Viral Diarrhea Virus

BVDV antiviral assays were carried out in the MDBK cell lines. Neither ToP-DNJ nor α-tocopherol had an effect on the either the amount of viral RNA secreted as measured by quantitative reverse transcription-PCR (qRT-PCR, Figure 6.12A), which is consistent with an iminosugar that does not inhibit ER α-glucosidases.[180;361] Like HCV, BVDV has a p7 viroporin, and the antiviral properties of long chain DNJs and DGJs are explained, at least in part, by inhibition of this protein.[180] Iminosugars that act via p7 inhibition normally only demonstrate the effect via the infectivity assay. The infectivity of virus produced by ToP-DNJ treated cells showed no effect due to the drug. Although not conclusive, this indicates that ToP-DNJ is not a p7 inhibitor at the concentrations tested.

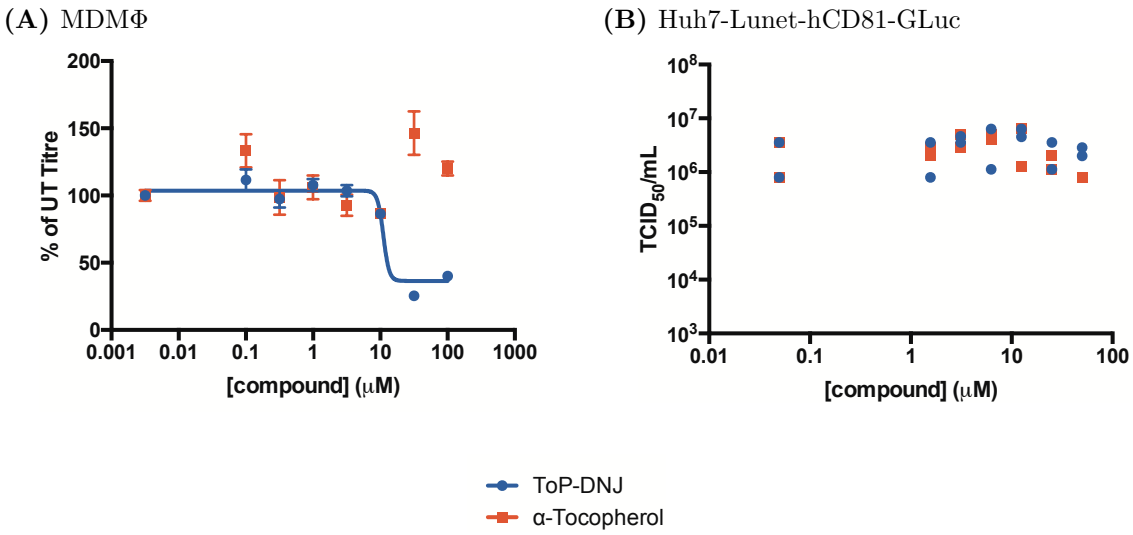

Figure 6.11: *Effect of ToP-DNJ on DENV Infection.* (A): Primary human MDMΦ cells were infected with DENV and then incubated with media containing either ToP-DNJ **105** or α-tocopherol **97** with each concentration measured in triplicate. After 2 d, the cell supernatant was harvested, and the titer of infectious virus from each well was measured in triplicate by plaque assay on LLC-MK$_2$ monolayers. For each of the 7 donors, the average titer for each treatment was determined and converted to a percentage of the average untreated titer for that donor, with propagated error indicated as standard error of the mean for each point. In order to carry out a Kruskall-Wallis test, each individual titer (including untreated) was converted to a percentage out of average untreated titer. The ranked test indicated ($p < 0.0001$) deviation amongst the medians, with a subsequent Dunn's multiple comparisons test identifying the higher doses as significantly different from untreated ($p < 0.0001$ for both 30 and 100 μM). (B): Huh7-Lunet-hCD81-GLuc cells were infected with DENV and then incubated with media containing either ToP-DNJ **105** or α-tocopherol **97** with each concentration measured in duplicate. After 2 d, the cell supernatant was harvested, and the titer of infectious virus from each well was measured by an immunofluorescence endpoint dilution assay on LLC-MK$_2$ cells. Because the hepatoma cell line does not come from various donors from an outbred population, titers were consistent between experiments and raw TCID$_{50}$ values are reported rather than as a percentage. *Data collected in collaboration with Dr. J. Miller.*

6.7.3 Hepatitis C Virus

The ability of ToP-DNJ to inhibit HCV was tested in Huh7-Lunet-hCD81-GLuc cells, using α-tocopherol as a control (Figure 6.13). In the case of both drugs, statistical analysis indicated that a horizontal line was a better fit for TCID$_{50}$ *vs.* concentration curves than a sigmoidal Hill curve, suggesting neither compound provides a dose dependent antiviral effect in the system.

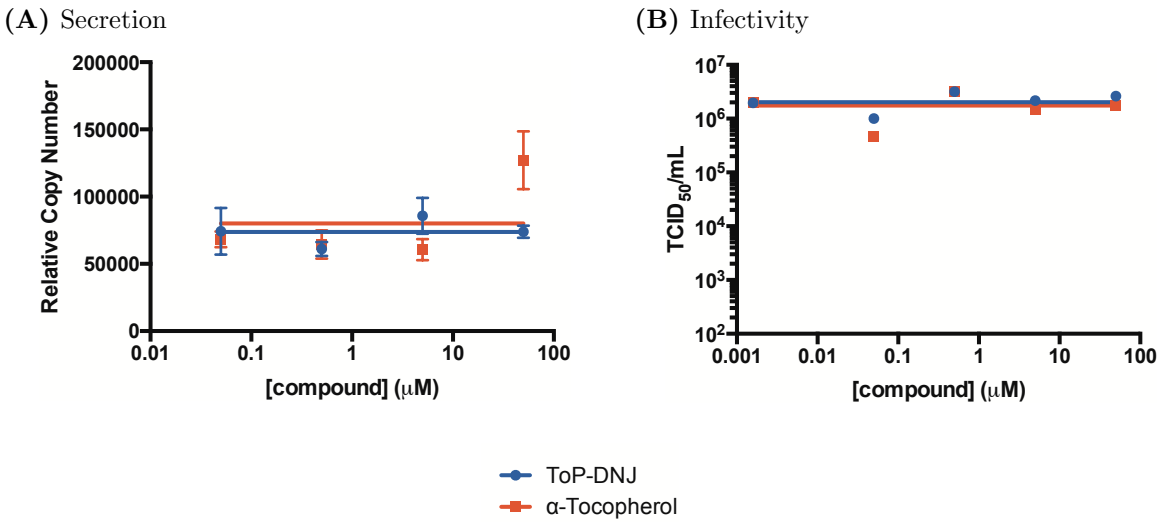

Figure 6.12: *Effect of ToP-DNJ on BVDV Infection.* MDBK cells were infected with Pe515 ncp BVDV (MOI = 10) and then incubated with media containing the indicated drug treatment in duplicate. After 2 d, the cell supernatant was harvested. (A) Viral RNA was isolated from the supernatant and quantified by RT-qPCR). (B) The titer of infectious virus in the supernatant from each well was measured by immunofluorescence endpoint dilution assay on naive MDBK cells, calculating by the method or Reed and Muench.[212] Data were fitted using Prism. Points represent the mean with error bars indicating the standard error of the mean. In both cases, the data were fitted using Prism 6, with a comparison of fits between a horizontal line and a three parameter Hill plot, using the extra sum-of-squares F test to determine the better fit. In both instances, the horizontal line was identified as the better fit for ToP-DNJ and α-tocopherol. *Data collected in collaboration with M. Hill.*

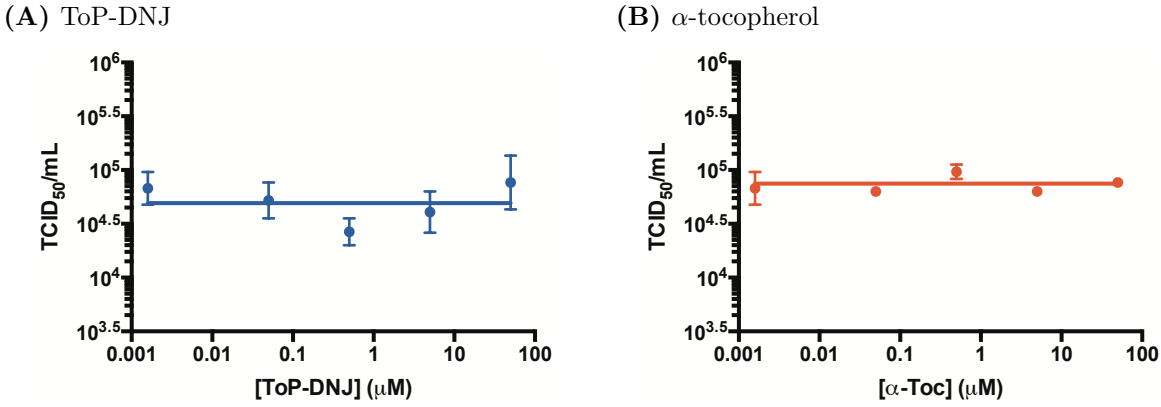

Figure 6.13: *Effect of ToP-DNJ on HCV Infectivity.* Huh7-Lunet-hCD81-GLuc cells were infected with Jc1 HCV (MOI = 0.2) and then incubated with media containing the indicated drug treatment in duplicate. After 4 d, the cell supernatant was harvested, and the titer of infectious virus from each well was measured by immunofluorescence endpoint dilution assay on naive Huh7-Lunet-hCD81-GLuc cells, calculating by the method or Reed and Muench.[212] Points represent the mean with error bars indicating the standard error of the mean. In both cases, the data were fitted using Prism 6, with a comparison of fits between a horizontal line and a three parameter Hill plot, using the extra sum-of-squares F test to determine the better fit. The horizontal line was identified as the better fit for ToP-DNJ and α-tocopherol.

6.7.4 HIV

The effects of ToP-DNJ on HIV secretion were examined in a two-step, two cell line assay. HEK 293T cells were transiently transfected with Lai strain HIV DNA, and incubated with ToP-DNJ for two days. The cells lack the proper receptors to be infected, so the effects only represent a "single round" of infection, with no convolution due to subsequent infection. The amount of secreted virus was evaluated by enzyme-linked immunosorbent assay (ELISA) measurement of HIV p24 protein. To measure infectivity, the virus produced by treated cells was diluted to equalize with respect to p24 concentration, and these dilutions were used to inoculate TZM-bl cells. These are a reporter cell line, which expresses firefly luciferase under control of the HIV-1 promoter. ToP-DNJ had no effect on either HIV secretion or infectivity (Figure 6.14).

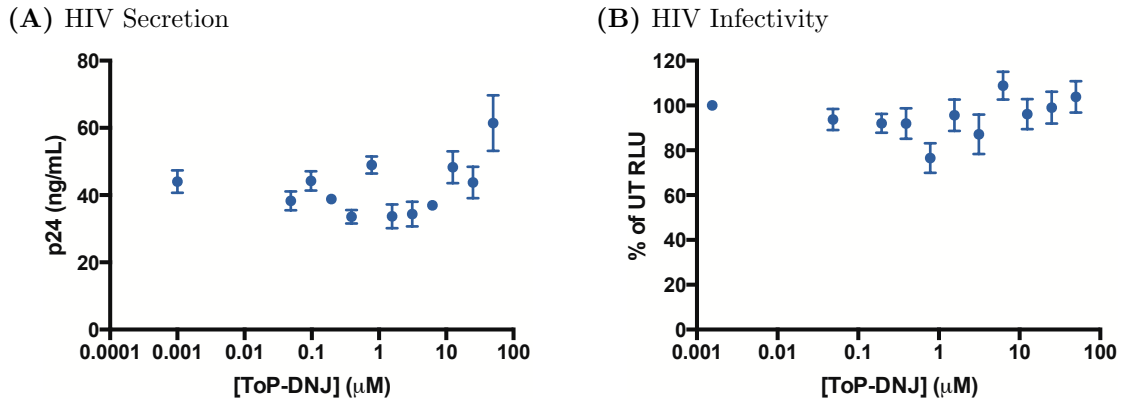

Figure 6.14: *Effect of ToP-DNJ on HIV Infection.* (A) HEK 293T cells were transfected with Lai strain HIV DNA using lipofectamine and subsequently incubated with the indicated concentration of ToP-DNJ in growth media for 2 d. The supernatant was harvested, and the amount of p24 quantified by ELISA. (B) Using the ELISA data, the supernatant of each sample was diluted to equalize the concentration of p24 and used to inoculate TZM-bl reporter cells. After incubating for 2 d, the amount of luciferase was measured using the Bright-Glo™ Luciferase Assay System. *Data collected by S. Spiro.*

6.7.5 Hepatitis B Virus

Similar to HIV, HBV antiviral assays employ a two cell line system, with the first (HepG2.2.2.15) simply expressing virus and the second (differentiated HepaRG)[362] allowing infection. In experiments conducted by Dr. N. Branza-Nichita (Institute of

Biochemistry, Romanian Academy; Bucharest, Romania) ToP-DNJ had a small, but statistically not significant, effect on HBV secretion (Figure 6.15A) and infectivity (Figure 6.15B), showing a maximum of 18% and 29% reduction, respectively.

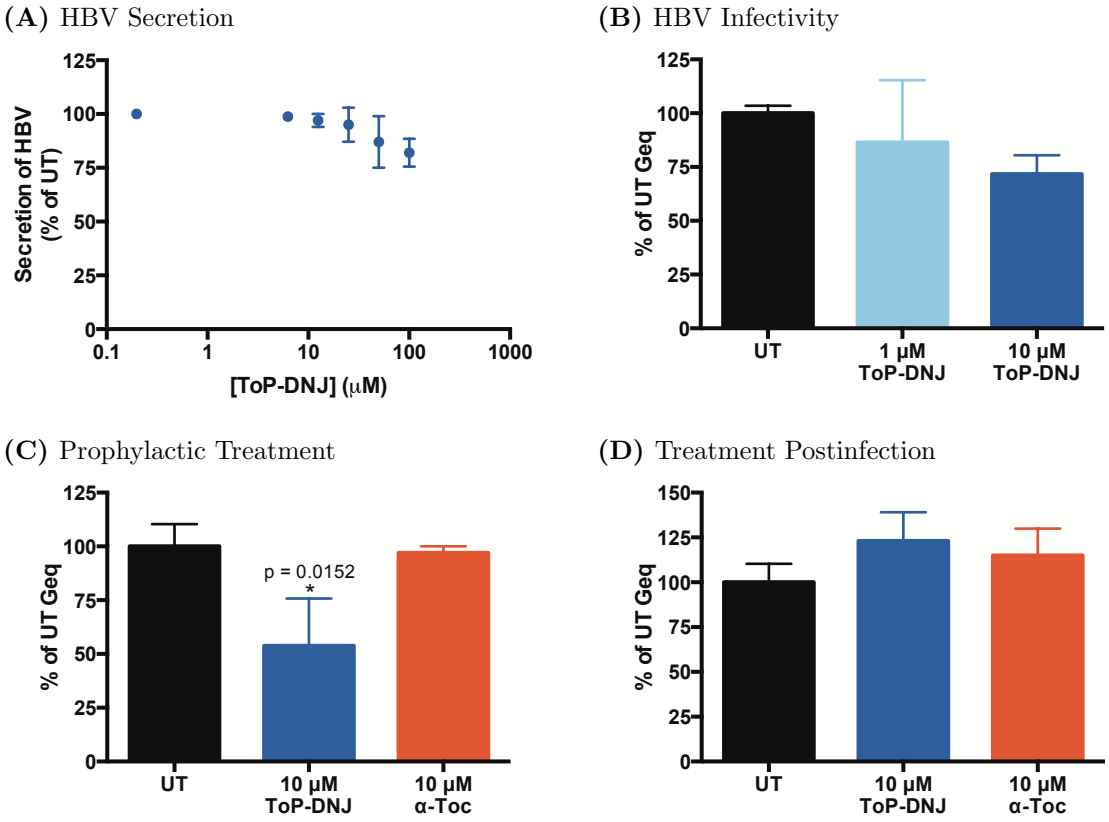

Figure 6.15: *Effect of ToP-DNJ on Hepatitis B Infection.* (A) HepG2.2.2.15 cells stably transfected with two copies of the HBV genome were treated for 4 d. Secretion of HBsAg was quantified by ELISA, and values were normalized to the total number of cells. Data represent the means and standard deviations of triplicates from three independent experiments and are presented as percentages of the values for untreated samples. (B) HBV was purified from HepG2.2.215 cells treated with either 1 or 10 µM ToP-DNJ for 5 d, by ultracentrifugation on 20% sucrose cushion. Encapsidated HBV genomes (Geq) were quantified by qPCR . Equal amounts of Geq were used to infect differentiated HepaRG cells. The amount of HBV nucleocapsids in infected cells was quantified by qPCR at day 14 post infection. (C) HBV was purified from untreated HepG2.2.215 cells, by ultracentrifugation on 20% sucrose cushion. Encapsidated HBV Geq were quantified by qPCR . Equal amounts of Geq were used to infect differentiated HepaRG cells either pre-treated with 10 µM ToP-DNJ, α-tocopherol, or untreated for 3 d. The amount of HBV nucleocapsids in infected cells was quantified by qPCR at day 14 post infection. (D) The experiment of panel C was repeated except the cells were treated with drugs at 24 h post infection for 3 d, rather than prior to infection. *Data collected by Dr. N. Branza-Nichita.*

One of the most effective treatments of HBV previously demonstrated *in vitro* was removal of cellular cholesterol, a key component of lipid nanodomains.[363] Glycosph-

ingolipids are also a critical component of these "rafts"; with lipidomic confirmation that ToP-DNJ reduces glycosphingolipid levels in hepatoma cells at 10 µM, HepaRG cells were pretreated with this condition for 3 d before inoculating with HBV to see whether disrupting rafts in this alternate way is also antiviral. This resulted in a statistically significant (p = 0.0152) reduction in viral Geq levels by 46.2% at 14 d post infection (Figure6.15C), an effect that was not seen either with prophylactic treatment with α-tocopherol or treatment with either drug at 24 h post infection(6.15D).

6.7.6 Prophylactic ToP-DNJ Treatment

After observing that pretreatment of cells with ToP-DNJ reduces their "infectability" with respect to HBV, it was determined that similar assays should be carried out with the other investigated viruses. Preliminary results indicate that a similar effect occurs in both the HCV and HIV cell culture systems upon 4 d pretreatment with 10 µM ToP-DNJ (Figure 6.16).

In the HCV system, both prophylactic only treatment and continued treatment (prophylactic and post infection treatment) were examined. Drug treatment induced a significant effect on viral $TCID_{50}$ ($p = 0.008$), though multiple comparisons revealed no single treatment as being significantly different from untreated. Qualitative treatment of the data showed ToP-DNJ exerted an antiviral effect, while α-tocopherol induced an apparent proviral effect. There was no significant effect of treatment duration, suggesting that glycosphingolipid turnover in Huh7-Lunet-hCD81-GLuc cells under the assay conditions is not fast enough for removal of the drug to revive infectability of the cells within the time course of the assay.

Though a statistically significant ($p = 0.001$) reduction in luciferase was observed in the HIV assay, it is important to remember that this is a reporter cell line, developed to express HIV receptors at high levels. Experiments are currently under way to examine whether the effect is recapitulated in periphery blood mononuclear cells.

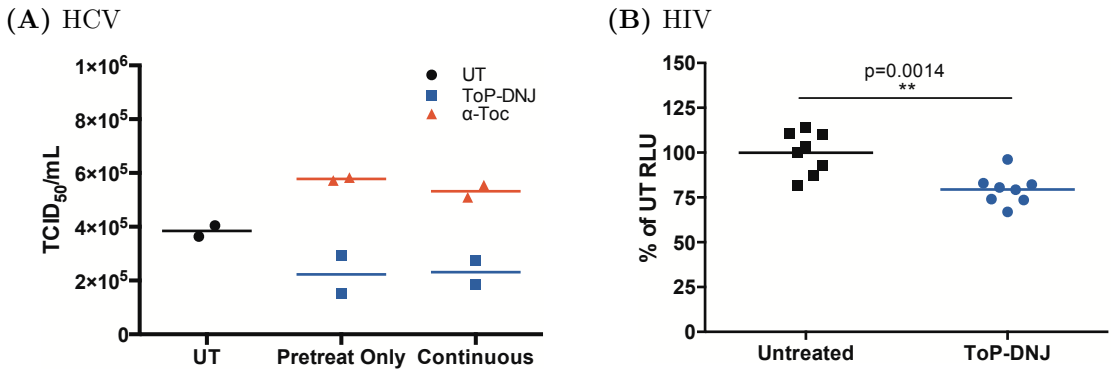

Figure 6.16: *Antiviral Effect of Prophylactic ToP-DNJ Treatment.* (A) Huh7-Lunet-hCD81-GLuc cells were incubated for 3 d, in media alone or supplemented with 10 µM of respective drug (ToP-DNJ or α-tocopherol). The cells were then infected with Jc1 HCV (MOI = 0.2). The untreated were continued to be incubated in untreated media after infection, while the drug pretreated cells were separated into pretreat only (incubated in untreated media after infection) and continuous (incubated in media with the same drug treatment before and after infection). 4 d after infection, the cell supernatant was harvested, and the titer of infectious virus from each well was measured by immunofluorescence endpoint dilution assay on naive Huh7-Lunet-hCD81-GLuc cells, calculating by the method of Reed and Muench.[212] Data were analysed using Prism 6 to perform a two-way ANOVA. There was a statistically significant effect of drug treatment ($p = 0.008$). (B) TZM-bl cells were incubated for 3 d, in media alone or supplemented with 10 µM ToP-DNJ. The cells were then inoculated with HIV at a titer corresponding to a p24 concentration of 2.5 ng/mL, then the media replaced with fresh untreated media. After incubating for 2 d, the amount of luciferase was measured using the Bright-Glo™ Luciferase Assay System. Data were analysed using Prism 6 to perform a one-way ANOVA. There was a statistically significant effect of drug treatment ($p = 0.001$). *Data in Panel B collected by S. Spiro.*

6.8 Disruption of Lipid Rafts

Having demonstrated the effect of ToP-DNJ on glycosphingolipid levels in cells, it was sought to observe whether this had a functional effect given the critical role played by glycosphingolipids in lipid nanodomains. Collaborating with Dr. J. Chojnacki and Prof. C. Eggeling (Weatherall Institute of Molecular Medicine, University of Oxford; Oxford, U.K.), stimulated emission depletion (STED) microscopy experiments were carried out to examine the behavior of lipids in the plasma membrane of Huh7.5 cells. After 4 d pretreatment with ToP-DNJ, α-tocopherol or DMSO (vehicle control), cells were labeled with either a fluorescent sphingomyelin (SM) or fluorescent phosphoethanolamine (PE) lipid and measured by fluorescence correlation spectroscopy to determine lipid transit times. As SM is a component of lipid nanodomains, it moves

less freely than the control PE, displaying a longer transit time.

Indeed, the expected relative transit times of the two lipids are observed in the untreated control, with the SM displaying a transit time more than twice as long as PE (Figure 6.17). ToP-DNJ treatment has no effect on PE, as predicted given that the lipid does not associate with lipid rafts. In contrast, ToP-DNJ treatment results in a statistically significant ($p = 0.0210$) reduction in the transit time of SM (*i.e.*, SM is moving faster, on average), indicating disruption of the lipid nanodomains. While the drug caused reduction in SM transit time, SM motion remained slower than the freely diffusing PE, suggesting that lipid rafts, though effected, have not been completely ablated.

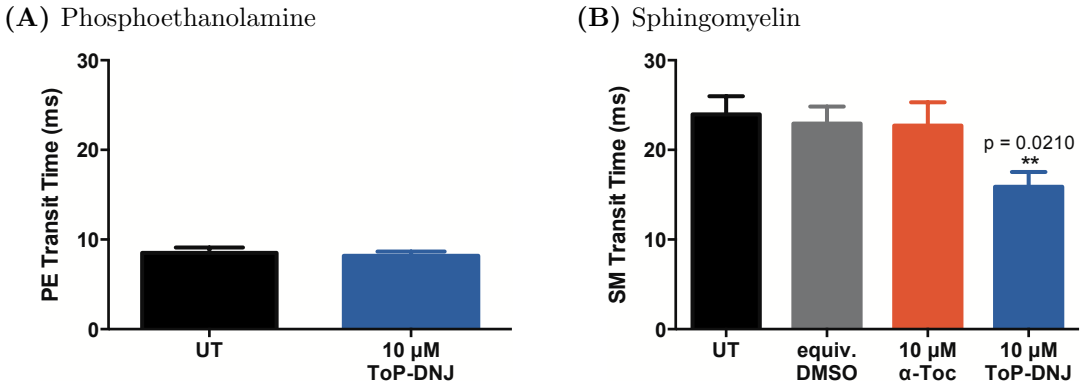

Figure 6.17: *Effects of ToP-DNJ on Membrane Lipid Diffusion Times.* Huh7.5 cells were incubated for 4 d with the indicated drug treatment. At the end of this time, the cells were washed with PBS, blocked with BSA and incubated with Atto647N labeled lipid (either SM or PE). Fluorescence correlation spectroscopy was then carried out using STED microscopy. *Data collected in collaboration with Dr. J. Chojnacki.*

6.9 Pharmacokinetics and Biodistribution

As one of the original goals was to improve bioavailability, a mouse study was performed in collaboration with Sai Life Sciences (India) (For the complete experimental report, consult Appendix E). ToP-DNJ was provided in a single dose to male BALB/c mice either by IV at 2 mg/kg or orally (PO) at 10 mg/kg. Serum was collected from the mice at 8 time points over the course of 24 h (Figure 6.18). In the instance of IV administration, ToP-DNJ concentration stayed above 10 µM (the concentration

employed for HBV and lipidomics studies) up to 4 h post treatment. Serum concentration of ToP-DNJ was above the IC_{50} (50 nM) observed for GM3 levels in HL60 cells at all time points measured. Despite the higher amount of drug administered PO, much lower serum concentrations were observed, with a maximum of 45 µM at 8 h. Of note, absorption of vitamin E is diet dependent. As a fat soluble vitamin, statistically significant changes in serum levels result from consuming the tocopherol together with fats (e.g. butter and whole milk), with a further effect from the fat source.[364] As ToP-DNJ has been observed to have higher solubility in organic solvents than aqueous buffers, follow-up bioavailibility studies coupling the drug with modified diets are warranted.

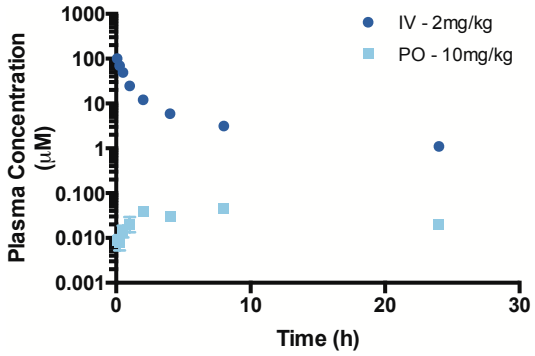

Figure 6.18: *Time Course of ToP-DNJ Concentration in Mouse Serum.* Mice were treated with a single dose of ToP-DNJ either by oral gavage (PO, 10 mg/kg) or by IV (2 mg/kg). Blood was collected at the indicated time point, and the circulating level of ToP-DNJ quantified by HPLC. *Data collected by SAI Life Sciences Ltd.*

One of the aims of tocopherol conjugation to DNJ was to lengthen the iminosugar's biological half-life. The terminal half-life of ToP-DNJ (based upon the IV treatment) is 8.79 h, an improvement of nearly 4-fold from the anti-HCV clinical candidate UT231B (*N*-(6-ethoxyhexyl)-6-deoxy-D-DGJ, $t_{1/2}$ = 2.25 h). A half-life could not be accurately calculated for the mice administered with ToP-DNJ orally, as there were not sufficient time points measured after the maximum observed concentration at 8 h. Although this demonstrates an appreciable improvement over the serum lifetime of other iminosugars, the half-life of ToP-DNJ is still less than that of α-tocopherol ($t_{1/2}$ = 2 – 100 d).[338;365–370] The evaluation of α-tocopherol's half-life depends upon the length of the study, as initial half-life (typically 2 d) depends on the lifetime

of the chylomicrons used to transport tocopherol to the liver, while measurements of longer experiments (70 – 460 d) represent the turnover of α-tocopherol that has been packaged by α-tocopherol transport protein (α-TTP) and stored, giving higher estimates of vitamin E half-life (18 – 105 d).[370]

Further to the effect on serum half-life, ToP-DNJ has improved distribution to and retention in the liver (Figure 6.19) relative to *N*B-DNJ,[371] and even relative to the lipophilic *N*-*n*-octadecyl-DNJ (*N*Od-DNJ).[198] Whereas *N*B-DNJ is quickly excreted in urine, showing the highest concentrations in kidneys and bladder after p.o. administration, ToP-DNJ reaches the highest concentrations in the liver, regardless of administration method. While *N*Od-DNJ also accumulates primarily in the liver, the liver concentration decreases by >84% between 5 and 24 h post treatment. In contrast, the liver concentration of ToP-DNJ shows no drop over the same time interval and decreases by less that 50% over the course of the entire 24 h, indicating a long liver half-life, ideal for treatment of HCV and HBV.

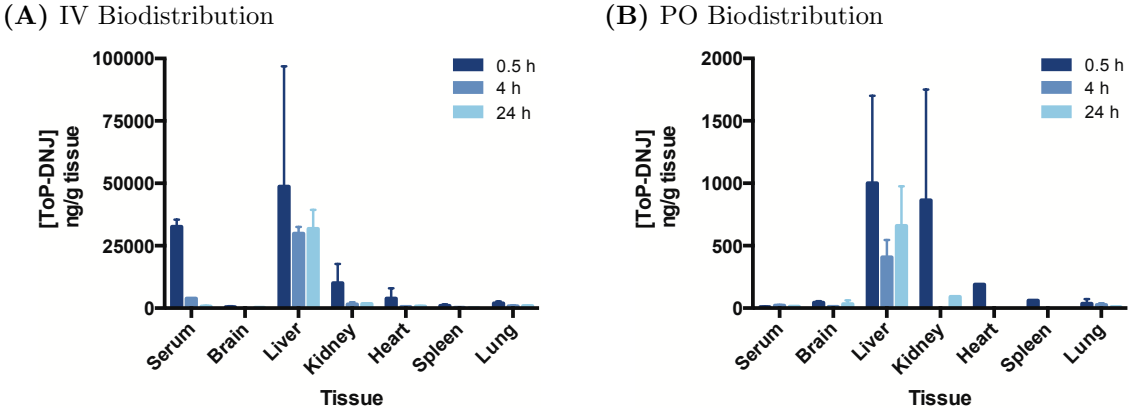

Figure 6.19: *Mouse Biodistribution of ToP-DNJ.* Mice were treated with a single dose of ToP-DNJ either by oral gavage (PO, 10 mg/kg) or by IV (2 mg/kg). The mice were sacrificed at 30 min, 4 h, and 24 h after ToP-DNJ administration, and the indicated tissues homogenized and analyzed for ToP-DNJ by HPLC. *Data collected by SAI Life Sciences Ltd.*

6.10 Conclusions and Future Directions

Conjugating vitamin E to an iminosugar gave rise to an iminosugar with a promising and unexpected profile of biological activity. Although lengthening the alkyl chain has generally been synonymous with increased inhibition of glucosidases and increased toxicity, ToP-DNJ displays potent inhibition of glycolipid, rather than glycoprotein, processing pathways. ER α-glucosidase inhibition effects were found to be cell type dependent, and selective for the second reaction of ER GluII in those cell lines where it was observed. The effected cell types (primary human MDMΦ and HL60) are both immune cells of the myeloid lineage. This might indicated that ToP-DNJ is specific to this class. To investigate this, further studies of other cell types (other myeloid immune cells, lymphoid immune cells and non-immune cells) are currently under way.

Comparative DENV studies in two different cell lines reinforced the concept that the inhibition of DENV by iminosugars is driven by inhibition of the ER α-glucosidases, with the antiviral effect only observed in MDMΦ, where ToP-DNJ induced FOS. Because there were only monoglucosylated species and neither di- nor triglucosylated species observed by FOS analysis, this suggests that inhibition of ER GluII alone is sufficient to induce an anti-DENV effect. It is unclear whether the lack of diglucosylated species is due to a selective inhibition by ToP-DNJ or reflects the kinetics of glycan processing in the ER. Inhibition studies with the isolated enzyme are being performed in order to try and tease out this information. If ToP-DNJ is truly selective for inhibiting only the second hydrolysis catalyzed by ER GluII, it could prove to be a useful tool in biological experiments, trapping glycans at the stage where they may interact with CNX/CRT. Regardless of whether it inhibits only the second reaction or both of ER Glu II, identification of this enzyme as antiviral without inhibition of ER Glu I allows for targeting of future antivirals to a single enzyme, and ToP-DNJ serves as a starting point for studies of the iminosugar structural requirements for this specificity.

The lack of an antiviral effect by ToP-DNJ with respect to BVDV and HCV suggests that it is not a p7 inhibitor.

The influence of ToP-DNJ has been demonstrated to extend beyond attenuating the amount of glycosphingolipids, with a demonstrated functional effect- interference with lipid rafts. Direct observations of the plasma membrane were made that show drug treatment increased the diffusion speed of SM without influencing the rate of diffusion for PC. To better characterize the effect as either mechanical or metabolic, treatment time courses are under way. By performing a drug titration, data may also be correlated with the planned measurements of GlcCer levels to elucidate the mechanism of lipid nanodomain disruption more fully.

Given the dependence of HCV in particular on lipid rafts, as well as the presence of receptors for HIV and DENV in lipid rafts, the lack of antiviral effect of ToP-DNJ towards these viruses is perhaps unexpected. However, glycolipid turnover rates are known to be growth dependent and as slow as several days.[151] It is possible that the design of the antiviral assays means that by the time glycolipid turnover has taken place at the plasma membrane, the infection level is already so high that the effect of the drug is not statistically significant. Indeed, the promising results in antiviral assays of HBV, HCV and HIV after pretreatment with ToP-DNJ suggest that there is an antiviral effect of the drug that is not achieved with treatment post infection. Further pretreatment studies, as well as antiviral assays with lower initial MOI will provide more clarity about the nature of this prophylactic effect.

ToP-DNJ is simply the beginning. In order to fully understand the structure-activity relationships of ToP-DNJ with its inhibitory targets, analogues will have to be synthesized and tested, varying the iminosugar, linker and conjugate. Incorporating the knowledge from investigations of iminosugar stereochemistry (Chapter 5), a ToP-iminosugar with L-*ido* or L-*talo* stereochemistry could be prepared with potentially higher potency, and as different stereochemistries seem to give different selectivity for catabolism vs. anabolism inhibition, activity could also be tailored in this way to increase antiviral and reduce potentially proviral effects.

One of the biggest difficulties in working with ToP-DNJ has been its low solubility in aqueous media. In this regard, variations in the linker hold the most promise as DNJ and D-α-tocopherol are each soluble in water by themselves. By incorporating hydrogen bond donors and acceptors, for example ethers or amines, it is possible that higher solubility in water will be obtained. The introduction of these heteroatoms also opens the possibility of tuning the pK_a of the endocyclic nitrogen atom, a quality that could influence its inhibition in the acidic environment of the lysozyme where the affected β-glucosidase resides.

Mirroring the lack of solubility in cell culture media, ToP-DNJ had poor bioavailability when administered orally. In this instance, as an alternative to analoguing the iminosugar, absorption could potentially be improved by administering with a lipid-rich meal. Despite the poor bioavailability, the desired effect of directing the iminosugar to the liver with α-tocopherol was successful, and the serum half-life of the drug improved more than 3-fold over other members of the iminosugar class. Given this influence of the tocopherol, subsequent studies to investigate the interaction of ToP-DNJ with tocopherol receptors (α-TTP, SR-BI, LDLr and NPC1-L1) will be important for understanding if it is mimicry of the natural lipid or some other mechanism that imparts these pharmacological improvements to the drug.

With regard to conjugation, opportunity lies both in using natural analogues of the tocopherol studied here, with variations in the methylation of the chroman as well as the stereochemistry and saturation of the isoprene side chain.

As noted after characterizing the enzymatic inhibition profile of ToP-DNJ, it represents not simply an iminosugar, but perhaps more accurately an iminoglycolipid. With this thought in mind, conjugation of full membrane components to iminosugars and subtle blends of these two classes of natural products represent a novel avenue for further research.

6.11 Biological Materials and Methods

MTS viability, HCV, DENV, and BVDV antiviral assays were carried out according to the procedures described in §4.8, with the exception that the $TCID_{50}$ assay to analyze the HCV pretreatment employed eight 2-fold dilutions of the analyte beginning at a $1{:}10^{2.5}$ dilution.

6.11.1 DENV MDMΦ Assay

Primary human MDMΦ were generated from human monocytes isolated from buffy coats (NHS Blood and Transplant, surplus to clinical requirements) as described previously[372] and incubated with 25 ng/mL recombinant human interleukin-4 (Peprotech) for 3 days prior to DENV infection to enhance their susceptibility to DENV infection. The use of human blood was approved by the NHS National Research Ethics Service (09/H0606/3).

MDMΦ cells were inoculated for 2 h with DENV2 16681 strain at an MOI of 1. The inoculum was removed and replaced with X-VIVO media (Cambrex) supplemented with 1% autologous human plasma and the drug treatment at the indicated concentration or untreated in triplicate, and the infected cells were incubated with drug for 2 d. The supernatant was harvested and stored at –80 °C until analysis by plaque assay (§4.8.6.2)

6.11.2 ApoToxGlo Assay

The ApoToxGlo Assay (Promega) was performed according to the manufacturer's instructions on MDMΦ seeded in a sterile 96-well plate at 2×10^5 cells/well in 200 µL of supplemented with 1% autologous human plasma and the drug treatment at the indicated concentration in triplicate. As controls, wells with 200 µL growth media with and without cells were also included in triplicate.

6.11.3 BVDV qRT-PCR Assay

Viral RNA was extracted from 140 µL of supernatant using the QIAamp Viral RNA Mini Kit (Qiagen) as per manufacturer's instructions. The extracted RNA was treated with 5 U DNase I (Roche), incubating at 37 °C for 1 h, followed by inactivation at 80 °C for 20 min. qRT-PCR was set up (Table 6.4) using QuantiTect SYBR® Green RT-PCR kit (Qiagen) and two primers for the NS2 coding sequence: forward primer (NS2-F), 5′-TAG GGC AAA CCA TCT GGA AG-3′; reverse primer (NS2-R), 5′-ACT TGG AGC TAC AGG CCT CA-3′. The RT step was effected by incubation at 50 °C, for 30 min. The hot start polymerase was activated by incubation at 95 °C for 15 min. The DNA was then amplified by PCR (35 cycles of 95 °C for 15 s, 50 °C for 1 min, 72 °C for 1 min; final extension at 72 °C for 7 min) on a DNA Engine Opticon® 2 System (Bio-Rad). Melting curves were measured once every 1 °C for 45 – 95 °C, holding at each temperature for 1 s.

Table 6.4: *BVDV qRT-PCR Reaction Preparation*

Component	1× Reaction (µL)
2× SYBR Green Mastermix	12.5
NS2-F (100 µM)	0.125
NS2-R (100 µM)	0.125
RT Mix	0.25
H_2O	2.5
RNA Analyte	10
Total Volume	25

To normalize the amount of viral RNA between experiments, 140 µL of 1×10^7 ffu/mL was extracted with the QIAamp Viral RNA Mini Kit as described for supernatants. 6 serial 10-fold dilutions were prepared from the isolated RNA, and the 7 standards, together with a H_2O-only blank were included in duplicate on every qRT-PCR plate to produce a standard curve.

6.11.4 Lipidomics

Experiments were carried out starting with either naive Huh7.5 or cells of the same cell line infected with Jc1 HCV at a level of 90% as measured by IF. The cells were seeded at 3×10^5 cells/flask in 25 cm^2 tissue culture flasks in 6 mL of growth media supplemented with the indicated treatment (either untreated or 10 µM ToP-DNJ). After 96 h, the supernatant was removed, and the cells washed twice with PBS and lifted with trypsin + EDTA, which was then diluted with DMEM + 10% FCS. The cells were pelleted (290 × *g*, 5 min, 4 °C) and resuspended twice with DMEM + 10% FCS. The cells were subsequently pelleted (290 × *g*, 10 min, 4 °C) and resuspended with PBS (10 mL) three times. 250 µL of the PBS-suspended cells was set aside for Bradford assay, and the remainder pelleted (290 × *g*, 10 min, 4 °C). The pellet was resuspended in 1 mL of 1:1 MeOH:acetone and submitted to Prof. C. Wolf for lipidomic study.[346–353]

In addition to the results discussed in the chapter, the complete lipidomic report is included in Appendix D.

6.11.5 Bradford Assay

The sample to be assayed for protein was subjected to three freeze-thaw cycles to effect cell lysis. 10 µL of analyte was diluted in 140 µL of H_2O in a well of a clear-bottom 96-well plate, with triplicate wells evaluated for each sample. A standard curve of BSA (20, 15, 10, 5 and 2.5 µg/mL) was prepared and treated identically to analytes. Immediately before plate reading, 150 µL of Bradford Quick Start Reagent (Bio-Rad) was added to each well, and the absorbance read at 595 and 450 nm. The ratio of absorbances (A_{595}/A_{450}) was calculated and used to determine protein concentration.

6.11.6 Fluorescence Correlation Spectroscopy

Huh7.5 cells were seeded at 3×10^5 cells/flask in 25 cm^2 tissue culture flasks in 6 mL of growth media supplemented with the indicated treatment (untreated, 10 µM ToP-DNJ, 10 µM D-α-tocopherol, or 0.2 % DMSO). After 72 h, the supernatant was collected and the cells were scraped and resuspended in 4 mL of PBS. 6×10^5 cells were pelleted and resuspended in their original supernatant, and plated in triplicate onto sterile microscope slides (25 mm diameter, No. 1 thickness, Marienfeld) in a sterile 6-well plate. The cells were allowed to adhere for 18 h before addition of labelled lipid and measuring as previously described.[373;374]

6.12 Selected Synthesis Experimental Data

For general synthetic procedures, see Section 4.9.

All tabulated NMR spectra described in this section may be found in Appendix F.

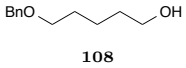

108

5-(benzyloxy)pentan-1-ol 108: 1,5-pentanediol **107** (2.10 mL, 20.0 mmol, 1.0 equiv) was dissolved in CH_2Cl_2 (100 mL). Ag_2O (6.95 g, 30.0 mmol, 1.5 equiv) and BnBr (2.62 mL, 22.0 mmol, 1.1 equiv) were added to the solution sequentially. The flask was wrapped with aluminium foil, and the solution was stirred at room temperature for 18 h. The solution was filtered through a pad of Celite, eluting with CH_2Cl_2, and concentrated under reduced pressure. The residue was purified by flash column chromatography (silica gel, EtOAc:pet ether) = 3:17 → 1:1) to give alcohol **108** as a colorless oil. **108**: ^{1}H NMR (500 MHz, $CDCl_3$): δ = 7.37 – 7.26 (m, 5 H), 4.50 (s, 2 H), 3.64 (t, J = 6.5 Hz, 2 H), 3.49 (t, J = 6.5 Hz, 2 H), 1.70 – 1.63 (m, 2 H), 1.62 – 1.55 (m, 2 H), 1.50 – 1.42 (m, 2 H), 1.34 (br s, 1 H) ppm; ^{13}C NMR (125 MHz, $CDCl_3$): δ = 138.8, 128.6, 127.8, 127.7, 73.2, 70.5, 63.1, 32.8, 29.7, 22.7 ppm; LRMS (ESI): 217 ($C_{12}H_{18}O_2$ + Na^+).

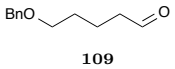

109

5-(benzyloxy)pentanal 109: Alcohol **108** (assumed 20.0 mmol) was dissolved in CH_2Cl_2 (100 mL). Dess–Martin periodinane (8.70 g, 20.5 mmol, 1 equiv) was added, and the resulting solution stirred at room temperature for 18 h. The reaction mixture was then diluted with sat. aq. $NaHCO_3$ (50 mL) and sat. aq. NaS_2O_3 (50 mL). The layers were separated, and the aqueous layer extracted with CH_2Cl_2 (2 × 100 mL). The combined organic layers were washed with sat. aq. $NaHCO_3$ (100 mL) and brine (2 × 100 mL), dried ($MgSO_4$), filtered, and concentrated under reduced pressure. The residue was purified by flash column chromatography (silica gel, EtOAc:pet ether = 1:2 → 2:3) to give aldehyde **109** (2.85 g, 14.8 mmol, 75% yield from **107**) as a colorless oil. **109**: ^{1}H NMR (500 MHz, $CDCl_3$): δ = 9.76 (t, J = 1.7 Hz, 1 H), 7.37 – 7.26 (m, 5 H), 4.50 (s, 2 H), 3.49 (t, J = 6.2 Hz, 2 H), 2.46 (td, J = 7.2, 1.8 Hz, 2 H), 1.79 – 1.71 (m, 2

H), 1.70 – 1.61 (m, 2 H) ppm; ^{13}C NMR (125 MHz, $CDCl_3$): δ = 202.6, 138.7, 128.6, 127.84, 127.79, 73.2, 70.0, 43.8, 29.4, 19.2 ppm; LRMS (ESI): 215 ($C_{12}H_{16}O_2$ + Na^+).

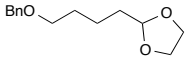

110

2-(4-(benzyloxy)butyl)-1,3-dioxolane 110: Aldehyde **109** (2.85 g, 14.8 mmol, 1.0 equiv) was dissolved in benzene (130 mL). Ethylene glycol (1.1 mL, 19.7 mmol, 1.33 equiv) and TsOH (catalytic) were added. The solution was heated at reflux with a Dean–Stark apparatus for 12 h. The solution was then cooled to room temperature and diluted with sat. aq. $NaHCO_3$ (100 mL) and CH_2Cl_2 (300 mL). The layers were separated, and the aqueous layer was extracted with CH_2Cl_2 (2 × 100 mL). The combined organic layers were then dried (Na_2SO_4), filtered and concentrated under reduced pressure. The residue was purified by flash column chromatography (silica gel, EtOAc:pet ether = 1:9 → 3:17) to give acetal **110** (2.49 g, 10.5 mmol, 71% yield) as a colorless oil. **110**: R_f = 0.43 (silica gel, EtOAc:pet ether = 1:2); ^{1}H NMR (500 MHz, $CDCl_3$): δ = 7.37 – 7.26 (m, 5 H), 4.86 (t, J = 4.8 Hz, 1H), 4.50 (s, 2 H), 4.00 – 3.92 (m, 2 H), 3.88 – 3.81 (m, 2 H), 3.48 (t, J = 6.6 Hz, 2 H), 1.72 – 1.64 (m, 4 H), 1.57 – 1.48 (m, 2 H) ppm; ^{13}C NMR (125 MHz, $CDCl_3$): δ = 138.9, 128.5, 127.8, 127.7, 104.8, 104.7, 73.1, 70.5, 65.1, 33.9, 29.9, 21.0 ppm; LRMS (ESI): 259 ($C_{14}H_{20}O_3$ + Na^+).

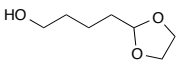

111

4-(1,3-dioxolan-2-yl)butan-1-ol 111: Benzyl ether **110** (2.00 g, 8.46 mmol, 1.0 equiv) was dissolved under argon in 1,4-dioxane (20 mL). Pd/C (10% Pd, 50 mg, 2.5 weight-%) was added. The mixture was purged with argon, and subsequently with H_2. The mixture was stirred at room temperature for 16 h. The solution was filtered (GF/C glass microfiber) and concentrated under reduced pressure to give alcohol **111** (1.24 g, 8.46 mmol, 100% yield) as a clear, colorless oil which was used in the next step without further purification. **111**: R_f = 0.27 (silica gel, EtOAc:pet ether = 3:1); ^{1}H NMR (500 MHz, $CDCl_3$): δ = 4.86 (t, J = 4.7 Hz, 1 H), 4.00 – 3.91 (m, 2 H), 3.90 – 3.80 (m, 2 H), 3.65 (t, J = 6.5 Hz, 2 H), 1.74 – 1.66 (m, 2 H), 1.66 – 1.58 (m, 2 H), 1.56 – 1.46 (m, 2 H), 1.40 (br s, 1 H) ppm; LRMS (ESI): 169 ($C_7H_{14}O_3$ + Na^+).

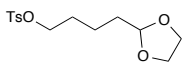

106

4-(1,3-dioxolan-2-yl)butyl 4-methylbenzenesulfonate 106: To a stirred solution of **111** (0.50 g, 3.4 mmol, 1.0 equiv) in CH_2Cl_2 (50 mL) at room temperature was added Et_3N (0.62 mL, 4.4 mmol, 1.3 equiv) followed by TsCl (0.71 g, 3.7 mmol, 1.1 equiv) and DMAP (50 mg, 0.4 mmol, 0.1 equiv). The resulting mixture was stirred at the same temperature for 8 h. The mixture was diluted with CH_2Cl_2 (100 mL) washed with sat. aq. $NaHCO_3$ (100 mL) and brine (2 × 100 mL), dried ($MgSO_4$), filtered, and concentrated under reduced pressure to give tosylate **106**. While concentrating, the temperature was maintained below 40 °C, as the compound has been reported as unstable above this temperature.[375] Due to this instability, the compound was immediately used in the next step. **106**: R_f = 0.29 (silica gel, EtOAc:pet ether = 1:3); ^{1}H NMR (500 MHz, $CDCl_3$): δ = 7.79 (d, J = 8.3 Hz, 2 H), 7.34 (d, J = 8.4 Hz, 2 H), 4.80 (t, J = 4.6 Hz, 1 H), 4.03 (t, J = 6.5 Hz, 2 H), 3.96 – 3.88 (m, 2 H), 3.87 – 3.78 (m, 2 H), 2.45 (s, 3 H), 1.75 – 1.65 (m, 2 H), 1.65 – 1.57 (m, 2 H), 1.50 – 1.41 (m, 2 H) ppm; ^{13}C NMR (125 MHz, $CDCl_3$): δ = 144.9, 133.5, 130.0, 128.1, 104.4, 70.6, 65.1, 33.3, 29.0, 20.1, 14.4 ppm; LRMS (ESI): 323 ($C_{14}H_{20}O_5S$ + Na^+).

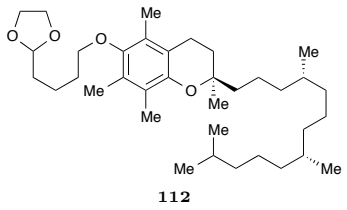

112

(*R*)-6-(4-(1,3-dioxolan-2-yl)butoxy)-2,5,7,8-tetramethyl-2-((4*R*, 8*R*)-4,8,12-trimethyltridecyl)chroman 112: To a stirred solution of D-α-tocopherol (1.54 g, 3.6 mmol, 1.1 equiv) in DMF (30 mL) at 0 °C (ice/water bath) was added NaH (60% in mineral oil, 0.30 g, 7.5 mmol, 2.2 equiv) in a single portion. After H_2 gas was no longer being visibly evolved, the cooling bath was removed, and the mixture stirred at room temperature for 1 h. A solution of **106** (crude from previous step, assumed 3.4 mmol, 1.0 equiv) in DMF (10 mL) was added to the reaction mixture at room temperature. The mixture was stirred at 80 °C for 20 h. Solvent was removed by coevaporation with toluene (3 × 50 mL). The residue was taken up in EtOAc (250 mL). The solution was then washed with sat. aq. $NaHCO_3$ (50 mL) and brine (50 mL). The combined aqueous fractions were extracted with EtOAc (2 × 50 mL). The combined organic fractions were then

dried ($MgSO_4$), filtered, and concentrated under reduced pressure. The residue was purified by flash column chromatography (silica gel, pet ether → EtOAc:pet ether = 1:9) to give **112** (1.65 g, 3.0 mmol, 86% yield) as a colorless oil. **112**: $R_f = 0.26$ (silica gel, EtOAc:pet ether = 1:9); ^{1}H NMR (500 MHz, $CDCl_3$): δ = 4.93 (t, J = 4.7 Hz, 1 H), 4.05 – 3.94 (m, 2 H), 3.92 – 3.84 (m, 2 H), 3.68 (t, J = 6.6 Hz, 2 H), 2.60 (t, J = 6.9 Hz, 2 H), 2.20 (s, 3 H), 2.16 (s, 3 H), 2.12 (s, 3 H), 1.93 – 1.05 (m, 29 H), 1.27 (s, 3 H), 0.97 – 0.83 (m, 12 H) ppm; ^{13}C NMR (125 MHz, $CDCl_3$): δ = 148.6, 147.8, 127.9, 125.9, 122.9, 117.6, 104.7, 74.8, 72.9, 65.0, 40.3, 39.6, 37.67, 37.65, 37.6, 37.5, 34.1, 33.0, 32.9, 31.5, 30.4, 28.2, 25.0, 24.6, 24.1, 22.9, 22.8, 21.2, 21.0, 20.8, 19.94, 19.85, 12.9, 12.03, 11.9 ppm; HRMS (ESI): calcd for $C_{36}H_{62}O_4$ [M + H^+]: 559.4721, found 559.4719.

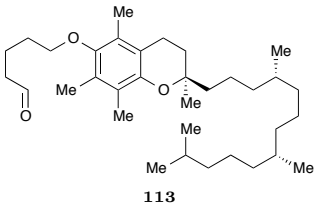

113

5-(((*R*)-2,5,7,8-tetramethyl-2-((4*R*,8*R*)-4,8,12-trimethyltridecyl)chroman-6-yl)oxy)pentanal 113: To a stirred solution of **112** (534.1 mg, 1.03 mmol, 1.0 equiv) in 1,4-dioxane (8 mL) at room temperature was added H_2O (1 mL), followed by addition of $TsOH \cdot H_2O$ (0.40 g, 2.10 mmol, 2.0 equiv) in a single portion. The mixture was stirred at 90 °C. Over the next 2 h, H_2O (2 mL) was slowly added. The mixture was then stirred at 90 °C for a further 3 h. The reaction mixture was quenched with sat. aq. $NaHCO_3$ (15 mL) and then extracted with EtOAc (3 × 20 mL). The combined organic fractions were then dried ($MgSO_4$), filtered, and concentrated under reduced pressure to give **113** (486.5 mg, 1.03 mmol, 99% yield) as a colorless oil which was used directly in the next step. A sample was purified by flash column chromatography (silica gel, EtOAc:pet ether = 1:19 → 13:187) for characterization. **113**: $R_f = 0.26$ (silica gel, EtOAc:pet ether = 1:9); ^{1}H NMR (500 MHz, $CDCl_3$): δ = 9.83 (t, J = 1.6 Hz, 1 H), 3.68 (t, J = 6.1 Hz, 2 H), 2.65 – 2.50 (m, 4 H), 2.19 (s, 3 H), 2.14 (s, 3 H), 2.11 (s, 3 H), 1.98 – 1.72 (m, 6 H), 1.72 – 1.03 (m, 21 H), 1.26 (s, 3 H), 0.96 – 0.82 (m, 12 H) ppm; ^{13}C NMR (125 MHz, $CDCl_3$): δ = 202.3, 148.4, 147.9, 127.9, 125.8, 123.0, 117.7, 74.9, 72.5, 44.0, 40.3, 39.6, 37.68, 37.65, 37.6, 37.5, 33.0, 32.9, 31.5, 30.0, 28.2, 25.0, 24.6,

24.1, 22.9, 22.8, 21.2, 20.9, 19.94, 19.86, 19.3, 12.9, 12.04, 11.96 ppm; HRMS (ESI): calcd for $C_{34}H_{58}NaO_3$ [M + Na^+]: 537.4278, found 537.4268.

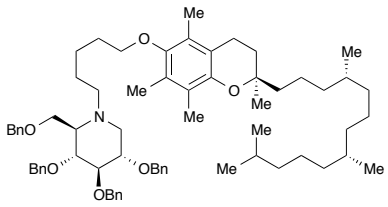

115

2,3,4,6-tetra-*O*-benzyl Top-DNJ 115: To a stirred solution of **114**[337] (277.0 mg, 0.53 mmol, 1.0 equiv) and **113** (408.5 mg, 0.79 mmol, 1.5 equiv) in EtOH (3 mL) at room temperature was added AcOH (0.3 mL), followed by addition of Pd/C (10% Pd, 30 mg, 10 weight-%) in a single portion. The mixture was purged with argon, and subsequently with H_2. The mixture was stirred under H_2 balloon at 60 °C. After 12 h, a further portion of Pd/C (10% Pd, 30 mg, 10 weight-%) was added at room temperature. The reaction mixture was then stirred at 60 °C for a further 36 h. The solution was filtered (GF/A glass microfiber) and concentrated under reduced pressure to give protected Top-DNJ **115** as a clear, colorless oil which was used in the next step without further purification. **115**: HRMS (ESI): calcd for $C_{68}H_{96}NO_6$ [M + H^+]: 1022.7232, found 1022.7260.

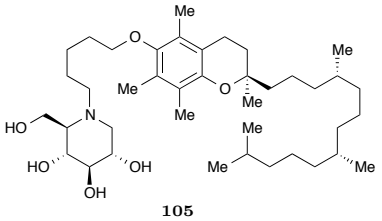

105

Top-DNJ 105: To a stirred solution of **115** (crude from previous step, assumed 0.78 mmol, 1.0 equiv) in 1:1 MeOH:EtOH (50 mL) at room temperature were added cyclohexene (0.8 mL, 7.8 mmol, 10. equiv), HCO_2NH_4 (500 mg, 7.8 mmol, 10. equiv), Pd/C (10% Pd, 200 mg, 25 weight-%), and $Pd(OH)_2$/C (20% $Pd(OH)_2$, 200 mg, 25 weight-%). The mixture was purged with argon, and stirred at reflux for 24 h. Further portions of cyclohexene (0.8 mL, 7.8 mmol, 10. equiv) and HCO_2NH_4 (500 mg, 7.8 mmol, 10. equiv) were added and the reaction mixture stirred at reflux for a further 48 h. The solution was filtered (GF/A glass microfiber), washing the catalyst sequentially with EtOH, MeOH, H_2O, MeOH and EtOH. The combined filtrates were concentrated under reduced pressure. The crude residue was purified by flash column chromatography (silica gel, EtOAc:MeOH = 19:1 → 17:3) to give **105** (56 mg, 8.5 µmol, 11% yield from **113**) as a colorless foam. **105**: ^1H

NMR (500 MHz, CD_3OD): δ = 3.88 (ddd, J = 14.8, 12.1, 2.7 Hz, 2 H), 3.63 (t, J = 6.3 Hz, 2 H), 3.50 (ddd, J = 10.3, 9.2, 4.8 Hz, 1 H), 3.38 (t, J = 9.3 Hz, 1 H), 3.16 (t, J = 9.1 Hz, 1 H), 3.04 (dd, J = 11.2, 4.8 Hz, 1 H), 2.89, (ddd, J = 13.4, 9.3, 6.6 Hz, 1 H), 2.72 – 2.61 (m, 1 H), 2.57 (t, J = 6.8 Hz, 2 H), 2.25 (t, J = 10.9 Hz, 1 H), 2.20 (br d, J = 9.5 Hz, 1 H), 2.13 (s, 3 H), 2.09 (s, 3 H), 2.04 (s, 3 H), 1.87 – 1.67 (m, 4 H), 1.67 – 1.01 (m, 25 H), 1.21 (s, 3 H), 0.93 – 0.79 (m, 12 H) ppm; ^{13}C NMR (125 MHz, CD_3OD): δ = 149.5, 148.9, 128.5, 126.7, 123.7, 118.7, 111.4, 80.4, 75.7, 73.9, 71.9, 70.6, 67.4, 59.3, 57.6, 53.8, 40.63, 40.55, 38.5, 38.4, 38.3, 33.9, 33.7, 32.8, 31.2, 29.1, 25.9, 25.4, 25.33, 25.25, 24.3, 23.2, 23.1, 22.0, 21.6, 20.3, 13.1, 12.2, 12.1 ppm; HRMS (ESI): calcd for $C_{40}H_{72}NO_6$ [M + H^+]: 662.5354, found 662.5349.

I may not have gone where I intended to go,
but I think I have ended up where I needed to be.
—Douglas Adams, *The Long Dark Tea-Time of the Soul*

7
The Way Forward

Throughout Chapters 4 – 6, a variety of different iminosugars have been examined. Collectively, the studies characterized the importance of structural variation in the iminosugar core and the *N*-alkylation for both enzyme inhibition and inhibition of three members of the *Flaviviridae* family: HCV, BVDV, and DENV.

Overall, the data predominantly fall in line with the standard explanation for antiviral effect: inhibition of ER α-glucosidases I and II. All of the D-DNJ compounds studied in Chapter 4 inhibited ER GluII *in vitro* (Table 4.1) and inhibited all three studied viruses in the respective cell culture systems (Figure 4.13). ToP-DNJ further informed the critical nature of this mechanism in that the molecule was only antiviral (Figure 6.11) when tested in cells where it inhibited ER GluII (Figure 6.7). This observation of ToP-DNJ also demonstrated that inhibition of ER GluII alone (i.e. without inhibition of ER GluI) is sufficient to impart an antiviral effect.

Although all D-DNJ compounds inhibited all three viruses, there was more than one trend across the alkylation homologue series, with comparable effect of alkylation against HCV and BVDV, while DENV showed a different pattern. Because the HCV

and DENV antiviral assays were performed in the same (Huh7-Lunet-hCD81-GLuc) cell line, this is unlikely to be due to cellular uptake of the iminosugars, unless the virus itself influences the absorption and distribution of the drug by the cell. Instead these divergent trends are more probably due to differences in the iminosugar mechanism of action. That is to say different effects of the iminosugar create more or less of an antiviral effect in each case.

One possible explanation for the difference is inhibition of the viral ion channel, p7, which is present in HCV and BVDV but not DENV. It is known that *N*B-D-DNJ does not inhibit the viroporin, while *N*N-D-DNJ does. While the intermediate length alkyl iminosugars have never been tested, it is possible that increasing chain length gradually increases p7 inhibition ability, resulting in the observed trend of the D-DNJ series. To confirm this, however, electrophysiology studies with the isolated p7 protein of each virus will need to be performed to see whether then N- pentyl, hexyl, heptyl and octyl iminosugars do indeed disrupt the ion channel.

A second proposed mechanism of anti-HCV and anti-BVDV activity was glycolipid metabolism disruption, as the iminosugars with *N*-butyl or longer alkylation were increasingly more potent at inhibiting enzymes in this pathway than those with shorter alkyl chains. This hypothesis was further strengthened by the fact that *N*N-D-DMJ **95D** and *N*N-D-DTJ **93D** (both inhibitors of the glucosylceramide synthase and glucocerebrosidase) were also found to be antiviral. However, the fact that *N*B-D-DTJ, an inhibitor of glucosylceramide synthase, was not antiviral against any of the three viruses studied, indicated that inhibition of the anabolic pathway does not correlate with antiviral ability. ToP-DNJ **105**, like the *N*-nonyl compounds, potently inhibited both of the glucosylceramide related enzymes, however it demonstrated no antiviral effect against either HCV or BVDV in the same viral assays (Figure 6.12 and Figure 6.13). Overall, the negative antiviral results of ToP-DNJ and *N*B-D-DTJ indicate that it is unlikely the disruption of glycosphingolipid metabolism that leads to the antiviral effect of the other alkyl iminosugars.

While glycolipid disruption does not correlate with antiviral ability in the general assay used, a preliminary prophylactic assay with ToP-DNJ did show an antiviral trend with respect to HCV, HBV and HIV. This indicates that interruption of these pathways could be antiviral but require longer turnover for the metabolic changes to result in the functional antiviral effect. As discussed in Chapter 6, ongoing work with further pretreatment assays will better characterize this effect. A number of the other iminosugars will serve as excellent controls given their selective effect on only the anabolic part of the pathway or complete lack of influence on glycosphingolipids.

Indeed, even the partial library of DNJ stereoisomers prepared so far has resulted in a variety of inhibition profiles. The use of them as controls for glycolipid studies demonstrates the ongoing utility they will have even after initial screening as antiviral compounds. The particular importance of *R*-stereochemistry at C4 for iminopyranose inhibition of α-glucosidases has been identified, while the other stereocenters appear less critical (Table 5.1). In terms of antiviral activity, even before this work, *N*N-D-DNJ was a known inhibitor of HCV, BVDV and DENV (as well as other viruses),[177;178;180] and *N*N-D-DGJ, an inhibitor of HCV and BVDV.[177;180] *N*N-D-DMJ and *N*N-D-DTJ have now been added to this list of antiviral iminosugars (Figure 5.2),

To take advantage of the diversity of antiviral stereochemistries, new synthetic targets can be approached that mimic more than one glycose stereochemistry (Figure 7.1). As the route to the isomers described in Chapter 5 isolates each carbon for manipulation, it serves as a starting point from which these deoxy- and fluoroiminosugars may be prepared. Limited structures from these two classes have been prepared previously, but were examined against neither a large panel of enzymes nor any viruses for inhibition.[376;377] Particularly if iminosugars with separate stereochemistries act by different mechanisms of action, these hybrid isomers could act as a cocktail of the two in a single compound.

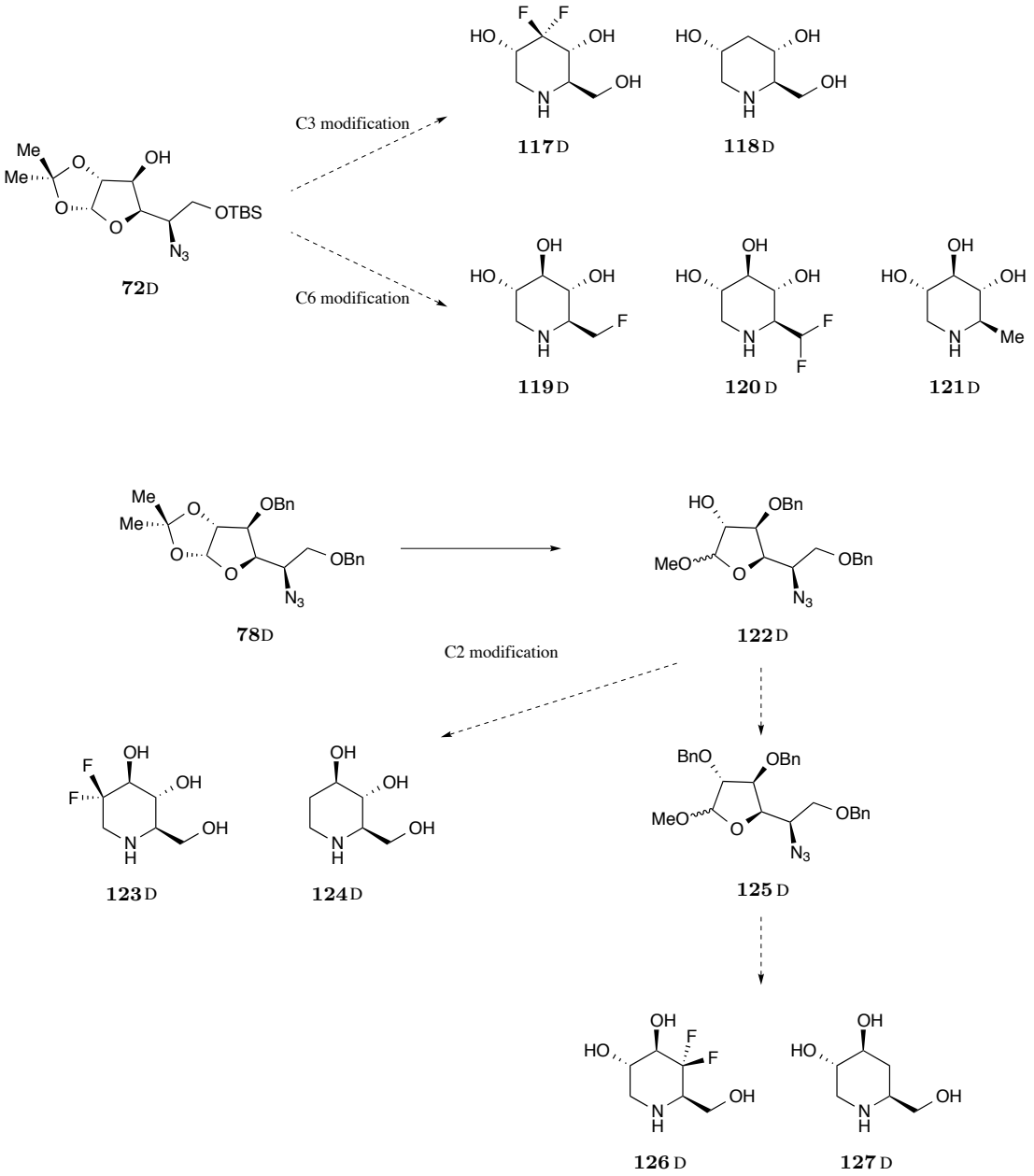

Figure 7.1: *Proposed Deoxy- and Fluoroiminosugar Dual Mimics.* As several iminosugar stereochemistries (D-*gluco*, D-*galacto*, D-*manno*, and D-*talo*) have now been demonstrated to have antiviral properties, iminosugars that inhibit more than a single monosaccharide are now proposed by either removing hydroxylation or replacing a single hydroxyl group with two fluorines. Fluorine is a traditional bioisostere of both hydrogen (having similar size) and of a hydroxyl group (given its electronegative nature and ability to act as hydrogen bond acceptor). Compounds **117D** and **118D** mimic both D-*gluco* and D-*allo* stereochemistry; **123D** and **124D**, D-*gluco* and D-*manno*; **126D** and **127D**, D-*gluco* and D-*galacto*. While C6 is not a stereocenter, performing similar manipulations will both provide insight to the importance of hydroxylation at that carbon atom. Further, because the removal of hydroxylation or introduction of electronegative fluorine will have effects besides those on stereochemistry (*e.g.* influencing the pK_a of the iminosugar), the C6 compounds will serve as useful controls. While all of the examples in this figure show D-*gluco* hybrids, the stereochemical manipulations of Chapter 5 allow for others, such as D-*manno* and D-*talo*.

The first research on iminosugars as antivirals began three decades ago. With the tool of chemical synthesis in hand, iminosugar biological activity becomes less foreboding terrain. By synthesizing carefully designed libraries of compounds and fully characterizing them in terms of biological activity, there will hopefully eventually be sufficient data from which to design a combination of iminosugar head group and alkylation for any specific set of desired biological properties. The structure–activity relationships described herein bring us closer to understanding the mechanisms by which the compounds exert their effects, but much work remains to be done. The structural diversity of the class leaves much of the full spectrum of potential for the iminosugars to be elucidated; however, by continuing the studies commenced here, light can be brought to the furthest corners of the iminosugar landscape.

Appendices

A

Selected NMR Spectra of the Shishijimicin A Carboline Disaccharide Domain and its Precursors

^{1}H spectrum of **16** (600 MHz, DMSO-d_6)

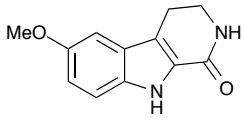

16

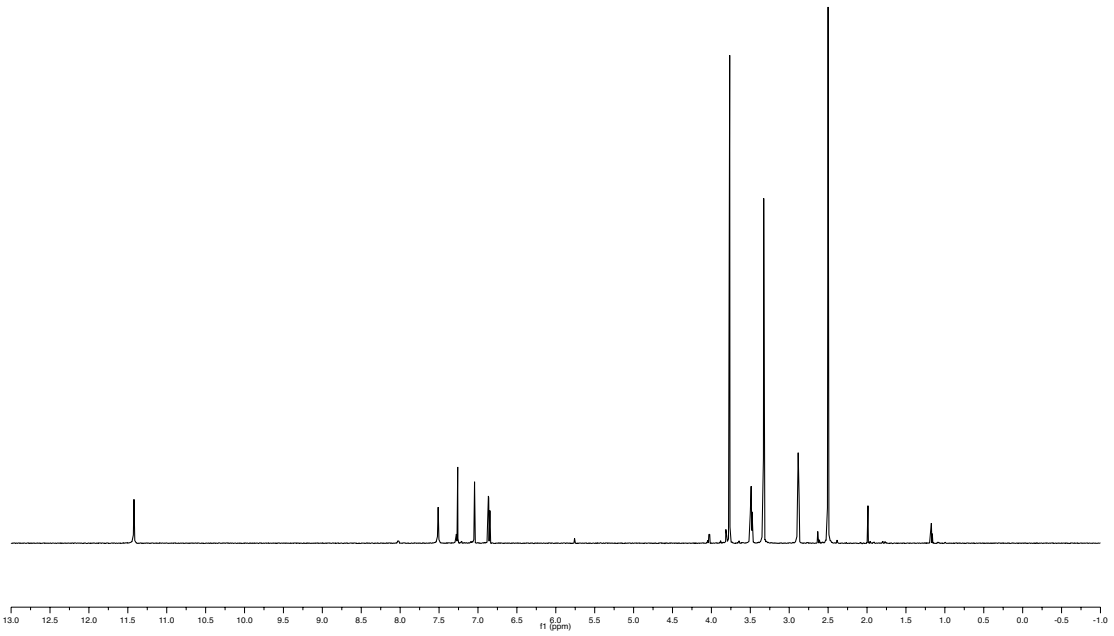

^{13}C spectrum of **16** (150 MHz, DMSO-d_6)

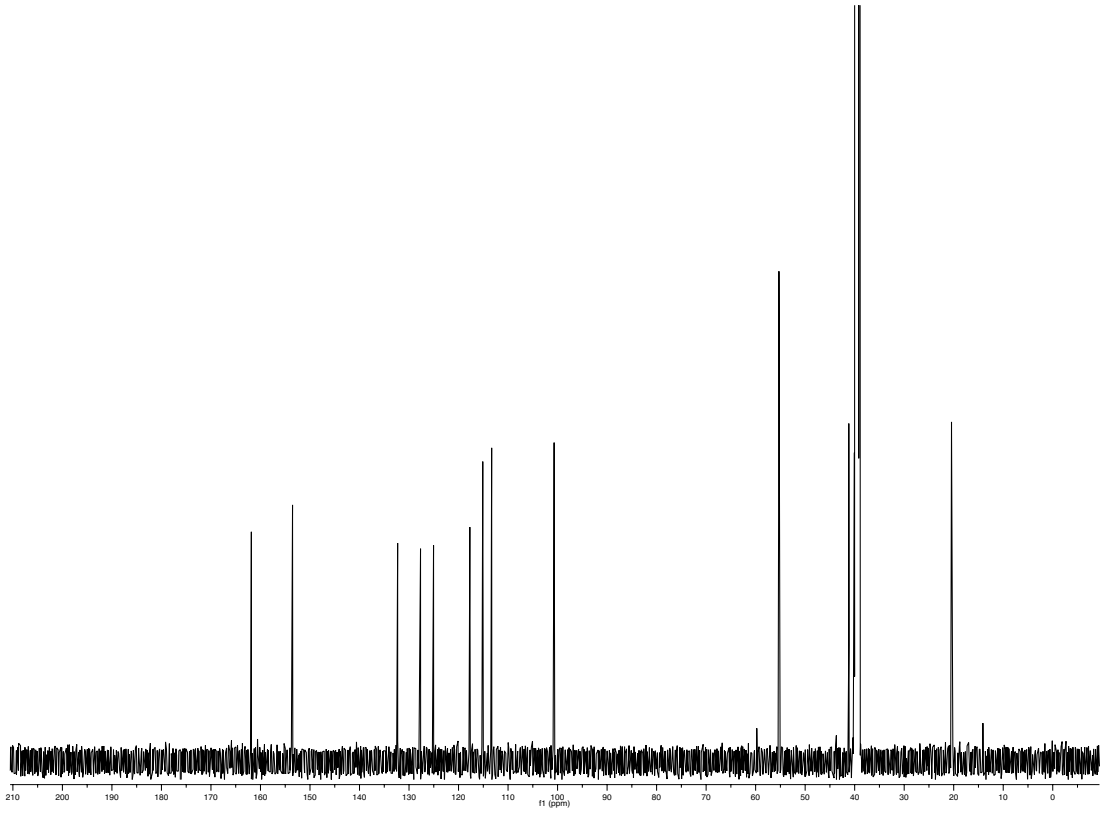

^{1}H spectrum of **17** (500 MHz, DMSO-d_6)

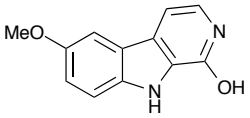

17

^{13}C spectrum of **17** (150 MHz, DMSO-d_6)

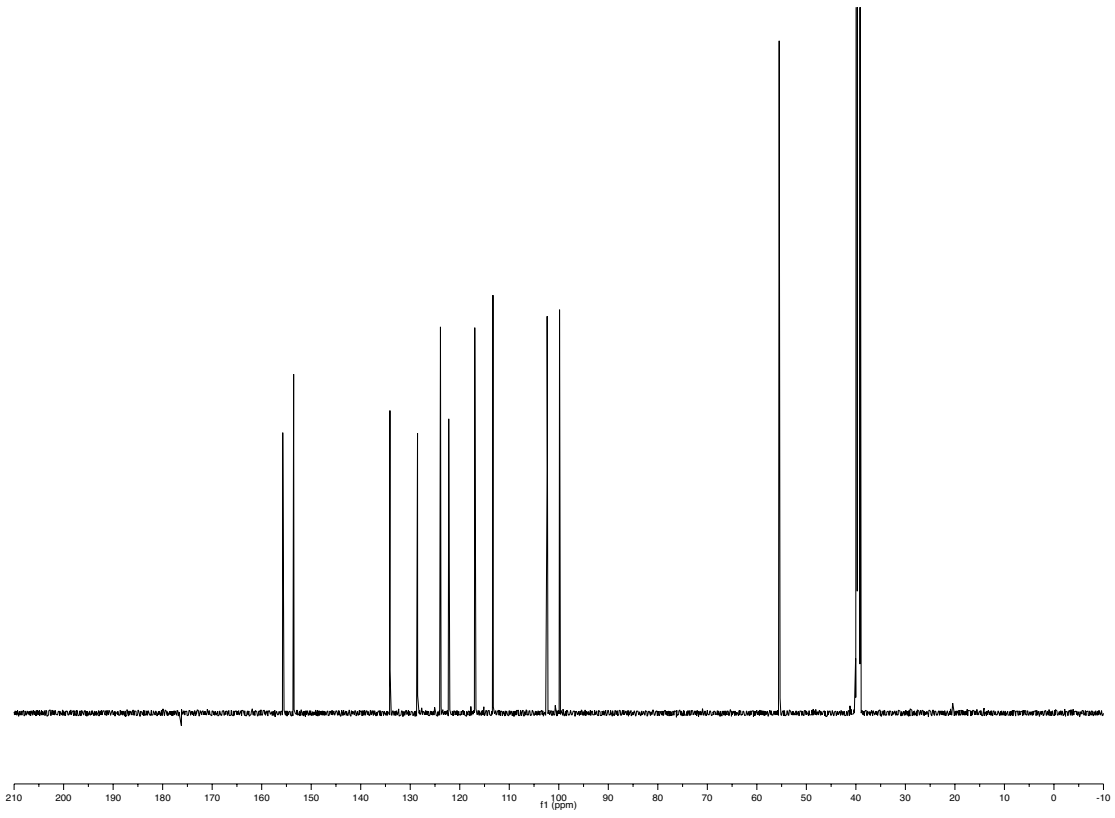

^{1}H spectrum of **18** (600 MHz, C_6D_6)

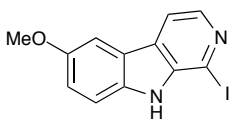

18

^{13}C spectrum of **18** (150 MHz, C_6D_6)

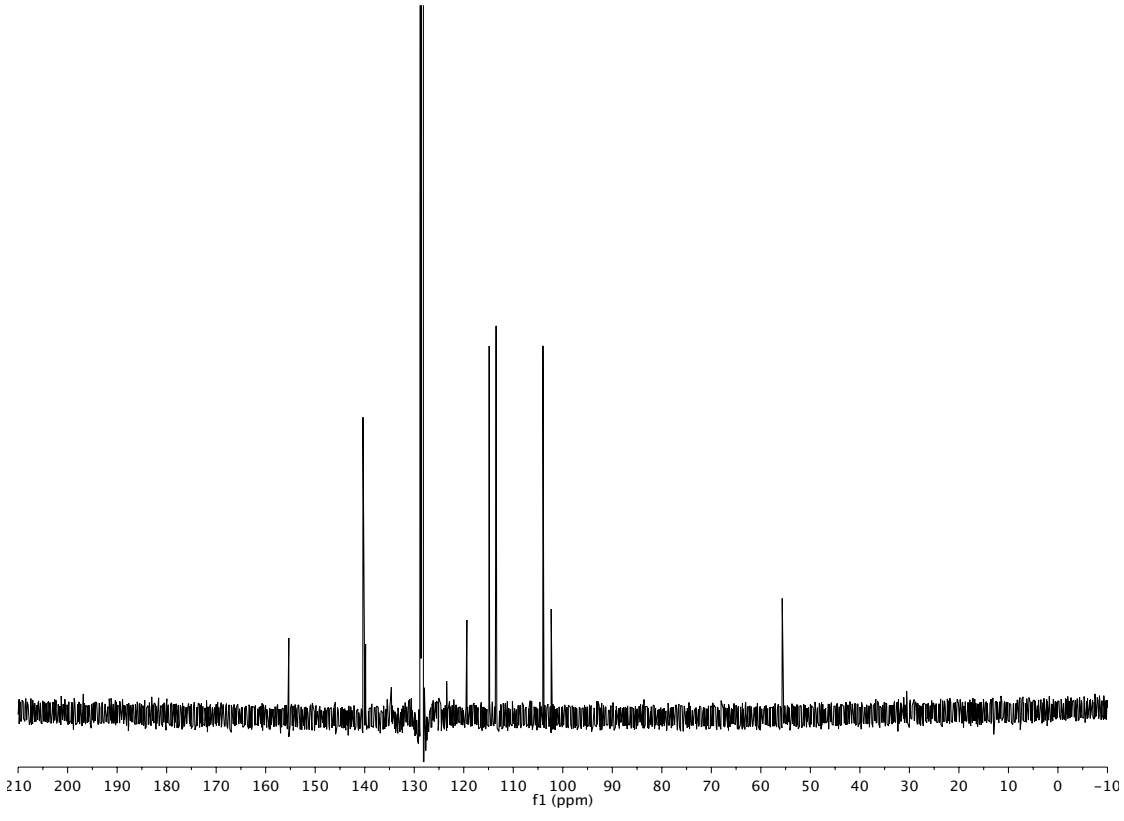

^{1}H spectrum of **12** (400 MHz, C_6D_6)

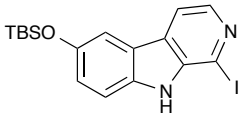

12

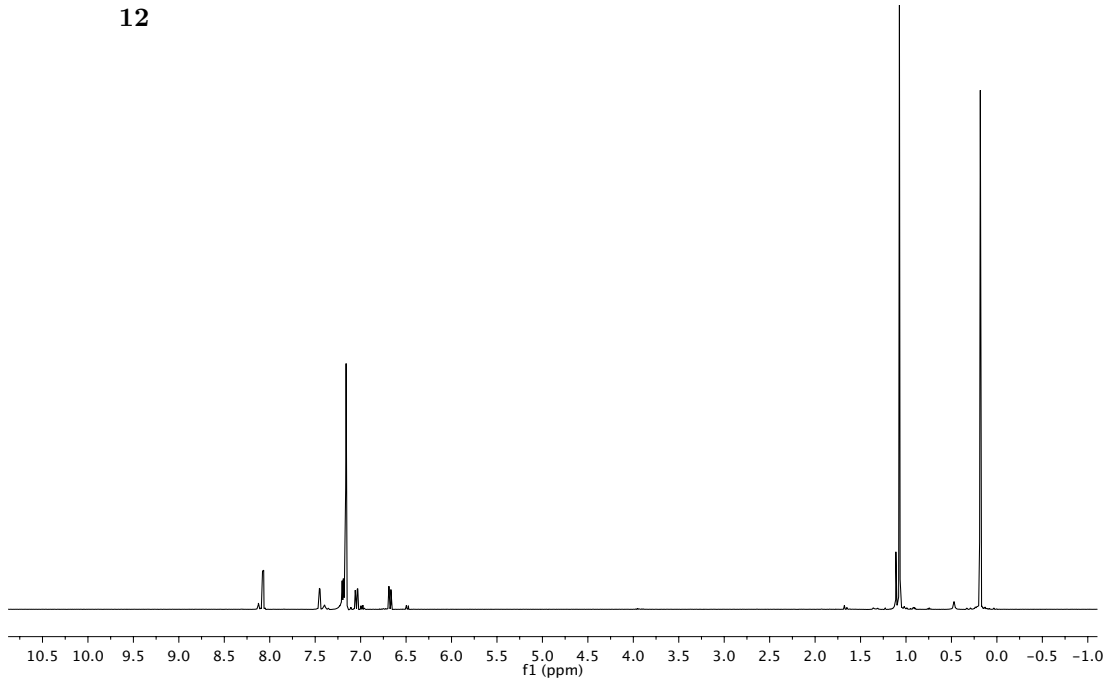

^{13}C spectrum of **12** (100 MHz, C_6D_6)

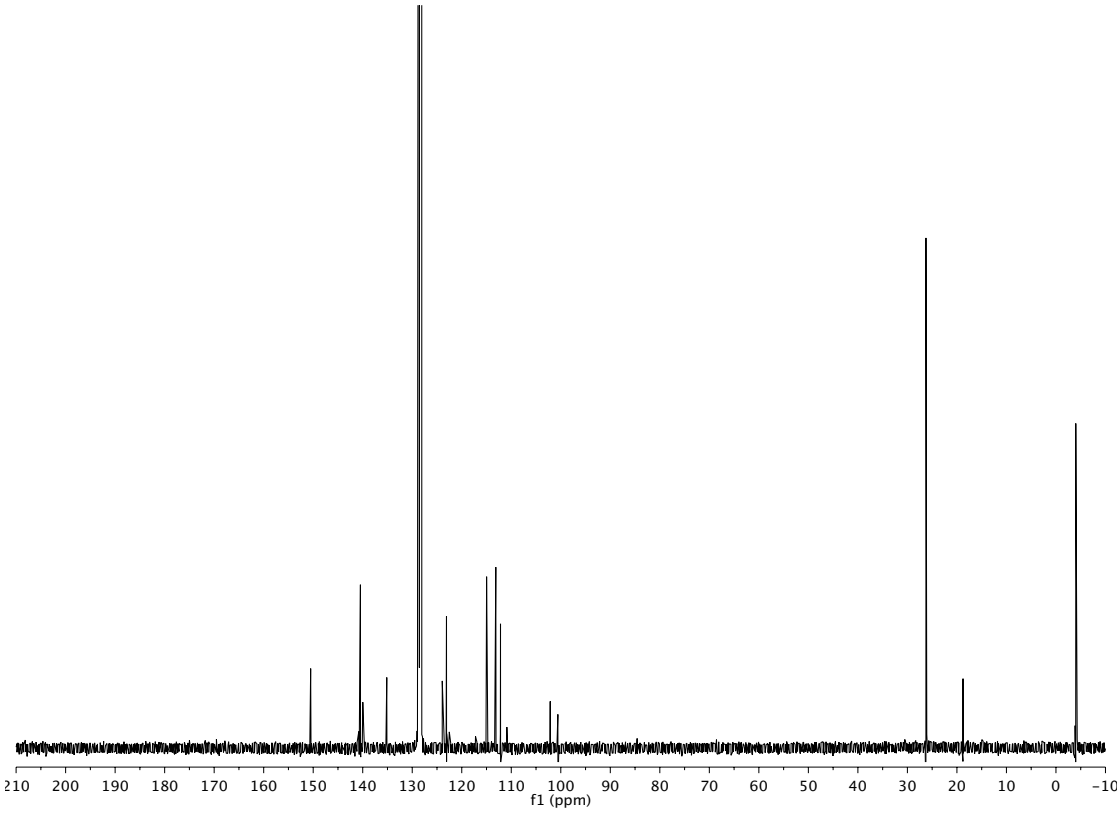

^{1}H spectrum of **20** (400 MHz, $CDCl_3$)

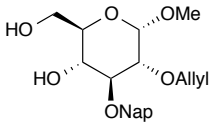

20

^{13}C spectrum of **20** (100 MHz, $CDCl_3$)

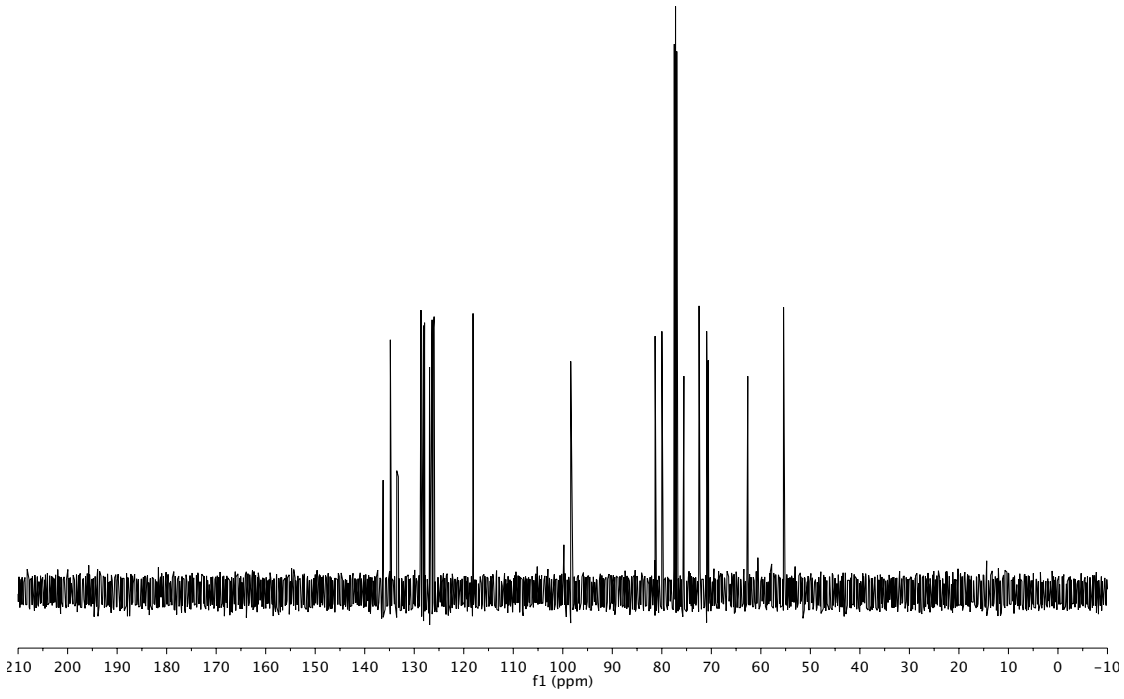

^{1}H spectrum of **21** (500 MHz, $CDCl_3$)

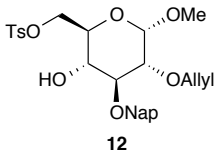

12

^{13}C spectrum of **21** (125 MHz, $CDCl_3$)

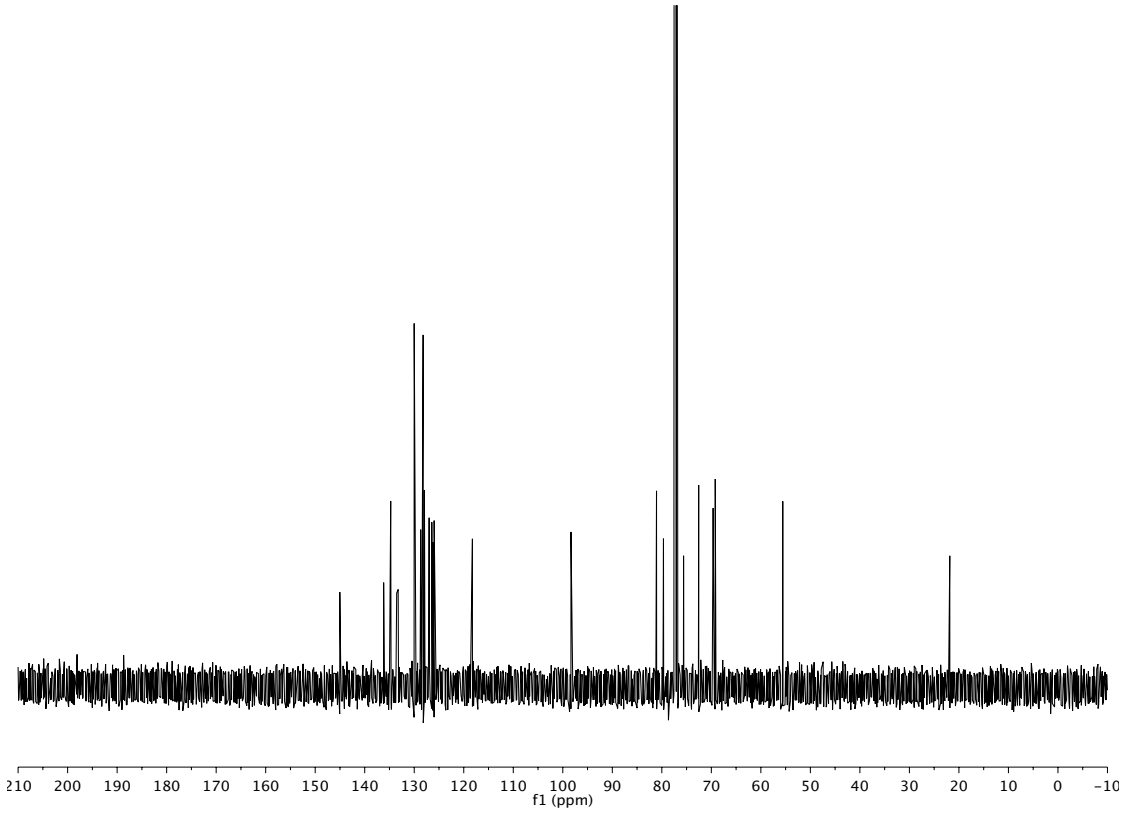

^{1}H spectrum of **22** (500 MHz, $CDCl_3$)

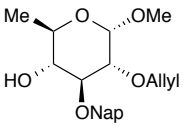

22

^{13}C spectrum of **22** (125 MHz, $CDCl_3$)

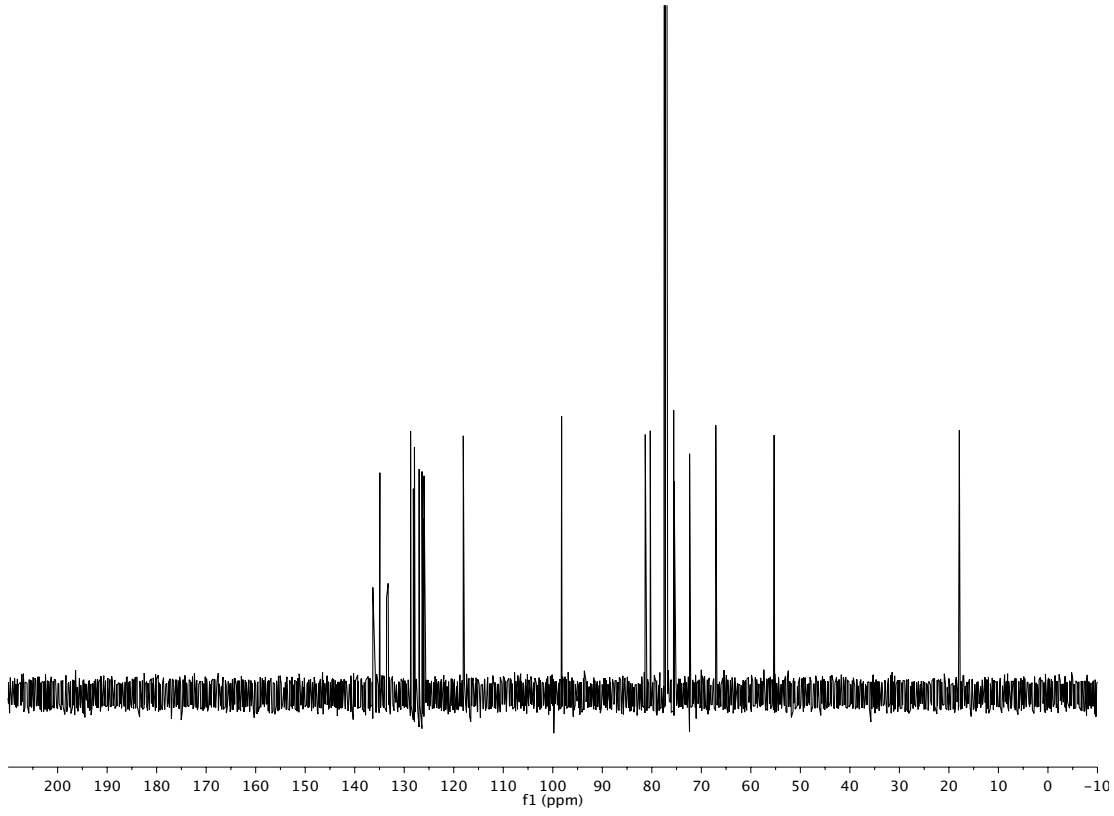

^{1}H spectrum of **23** (600 MHz, $CDCl_3$)

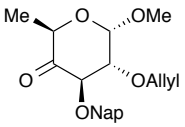

23

^{13}C spectrum of **23** (150 MHz, $CDCl_3$)

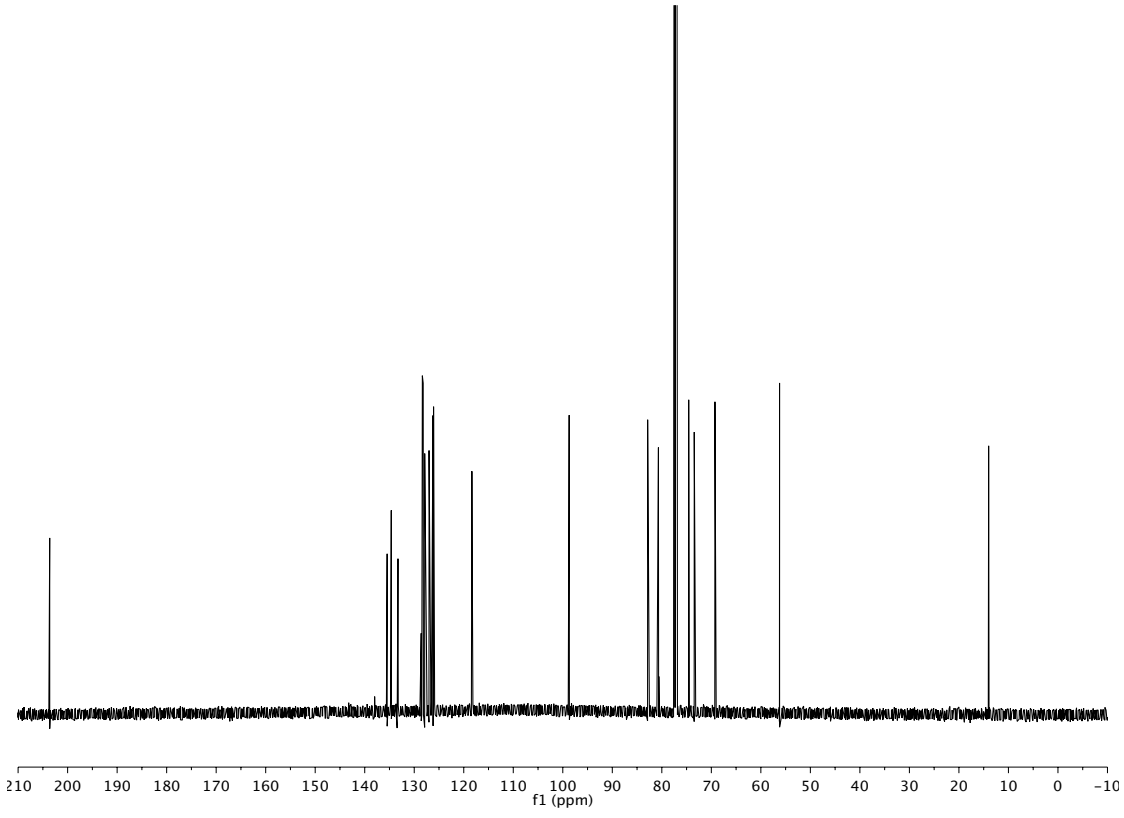

^{1}H spectrum of **24** (600 MHz, $CDCl_3$)

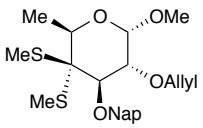

24

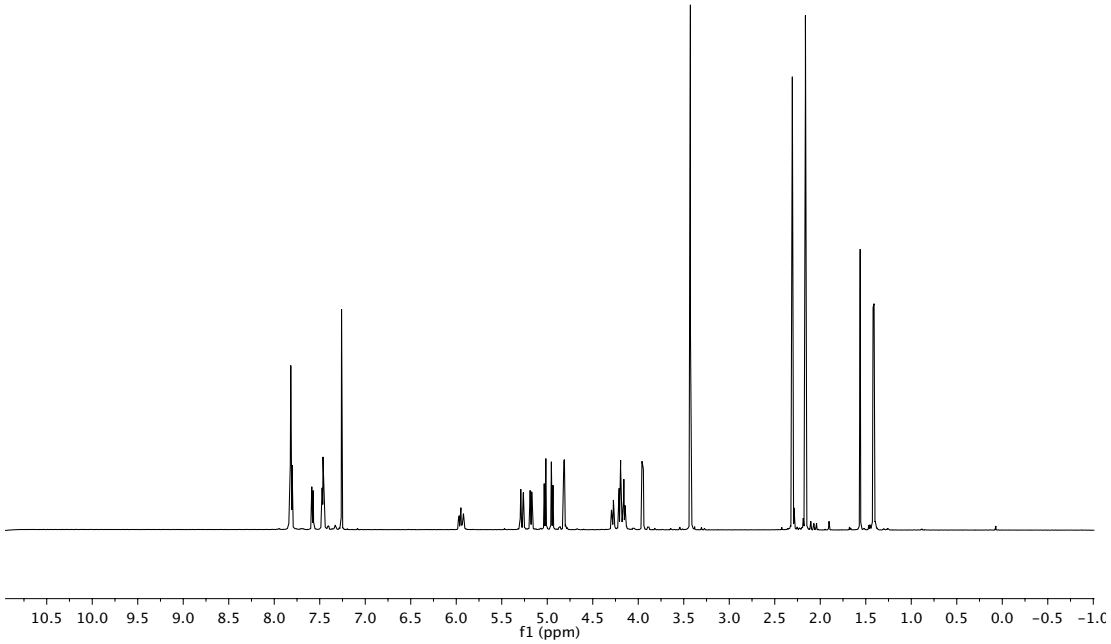

^{13}C spectrum of **24** (150 MHz, $CDCl_3$)

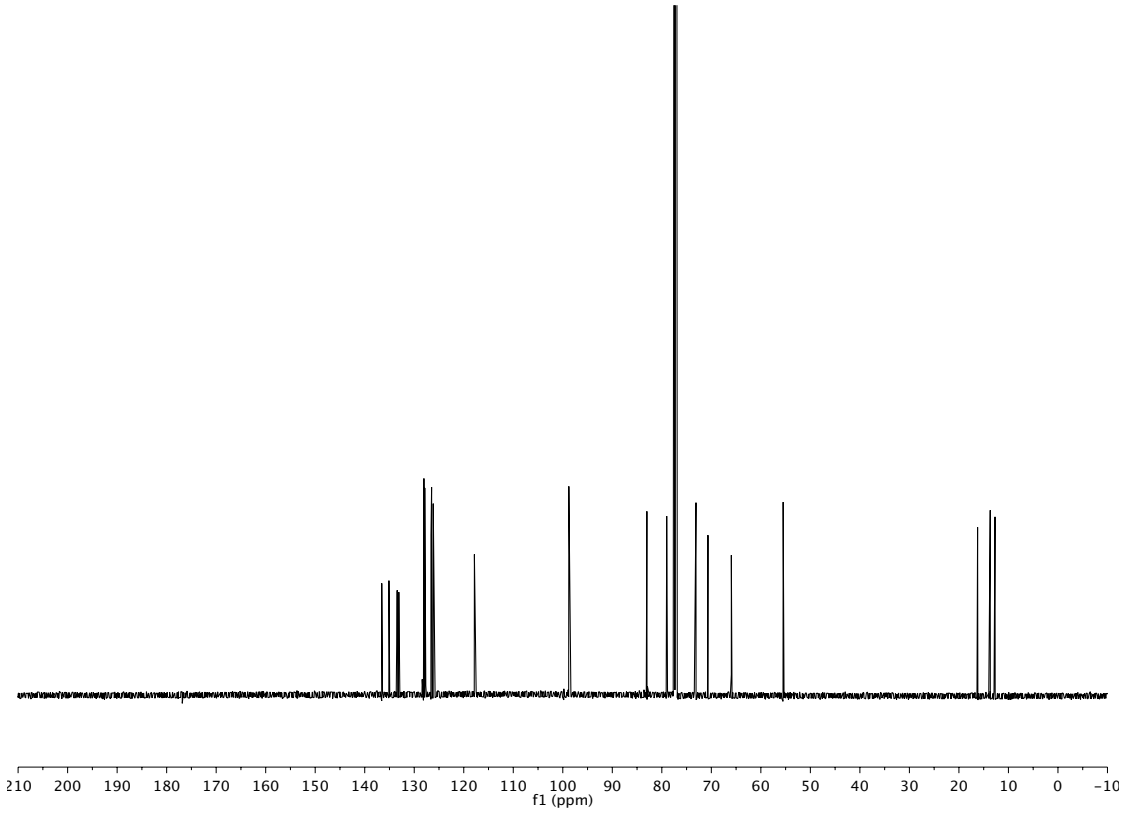

^{1}H spectrum of **25** (600 MHz, $CDCl_3$)

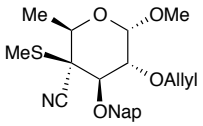

25

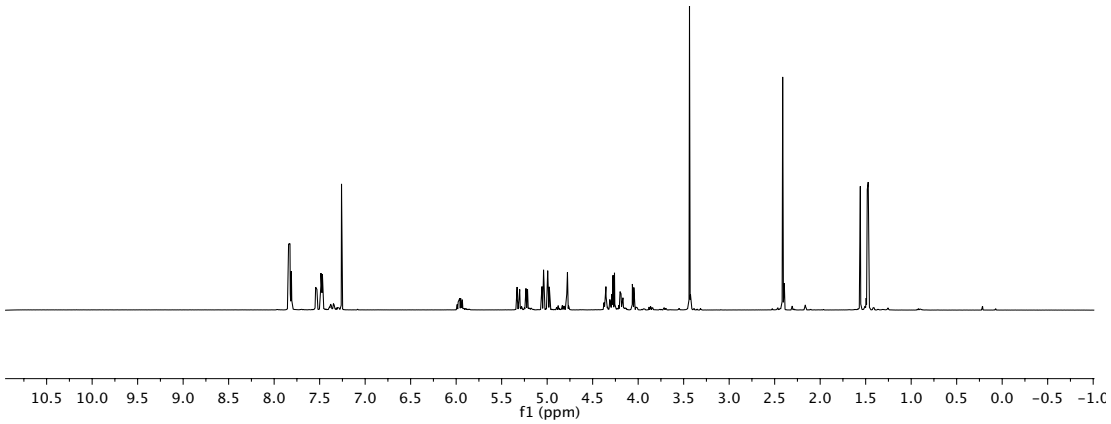

^{13}C spectrum of **25** (150 MHz, $CDCl_3$)

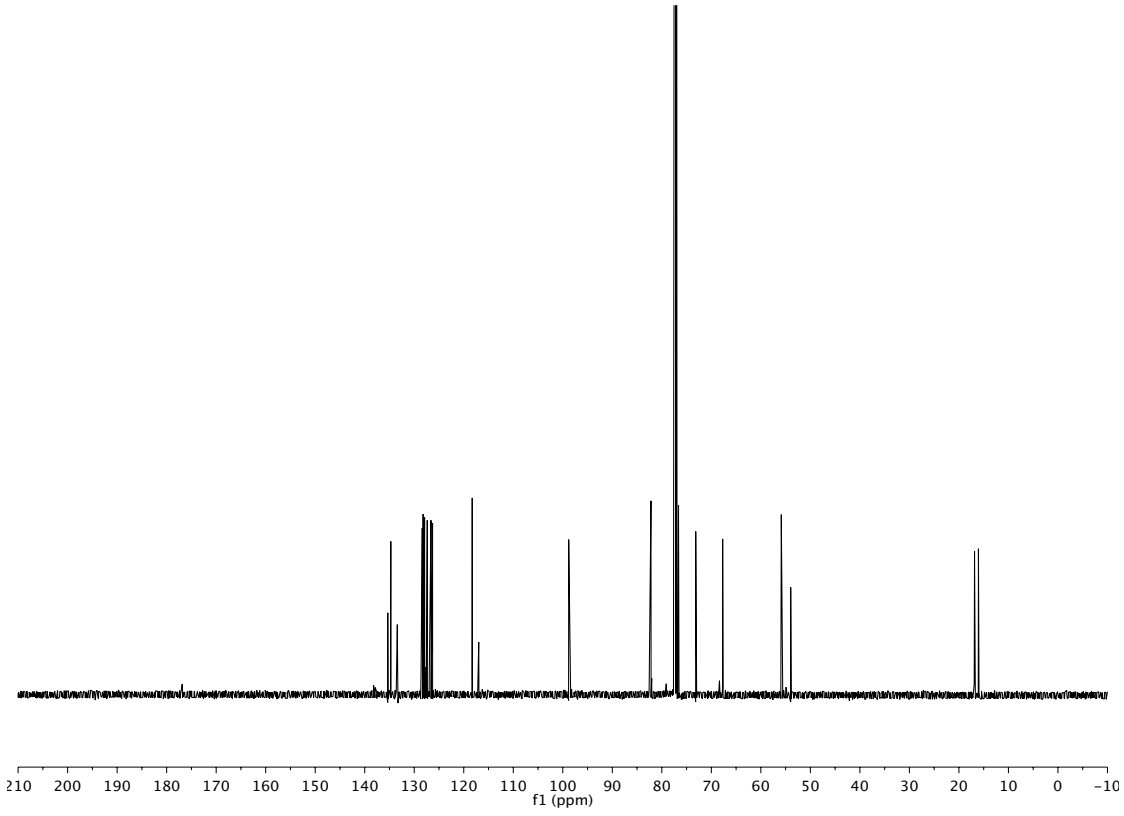

^{1}H spectrum of **4-*epi*-25** (600 MHz, $CDCl_3$)

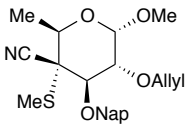

4-*epi*-25

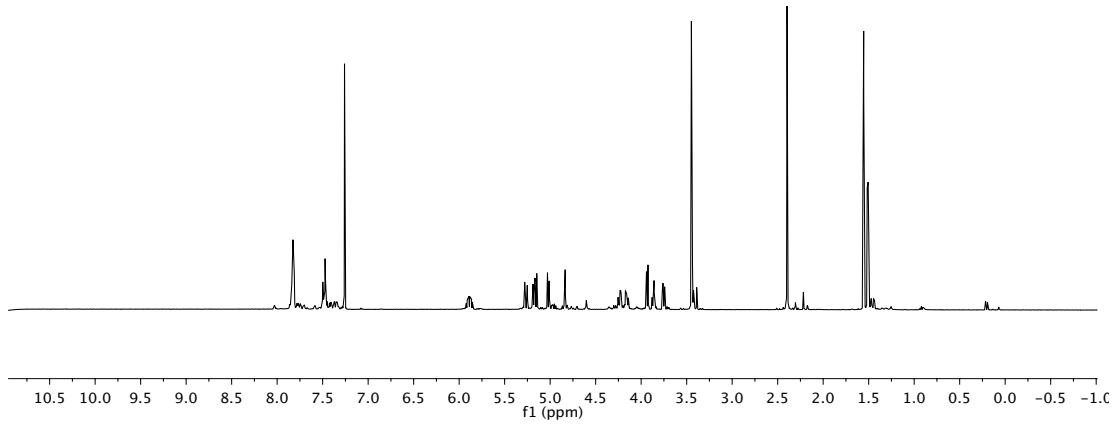

^{13}C spectrum of **4-*epi*-25** (150 MHz, $CDCl_3$)

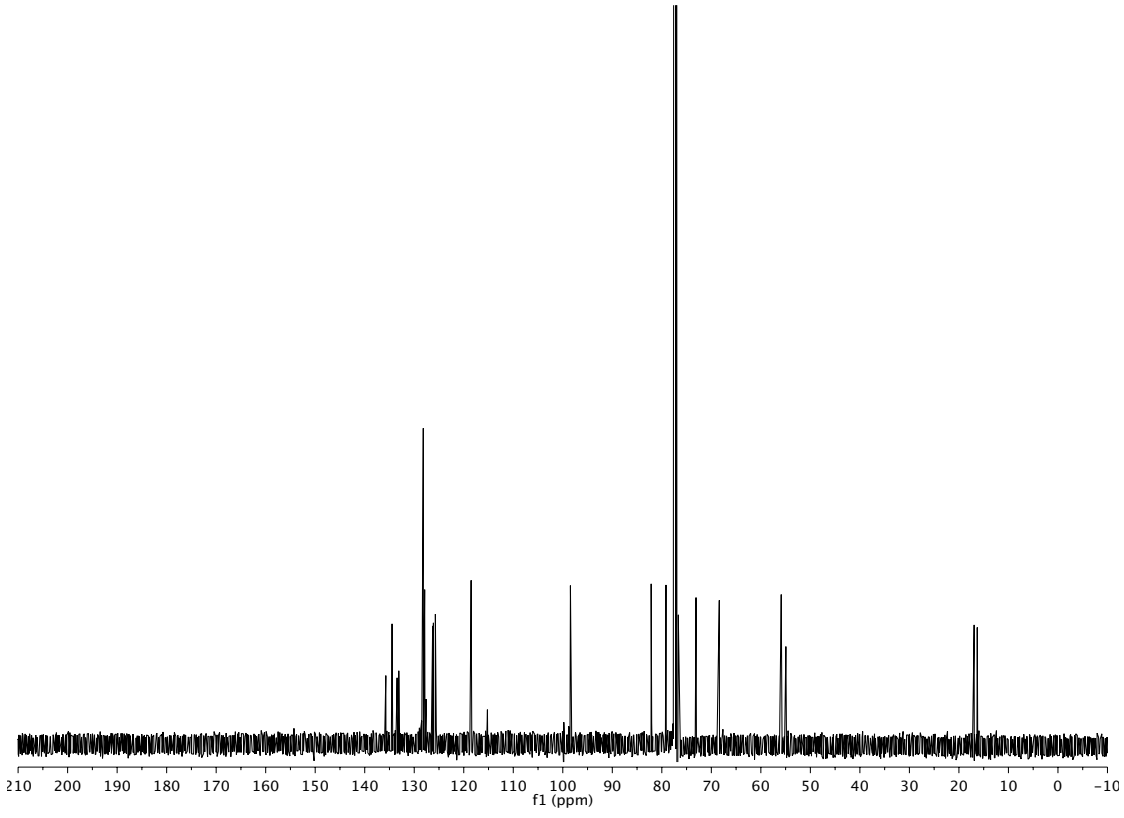

^{1}H spectrum of **13** (600 MHz, $CDCl_3$)

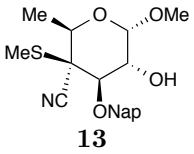

13

^{13}C spectrum of **13** (150 MHz, $CDCl_3$)

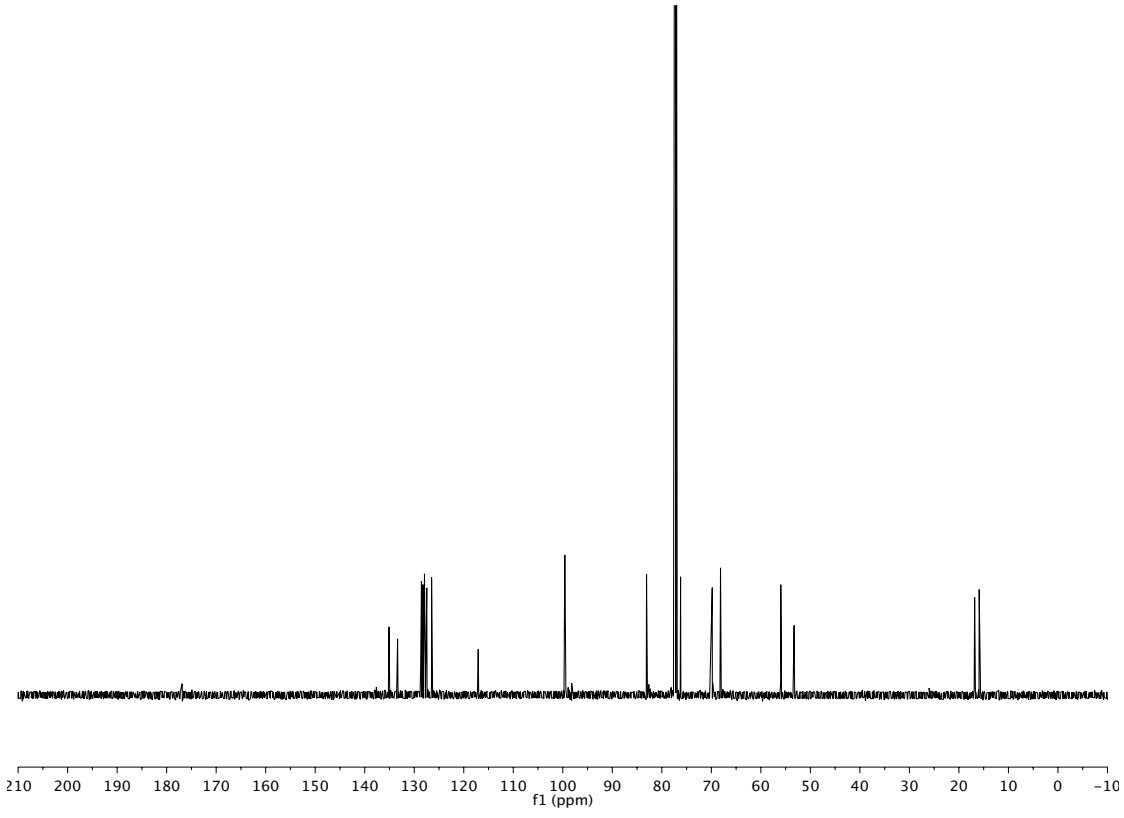

^{1}H spectrum of **27** (600 MHz, $CDCl_3$

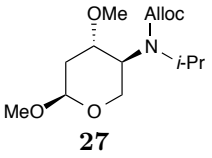

27

^{13}C spectrum of **27** (150 MHz, $CDCl_3$)

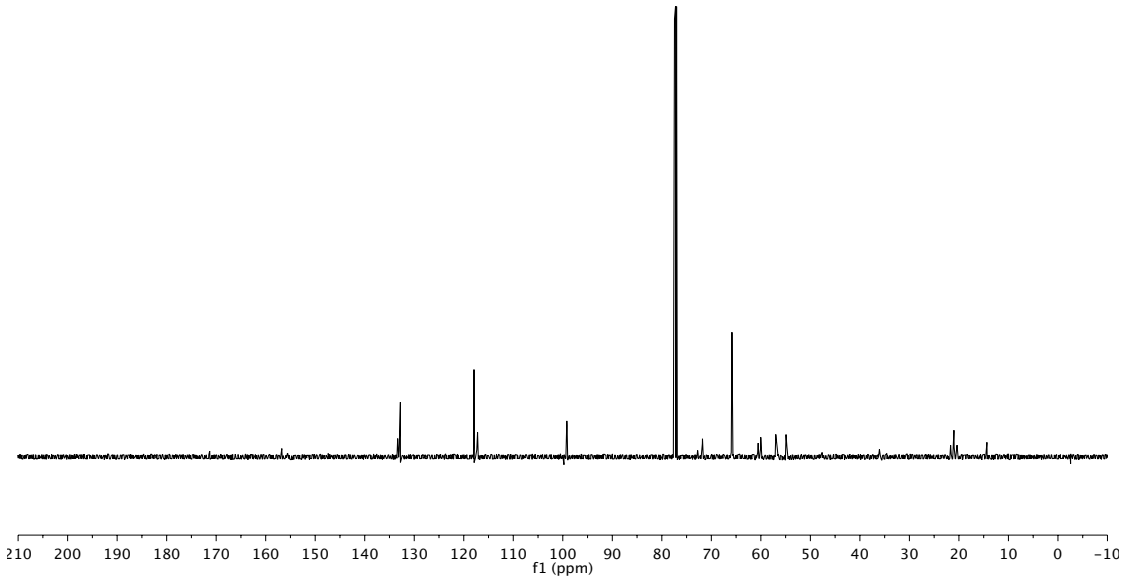

^{1}H spectrum of **28** (500 MHz, toluene-d_8, 80 °C)

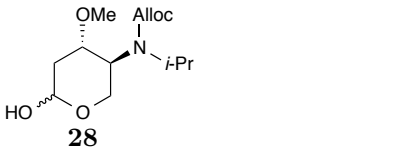

28

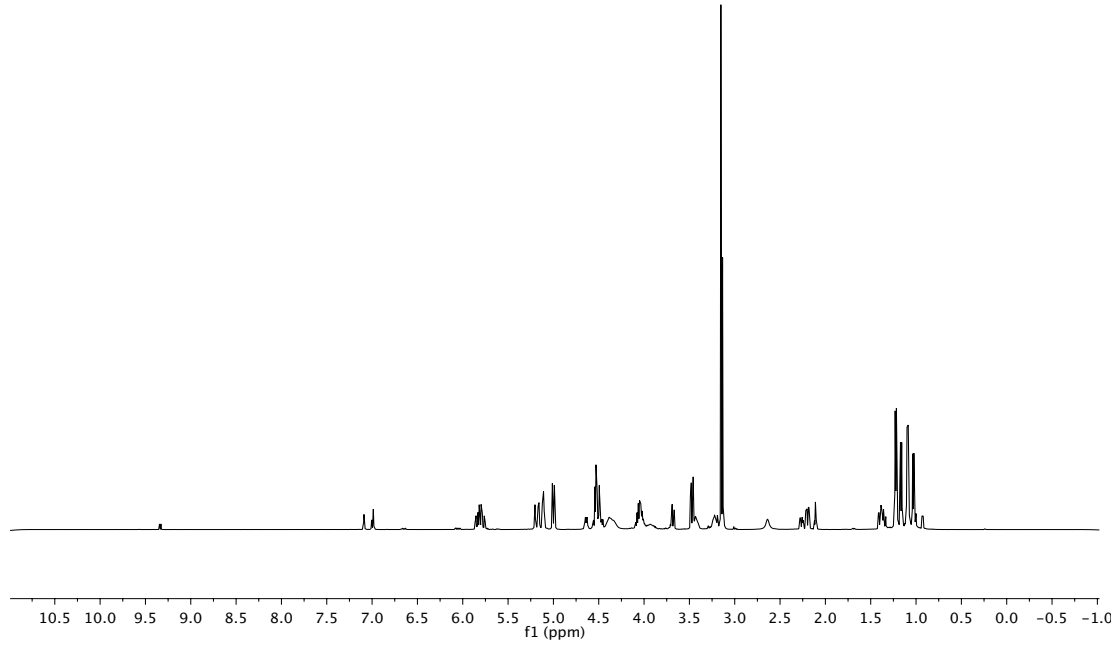

^{13}C spectrum of **28** (125 MHz, toluene-d_8, 80 °C)

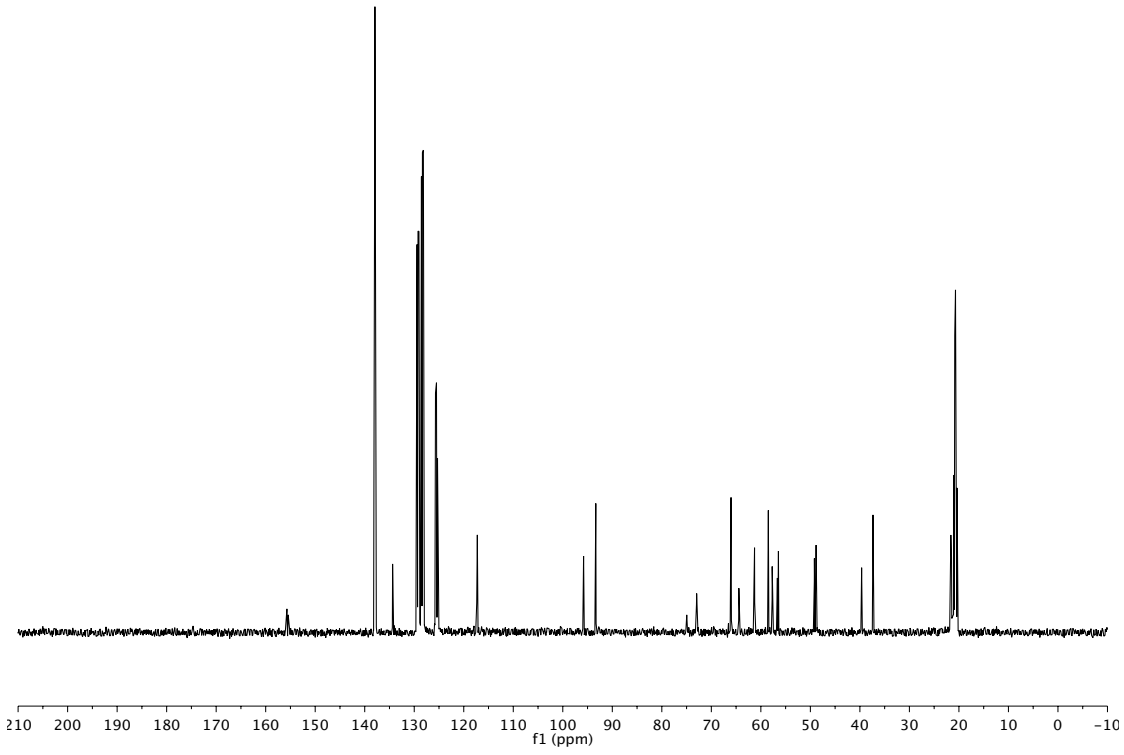

^{1}H spectrum of **14** (600 MHz, $CDCl_3$)

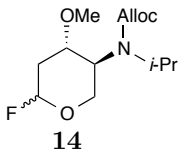

14

^{13}C spectrum of **14** (150 MHz, $CDCl_3$)

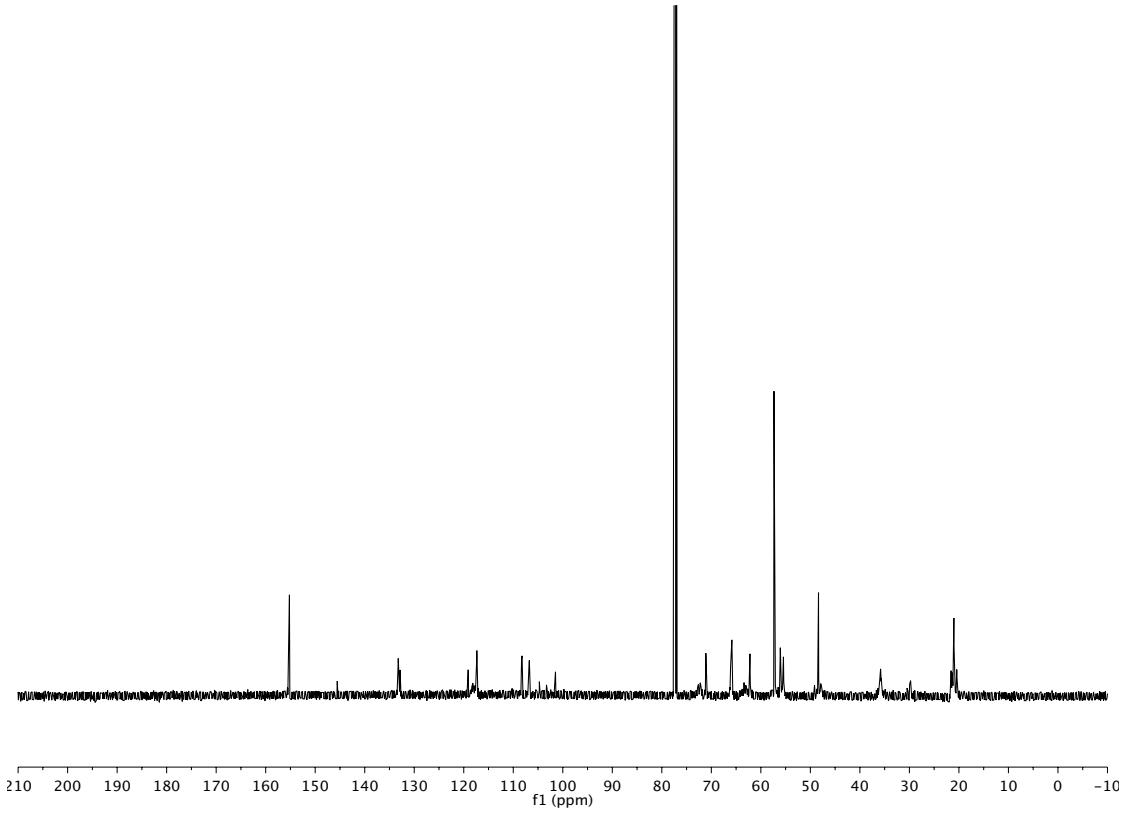

^{1}H spectrum of **29** (500 MHz, toluene-d_8, 80 °C)

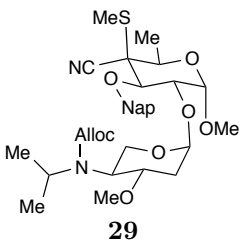

29

^{13}C spectrum of **29** (125 MHz, toluene-d_8, 80 °C)

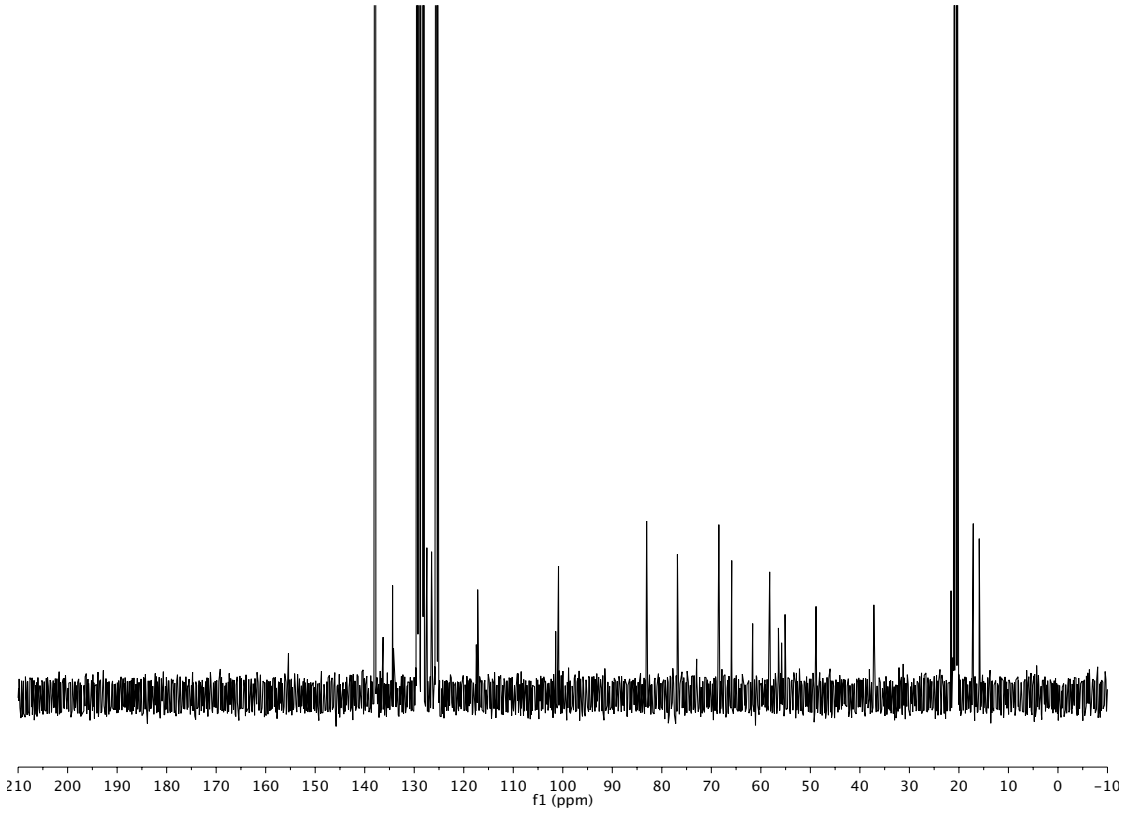

^{1}H spectrum of **30** (500 MHz, toluene-d_8, 70 °C)

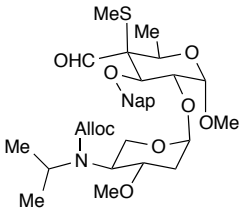

30

^{13}C spectrum of **30** (125 MHz, toluene-d_8, 50 °C)

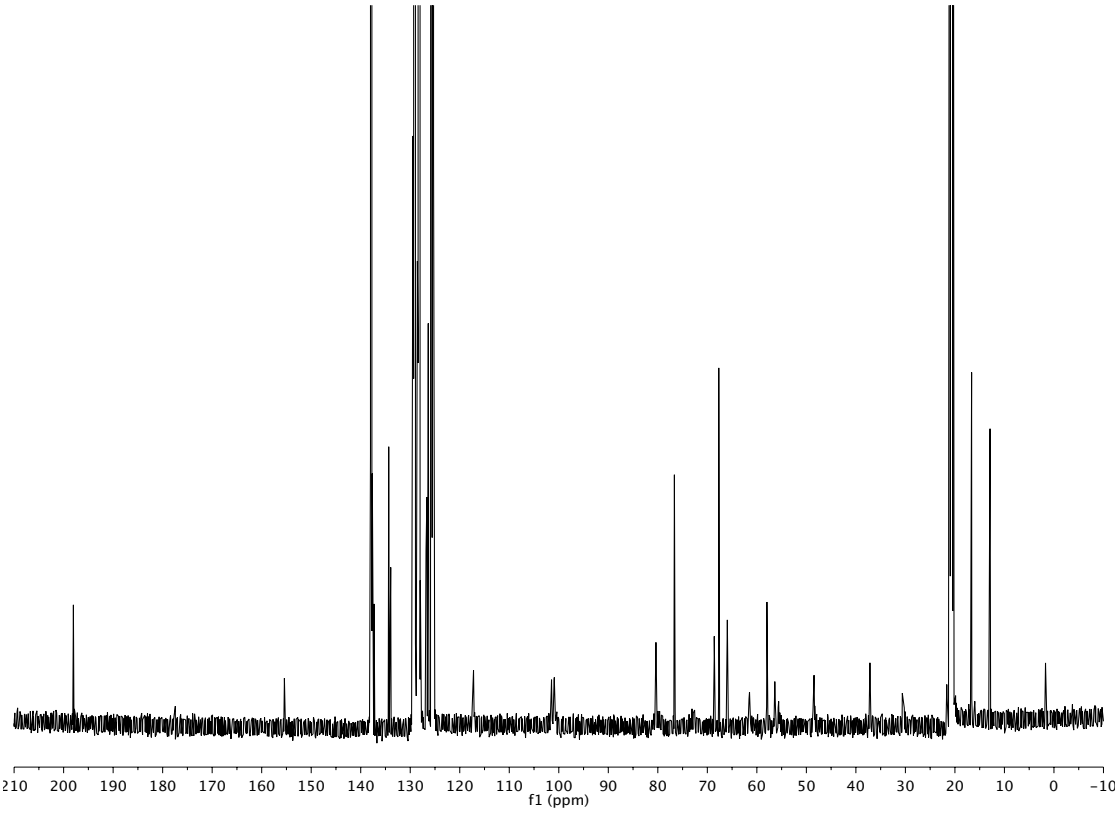

^{1}H spectrum of **11** (500 MHz, toluene-d_8, 65 °C)

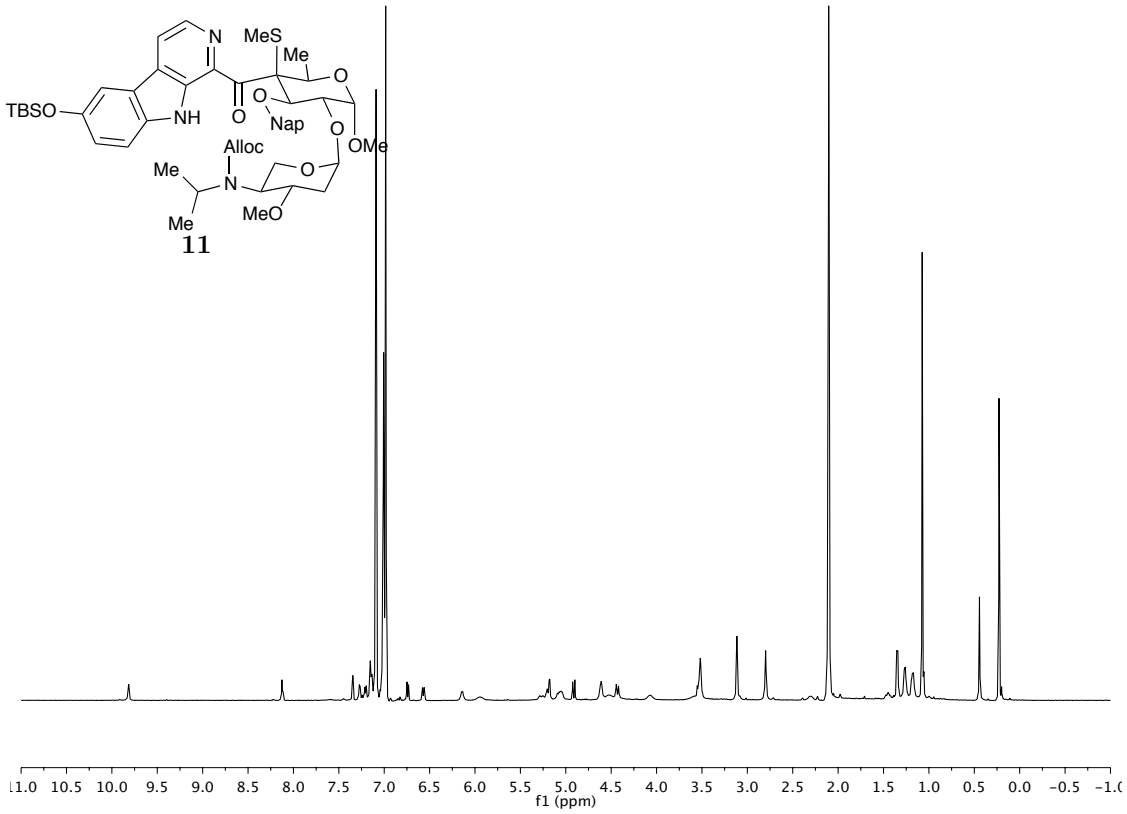

^{13}C spectrum of **11** (125 MHz, toluene-d_8, 65 °C)

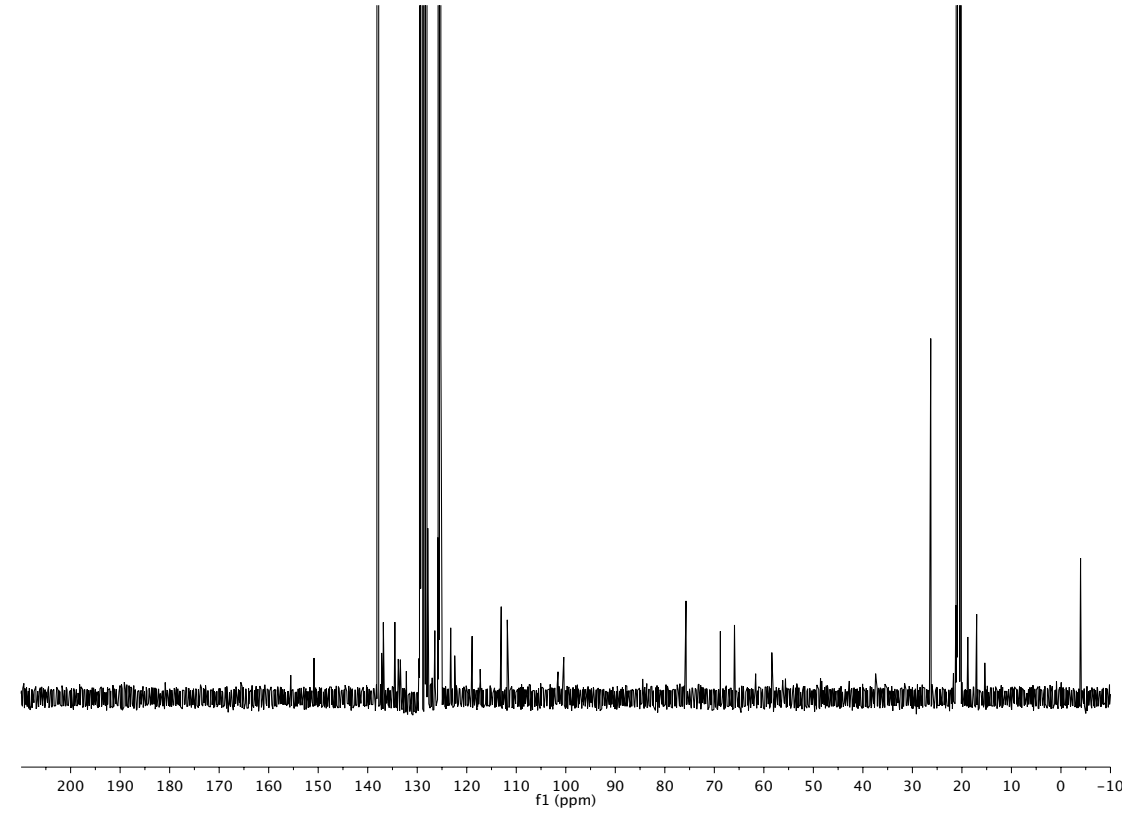

HMBC spectrum of **11** (600 MHz, toluene-d_8, 60 °C)

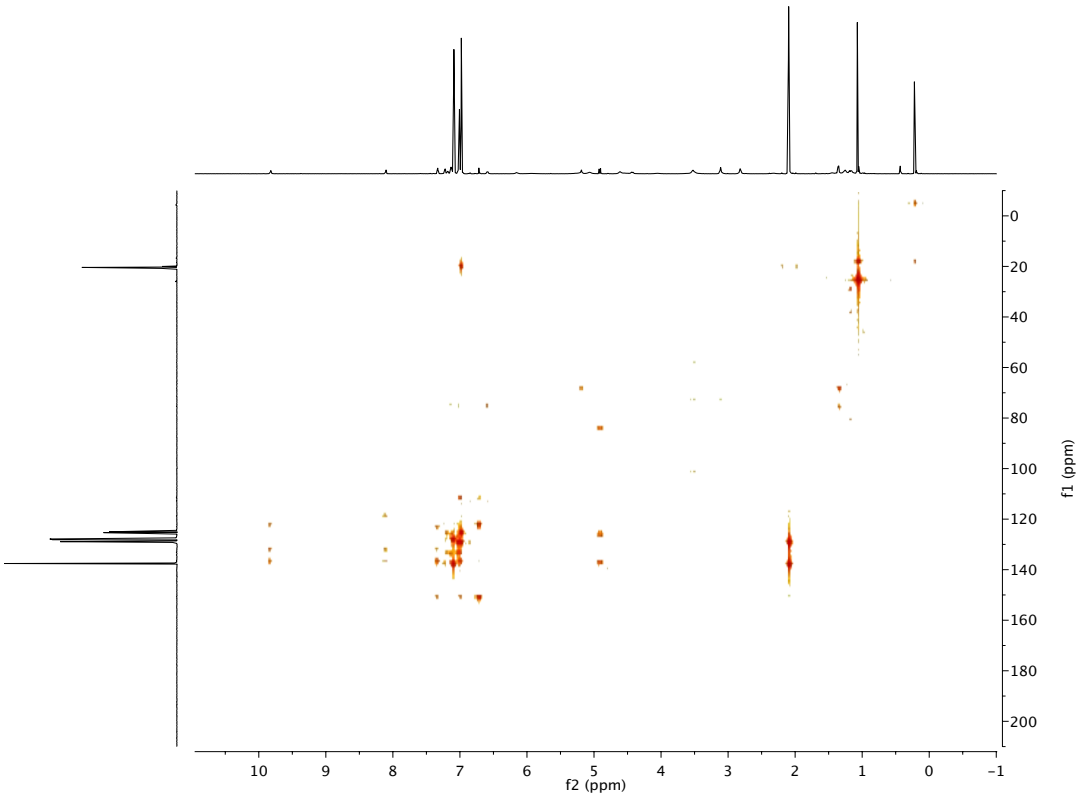

B

Selected NMR Spectra of DNJ Stereoisomers and Alkyl Homologs

^{1}H spectrum of **33D** (500 MHz, D_2O)

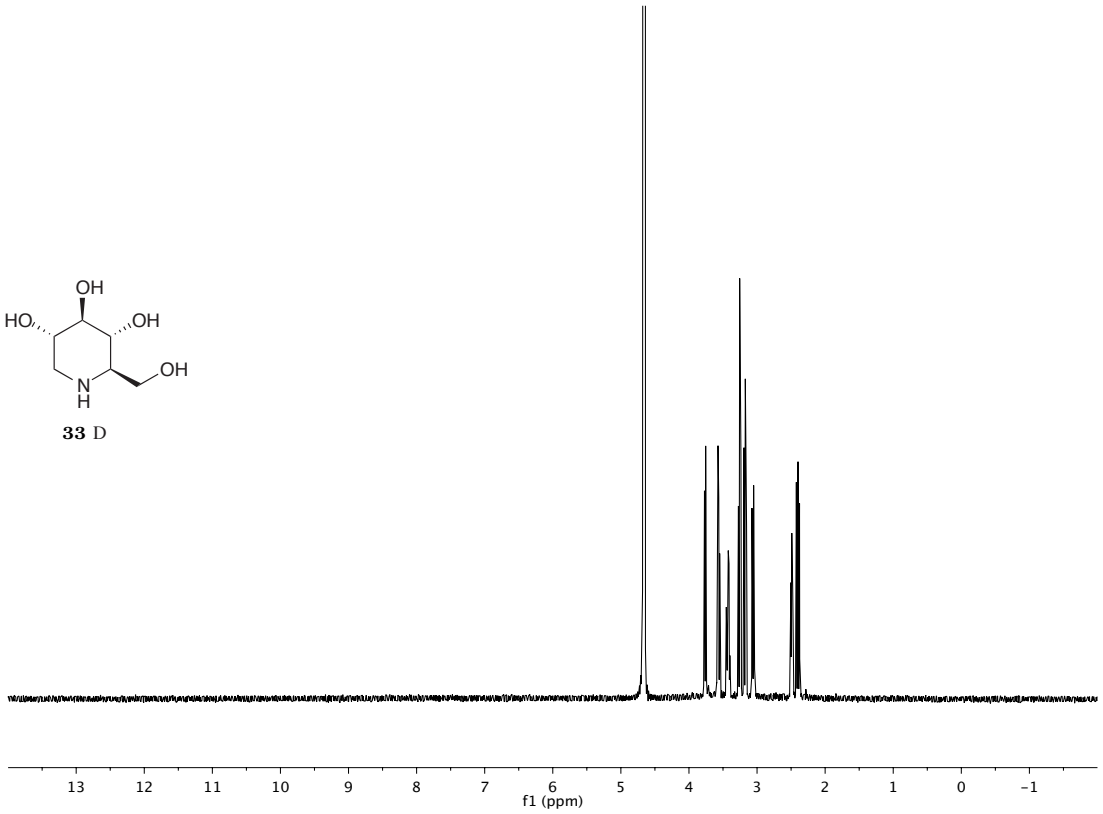

33 D

^{1}H spectrum of **54D** (500 MHz, D_2O)

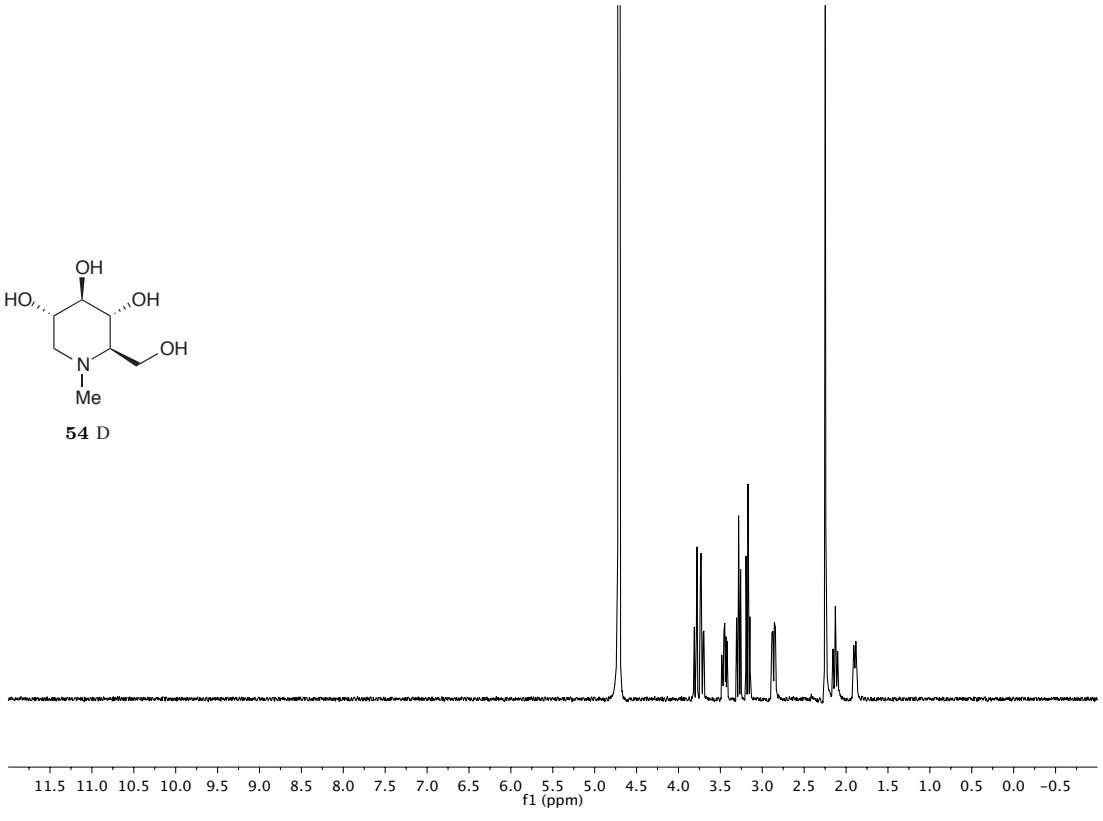

54 D

^{1}H spectrum of **55D** (500 MHz, D_2O)

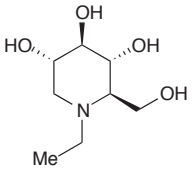

55 D

^{1}H spectrum of **56D** (500 MHz, CD_3OD)

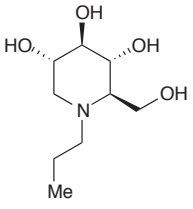

56 D

^{1}H spectrum of **47D** (500 MHz, CD_3OD)

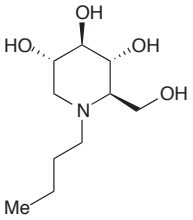

47 D

^{1}H spectrum of **57D** (500 MHz, CD_3OD)

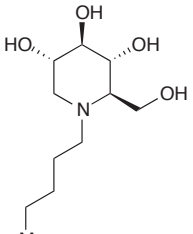

57 D

^{1}H spectrum of **58D** (500 MHz, CD_3OD)

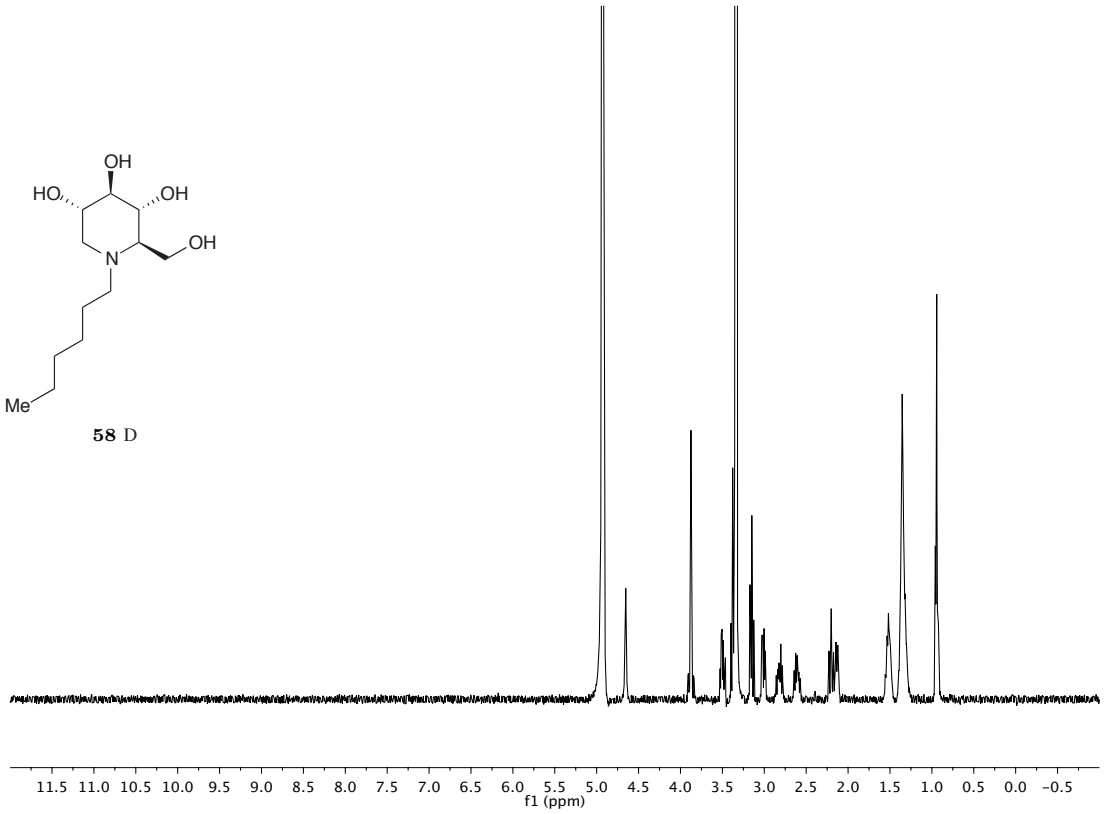

58 D

^{1}H spectrum of **48D** (500 MHz, CD_3OD)

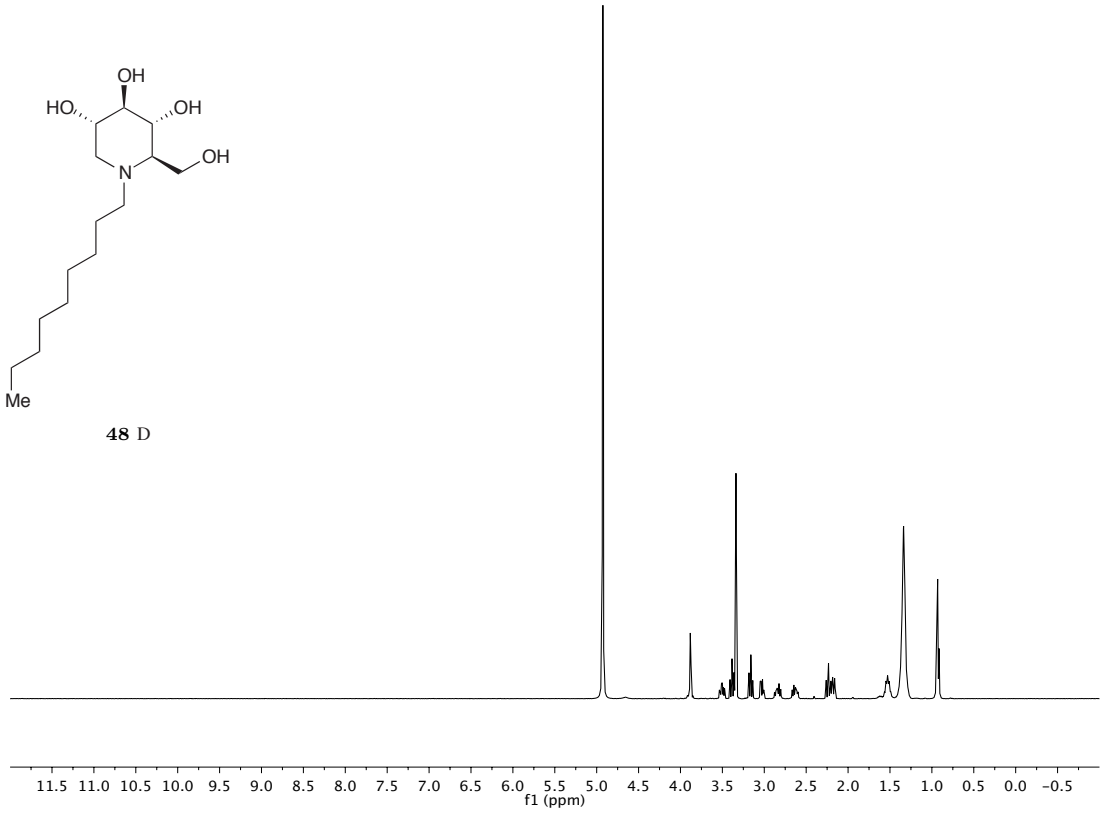

48 D

^{1}H spectrum of **63D** (500 MHz, D_2O)

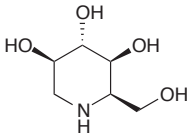

63 D

^{1}H spectrum of **90D** (500 MHz, CD_3OD)

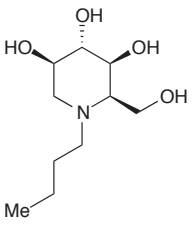

90 D

^{1}H spectrum of **91D** (500 MHz, CD_3OD)

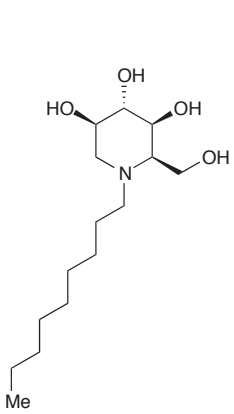

91 D

^{1}H spectrum of **61D** (500 MHz, D_2O)

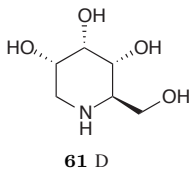

61 D

^{1}H spectrum of **64D** (500 MHz, D_2O)

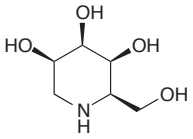

64 D

^{1}H spectrum of **92D** (500 MHz, CD_3OD)

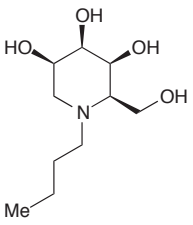

92 D

^{1}H spectrum of **93D** (500 MHz, CD_3OD)

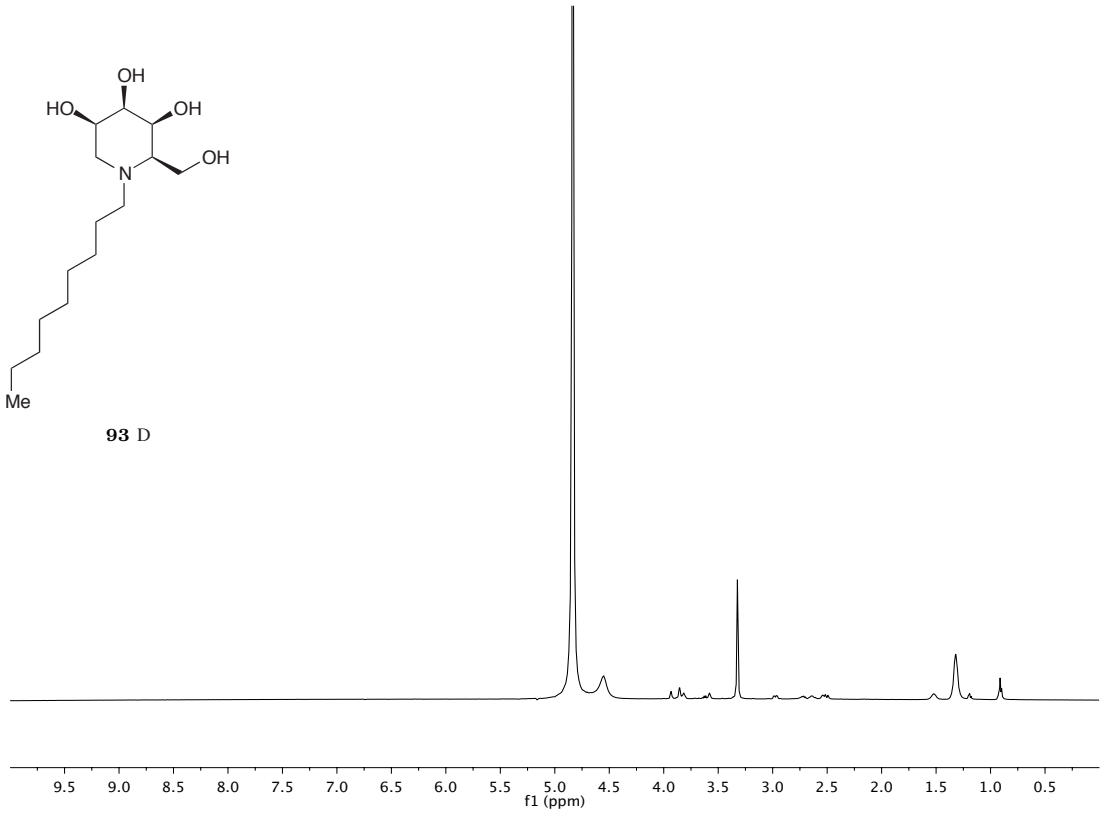

93 D

^{1}H spectrum of **45D** (500 MHz, D_2O)

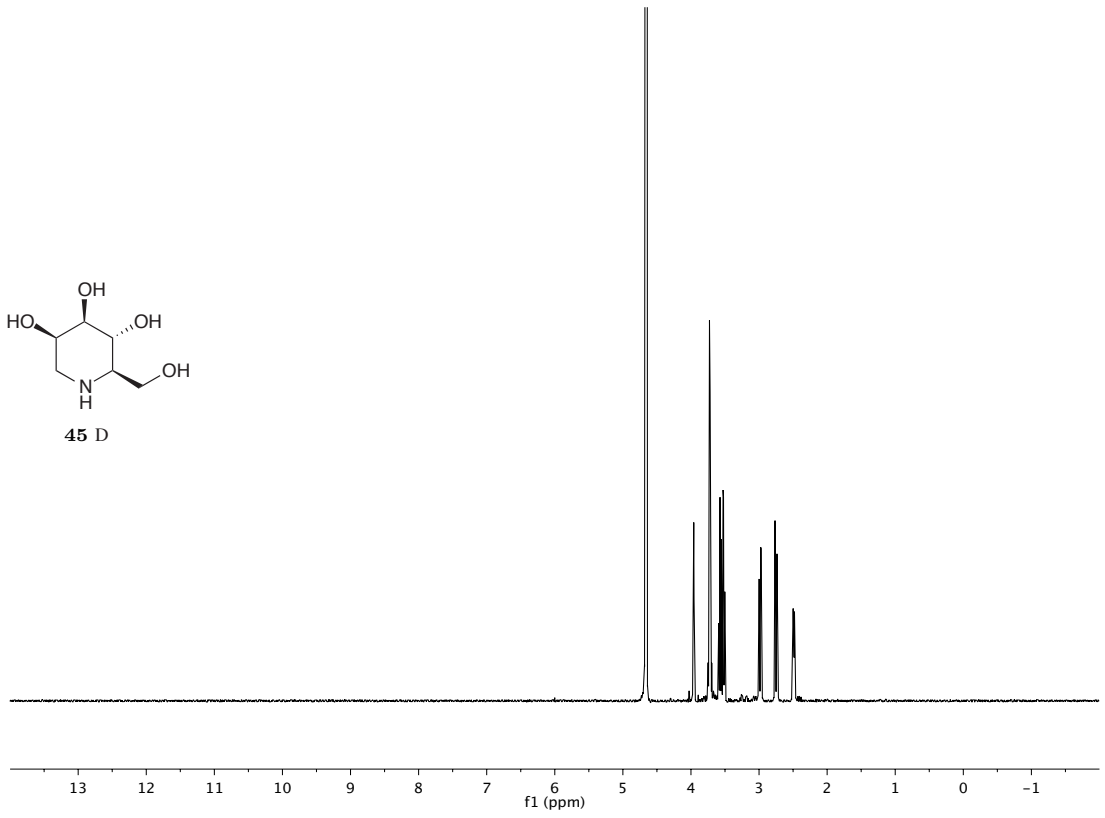

45 D

^{1}H spectrum of **94D** (500 MHz, CD_3OD)

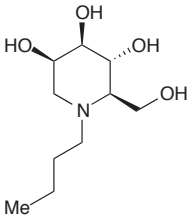

94 D

^{1}H spectrum of **95D** (500 MHz, CD_3OD)

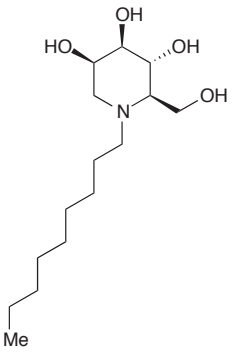

95 D

^{1}H spectrum of **65D** (400 MHz, D_2O)

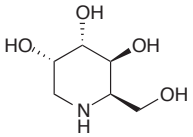

65 D

^{1}H spectrum of **66D** (500 MHz, D_2O)

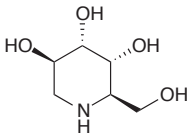

66 D

^{1}H spectrum of **62D** (500 MHz, D_2O)

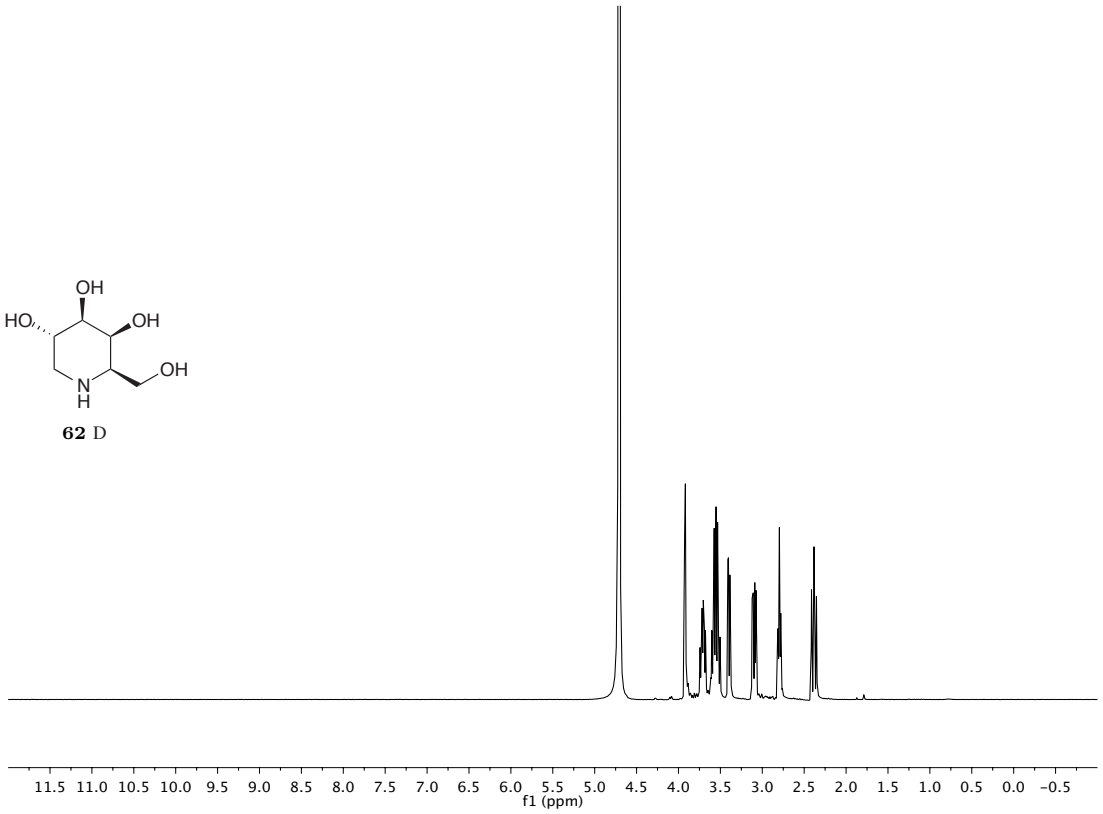

62 D

C

Free Oligosaccharide Chromatograms

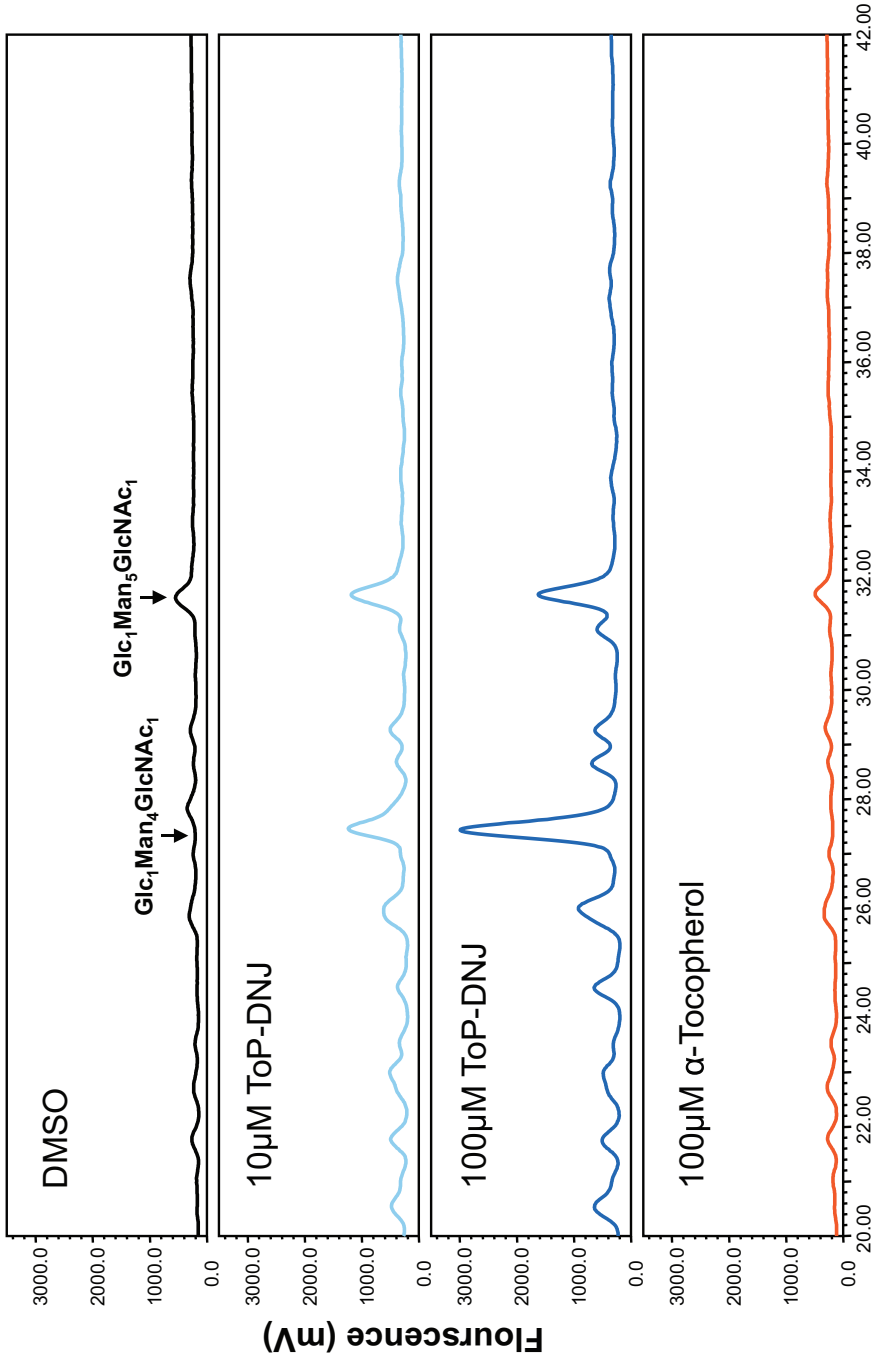

Figure C.1: *Chromatogram of Treated MDMΦFree Oligosaccharides.* MDMΦ cells were incubated with the indicated treatment for 48 h. FOS were isolated and characterized by HPLC as previously described.[145] Cells treated with ToP-DNJ demonstrated a dose-dependent accumulation of Glc_1 species, but no accumulation of either Glc_2 or Glc_3.

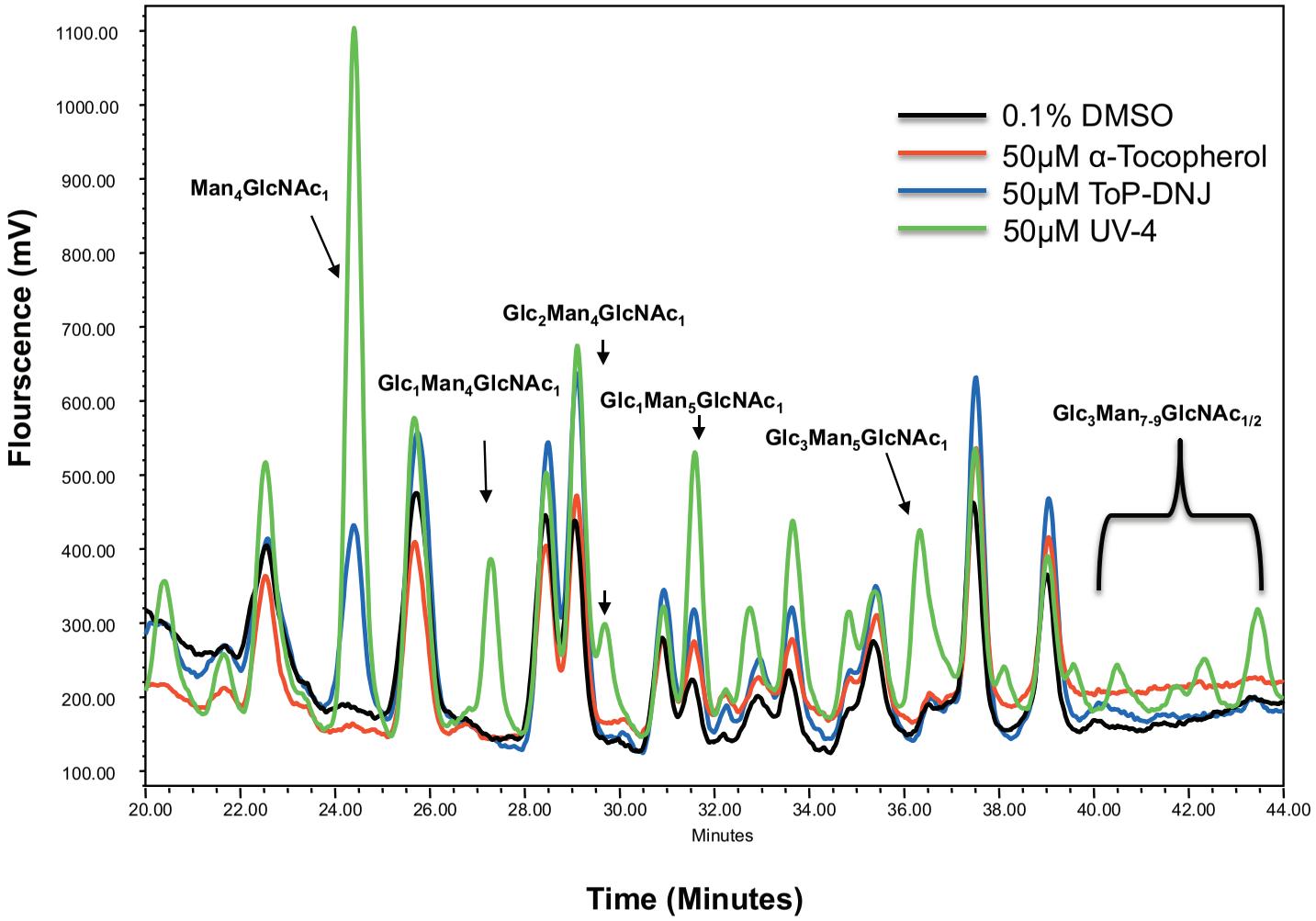

Figure C.2: *Chromatogram of Treated Huh7.5 Free Oligosaccharides.* Huh7.5 cells were incubated with the indicated treatment for 24 h. FOS were isolated and characterized by HPLC as previously described.[145] The positive control, M*O*N-DNJ, induced accumulation of Glc_1, Glc_2, and Glc_3 species indicating inhibition of ER α-GluI and both reactions of ER α-GluII. In contrast, ToP-DNJ, like the two negative controls (α-tocopherol and DMSO), showed no appreciable levels of any of these species.

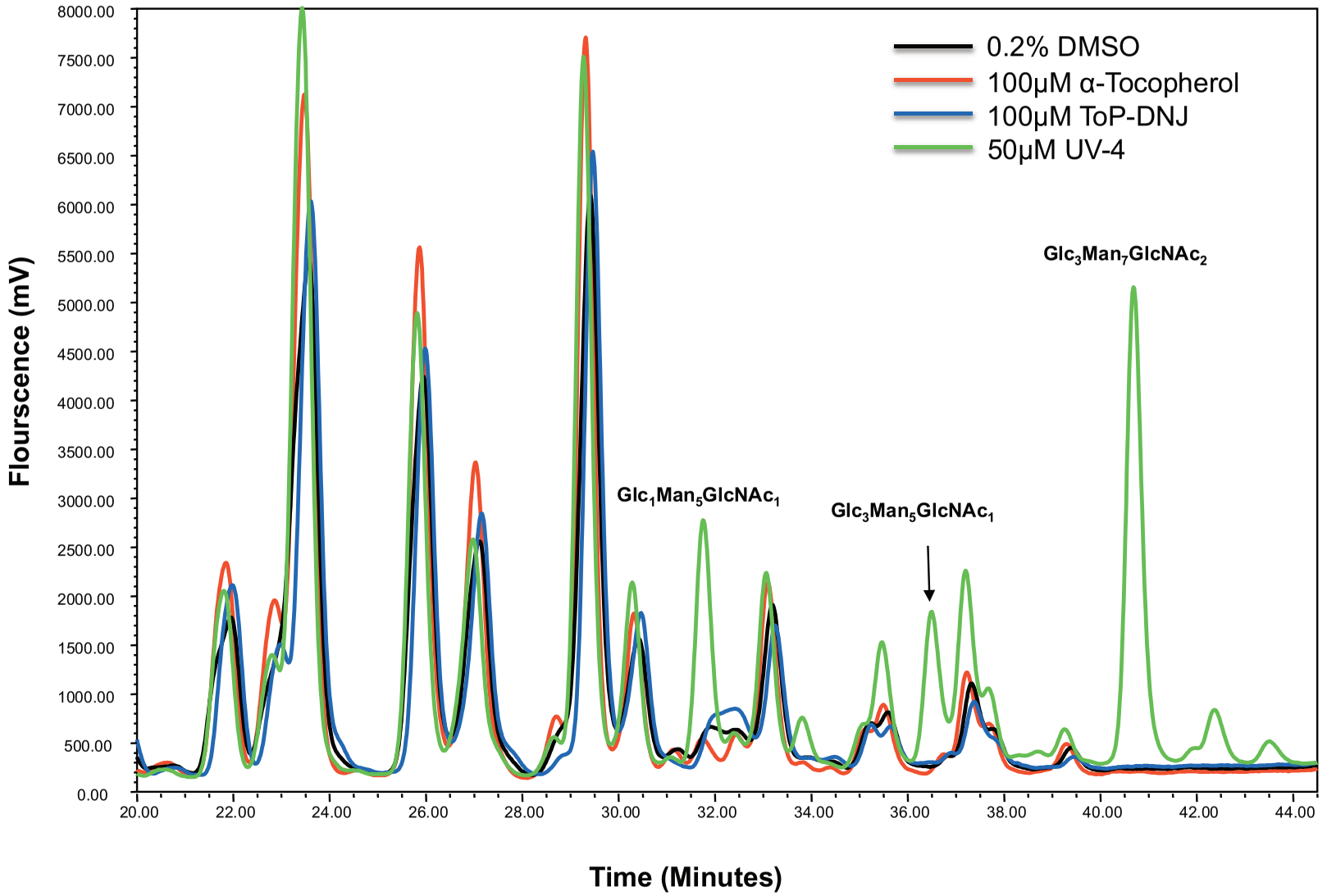

Figure C.3: *Chromatogram of Treated MDBK Free Oligosaccharides.* MDBK cells were incubated with the indicated treatment for 24 h. FOS were isolated and characterized by HPLC as previously described.[145] The positive control, M*O*N-DNJ, induced accumulation of Glc_1, Glc_2, and Glc_3 species indicating inhibition of ER α-GluI and both reactions of ER α-GluII. In contrast, ToP-DNJ, like the two negative controls (α-tocopherol and DMSO), showed no appreciable levels of any of these species.

D

ToP-DNJ Lipidomics Report

Samples 1-33 received from Stephanie on 4th March 2013. Extraction on 5th March 2013. Samples 34-45 received from Stephanie on 5th April 2013. Extraction and processed 6th April.

Sample volume is 2ml (methanol/acetone) corresponding to one T25 cell plate. 0.25 ml (1/4th of T25) is sampled for FAME profile and 0.25 ml (1/4th of T25) for total cholesterol (GCMS).

1ml (1/2 of a T25 plate) is kept for HPLC-MS2 lipidomics.

Sample ID	HCVcc un/infected	Treatment	Conc. (uM)	total protein (mg)	% HCV positive cells	HCV RNA copies secreted (per ml)
samples sent: 4 march 2013						
1	infected	DNJ	1000	0,138	91,31	3,26E+04
2	infected	DNJ	1000	0,120	88,14	3,15E+04
3	infected	DNJ	1000	0,114	84,83	3,03E+04
4	infected	untreated		0,156	86,77	3,10E+04
5	infected	untreated		0,204	92,93	3,32E+04
6	infected	untreated		0,194	89,81	3,21E+04
7	infected	NB-DGJ	1000	0,116	72,27	2,58E+04
8	infected	NB-DGJ	1000	0,095	77,81	2,78E+04
9	infected	NB-DGJ	1000	0,179	63,64	2,27E+04
10	infected	UV4	50	0,137	79,63	2,84E+04
11	infected	UV4	50	0,123	76,65	2,74E+04
12	infected	UV4	50	0,078	74,29	2,65E+04
13	infected	ToP-DNJ	10	0,216	60,63	2,16E+04
14	infected	ToP-DNJ	10	0,224	62,31	2,22E+04
15	infected	ToP-DNJ	10	0,107	66,88	2,39E+04
16	uninfected	untreated		0,283		
17	uninfected	untreated		0,250		
18	uninfected	untreated		0,341		
19	uninfected	ToP-DNJ	10	0,270		
20	uninfected	ToP-DNJ	10	0,323		
21	uninfected	ToP-DNJ	10	0,254		
22	uninfected	DNJ	1000	0,289		
23	uninfected	DNJ	1000	0,330		
24	uninfected	DNJ	1000	0,231		
25	uninfected	NB-DGJ	1000	0,213		
26	uninfected	NB-DGJ	1000	0,250		
27	uninfected	NB-DGJ	1000	0,181		
28	uninfected	UV4	50	0,161		
29	uninfected	UV4	50	0,185		
30	uninfected	UV4	50	0,198		
31	uninfected	Horse serum	10%	0,214		
32	uninfected	Horse serum	10%	0,168		
33	uninfected	Horse serum	10%	0,184		

samples sent on 3 April 2013				
34	uninfected	untreated 6h		0,306
35	uninfected	untreated 6h		0,324
36	uninfected	untreated 6h		0,303
37	uninfected	untreated 24h		0,326
38	uninfected	untreated 24h		0,302
39	uninfected	untreated 24h		0,342
40	uninfected	UV4 6h	50	0,320
41	uninfected	UV4 6h	50	0,325
42	uninfected	UV4 6h	50	0,284
43	uninfected	UV4 24h	50	0,286
44	uninfected	UV4 24h	50	0,290
45	uninfected	UV4 24h	50	0,273

1- Fatty Acid (FA) composition of total lipid extracts from HCVcc infected (sample 1 to 15) and uninfected cultured Huh7.5 cell plates (s. 16 to 30 and horse serum supplemented).

The FA profile of total lipids comprised in the total lipid extract is obtained by GCMS after acid transmethylation of lipids. All lipids contribute to the total FA profile; Glycerolipids (2 or 3 FA/molecule), cholesterol esters (1 FA/molecule) and sphingolipids (1 FA/molecule). FA methyl esters (FAME) are separated by GC and specific M+ NH_4^+ adducts are assayed in the chemical ionization mode of acquisition with ammonia as the reagent gas. Results are normalized relative to the internal standard of C17:0 (10 mcg/sample (1/4th of T25 plate)).

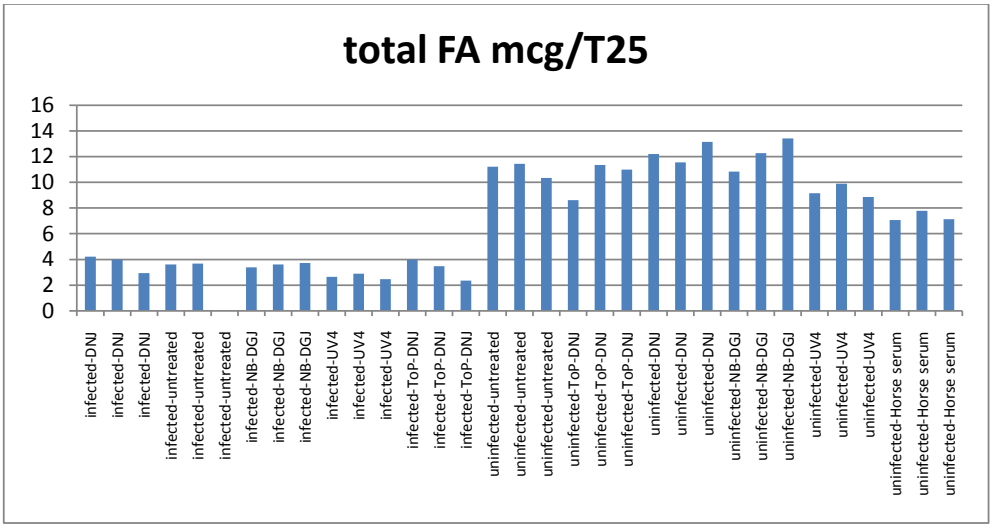

NB: A data point for an infected-untreated sample is missing for total FA quantification.
FA amounts are shown separately for infected and infected cell plates below (red cross = mean value).

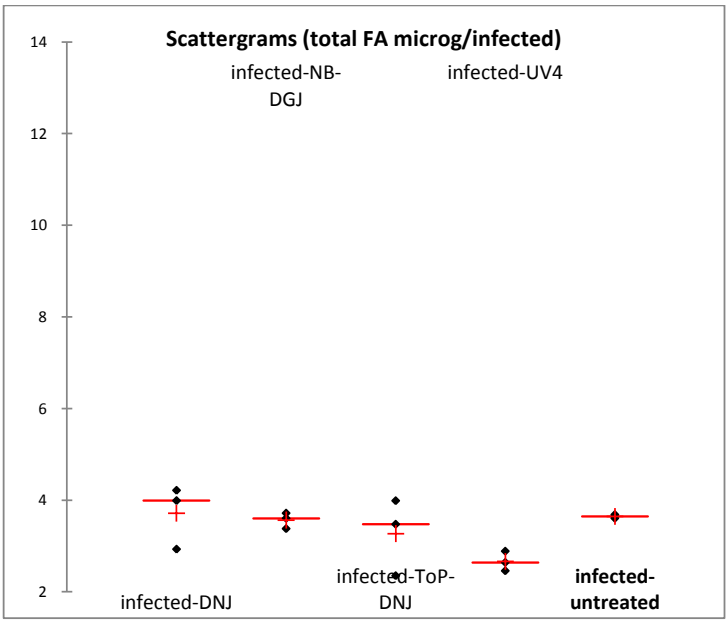

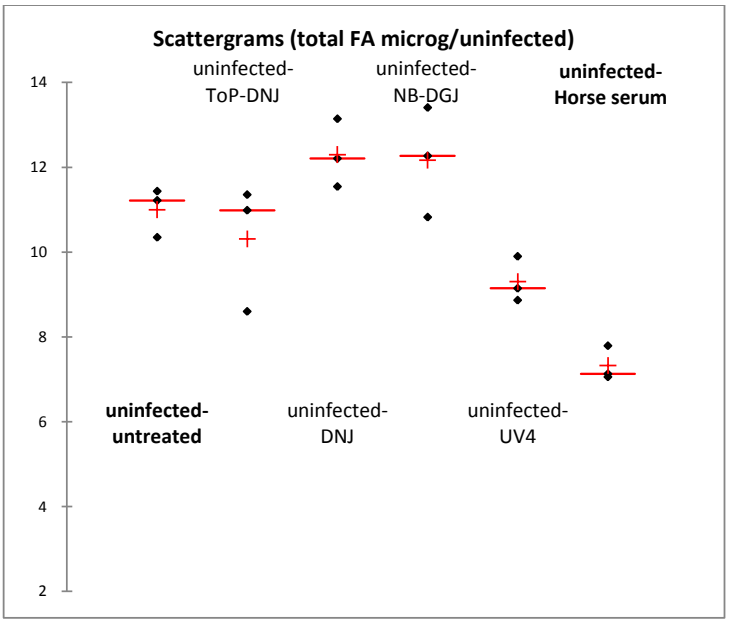

The total amount of FA is indicative of the total lipid content in the extract, disregarding a change in the proportions of the different lipid classes comprised of 1, 2 or 3 FA/molecule. The FA total amount is considerably reduced (-66%) by infection (proteins are reduced from 0.291 to 0.184; -36%). The reduction is observed whether or not the cells have been treated. Uninfected plates supplemented by horse serum contain LESS (X0.55) FA (≈less lipids) than bovine serum supplemented plates. The following study of FA profile shows that horse serum supplemented cell plates have a reduced *de novo* lipogenesis (DNL) rate.

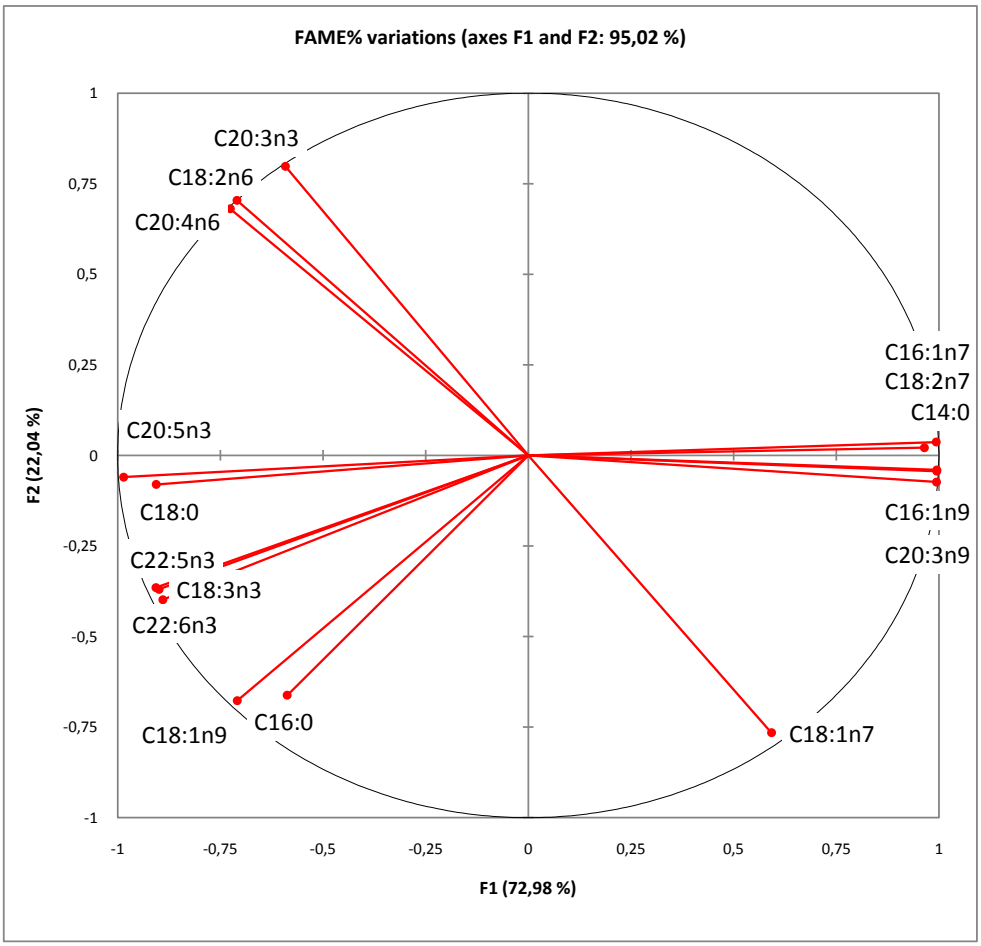

The variations in the profiles are summarized by the principal components analysis of FAME% (above).

The load-plot shows FA products of the correlation of characteristic *de novo* lipidogenesis biomarkers of DNL in the right quadrants (except C16:0, 18:0 and 18:1n9 which are abundantly supplied by the culture medium in the lower right quadrant). Their variations are diametrically opposite to essential fatty acids (EFA n3 and n6 series) as well as (non essential) FA C16:0, C18:0 and C18:1n9 (oleic acid). Exogenous FA such as C16:0, C18:0 and C18:1n9 serve as precursor for conversion by desaturases and elongases in the DNL pathway (16:0>16:1n7-9; 18:0>18:1n7-9>18:2n7-9>20:3n7-9). GCMS analysis has evidenced the occurrence of 18:2n7-9, a precursor of 20:3n7-9. The variations of FAs after infection can be understood as a wide reduction of the very high DNL rate (endogenous synthesis of FA). Such accelerated DNL is resulting of a low exogenous supply of the Huh cells cultures supplemented with (10% v/v) bovine serum. Infected/non infected status modifies the DNL rate but from its very accelerated rate under the common culture conditions. This can be proven by the horse serum supplementation test.

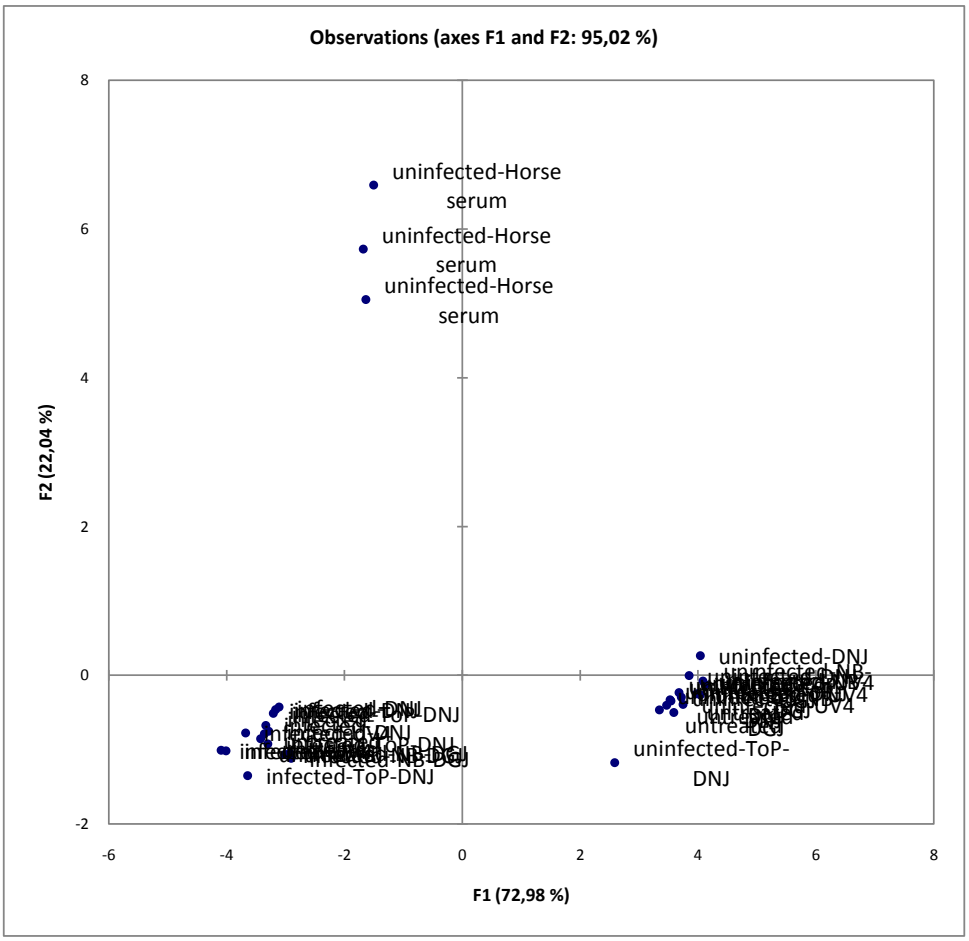

The score plot illustrates the separation in 3 sub-groups, which shows:
1) The enrichment in EFAn3 and n6, SAT and oleic acid of infected plates (in the lower left quadrant)
2) Uninfected plates are enriched in DNL produced FA (in the right quadrants)
3) Separation of horse serum supplemented cells results of an enrichment in PUFA (18:2n6 (LA), 20:3n3 and 20:4n6 (AA)). In turn, PUFA exert its inhibition on DNL (scores in the right quadrant).

The proportions of DNL products in the profiles are shown as percentage (below).
C20:3n9 (mead acid) is the most sensitive markers of DNL in the culture showing the largest increase in the uninfected plates (0.78+/-0.07 to 7.91%+/-0.67).
C18:2n6 and 20:4n6 (PUFA) percentages show EFA enrichment (relative to DNL biomarkers) in infected cells (LA; 5.12+/-0.42 vs 0.79%+/-0.06: AA; 7.99%+/-0.57 vs 3.21%+/-0.41).
Uninfected horse serum supplemented cells show even much higher levels of essential FA (LA 12.50%+/-0.54: AA 15.23%+/-1.56) and much lower DNL markers.

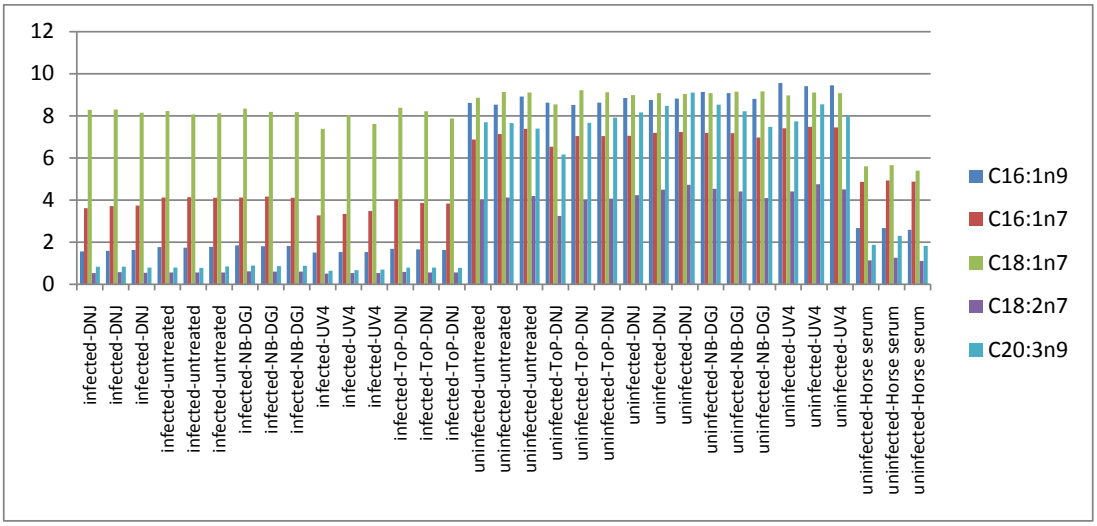

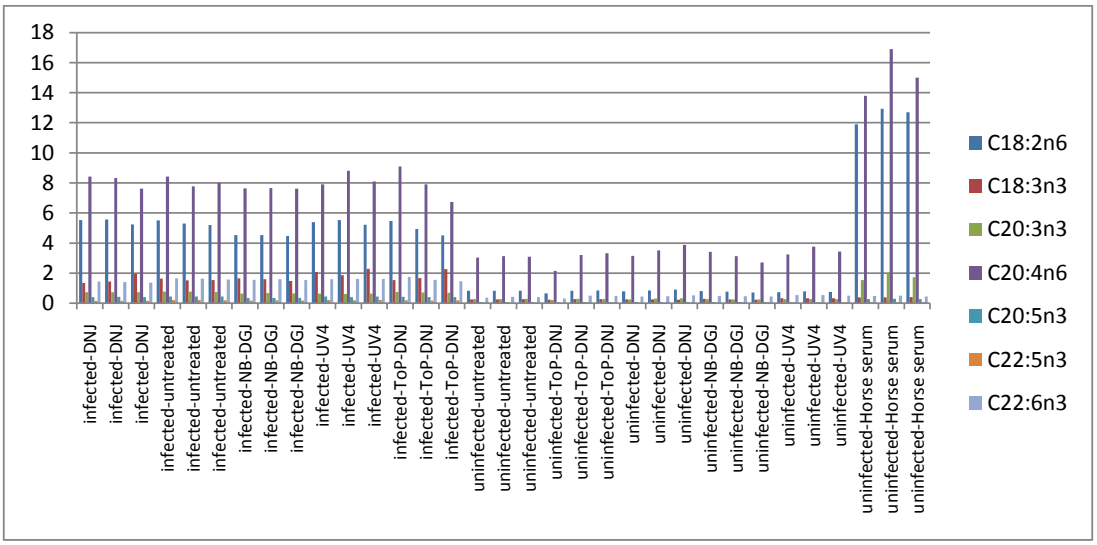

Treatment by UV4 has no significant influence on the total FAME amounts at 6 and 24 hours.

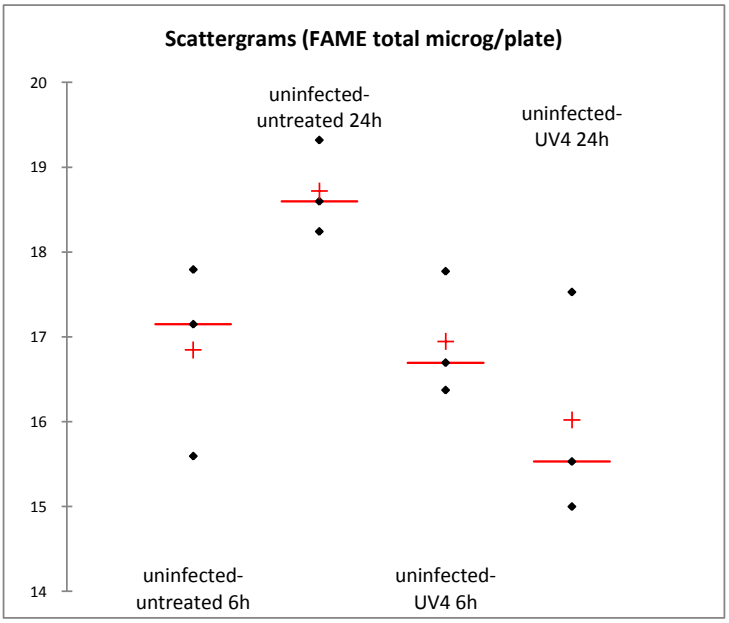

However a separation of 6h and 24h treated plates is detected suggesting a change in the FAME% profile.

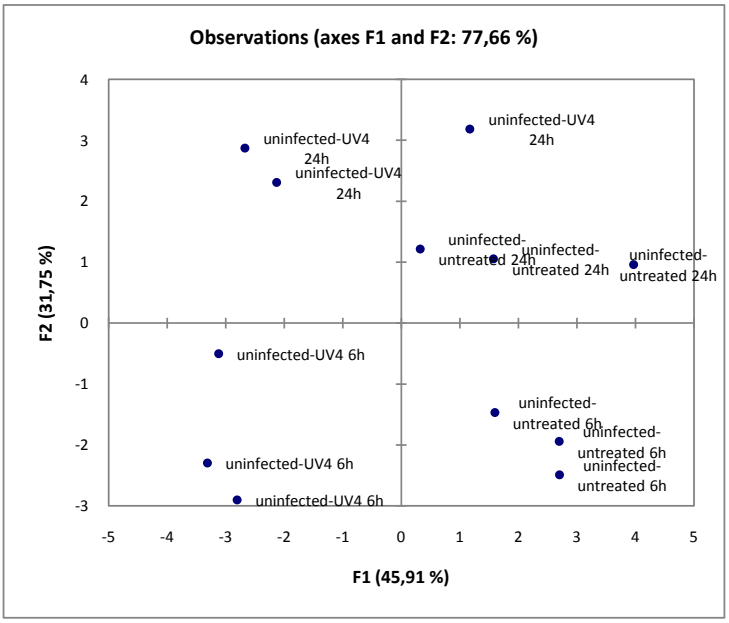

The separation of treated plates in the left quadrants (negative loading on F1) is related to the enrichment in the profile of DHA+ ALA at the expense of DNL products (16:1):

	F1	F2
C22:6n3	-0,822	-0,381
C18:3	-0,746	0,399
C20:3n9	-0,706	-0,610
C20:3n3	-0,702	-0,312
C18:1n9	-0,616	0,764
C18:1n7	-0,490	-0,521
C18:2n7	-0,475	-0,732
C18:0	-0,465	-0,818
C20:4n6	-0,250	-0,189
C18:2n6	0,611	0,391
C16:1n9	0,741	-0,679
C16:0	0,796	-0,479
C14:0	0,806	0,827
C16:1n7	0,935	0,222

2- Total cholesterol assayed by GCMS from HCVcc infected (samples 1 to 15) and uninfected Huh7.5 cell plates (s. 16 to 30 and horse serum supplemented).

No other sterols than cholesterol (including oxidized sterols or cholesterol precursors such as 7DHC, lathosterol) is detected by MS fragmentography in the present cultures.

The total cholesterol (including non-esterified and esterified cholesterol) is assayed after acid transmethylation of FA and trimethylsilylation of 3 beta OH-cholesterol. TMSi-Sterols are quantitifed with GCMS relative to the internal standard of epicoprostanol (20 mcg added to a volume of extract corresponding to 1/4th of T25 plate).

NB: A data-point is missing for infected-UV4 sample (sample 11).

The total cholesterol amount (microgram/T25 flask) is reduced by HVC infection (-47%).

Horse serum supplementation reduces also the total cholesterol level by -24%. No significant reduction is brought about by UV4 after 48 hrs as compared to untreated samples.

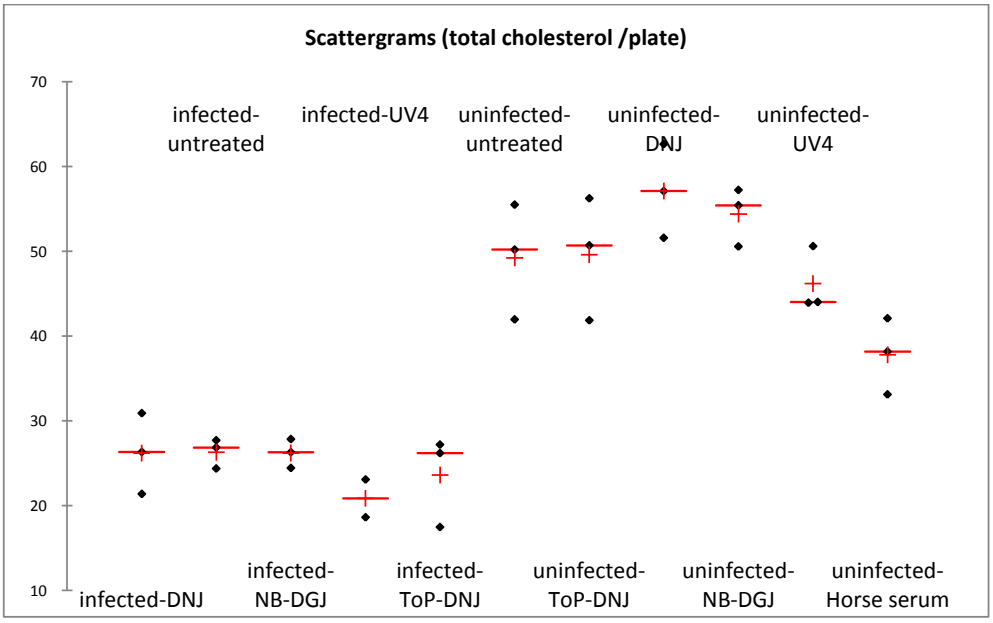

	infec-DNJ	infected-untreated	infected-NB-DGJ	infect-UV4	infected-ToP-DNJ	uninfected-untreated	uninfected-ToP-DNJ	uninf-DNJ	uninfected-NB-DGJ	uninfe-UV4	uninfected-horse serum
M	26,194	26,298	26,201	20,844	23,608	49,219	49,606	57,109	54,411	46,197	37,801
SD	4,764	1,725	1,704	3,151	5,343	6,808	7,263	5,531	3,441	3,827	4,497

Also, UV4 treatment has no significant influence at 6h, 24h (and 48h figure above) on the total cholesterol level in cultured cells.
NB: At 6, 24 and 48hrs the total amounts of cholesterol are not in proportion with the total amounts of proteins (at 48hrs) or with the total amounts of FAME (at 48hrs).

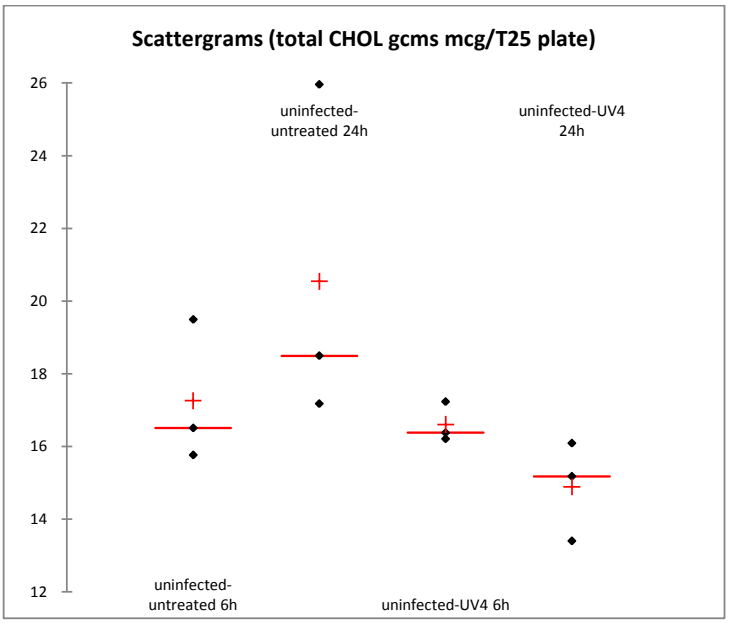

Cholesteryl esters are (slightly) decreased by infection (28.9+/-6.0 to 23.4+/-2.9 nmoles). CE amounts (average MW of ≈690) correspond to 17 mcg as compared with ≈ 50 mcg of total cholesterol (assayed by GCMS).

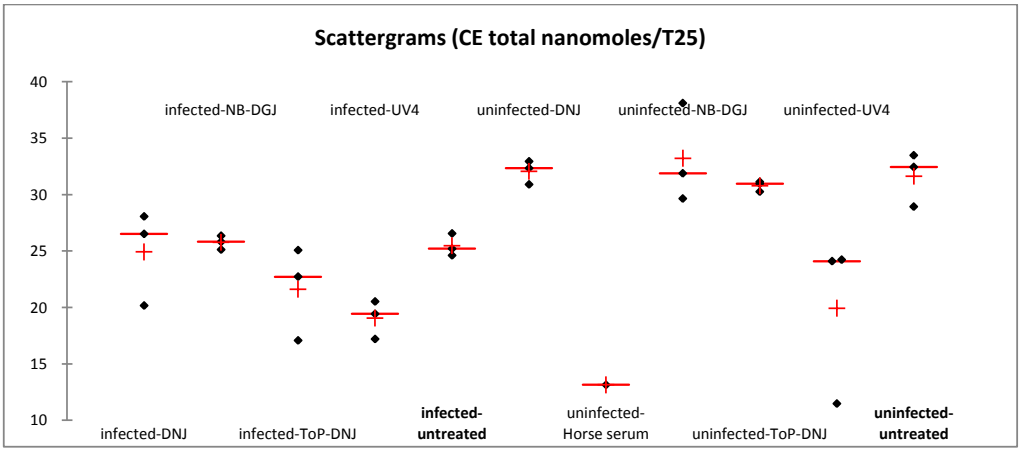

Whereas no significant variations of CE are detected, large variations in the molecular species profile are observed reflecting the reduction of DNL markers in the infected cells (16-0, 16-1, 18-1, 14-1, 14-0) at the expense of PUFA (20-3 (n?), 20-4, 22-4, 20-5, 22-6, 22-4, 22-5). The change in the molecular species profile allows a complete separation of uninfected/infected plates in the score-plot.

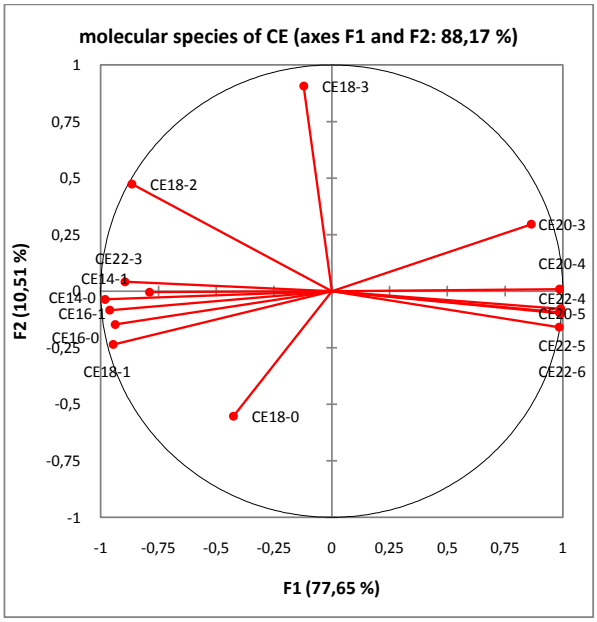

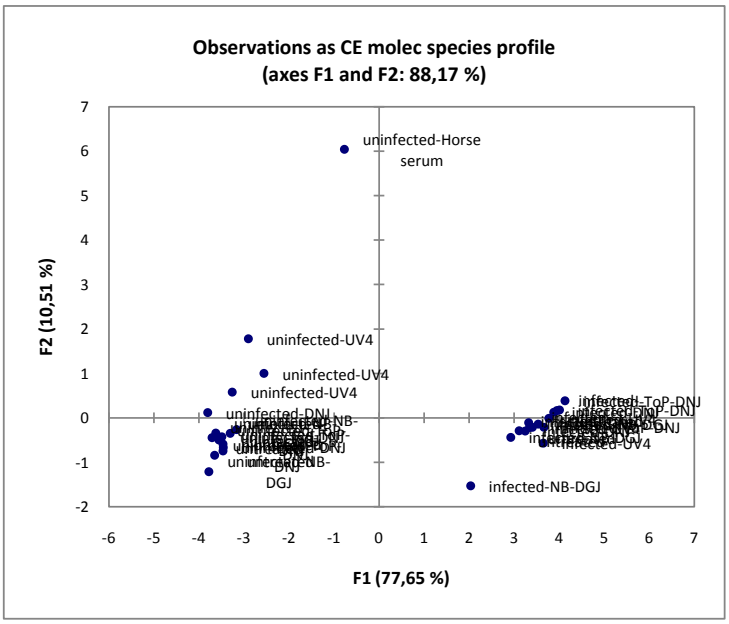

(NB: only 1 data point is reported for horse serum supplemented cultures).

As a function of time there is only a limited influence of UV4 on the total CE levels.

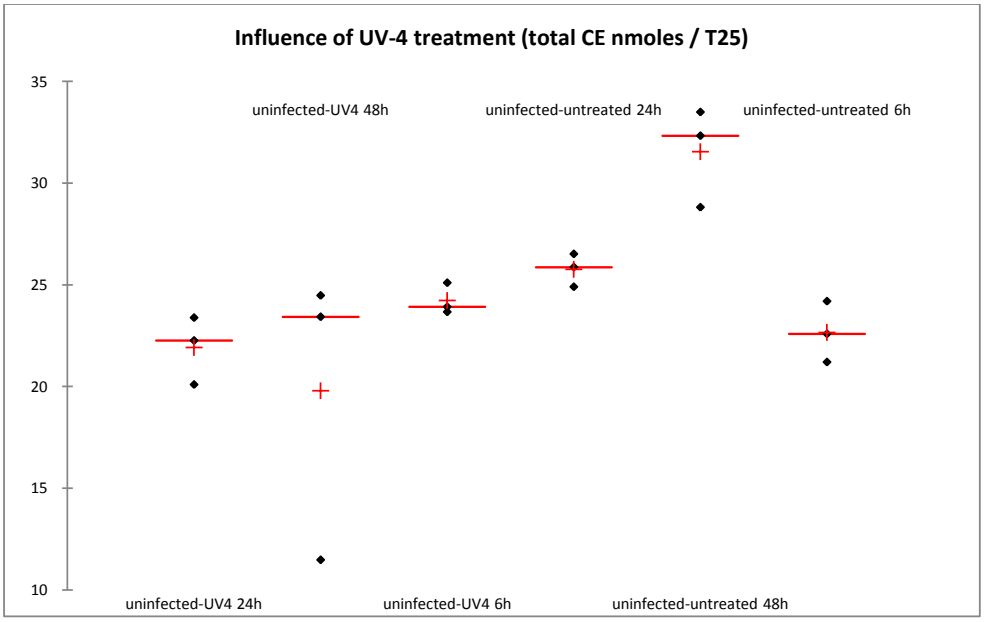

Whereas no influence of the treatment is detected on the total CE amounts, the influence on the FA composition of CE is evidenced in the score-plot as a function of the culture time:

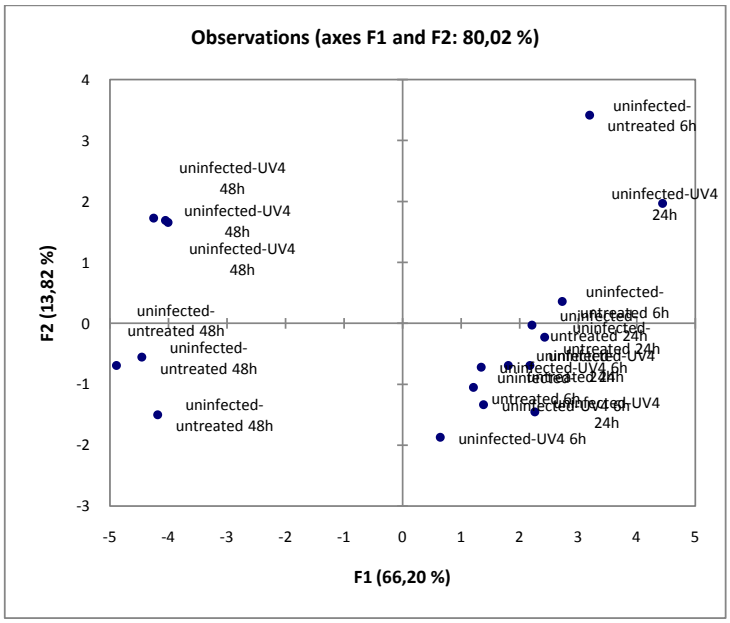

The separation of samples collected at 48h is related to their enrichment in 18:2 (n?) and FA products of the DNL pathway (C14, C16:1) at the expense of PUFA. However there is no separation under the influence of UV4 treatment detected in the score-plot

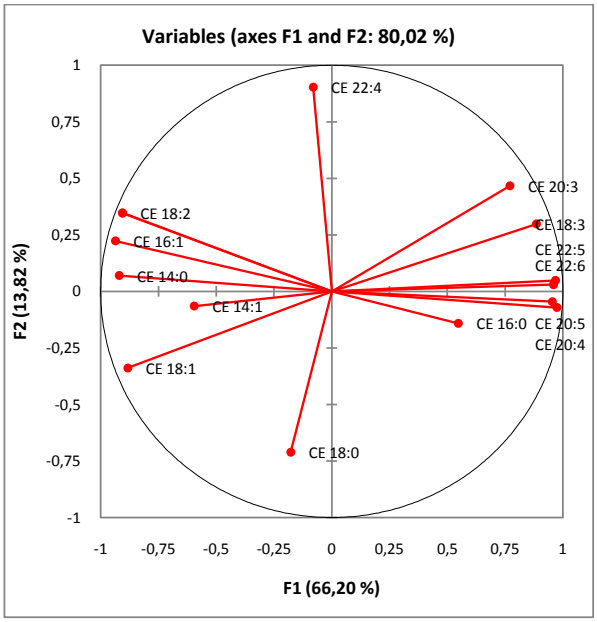

3- Total triglycerides (TAG) in lipids extracted from HCVcc infected (samples 1 to 15) and uninfected Huh7.5 cell plates (s. 16 to 30 and BCS/horse serum supplemented).

167 molecular species are assayed by tandem MS. The total TAG amounts are quantified relatively to an internal standard of 2 nmoles triheptadecanoyl (tri C17:0) TAG added to the lipid extract.

Infection reduces the TAG content of plates by **-77%** (71.15+/-4.38 > 17.56+/-2.25 nmoles).

UV4 treatment reduces the TAG content in uninfected cells by -45% (67.7+/-2.8 nmoles>37.8+/-12.4 nmoles). This reduction is not observed for cultured cells collected at 6 and 24 hrs where the TAG levels are considerably lower (≈23 nmoles) than 48 hrs (see below).

Plates supplemented by **horse serum** instead of bovine calf serum show a reduced TAG content (67.7+/-2.8 > 18.3+/-1.2; **-74%**). This large decrease in TAG is consistent with a reduced DNL rate previously described in the composition of FAME%.

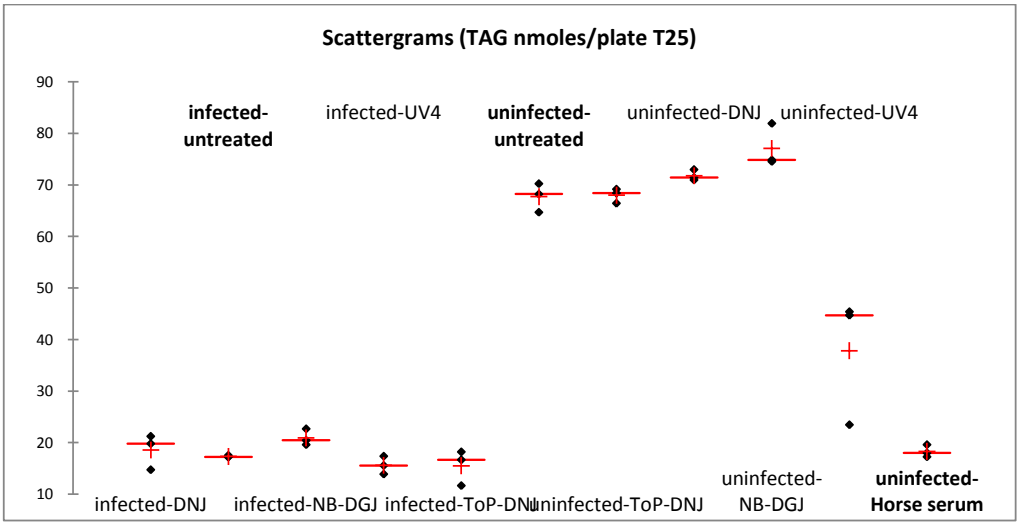

	infected-DNJ	**infected-untreated**	infected-NB-DGJ	infected-UV4	infected-ToP-DNJ	**uninfected-untreated**	uninfected-ToP-DNJ	uninfected-DNJ	uninfected-NB-DGJ	uninfected-UV4	**uninfected-Horse serum**
Ave	18,6	17,3	20,9	15,6	15,5	67,7	68,0	71,8	77,1	37,8	18,3
SD	3,4	0,2	1,6	1,7	3,4	2,8	1,4	1,0	4,2	12,5	1,2

The molecular species composition of TAG shows also large variations correlated with the total TAG content, which can be interpreted as a variation in the DNL rate. The scoring of TAG profile is mostly influenced by TAG marking high DNL rate.
The score-plot shows the separation of 4 sub-groups (uninfected-horse serum supplemented plates, infected, uninfected plates and infected-UV4 treated plates) in 2 factorial plans F1, F2 and F1, F3 representing altogether 95% of the total variability.

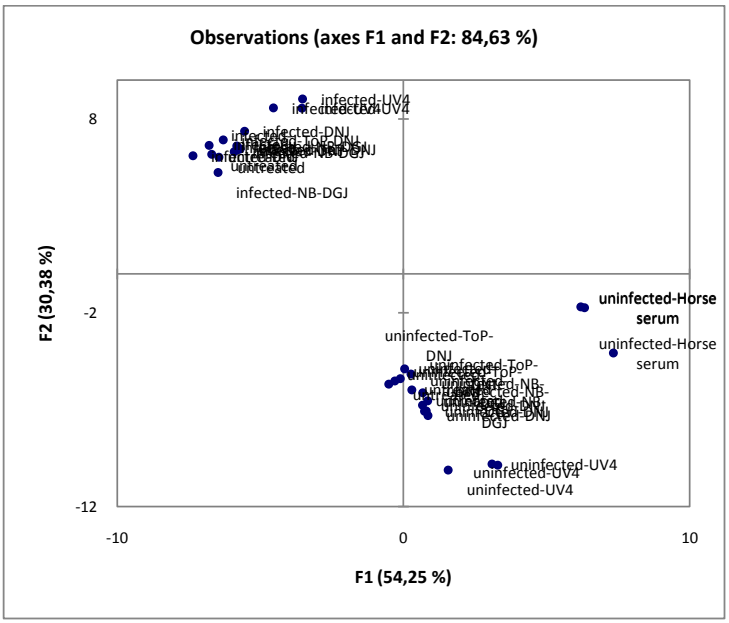

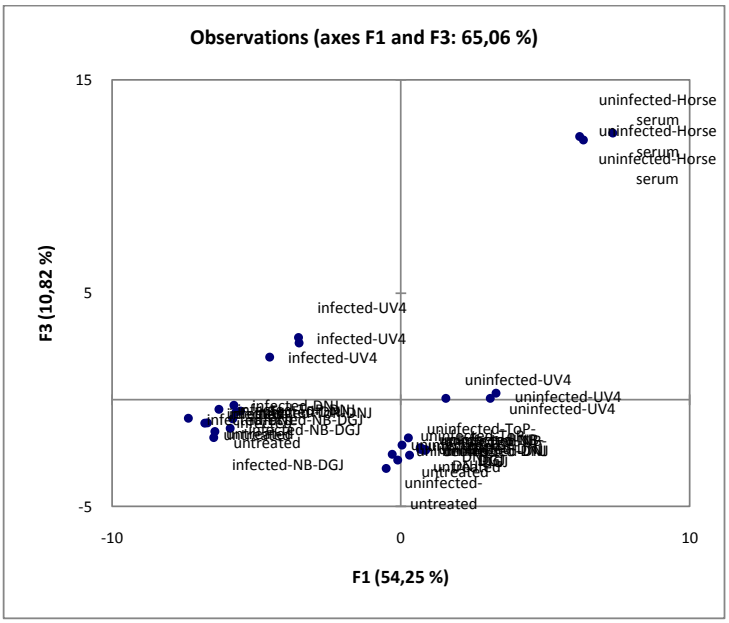

The corresponding load-plots collecting the variations of 167 molecular species of TAG for the 33 samples reveals most influential species along F1, F2 and F3 components (Factor loadings are shown in the Table below).

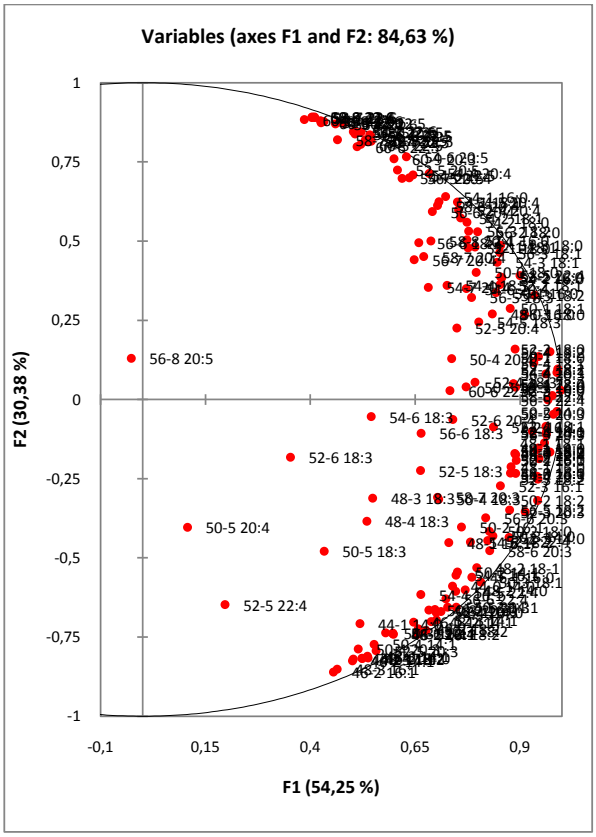

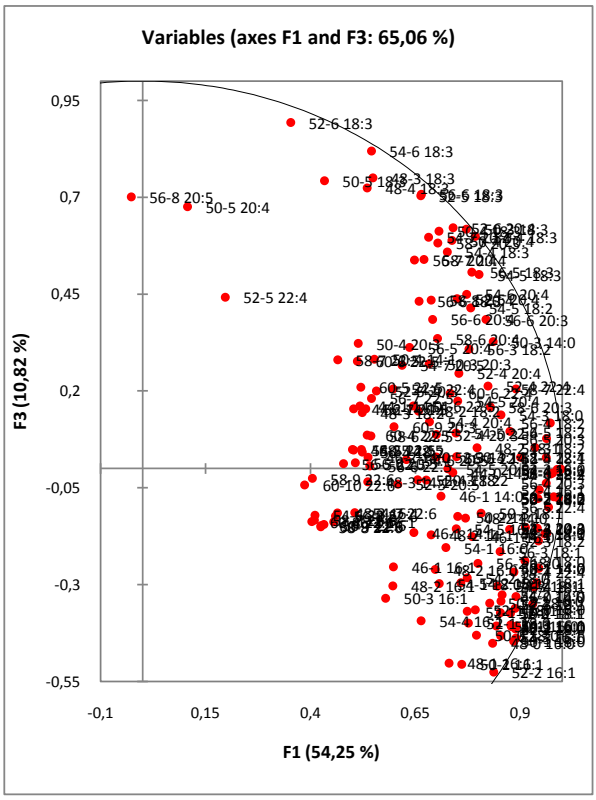
Variables (axes F1 and F3: 65,06 %)
F3 (10,82 %)
F1 (54,25 %)
0,95
0,7
0,45
0,2
-0,05
-0,3
-0,55
-0,1
0,15
0,4
0,65
0,9
52-6 18:3
54-6 18:3
56-8 20:5
50-5 20:4
52-5 22:4
52-2 16:1

Table of Factors loadings. Only the 10 highest and lowest loadings in the TAG profile are shown. Their contributions in the principal component axis F1, F2 and F3 are given. Molecular species are given as xx:yy zz (xx = carbon number comprised in the 3 acyl chains; yy = total double-bond number; zz = neutral loss by cleavage of one FA (the NL is used for MS2 detection after CID of TAG species).

	F1		**F2**		**F3**
52-3 16:0	0,997	58-7 22:6	0,892	52-6 18:3	0,893
52-2 18:2	0,990	58-9 22:6	0,892	54-6 18:3	0,819
54-4 18:1	0,988	60-8 22:6	0,891	48-3 18:3	0,750
50-2 14:0	0,988	54-6 22:6	0,890	50-5 18:3	0,743
58-5 20:3	0,979	60-10 22:6	0,884	48-4 18:3	0,724
58-6 22:4	0,977	58-8 22:6	0,880	56-6 18:3	0,707
54-4 18:2	0,972	56-7 22:6	0,877	52-5 18:3	0,704
56-4 18:2	0,971	60-9 22:6	0,874	56-8 20:5	0,701
56-5 22:4	0,967	56-5 22:5	0,872	50-5 20:4	0,676
52-4 14:0	0,963	56-8 22:6	0,870	52-6 20:4	0,622
56-5 20:3	0,962	54-7 22:6	0,846	50-3 18:3	0,617
60-9 22:6	0,425	50-4 14:1	-0,773	50-2 16:0	-0,407
58-8 22:6	0,424	50-4 20:3	-0,788	48-1 16:0	-0,408
54-6 22:6	0,411	52-5 20:3	-0,793	52-2 18:0	-0,414
58-7 22:6	0,409	48-3 14:1	-0,810	50-0 18:0	-0,430
58-9 22:6	0,404	46-2 14:0	-0,816	52-3 16:1	-0,432
60-8 22:6	0,403	50-4 18:2	-0,817	54-3 16:0	-0,438
60-10 22:6	0,386	48-3 18:2	-0,818	50-1 18:0	-0,446
52-6 18:3	0,353	44:2 14:1	-0,820	48-0 16:0	-0,452
52-5 22:4	0,197	46-2 14:1	-0,825	48-1 16:1	-0,502
50-5 20:4	0,107	48-3 16:1	-0,852	50-2 16:1	-0,506
56-8 20:5	-0,027	46-2 16:1	-0,860	52-2 16:1	-0,526

Interpretation of the compositional variations in TAG (PCA):

Factor F1 separates observations as a function of the double-bond numbers; high loadings are 4 unsaturations (average nDB=4; nC=54,36) *versus* lower loadings values (nDB=6,2; nC=55,8).

F2 separates observations for their enrichment in DHA (corresponding to highly positive loading factors with nC=57,27 and nDB=6,73) *versus* DNL products with low nC (48) and low nDB (3,09) values (corresponding to negative loadings).

F3 separates observations as a function of ALA (18:3) enrichment (positive loadings) *versus* SAT and MUFA (16:0, 18:0, 16:1; negative values).

Finally, the comparison of score- and load-plots reveals that;

1. Infected Huh7.5 plates (low F1, high F2) contain low levels of TAG enriched in polyunsaturated FA, especially DHA (low F1 loadings, high F2 loadings). The high PUFA levels is at the expense of DNL markers (low F2, low F3).

2. Treatment by UV4 in infected cells collected at 48 hrs show higher F2 and F3 loadings consistent with higher DHA- and ALA-containing TAG, respectively, as compared with untreated and other inhibitors. In uninfected cultures UV4 treatment, the loadings are shifted to lower F2 (lower DHA) but higher F3 (higher ALA). (blockade of the ALA interconversion to DHA?).
3. Horse serum supplemented uninfected plates form a distinct sub-group regarding the TAG composition with much higher F1 and higher F3 than other plates. This shift corresponds to lower DHA levels but higher ALA-containing TAG (blockade of the ALA interconversion to DHA?).

The measurement of UV4 activity on total TAG levels reveals a reduction after 48 h culture but (low) levels are not influenced by UV4 treatment at 6 and 24h.

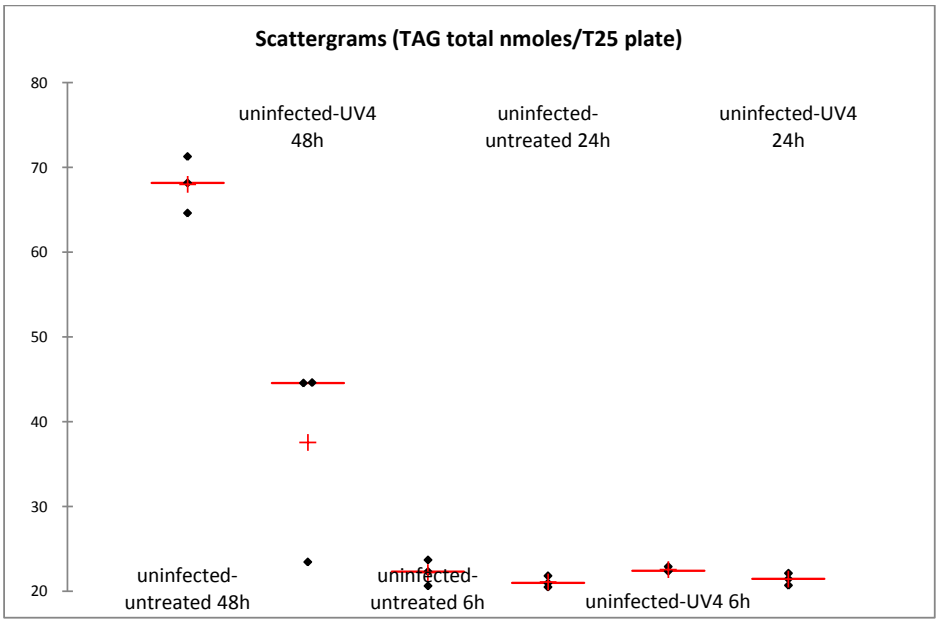

As a function of time the FA composition of TAG is shifted. The changes in TAG profile result in the separation of 6h, 24 h and 48 h scores. The separation of UV4-treated/untreated cultures is only detected at 48h (not at 6 and 24 hrs culture times).

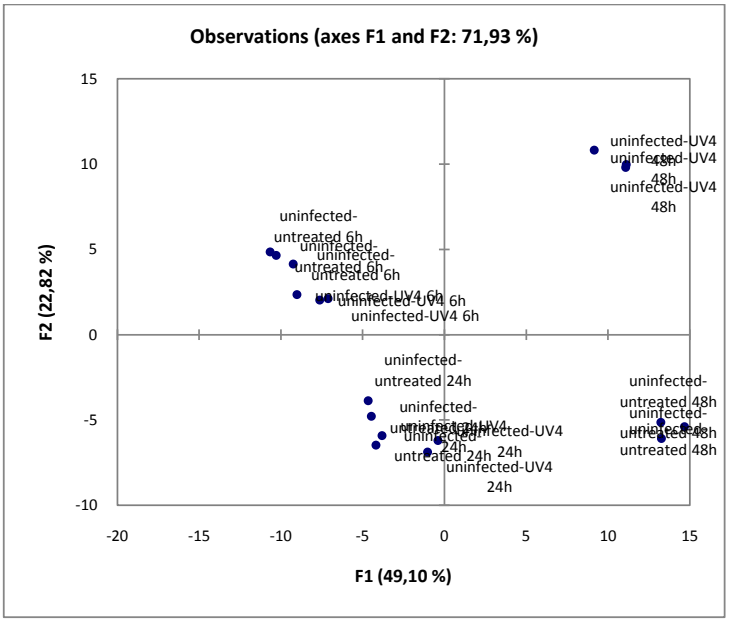

The separation of 48h data-points along F1 is consistent with the enrichment in TAG species (nC=55, nDB=3,27) with a positive contribution such as indicated in the table (Molecular species are given as xx:yy zz (xx = carbon number comprised in the 3 acyl chains; yy = total double-bond number; zz = neutral loss Induced by Dissociation (cleavage) of one in 3 FAs (the NL is used for MS2 detection after CID of TAG species).

	F1
54-3 18:0	0,963
52-2 18:1	0,962
56-3 18:2	0,952
56-3 18:1	0,950
52-4 14:0	0,937
54-2 18:1	0,926
54-1 18:0	0,919
58-5 20:3	0,899
60-6 22:4	0,897
56-4 18:1	0,895
54-3 16:1	0,888

The shift of 6h- and 24h-samples (treated as well as untreated) relatively to 48 h-samples is consistent with polyunsaturated species with a negative contribution (nDB=4,09) along F1:

54-7 20:4	-0,945
50-3 18:1	-0,946
54-5 18:2	-0,948
56-7 20:5	-0,948
54-6 20:4	-0,949
52-4 18:2	-0,955
50-2 16:1	-0,961
50-4 18:2	-0,962
56-6 20:3	-0,962

3- Diacylglycerol (DAG) extracted from HCVcc infected (samples 1 to 15) and uninfected Huh7.5 cell plates (s. 16 to 30 and horse serum supplemented).

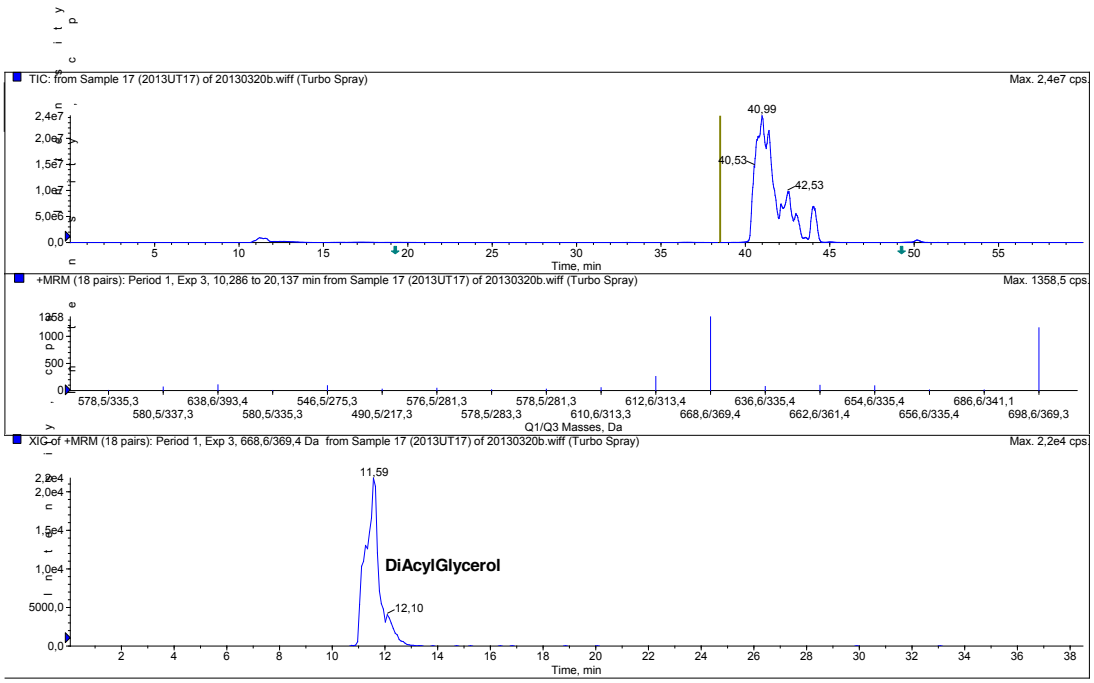

Infection reduces the level of DAG in cell plates from ≈ 1.31 to 0.86 nmoles.
UV4 treatment and horse serum supplementation decreases also DAG level in uninfected plate as already noted for total FA and TAG levels.

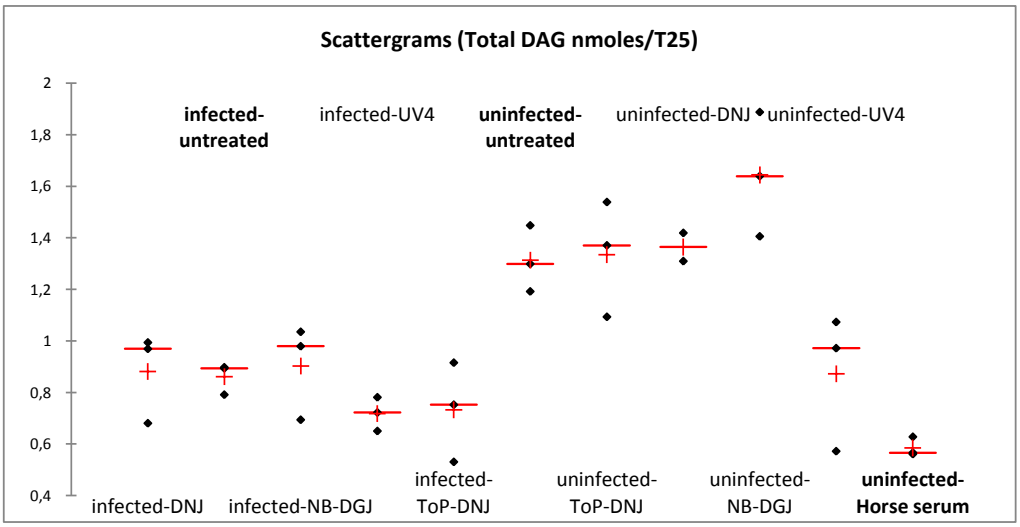

	infected-DNJ	**infected-untreated**	infected-NB-DGJ	infected-UV4	infected-ToP-DNJ	**uninfected-untreated**	uninfected-ToP-DNJ	uninfected-DNJ	uninfected-NB-DGJ	uninfected-UV4	**uninfected-Horse serum**
Av.	0,88	0,86	0,90	0,72	0,73	1,31	1,33	1,36	1,64	0,87	0,58
SD	0,17	0,06	0,18	0,07	0,19	0,13	0,22	0,08	0,24	0,27	0,04

Altogether the variations of end-products (FA, TAG, CE) and intermediary metabolites (DAG) are consistent with a reduced DNL rate by infection, UV4 treatment and horse serum supplementation.

No separation between any sub-groups is detected in the score-plot based on the composition of DAG.

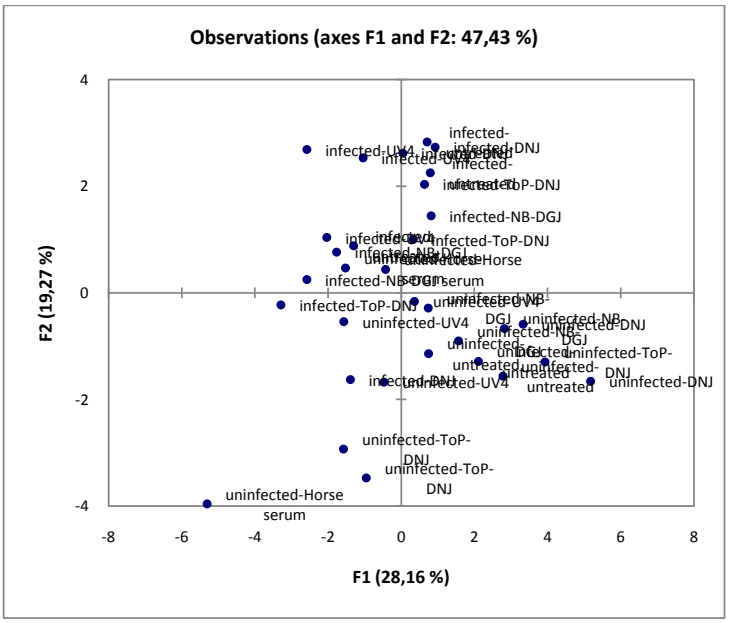

No influence on the DAG level is observed after UV4 treatment at 6, 24 (below).

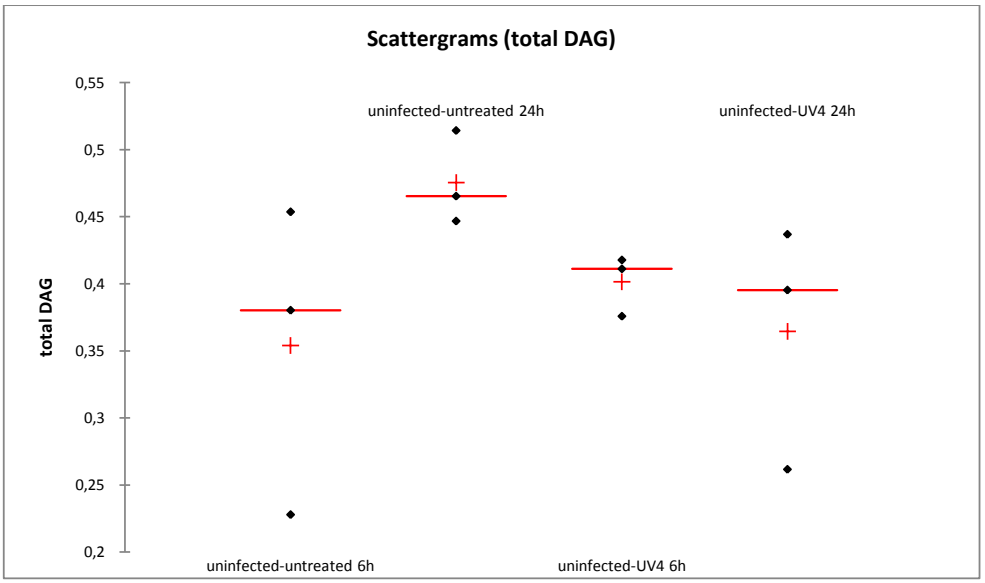

4- Total phosphatidylcholines (PC) and lysophosphatidylcholines (LPC) extracted from HCVcc infected (samples 1 to 15) and uninfected Huh7.5 cell plates (s. 16 to 30 and horse serum supplemented).

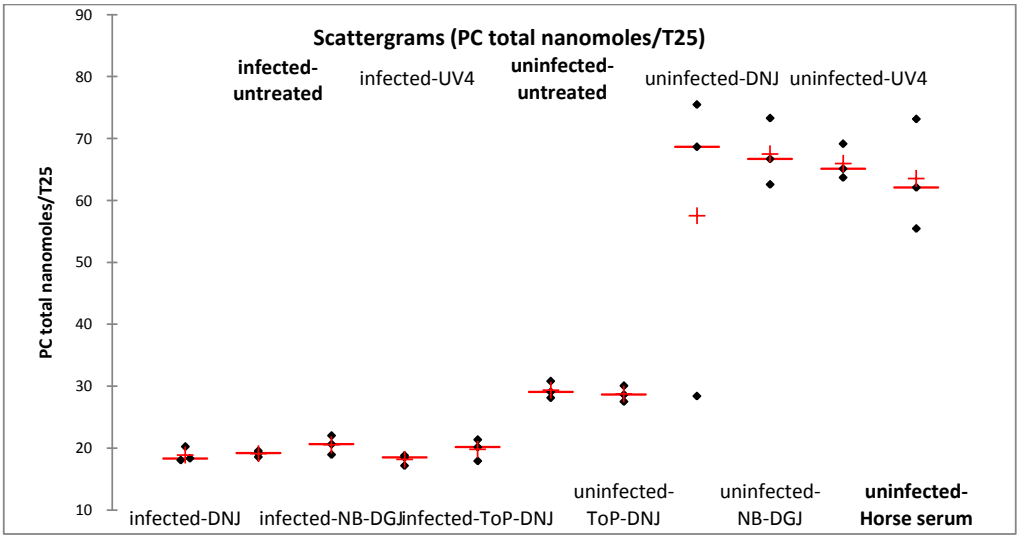

	infected -DNJ	**infected-untreated**	infected-NB-DGJ	infected -UV4	infected-ToP-DNJ	**uninfected-untreated**	uninfected-ToP-DNJ	uninfecte d-DNJ	uninfected-NB-DGJ	uninfect -UV4	**uninfected-Horse serum**
Av	18,9	19,1	20,5	18,2	19,8	29,4	28,8	57,5	67,5	66,0	63,6
SD	1,2	0,5	1,5	0,9	1,7	1,4	1,3	25,4	5,4	2,8	8,9

Total PC is lowered by infection (19.1 +/- 0.5 nmoles/T25) as compared to uninfected-untreated samples (29.4 +/-1.4 nmoles).

NB: *Treatments by DNJ, NB-DGJ, UV4 and supplementation with horse serum increase considerably the total PC amounts to ≈60 nanomoles as compared with uninfected untreated plates (≈29 nmoles). (IS response are lowered (checked) in the corresponding recordings; I suspect a quantification inconsistency for the corresponding samples). Such an influence of DNJ, NB-DGJ, UV4 treatment was not noticed previously.*

As indicated by the compositional study of PC, 3 subgroups (infected, uninfected, horse serum supplemented) can be separated.
The score-plot does not show a separation as a function of the treatment.
The load-plot shows the enrichment in PUFA-containing PC species 36:4, 38:4 and 38:5 in horse serum supplemented plates (lower quadrant).

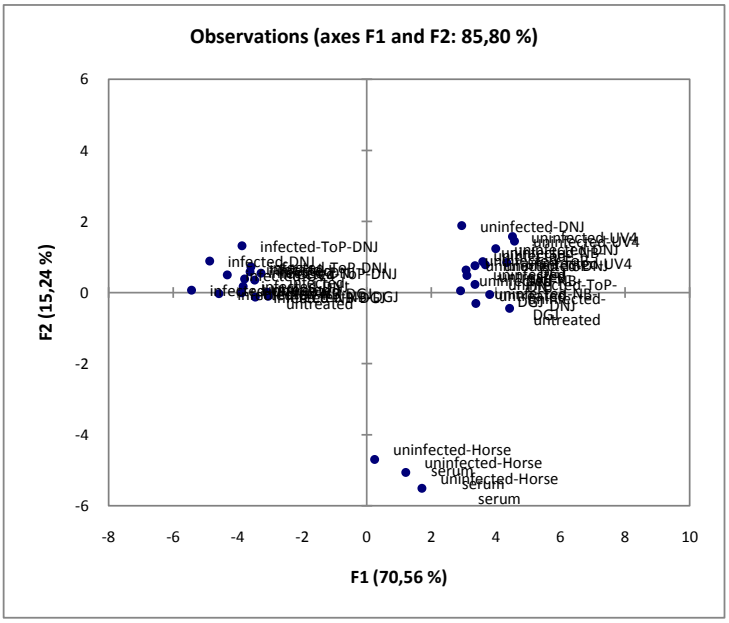
Observations (axes F1 and F2: 85,80 %)
F2 (15,24 %)
F1 (70,56 %)
6
4
2
0
-2
-4
-6
-8
-6
-4
-2
0
2
4
6
8
10
uninfected-DNJ
infected-ToP-DNJ
uninfected-Horse
uninfected-Horse
serum
serum

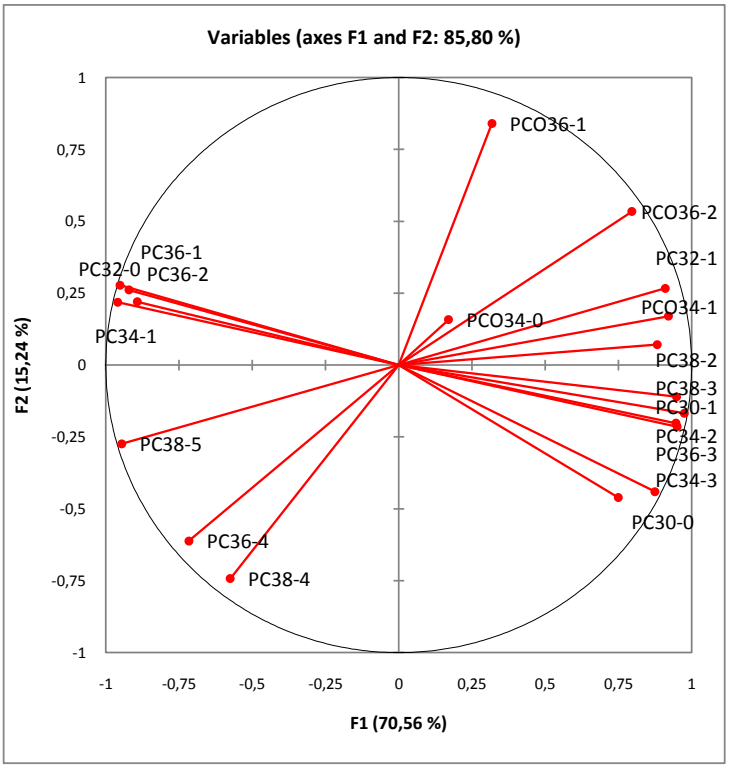
Variables (axes F1 and F2: 85,80 %)
F2 (15,24 %)
F1 (70,56 %)
1
0,75
0,5
0,25
0
-0,25
-0,5
-0,75
-1
-1
-0,75
-0,5
-0,25
0
0,25
0,5
0,75
1
PCO36-1
PCO36-2
PC32-1
PCO34-1
PC38-2
PC38-3
PC30-1
PC34-2
PC36-3
PC34-3
PC30-0
PC36-1
PC32-0
PC36-2
PC34-1
PCO34-0
PC38-5
PC36-4
PC38-4

The influence of the culture time-duration is manifest on the PC composition:

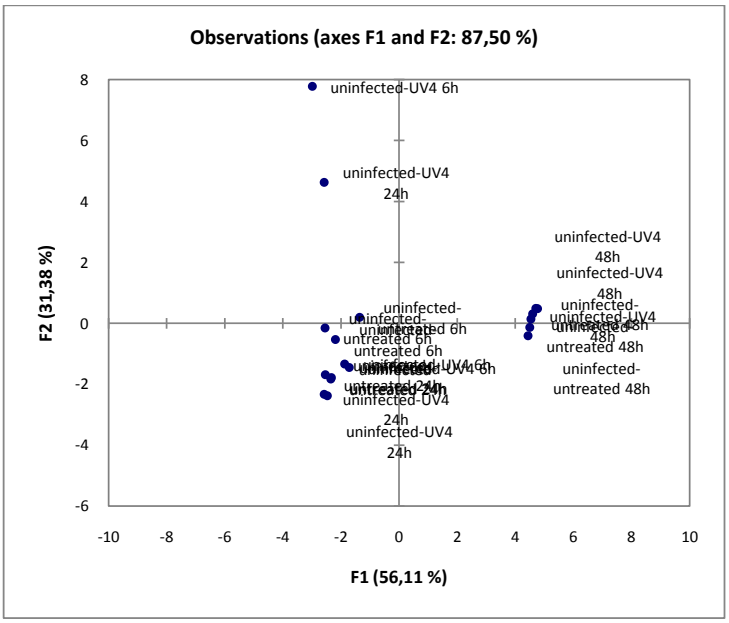

The separation of 48h data-points is based on molecular species with positive loadings along the principal component F1 such as:

PCO-34-1	0,831
PC38-4	0,884
PCO-36-2	0,888
PCO-34-0	0,925
PCO-36-1	0,963
PC38-2	0,970
PC38-3	0,975

The total lysoPC content shows only little difference as a function of infection and treatment.LPC is an index of phospholipase activity.

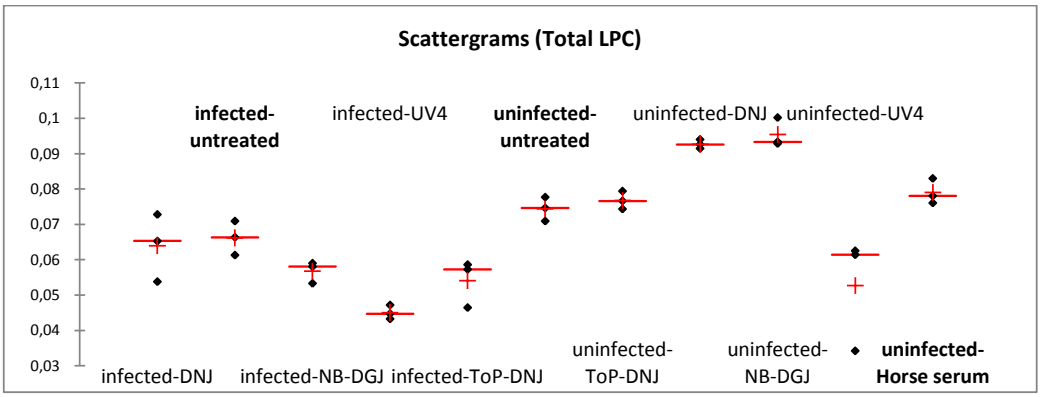

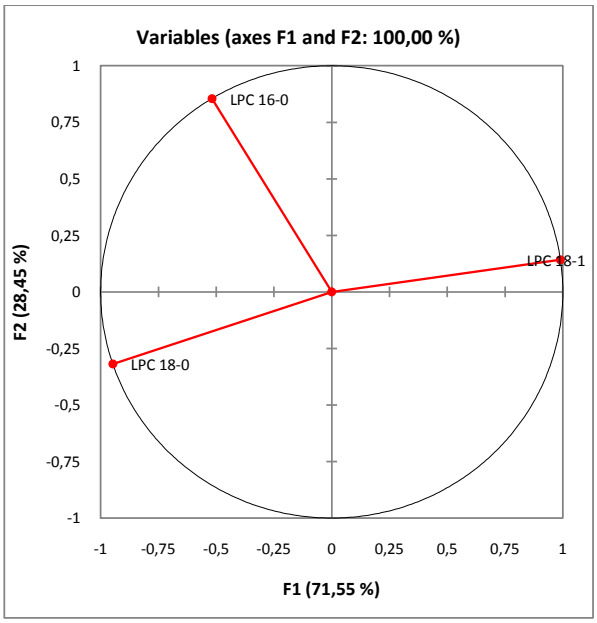

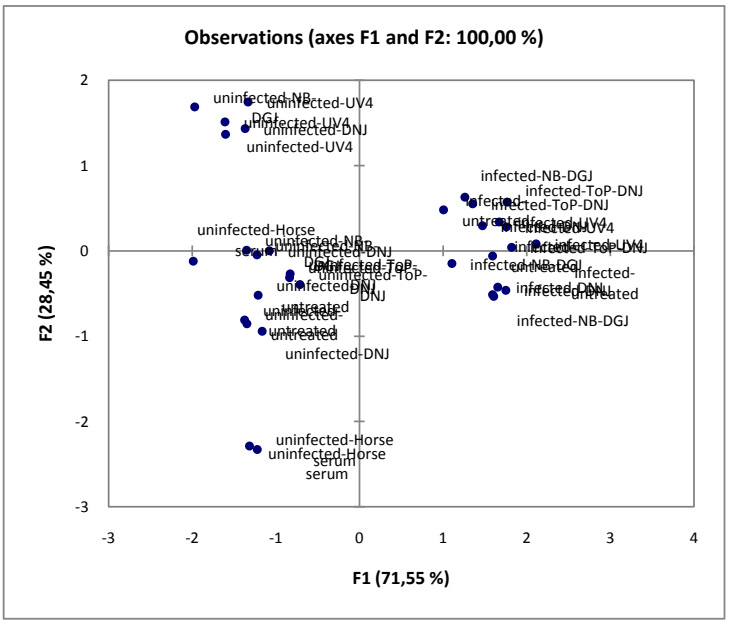

In infected plates LPC18-1 is higher than saturated LPC (LPC16-0 and 18-0). This is consistent with higher PC34-1, 36-1 and 36-2 (18-1/18-1) serving as precursor of LPC by activated PLA2 in infected plates (no PUFA-containing LPC detected; see above).

5- Sphingomyelin (SM) in extracts from HCVcc infected (samples 1 to 15) and uninfected Huh7.5 cell plates (s. 16 to 30 and horse serum supplemented).

Infection reduces the mean amount of SM from 14.08+/-2.61 nmoles/T25 plate to 9.35+/-1.55 (Internal Standard for SM is synthetic analogue SM-C12 (0.05 nmoles added for ½ T25 cell plate).

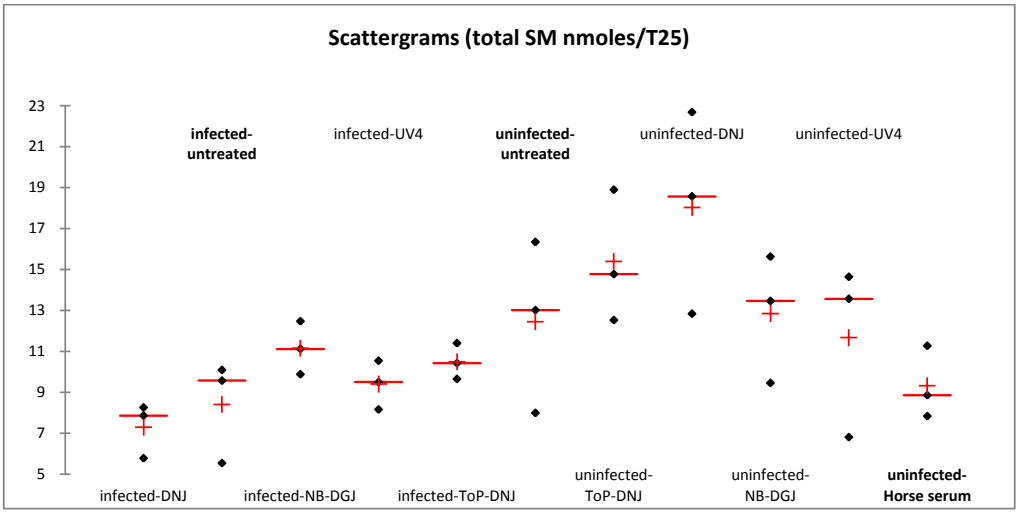

Infection and treatment change the proportions in very long chain (C24)-SM versus C16 and C18 chain SM as shown in the load-plot of the compositional study (below).

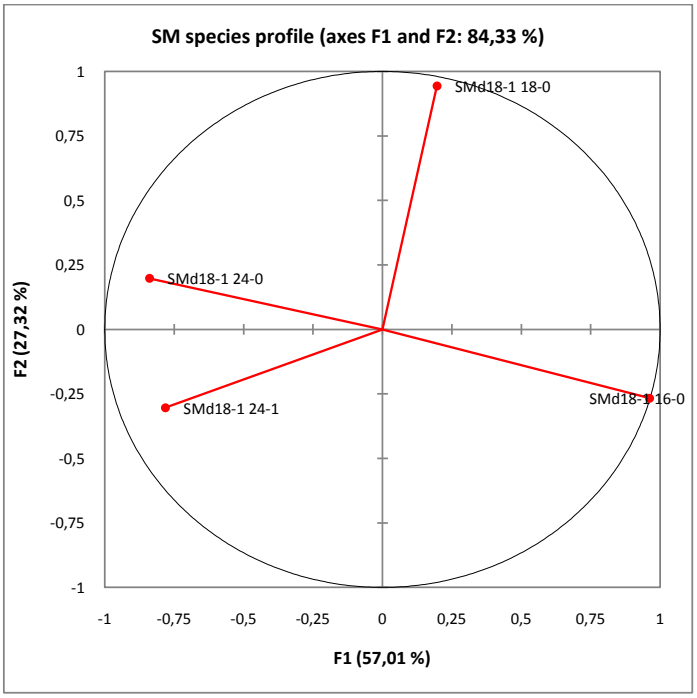

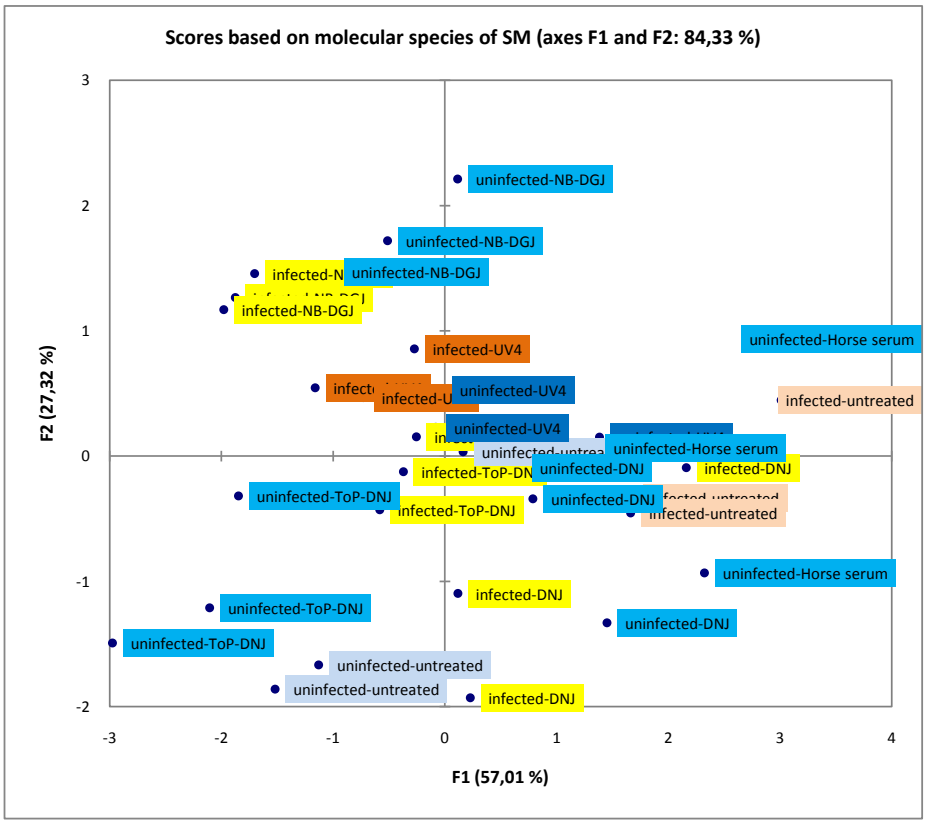

The ratio of C24:0/(C16+18)-SM is (slightly) heighted in infected **and** uninfected NB-DGJ treated plates. The ratio of C24:1/(C16+18)-SM is augmented in uninfected ToP-DNJ treated plates. Uninfected horse serum supplemented show higher C16 + C18 species.

The scatterograms show the percentages of C24:1 and 24:0-SM as a function of infection status and treatments:

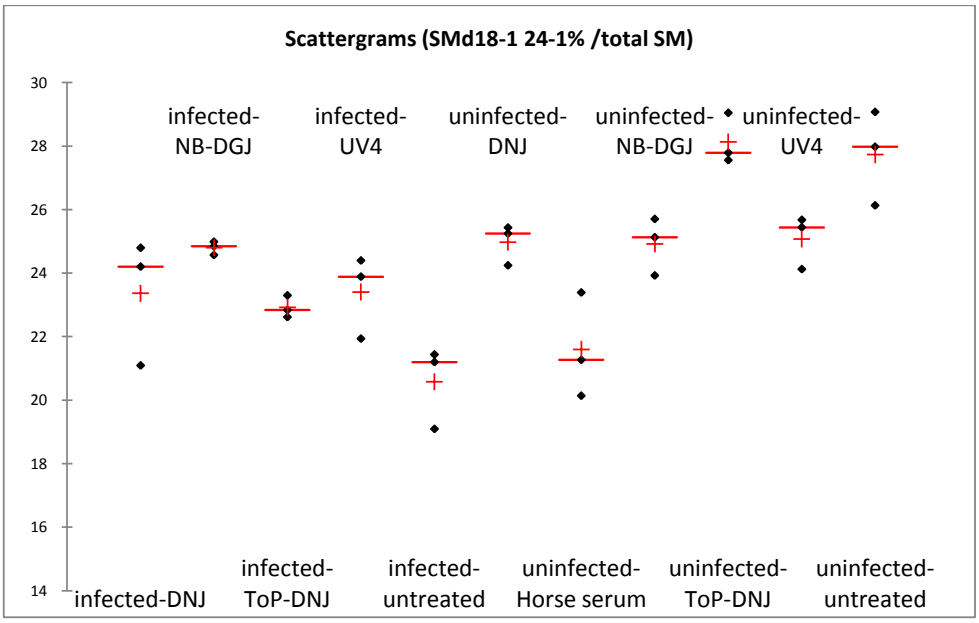

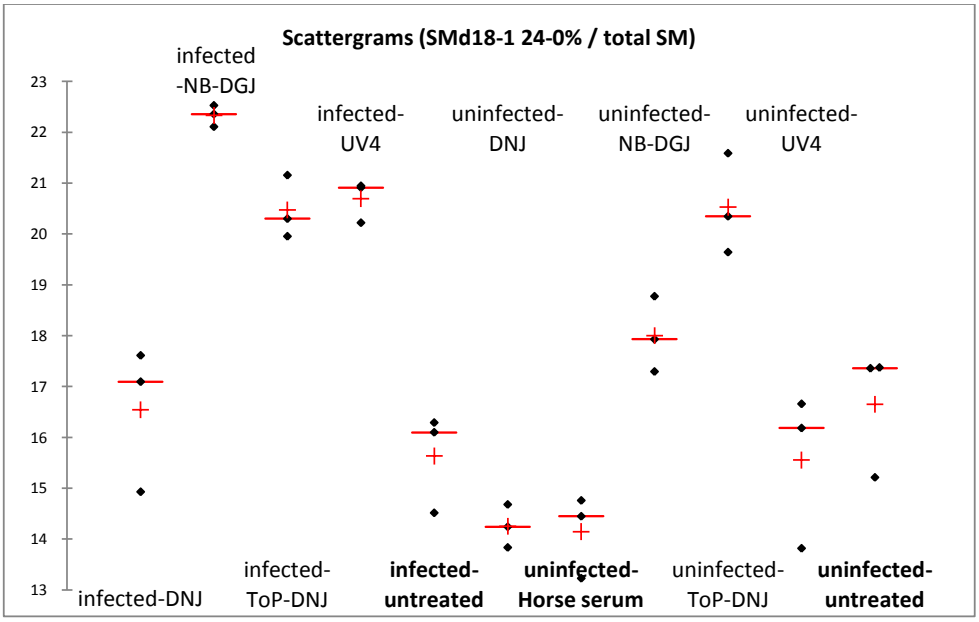

No influence of UV4 is detected on SM content.

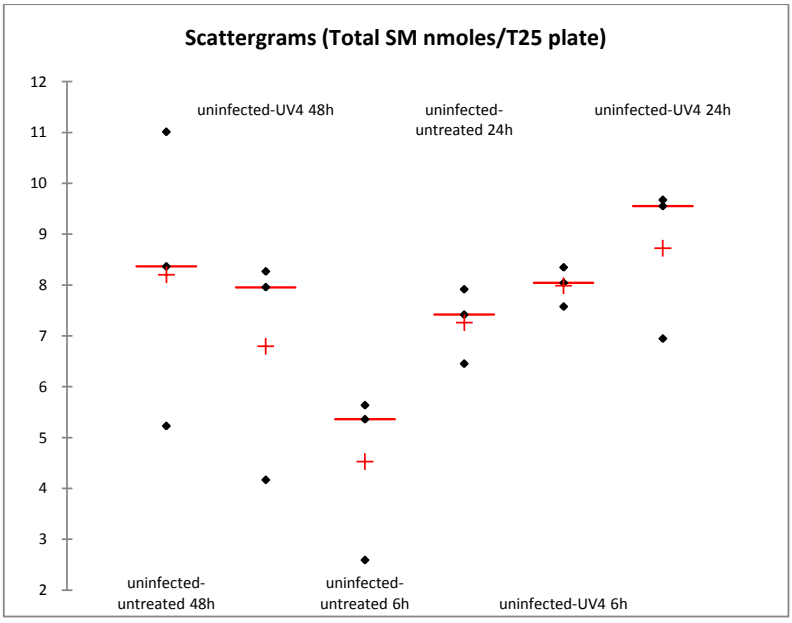

6- Ceramides (CER), HexosylCeramides (HexosylCER) and LactosylCeramides (LactosylCER) in extracts from HCVcc infected (sample 1 to 15) and uninfected Huh7.5 cell plates (s. 16 to 30 and horse serum supplemented).

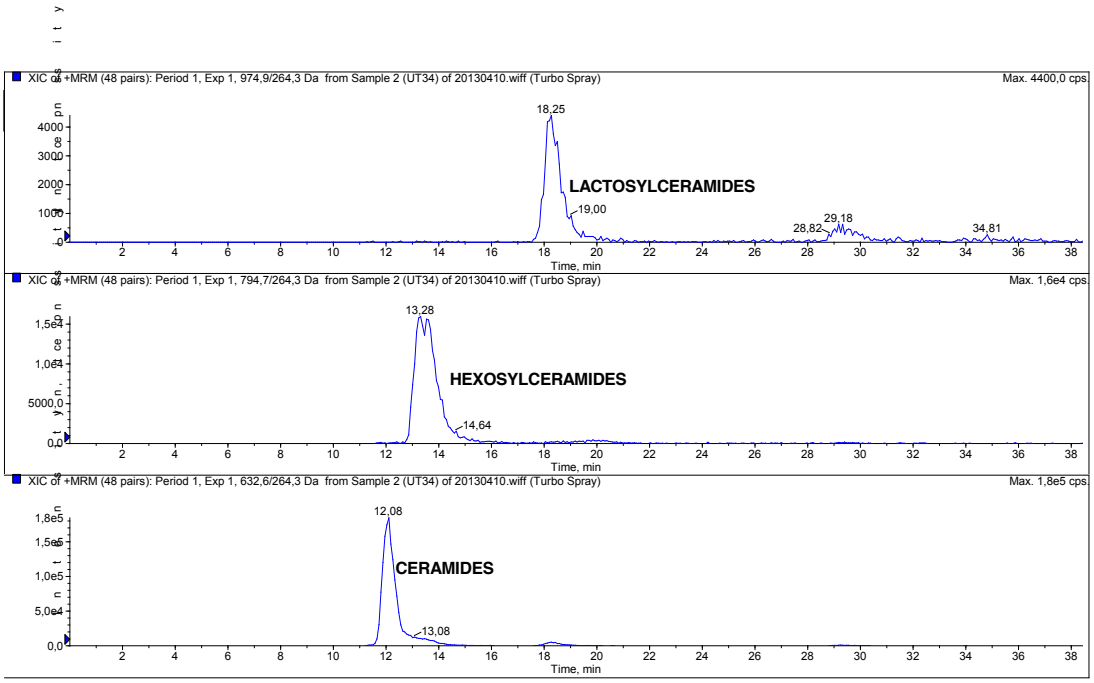

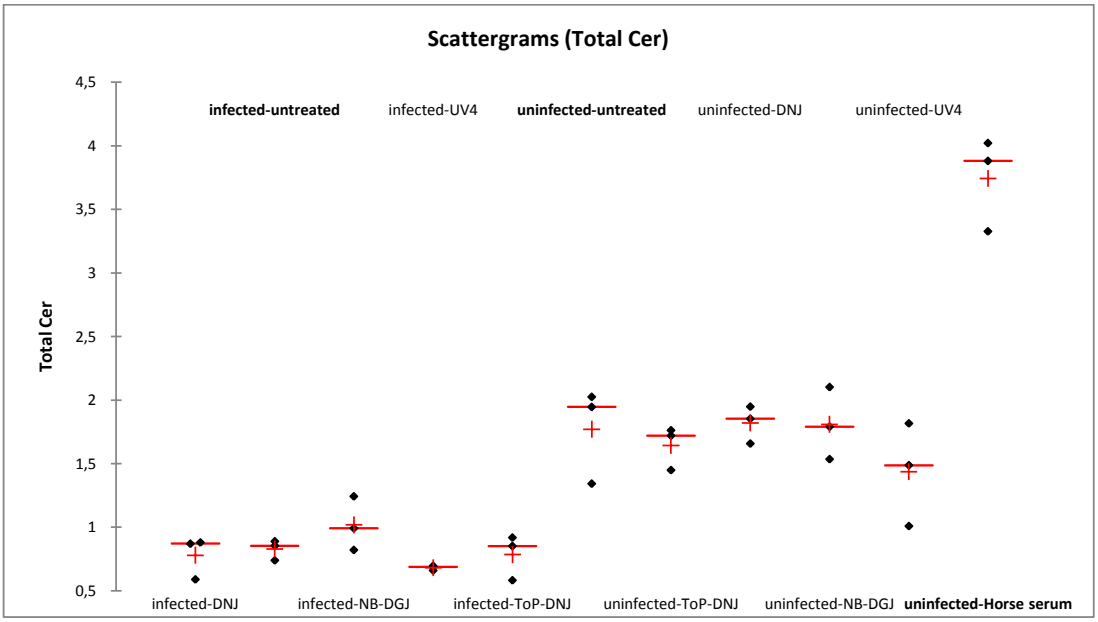

	infected -DNJ	**infected-untreated**	infected-NB-DGJ	infected -UV4	infected-ToP-DNJ	**uninfected-untreated**	uninfected-ToP-DNJ	uninfected-DNJ	uninfected-NB-DGJ	uninfected-UV4	**uninfected-Horse serum**
AVSD	0,78	0,83	1,02	0,68	0,78	1,77	1,64	1,82	1,81	1,44	3,74
	0,17	0,08	0,21	0,02	0,18	0,37	0,17	0,15	0,28	0,41	0,37

Ceramides are 0.83+/-0.08 nmoles in infected plates and 1.77+/-0.37 in uninfected plates. Horse serum supplementation increases considerably the level up to 3.74 +/- 0.37 nmoles.

A change in the fatty acid composition is associated with the change in total ceramide amounts. The compositional study discriminates infected, uninfected and uninfected horse serum supplemented plates (see score plot below). Infected plates are enriched in CER C16 and C18-0 while uninfected plates are enriched in very long chain fatty acids C24 and C26 (*inhibition of the peroxysomal conversion to VLCFA by infection*?). Horse serum supplemented plates ceramides are enriched in C22-0.

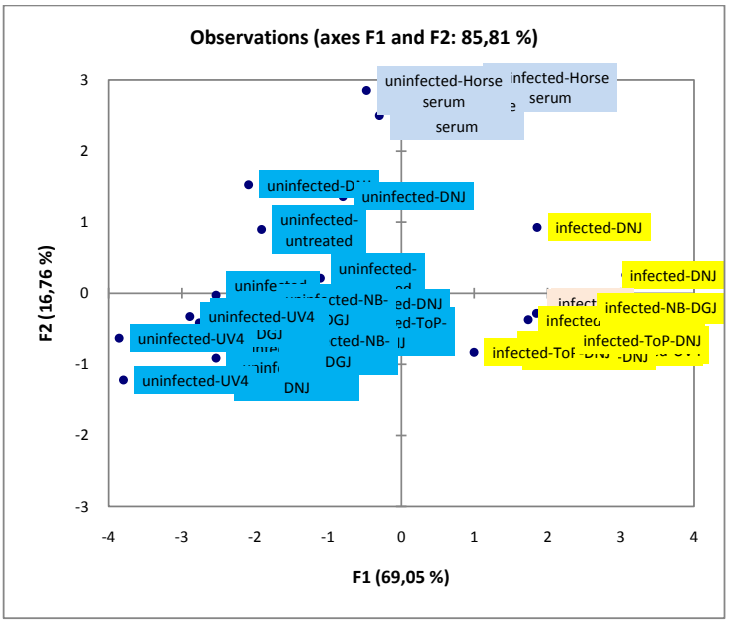

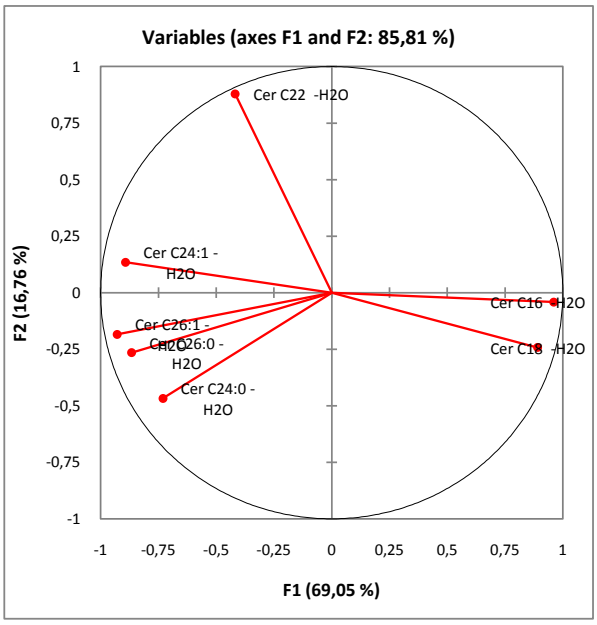

The variations in HexosylCeramide amounts (quantified relatively to glucosylCER C12 (0.05 nmoles added per ½ T25 plate)) are <u>widely influenced by the treatment</u>.

DNJ (and possibly ToP-DNJ) depress hexosylCER to a lesser degree than other inhibitors acting as complete blockers (-98.7% for UV4 50 microM: -97.4% for NB-DGJ 1000 microM).

NB: *HexosylCeramide level is considerably decreased in horse serum supplemented uninfected plates as compared with bovine serum*.

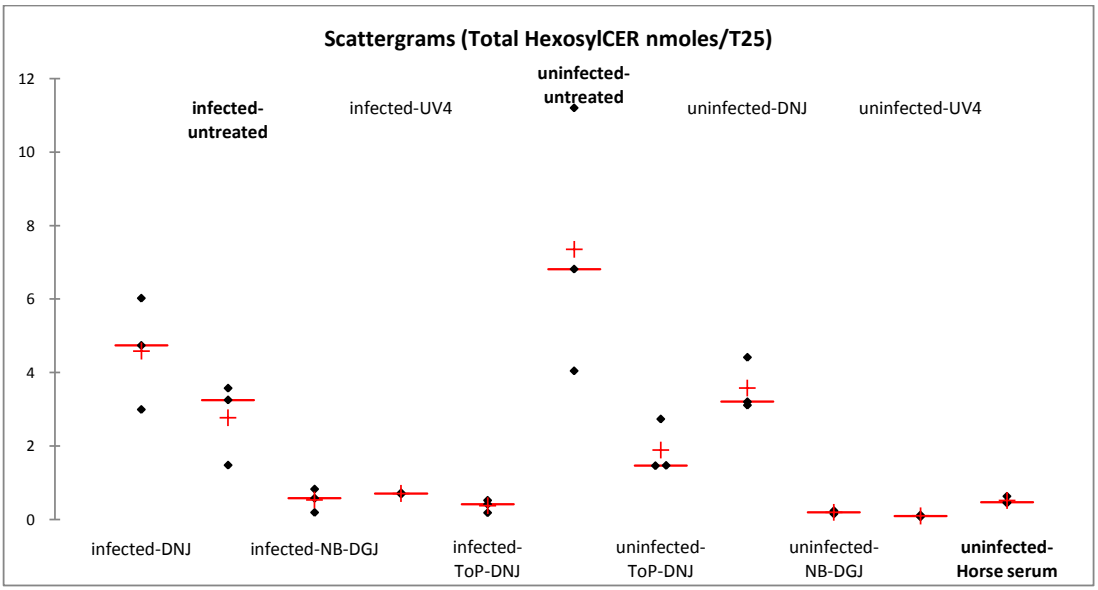

	infected-DNJ	**infected-untreated**	infected-NB-DGJ	infected-UV4	infected-ToP-DNJ	**uninfected-untreated**	uninfected-ToP-DNJ	uninfected-DNJ	uninfected-NB-DGJ	uninfected-UV4	**uninfected-Horse serum**
AVS	4,585	2,766	0,533	0,707	0,371	7,353	1,886	3,576	0,193	0,096	0,517
D	1,522	1,126	0,320	0,016	0,173	3,608	0,731	0,725	0,041	0,023	0,101

LactosylCeramides are influenced by infection status and by treatments.

NB: *Opposite to hexosylceramides lactosylCer are heightened by NB-DGJ and horse serum supplementation which suggests an accelerated glycosylation of HexCER to LacCER (?).*

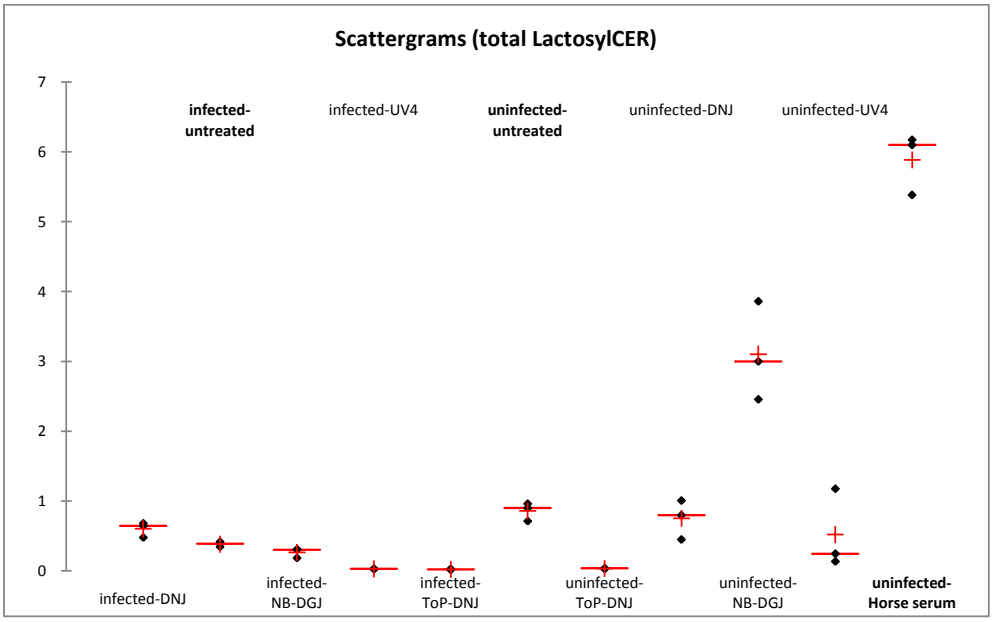

	infected-DNJ	**infected-untreated**	infected-NB-DGJ	infected-UV4	infected-ToP-DNJ	**uninfected-untreated**	uninfected-ToP-DNJ	uninfected-DNJ	uninfected-NB-DGJ	uninfected-UV4	**uninfected-Horse serum**
AVS	0,601	0,382	0,263	0,027	0,020	0,858	0,033	0,750	3,103	0,518	5,884
D	0,108	0,037	0,070	0,000	0,005	0,130	0,005	0,281	0,708	0,571	0,436

The fatty acid composition of lactosylceramides is widely changed by UV4-treatment which shows enrichment in C22 & C24-0 at the expense of C16-0 lactosylceramides in the uninfected plates.

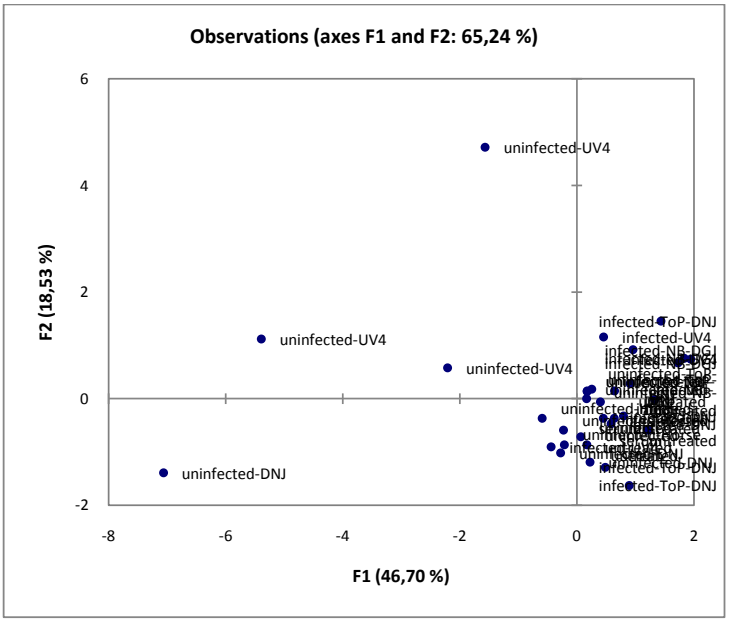

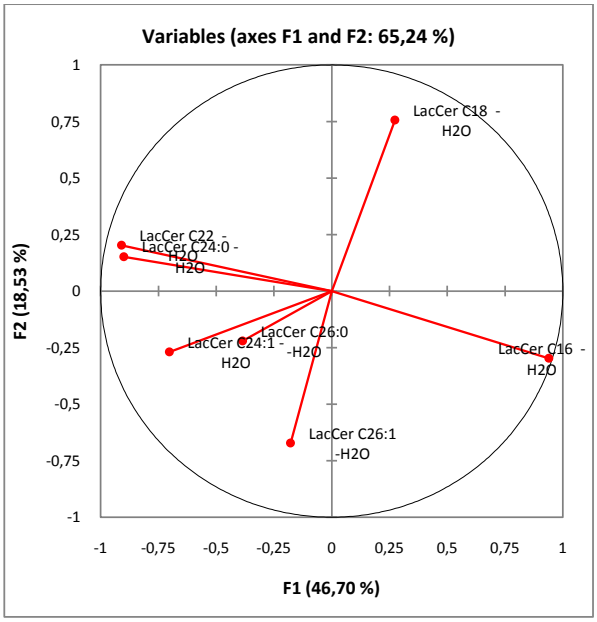

Based on total ceramide, hexosylceramide and lactosylceramide levels PCA analysis separates clearly uninfected-untreated, uninfected horse serum supplemented and infected-DNJ plates from other infection status/treatments.

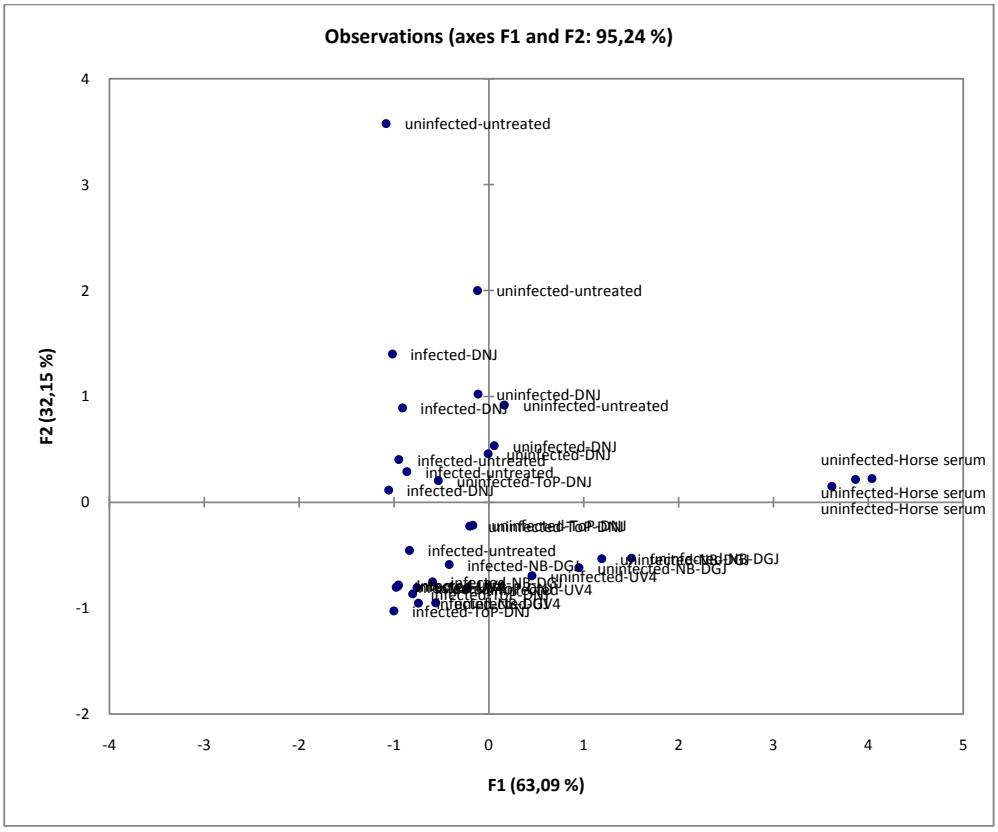

F1 component indicates Ceramides and Lactosylceramides (highly correlated) enrichment in horse serum supplemented cultures. F2 discriminates for HexosylCeramides of which the synthesis is blocked by inhibitors (except less active DNJ).

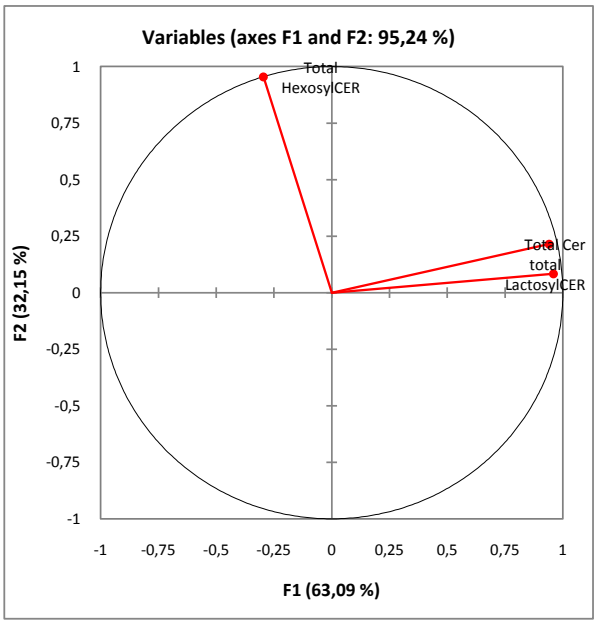

7. Kinetics of UV-4 activity on CER in uninfected plates; untreated 6h (plates 34-36), 24h (37-39) and 48 hours (16-18) *versus* UV-treated 4 (40-42, 43-45, 28-30).

	uninfected-untreated 6h	**uninfected-untreated 24h**	**uninfected-untreated 48h**	**uninfected-UV4 6h**	**uninfected-UV4 24h**	**uninfected-UV4 48h**
CER AV.	1,30	2,01	1,77	1,34	1,59	1,44
SD	0,16	0,11	0,37	0,10	0,29	0,41
HexCER	0,56	0,10	1,25	1,64	7,35	1,08
SD	0,23	0,02	0,17	0,39	3,61	0,30
LacCER	0,10	0,52	0,15	0,21	0,86	0,19
SD	0,04	0,57	0,03	0,02	0,13	0,02
HexCER/CER	0,43	0,05	0,71	1,22	4,63	0,75
LacCER/HexCER	0,18	5,42	0,12	0,13	0,12	0,18

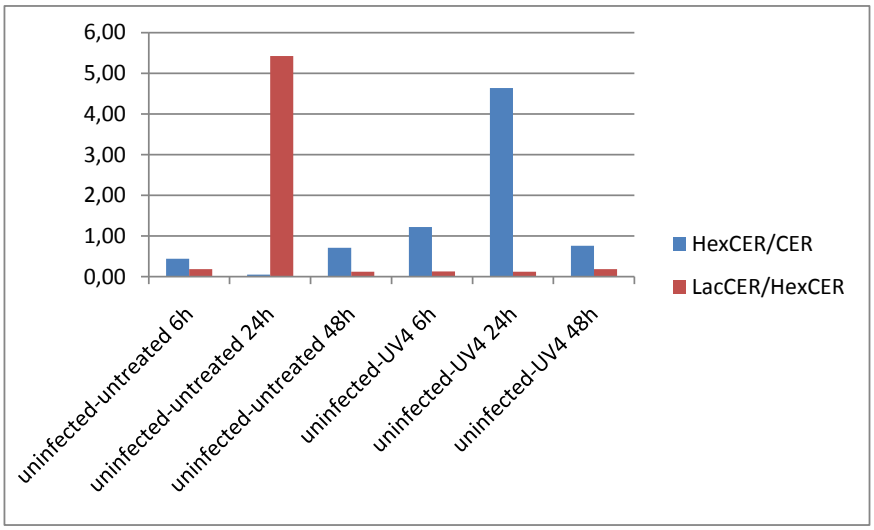

Whereas the total amounts of ceramides appears unchanged their molecular composition is changed after 48 hours culture.

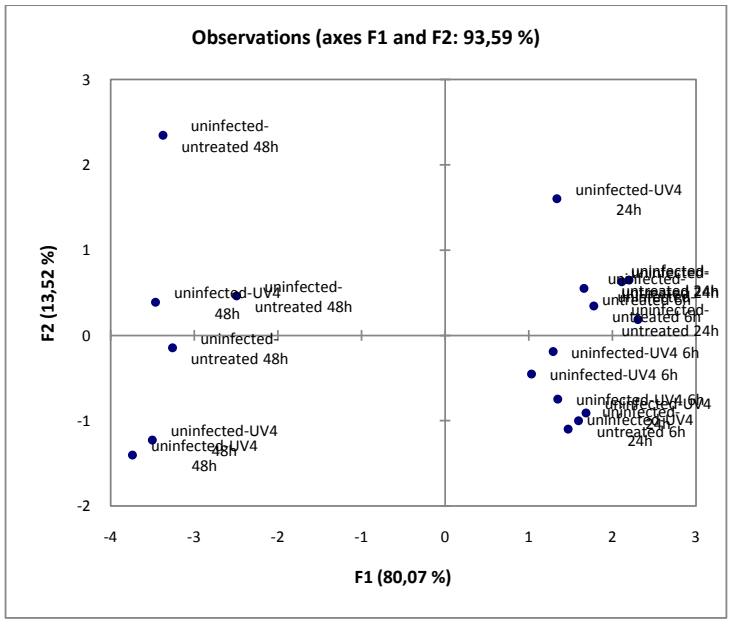

The shift to negative values corresponds to the enrichment of CER in C24:0, C26:0 and C26:1 at the expense of C22:00, C18:0 and C24:1-CER at shorter culture times.

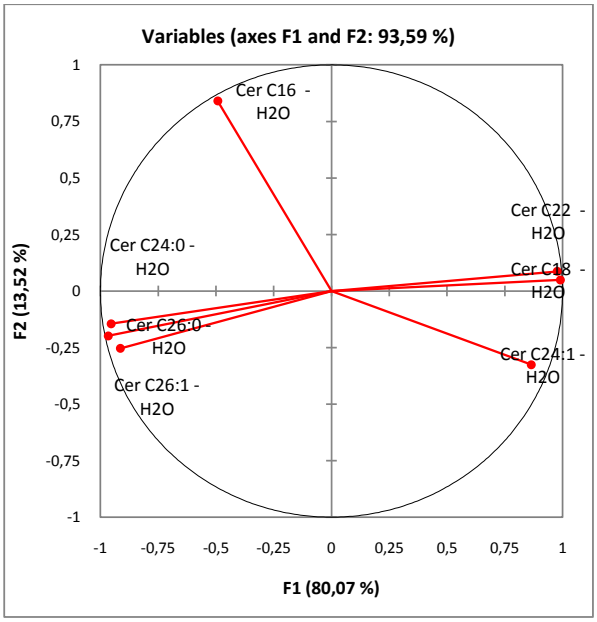

E

ToP-DNJ Pharmacokinetic Report

LIST OF ABBREVIATIONS

ACN	Acetonitrile
AUC	Area Under the Curve
CPCSEA	Committee for the Purpose of Control and Supervision of Experiments on Animals
CV	Coefficient of Variation
CL	Clearance
IAEC	Institutional Animal Ethics Committee
i.v.	Intravenous
LLOQ	Lower Limit of Quantification
LC-MS/MS	Liquid Chromatography tandem Mass Spectrometry
NA	Not Applicable
NCA	Non-Compartmental Analysis
p.o.	Per oral
SD	Standard Deviation
SOP	Standard Operating Procedures
$T_{1/2}$	Terminal elimination half-life

1.0 Summary

The objective of this study was to investigate the plasma pharmacokinetics and tissue distribution of Deoxynojirimycin in male BALB/c mice following a single intravenous and oral dose administration. A group of eighteen male mice were divided into two groups as Group 1(i.v., 2 mg/kg) and Group 2 (p.o., 10 mg/kg). Group 1 and Group 2 were administered with Deoxynojirimycin solution formulation prepared using DMSO stock (97.2 mg/mL) in 5 % NMP, 5% solutol in normal saline intravenously and orally respectively. The blood samples were collected from a set of three mice under light isoflurane anesthesia at Pre-dose, 0.08, 0.25, 0.5, 1, 2, 4, 8 and 24 hr (i.v.) and Pre-dose, 0.25, 0.5, 1 , 2, 4, 6, 8 and 24 hr (p.o.) in labeled micro centrifuge tube containing K_2EDTA as an anticoagulant. Immediately after blood collection, plasma was harvested by centrifugation and stored at -70ºC until analysis. Following blood collection, animals in Group 1 and Group 2 were euthanized by CO_2 asphyxiation at 0.5, 4 and 24 hr to collect spleen, brain, liver, kidney, heart and lung. Collected tissues were dipped in 20 mL fresh phosphate buffer saline (pH 7.4) thrice, dried on blotted paper and weighed. Tissue samples were homogenized using ice-cold phosphate buffer saline (pH 7.4) and homogenates were stored below -70ºC until analysis. Total homogenate volume was three times for lung, spleen, brain, kidney, heart and ten times the liver weight. All samples were processed for analysis by protein precipitation using acetonitrile and analyzed with fit-for-purpose LC-MS/MS method (LLOQ = 1.02 ng/mL in plasma and brain, 2.04 ng/mL in liver, spleen and lung, 10.21 ng/mL in heart and kidney). Pharmacokinetic parameters were calculated using the non-compartmental analysis tool of Phoenix WinNonlin® (Version 6.3). The overall exposure data is summarized below:

Compound	Matrix	Route	T_{max} (hr)	[a]$C0/C_{max}$ (ng/mL)	AUC_{last} (ng/mL*hr)	AUC_{inf} (ng/mL*hr)	$T_{1/2}$ (hr)	CL (mL/min/kg)	Vss (L/kg)	%F[b]
Deoxynojirimycin	Plasma	i.v.	-	78977.95	96067.91	104975.00	8.79	0.32	0.13	-
		p.o.	8.00	30.17	497.68	NR	-	-	-	0.1%

a – extrapolated concentration for i.v. administration,
b - AUC_{last} was considered for calculation of bioavailability
NR – not reported since AUC_{inf} is 20% more than AUC_{last}

Following a single intravenous administration of Deoxynojirimycin to male BALB/c mice at 2 mg/kg dose, plasma clearance was low (0.32 mL/min/kg, normal hepatic blood flow in mice is 90 mL/min/kg) with elimination half-life of 8.8 hr. Volume of distribution was less than the total body water (0.7 L/kg).

Following a single dose administration of Deoxynojirimycin to male BALB/c mice at 10 mg/kg dose, plasma concentrations were detected upto 24 hr with T_{max} of 8.0 hr. Oral solution bioavailability was low (0.1%).

Tissue to plasma concentration ratio of Deoxynojirimycin following single intravenous (Dose: 2 mg/kg) and single oral (Dose: 10 mg/kg) administration in male BALB/c mice

	Tissue to plasma concentration ratio						
Time (hr)	**Route**	**Brain**	**Liver**	**Kidney**	**Heart**	**Spleen**	**Lung**
0.5	i.v.	0.01	1.49	0.31	0.12	0.03	0.06
4		0.02	7.65	0.40	0.14	0.04	0.21
24		NA	43.70	2.38	1.00	0.18	1.17
0.5	p.o.	8.65	193.51	167.15	NA	NA	6.97
4		0.40	16.00	NA	NA	NA	1.03
24		2.48	50.41	NA	NA	NA	0.66

Following a single intravenous administration, brain-to-plasma ratio ranged between 0.01-0.02, liver to plasma ratio was 1.49-43.70, kidney-to-plasma ratio was 0.31 to 2.38, heart-to-plasma ratio was 0.12 - 1.00, spleen-to-plasma ratio was 0.03-0.18 and lung-to-plasma ratio was 0.06-1.17

Following a single oral administration, brain to plasma ratio ranged between 0.40-8.65, liver-to-plasma ratio was 16-193 and lung-to-plasma ratio was 0.66-6.97 while, concentrations were not detectable in heart and spleen. Concentrations in kidney was detectable at only 0.5 hr and the kidney-to-plasma ratio was 167.15 (0.5 hr).

2.0 Study Objective

To determine the pharmacokinetics and tissue (spleen, brain, liver, kidney, heart and lung) distribution of Deoxynojirimycin following a single intravenous and oral administration to male BALB/c mice

3.0 Test Guidelines / SOPs

The study was conducted at Sai Life Sciences Limited, Pune, India, in accordance with the Study Plan SAIDMPK/PK-14-03-090 and the guidelines of the Institutional Animal Ethics Committee (IAEC). The study was conducted under non Good Laboratory Practice; however, all relevant study documents were maintained in the study file. In-house SOPs were followed for the conduct of the study.

4.0 Animal Welfare

All procedures of the present study were in accordance with the guidelines provided by the Committee for the Purpose of Control and Supervision of Experiments on Animals (CPCSEA) as published in The Gazette of India, December 15, 1998. Prior approval of the Institutional Animal Ethics Committee (IAEC) was obtained before initiation of the study.

5.0 Experimental

5.1. Test Compound

The test Deoxynojirimycin (Batch No: JLK-IV-50: Mol wt: 662.009; Purity: Considered 100%) was received Oxford Glycobiology Institute.

5.2. Test System

Healthy male BALB/c mice (8-12 weeks old) weighing between 20 to 35 g were procured from ACTREC, Mumbai, India. Maximum three mice were housed in each polycarbonate cage. Temperature and humidity were maintained at 22 ± 3ºC and 40-70%, respectively and illumination was controlled to give a sequence of 12 hr light and 12 hr dark cycle. The temperature and humidity were recorded by auto-controlled data logger system. Animals were provided laboratory rodent diet

(Vetcare India Pvt. Ltd, Bengaluru) *ad libitum* and were provided fresh reverse osmosis water treated with UV light *ad libitum*.

5.3. Study Design

A group of eighteen male mice were divided into two groups as Group 1(i.v., 2 mg/kg) and Group 2 (p.o., 10 mg/kg). Group 1 and Group 2 were administered with Deoxynojirimycin solution formulation intravenously and orally respectively. Dosing volume administered was 5 mL/kg for intravenous and 10 mL/kg for oral administration. Assignment of animals was as below.

Group	Route	Mice ID
1	i.v.	1-9
2	p.o.	10-18

5.4. Formulation Preparation

DMSO stock was prepared by adding 200 μL to the bottle to prepare strength of 97.2 mg/mL. Formulation strength prepared was 0.4 mg/mL (i.v.) and 1 mg/mL (p.o.).

IV formulation: Accurately 0.0103 mL of DMSO stock was added into a bottle. To this bottle 0.115 mL volume of NMP, 0.125 mL volume of solutol and 2.25 mL volume of normal saline were added. Formulation was vortexed for 2 minutes followed by sonication for 2 minutes to obtain a clear solution.

PO formulation: Accurately 0.0514 mL of DMSO stock was added into a bottle. To this bottle 0.200 mL volume of NMP, 0.250 mL volume of solutol and 4.5 mL volume of normal saline were added. Formulation was vortexed for 2 minutes followed by sonication for 2 minutes to obtain a clear solution.

5.4.1. Formulation Results

After preparation of formulations, a volume of 200 μL was aliquoted for analysis. The i.v. and p.o. formulation were analyzed and the concentration was found to be 0.45 mg/mL and 1.16 mg/mL respectively. The formulations were found to be

within the acceptance criteria (in-house acceptance criteria is ± 20% from the nominal value) Formulation were prepared freshly prior to dosing.

COMPOUND	FORMULATION NAME	THEORETICAL CONC. (mg/mL)	CONC. FOUND (mg/mL)	% CHANGE
Deoxynojirimycin	i.v.	0.4	0.45	12.5
	p.o.	1.0	1.16	16.0

5.5. Sample Collection

Blood samples (Approximately 60 µL) were collected from retro- orbital plexus of each mouse under light isoflurane anesthesia at Pre-dose, 0.08, 0.25, 0.5, 1, 2, 4, 8 and 24 hr (i.v.) and Pre-dose, 0.25, 0.5, 1 , 2, 4, 6, 8 and 24 hr (p.o.) in labeled micro centrifuge tube containing K_2EDTA as an anticoagulant. Following blood collection, animals in Group 1 and Group 2 were euthanized by CO_2 asphyxiation at 0.5, 4 and 24 hr to collect spleen, brain, liver, kidney, heart and lung. Collected tissues were dipped in 20 mL fresh phosphate buffer saline (pH 7.4) thrice, dried on blotted paper and weighed. Tissue samples were homogenized using ice-cold phosphate buffer saline (pH 7.4) and homogenates were stored below -70ºC until analysis. Total homogenate volume was three times for lung, spleen, brain, kidney, heart and ten times the liver weight.

5.6. Bioanalysis

Concentrations of Deoxynojirimycin in mouse plasma, spleen, brain, liver, kidney, heart and lung samples were determined by fit for purpose LC-MS/MS method. The sample processing and extraction procedure, chromatographic, mass spectrometric conditions, calibration curve and calibration curve data and the chromatograms were presented in Annexure 1.

6.0 Data analysis

The plasma, spleen, brain, liver, kidney, heart and lung concentration-time data (ng/mL) for Deoxynojirimycin were provided for data analysis by bioanalytical group of Sai Life Sciences Ltd, Pune. The plasma, spleen, brain, liver, kidney, heart

and lung concentration-time data were used for the pharmacokinetic analysis. Non-Compartmental-Analysis module in Phoenix WinNonlin® (Version 6.3) was used to assess the pharmacokinetic parameters. Peak plasma concentrations (C_{max}) and time for the peak plasma concentrations (T_{max}) were the observed values. The areas under the concentration time curve (AUC_{last} and AUC_{inf}) were calculated by linear trapezoidal rule. The terminal elimination rate constant, ke was determined by regression analysis of the linear terminal portion of the log plasma concentration-time curve. The terminal half-life ($T_{1/2}$) was estimated as 0.693/ke. CL_{iv}= Dose/$AUC_{inf;}$ V_{ss}= MRT X $CL_{iv;}$ %F = [(Mean $AUC_{p.o.}$ × $Dose_{i.v.}$) / (Mean $AUC_{i.v.}$ × $Dose_{p.o.}$)] × 100.

7.0 Results

Following a single intravenous administration of Deoxynojirimycin to male BALB/c mice at 2 mg/kg dose, plasma clearance was low (0.32 mL/min/kg, normal hepatic blood flow in mice is 90 mL/min/kg) with elimination half-life of 8.8 hr. Volume of distribution was less than the total body water (0.7 L/kg).

Following a single dose administration of Deoxynojirimycin to male BALB/c mice at 10 mg/kg dose, plasma concentrations were detected upto 24 hr with Tmax of 8.0 hr. Oral solution bioavailability was low (0.1%).

Following a single intravenous administration, brain-to-plasma ratio ranged between 0.01-0.02, liver to plasma ratio was 1.49-43.70, kidney-to-plasma ratio was 0.31 to 2.38, heart-to-plasma ratio was 0.12 - 1.00, spleen-to-plasma ratio was 0.03-0.18 and lung-to-plasma ratio was 0.06-1.17

Following a single oral administration, brain to plasma ratio ranged between 0.40-8.65, liver-to-plasma ratio was 16-193 and lung-to-plasma ratio was 0.66-6.97 while, concentrations were not detectable in heart and spleen. Concentrations in kidney was detectable at only 0.5 hr and the kidney-to-plasma ratio was 167.15 (0.5 hr).

Pharmacokinetic parameters of Deoxynojirimycin following a single intravenous and oral dose administration are tabulated in Table 1. Individual plasma

concentrations are presented in Table 2-3. Individual tissue concentrations of Deoxynojirimycin following intravenous and oral administration are presented in Tables 4-15. Tissue to plasma concentration ratio following intravenous and oral administration are presented in Table 16-27. The mean plasma concentration-time profiles of Deoxynojirimycin are presented in Figure 1.

8.0 Data Archiving

All raw data, study protocol and final report were documented and archived. The materials (hard and soft copies) will be retained for 1 year from the date of approval of final report. Thereafter, the archived material will be destroyed or stored for extended period as per written consent from the sponsor.

Table 1: Pharmacokinetic parameters of Deoxynojirimycin following a single intravenous (Dose: 2 mg/kg) and single oral (Dose: 10 mg/kg) administration in male BALB/c mice

Compound	Matrix	Route	T_{max} (hr)	[a]$C0/C_{max}$ (ng/mL)	AUC_{last} (ng/mL*hr)	AUC_{inf} (ng/mL*hr)	$T_{1/2}$ (hr)	CL (mL/min/kg)	Vss (L/kg)	%F[b]
Deoxynojirimycin	Plasma	i.v.	-	78977.95	96067.91	104975.00	8.79	0.32	0.13	-
		p.o.	8.00	30.17	497.68	NR	-	-	-	0.1%

a – extrapolated concentration for i.v. administration,
b - AUC_{last} was considered for calculation of bioavailability
NR – not reported since AUC_{inf} is 20% more than AUC_{last}

Table 2: Individual plasma concentration-time data of Deoxynojirimycin following a single intravenous administration to male BALB/c mice (Dose: 2 mg/kg)

	Plasma Concentration (ng/mL)								
	Time (hr)								
Mice ID	**Predose**	**0.08**	**0.25**	**0.5**	**1**	**2**	**4**	**8**	**24**
1	0.00	69860.79		30568.81					
2	0.00	66656.68		35910.16					
3	0.00	62838.73		31388.10					
4			52017.33		16012.05		3861.39		
5			41566.66		16842.56		3926.89		
6			44537.24		16384.25		3940.34		
7						6227.07		1520.67	618.72
8						9702.05		2599.92	990.32
9						8080.07		2131.06	572.97
Mean	**0.00**	**66452.07**	**46040.41**	**32622.36**	**16412.95**	**8003.06**	**3909.54**	**2083.88**	**727.33**
SD	0.00	3515.50	5385.05	2876.64	416.00	1738.77	42.24	541.17	228.89
CV%	NA	5.3	11.7	8.8	2.5	21.7	1.1	26.0	31.5

LLOQ = 1.02 ng/mL
NA – not applicable

Table 3: Individual plasma concentration-time data of Deoxynojirimycin following a single oral administration to male BALB/c mice (Dose: 10 mg/kg)

	Plasma Concentration (ng/mL)								
	Time (hr)								
Mice ID	**Predose**	**0.25**	**0.5**	**1**	**2**	**4**	**6**	**8**	**24**
10	0.00	7.08	4.19						
11	0.00	5.52	3.28						
12	0.00	5.19	8.03						
13				10.29	20.19	30.90			
14				5.51	11.27	19.01			
15				11.76	8.07	26.38			
16							25.25	35.58	11.67
17							19.91	29.81	14.68
18							15.64	25.13	12.89
Mean	**0.00**	**5.93**	**5.17**	**9.19**	**13.18**	**25.43**	**20.27**	**30.17**	**13.08**
SD	0.00	1.01	2.52	3.27	6.28	6.00	4.81	5.24	1.51
CV%	NA	17.1	48.8	35.5	47.7	23.6	23.8	17.4	11.6

LLOQ = 1.02 ng/mL
NA – not applicable

Table 4: Individual brain concentration-time data of Deoxynojirimycin following a single intravenous administration to male BALB/c mice (Dose: 2 mg/kg)

Mice ID	Brain Conc. (ng/mL) Time (hr)			[a]Brain Conc. (ng/g) Time (hr)		
	0.5	**4.0**	**24.0**	**0.5**	**4.0**	**24.0**
1	271.13			813.38		
2	92.58			277.74		
3	72.65			217.94		
4		18.87			56.62	
5		51.76			155.28	
6		12.33			36.98	
7			58.66			175.99
8			0.00			0.00
9			0.00			0.00
Mean	**145.45**	**27.65**	**58.66[e]**	**436.36**	**82.96**	**175.99[e]**
SD	109.29	21.13	NA	327.88	63.40	NA
CV%	75.1	76.4	NA	75.1	76.4	NA

LLOQ = 1.02 ng/mL, e – one value reported
a - The density of brain homogenate was considered as 1 which is equivalent to plasma density (1)
No peaks or values below LLOQ were considered zero

Table 5: Individual liver concentration-time data of Deoxynojirimycin following a single intravenous administration to male BALB/c mice (Dose: 2 mg/kg)

Mice ID	Liver Conc. (ng/mL) Time (hr)			[a]Liver Conc. (ng/g) Time (hr)		
	0.5	**4.0**	**24.0**	**0.5**	**4.0**	**24.0**
1	10402.40			104024.02		
2	2631.83			26318.34		
3	1585.19			15851.89		
4		3209.63			32096.32	
5		2690.97			26909.66	
6		3069.11			30691.06	
7			3010.27			30102.67
8			4004.87			40048.69
9			2520.12			25201.19
Mean	**4873.14**	**2989.90**	**3178.42**	**48731.42**	**29899.01**	**31784.18**
SD	4816.99	268.25	756.52	48169.91	2682.51	7565.23
CV%	98.8	9.0	23.8	98.8	9.0	23.8

LLOQ = 2.04 ng/mL
a - The density of liver homogenate was considered as 1 which is equivalent to plasma density (1)

Table 6: Individual kidney concentration-time data of Deoxynojirimycin following a single intravenous administration to male BALB/c mice (Dose: 2 mg/kg)

Mice ID	kidney Conc. (ng/mL) Time (hr)			[a] kidney Conc. (ng/g) Time (hr)		
	0.5	**4.0**	**24.0**	**0.5**	**4.0**	**24.0**
1	5703.74			17111.21		
2	3712.02			11136.07		
3	649.84			1949.51		
4		316.77			950.31	
5		813.57			2440.70	
6		436.65			1309.96	
7			591.04			1773.11
8			652.10			1956.30
9			487.12			1461.36
Mean	**3355.20**	**522.33**	**576.75**	**10065.60**	**1566.99**	**1730.26**
SD	2545.78	259.24	83.41	7637.33	777.73	250.24
CV%	75.9	49.6	14.5	75.9	49.6	14.5

LLOQ = 10.21 ng/mL

a - The density of kidney homogenate was considered as 1 which is equivalent to plasma density (1)

Table 7: Individual heart concentration-time data of Deoxynojirimycin following a single intravenous administration to male BALB/c mice (Dose: 2 mg/kg)

Mice ID	Heart Conc. (ng/mL) Time (hr)			[a] Heart Conc. (ng/g) Time (hr)		
	0.5	**4.0**	**24.0**	**0.5**	**4.0**	**24.0**
1	2847.87			8543.60		
2	513.79			1541.38		
3	520.39			1561.16		
4		226.39			679.16	
5		110.85			332.54	
6		217.58			652.73	
7			179.99			539.96
8			266.22			798.66
9			278.24			834.72
Mean	**1294.02**	**184.94**	**241.48**	**3882.05**	**554.81**	**724.45**
SD	1345.68	64.32	53.59	4037.04	192.95	160.78
CV%	104.0	34.8	22.2	104.0	34.8	22.2

LLOQ = 10.21 ng/mL

a - The density of heart homogenate was considered as 1 which is equivalent to plasma density (1)

Table 8: Individual spleen concentration-time data of Deoxynojirimycin following a single intravenous administration to male BALB/c mice (Dose: 2 mg/kg)

Mice ID	Spleen Conc. (ng/mL) Time (hr)			[a]Spleen Conc. (ng/g) Time (hr)		
	0.5	**4.0**	**24.0**	**0.5**	**4.0**	**24.0**
1	117.49			352.48		
2	481.46			1444.37		
3	388.81			1166.44		
4		62.41			187.24	
5		84.10			252.29	
6		24.00			72.00	
7			26.38			79.13
8			87.07			261.22
9			18.39			55.17
Mean	**329.25**	**56.84**	**43.95**	**987.76**	**170.51**	**131.84**
SD	189.15	30.44	37.56	567.45	91.30	112.69
CV%	57.4	53.5	85.5	57.4	53.5	85.5

LLOQ = 2.04 ng/mL

a - The density of spleen homogenate was considered as 1 which is equivalent to plasma density (1)

Table 9: Individual lung concentration-time data of Deoxynojirimycin following a single intravenous administration to male BALB/c mice (Dose: 2 mg/kg)

Mice ID	Lung Conc. (ng/mL) Time (hr)			[a]Lung Conc. (ng/g) Time (hr)		
	0.5	**4.0**	**24.0**	**0.5**	**4.0**	**24.0**
1	840.44			2521.33		
2	731.97			2195.92		
3	369.14			1107.43		
4		377.52			1132.57	
5		291.53			874.58	
6		157.16			471.49	
7			254.74			764.22
8			282.38			847.13
9			310.54			931.63
Mean	**647.19**	**275.40**	**282.55**	**1941.56**	**826.21**	**847.66**
SD	246.83	111.06	27.90	740.48	333.18	83.70
CV%	38.1	40.3	9.9	38.1	40.3	9.9

LLOQ = 2.04 ng/mL

a - The density of Lung homogenate was considered as 1 which is equivalent to plasma density (1)

Table 10: Individual brain concentration-time data of Deoxynojirimycin following a single oral administration to male BALB/c mice (Dose: 10 mg/kg)

Mice ID	Brain Conc. (ng/mL) Time (hr)			[a]Brain Conc. (ng/g) Time (hr)		
	0.5	**4.0**	**24.0**	**0.5**	**4.0**	**24.0**
10	12.23			36.69		
11	17.59			52.77		
12	0.00			0.00		
13		0.00			0.00	
14		3.85			11.54	
15		2.91			8.74	
16			17.91			53.72
17			3.70			11.11
18			0.00			0.00
Mean	**14.91[d]**	**3.38[d]**	**10.81[d]**	**44.73[d]**	**10.14[d]**	**32.43[d]**
SD	NA	NA	NA	NA	NA	NA
CV%	NA	NA	NA	NA	NA	NA

LLOQ = 1.02 ng/mL, d – average of two values reported
a - The density of brain homogenate was considered as 1 which is equivalent to plasma density (1)
No peaks or values below LLOQ were considered zero

Table 11: Individual liver concentration-time data of Deoxynojirimycin following a single oral administration to male BALB/c mice (Dose: 10 mg/kg)

Mice ID	Liver Conc. (ng/mL) Time (hr)			[a]Liver Conc. (ng/g) Time (hr)		
	0.5	**4.0**	**24.0**	**0.5**	**4.0**	**24.0**
10	116.98			1169.77		
11	160.08			1600.79		
12	23.09			230.91		
13		50.57			505.68	
14		0.00			0.00	
15		30.82			308.18	
16			54.95			549.54
17			101.64			1016.41
18			41.21			412.06
Mean	**100.05**	**40.70[d]**	**65.93**	**1000.49**	**406.95[d]**	**659.34**
SD	70.05	NA	31.68	700.45	NA	316.78
CV%	70.0	NA	48.0	70.0	NA	48.0

LLOQ = 2.04 ng/mL, d – average of two values reported
a - The density of liver homogenate was considered as 1 which is equivalent to plasma density (1)
No peaks or values below LLOQ were considered zero

Table 12: Individual kidney concentration-time data of Deoxynojirimycin following a single oral administration to male BALB/c mice (Dose: 10 mg/kg)

Mice ID	kidney Conc. (ng/mL) Time (hr)			[a] kidney Conc. (ng/g) Time (hr)		
	0.5	**4.0**	**24.0**	**0.5**	**4.0**	**24.0**
10	497.03			1491.09		
11	0.00			0.00		
12	79.11			237.34		
13		0.00			0.00	
14		0.00			0.00	
15		0.00			0.00	
16			0.00			0.00
17			30.52			91.57
18			0.00			0.00
Mean	**288.07[d]**	**0.00**	**30.52[e]**	**864.21[d]**	**0.00**	**91.57[e]**
SD	NA	0.00	NA	NA	0.00	NA
CV%	NA	NA	NA	NA	NA	NA

LLOQ = 10.21 ng/mL, d – average of two values reported, e – one value reported
a - The density of kidney homogenate was considered as 1 which is equivalent to plasma density (1)
No peaks or values below LLOQ were considered zero

Table 13: Individual heart concentration-time data of Deoxynojirimycin following a single oral administration to male BALB/c mice (Dose: 10 mg/kg)

Mice ID	Heart Conc. (ng/mL) Time (hr)			[a] Heart Conc. (ng/g) Time (hr)		
	0.5	**4.0**	**24.0**	**0.5**	**4.0**	**24.0**
10	63.23			189.70		
11	0.00			0.00		
12	0.00			0.00		
13		0.00			0.00	
14		0.00			0.00	
15		0.00			0.00	
16			0.00			0.00
17			0.00			0.00
18			0.00			0.00
Mean	**63.23[e]**	**0.00**	**0.00**	**189.70[e]**	**0.00**	**0.00**
SD	NA	0.00	0.00	NA	0.00	0.00
CV%	NA	NA		NA	NA	NA

LLOQ = 10.21 ng/mL, e – one value reported
a - The density of heart homogenate was considered as 1 which is equivalent to plasma density (1)
No peaks or values below LLOQ were considered zero

Table 14: Individual spleen concentration-time data of Deoxynojirimycin following a single oral administration to male BALB/c mice (Dose: 10 mg/kg)

Mice ID	Spleen Conc. (ng/mL) Time (hr)			[a]Spleen Conc. (ng/g) Time (hr)		
	0.5	**4.0**	**24.0**	**0.5**	**4.0**	**24.0**
10	20.15			60.45		
11	0.00			0.00		
12	0.00			0.00		
13		0.00			0.00	
14		0.00			0.00	
15		0.00			0.00	
16			0.00			0.00
17			0.00			0.00
18			0.00			0.00
Mean	**20.15[e]**	**0.00**	**0.00**	**60.45[e]**	**0.00**	**0.00**
SD	NA	0.00	0.00	NA	0.00	0.00
CV%	NA	NA	NA	NA	NA	NA

LLOQ = 2.04 ng/mL, e – one value reported
a - The density of spleen homogenate was considered as 1 which is equivalent to plasma density (1)
No peaks or values below LLOQ were considered zero

Table 15: Individual lung concentration-time data of Deoxynojirimycin following a single oral administration to male BALB/c mice (Dose: 10 mg/kg)

Mice ID	Lung Conc. (ng/mL) Time (hr)			[a]Lung Conc. (ng/g) Time (hr)		
	0.5	**4.0**	**24.0**	**0.5**	**4.0**	**24.0**
10	20.65			61.94		
11	0.00			0.00		
12	3.36			10.08		
13		5.69			17.08	
14		0.00			0.00	
15		11.85			35.54	
16			0.00			0.00
17			2.89			8.66
18			2.89			8.67
Mean	**12.01[d]**	**8.77[d]**	**2.89[d]**	**36.02[d]**	**26.31[d]**	**8.67[d]**
SD	NA	NA	NA	NA	NA	NA
CV%	NA	NA	NA	NA	NA	NA

LLOQ = 2.04 ng/mL, d – average of two values reported
a - The density of Lung homogenate was considered as 1 which is equivalent to plasma density (1)
No peaks or values below LLOQ were considered zero

Table 16: Brain-to-plasma concentration ratio of Deoxynojirimycin following a single intravenous administration to male BALB/c mice (Dose: 2 mg/kg)

[c]Brain/Plasma ratio			
Time (hr)	**Plasma Concentration (ng/mL)**	**Brain Concentration (ng/g)**	**Ratio**
0.5	32622.56 ± 2876.64	436.36 ± 327.88	0.01
4	3909.54 ± 42.24	82.96 ± 63.40	0.02
24	727.33 ± 228.89	NA	NA

c – Brain conc. as ng/g, density of brain tissue was considered as 1 which is equivalent to plasma density (1); NA- Not applicable

Table 17: Liver-to-plasma concentration ratio of Deoxynojirimycin following a single intravenous administration to male BALB/c mice (Dose: 2 mg/kg)

[c]Liver/Plasma ratio			
Time (hr)	**Plasma Concentration (ng/mL)**	**Liver Concentration (ng/g)**	**Ratio**
0.5	32622.56 ± 2876.64	48731.42 ± 48169.91	1.49
4	3909.54 ± 42.24	29899.01 ± 2682.51	7.65
24	727.33 ± 228.89	31784.18 ± 7565.23	43.70

c – Liver conc. as ng/g, density of liver tissue was considered as 1 which is equivalent to plasma density (1); NA- Not applicable

Table 18: Kidney-to-plasma concentration ratio of Deoxynojirimycin following a single intravenous administration to male BALB/c mice (Dose: 2 mg/kg)

[c]Kidney/Plasma ratio			
Time (hr)	**Plasma Concentration (ng/mL)**	**Kidney Concentration (ng/g)**	**Ratio**
0.5	32622.56 ± 2876.64	10065.60 ± 7637.33	0.31
4	3909.54 ± 42.24	1566.99 ± 777.73	0.40
24	727.33 ± 228.89	1730.26 ± 250.24	2.38

c – Kidney conc. as ng/g, density of kidney tissue was considered as 1 which is equivalent to plasma density (1); NA- Not applicable

Table 19: Heart-to-plasma concentration ratio of Deoxynojirimycin following a single intravenous administration to male BALB/c mice (Dose: 2 mg/kg)

[c]Heart/Plasma ratio			
Time (hr)	**Plasma Concentration (ng/mL)**	**Heart Concentration (ng/g)**	**Ratio**
0.5	32622.56 ± 2876.64	3882.05 ± 4037.04	0.12
4	3909.54 ± 42.24	554.81 ± 192.95	0.14
24	727.33 ± 228.89	724.45 ± 160.78	1.00

c – Heart conc. as ng/g, density of heart tissue was considered as 1 which is equivalent to plasma density (1); NA- Not applicable

Table 20: Spleen-to-plasma concentration ratio of Deoxynojirimycin following a single intravenous administration to male BALB/c mice (Dose: 2 mg/kg)

[c]Spleen/Plasma ratio			
Time (hr)	**Plasma Concentration (ng/mL)**	**Spleen Concentration (ng/g)**	**Ratio**
0.5	32622.56 ± 2876.64	987.76 ± 567.45	0.03
4	3909.54 ± 42.24	170.51 ± 91.30	0.04
24	727.33 ± 228.89	131.84 ± 112.69	0.18

c – Spleen conc. as ng/g, density of spleen tissue was considered as 1 which is equivalent to plasma density (1); NA- Not applicable

Table 21: Lung-to-plasma concentration ratio of Deoxynojirimycin following a single intravenous administration to male BALB/c mice (Dose: 2 mg/kg)

[c]Lung/Plasma ratio			
Time (hr)	**Plasma Concentration (ng/mL)**	**Lung Concentration (ng/g)**	**Ratio**
0.5	32622.56 ± 2876.64	1941.56 ± 740.48	0.06
4	3909.54 ± 42.24	826.21 ± 333.18	0.21
24	727.33 ± 228.89	847.66 ± 83.70	1.17

c – Lung conc. as ng/g, density of lung tissue was considered as 1 which is equivalent to plasma density (1); NA- Not applicable

Table 22: Brain-to-plasma concentration ratio of Deoxynojirimycin following a single oral administration to male BALB/c mice (Dose: 10 mg/kg)

[c]Brain/Plasma ratio			
Time (hr)	**Plasma Concentration (ng/mL)**	**Brain Concentration (ng/g)**	**Ratio**
0.5	5.17 ± 2.52	44.73 ± NA	8.65
4	25.43 ± 6.00	10.14 ± NA	0.40
24	13.08 ± 1.51	32.43 ± NA	2.48

c – Brain conc. as ng/g, density of brain tissue was considered as 1 which is equivalent to plasma density (1); NA- Not applicable

Table 23: Liver-to-plasma concentration ratio of Deoxynojirimycin following a single oral administration to male BALB/c mice (Dose: 10 mg/kg)

[c]Liver/Plasma ratio			
Time (hr)	**Plasma Concentration (ng/mL)**	**Liver Concentration (ng/g)**	**Ratio**
0.5	5.17 ± 2.52	1000.49 ± 700.45	193.51
4	25.43 ± 6.00	406.95 ± NA	16.00
24	13.08 ± 1.51	659.34 ± 316.78	50.41

c – Liver conc. as ng/g, density of liver tissue was considered as 1 which is equivalent to plasma density (1); NA- Not applicable

Table 24: Kidney-to-plasma concentration ratio of Deoxynojirimycin following a single oral administration to male BALB/c mice (Dose: 10 mg/kg)

[c]Kidney/Plasma ratio			
Time (hr)	**Plasma Concentration (ng/mL)**	**Kidney Concentration (ng/g)**	**Ratio**
0.5	5.17 ± 2.52	864.21 ± NA	167.15
4	25.43 ± 6.00	NA	NA
24	13.08 ± 1.51	NA	NA

c – Kidney conc. as ng/g, density of kidney tissue was considered as 1 which is equivalent to plasma density (1); NA- Not applicable

Table 25: Heart-to-plasma concentration ratio of Deoxynojirimycin following a single oral administration to male BALB/c mice (Dose: 10 mg/kg)

[c]Heart/Plasma ratio			
Time (hr)	**Plasma Concentration (ng/mL)**	**Heart Concentration (ng/g)**	**Ratio**
0.5	5.17 ± 2.52	NA	NA
4	25.43 ± 6.00	NA	NA
24	13.08 ± 1.51	NA	NA

c – Heart conc. as ng/g, density of heart tissue was considered as 1 which is equivalent to plasma density (1); NA- Not applicable

Table 26: Spleen-to-plasma concentration ratio of Deoxynojirimycin following a single oral administration to male BALB/c mice (Dose: 10 mg/kg)

[c]Spleen/Plasma ratio			
Time (hr)	**Plasma Concentration (ng/mL)**	**Spleen Concentration (ng/g)**	**Ratio**
0.5	5.17 ± 2.52	NA	NA
4	25.43 ± 6.00	NA	NA
24	13.08 ± 1.51	NA	NA

c – Spleen conc. as ng/g, density of spleen tissue was considered as 1 which is equivalent to plasma density (1); NA- Not applicable

Table 27: Lung-to-plasma concentration ratio of Deoxynojirimycin following a single oral administration to male BALB/c mice (Dose: 10 mg/kg)

[c]Lung/Plasma ratio			
Time (hr)	**Plasma Concentration (ng/mL)**	**Lung Concentration (ng/g)**	**Ratio**
0.5	5.17 ± 2.52	36.02 ± NA	6.97
4	25.43 ± 6.00	26.31 ± NA	1.03
24	13.08 ± 1.51	8.67 ± NA	0.66

c – Lung conc. as ng/g, density of lung tissue was considered as 1 which is equivalent to plasma density (1); NA- Not applicable

Figure 1: Mean plasma concentration-time profiles of Deoxynojirimycin following a single intravenous (Dose: 2 mg/kg and oral (Dose: 10 mg/kg) administration to male BALB/c mice

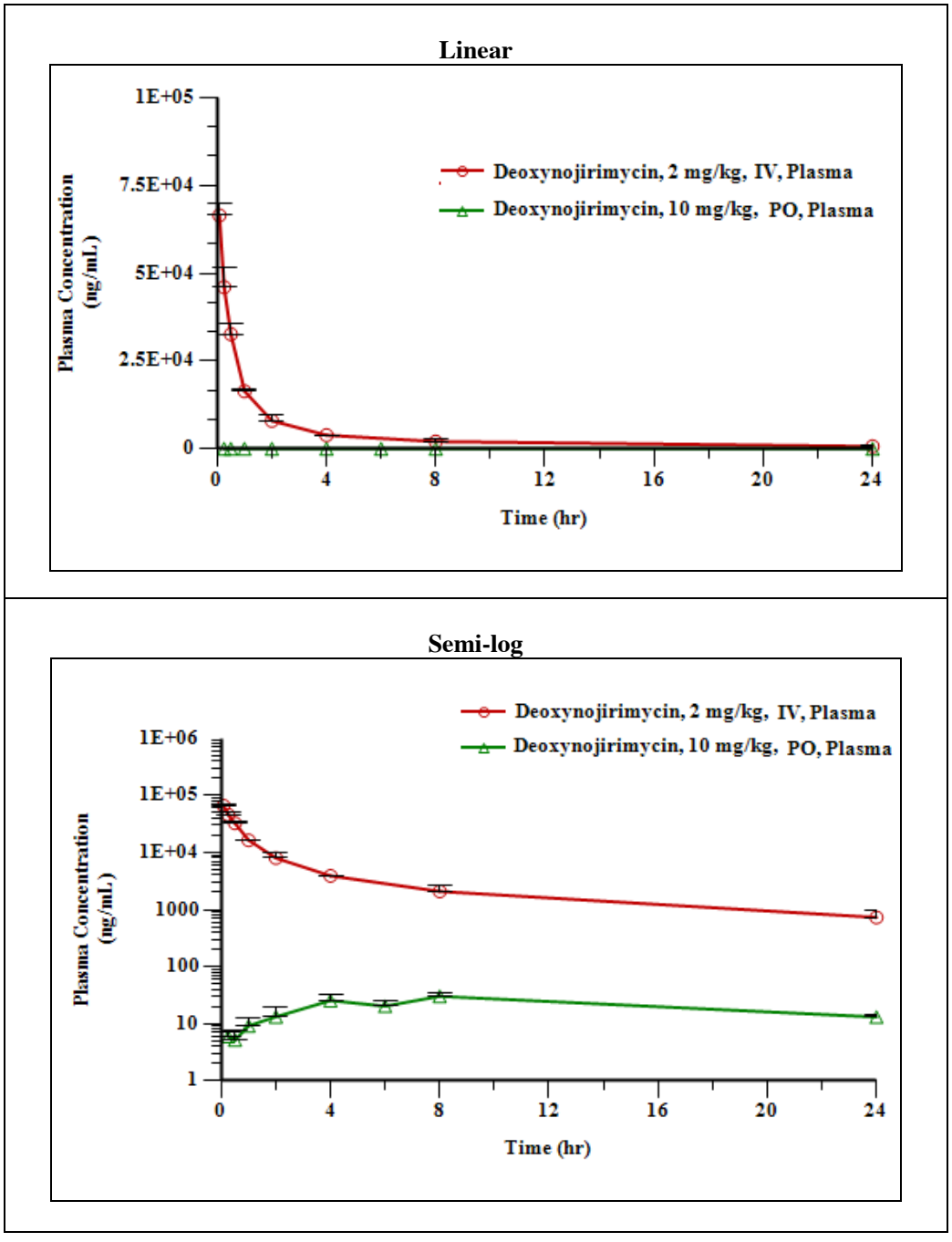

Annexure I

Bioanalytical Summary

HPLC and MS Conditions

Chromatographic Mode	**:**	LC/MS/MS
MS System Used	**:**	AB Sciex API-4000 (Q-Trap)
Software Version	**:**	Analyst 1.5
Scan Type	**:**	MRM
Polarity	**:**	Positive
Ion Source	**:**	Turbospray
Mobile Phase	**:**	A**:** 0.1 % Formic acid in acetonitrile B**:** 0.1 % Formic acid in water
Flow Rate (mL/min)	**:**	0.8
Draw Speed (μL/min)	**:**	200
Splitter	**:**	Approximately 50 % Out
Probe Position	**:**	5 mm vertical, and 5 horizontal
Injection Volume (μL)	**:**	20
Auto Sampler Temperature (ºC)	**:**	4
Column Oven Temperature (ºC)	**:**	40
Column Used (length x width in mm, Particle size)	**:**	Waters, XBridge, C18, (50×3.0, 3.5μm)
Retention Time (in min)	**:**	Deoxynojirimycin – 2.80 Glipizide (IS) – 2.33
Run Time (in min)	**:**	5.00

HPLC Gradient Used: TOP-deoxynojirimycin_GD-01_050314.dam

A**:** 0.1 % Formic acid in acetonitrile

B**:** 0.1 % Formic acid in water

Time (min)	**Flow (mL/min)**	**PUMP A (% Conc.)**	**PUMP B (% Conc.)**
0.01	0.8	5	95
0.50	0.8	5	95
1.00	0.8	98	2
3.40	0.8	98	2
3.80	0.8	5	95
5.00	0.8	5	95

MRM Transitions

Q1 Mass (Da)	Q3Mass (Da)	I.D.	Dwell time (msec)	DP	CE	CXP
662.50	148.90	Deoxynojirimycin_148	60	121.0	77.0	25.0
446.30	347.00	GLIPI_POS	60	40.0	22.0	12.0
Source Parameters						
CAD			Medium			
CUR			20			
GS1			60			
GS2			40			
Ion Spray Voltage			5500			
Temperature			550			
Interface Heater			ON			
EP			10			

Extraction Procedure

The extraction procedure for plasma, brain, liver, kidney, heart, spleen and lungs samples and the spiked calibration standards were identical.

A 25 μL of study sample (Dilution Factor applied to few samples) or spiked calibration standard was added to individual pre-labeled micro-centrifuge tubes followed by 100 μL of internal standard prepared in acetonitrile (Glipizide, 500 ng/mL) was added except for blank, where 100 μL of acetonitrile was added. Samples were vortexed for 5 minutes. Samples were centrifuged for 10 minutes at a speed of 4000 rpm at 4 °C. Following centrifugation, 100 μL of clear supernatant was transferred in 96 well plates and analyzed using LC-MS/MS.

Calibration Curve Details

Calibration Curve Data of Deoxynojirimycin in Mice Plasma

CC Sample Name	Nominal Conc (ng/mL)	Calculated Conc (ng/mL)	% Accuracy
DEOXYNOJIRIMYCIN_P_CS-01	1.02	0.98	96.26
DEOXYNOJIRIMYCIN_P_CS-02	2.04	2.12	104.06
DEOXYNOJIRIMYCIN_P_CS-03	10.21	12.13	118.78
DEOXYNOJIRIMYCIN_P_CS-04#	51.03	31.72	62.16
DEOXYNOJIRIMYCIN_P_CS-05	102.06	86.35	84.61
DEOXYNOJIRIMYCIN_P_CS-06#	510.30	353.64	69.30
DEOXYNOJIRIMYCIN_P_CS-07	1020.60	906.12	88.78
DEOXYNOJIRIMYCIN_P_CS-08	2551.50	1979.70	77.59
DEOXYNOJIRIMYCIN_P_CS-09	5103.00	5960.48	116.80
DEOXYNOJIRIMYCIN_P_CS-10	10206.00	11544.39	113.11
Regression Equation	Y = mx+c		
Slope	0.0000145		
Intercept	0.0000173		
R	0.9860		

Calibration standard not meeting acceptance criteria

Calibration Curve of Deoxynojirimycin in Mice Plasma

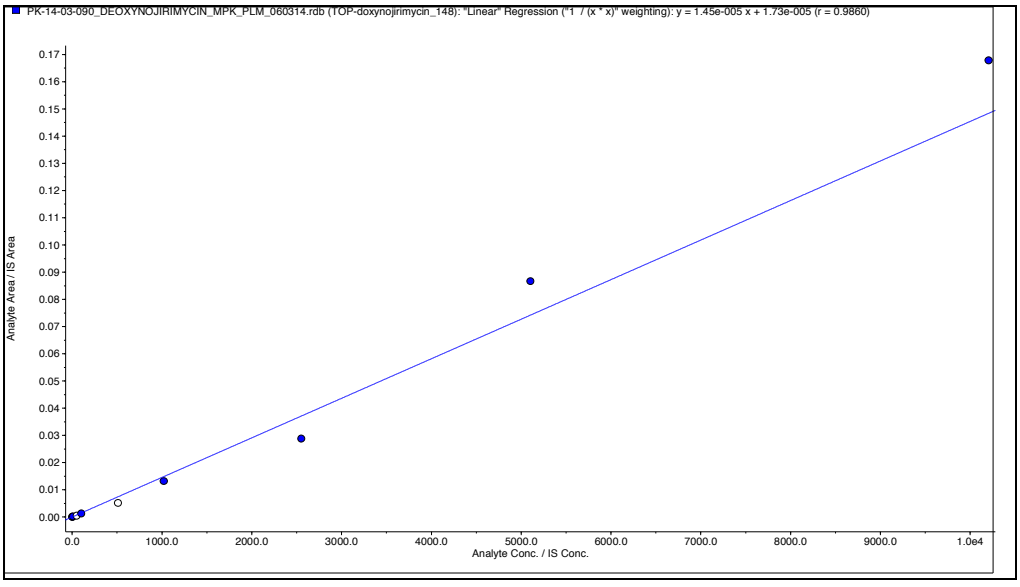

Calibration Curve Data of Deoxynojirimycin in Mice Brain

CC Sample Name	Nominal Conc (ng/mL)	Calculated Conc (ng/mL)	% Accuracy
DEOXYNOJIRIMYCIN_BR_CS-01	1.02	1.01	99.23
DEOXYNOJIRIMYCIN_BR_CS-02#	2.04	10.78	528.64
DEOXYNOJIRIMYCIN_BR_CS-03	10.20	10.84	106.17
DEOXYNOJIRIMYCIN_BR_CS-04#	51.03	31.23	61.20
DEOXYNOJIRIMYCIN_BR_CS-05	102.06	122.49	120.02
DEOXYNOJIRIMYCIN_BR_CS-06	510.30	404.99	79.36
DEOXYNOJIRIMYCIN_BR_CS-07	1020.60	971.80	95.22
Regression Equation	Y = mx+c		
Slope	0.00000154		
Intercept	0.00005		
R	0.9884		

Calibration standard not meeting acceptance criteria

Calibration Curve of Deoxynojirimycin in Mice Brain

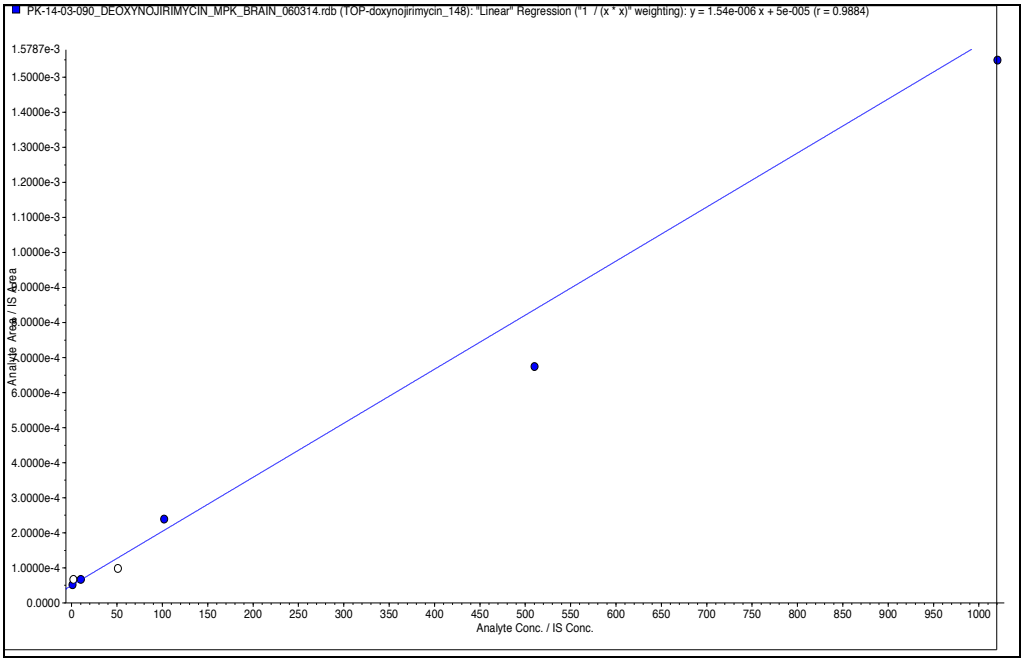

Calibration Curve Data of Deoxynojirimycin in Mice Lungs

CC Sample Name	Nominal Conc (ng/mL)	Calculated Conc (ng/mL)	% Accuracy
DEOXYNOJIRIMYCIN_LUN_CS-01	2.04	1.99	97.43
DEOXYNOJIRIMYCIN_LUN_CS-02	10.21	11.48	112.39
DEOXYNOJIRIMYCIN_LUN_CS-03[#]	51.03	36.66	71.84
DEOXYNOJIRIMYCIN_LUN_CS-04	102.06	105.72	103.58
DEOXYNOJIRIMYCIN_LUN_CS-05	510.30	545.10	106.82
DEOXYNOJIRIMYCIN_LUN_CS-06[#]	1020.60	1537.37	150.63
DEOXYNOJIRIMYCIN_LUN_CS-07	2551.50	2728.25	106.93
DEOXYNOJIRIMYCIN_LUN_CS-08	5103.00	4694.24	91.99
DEOXYNOJIRIMYCIN_LUN_CS-09	10206.00	8252.70	80.86
Regression Equation	Y = mx+c		
Slope	0.0000125		
Intercept	0.0000178		
R	0.9938		

[#] Calibration standard not meeting acceptance criteria

Calibration Curve of Deoxynojirimycin in Mice Lungs

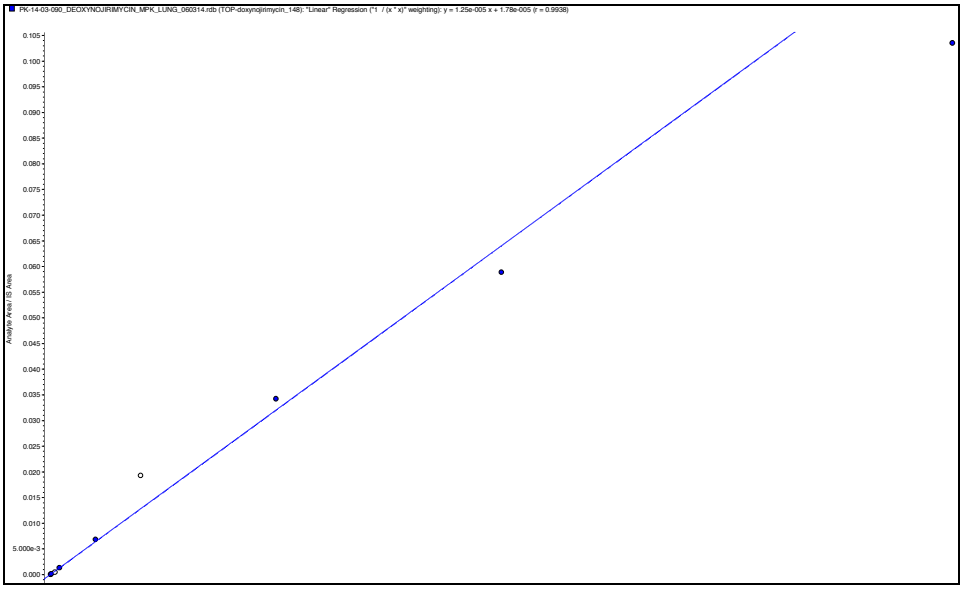

Calibration Curve Data of Deoxynojirimycin in Mice Kidney

CC Sample Name	Nominal Conc (ng/mL)	Calculated Conc (ng/mL)	% Accuracy
DEOXYNOJIRIMYCIN_KDNY_CS-03	10.21	10.21	100.03
DEOXYNOJIRIMYCIN_KDNY_CS-04	51.03	51.52	100.95
DEOXYNOJIRIMYCIN_KDNY_CS-05[#]	102.06	216.49	212.12
DEOXYNOJIRIMYCIN_KDNY_CS-06	510.30	481.91	94.44
DEOXYNOJIRIMYCIN_KDNY_CS-07	1020.60	937.26	91.83
DEOXYNOJIRIMYCIN_KDNY_CS-08	2551.50	2157.75	84.57
DEOXYNOJIRIMYCIN_KDNY_CS-09	5103.00	5356.17	104.96
DEOXYNOJIRIMYCIN_KDNY_CS-10	10206.00	12575.54	123.22
Regression Equation	Y = mx+c		
Slope	0.000000742		
Intercept	0.0000607		
R	0.9920		

[#] Calibration standard not meeting acceptance criteria

Calibration Curve of Deoxynojirimycin in Mice Kidney

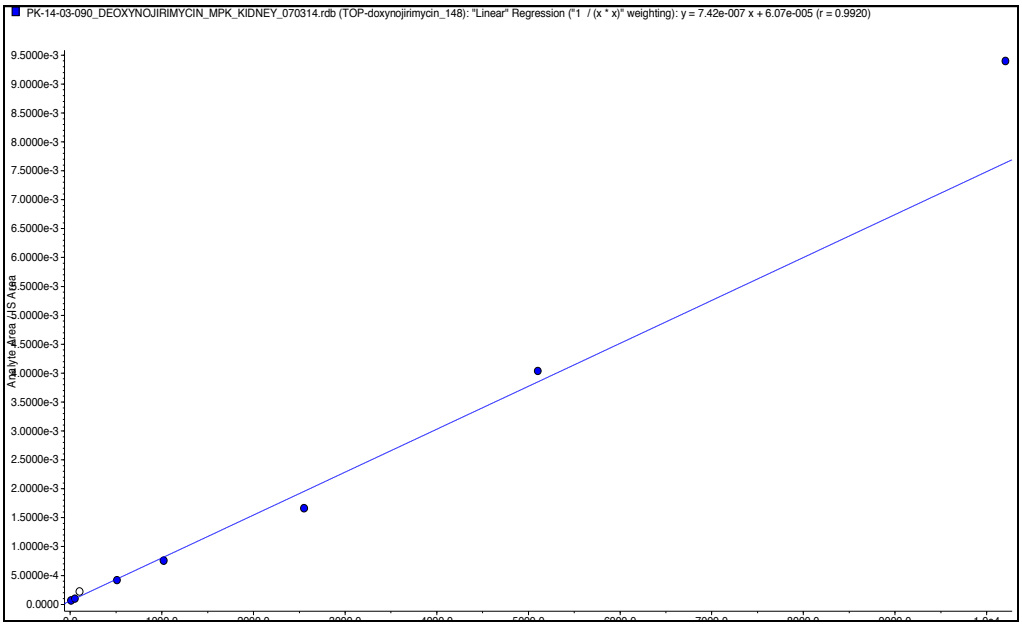

Calibration Curve Data of Deoxynojirimycin in Mice Liver

CC Sample Name	Nominal Conc (ng/mL)	Calculated Conc (ng/mL)	% Accuracy
DEOXYNOJIRIMYCIN_LVR_CS-02	2.04	2.06	100.90
DEOXYNOJIRIMYCIN_LVR_CS-03[#]	10.21	14.22	139.24
DEOXYNOJIRIMYCIN_LVR_CS-04	51.03	39.54	77.48
DEOXYNOJIRIMYCIN_LVR_CS-05	102.06	99.53	97.52
DEOXYNOJIRIMYCIN_LVR_CS-06	510.30	582.72	114.19
DEOXYNOJIRIMYCIN_LVR_CS-07	1020.60	1020.90	100.03
DEOXYNOJIRIMYCIN_LVR_CS-08	2551.50	2260.59	88.60
DEOXYNOJIRIMYCIN_LVR_CS-09	5103.00	5467.53	107.14
DEOXYNOJIRIMYCIN_LVR_CS-10	10206.00	11649.16	114.14
Regression Equation	Y = mx+c		
Slope	0.00000391		
Intercept	0.00022		
R	0.9921		

[#] Calibration standard not meeting acceptance criteria

Calibration Curve of Deoxynojirimycin in Mice Liver

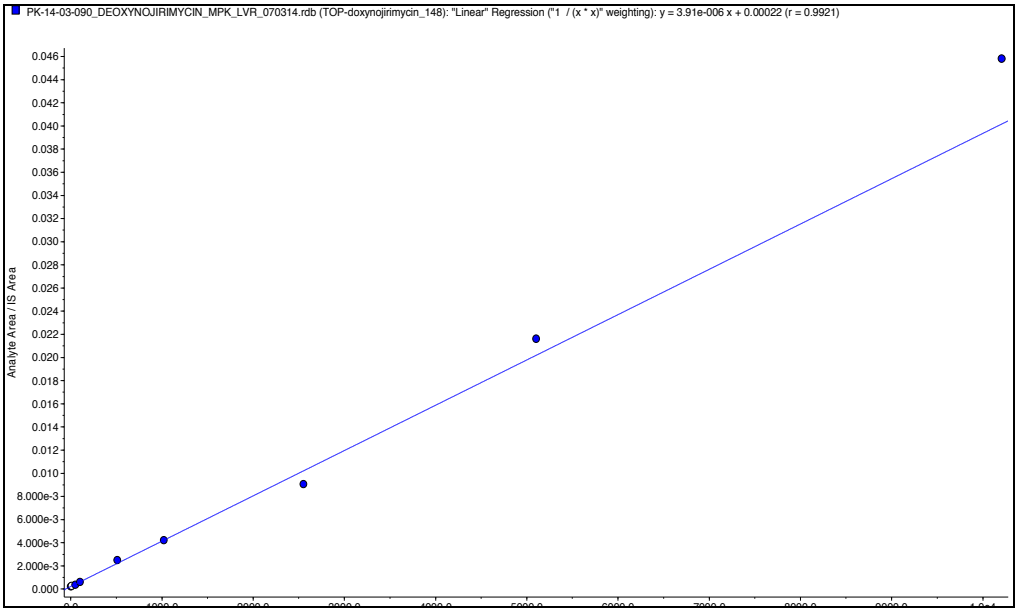

Calibration Curve Data of Deoxynojirimycin in Mice Heart

CC Sample Name	Nominal Conc (ng/mL)	Calculated Conc (ng/mL)	% Accuracy
DEOXYNOJIRIMYCIN_HRT_CS-03	10.21	10.30	100.86
DEOXYNOJIRIMYCIN_HRT_CS-04	51.03	51.85	101.60
DEOXYNOJIRIMYCIN_HRT_CS-05	102.06	87.33	85.57
DEOXYNOJIRIMYCIN_HRT_CS-06	510.30	577.24	113.12
DEOXYNOJIRIMYCIN_HRT_CS-07	1020.60	1065.66	104.41
DEOXYNOJIRIMYCIN_HRT_CS-08	2551.50	2144.40	84.04
DEOXYNOJIRIMYCIN_HRT_CS-09	5103.00	5633.45	110.39
Regression Equation	Y = mx+c		
Slope	0.00000319		
Intercept	0.0000874		
R	0.9929		

Calibration Curve of Deoxynojirimycin in Mice Heart

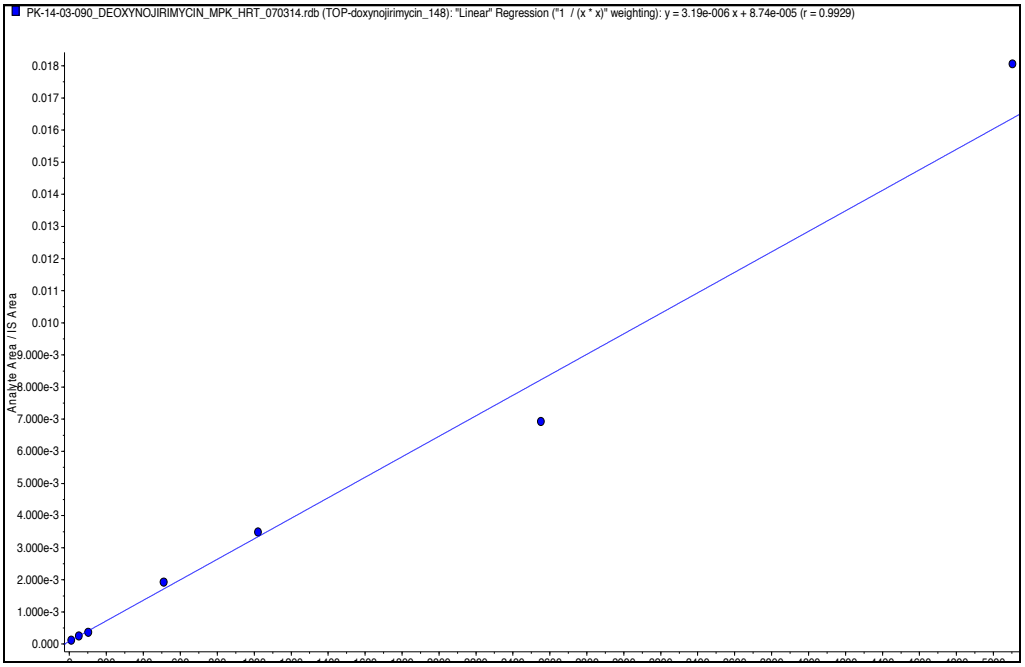

Calibration Curve Data of Deoxynojirimycin in Mice Spleen

CC Sample Name	Nominal Conc (ng/mL)	Calculated Conc (ng/mL)	% Accuracy
DEOXYNOJIRIMYCIN_SPLN_CS-02	2.04	2.04	99.77
DEOXYNOJIRIMYCIN_SPLN_CS-03	10.21	10.00	97.96
DEOXYNOJIRIMYCIN_SPLN_CS-04	51.03	54.12	106.06
DEOXYNOJIRIMYCIN_SPLN_CS-05	102.06	124.47	121.95
DEOXYNOJIRIMYCIN_SPLN_CS-06	510.30	462.12	90.56
DEOXYNOJIRIMYCIN_SPLN_CS-07	1020.60	1050.96	102.97
DEOXYNOJIRIMYCIN_SPLN_CS-08	2551.50	2161.35	84.71
DEOXYNOJIRIMYCIN_SPLN_CS-09	5103.00	5037.95	98.73
DEOXYNOJIRIMYCIN_SPLN_CS-10	10206.00	9928.75	97.28
Regression Equation	Y = mx+c		
Slope	0.0000964		
Intercept	0.000172		
R	0.9943		

Calibration Curve of Deoxynojirimycin in Mice Spleen

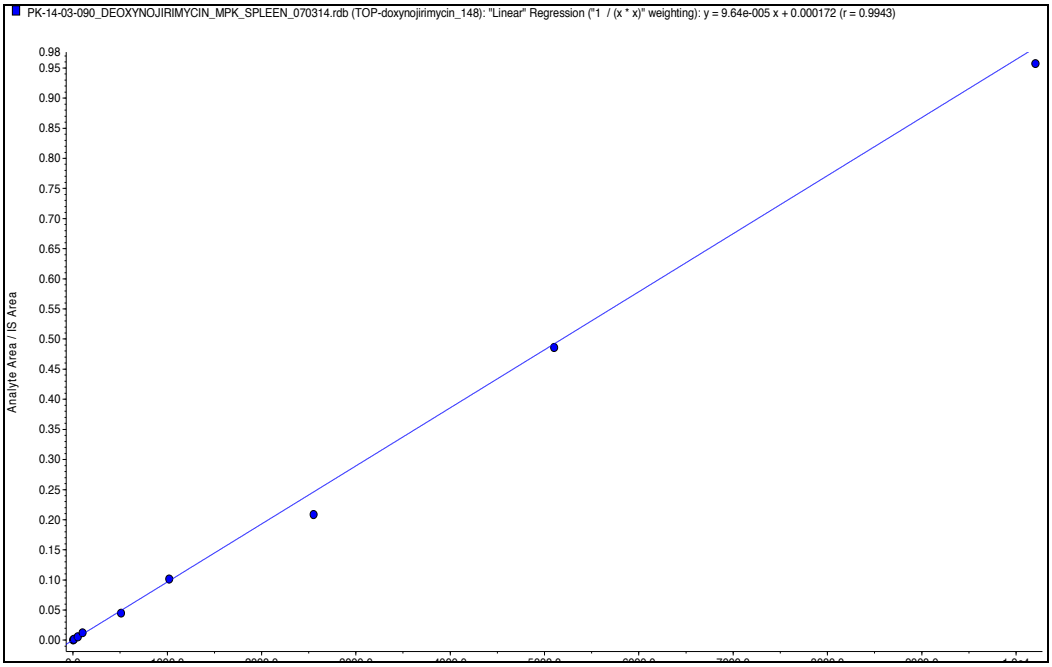

Representative chromatogram of blank plasma matrix in the LC-MS/MS analysis of Deoxynojirimycin

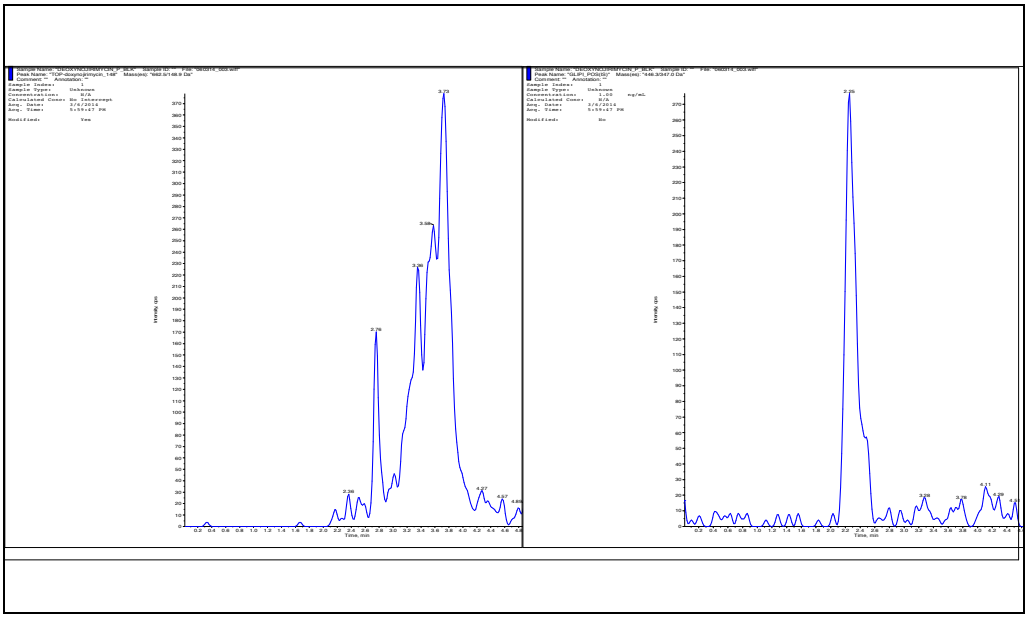

Representative LC-MS/MS chromatogram of Deoxynojirimycin calibration standard and Glipizide (IS) in mice plasma

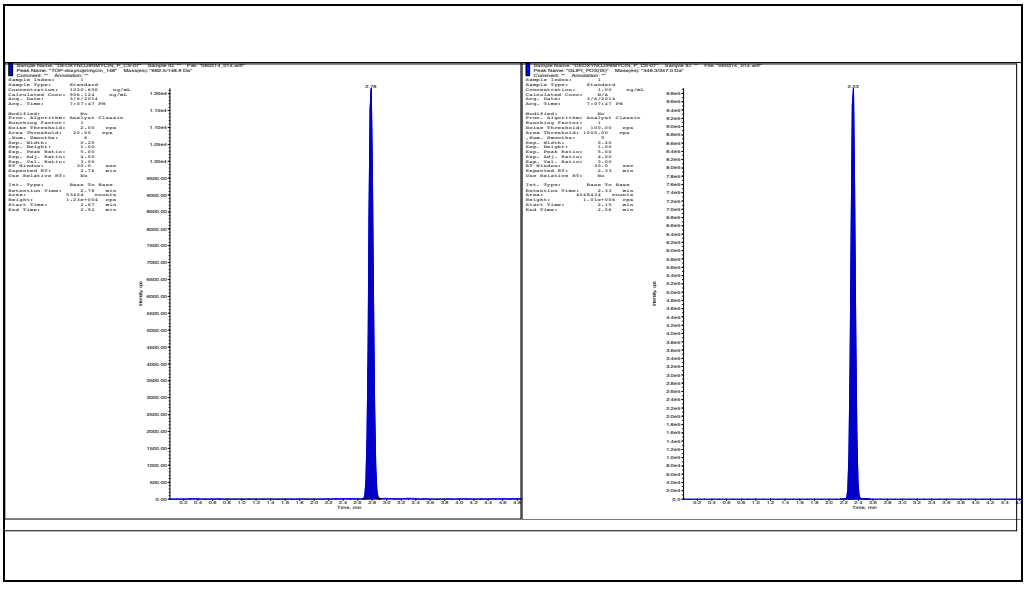

Representative LC-MS/MS chromatogram of Deoxynojirimycin intravenous study sample (plasma) and Glipizide (IS)

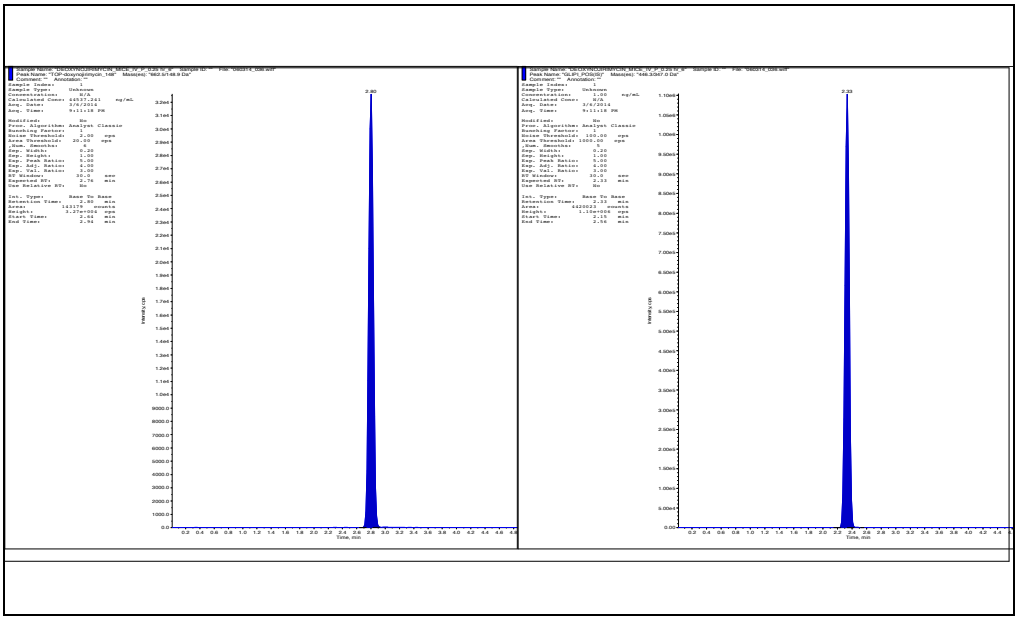

Representative LC-MS/MS chromatogram of Deoxynojirimycin peroral study sample (plasma) and Glipizide (IS)

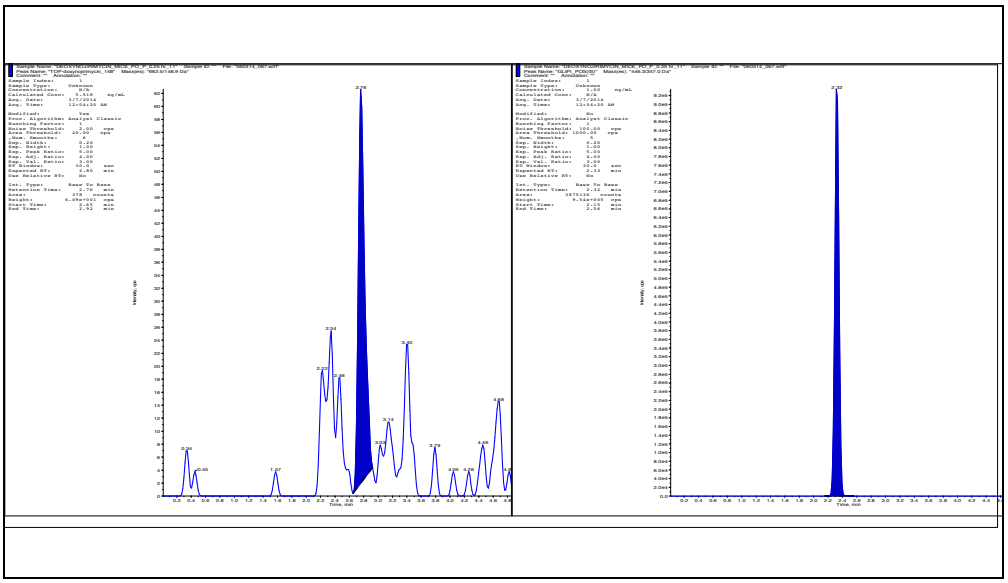

Representative chromatogram of blank brain matrix in the LC-MS/MS analysis of Deoxynojirimycin

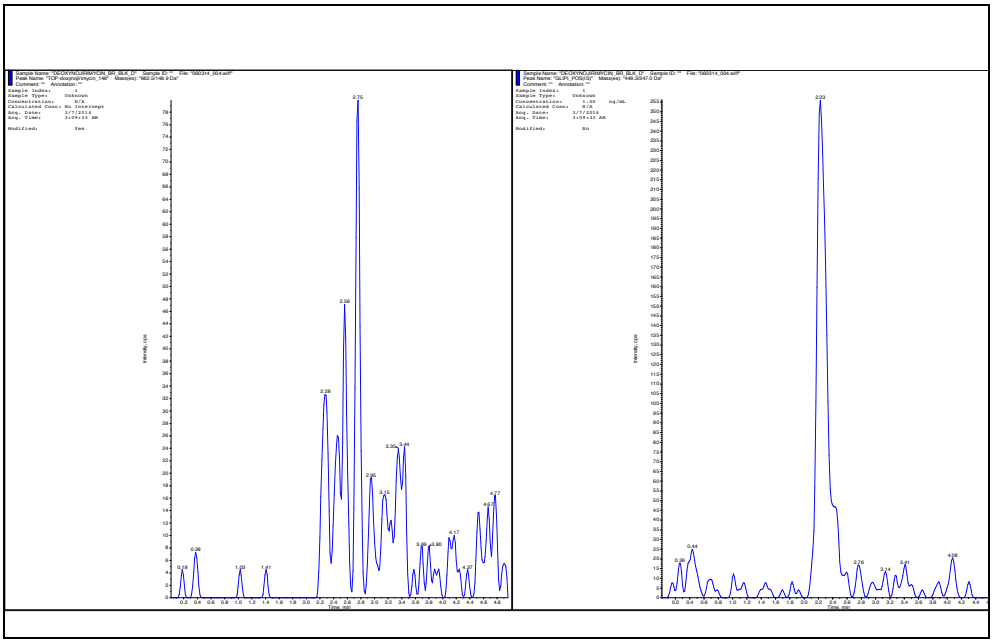

Representative LC-MS/MS chromatogram of Deoxynojirimycin calibration standard and Glipizide (IS) in mice brain

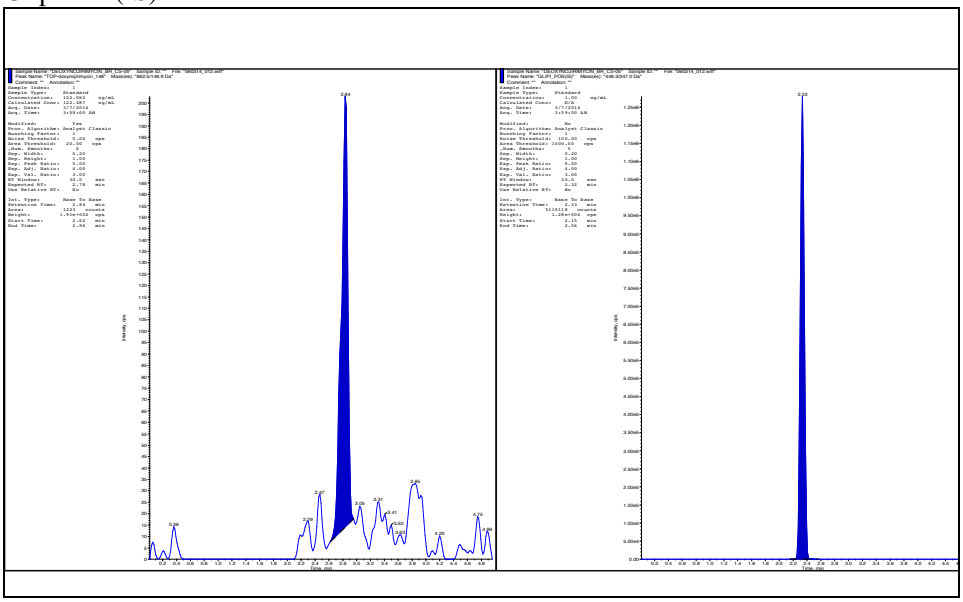

Representative LC-MS/MS chromatogram of Deoxynojirimycin intravenous study sample (brain) and Glipizide (IS)

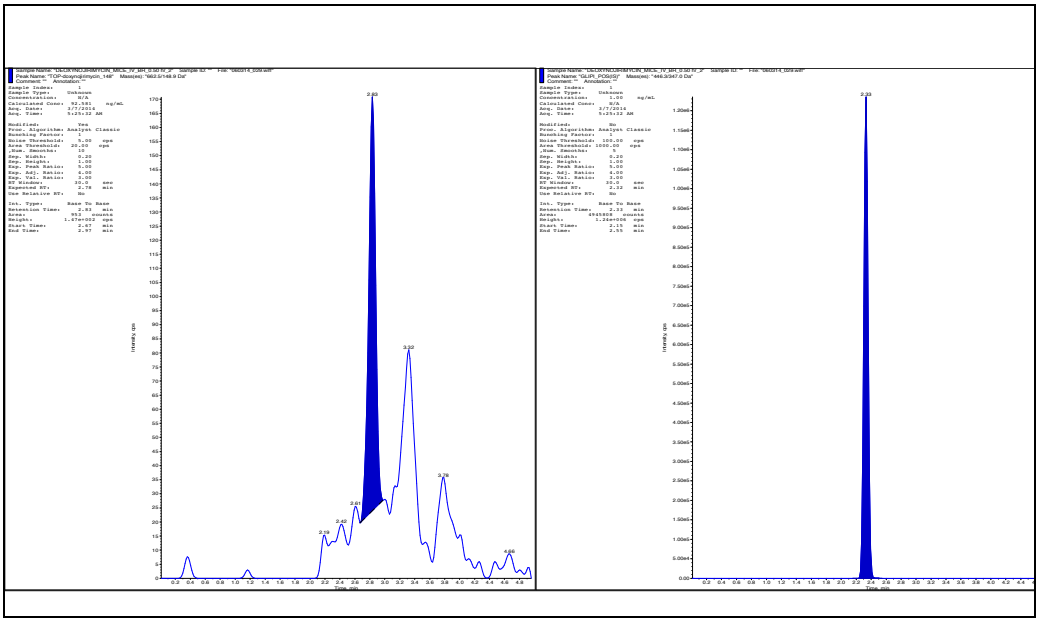

Representative LC-MS/MS chromatogram of Deoxynojirimycin per oral study sample (brain) and Glipizide (IS)

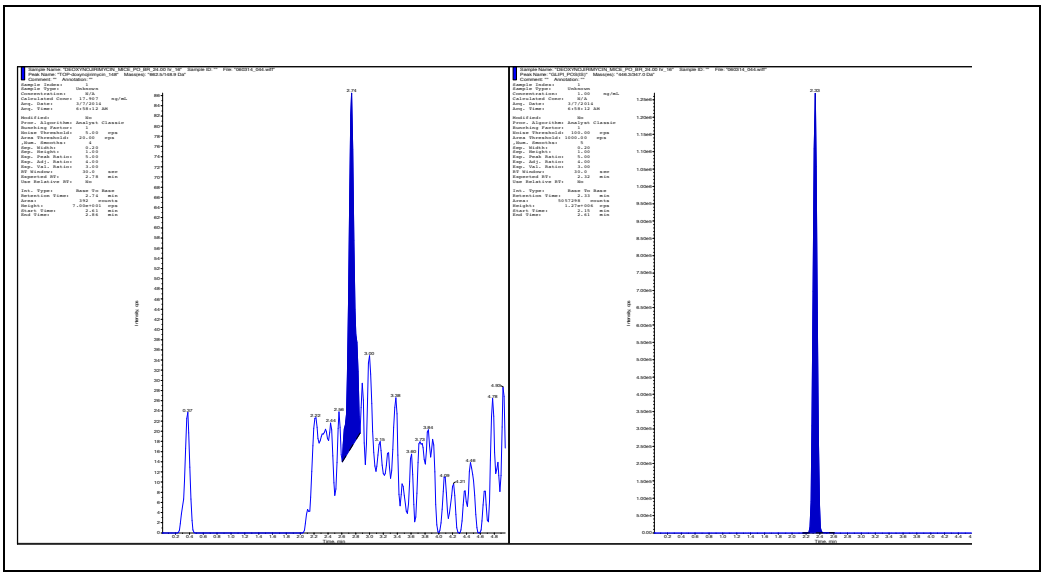

Representative chromatogram of blank lungs matrix in the LC-MS/MS analysis of Deoxynojirimycin

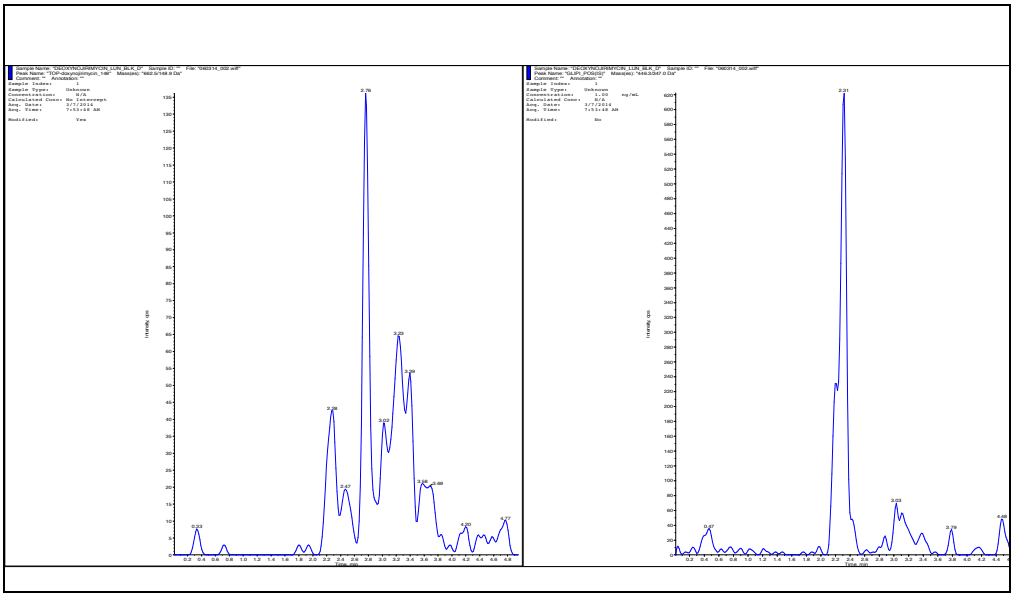

Representative LC-MS/MS chromatogram of Deoxynojirimycin calibration standard and Glipizide (IS) in mice lungs

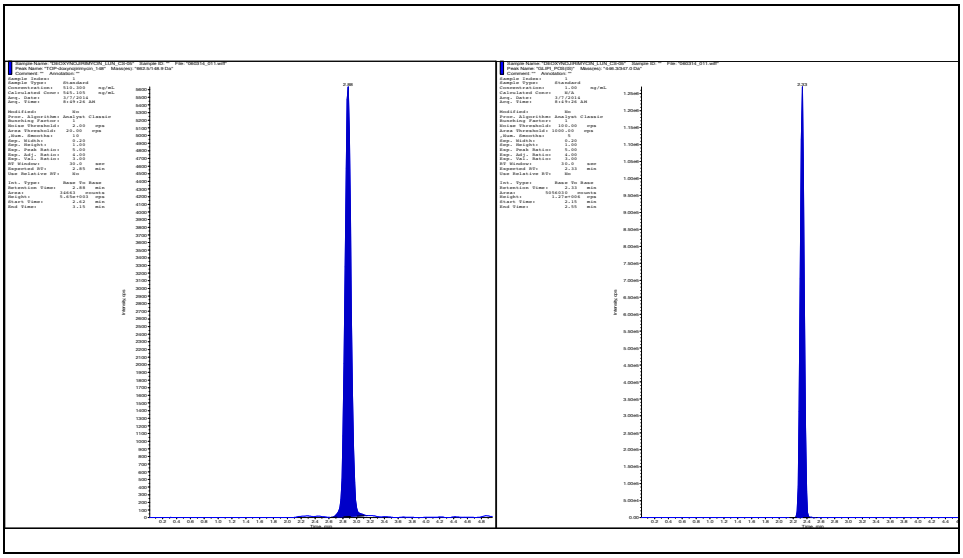

Representative LC-MS/MS chromatogram of Deoxynojirimycin intravenous study sample (lungs) and Glipizide (IS)

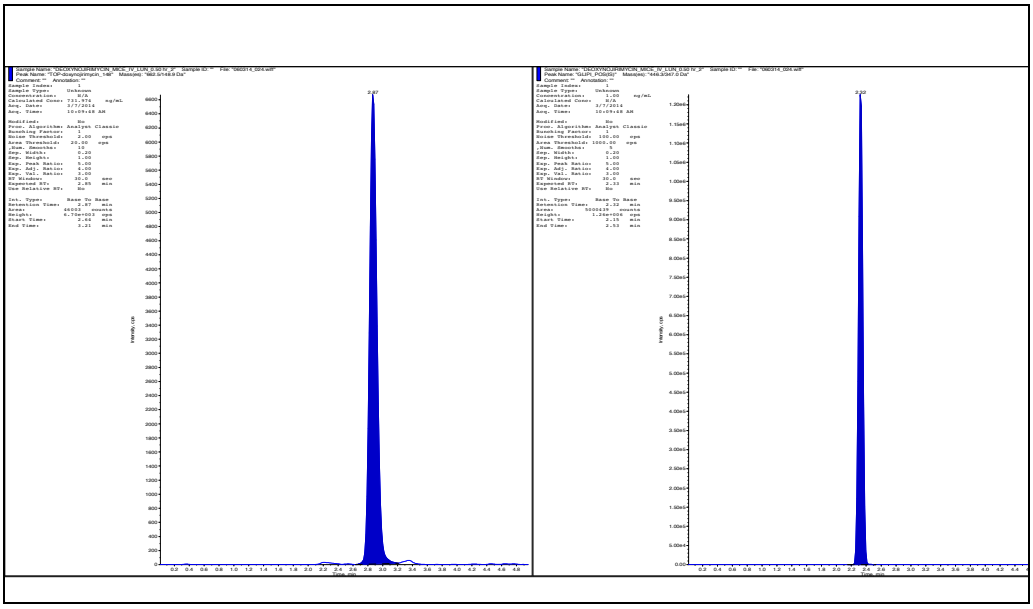

Representative LC-MS/MS chromatogram of Deoxynojirimycin per oral study sample (lungs) and Glipizide (IS)

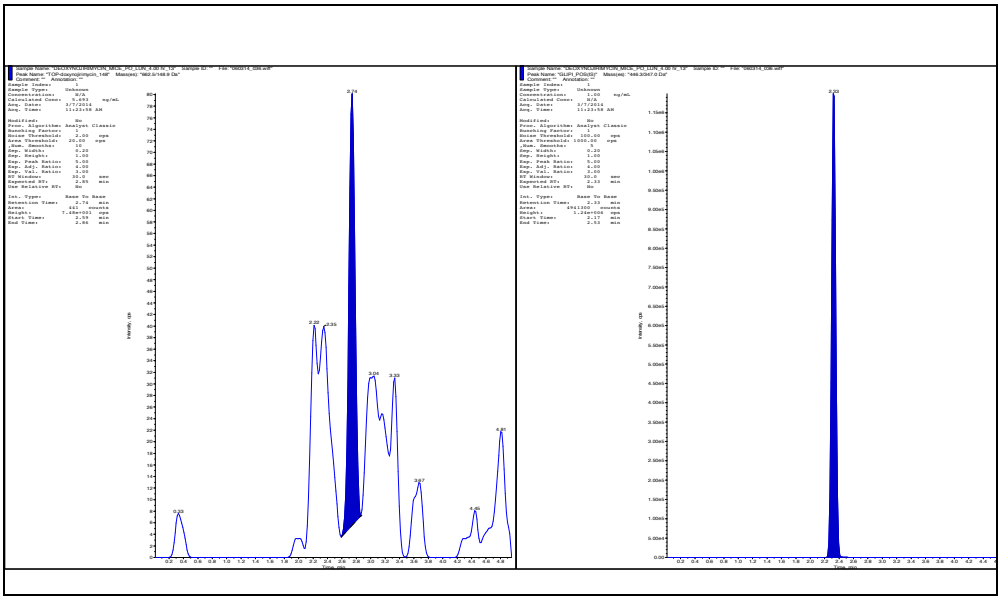

Representative chromatogram of blank kidney matrix in the LC-MS/MS analysis of Deoxynojirimycin

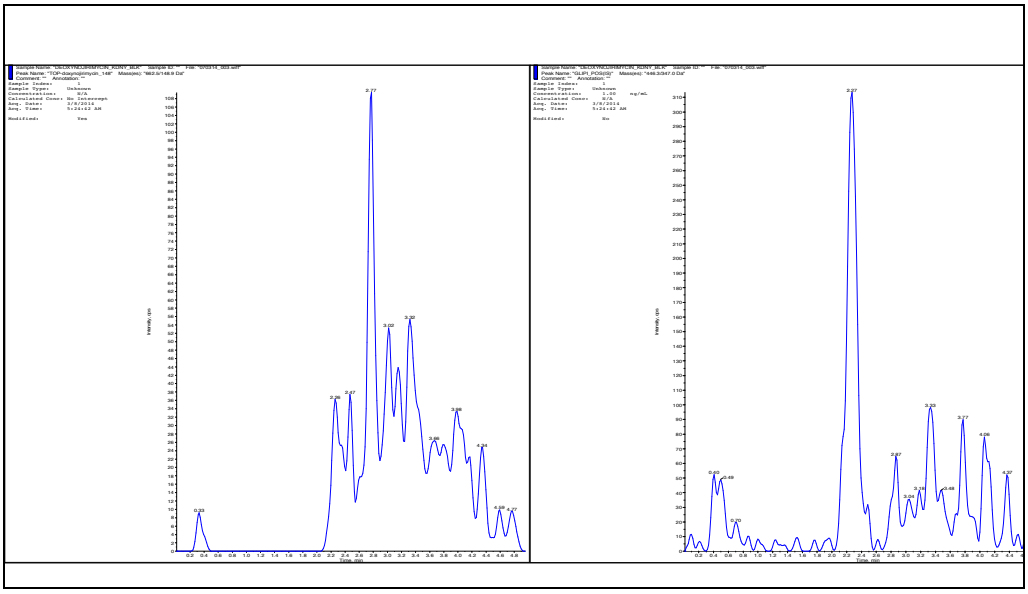

Representative LC-MS/MS chromatogram of Deoxynojirimycin calibration standard and Glipizide (IS) in mice kidney

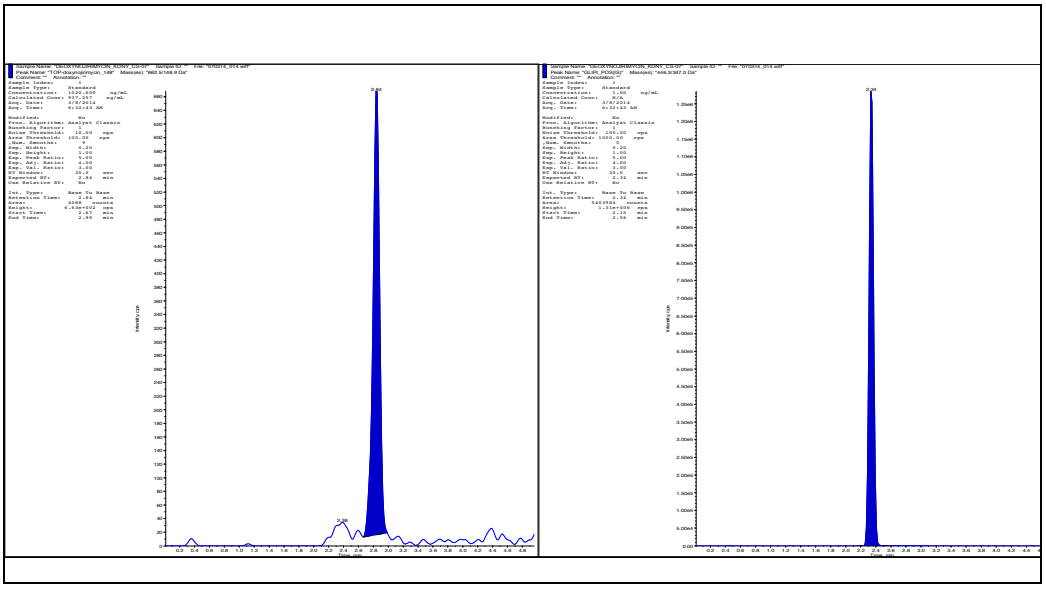

Representative LC-MS/MS chromatogram of Deoxynojirimycin intravenous study sample (kidney) and Glipizide (IS)

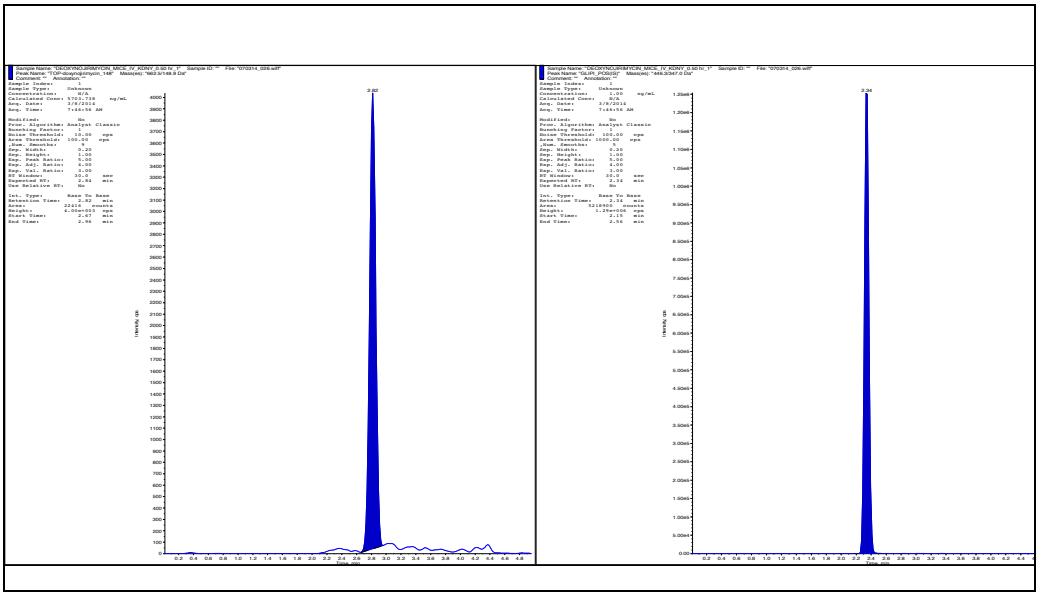

Representative LC-MS/MS chromatogram of Deoxynojirimycin peroral study sample (kidney) and Glipizide (IS)

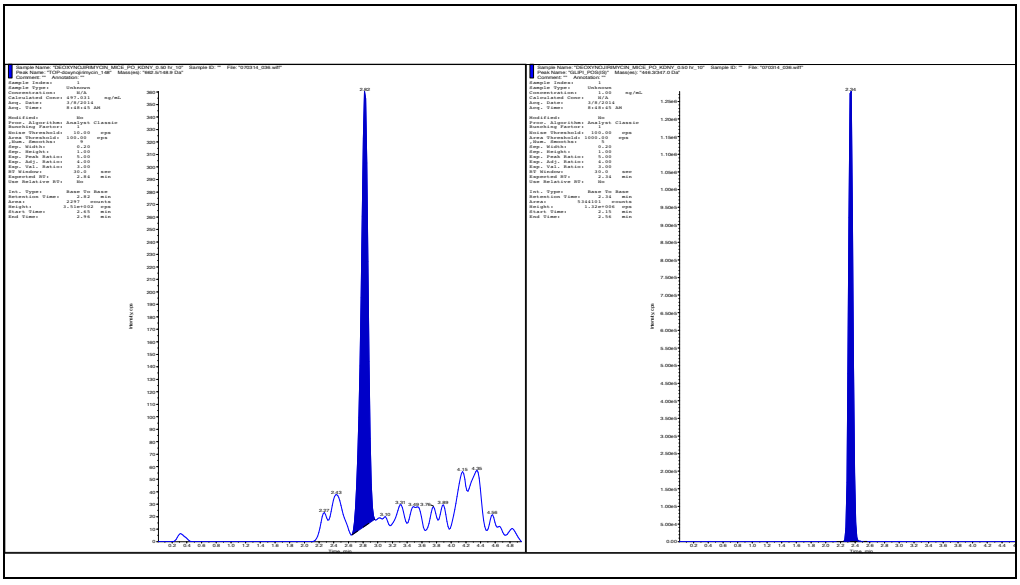

Representative chromatogram of blank liver matrix in the LC-MS/MS analysis of Deoxynojirimycin

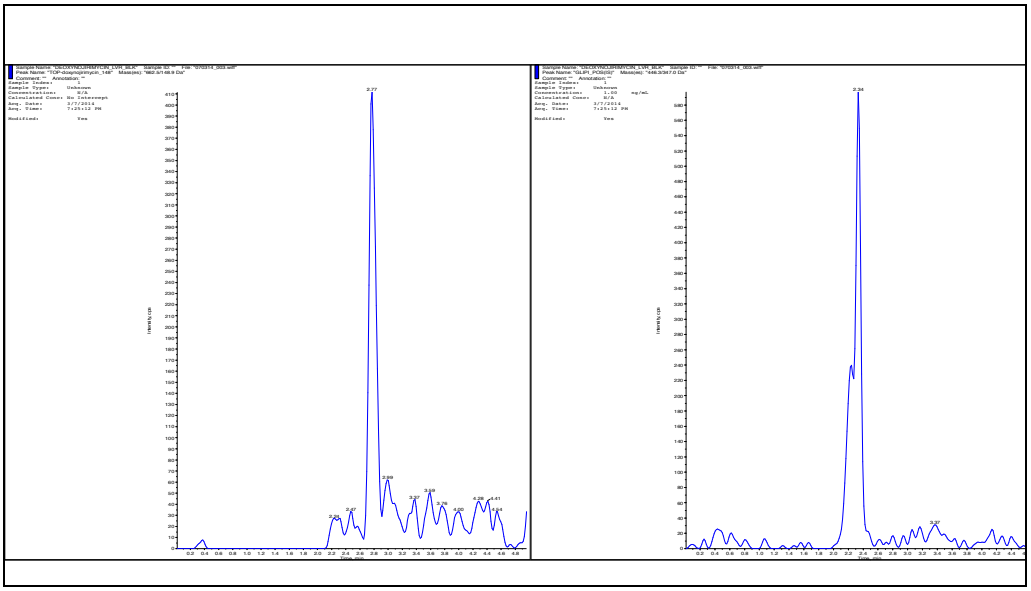

Representative LC-MS/MS chromatogram of Deoxynojirimycin calibration standard and Glipizide (IS) in mice liver

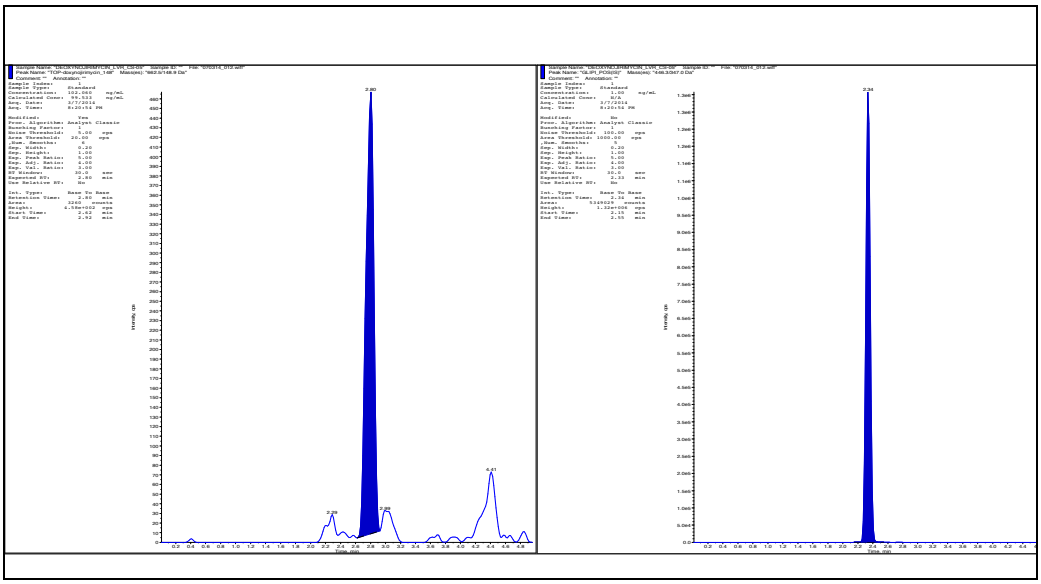

Representative LC-MS/MS chromatogram of Deoxynojirimycin intravenous study sample (liver) and Glipizide (IS)

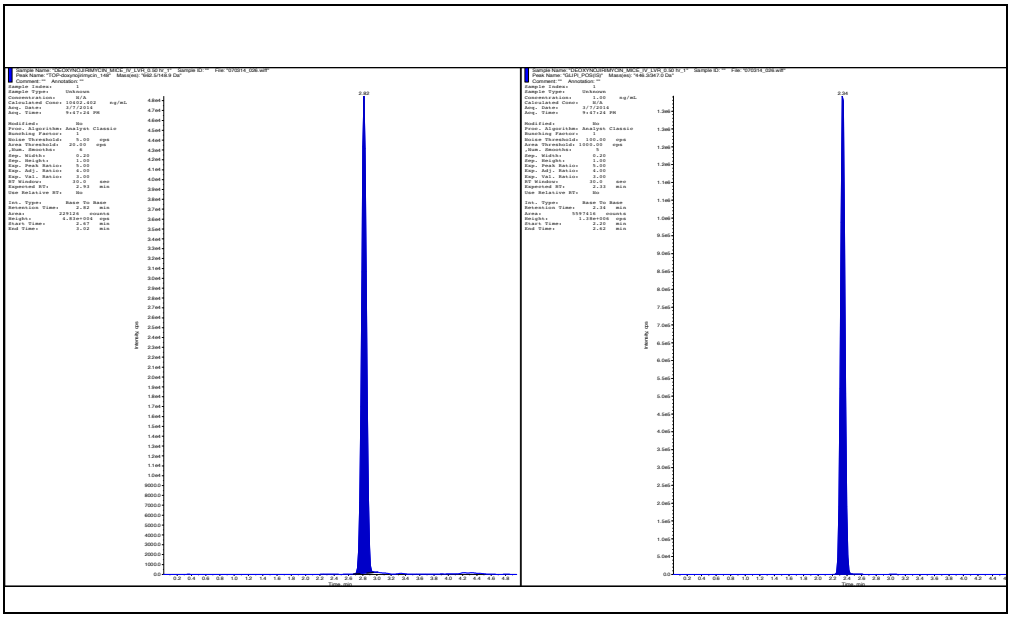

Representative LC-MS/MS chromatogram of Deoxynojirimycin per oral study sample (liver) and Glipizide (IS)

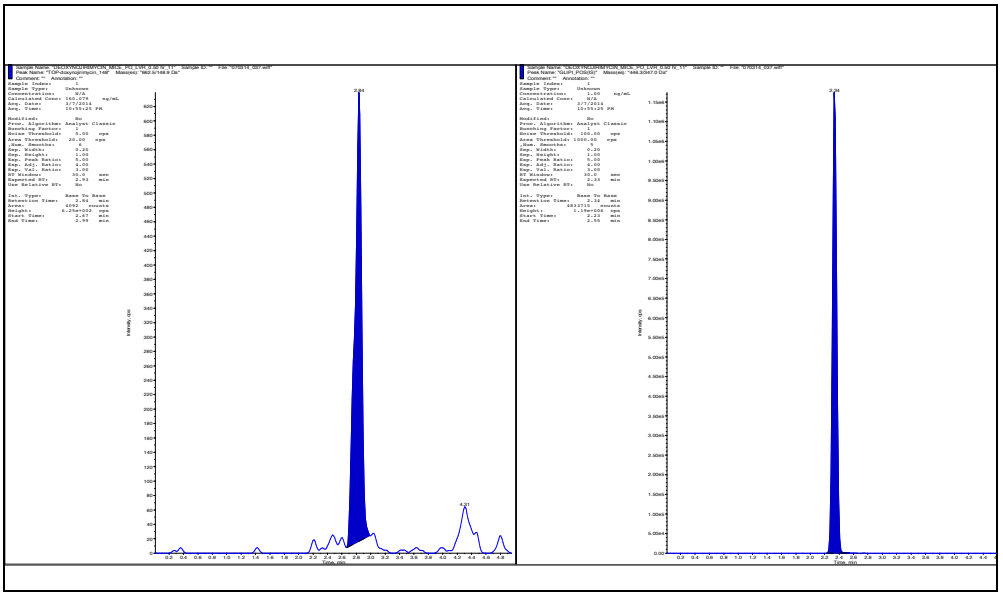

Representative chromatogram of blank heart matrix in the LC-MS/MS analysis of Deoxynojirimycin

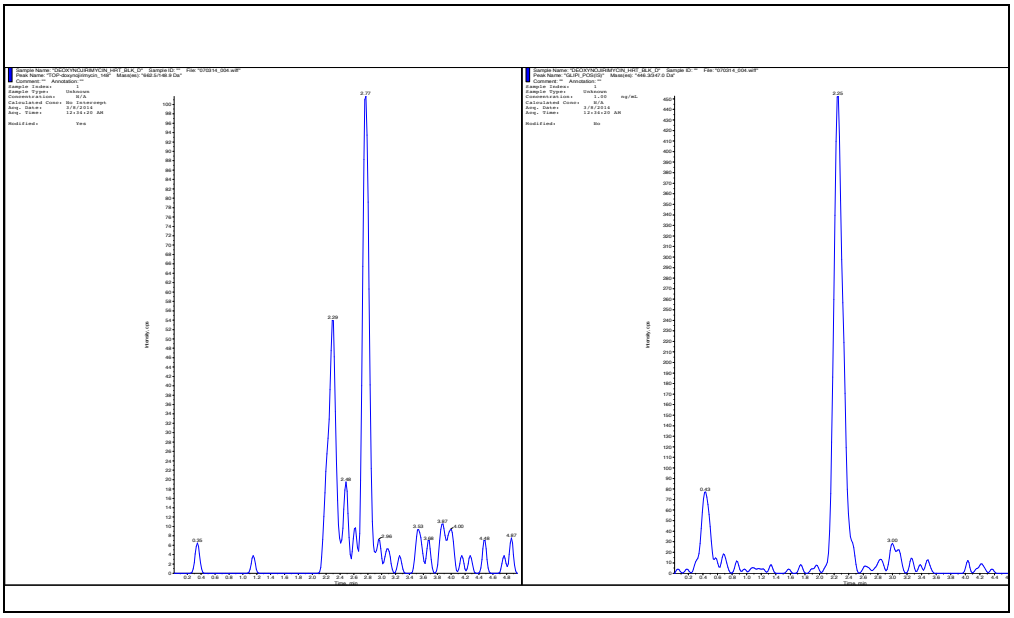

Representative LC-MS/MS chromatogram of Deoxynojirimycin calibration standard and Glipizide (IS) in mice heart

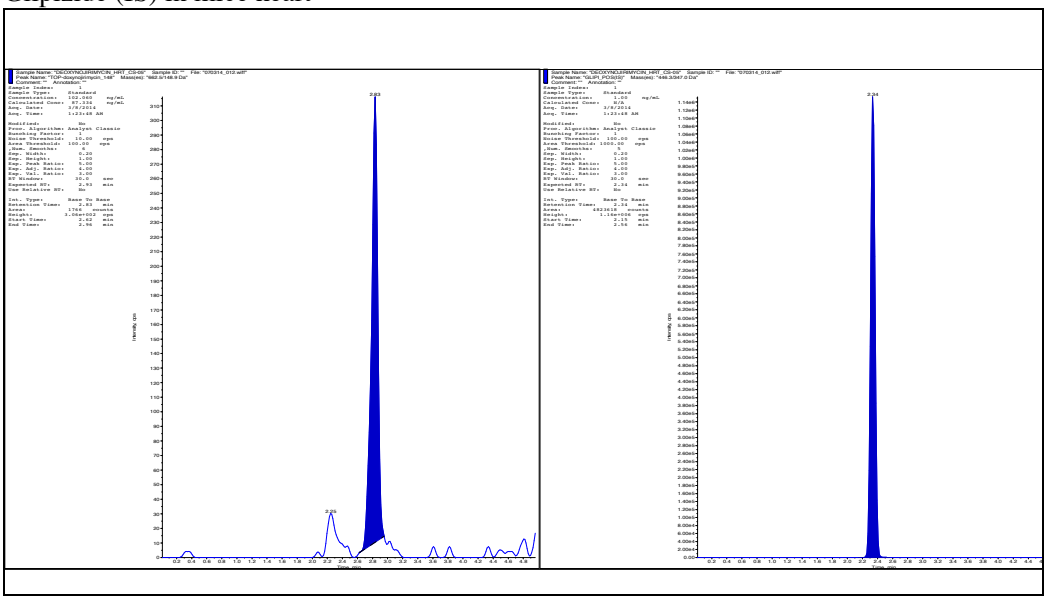

Representative LC-MS/MS chromatogram of Deoxynojirimycin intravenous study sample (heart) and Glipizide (IS)

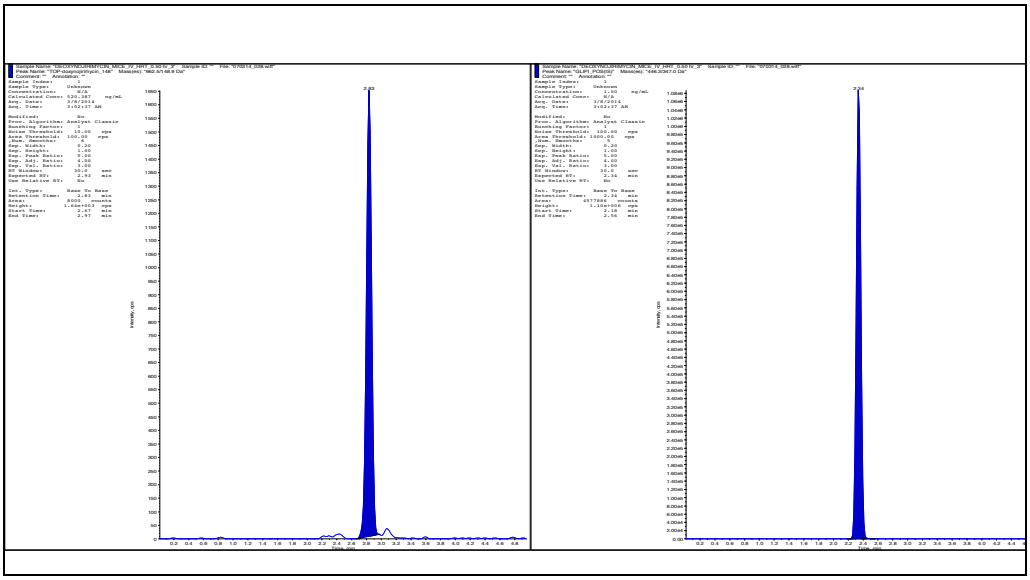

Representative LC-MS/MS chromatogram of Deoxynojirimycin per oral study sample (heart) and Glipizide (IS)

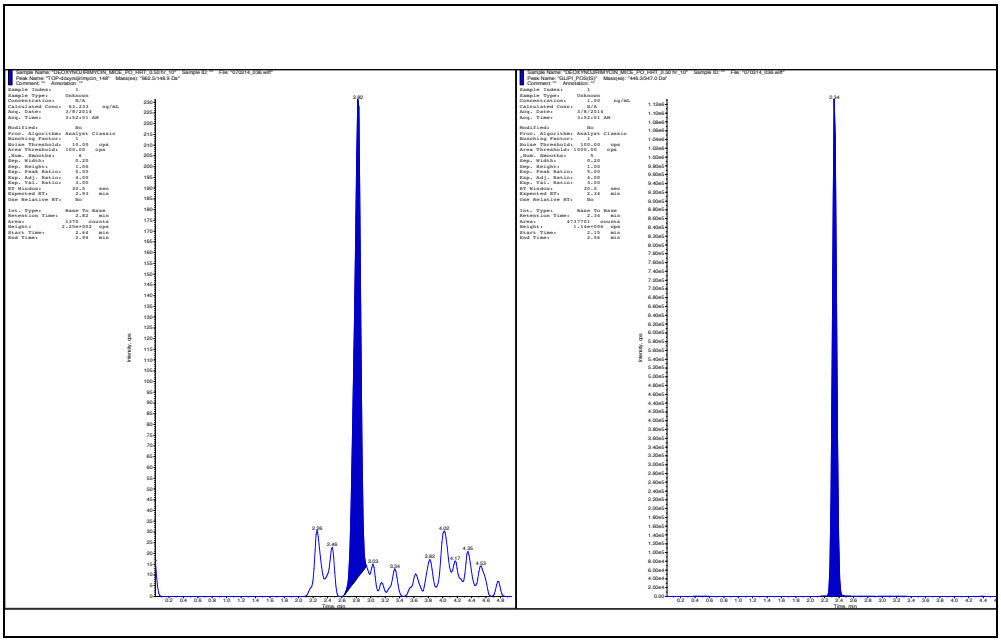

Representative chromatogram of blank spleen matrix in the LC-MS/MS analysis of Deoxynojirimycin

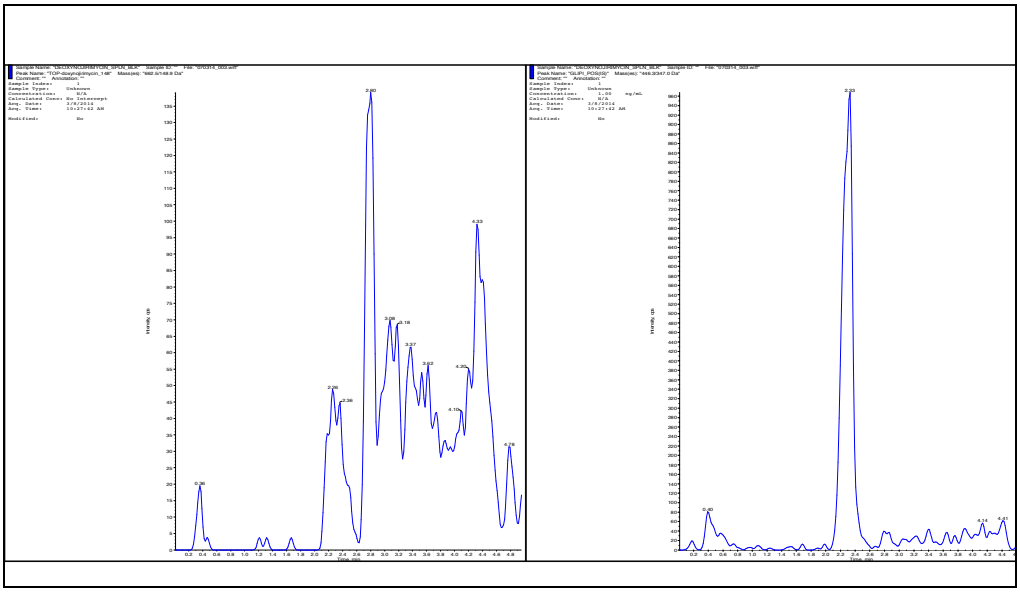

Representative LC-MS/MS chromatogram of Deoxynojirimycin calibration standard and Glipizide (IS) in mice spleen

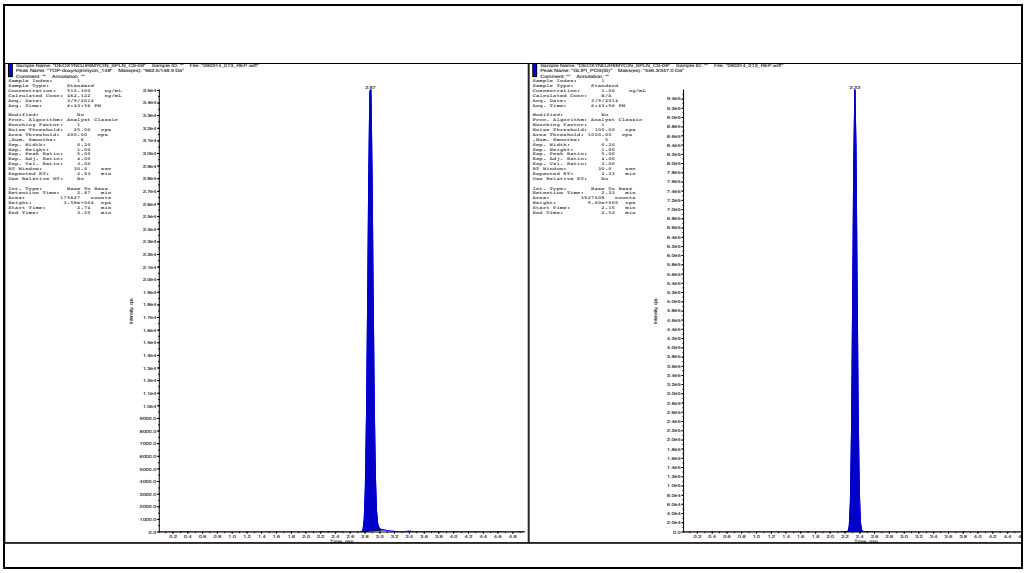

Representative LC-MS/MS chromatogram of Deoxynojirimycin intravenous study sample (spleen) and Glipizide (IS)

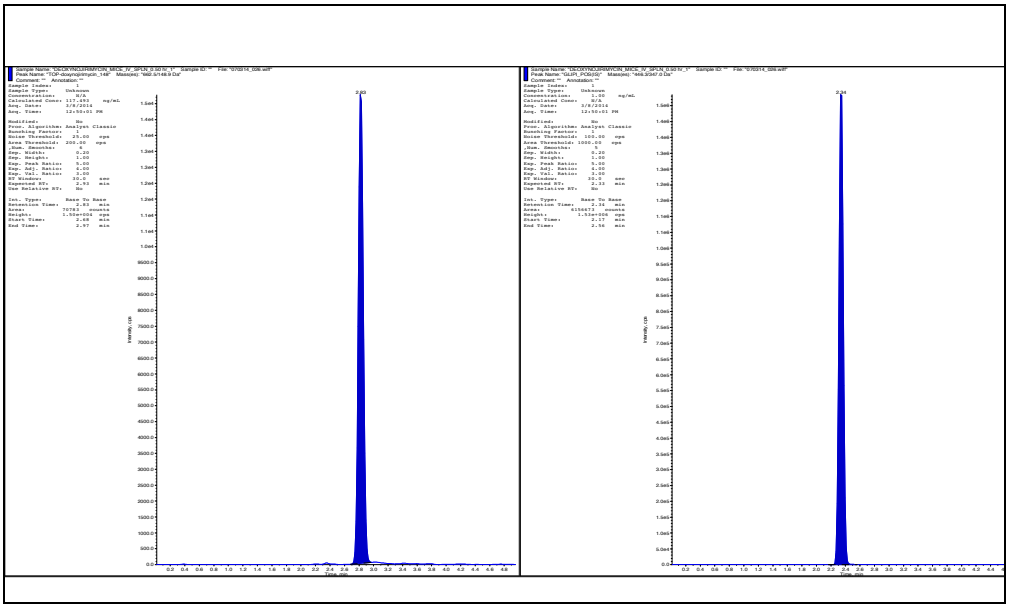

Representative LC-MS/MS chromatogram of Deoxynojirimycin per oral study sample (spleen) and Glipizide (IS)

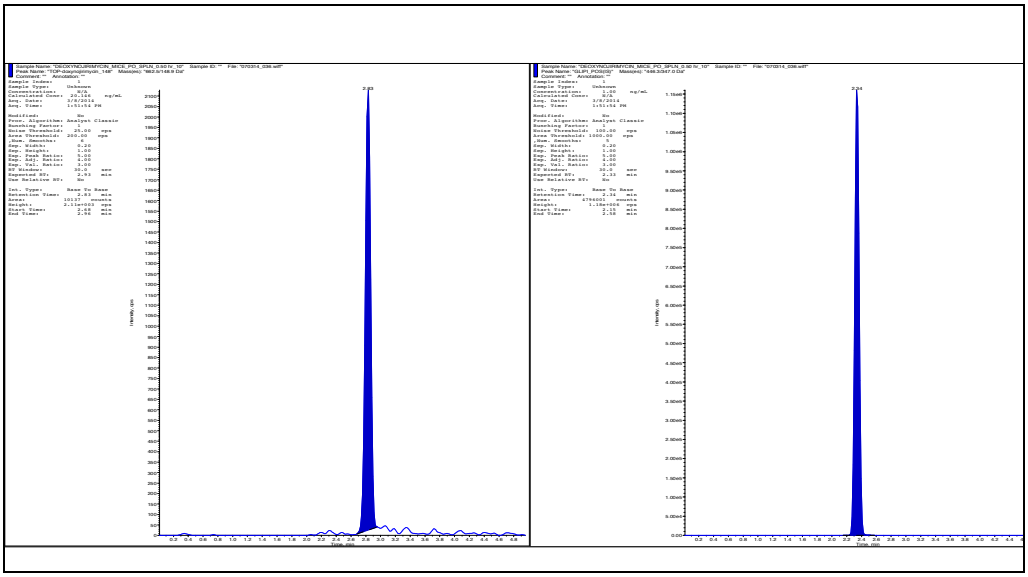

F

Selected NMR Spectra of ToP-DNJ and its Precursors

^{1}H spectrum of **108** (500 MHz, $CDCl_3$)

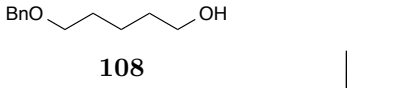

108

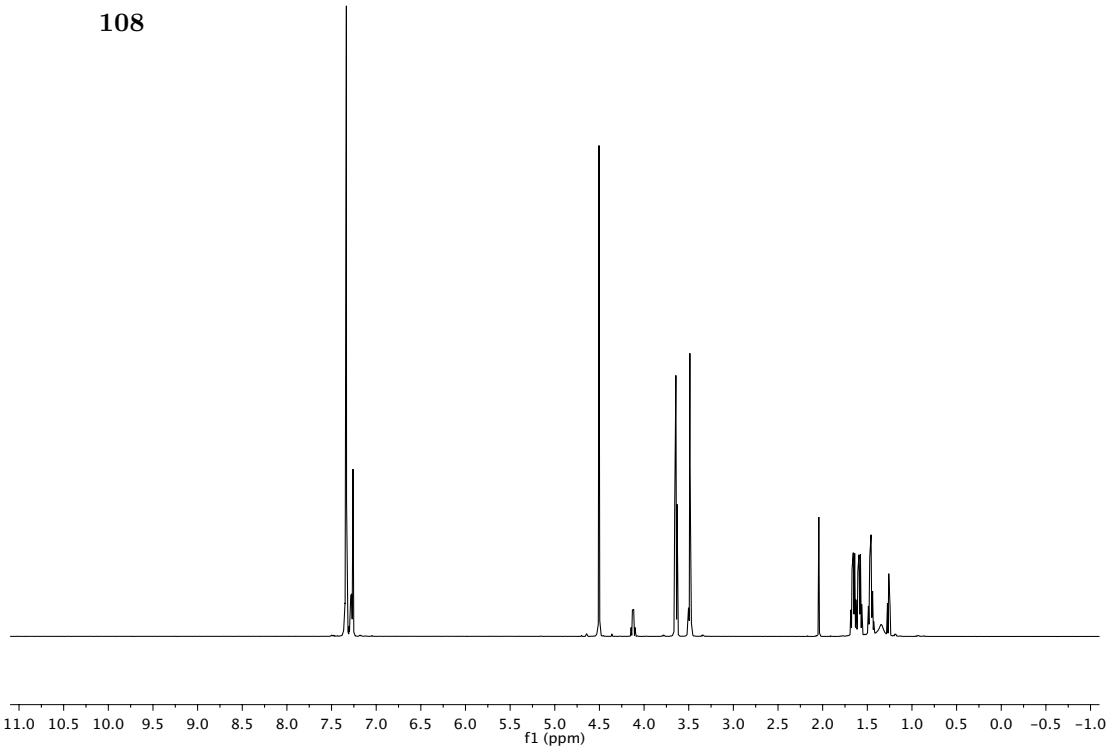

^{13}C spectrum of **108** (125 MHz, $CDCl_3$)

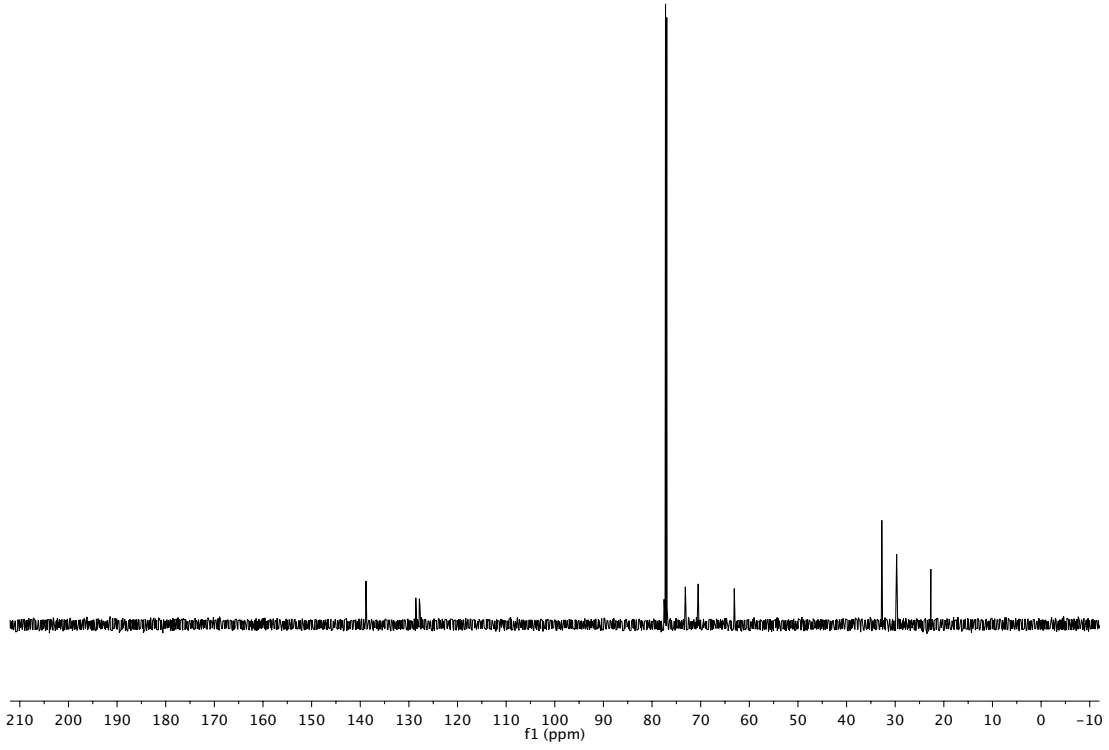

^{1}H spectrum of **109** (500 MHz, $CDCl_3$)

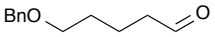

109

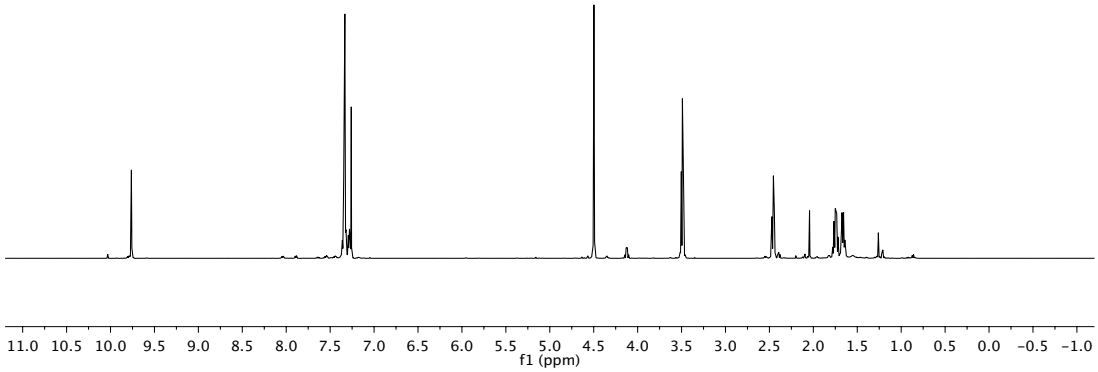

^{13}C spectrum of **109** (125 MHz, $CDCl_3$)

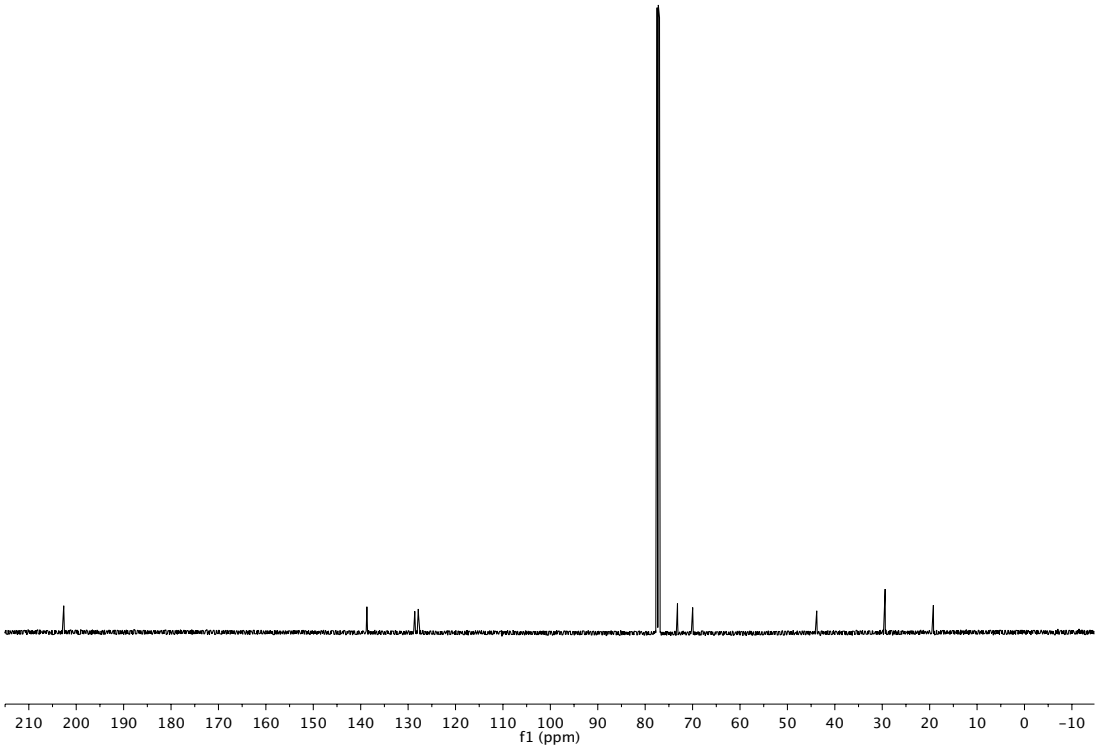

^{1}H spectrum of **110** (500 MHz, $CDCl_3$)

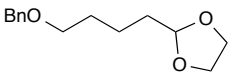

110

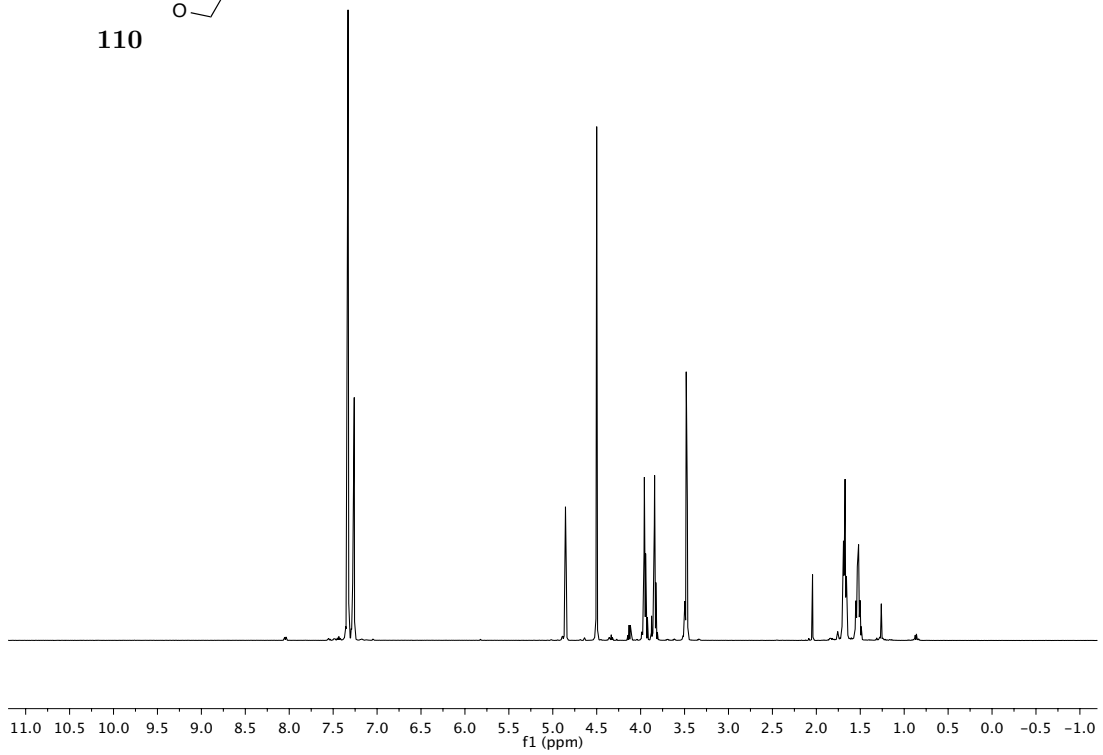

^{13}C spectrum of **110** (125 MHz, $CDCl_3$)

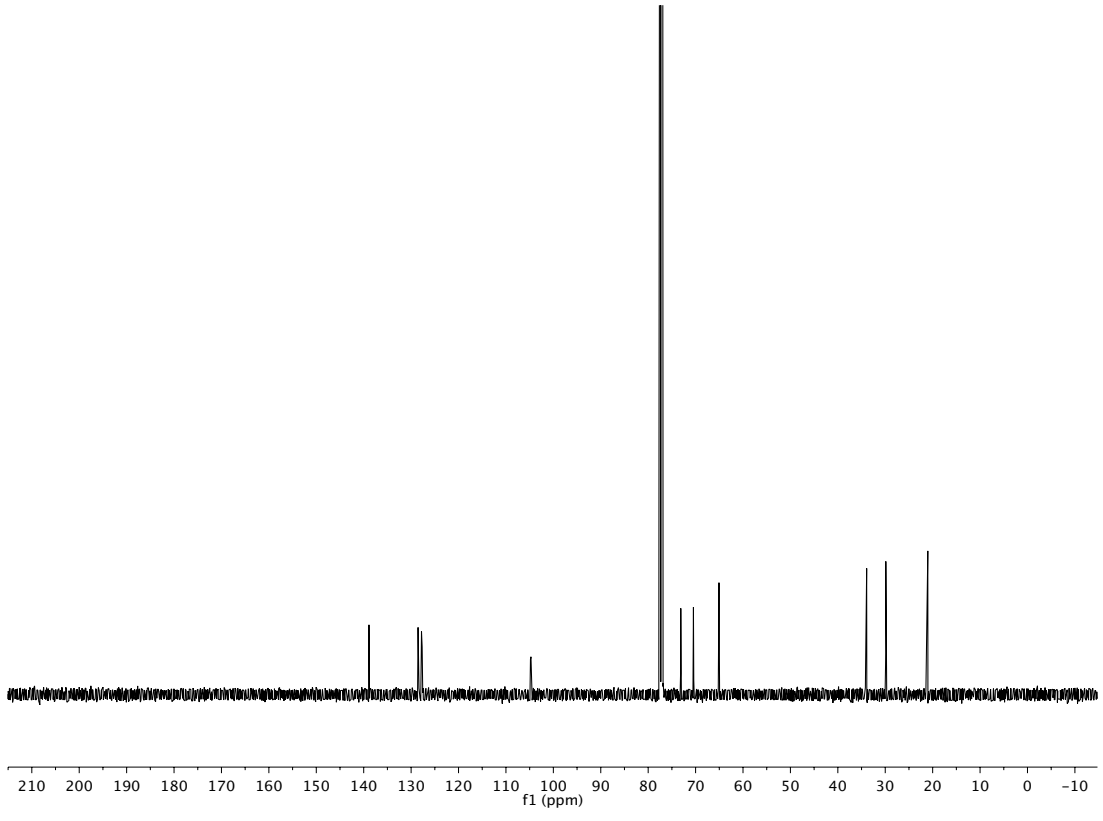

^{1}H spectrum of **111** (400 MHz, $CDCl_3$)

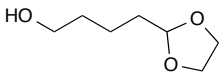

111

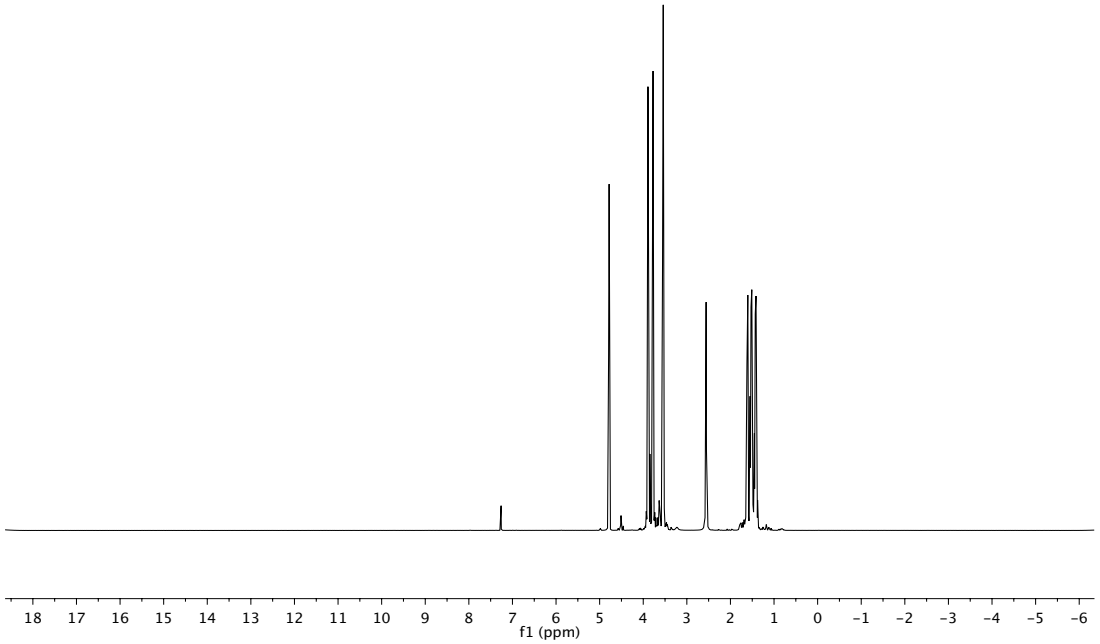

^{13}C spectrum of **111** (100 MHz, $CDCl_3$)

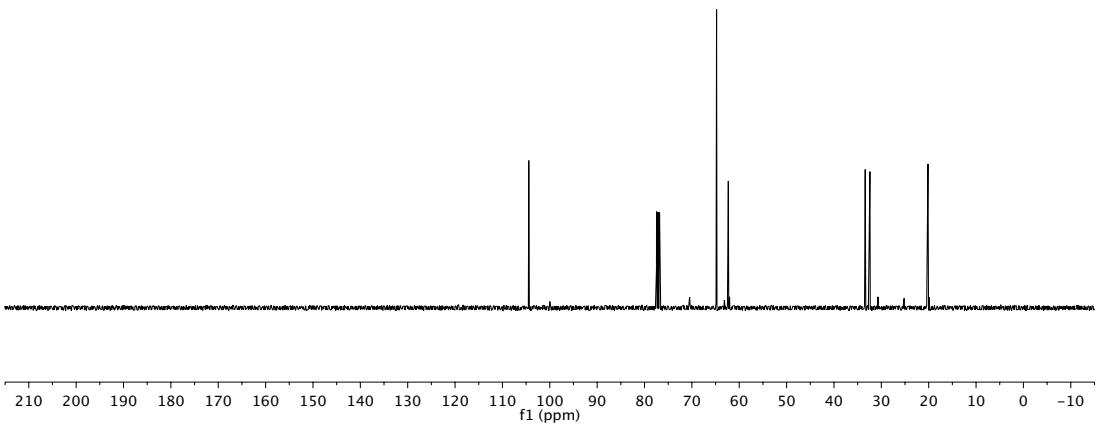

^{1}H spectrum of **106** (500 MHz, $CDCl_3$)

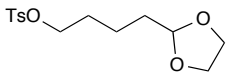

106

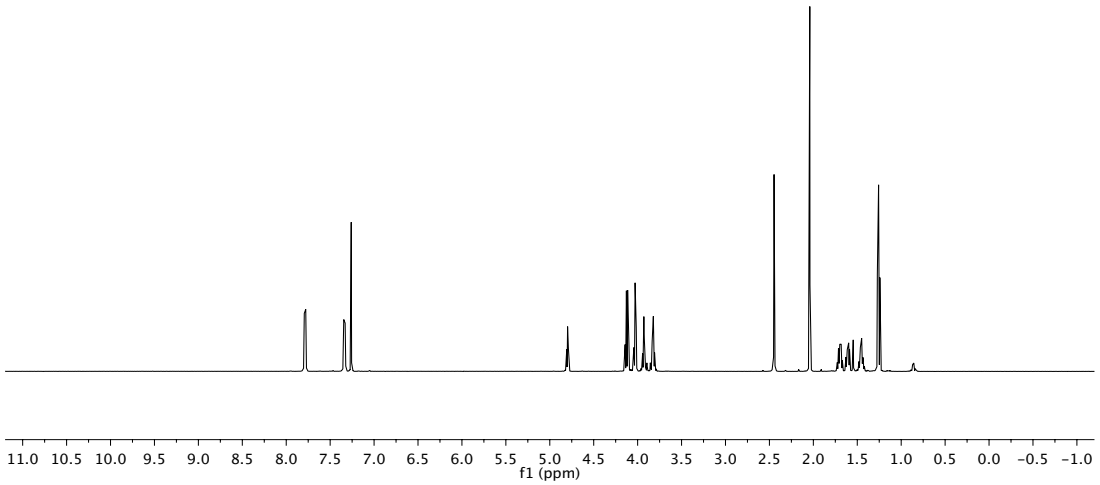

^{13}C spectrum of **106** (125 MHz, $CDCl_3$)

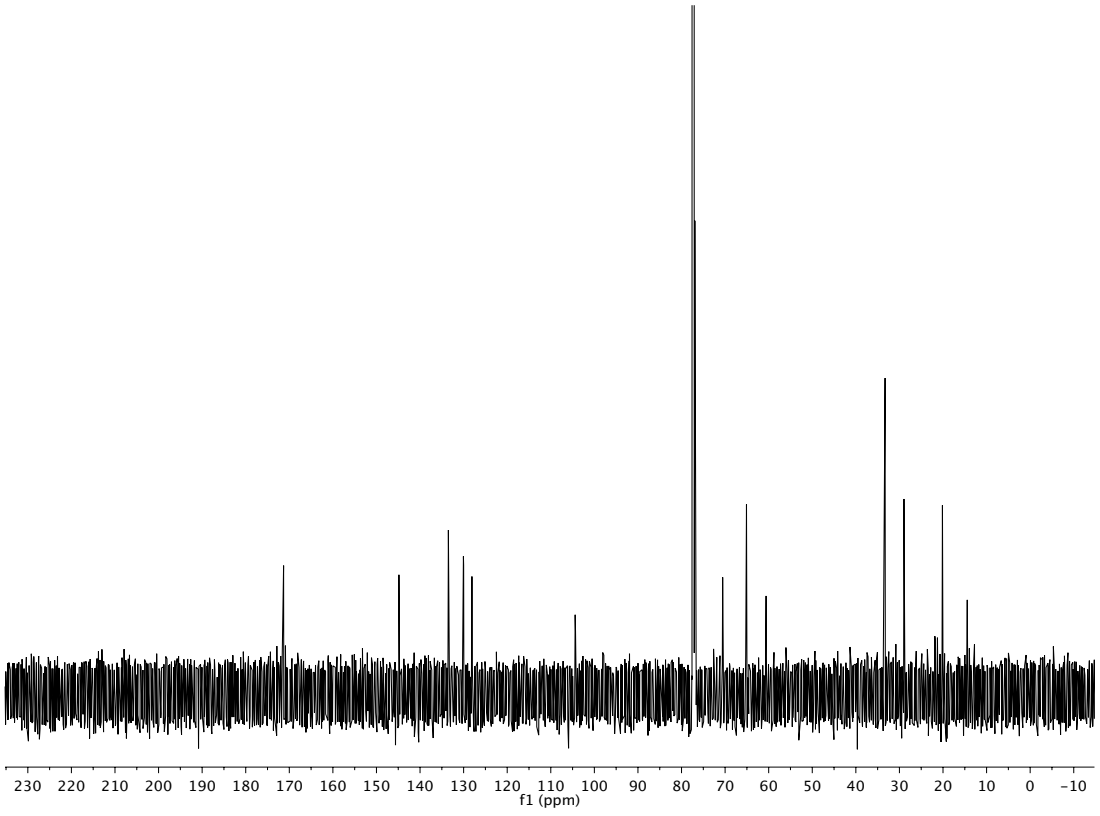

^{1}H spectrum of **112** (500 MHz, $CDCl_3$)

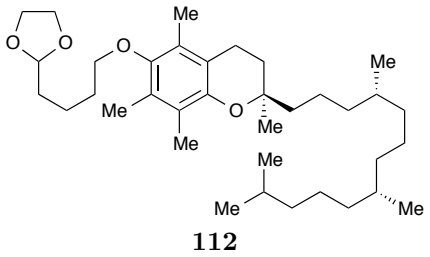

112

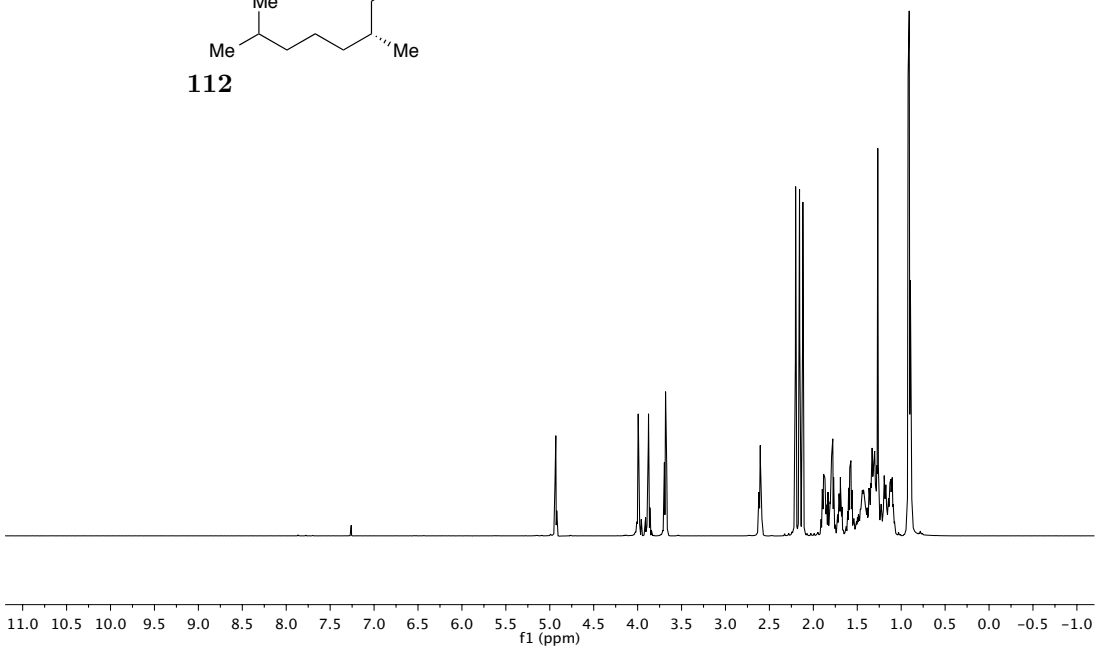

^{13}C spectrum of **112** (125 MHz, $CDCl_3$)

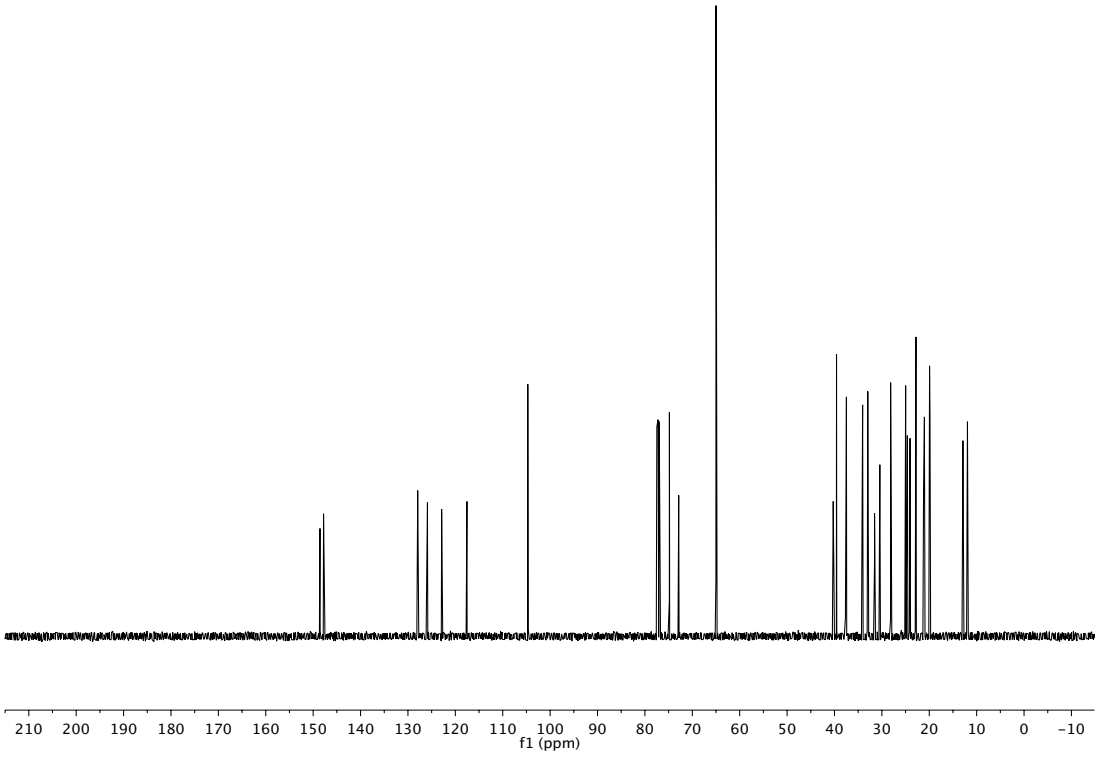

^{1}H spectrum of **113** (500 MHz, $CDCl_3$)

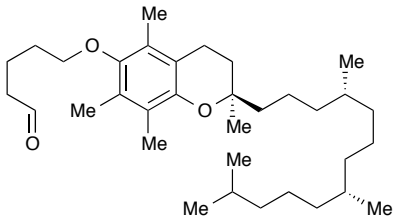

113

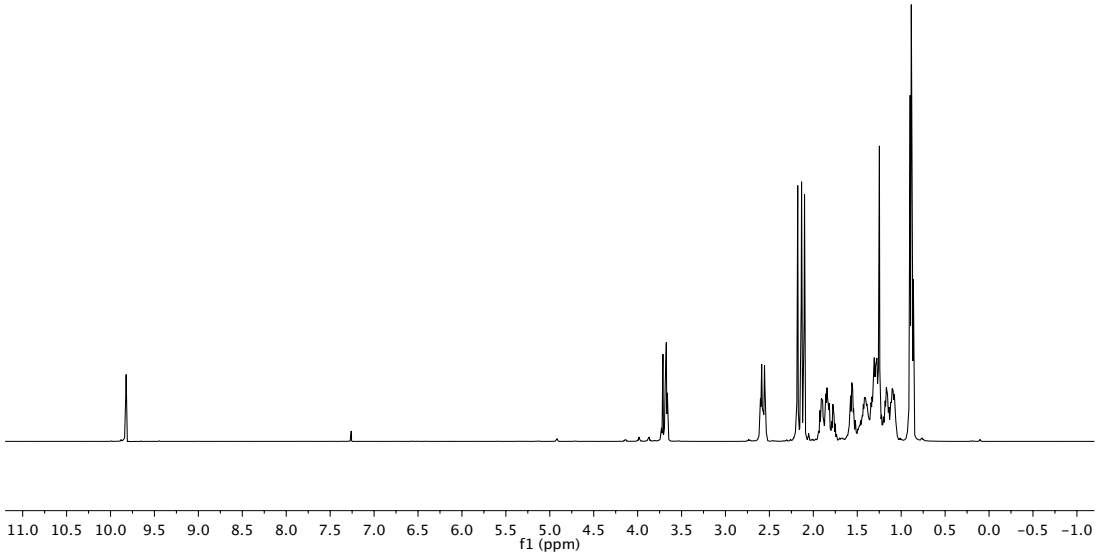

^{13}C spectrum of **113** (125 MHz, $CDCl_3$)

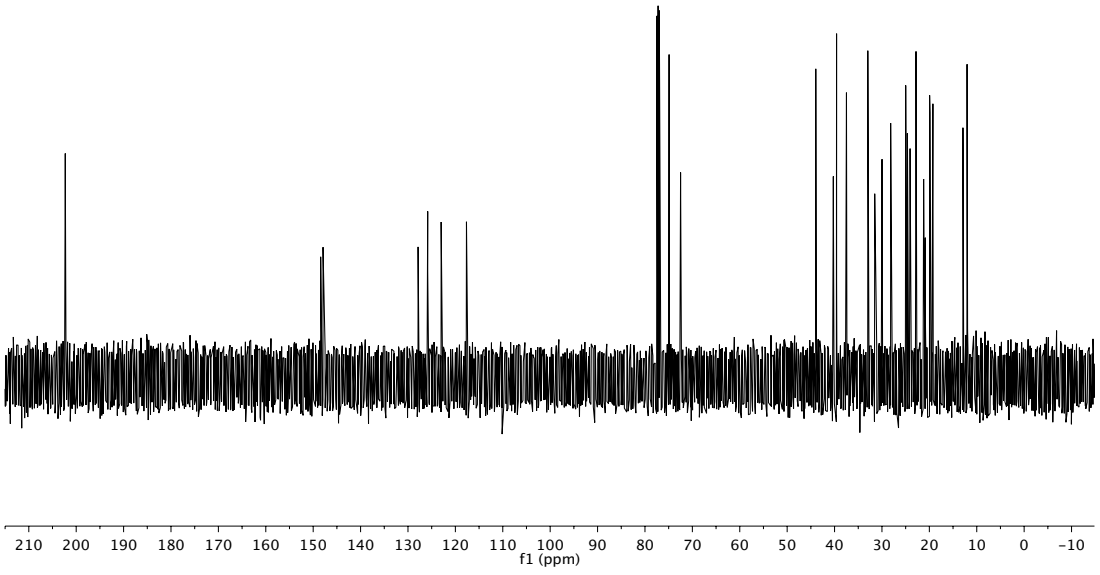

^{1}H spectrum of **105** (500 MHz, CD_3OD)

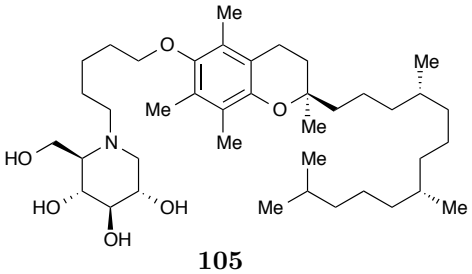

105

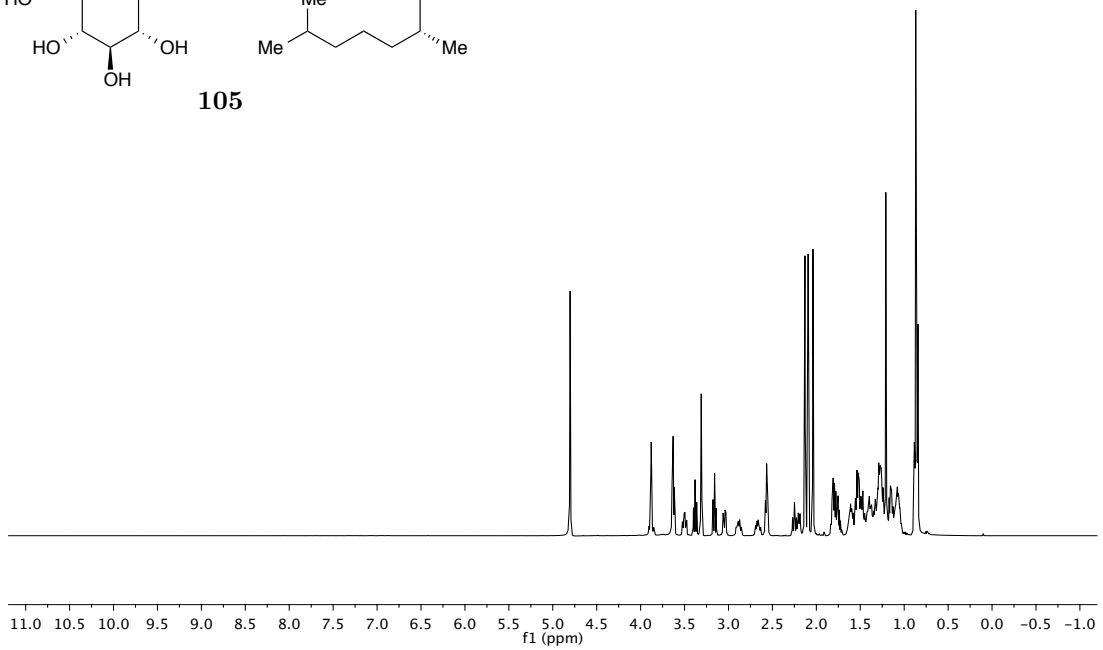

^{13}C spectrum of **105** (125 MHz, CD_3OD)

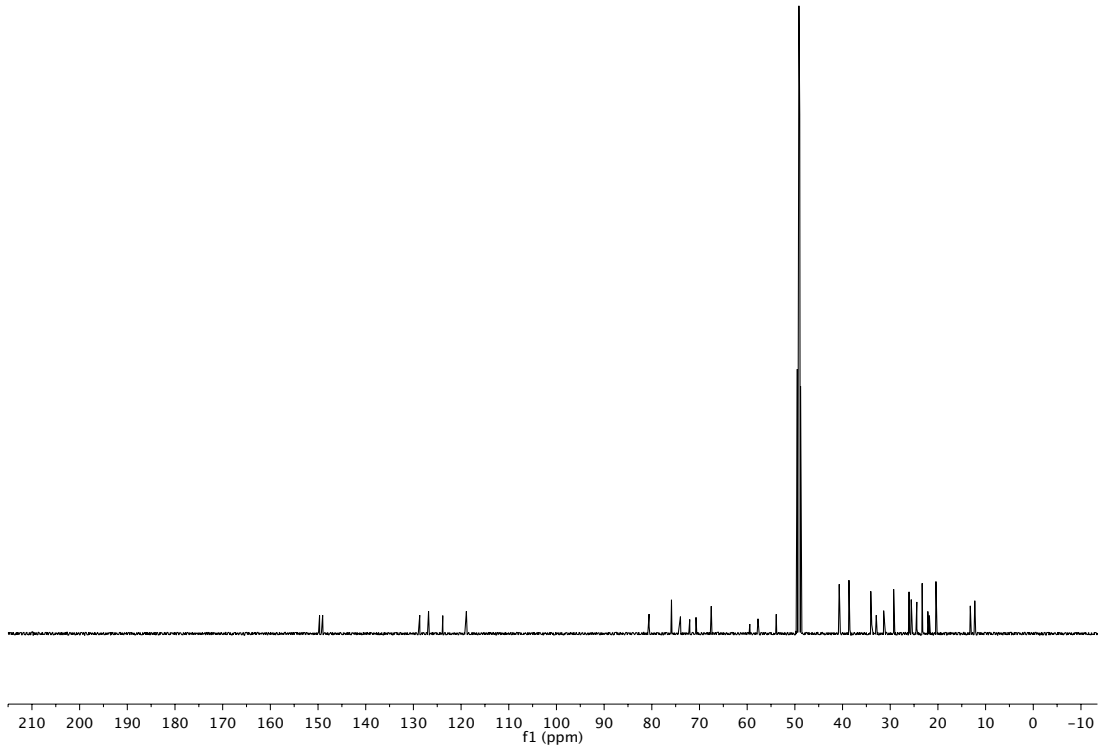

References

[1] McNaught, A. D. *Carbohyd. Res.* **1997**, *297*, 1–92.

[2] Harvey, D. J.; Merry, A. H.; Royle, L.; Campbell, M. P.; Dwek, R. A.; Rudd, P. M. *Proteomics* **2009**, *9*, 3796–3801.

[3] Berg, J. M.; Tymoczko, J. L.; Stryer, L. *Biochemistry*, 6th ed.; W. H. Freeman: New York, 2007.

[4] Whelan, W. J. *Protein Sci.* **1998**, *7*, 2038–2041.

[5] Nicolaou, K. C.; Kiappes, J. L.; Tian, W.; Gondi, V. B.; Becker, J. *Org. Lett.* **2011**, *13*, 3924–3927.

[6] Oku, N.; Matsunaga, S.; Fusetani, N. *J. Am. Chem. Soc.* **2003**, *125*, 2044–2045.

[7] McDonald, L. A.; Capson, T. L.; Krishnamurthy, G.; Ding, W. D.; Ellestad, G. A.; Bernan, V. S.; Maiese, W. M.; Lassota, P.; Discafani, C.; Kramer, R. A.; Ireland, C. M. *J. Am. Chem. Soc.* **1996**, *118*, 10898–10899.

[8] Witczak, Z. J. *J. Carbohydr. Chem.* **1996**, *15*, 649–650.

[9] Mayor, A.; Hayes, A. *Princeton/Stanford Working Papers in Classics* **2011**, 1–30.

[10] Myers, A. G.; Cohen, S. B.; Kwon, B. M. *J. Am. Chem. Soc.* **1994**, *116*, 1255–1271.

[11] Clive, D.; Bo, Y. X.; Selvakumar, N.; McDonald, R.; Santarsiero, B. D. *Tetrahedron* **1999**, *55*, 3277–3290.

[12] Nicolaou, K. C.; Ogawa, Y.; Zuccarello, G.; Schweiger, E. J.; Kumazawa, T. *J. Am. Chem. Soc.* **1988**, *110*, 4866–4868.

[13] Hangeland, J. J.; De Voss, J. J.; Heath, J. A.; Townsend, C. A.; Ding, W.-D.; Ashcroft, J. S.; Ellestad, G. A. *J. Am. Chem. Soc.* **1992**, *114*, 9200–9202.

[14] Ikemoto, N.; Kumar, R. A.; Ling, T. T.; Ellestad, G. A.; Danishefsky, S. J.; Patel, D. J. *Proc. Natl. Acad. Sci. U.S.A.* **1995**, *92*, 10506–10510.

[15] Zeman, S. M.; Depew, K. M.; Danishefsky, S. J.; Crothers, D. M. *Proc. Natl. Acad. Sci. U.S.A.* **1998**, *95*, 4327–4332.

[16] Drak, J.; Iwasawa, N.; Danishefsky, S.; Crothers, D. M. *Proc. Natl. Acad. Sci. U.S.A.* **1991**, *88*, 7464–7468.

[17] Ho, S. N.; Boyer, S. H.; Schreiber, S. L.; Danishefsky, S. J.; Crabtree, G. R. *Proc. Natl. Acad. Sci. U.S.A.* **1994**, *91*, 9203–9207.

[18] Nicolaou, K. C.; Dai, W. M. *Angew. Chem., Int. Ed. Engl.* **1991**, *30*, 1387–1416.

[19] Smith, A. L.; Nicolaou, K. C. *J. Med. Chem.* **1996**, *39*, 2103–2117.

[20] Grissom, J. W.; Gunawardena, G. U.; Klingberg, D.; Huang, D. H. *Tetrahedron* **1996**, *52*, 6453–6518.

[21] Thorson, J.; Sievers, E.; Ahlert, J.; Shepard, E.; Whitwam, R.; Onwueme, K.; Ruppen, M. *Curr. Pharm. Des.* **2000**, *6*, 1841–1879.

[22] Jones, G. B.; Fouad, F. S. *Curr. Pharm. Des.* **2002**, *8*, 2415–2440.

[23] Liang, Z.-X. *Nat. Prod. Rep.* **2010**, *27*, 499–528.

[24] Joshi, M. C.; Rawat, D. S. *Chem. Biodivers.* **2012**, *9*, 459–498.

[25] Hamann, P. R.; Hinman, L. M.; Hollander, I.; Beyer, C. F.; Lindh, D.; Holcomb, R.; Hallett, W.; Tsou, H.-R.; Upeslacis, J.; Shochat, D.; Mountain, A.; Flowers, D. A.; Bernstein, I. *Bioconjugate Chem.* **2002**, *13*, 47–58.

[26] Advani, A.; Coiffier, B.; Czuczman, M. S.; Dreyling, M.; Foran, J.; Gine, E.; Gisselbrecht, C.; Ketterer, N.; Nasta, S.; Rohatiner, A.; Schmidt-Wolf, I. G. H.; Schuler, M.; Sierra, J.; Smith, M. R.; Verhoef, G.; Winter, J. N.; Boni, J.; Vandendries, E.; Shapiro, M.; Fayad, L. *J. Clin. Oncol.* **2010**, *28*, 2085–2093.

[27] Ricart, A. D. *Clin. Cancer Res.* **2011**, *17*, 6417–6427.

[28] Smythies, J. R.; Antun, F. *Nature* **1969**, *223*, 1061–1063.

[29] Duportail, G.; Lami, H. *Biochim. Biophys. Acta* **1975**, *402*, 20–30.

[30] Hayashi, K.; Nagao, M.; Sugimura, T. *Nucleic Acids Res.* **1977**, *4*, 3679–3685.

[31] Pezzuto, J. M.; Lau, P. P.; Luh, Y.; Moore, P. D.; Wogan, G. N.; Hecht, S. M. *Proc. Natl. Acad. Sci. U.S.A.* **1980**, *77*, 1427–1431.

[32] Duportail, G. *Int. J. Biol. Macromol.* **1981**, *3*, 188–192.

[33] McPherson, D. D.; Pezzuto, J. M. *J. Chromatogr.* **1983**, *281*, 348–354.

[34] Feigon, J.; Denny, W. A.; Leupin, W.; Kearns, D. R. *J. Med. Chem.* **1984**, *27*, 450–465.

[35] Funayama, Y.; Nishio, K.; Wakabayashi, K.; Nagao, M.; Shimoi, K.; Ohira, T.; Hasegawa, S.; Saijo, N. *Mutat. Res.* **1996**, *349*, 183–191.

[36] Taira, Z.; Kanzawa, S.; Dohara, C.; Ishida, S.; Matsumoto, M.; Sakiya, Y. *Jpn. J. Tox. Env. Health* **1997**, *43*, 83–91.

[37] Tamura, S.; Konakahara, T.; Komatsu, H.; Ozaki, T.; Ohta, Y.; Takeuchi, H. *Heterocycles* **1998**, *48*, 2477–2480.

[38] Xiao, S. L.; Lin, W.; Wang, C.; Yang, M. *Bioorg. Med. Chem. Lett.* **2001**, *11*, 437–441.

[39] Toshima, K.; Okuno, Y.; Nakajima, Y. *Bioorg. Med. Chem. Lett.* **2002**, *12*, 671–673.

[40] Nicolaou, K. C.; Hummel, C. W.; Pitsinos, E. N.; Nakada, M.; Smith, A. L.; Shibayama, K.; Saimoto, H. *J. Am. Chem. Soc.* **1992**, *114*, 10082–10084.

[41] Groneberg, R. D.; Miyazaki, T.; Stylianides, N. A.; Schulze, T. J.; Stahl, W.; Schreiner, E. P.; Suzuki, T.; Iwabuchi, Y.; Smith, A. L.; Nicolaou, K. C. *J. Am. Chem. Soc.* **1993**, *115*, 7593–7611.

[42] Smith, A. L.; Pitsinos, E. N.; Hwang, C. K.; Mizuno, Y.; Saimoto, H.; Scarlato, G. R.; Suzuki, T.; Nicolaou, K. C. *J. Am. Chem. Soc.* **1993**, *115*, 7612–7624.

[43] Nicolaou, K. C.; Hummel, C. W.; Nakada, M.; Shibayama, K.; Pitsinos, E. N.; Saimoto, H.; Mizuno, Y.; Baldenius, K. U.; Smith, A. L. *J. Am. Chem. Soc.* **1993**, *115*, 7625–7635.

[44] Hitchcock, S. A.; Chu-Moyer, M. Y.; Boyer, S. H.; Olson, S. H.; Danishefsky, S. J. *J. Am. Chem. Soc.* **1995**, *117*, 5750–5756.

[45] Bracher, F.; Hildebrand, D. *Tetrahedron* **1994**, *50*, 12329–12336.

[46] Kuwada, T.; Fukui, M.; Hata, T.; Choshi, T.; Nobuhiro, J.; Ono, Y.; Hibino, S. *Chem. Pharm. Bull.* **2003**, *51*, 20–23.

[47] Maloney, K. M.; Nwakpuda, E.; Kuethe, J. T.; Yin, J. *J. Org. Chem.* **2009**, *74*, 5111–5114.

[48] Wang, C.-C.; Lee, J.-C.; Luo, S.-Y.; Kulkarni, S. S.; Huang, Y.-W.; Lee, C.-C.; Chang, K.-L.; Hung, S.-C. *Nature* **2007**, *446*, 896–899.

[49] Wang, C.-C.; Kulkarni, S. S.; Lee, J.-C.; Luo, S.-Y.; Hung, S.-C. *Nat. Protoc.* **2008**, *3*, 97–113.

[50] Reetz, M. T.; Müller-Starke, H. *Tetrahedron Lett.* **1984**, *25*, 3301–3304.

[51] Nicolaou, K. C.; Groneberg, R. D.; Stylianides, N. A.; Miyazaki, T. *J. Chem. Soc., Chem. Commun.* **1990**, 1275–1277.

[52] Crotti, P.; Di Bussolo, V.; Favero, L.; Macchia, F.; Pineschi, M. *Tetrahedron: Asymmetry* **1996**, *7*, 779–786.

[53] Weinstein, D. S.; Nicolaou, K. C. *J. Chem. Soc., Perkin Trans. 1* **1999**, 545–558.

[54] Mukaiyama, T.; Hashimoto, Y.; Shoda, S.-i. *Chem. Lett.* **1983**, 935–938.

[55] Nicolaou, K. C.; Randall, J. L.; Furst, G. T. *J. Am. Chem. Soc.* **1985**, *107*, 5556–5558.

[56] Gottlieb, H. E.; Kotlyar, V.; Nudelman, A. *J. Org. Chem.* **1997**, *62*, 7512–7515.

[57] Inouye, S.; Tsuruoka, T.; Nida, T. *J. Antibiot.* **1966**, *19*, 288–292.

[58] Inouye, S.; Tsuruoka, T.; Ito, T.; Niida, T. *Tetrahedron* **1968**, *24*, 2125–2144.

[59] Compain, P., Martin, O. R., Eds. *Iminosugars: From Synthesis to Therapeutic Applications*, 1st ed.; John Wiley & Sons: Chichester, 2007.

[60] Paulsen, H. *Angew. Chem., Int. Ed. Engl.* **1962**, *1*, 454–454.

[61] Paulsen, H. *Angew. Chem., Int. Ed. Engl.* **1962**, *1*, 597–597.

[62] Jones, J. K. N.; Turner, J. C. *J. Chem. Soc.* **1962**, 4699–4703.

[63] Jones, J. K. N.; Szarek, W. A. *Can. J. Chem.* **1963**, *41*, 636–640.

[64] Hanessian, S.; Haskell, T. H. *J. Org. Chem.* **1963**, *28*, 2604–2610.

[65] Hanessian, S. *Chem. Commun. (London)* **1966**, 796–798.

[66] Paulsen, H.; Todt, K. *Adv. Carbohydr. Chem. Biochem.* **1968**, *23*, 115–232.

[67] Paulsen, H. *Angew. Chem., Int. Ed. Engl.* **1966**, *5*, 495–510.

[68] Paulsen, H.; Todt, K. *Chem. Ber.* **1967**, *100*, 3385–3396.

[69] Paulsen, H.; Todt, K. *Chem. Ber.* **1967**, *100*, 3397–3404.

[70] Yoshikaki, A.; Hivonu, M. *Nippon Nogeik. Kaishi* **1976**, *50*, 571–572.

[71] Yin, H.; Shi, X.-q.; Sun, B.; Ye, J.-j.; Duan, Z.-a.; Zhou, X.-l.; Cui, W.-z.; Wu, X.-f. *J. Zhejiang Univ. Sci. B* **2010**, *11*, 286–291.

[72] Dwek, R. A.; Butters, T. D.; Platt, F. M.; Zitzmann, N. *Nat. Rev. Drug Discov.* **2002**, *1*, 65–75.

[73] Butters, T. D.; Dwek, R. A.; Platt, F. M. *Glycobiology* **2005**, *15*, 43R–52R.

[74] Dalziel, M.; Crispin, M.; Scanlan, C. N.; Zitzmann, N.; Dwek, R. A. *Science* **2014**, *343*, 1235681.

[75] Davis, B. G.; Hull, A.; Smith, C.; Nash, R. J.; Watson, A. A. *Tetrahedron: Asymmetry* **1998**, *9*, 2947–2960.

[76] Lee, J. C.; Francis, S.; Dutta, D.; Gupta, V.; Yang, Y.; Zhu, J.-Y.; Tash, J. S.; Schönbrunn, E.; Georg, G. I. *J. Org. Chem.* **2012**, *77*, 3082–3098.

[77] Lenagh-Snow, G. M. J.; Araújo, N.; Jenkinson, S. F.; Martínez, R. F.; Shimada, Y.; Yu, C.-Y.; Kato, A.; Fleet, G. W. J. *Org. Lett.* **2012**, *14*, 2142–2145.

[78] Li, H.; Blériot, Y.; Chantereau, C.; Mallet, J.-M.; Sollogoub, M.; Zhang, Y.; Rodríguez-García, E.; Vogel, P.; Jiménez-Barbero, J.; Sinaÿ, P. *Org. Biomol. Chem.* **2004**, *2*, 1492–1499.

[79] Orwig, S. D.; Tan, Y. L.; Grimster, N. P.; Yu, Z.; Powers, E. T.; Kelly, J. W.; Lieberman, R. L. *Biochemistry* **2011**, *50*, 10647–10657.

[80] Araújo, N.; Jenkinson, S. F.; Martínez, R. F.; Glawar, A. F. G.; Wormald, M. R.; Butters, T. D.; Nakagawa, S.; Adachi, I.; Kato, A.; Yoshihara, A.; Akimitsu, K.; Izumori, K.; Fleet, G. W. J. *Org. Lett.* **2012**, *14*, 4174–4177.

[81] Wrodnigg, T. M. *Monatsh. Chem.* **2002**, *133*, 393–426.

[82] Ayers, B. J.; Ngo, N.; Jenkinson, S. F.; Martínez, R. F.; Shimada, Y.; Adachi, I.; Weymouth-Wilson, A. C.; Kato, A.; Fleet, G. W. J. *J. Org. Chem.* **2012**, *77*, 7777–7792.

[83] Welter, A.; Jadot, J.; Dardenne, G.; Marlier, M.; Casimir, J. *Phytochemistry* **1976**, *15*, 747–749.

[84] Sinnott, M. L. *Chem. Rev.* **1990**, *90*, 1171–1202.

[85] Gloster, T. M.; Davies, G. J. *Org. Biomol. Chem.* **2009**, *8*, 305–320.

[86] Terwisscha van Scheltinga, A. C.; Armand, S.; Kalk, K. H.; Isogai, A.; Henrissat, B.; Dijkstra, B. W. *Biochemistry* **1995**, *34*, 15619–15623.

[87] Tews, I.; Perrakis, A.; Oppenheim, A.; Dauter, Z.; Wilson, K. S.; Vorgias, C. E. *Nat. Struct. Biol.* **1996**, *3*, 638–648.

[88] Marković-Housley, Z.; Miglierini, G.; Soldatova, L.; Rizkallah, P. J.; Müller, U.; Schirmer, T. *Structure* **2000**, *8*, 1025–1035.

[89] Knapp, S.; Vocadlo, D.; Gao, Z.; Kirk, B.; Lou, J.; Withers, S. G. *J. Am. Chem. Soc.* **1996**, *118*, 6804–6805.

[90] Macauley, M. S.; Whitworth, G. E.; Debowski, A. W.; Chin, D.; Vocadlo, D. J. *J. Biol. Chem.* **2005**, *280*, 25313–25322.

[91] Umekawa, M.; Huang, W.; Li, B.; Fujita, K.; Ashida, H.; Wang, L.-X.; Yamamoto, K. *J. Biol. Chem.* **2008**, *283*, 4469–4479.

[92] Abbott, D. W.; Macauley, M. S.; Vocadlo, D. J.; Boraston, A. B. *J. Biol. Chem.* **2009**, *284*, 11676–11689.

[93] Watts, A. G.; Damager, I.; Amaya, M. L.; Buschiazzo, A.; Alzari, P.; Frasch, A. C.; Withers, S. G. *J. Am. Chem. Soc.* **2003**, *125*, 7532–7533.

[94] Damager, I.; Buchini, S.; Amaya, M. F.; Buschiazzo, A.; Alzari, P.; Frasch, A. C.; Watts, A.; Withers, S. G. *Biochemistry* **2008**, *47*, 3507–3512.

[95] McCarter, J. D.; Withers, S. G. *Curr. Opin. Struct. Biol.* **1994**, *4*, 885–892.

[96] Bols, M. *Acc. Chem. Res.* **1998**, *31*, 1–8.

[97] Withers, S. G.; Namchuk, M.; Mosi, R. Potent Glycoside Inhibitors: Transition State Mimics or Simply Fortuitous Binders? In *Iminosugars as Glycosidase Inhibitors*; Wiley-VCH Verlag GmbH & Co. KGaA: Weinheim, FRG, 1998; pp 188–206.

[98] Zechel, D. L.; Boraston, A. B.; Gloster, T.; Boraston, C. M.; Macdonald, J. M.; Tilbrook, D. M. G.; Stick, R. V.; Davies, G. J. *J. Am. Chem. Soc.* **2003**, *125*, 14313–14323.

[99] Gloster, T. M.; Meloncelli, P.; Stick, R. V.; Zechel, D.; Vasella, A.; Davies, G. J. *J. Am. Chem. Soc.* **2007**, *129*, 2345–2354.

[100] López, O.; Qing, F.-L.; Pedersen, C. M.; Bols, M. *Bioorg. Med. Chem.* **2013**, *21*, 4755–4761.

[101] Casey, J. R.; Grinstein, S.; Orlowski, J. *Nat. Rev. Mol. Cell. Biol.* **2009**, *11*, 50–61.

[102] Marshall, R. D. *Annu. Rev. Biochem.* **1972**, *41*, 673–702.

[103] Stenflo, J.; Fernlund, P. *J. Biol. Chem.* **1982**, *257*, 12180–12190.

[104] Gil, G.-C.; Velander, W. H.; Van Cott, K. E. *Proteomics* **2009**, *9*, 2555–2567.

[105] Chi, Y. H.; Koo, Y. D.; Dai, S. Y.; Ahn, J.-E.; Yun, D.-J.; Lee, S. Y.; Zhu-Salzman, K. *Comp. Biochem. Physiol. B* **2010**, *156*, 40–47.

[106] Matsui, T.; Takita, E.; Sato, T.; Kinjo, S.; Aizawa, M.; Sugiura, Y.; Hamabata, T.; Sawada, K.; Kato, K. *Glycobiology* **2011**, *21*, 994–999.

[107] Katsuri, L.; Eshleman, J. R.; Wunner, W. H.; Shakin-Eshleman, S. H. *J. Biol. Chem.* **1995**, *270*, 14756–14761.

[108] Katsuri, L.; Chen, H. G.; Shakin-Eshleman, S. H. *Biochem. J.* **1997**, *323*, 415–419.

[109] Schulz, B. L. Beyond the Sequon: Sites of N-Glycosylation. In *Glycosylation*; Petrescu, S. M., Ed.; InTech, 2012; pp 21–40.

[110] te Heesen, S.; Lehle, L.; Weissmann, A.; Aebi, M. *Eur. J. Biochem.* **1994**, *224*, 71–79.

[111] Couto, J. R.; Huffaker, T. C.; Robbins, P. W. *J. Biol. Chem.* **1984**, *259*, 378–382.

[112] Cipollo, J. F.; Trimble, R. B.; Chi, J. H.; Yan, Q.; Dean, N. *J. Biol. Chem.* **2001**, *276*, 21828–21840.

[113] Bickel, T.; Lehle, L.; Schwarz, M.; Aebi, M.; Jakob, C. A. *J. Biol. Chem.* **2005**, *280*, 34500–34506.

[114] O'Reilly, M. K.; Zhang, G.; Imperiali, B. *Biochemistry* **2006**, *45*, 9593–9603.

[115] O'Reilly, M. K. Investigating the pathway of asparagine-linked glycoprotein biosynthesis. Ph.D. thesis, Massachusetts Institute of Technology, 2006.

[116] Kampf, M.; Absmanner, B.; Schwarz, M.; Lehle, L. *J. Biol. Chem.* **2009**, *284*, 11900–11912.

[117] Sanyal, S.; Frank, C. G.; Menon, A. K. *Biochemistry* **2008**, *47*, 7937–7946.

[118] Snider, M. D.; Rogers, O. C. *Cell* **1984**, *36*, 753–761.

[119] Rush, J. S.; van Leyen, K.; Ouerfelli, O.; Wolucka, B.; Waechter, C. J. *Glycobiology* **1998**, *8*, 1195–1205.

[120] Rush, J. S.; Waechter, C. J. *J. Cell Biol.* **1995**, *130*, 529–536.

[121] Helenius, A.; Aebi, M. *Annu. Rev. Biochem.* **2004**, *73*, 1019–1049.

[122] Aebi, M.; Gassenhuber, J.; Domdey, H.; te Heesen, S. *Glycobiology* **1996**, *6*, 439–444.

[123] Burda, P.; Aebi, M. *Glycobiology* **1998**, *8*, 455–462.

[124] Cipollo, J. F.; Trimble, R. B. *J. Biol. Chem.* **2000**, *275*, 4267–4277.

[125] Sharma, C. B.; Knauer, R.; Lehle, L. *Biol. Chem.* **2001**, *382*, 321–328.

[126] Cipollo, J. F.; Trimble, R. B. *Glycobiology* **2002**, *12*, 749–762.

[127] Frank, C. G.; Aebi, M. *Glycobiology* **2005**, *15*, 1156–1163.

[128] Breitling, J.; Aebi, M. *Cold Spring Harb. Perspect. Biol.* **2013**, *5*, a013359.

[129] Gilchrist, A.; Au, C. E.; Hiding, J.; Bell, A. W.; Fernandez-Rodriguez, J.; Lesimple, S.; Nagaya, H.; Roy, L.; Gosline, S. J. C.; Hallett, M.; Paiement, J.; Kearney, R. E.; Nilsson, T.; Bergeron, J. J. M. *Cell* **2006**, *127*, 1265–1281.

[130] Pan, S.; Wang, S.; Utama, B.; Huang, L.; Blok, N.; Estes, M. K.; Moremen, K. W.; Sifers, R. N. *Mol. Biol. Cell* **2011**, *22*, 2810–2822.

[131] Rymen, D.; Peanne, R.; Millón, M. B.; Race, V.; Sturiale, L.; Garozzo, D.; Mills, P.; Clayton, P.; Asteggiano, C. G.; Quelhas, D.; Cansu, A.; Martins, E.; Nassogne, M.-C.; Gonçalves-Rocha, M.; Topaloglu, H.; Jaeken, J.; Foulquier, F.; Matthijs, G. *PLoS Genet.* **2013**, *9*, e1003989.

[132] Elbein, A. D. *FASEB J.* **1991**, *5*, 3055–3063.

[133] Mellor, H. R.; Neville, D. C. A.; Harvey, D. J.; Platt, F. M.; Dwek, R. A.; Butters, T. D. *Biochem. J.* **2004**, *381*, 867–875.

[134] Branza-Nichita, N.; Petrescu, A. J.; Negroiu, G.; Dwek, R. A.; Petrescu, S. M. *Chem. Rev.* **2000**, *100*, 4697–4711.

[135] Negroiu, G.; Dwek, R. A.; Petrescu, S. M. *J. Biol. Chem.* **2000**, *275*, 32200–32207.

[136] Ellgaard, L.; Helenius, A. *Nat. Rev. Mol. Cell. Biol.* **2003**, *4*, 181–191.

[137] Branza-Nichita, N.; Lazar, C.; Dwek, R. A.; Zitzmann, N. *Biochem. Biophys. Res. Commun.* **2004**, *319*, 655–662.

[138] Williams, D. B. *J. Cell. Sci.* **2006**, *119*, 615–623.

[139] Hebert, D. N.; Molinari, M. *Physiol. Rev.* **2007**, *87*, 1377–1408.

[140] Petrescu, S. M.; Branza-Nichita, N.; Negroiu, G.; Petrescu, A. J.; Dwek, R. A. *Biochemistry* **2000**, *39*, 5229–5237.

[141] Gonzalez, D. S.; Karaveg, K.; Vandersall-Nairn, A. S.; Lal, A.; Moremen, K. W. *J. Biol. Chem.* **1999**, *274*, 21375–21386.

[142] Iannotti, M. J.; Figard, L.; Sokac, A. M.; Sifers, R. N. *J. Biol. Chem.* **2014**, *289*, 11844–11858.

[143] Sousa, M. C.; Ferrero-Garcia, M. A.; Parodi, A. J. *Biochemistry* **1992**, *31*, 97–105.

[144] Wang, T.; Hebert, D. N. *Nat. Struct. Biol.* **2003**, *10*, 319–321.

[145] Alonzi, D. S.; Neville, D. C. A.; Lachmann, R. H.; Dwek, R. A.; Butters, T. D. *Biochem. J.* **2008**, *409*, 571–580.

[146] Branza-Nichita, N.; Petrescu, A. J.; Dwek, R. A.; Wormald, M. R.; Platt, F. M.; Petrescu, S. M. *Biochem. Biophys. Res. Commun.* **1999**, *261*, 720–725.

[147] Petrescu, S. M.; Petrescu, A. J.; Titu, H. N.; Dwek, R. A.; Platt, F. M. *J. Biol. Chem.* **1997**, *272*, 15796–15803.

[148] Simons, K.; Ikonen, E. *Nature* **1997**, *387*, 569–572.

[149] Simons, K.; van Meer, G. *Biochemistry* **1988**, *27*, 6197–6202.

[150] Simons, K.; Ehehalt, R. *J. Clin. Invest.* **2002**, *110*, 597–603.

[151] Tettamanti, G. *Glycoconj. J.* **2004**, *20*, 301–317.

[152] Basu, S.; Kaufman, B.; Roseman, S. *J. Biol. Chem.* **1973**, *248*, 1388–1394.

[153] Ichikawa, S.; Sakiyama, H.; Suzuki, G.; Hidari, K. I.; Hirabayashi, Y. *Proc. Natl. Acad. Sci. U.S.A.* **1996**, *93*, 4638–4643.

[154] Paul, P.; Kamisaka, Y.; Marks, D. L.; Pagano, R. E. *J. Biol. Chem.* **1996**, *271*, 2287–2293.

[155] Morell, P.; Radin, N. S. *Biochemistry* **1969**, *8*, 506–512.

[156] Basu, S.; Schultz, A. M.; Basu, M.; Roseman, S. *J. Biol. Chem.* **1971**, *246*, 4272–4279.

[157] Butters, T. D.; Mellor, H. R.; Narita, K.; Dwek, R. A.; Platt, F. M. *Philos. Trans. R. Soc. Lond., B, Biol. Sci.* **2003**, *358*, 927–945.

[158] Mellor, H. R.; Neville, D. C. A.; Harvey, D. J.; Platt, F. M.; Dwek, R. A.; Butters, T. D. *Biochem. J.* **2004**, *381*, 861–866.

[159] *Zavesca (miglustat) full prescribing information*; Actelion Pharmaceuticals, 2014.

[160] Orsi, F.; D'Almeida, C. *Curr. Opin. HIV AIDS* **2010**, *5*, 237–241.

[161] Nachega, J. B.; C Marconi, V.; U van Zyl, G.; M Gardner, E.; Preiser, W.; Y Hong, S.; J Mills, E.; Gross, R. *IDDT* **2011**, *11*, 167–174.

[162] Wilkins, T.; Malcolm, J. K. *Am. Fam. Physician* **2010**, *81*, 1351–1357.

[163] Cooper, C. *Clin. Infect. Dis.* **2012**, *55*, 418–425.

[164] Welsch, C.; Shimakami, T.; Hartmann, C.; Yang, Y.; Domingues, F. S.; Lengauer, T.; Zeuzem, S.; Lemon, S. M. *Gastroenterology* **2012**, *142*, 654–663.

[165] *Dengue and Severe Dengue Fact Sheet No. 117*; World Health Organization, 2014.

[166] *Hepatitis B Fact Sheet No. 204*; World Health Organization: Geneva, 2012.

[167] *Hepatitis C Fact Sheet No. 164*; World Health Organization: Geneva, 2012.

[168] *HIV/AIDS Fact Sheet No. 360*; World Health Organization: Geneva, 2014.

[169] Pan, Y. T.; Hori, H.; Saul, R.; Sanford, B. A.; Molyneux, R. J.; Elbein, A. D. *Biochemistry* **1983**, *22*, 3975–3984.

[170] Karpas, A.; Fleet, G. W. J.; Dwek, R. A.; Petursson, S.; Namgoong, S. K.; Ramsden, N. G.; Jacob, G. S.; Rademacher, T. W. *Proc. Natl. Acad. Sci. U.S.A.* **1988**, *85*, 9229–9233.

[171] Fleet, G. W. J.; Karpas, A.; Dwek, R. A.; Fellows, L. E.; Tyms, A. S.; Petursson, S.; Namgoong, S. K.; Ramsden, N. G.; Smith, P. W.; Son, J. C.; Wilson, F.; Witty, D. R.; Jacob, G. S.; Rademacher, T. W. *FEBS Letters* **1988**, *237*, 128–132.

[172] Takatsuki, A.; Tamura, G. *J. Antibiot.* **1971**, *24*, 224–231.

[173] Doerrler, W. T.; Lehrman, M. A. *Proc. Natl. Acad. Sci. U.S.A.* **1999**, *96*, 13050–13055.

[174] Block, T. M.; Lu, X. Y.; Platt, F. M.; Foster, G. R.; Gerlich, W. H.; Blumberg, B. S.; Dwek, R. A. *Proc. Natl. Acad. Sci. U.S.A.* **1994**, *91*, 2235–2239.

[175] Zitzmann, N.; Mehta, A. S.; Carrouée, S.; Butters, T. D.; Platt, F. M.; McCauley, J.; Blumberg, B. S.; Dwek, R. A.; Block, T. M. *Proc. Natl. Acad. Sci. U.S.A.* **1999**, *96*, 11878–11882.

[176] Wu, S. F.; Lee, C. J.; Liao, C. L.; Dwek, R. A.; Zitzmann, N.; Lin, Y. L. *J. Virol.* **2002**, *76*, 3596–3604.

[177] Steinmann, E.; Whitfield, T.; Kallis, S.; Dwek, R. A.; Zitzmann, N.; Pietschmann, T.; Bartenschlager, R. *Hepatology* **2007**, *46*, 330–338.

[178] Miller, J. L.; Lachica, R.; Sayce, A. C.; Williams, J. P.; Bapat, M.; Dwek, R.; Beatty, P. R.; Harris, E.; Zitzmann, N. *Antimicrob. Agents Chemother.* **2012**, *56*, 6379–6386.

[179] Chang, J.; Block, T. M.; Guo, J.-T. *Antiviral Res.* **2013**, *99*, 251–260.

[180] Durantel, D.; Branza-Nichita, N.; Carrouée-Durantel, S.; Butters, T. D.; Dwek, R. A.; Zitzmann, N. *J. Virol.* **2001**, *75*, 8987–8998.

[181] Pavlović, D.; Neville, D. C. A.; Argaud, O.; Blumberg, B.; Dwek, R. A.; Fischer, W. B.; Zitzmann, N. *Proc. Natl. Acad. Sci. U.S.A.* **2003**, *100*, 6104–6108.

[182] Pavlović, D.; Fischer, W.; Hussey, M.; Durantel, D.; Durantel, S.; Branza-Nichita, N.; Woodhouse, S.; Dwek, R. A.; Zitzmann, N. *Adv. Exp. Med. Biol.* **2005**, *564*, 3–4.

[183] Lu, X.; Tran, T.; Simsek, E.; Block, T. M. *J. Virol.* **2003**, *77*, 11933–11940.

[184] Weber, K. T.; Hammache, D.; Fantini, J.; Ganem, B. *Bioorg. Med. Chem. Lett.* **2000**, *10*, 1011–1014.

[185] Nguyen, D. H.; Taub, D. D. *Mol. Interv.* **2004**, *4*, 318–320.

[186] Sakamoto, H.; Okamoto, K.; Aoki, M.; Kato, H.; Katsume, A.; Ohta, A.; Tsukuda, T.; Shimma, N.; Aoki, Y.; Arisawa, M.; Kohara, M.; Sudoh, M. *Nat. Chem. Biol.* **2005**, *1*, 333–337.

[187] Amemiya, F.; Maekawa, S.; Itakura, Y.; Kanayama, A.; Matsui, A.; Takano, S.; Yamaguchi, T.; Itakura, J.; Kitamura, T.; Inoue, T.; Sakamoto, M.; Yamauchi, K.; Okada, S.; Yamashita, A.; Sakamoto, N.; Itoh, M.; Enomoto, N. *J. Infect. Dis.* **2008**, *197*, 361–370.

[188] Tatematsu, K.; Tanaka, Y.; Sugiyama, M.; Sudoh, M.; Mizokami, M. *J. Med. Virol.* **2011**, *83*, 587–593.

[189] Sayce, A. C.; Miller, J. L.; Zitzmann, N. *Trends Microbiol.* **2010**, *18*, 323–330.

[190] Asano, N.; Nishida, M.; Kato, A.; Kizu, H.; Matsui, K.; Shimada, Y.; Itoh, T.; Baba, M.; Watson, A. A.; Nash, R. J.; Lilley, P. M.; Watkin, D. J.; Fleet, G. W. J. *J. Med. Chem.* **1998**, *41*, 2565–2571.

[191] Tierney, M.; Pottage, J.; Kessler, H.; Fischl, M.; Richman, D.; Merigan, T.; Powderly, W.; Smith, S.; Karim, A.; Sherman, J. *J. Acquir. Immune Defic. Syndr. Hum. Retrovirol.* **1995**, *10*, 549–553.

[192] Mehta, A.; Carrouée, S.; Conyers, B.; Jordan, R.; Butters, T.; Dwek, R. A.; Block, T. M. *Hepatology* **2001**, *33*, 1488–1495.

[193] Gu, B.; Mason, P.; Wang, L.; Norton, P.; Bourne, N.; Moriarty, R.; Mehta, A.; Despande, M.; Shah, R.; Block, T. *Antivir. Chem. Chemother.* **2007**, *18*, 49–59.

[194] Pollock, S.; Dwek, R. A.; Burton, D. R.; Zitzmann, N. *AIDS* **2008**, *22*, 1961–1969.

[195] Chang, J.; Wang, L.; Ma, D.; Qu, X.; Guo, H.; Xu, X.; Mason, P. M.; Bourne, N.; Moriarty, R.; Gu, B.; Guo, J.-T.; Block, T. M. *Antimicrob. Agents Chemother.* **2009**, *53*, 1501–1508.

[196] Qu, X.; Pan, X.; Weidner, J.; Yu, W.; Alonzi, D.; Xu, X.; Butters, T.; Block, T.; Guo, J.-T.; Chang, J. *Antimicrob. Agents Chemother.* **2011**, *55*, 1036–1044.

[197] Bush, C. O.; Pokrovskii, M. V.; Saito, R.; Morganelli, P.; Canales, E.; Clarke, M. O.; Lazerwith, S. E.; Golde, J.; Reid, B. G.; Babaoglu, K.; Pagratis, N.; Zhong, W.; Delaney, W. E.; Paulson, M. S.; Beran, R. K. F. *Antimicrob. Agents Chemother.* **2014**, *58*, 386–396.

[198] Mellor, H. R.; Nolan, J.; Pickering, L.; Wormald, M. R.; Platt, F. M.; Dwek, R. A.; Fleet, G. W. J.; Butters, T. D. *Biochem. J.* **2002**, *366*, 225–233.

[199] Schnaar, R. L.; Suzuki, A.; Stanley, P. Glycosphingolipids. In *Essentials of Glycobiology*; Varki, A., Cummings, R. D., Esko, J. D., Freeze, H. H., Stanley, P., Bertozzi, C. R., Hart, G. W., Etzler, M. E., Eds.; Cold Spring Harbor Laboratory Press, Cold Spring Harbor (NY): Cold Spring Harbor (NY), 2009.

[200] Mellor, H. R.; Platt, F. M.; Dwek, R. A.; Butters, T. D. *Biochem. J.* **2003**, *374*, 307–314.

[201] Russell, P. K.; Nisalak, A.; Sukhavachana, P.; Vivona, S. *J. Immunol.* **1967**, *99*, 285–290.

[202] Lin, Y. L.; Liu, C. C.; Lei, H. Y.; Yeh, T. M.; Lin, Y. S.; Chen, R. M.; Liu, H. S. *J. Med. Virol.* **2000**, *60*, 425–431.

[203] Ang, F.; Wong, A. P. Y.; Ng, M. M.-L.; Chu, J. J. H. *Virol. J.* **2010**, *7*, 24.

[204] McCormick, K. D.; Liu, S.; Jacobs, J. L.; Marques, E. T. A.; Sluis-Cremer, N.; Wang, T. *Antimicrob. Agents Chemother.* **2012**, *56*, 3399–3401.

[205] Cruz, D. J. M.; Koishi, A. C.; Taniguchi, J. B.; Li, X.; Milan Bonotto, R.; No, J. H.; Kim, K. H.; Baek, S.; Kim, H. Y.; Windisch, M. P.; Pamplona Mosimann, A. L.; de Borba, L.; Liuzzi, M.; Hansen, M. A. E.; Duarte dos Santos, C. N.; Freitas-Junior, L. H. *PLoS Negl. Trop. Dis.* **2013**, *7*, e2073.

[206] Jessie, K.; Fong, M. Y.; Devi, S.; Lam, S. K.; Wong, K. T. *J. Infect. Dis.* **2004**, *189*, 1411–1418.

[207] Balsitis, S. J.; Coloma, J.; Castro, G.; Alava, A.; Flores, D.; McKerrow, J. H.; Beatty, P. R.; Harris, E. *Am. J. Trop. Med. Hyg.* **2009**, *80*, 416–424.

[208] Manning, J. S.; Collins, J. K. *J. Clin. Microbiol.* **1979**, *10*, 235–239.

[209] Pietschmann, T.; Lohmann, V.; Rutter, G.; Kurpanek, K.; Bartenschlager, R. *J. Virol.* **2001**, *75*, 1252–1264.

[210] Scholle, F.; Li, K.; Bodola, F.; Ikeda, M.; Luxon, B. A.; Lemon, S. M. *J. Virol.* **2004**, *78*, 1513–1524.

[211] Nelson, H. B.; Tang, H. *J. Virol.* **2006**, *80*, 1181–1190.

[212] Reed, L. J.; Muench, H. *Am. J. Hyg.* **1938**, *27*, 493–497.

[213] Bitzegeio, J.; Bankwitz, D.; Hueging, K.; Haid, S.; Brohm, C.; Zeisel, M. B.; Herrmann, E.; Iken, M.; Ott, M.; Baumert, T. F.; Pietschmann, T. *PLoS Pathog.* **2010**, *6*, e1000978.

[214] Koutsoudakis, G.; Kaul, A.; Steinmann, E.; Kallis, S.; Lohmann, V.; Pietschmann, T.; Bartenschlager, R. *J. Virol.* **2006**, *80*, 5308–5320.

[215] Gentzsch, J.; Hinkelmann, B.; Kaderali, L.; Irschik, H. *Antiviral Res.* **2011**, *89*, 136–148.

[216] Barbier, J.; Wegner, J.; Benson, S.; Gentzsch, J.; Pietschmann, T.; Kirschning, A. *Chem. Eur. J.* **2012**, *18*, 9083–9090.

[217] Best, D.; Wang, C.; Weymouth-Wilson, A. C.; Clarkson, R. A.; Wilson, F. X.; Nash, R. J.; Miyauchi, S.; Kato, A.; Fleet, G. W. J. *Tetrahedron: Asymmetry* **2010**, *21*, 311–319.

[218] Butters, T. D.; van den Broek, L.; Fleet, G. W. J.; Krulle, T. M.; Wormald, M. R.; Dwek, R. A.; Platt, F. M. *Tetrahedron: Asymmetry* **2000**, *11*, 113–124.

[219] Kato, T.; Date, T.; Murayama, A.; Morikawa, K.; Akazawa, D.; Wakita, T. *Nat. Protoc.* **2006**, *1*, 2334–2339.

[220] Fischer, E. *Ber. Dtsch. Chem. Ges.* **1894**, *27*, 2985–2993.

[221] Jenkinson, S. F.; Fleet, G. W. J.; Nash, R. J.; Koike, Y.; Adachi, I.; Yoshihara, A.; Morimoto, K.; Izumori, K.; Kato, A. *Org. Lett.* **2011**, *13*, 4064–4067.

[222] Balzarini, J. *FEBS Letters* **2007**, *581*, 2060–2064.

[223] Saeki, H.; Ohki, E. *Chem. Pharm. Bull.* **1968**, *16*, 2477–2481.

[224] Kinast, G.; Schedel, M. *Angew. Chem.* **1981**, *93*, 799–800.

[225] Vasella, A.; Voeffray, R. *Helv. Chim. Acta* **1982**, *65*, 1134–44.

[226] Bernotas, R. C.; Ganem, B. *Tetrahedron Lett.* **1984**, *25*, 165–168.

[227] Fleet, G. W. J.; Smith, P. W. *Tetrahedron Lett.* **1985**, *26*, 1469–1472.

[228] Legler, G.; Pohl, S. *Carbohyd. Res.* **1986**, *155*, 119–129.

[229] Fleet, G. W. J.; Fellows, L. E.; Smith, P. W. *Tetrahedron* **1987**, *43*, 979–990.

[230] Bernotas, R. C.; Pezzone, M. A.; Ganem, B. *Carbohyd. Res.* **1987**, *167*, 305–311.

[231] Fleet, G. W. J.; Ramsden, N. G.; Molyneux, R. J.; Jacob, G. S. *Tetrahedron Lett.* **1988**, *29*, 3603–3606.

[232] Fleet, G. W. J.; Ramsden, N. G.; Witty, D. R. *Tetrahedron Lett.* **1988**, *29*, 2871–2874.

[233] Pederson, R. L.; Kim, M.-J.; Wong, C.-H. *Tetrahedron Lett.* **1988**, *29*, 4645–4648.

[234] Broxterman, H. J. G.; Neefjes, J. J.; Van der Marel, G. A.; Ploegh, H. L.; Van Boom, J. H. *J. Carbohydr. Chem.* **1988**, *7*, 593–603.

[235] Hashimoto, H.; Hayakawa, M. *Chem. Lett.* **1989**, 1881–1884.

[236] Pederson, R. L.; Wong, C.-H. *Heterocycles* **1989**, *28*, 477–80.

[237] Fleet, G. W. J.; Ramsden, N. G.; Witty, D. R. *Tetrahedron* **1989**, *45*, 319–326.

[238] Paulsen, H.; Matzke, M.; Orthen, B.; Nuck, R.; Reutter, W. *Liebigs Ann. Chem.* **1990**, 953–63.

[239] Reitz, A. B.; Baxter, E. W. *Tetrahedron Lett.* **1990**, *31*, 6777–6780.

[240] Anzeveno, P. B.; Creemer, L. J. *Tetrahedron Lett.* **1990**, *31*, 2085–2088.

[241] Heiker, F.-R.; Schueller, A. M. *Carbohyd. Res.* **1990**, *203*, 314–318.

[242] Aoyagi, S.; Fujimaki, S.; Yamazaki, N.; Kibayashi, C. *J. Org. Chem.* **1991**, *56*, 815–819.

[243] Behling, J.; Farid, P.; Medich, J. R.; Scaros, M. G.; Prunier, M.; Weier, R. M.; Khanna, I. *Synthetic Commun.* **1991**, *21*, 1383–1386.

[244] Kajimoto, T.; Chen, L.; Liu, K. K. C.; Wong, C.-H. *J. Am. Chem. Soc.* **1991**, *113*, 6678–6680.

[245] de Raadt, A.; Stütz, A. E. *Tetrahedron Lett.* **1992**, *33*, 189–192.

[246] Lees, W. J.; Whitesides, G. M. *Bioorg. Chem.* **1992**, *20*, 173–179.

[247] Baxter, E. W.; Reitz, A. B. *Bioorg. Med. Chem. Lett.* **1992**, *2*, 1419–1422.

[248] Chida, N.; Furuno, Y.; Ikemoto, H.; Ogawa, S. *Carbohyd. Res.* **1992**, *237*, 185–194.

[249] Smid, P.; Schipper, F. J. M.; Broxterman, H. J. G.; Boons, G. J. P. H.; Van der Marel, G. A.; Van Boom, J. H. *Recl. Trav. Chim. Pays-Bas* **1993**, *112*, 451–6.

[250] Zhou, P.; Salleh, H. M.; Chan, P. C. M.; Lajoie, G.; Honek, J. F.; Nambiar, P. T. C.; Ward, O. P. *Carbohyd. Res.* **1993**, *239*, 155–166.

[251] Fowler, P. A.; Haines, A. H.; Taylor, R. J. K.; Chrystal, E. J. T.; Gravestock, M. B. *Carbohyd. Res.* **1993**, *246*, 377–381.

[252] Chida, N.; Tanikawa, T.; Tobe, T.; Ogawa, S. *J. Chem. Soc., Chem. Commun.* **1994**, 1247–1248.

[253] Park, K. H.; Yoon, Y. J.; Lee, S. G. *J. Chem. Soc., Perkin Trans. 1* **1994**, 2621–2623.

[254] Rudge, A. J.; Collins, I.; Holmes, A. B.; Baker, R. *Angew. Chem.* **1994**, *106*, 2416–2418.

[255] Poitout, L.; Le Merrer, Y.; Depezay, J.-C. *Tetrahedron Lett.* **1994**, *35*, 3293–3296.

[256] Asano, N.; Oseki, K.; Kaneko, E.; Matsui, K. *Carbohyd. Res.* **1994**, *258*, 255–266.

[257] Park, K. H. *B. Kor. Chem. Soc.* **1995**, *16*, 985–988.

[258] Johnson, C. R.; Golebiowski, A.; Sundram, H.; Miller, M. W.; Dwaihy, R. L. *Tetrahedron Lett.* **1995**, *36*, 653–654.

[259] Johnson, C. R.; Golebiowski, A.; Schoffers, E.; Sundram, H.; Braun, M. P. *Synlett* **1995**, *1995*, 313–314.

[260] Altenbach, H.-J.; Himmeldirk, K. *Tetrahedron: Asymmetry* **1995**, *6*, 1077–1080.

[261] Gradnig, G.; Legler, G.; Stütz, A. E. *Carbohyd. Res.* **1996**, *287*, 49–57.

[262] Poitout, L.; Le Merrer, Y.; Depezay, J.-C. *Tetrahedron Lett.* **1996**, *37*, 1609–1612.

[263] Barili, P. L.; Berti, G.; Catelani, G.; D'Andrea, F.; DeRensis, F. *Tetrahedron* **1997**, *53*, 8665–8674.

[264] Le Merrer, Y.; Poitout, L.; Depezay, J.-C.; Dosbaa, I.; Geoffroy, S.; Foglietti, M.-J. *Bioorg. Med. Chem.* **1997**, *5*, 519–533.

[265] Grandel, R.; Kazmaier, U. *Tetrahedron Lett.* **1997**, *38*, 8009–8012.

[266] Hügel, H. M.; Hughes, A. B.; Khalil, K. *Aust. J. Chem.* **1998**, *51*, 1149.

[267] Kazmaier, U.; Grandel, R. *Eur. J. Org. Chem.* **1998**, *1998*, 1833–1840.

[268] Lindström, U. M.; Somfai, P. *Tetrahedron Lett.* **1998**, *39*, 7173–7176.

[269] Schaller, C.; Vogel, P.; Jäger, V. *Carbohyd. Res.* **1998**, *314*, 25–35.

[270] Ruiz, M.; Ojea, V.; Quintela, J. M. *Synlett* **1999**, *1999*, 204–206.

[271] Uriel, C.; Santoyo-González, F. *Synlett* **1999**, *1999*, 593–595.

[272] Meyers, A. I.; Andres, C. J.; Resek, J. E.; Woodall, C. C.; McLaughlin, M. A.; Lee, P. H.; Price, D. A. *Tetrahedron* **1999**, *55*, 8931–8952.

[273] Lee, B. W.; Jeong, I.-Y.; Yang, M. S.; Choi, S. U.; Park, K. H. *Synthesis* **2000**, *2000*, 1305–1309.

[274] Martín, R.; Moyano, A.; Pericàs, M. A.; Riera, A. *Org. Lett.* **2000**, *2*, 93–95.

[275] Yokoyama, H.; Otaya, K.; Kobayashi, H.; Miyazawa, M.; Yamaguchi, S.; Hirai, Y. *Org. Lett.* **2000**, *2*, 2427–2429.

[276] Haukaas, M. H.; O'Doherty, G. A. *Org. Lett.* **2001**, *3*, 401–404.

[277] Spreitz, J.; Stütz, A. E.; Wrodnigg, T. M. *Carbohyd. Res.* **2002**, *337*, 183–186.

[278] Ruiz, M.; Ojea, V.; Ruanova, T. M.; Quintela, J. M. *Tetrahedron: Asymmetry* **2002**, *13*, 795–799.

[279] Joseph, C. C.; Regeling, H.; Zwanenburg, B.; Chittenden, G. J. F. *Carbohyd. Res.* **2002**, *337*, 1083–1087.

[280] Banwell, M. G.; Ma, X.; Asano, N.; Ikeda, K.; Lambert, J. N. *Org. Biomol. Chem.* **2003**, *1*, 2035–2037.

[281] Knight, J. G.; Tchabanenko, K. *Tetrahedron* **2003**, *59*, 281–286.

[282] Ostrowski, J.; Altenbach, H.-J.; Wischnat, R.; Brauer, D. J. *Eur. J. Org. Chem.* **2003**, *2003*, 1104–1110.

[283] Singh, O. V.; Han, H. *Tetrahedron Lett.* **2003**, *44*, 2387–2391.

[284] Takahata, H.; Banba, Y.; Ouchi, H.; Nemoto, H. *Org. Lett.* **2003**, *5*, 2527–2529.

[285] Dondoni, A.; Richichi, B.; Marra, A.; Perrone, D. *Synlett* **2004**, 1711–1714.

[286] Pyun, S.-J.; Lee, K.-Y.; Oh, C.-Y.; Ham, W.-H. *Heterocycles* **2004**, *62*, 333–341.

[287] Dhavale, D. D.; Markad, S. D.; Karanjule, N. S.; PrakashaReddy, J. *J. Org. Chem.* **2004**, *69*, 4760–4766.

[288] Amat, M.; Huguet, M.; Llor, N.; Bassas, O.; Gómez, A. M.; Bosch, J.; Badia, J.; Baldoma, L.; Aguilar, J. *Tetrahedron Lett.* **2004**, *45*, 5355–5358.

[289] Dhavale, D. D.; Kumar, K. S. A.; Chaudhari, V. D.; Sharma, T.; Sabharwal, S. G.; PrakashaReddy, J. *Org. Biomol. Chem.* **2005**, *3*, 3720–3726.

[290] Pyun, S.-J.; Lee, K.-Y.; Oh, C.-Y.; Joo, J.-E.; Cheon, S.-H.; Ham, W.-H. *Tetrahedron* **2005**, *61*, 1413–1416.

[291] Kato, A.; Kato, N.; Kano, E.; Adachi, I.; Ikeda, K.; Yu, L.; Okamoto, T.; Banba, Y.; Ouchi, H.; Takahata, H.; Asano, N. *J. Med. Chem.* **2005**, *48*, 2036–2044.

[292] Martín, R.; Murruzzu, C.; Pericàs, M. A.; Riera, A. *J. Org. Chem.* **2005**, *70*, 2325–2328.

[293] Boglio, C.; Stahlke, S.; Thorimbert, S.; Malacria, M. *Org. Lett.* **2005**, *7*, 4851–4854.

[294] Hong, B.-C.; Chen, Z.-Y.; Nagarajan, A.; Kottani, R.; Chavan, V.; Chen, W.-H.; Jiang, Y.-F.; Zhang, S.-C.; Liao, J.-H.; Sarshar, S. *Carbohyd. Res.* **2005**, *340*, 2457–2468.

[295] Boucheron, C.; Compain, P.; Martin, O. R. *Tetrahedron Lett.* **2006**, *47*, 3081–3084.

[296] Wei, B.-g.; Chen, J.; Lin, G.-j.; Huang, P.-q. *J. Xiamen Univ.* **2006**, *45*, 670–672.

[297] Maier, P.; Andersen, S. M.; Lundt, I. *Synthesis* **2006**, *2006*, 827–830.

[298] Ghosh, S.; Shashidhar, J.; Dutta, S. K. *Tetrahedron Lett.* **2006**, *47*, 6041–6044.

[299] Sugiyama, M.; Hong, Z.; Whalen, L. J.; Greenberg, W. A.; Wong, C.-H. *Adv. Synth. Catal.* **2006**, *348*, 2555–2559.

[300] Tzanetou, E. N.; Kasiotis, K. M.; Magiatis, P.; Haroutounian, S. A. *Molecules* **2007**, *12*, 735–744.

[301] Guaragna, A.; D'Errico, S.; D'Alonzo, D.; Pedatella, S.; Palumbo, G. *Org. Lett.* **2007**, *9*, 3473–3476.

[302] Sugiyama, M.; Hong, Z.; Liang, P.-H.; Dean, S. M.; Whalen, L. J.; Greenberg, W. A.; Wong, C.-H. *J. Am. Chem. Soc.* **2007**, *129*, 14811–14817.

[303] Malle, B. M.; Lundt, I.; Wrodnigg, T. M. *Org. Biomol. Chem.* **2008**, *6*, 1779–1786.

[304] Ruiz, M.; Ruanova, T. M.; Blanco, O.; Núñez, F.; Pato, C.; Ojea, V. *J. Org. Chem.* **2008**, *73*, 2240–2255.

[305] Zhou, Y.; Murphy, P. V. *Org. Lett.* **2008**, *10*, 3777–3780.

[306] Zhang, H.; Liu, H.; Chen, X.; Qu, L.; Zhao, Y. *Huaxue Tongbao* **2008**, *71*, 361–367.

[307] Concia, A. L.; Lozano, C.; Castillo, J. A.; Parella, T.; Joglar, J.; Clapés, P. *Chem. Eur. J.* **2009**, *15*, 3808–3816.

[308] Racine, E.; Bello, C.; Gerber-Lemaire, S.; Vogel, P.; Py, S. *J. Org. Chem.* **2009**, *74*, 1766–1769.

[309] Gupta, P.; Vankar, Y. D. *Eur. J. Org. Chem.* **2009**, *2009*, 1925–1933.

[310] Palyam, N.; Majewski, M. *J. Org. Chem.* **2009**, *74*, 4390–4392.

[311] Rengasamy, R.; Curtis-Long, M. J.; Ryu, H.-W.; Oh, K.-Y.; Park, K. H. *B. Kor. Chem. Soc.* **2009**, *30*, 1531–1534.

[312] Schitter, G.; Scheucher, E.; Steiner, A. J.; Stütz, A. E.; Thonhofer, M.; Tarling, C. A.; Withers, S. G.; Wicki, J.; Fantur, K.; Paschke, E.; Mahuran, D. J.; Rigat, B. A.; Tropak, M.; Wrodnigg, T. M. *Beilstein J. Org. Chem.* **2010**, *6*.

[313] Bagal, S. K.; Davies, S. G.; Lee, J. A.; Roberts, P. M.; Russell, A. J.; Scott, P. M.; Thomson, J. E. *Org. Lett.* **2010**, *12*, 136–139.

[314] Wennekes, T.; Meijer, A. J.; Groen, A. K.; Boot, R. G.; Groener, J. E.; van Eijk, M.; Ottenhoff, R.; Bijl, N.; Ghauharali, K.; Song, H.; O'Shea, T. J.; Liu, H.; Yew, N.; Copeland, D.; van den Berg, R. J.; van der Marel, G. A.; Overkleeft, H. S.; Aerts, J. M. *J. Med. Chem.* **2010**, *53*, 689–698.

[315] Karjalainen, O. K.; Passiniemi, M.; Koskinen, A. M. P. *Org. Lett.* **2010**, *12*, 1145–1147.

[316] van den Nieuwendijk, A. M. C. H.; Ruben, M.; Engelsma, S. E.; Risseeuw, M. D. P.; van den Berg, R. J. B. H. N.; Boot, R. G.; Aerts, J. M.; Brussee, J.; van der Marel, G. A.; Overkleeft, H. S. *Org. Lett.* **2010**, *12*, 3957–3959.

[317] Gandy, M. N.; Piggott, M. J.; Stubbs, K. A. *Aust. J. Chem.* **2010**, *63*, 1409–1412.

[318] Kumar, I.; Rode, C. V. *Tetrahedron: Asymmetry* **2010**, *21*, 2703–2708.

[319] Karjalainen, O. K.; Koskinen, A. M. P. *Org. Biomol. Chem.* **2011**, *9*, 1231–1236.

[320] Singh, A.; Kim, B.; Lee, W. K.; Ha, H.-J. *Org. Biomol. Chem.* **2011**, *9*, 1372–1380.

[321] Lamas, M.-C.; Malacria, M.; Thorimbert, S. *Eur. J. Org. Chem.* **2011**, *2011*, 2777–2780.

[322] Timmer, M. S. M.; Dangerfield, E. M.; Cheng, J. M. H.; Gulab, S. A.; Stocker, B. L. *Tetrahedron Lett.* **2011**, *52*, 4803–4805.

[323] Cho, J. K.; Rengasamy, R.; Curtis-Long, M. J.; Kim, J. H.; Lee, J. W.; Park, K. H. *J. Korean Soc. Appl. Biol. Chem.* **2011**, *54*, 881–888.

[324] Mettu, R.; Thatikonda, N. R.; Budde, M.; Vaidya, J. R. *ARKIVOC* **2012**, 287–302.

[325] Scarpi, D.; Bartali, L.; Casini, A.; Occhiato, E. G. *Eur. J. Org. Chem.* **2012**, *2012*, 2597–2605.

[326] Davies, S. G.; Figuccia, A. L. A.; Fletcher, A. M.; Roberts, P. M.; Thomson, J. E. *Org. Lett.* **2013**, *15*, 2042–2045.

[327] Hoecker, J.; Rudolf, G. C.; Bächle, F.; Fleischer, S.; Lindner, B. D.; Helmchen, G. *Eur. J. Org. Chem.* **2013**, *2013*, 5149–5159.

[328] Singh, P.; Manna, S. K.; Panda, G. *Tetrahedron* **2014**, *70*, 1363–1374.

[329] Bashyal, B. P.; Chow, H. F.; Fellows, L. E.; Fleet, G. W. J. *Tetrahedron* **1987**, *43*, 415–422.

[330] Best, D.; Chairatana, P.; Glawar, A. F. G.; Crabtree, E.; Butters, T. D.; Wilson, F. X.; Yu, C.-Y.; Wang, W.-B.; Jia, Y.-M.; Adachi, I.; Kato, A.; Fleet, G. W. J. *Tetrahedron Lett.* **2010**, *51*, 2222–2224.

[331] Glawar, A. F. G.; Best, D.; Ayers, B. J.; Miyauchi, S.; Nakagawa, S.; Aguilar-Moncayo, M.; García Fernández, J. M.; Ortiz Mellet, C.; Crabtree, E. V.; Butters, T. D.; Wilson, F. X.; Kato, A.; Fleet, G. W. J. *Chem. Eur. J.* **2012**, *18*, 9341–9359.

[332] Weymouth-Wilson, A. C.; Clarkson, R. A.; Jones, N. A.; Best, D.; Wilson, F. X.; Pino-González, M.-S.; Fleet, G. W. J. *Tetrahedron Lett.* **2009**, *50*, 6307–6310.

[333] Ratner, L.; Vander Heyden, N. *AIDS Res. Hum. Retroviruses* **1993**, *9*, 291–297.

[334] Brennan, T. M.; Taylor, D. L.; Bridges, C. G.; Leyda, J. P.; Tyms, A. S. *Antiviral Res.* **1995**, *26*, 173–187.

[335] Fischl, M. A.; Resnick, L.; Coombs, R.; Kremer, A. B.; Pottage, J. C.; Fass, R. J.; Fife, K. H.; Powderly, W. G.; Collier, A. C.; Aspinall, R. L. *J. Acquir. Immune Defic. Syndr.* **1994**, *7*, 139–147.

[336] Overkleeft, H. S.; Renkema, G. H.; Neele, J.; Vianello, P.; Hung, I. O.; Strijland, A.; van der Burg, A. M.; Koomen, G. J.; Pandit, U. K.; Aerts, J. *J. Biol. Chem.* **1998**, *273*, 26522–26527.

[337] Wennekes, T.; van den Berg, R. J. B. H. N.; Donker, W.; van der Marel, G. A.; Strijland, A.; Aerts, J. M. F. G.; Overkleeft, H. S. *J. Org. Chem.* **2007**, *72*, 1088–1097.

[338] Horwitt, M. K.; Harvey, C. C.; Duncan, G. D.; Wilson, W. C. *Am. J. Clin. Nutr.* **1956**, *4*, 408–419.

[339] Nakamura, M.; Hayashi, T. *Arch. Biochem. Biophys.* **1992**, *299*, 313–319.

[340] Bunyan, J.; McHale, D.; Green, J.; Marcinkiewicz, S. *Br. J. Nutr.* **1961**, *15*, 253–257.

[341] Weiser, H.; Vecchi, M.; Schlachter, M. *Int. J. Vitam. Nutr. Res.* **1986**, *56*, 45–56.

[342] Weiser, H.; Riss, G.; Kormann, A. W. *J. Nutr.* **1996**, *126*, 2539–2549.

[343] Traber, M. G.; Sies, H. *Annu. Rev. Nutr.* **1996**, *16*, 321–347.

[344] Drevon, C. A. *Free Radic. Res. Commun.* **1991**, *14*, 229–246.

[345] Bouzide, A.; Sauvé, G. *Tetrahedron Lett.* **1997**, *38*, 5945–5948.

[346] Bligh, E. G.; Dyer, W. J. *Can. J. Biochem. Physiol.* **1959**, *37*, 911–917.

[347] Chevy, F.; Illien, F.; Wolf, C.; Roux, C. *J. Lipid Res.* **2002**, *43*, 1192–1200.

[348] Chevy, F.; Humbert, L.; Wolf, C. *Prenatal Diagnosis* **2005**, *25*, 1000–1006.

[349] Ivanova, P. T.; Milne, S. B.; Byrne, M. O.; Xiang, Y.; Brown, H. A. *Meth. Enzymol.* **2007**, *432*, 21–57.

[350] Wolf, C.; Quinn, P. J. *Prog. Lipid Res.* **2008**, *47*, 15–36.

[351] Quinn, P. J.; Rainteau, D.; Wolf, C. **2009**, *579*, 127–159.

[352] Haimi, P.; Chaithanya, K.; Kainu, V.; Hermansson, M.; Somerharju, P. *Lipidomics* **2010**, 285–294.

[353] Myers, D. S.; Ivanova, P. T.; Milne, S. B.; Brown, H. A. *Biochim. Biophys. Acta* **2011**, *1811*, 748–757.

[354] Goti, D.; Reicher, H.; Malle, E.; Kostner, G. M.; Panzenboeck, U.; Sattler, W. *Biochem. J.* **1998**, *332*, 57–65.

[355] Mardones, P.; Quiñones, V.; Amigo, L.; Moreno, M.; Miquel, J. F.; Schwarz, M.; Miettinen, H. E.; Trigatti, B.; Krieger, M.; VanPatten, S.; Cohen, D. E.; Rigotti, A. *J. Lipid Res.* **2001**, *42*, 170–180.

[356] Goti, D.; Hrzenjak, A.; Levak-Frank, S.; Frank, S.; van der Westhuyzen, D. R.; Malle, E.; Sattler, W. *J. Neurochem.* **2001**, *76*, 498–508.

[357] Traber, M. G.; Kayden, H. J. *Am. J. Clin. Nutr.* **1984**, *40*, 747–751.

[358] Thellman, C. A.; Shireman, R. B. *J. Nutr.* **1985**, *115*, 1673–1679.

[359] Narushima, K.; Takada, T.; Yamanashi, Y.; Suzuki, H. *Mol. Pharmacol.* **2008**, *74*, 42–49.

[360] Rigotti, A. *Mol. Aspects Med.* **2007**, *28*, 423–436.

[361] Durantel, D.; Carrouée-Durantel, S.; Branza-Nichita, N.; Dwek, R. A.; Zitzmann, N. *Antimicrob. Agents Chemother.* **2004**, *48*, 497–504.

[362] Gripon, P.; Rumin, S.; Urban, S.; Le Seyec, J.; Glaise, D.; Cannie, I.; Guyomard, C.; Lucas, J.; Trépo, C.; Guguen-Guillouzo, C. *Proc. Natl. Acad. Sci. U.S.A.* **2002**, *99*, 15655–15660.

[363] Dorobantu, C.; Macovei, A.; Lazar, C.; Dwek, R. A.; Zitzmann, N.; Branza-Nichita, N. *J. Virol.* **2011**, *85*, 13373–13383.

[364] Jeanes, Y. M.; Hall, W. L.; Ellard, S.; Lee, E.; Lodge, J. K. *Br. J. Nutr.* **2004**, *92*, 575–579.

[365] Horwitt, M. K. *Am. J. Clin. Nutr.* **1960**, *8*, 451–461.

[366] Ferslew, K. E.; Acuff, R. V.; Daigneault, E. A.; Woolley, T. W.; Stanton, P. E. *J Clin. Pharmacol.* **1993**, *33*, 84–88.

[367] Traber, M. G.; Ramakrishnan, R.; Kayden, H. J. *Proc. Natl. Acad. Sci. U.S.A.* **1994**, *91*, 10005–10008.

[368] Hall, W. L.; Jeanes, Y. M.; Lodge, J. K. *J. Nutr.* **2005**, *135*, 58–63.

[369] Jeanes, Y. M.; Hall, W. L.; Lodge, J. K. *Br. J. Nutr.* **2005**, *94*, 92–99.

[370] Chuang, J. C.; Matel, H. D.; Nambiar, K. P.; Kim, S.-H.; Fadel, J. G.; Holstege, D. M.; Clifford, A. J. *J. Nutr.* **2011**, *141*, 1482–1488.

[371] Treiber, A.; Morand, O.; Clozel, M. *Xenobiotica* **2007**, *37*, 298–314.

[372] Miller, J. L.; deWet, B. M.; Martinez-Pomares, L. *PLoS Pathog.* **2008**, *4*, e17.

[373] Eggeling, C.; Ringemann, C.; Medda, R.; Schwarzmann, G.; Sandhoff, K.; Polyakova, S.; Belov, V. N.; Hein, B.; von Middendorff, C.; Schönle, A.; Hell, S. W. *Nature* **2009**, *457*, 1159–1162.

[374] Mueller, V.; Ringemann, C.; Honigmann, A.; Schwarzmann, G.; Medda, R.; Leutenegger, M.; Polyakova, S.; Belov, V. N.; Hell, S. W.; Eggeling, C. *Biophys. J.* **2011**, *101*, 1651–1660.

[375] Wennekes, T. Lipophilic iminosugars: synthesis and evaluation as inhibitors of glucosylceramide metabolism. Ph.D. thesis, Universiteit Leiden, Leiden, 2008.

[376] Dax, K.; Graßberger, V.; Stütz, A. E. *J. Carbohydr. Chem.* **1990**, *9*, 903–908.

[377] Wang, R.-W.; Qiu, X.-L.; Bols, M.; Ortega-Caballero, F.; Qing, F.-L. *J. Med. Chem.* **2006**, *49*, 2989–2997.

JOHN LEON KIAPPES, JR.

DEPARTMENT OF BIOCHEMISTRY • SOUTH PARKS ROAD • OXFORD OX1 3QU• UK

CURRENT POSITION

- **Lerner–Fink Postdoctoral Fellow in Medicinal Chemistry**
  Oxford Glycobiology Institute, Department of Biochemistry
  University of Oxford, Oxford, UK
  September 2014 – Present

EDUCATION

- **PhD in Organic Chemistry and DPhil in Biochemistry**

  Thesis: *Synthesis and Biological Characterization of Natural and Designed Sugars*
  University of Oxford, Lincoln College, Oxford, UK
  The Scripps Research Institute, La Jolla, California, USA
  August 2008 – August 2014
  GPA (4.00 scale): 4.00
- **B.S. in Chemistry (A.C.S. Certified), Summa Cum Laude, Wiess College of Natural Sciences**
  Rice University, Houston, Texas, USA
  August 2004 – May 2008
  GPA (4.00 scale): 4.10
  GRE: Quantitative: 800 (94th Percentile), Verbal: 660 (94th Percentile), Writing: 5.5
  GRE Chemistry: 910, 98th Percentile

AWARDS AND ACHIEVEMENTS

- Oxford University Glycobiology-Unither Virology Award *(2014)*
- Lincoln College Senior Scholarship *(2012 – 2013)*
- American Chemical Society Leadership Development Award *(2010)*
- Skaggs-Oxford Fellowship, University of Oxford and Scripps Research Institute *(2008 – 2014)*
- National Science Foundation Graduate Research Fellowship, NSF *(2008 – 2013)*
- Zevi and Bertha Salsburg Memorial Award in Chemistry, Rice University *(2008)*
- George Holmes Richter Memorial Fellowship in Chemistry, Rice University *(2007)*
- Arthur L. Draper Award in Chemistry, Rice University *(2007)*
- Rice Undergraduate Honors Research Fellowship *(2006 – 2007)*
- Silver Medalist at International Chemistry Olympiad *(2004*)

RESEARCH EXPERIENCE

- **Graduate Research Assistant, University of Oxford, Oxford, UK**

  Advisor: Prof. N. Zitzmann, Department of Biochemistry *(January 2011 – August 2014)*
  - Synthesis and evaluation of novel broad spectrum antivirals
  - Experience in synthesis of iminosugars, cell and virus culture, antiviral screening development, enzymology
- **Graduate Research Assistant, The Scripps Research Institute, La Jolla, California, USA**

  Advisor: Prof. K.C. Nicolaou, Department of Chemistry *(August 2008 – January 2011)*
  - Synthesis of the carboline disaccharide domain of shishijimicin
  - Experience in sugar synthesis
- **Undergraduate Research Assistant, Rice University, Houston, Texas, USA**

  Advisor: Prof. James M. Tour, Department of Chemistry *(August 2006 – May 2008)*

TEACHING EXPERIENCE

- **University of Oxford, Oxford, UK**
  Carbohydrate Chemistry (Department of Biochemistry, *HT 2015 – present)*
  Organic Chemistry for Biochemists (Lincoln College, *MT 2013 – present)*
  Biochemistry for Medics (Merton College, *MT 2012 – present*)
  Bench Supervision of one summer intern and four Part II students
  Admissions Interviews (Christ Church, *MT 2012)*
- **International Chemistry Olympiad**
  Representative of Americas, International Steering Committee (*July 2008 – July 2012*)
  Member of Scientific Committee for the 44th IChO (*2010 - 2012*)
  Member of United States delegation (Head Mentor *2011*, Scientific Observer *2007 – 2010*)
- **US Chemistry Olympiad, US Air Force Academy, Colorado Springs, Colorado, USA**
  Head Mentor (*2011*), Peer Mentor *(2006-2008)*
  - Instructed students on procedural and conceptual issues in a chemistry laboratory
  - Provided nightly tutoring regarding both laboratory and theoretical chemistry
- **Department of Chemistry, Rice University, Houston, Texas, USA**
  Honors Organic Chemistry Teaching Assistant *(Fall 2005-Spring 2008)*
  General Chemistry Teaching Assistant *(Spring 2007, Spring 2008)*

PUBLICATIONS

- Isolation and SAR Studies of Bicyclic Iminosugars from *Castanospermum australe* as Glycosidase Inhibitors; A. Kato, Y. Hirokami, K. Kinami, Y. Tsuji, S. Miyawaki, I. Adachi, J. Hollinshead, R. J. Nash, **J. L. Kiappes,** N. Zitzmann, J. K. Cha, R. J. Molyneux, G. W. J. Fleet, N. Asano; Phytochem. 111, 124-131 (2015).
- Synthesis of the Carboline Disaccharide Domain of Shishijimicin A; K. C. Nicolaou, **J. L. Kiappes**, W. Tian, V. B. Gondi, J. Becker; Org. Lett. 13(15), 3924-3927 (2011).
- Synthesis of Fluorescent Dye-Tagged Nanomachines for Single-Molecule Fluorescence Spectroscopy; G. Vives, J. M. Guerrero, J. Godoy, S. Khatua, Y.-P. Wang, **J. L. Kiappes**, S. Link, J. M. Tour; J. Org. Chem. 75(19), 6631-6643 (2010).
- Synthesis of a Porphyrin-Fullerene Pinwheel; T. Sasaki, A. J. Osgood**, J. L. Kiappes**, K. F. Kelly, J. M. Tour; Org. Lett. 10(7), 1377-1380 (2008).

PATENT APPLICATIONS

- Glycolipid Inhibition Using Iminosugars; T. Butters, D. Alonzi, S. Pollock, P. Laing, **J. L. Kiappes**, N. Zitzmann, R. A. Dwek; U.S. Patent Application 61929704, 2014.
- Novel Iminosugars and Their Applications; **J. L. Kiappes**, P. Laing, R. A. Dwek, N. Zitzmann; U.S. Patent Application 61656265, 2012.

BOOK CHAPTER

- S. Ching, D. Prieto-Centurion, **J. L. Kiappes**, and K. H. Whitmire. (2014) Bis[Bis(Triphenylphosphoranylidene)Ammonium] Undecacarbonyltriferrate(2–), in *Inorganic Syntheses*: Volume 36 (Eds. G. S. Girolami and A. P. Sattelberger), John Wiley & Sons , Inc., Hoboken, NJ, USA.

CONFERENCE PRESENTATIONS

- Antivirals in Stereo: Structure Activity Relationships of Iminosugars in Three Dimensions; **J. L. Kiappes**, J. L. Miller, M. Hill, A. Kato, R. A. Dwek, N. Zitzmann; Talk at Third Antivirals Congress, Amsterdam, Netherlands, October 2014.
- Evaluation and Mechanistic Characterization of a Novel Anti-HCV Iminosugar; **J. L. Kiappes**, S. Pollock, M. Hill, D. S. Alonzi, T. D. Butters, R. A. Dwek, N. Zitzmann; Poster presented at 19th International Symposium on Hepatitis C Virus and Related Viruses, Venice, Italy, October 2012.
- Chemistry Olympiad: Perspectives as a Student and Mentor; **J. L. Kiappes**; Invited talk at 21st Biennial Conference on Chemical Education, Denton, USA, August 2010.